NIR HYPERSPECTRAL IMAGING FOR PREDICTING THE COMPOSITION OF GRANULAR FOOD COMMODITIES

by

Nicola Caporaso

BSc, MSc

Thesis submitted to The University of Nottingham

in partial fulfilment of the requirements

for the degree of Doctor of Philosophy

in Food Sciences

Division of Food Sciences

School of Biosciences

University of Nottingham

December 2017

Acknowledgments

I would like to thank my supervisor, Professor Ian Fisk, for giving me the opportunity to undertake the research outlined in this thesis, as well as my secondary university supervisor, Dr. Stephen Grebby, who supported me during my PhD. The entire period of research has been carried out at Campden BRI, in a joint project that was set up within a network linking the University of Nottingham with Campden BRI and Buhler, to whom I am grateful for providing me with the opportunity of carrying out this project and making it successful. I am especially grateful to Buhler for providing the funding. I am thankful to Dr. Martin Whitworth for all the support he gave me, the training, guidance, continuous feedback and encouragement, and I feel fortunate that I met such a passionate and dedicated scientist. I am grateful to Dr. Timothy Kelf and Dr. Matthias Graeber for their innovative vision, their encouragement and positive feedback over these years. Mark Fowler is kindly acknowledged for giving me wise suggestions and helping me in taking a wider view on my project and my professional development. Dr. Alix Cornish, Dr. Simon Penson and Dr. Erika Georget are acknowledged for the useful scientific discussions. During these 3 years of work, I have met many people at Campden BRI and at the University of Nottingham, to whom my acknowledgments are expressed for their friendship and support: Dr. Charfedinne Ayed, Gloria (Chujiao) Liu, and all other PhD students and postgraduates (Clive, Vlad, Nicole, Wei, Su, Normando, Vincenzo, Filippo, Simone and many others). I also would like to thank my family for the continuous support; and especially one person. Just your presence, and talking to you, makes my life better and happier. Thanks for your patience and unconditional love.

Supervisory committee:

- Prof. Ian D. Fisk
- Dr. Martin B. Whitworth
- Dr. Stephen Grebby
- Dr. Timothy Kelf
- Dr. Matthias R. Graeber

TABLE OF CONTENTS

Abstract vii
1. **Introduction** 1
2. **Literature review** 6
2.1. Theory of NIR absorption 6
2.2. NIRS and HSI in agriculture and food research 11
2.3. Instrumentation 12
2.3.1. Machine vision technology 12
2.3.2. Hyperspectral imaging 13
2.4. Applications of HSI in food science and technology 19
2.4.1. Quality inspection of granular food commodities 26
2.4.2. Single grain analysis 30
2.4.3. On-line application of NIR and HSI 34
2.4.4. Limitations 36
2.4.5. Advantages of HSI 37
2.5. Data handling 38
2.5.1. Structure of the data cube (hypercube) 39
2.5.2. Image analysis 40
2.5.3. Chemometrics and multivariate analysis 42
2.5.4. Outlier identification and removal 47
2.5.5. Model validation and independence of the datasets 47
2.5.6. Application of calibrations 49
2.6. Wheat quality 50
2.6.1. HSI for wheat quality inspection 53
2.6.2. Prediction of wheat enzymatic activity 55
2.7. Cocoa quality 58
2.7.1. Cocoa composition 61
2.7.2. NIR and HSI applied for cocoa analysis 63
2.8. Coffee quality 65
2.8.1. Coffee composition 67
2.8.2. Coffee roasting 68
2.8.3. Coffee flavour generation 70
2.8.4. Variability of coffee aroma compounds 75
2.8.5. NIRS and HSI applied for coffee quality evaluation 77
3. **Wheat protein prediction in single kernels** 82
3.1. Introduction 82
3.2. Material and Methods 83
3.2.1. Wheat samples 83
3.2.2. Hyperspectral imaging 84

3.2.3. Analysis of hyperspectral data....85
3.2.4. Reference analysis for protein analysis....90
3.2.5. Data analysis and PLS calibration....91
3.2.6. Manual sorting of wheat kernels....92
3.3. Results and discussion....93
3.3.1. Single kernel protein variability....93
3.3.2. Protein prediction by HSI and application of the calibration....97
3.3.3. Bulk HSI protein prediction....103
3.3.4. Effect of kernel presentation, hardness and spectral range....105
3.3.5. Validation of single-kernel sorting....109
3.4. Conclusions....116
4. **Prediction of pre-germinated wheat kernels influencing Hagberg Falling Number**....118
4.1. Introduction....118
4.2. Materials and methods....120
4.2.1. Wheat samples....120
4.2.2. Hagberg Falling Number measurement....122
4.2.3. HSI data acquisition and treatment....123
4.2.4. Statistical treatment of the data....123
4.3. Results and Discussion....124
4.3.1. Distribution of HFN in wheat samples....124
4.3.2. PLS calibration for HFN prediction....125
4.3.3. Methods to apply calibrations to hyperspectral images....127
4.3.4. LDA for wheat classification related to sprouting problems....133
4.4. Conclusions....136
5. **Cocoa composition: lipid content prediction**....137
5.1. Introduction....137
5.2. Materials and Methods....139
5.2.1. Samples and reagents....139
5.2.2. Hyperspectral imaging analysis....141
5.2.3. Total fat analysis....141
5.2.4. Colour measurement....141
5.2.5. Data treatment and statistical analysis....142
5.2.6. Visualisation of chemical images....143
5.3. Results and Discussion....143
5.3.1. Reference analysis of fat content analysis....143
5.3.2. HSI for fat content prediction....146
5.3.3. Wavelength selection for multi-spectral imaging systems....155
5.3.4. Application of HSI calibration....156
5.3.5. HSI for colour prediction models....159
5.4. Conclusions....159

6. **Cocoa beans: fermentation index, antioxidant activity and total polyphenol prediction** 161
6.1. Introduction ... 161
6.2. Materials and Methods ... 163
6.2.1. Samples and reagents ... 163
6.2.2. Hyperspectral imaging ... 163
6.2.3. Fermentation index ... 164
6.2.4. Total polyphenols ... 164
6.2.5. Antioxidant activity ... 165
6.2.6. Statistical analysis ... 166
6.3. Results and Discussion ... 167
6.3.1. Reference measurements of TP, AA and FI ... 167
6.3.2. HSI calibrations for whole cocoa beans ... 172
6.3.3. Use of non-linear algorithms (SVM-R) ... 180
6.3.4. Visualisation of cocoa constituents at single bean level ... 180
6.4. Conclusions ... 184
7. **Coffee beans: prediction of moisture and fat content on single beans** ... 185
7.1. Introduction ... 185
7.2. Materials and Methods ... 187
7.2.1. Coffee samples ... 187
7.2.2. Reference analyses for moisture and fat ... 190
7.2.3. Hyperspectral imaging and data treatment ... 191
7.2.4. Statistical analysis ... 191
7.3. Results and Discussion ... 192
7.3.1. Descriptive statistics for reference measurements ... 192
7.3.2. Moisture and fat prediction in single green coffee beans ... 194
7.3.3. Wavelength selection ... 203
7.3.4. Application of PLS calibrations (chemical mapping) ... 206
7.3.5. Coffee bean species classification ... 209
7.4. Conclusions ... 211
8. **Prediction of sucrose, caffeine and trigonelline in single green coffee beans.** ... 212
8.1. Introduction ... 212
8.2. Materials and Methods ... 214
8.2.1. Coffee samples, chemicals and reagents ... 214
8.2.2. HSI analysis ... 214
8.2.3. Caffeine, sucrose and trigonelline extraction ... 214
8.2.4. HPLC/MS analysis ... 215
8.2.5. Recovery experiment, limits of detection and quantification ... 217
8.2.6. Data processing and statistical analysis ... 217
8.3. Results and Discussion ... 218
8.3.1. Coffee constituent variation and accuracy of reference measurement ... 218

8.3.2. PLS regression for prediction of coffee constituents 223
8.3.3. Application of the calibrations (chemical images) 236
8.4. Conclusions 239
9. **Coffee aroma generation prediction from green and roasted single coffee beans** 240
9.1. Introduction 240
9.2. Materials and Methods 243
9.2.1. Coffee samples and chemicals 243
9.2.2. Sample preparation and roasting 243
9.2.3. SPME-GC/MS analysis 244
9.2.4. Colour measurement 246
9.2.5. HSI acquisition, data treatment and statistical analysis 247
9.2.6. GC-MS analysis of sorted coffee beans 247
9.2.7. Sensory analysis of sorted coffee beans 247
9.3. Results and Discussion 250
9.3.1. Reference analysis of volatile compounds 250
9.3.2. Roasted coffee: HSI prediction of volatile compounds 257
9.3.3. Green coffee: HSI prediction of volatile compounds 262
9.3.4. Roasted coffee: prediction of chemical groups and aroma impact 266
9.3.5. Green coffee: prediction of chemical groups and odour impact 271
9.3.6. Application of calibrations (chemical images) 275
9.3.7. Manual sorting of coffee batches: GC-MS 277
9.3.8. Manual sorting of green coffee batches: sensory analysis 280
9.3.9. Discussion 283
9.4. Conclusions 288
10. **General discussion and Conclusions** 289
References 293
Appendix 314

ABSTRACT

Hyperspectral imaging (HSI) in the Near-Infrared (NIR) spectral range was applied for non-destructive characterisation of three staple food commodities: wheat, cocoa and coffee. Industrially-relevant properties such as moisture, fat and proteins were explored on a single seed basis. Prediction models were built for whole wheat kernels, cocoa seeds (de-shelled i.e., cotyledons or nibs) and green coffee beans. Major constituents were successfully predicted in the three commodities with performance allowing quantitative prediction for screening purposes and quality control. In addition, chemical compounds found at lower concentrations were analysed. This comprised indirect methods for enzymatic activity in wheat, polyphenols and antioxidant activity in cocoa, and sucrose, caffeine and trigonelline in green coffee beans. Calibration models built from HSI scanning of green and roasted coffee beans demonstrated the potential to predict generated volatile compounds upon roasting. This approach has been also performed to demonstrate the potential to understand variability at single kernel/seed basis, which can be used for quality improvement of food grains/seeds. HSI-based quantification for single seeds (as well as single pixel level) could be used as a selection tool to create different streams, e.g. for specific product characteristics or to obtain a more consistent composition of the final food product or segregating materials into different process streams with different commercial values. This research work is of strong practical interest, due to the potential applications.

List of abbreviations

AA	Antioxidant Activity
ABTS	2,2'-azino-bis(3-ethylbenzothiazoline-6-sulphonic acid
CCD	Charge-Coupled Device
CMOS	Complementary Metal Oxide Semiconductor
CV	Coefficient of Variation
DPPH	2,2-diphenyl-1-picrylhydrazyl
FI	Fermentation Index
PFA	Focal Plane Array
FT-IR	Fourier-Transform Infrared
GC-MS	Gas Chromatography-Mass Spectroscopy
HSI	Hyperspectral Imaging
LDA	Linear Discriminant Analysis
LV	Latent Variable
MIR	Mid-Infrared
MLR	Multiple Linear Regression
MSC	Multiple Scatter Correction
NIR	Near-Infrared
NIRS	Near-Infrared Spectroscopy
NMR	Nuclear Magnetic Resonance
PC	Principal Component
PCA	Principal Component Analysis
PCR	Principal Component Regression
PLS	Partial Least Square
PLS-DA	Partial Least Square Discriminant Analysis
PLSR	Partial Least Squares Regression
PTR-MS	Proton-Transfer Reaction Mass Spectrometry
RMSE	Root Mean Square Error
RMSEC	Root-Mean Square Error of Calibration
RMSECV	Root-Mean Square Error of Cross Validation
RMSEP	Root-Mean Square Error of Prediction
ROI	Region Of Interest
RPD	Ratio of Performance Deviation
SEL	Standard Error of the Laboratory
SPME	Solid-Phase Micro Extraction
SNV	Standard Normal Variate
SVM	Support Vector Machine
SWIR	Short Wave Infrared
TP	Total Polyphenols
UV	Ultraviolet
VIS	Visible

Peer-reviewed papers

- Caporaso, N., Whitworth, M. B., & Fisk, I. D. (2018) Near Infrared Spectroscopy and Hyperspectral Imaging for non-destructive quality assessment of cereal grains. *Applied Spectroscopy Reviews*. 1-21.
- Caporaso, N., Whitworth, M. B., & Fisk, I. D. (2017). Application of calibrations to hyperspectral images of food grains: example for wheat falling number. *Journal of Spectral Imaging*, *6*(a4), 1-15.
- Caporaso, N., Whitworth, M. B., & Fisk, I. D. (2018). Protein content prediction in single wheat kernels using hyperspectral imaging. *Food Chemistry*, *240*, 32-42.
- Caporaso, N., Whitworth, M. B., Fowler, M.., Fisk, I. D. (2018) Hyperspectral imaging for rapid non-destructive analysis of single cocoa beans: fermentation index, polyphenol content and antioxidant activity. Food *Chemistry. 30,* 343-351.
- Caporaso, N., Whitworth, M. B., Grebby, S., & Fisk, I. D. (2018). Rapid prediction of single green coffee bean moisture and lipid content by hyperspectral imaging. *Journal of Food Engineering*, *227*, 18-29.
- Caporaso, N., Whitworth, M. B., Grebby, S., Fisk, I. D. (2018). Non-destructive analysis of sucrose, caffeine and trigonelline on single green coffee beans by hyperspectral imaging. *Food Research International. 106*, 193-203.
- Caporaso, N., Whitworth, M. B, Fisk, I. D. (2018). Variability of single bean coffee volatile compounds of Arabica and robusta roasted coffees analysed by SPME-GC-MS. *Food Research International. 108,* 628-640.

Oral communications

- Hyperspectral imaging as a tool for the prediction of flavour potential (protein derived flavours) on a single UK wheat kernels basis. *3rd Nursten Postgraduate Flavour Symposium. Northumbria University, Newcastle. July 2015.*
- Applications of calibrations to Hyperspectral images: example for wheat Falling number. *IASIM 2016, 6th conference on Spectral Imaging, Chamonix-Mont Blanc, France. July 2016.*
- Investigating green coffee quality characteristics on a single bean basis by hyperspectral imaging: potential for aroma generation prediction. *4th Nursten Postgraduate Flavour Symposium. Reading University, UK. June 2016.* [RSC/SCI award for best contribution to flavour science]
- HSI for rapid screening of quality parameters in granular food commodities. *Hyperspectral Imaging & Applications Conference, Coventry, UK. October 2016*.
- Hyperspectral imaging as a tool for the screening and non-destructive evaluation of green coffee at a single coffee bean level. *5th Nursten Flavour Symposium. AFBI, Belfast, June 2017.*
- Hyperspectral imaging for the rapid non-destructive prediction of wheat kernel properties. *Nabim (National Association of British and Irish Millers) research and development annual meeting. London, November 2017*.

Scientific posters

- Caporaso, N., Whitworth, M. B., Fisk, I. D. Single coffee bean non-destructive chemical characterisation by hyperspectral imaging. London's ExCeL. *November 2017*.
- Caporaso, N., Whitworth, M. B., Fisk, I. D. Application of hyperspectral imaging for rapid screening of key quality parameters in cereal grains. *4th International Conference and Exhibition on Food Processing, London, UK. August 2015.*
- Caporaso, N., Whitworth, M. B., Fisk, I. D. Assessment of hyperspectral imaging for measurement of single kernel protein variation in UK wheat. *Joint ICC/AISTEC Conference at the World Expo, Milan, Italy. July 2015.*

1. INTRODUCTION

Spectral imaging is a combination of imaging and spectroscopy techniques. Hyperspectral imaging (HSI) acquires a large number (typically hundreds) of discrete, contiguous spectral bands so that a full spectrum is obtained for each pixel of the image. When working in the Near-Infrared (NIR) region, information is obtained on the chemical composition of a material. NIR Spectroscopy (NIRS) is characterised by its non-destructive nature and its ability to analyse products in a non-contact manner. It has the advantage of rapid analysis and little or no sample preparation. The food industry has the need to analyse the raw material, intermediate products and the final products to assess their composition and other parameters related to their quality, preferably with reduced costs and minimal or no sample preparation. Having a rapid non-destructive method that gives information on the product composition, for off-line or on-line applications, is important for quality assurance and quality control, and even more broadly to ensure the product quality.

However, standard NIRS offers information just on bulk, therefore variability that is naturally encountered in terms of chemical composition within a food product is averaged and not fully explored using this technique. In particular, food grains and seeds show large variation due to genetic and environmental factors, and differences can be observed even within the same batch.

Appropriate data treatment is required to extract useful and relevant information from the spectral data, to remove uninformative spectral variation. When the aim is to quantify the composition of a material, a calibration is required to build a relationship between the observed spectral characteristics and sample composition assessed by a reference measurement. As HSI contains hundreds of variables (spectral bands), multivariate statistical analysis is required to build prediction models, which require adequate numbers of samples with potentially the widest range of variation expected for future predictions.

The benefit of imaging is the addition of the spatial dimension to the spectral information. For practical applications, at both the laboratory and industrial scale, HSI offers the advantage to acquire an image for multiple seeds at a time and discriminate the results for each, contrary to

traditional NIR spectroscopy. This results in faster scanning and a higher throughput, which is of strong industrial interest. In addition, imaging offers the possibility to apply prediction models on food products at the single pixel level within an image, giving the capability to visualise the distribution of target compounds across a seed. Once a HSI calibration is built, automation is possible, thus allowing rapid inspection of the whole production and automatic evaluation of the target parameter.

This thesis will present several applications of HSI for the non-destructive study of granular food materials, which are basic ingredients for many food products. In particular, the aim of the current research was to explore the possibility of single object analysis, rather than applying averaged predictions on batches. Using this approach, once calibration models are developed, it is possible to report composition variability of single seeds within and between batches. It is possible to scan multiple seeds at a time so that a relatively high throughout can be analysed and seeds with composition outside the accepted range can be segregated.

The potential of HSI for the non-destructive analysis of granular food products has been explored, by focusing when possible at a single kernel or bean level. The aim was to carry out feasibility studies to demonstrate whether it is possible to measure commercially relevant chemical properties of these raw food ingredients in a rapid manner using HSI. This will be of benefit for industry and for research laboratories, e.g. breeding programmes. Even when quantification at an adequately low prediction error is not possible, HSI still offers the advantage to perform a rapid general screening, so that sub-fractions can be selected for further analyses using other more accurate methods. Whilst traditional NIR-based methods are often able to substitute chemical analyses, HSI provides the capability to study the distribution of properties within samples. However, generation of reference data for single grains for calibration purposes presents challenges.

The choice of the food products studied in this thesis was based on the evaluation and selection of the most important commodities on the international market, and on the potential suitability of HSI for rapid screening of key quality parameters related to the chemical composition. This was based on a detailed literature review to understand the most critical quality factors, especially

in terms of the chemical composition, and also considering a reasonable detection in the NIR spectrum. The general aim was to obtain a technology that successfully allows rapid analysis of grains and can potentially be implemented at a larger scale for automatic inspection and quality control. This would also enable sorting and segregation of kernels/beans with particular characteristics, for allocation to different production streams. In turn, this will lead to more consistent product, as a more consistent raw material is obtained. As a consequence, there is a potential for producers, traders and processors to obtain added value from the raw material.

Specific objectives of this thesis include:

- To build quantitative prediction models for total protein content in whole wheat kernels from different origins on a single kernel basis;
- To estimate Hagberg Falling Number value on whole wheat kernels and verify whether classification of kernels with excessive enzymatic activity can be done;
- To predict fat content in single whole cocoa beans or nibs (i.e. unshelled or shelled) from different origins;
- To estimate parameters such as antioxidant activity, total phenolic compounds and fermentation index in single cocoa beans or nibs;
- To predict moisture and lipid content of green coffee beans at a single bean basis;
- To estimate the concentration of coffee constituents such as caffeine, trigonelline and caffeine in single green coffee beans;
- To evaluate the feasibility of using HSI spectra from green and roasted coffee beans to predict the generation of volatile compounds in the resulting roasted coffee beans, at a single coffee bean level.

The research hypotheses investigated in the present thesis can be summarised as follows:

- Hyperspectral imaging (HSI) is able to predict the chemical composition of small seeds (kernels, beans) individually for quantification purposes.
- Compounds present at lower concentration commonly analysed by NIR spectroscopy or HSI can be predicted for screening purposes.

- Secondary properties of wheat kernels related to their enzymatic activity can be estimated using HSI.
- Whilst the cocoa shell is likely to prevent penetration of NIR radiation in the seed, it is still possible to predict internal chemical composition.
- The application of HSI quantitative calibrations allows the screening of batches to obtain information on the distribution of chemical composition in the population. When applied at single pixel level, it also allows visualising compound spatial distribution across single seeds.
- It is possible to sort grains according to their key quality parameters in a non-destructive way using HSI based on single seed composition, obtaining sub-fractions that are significantly different in composition.
- The sorting of single coffee beans according to the predicted aroma generated after roasting gives batches that are significantly different by sensory test.

Thesis structure. The thesis presents the development of a method to explore the chemical composition of food granular commodities on a single-object basis. It is organised into 10 chapters.

Following this introduction, Chapter 2 presents an overview of the theory behind HSI, the instrumentation and the application of HSI in the food industry with particular focus on calibrations for quality parameters of food granular commodities, as well as the data treatment (chemometrics) required to build prediction models. More information is reported in relation to the food products investigated in the present thesis, i.e. wheat, cocoa and coffee. Chapters 3 and 4 present applications of HSI for the study of whole wheat kernel composition and properties, to predict protein content in single kernels, and to estimate Hagberg Falling Number. Chapters 5 and 6 describe the application of HSI for single cocoa bean evaluation, to predict composition on seeds as unshelled or shelled cocoa nibs, in particular lipid content, total polyphenols and other parameters such as antioxidant activity, fermentation index and colour. Chapters 7, 8 and 9 report on the use of HSI for the study of single coffee beans. Moisture and lipid content were predicted

in single green coffee beans, in addition to classification models to discriminate for coffee species. The prediction of quality-related chemical compounds, namely sucrose, caffeine and trigonelline, in single green coffee beans is presented in Chapter 8, while Chapter 9 reports on the potential to predict coffee aroma generation in roasted coffee based on HSI measurements of single green beans. The prediction of aroma generated upon roasting has been investigated by scanning either the green coffee beans or the roasted coffee beans, to build quantitative prediction models for aroma groups and expected sensory impact. Finally, Chapter 10 gives a general discussion, conclusions and suggestions for future works.

2. LITERATURE REVIEW

2.1. THEORY OF NIR ABSORPTION

The term spectroscopy relates to the study of the interaction of matter with radiation. It is widely used in the food industry as it can be easily implemented for non-destructive analysis of food products (Burns & Ciurczak, 2007). The Near Infrared (NIR) region is defined as the region at 12821–4000 cm^{-1} (780-2500 nm) (Figure 2.1). It measures the overtone and combination bands of molecular vibrations, which differs from the infrared region (2500-25000nm) where the fundamental stretching, bending, wagging and scissoring absorbances can be directly measured (Workman & Weyer, 2012).

The interaction can occur in two ways, namely the selective absorption of energy at a given frequency by specific vibrational modes of molecular bonds, and scattering of energy through reflective, refractive and diffractive processes as a function of the number of interfaces between the matter and its surrounding medium (Shenk, Workman, & Westerhaus, 2001). The most interacting bonds are those having strong dipoles such as C-H, O-H and N-H. Functional groups do not produce distinct, identifiable bands as absorption bands are very broad and overlapped. This seems a disadvantage of NIR, due the difficult assignment of features to individual chemical compounds, but working in the NIR region allows easier sample presentation and greater penetrative power in the sample. NIR is particularly sensitive to the hydrogen bonds, thus it is readily applicable for the analysis of water, alcohols, proteins and sugars (Osborne et al., 1993).

Infrared (IR) spectroscopy studies the vibrations associated to molecules, through the measurement of the transmitted or reflected light that occurs at various wavelengths when a sample is irradiated with infrared radiation (Pelletier & Pelletier, 2010; Sasic, Ozaki, & (Eds.), 2011; Shenk et al., 2001; Workman & Weyer, 2012). The wavelengths at which molecules absorb, reflect, and transmit electromagnetic radiation are characteristics of their structure (Pelletier & Pelletier, 2010). This makes spectroscopy able to provide characteristic "fingerprints" of the sample composition by using these observed changes in molecular energy levels (Huang et al., 2014).

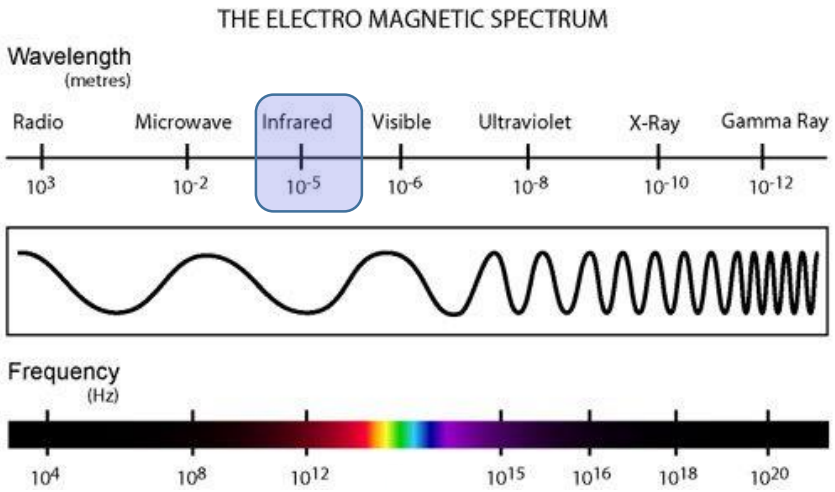


Figure 2.1 The electromagnetic spectrum highlighting the relationship between increased frequency and decreased wavelength (Modified from Wikimedia Commons [CC-BY-SA-2.5]).

The band assignment in NIR spectroscopy is much more difficult than Mid-Infrared (MIR, 5-40 μm wavelength) spectroscopy, due to the severe overlapping of the absorbance bands, which makes the interpretation complicated. Overtone and combination bands are about 10-100 times less intense than MIR absorption bands. Table 2.1 lists the absorption bands reported for specific chemical bonds, and the relative assignment for the chemical structure. NIR can be applied for analysing the chemical composition of materials, by giving information on the absorption of C-H, O-H and N-H chemical bonds. The carbonyl (C=O) group, which includes compounds such as aldehydes and ketones, has peak absorption at 2180, 2140, 2030, 1950, 1920, 1900, 1450 and 1160 nm. Absorption at 1960 nm has been attributed to aldehydes and ketones, while the region 1900-1950 nm is due to esters, 1920 nm to peptides and 1900 to carbonylic acids, which is close to a water absorption feature, i.e. 1940 nm. More generally, the C-H combination bands have higher absorption in the 1000-1100 and 2000-2500 nm regions (Osborne et al., 1993).

Table 2.1. Characteristic wavelengths in Near-Infrared (Shenk et al., 2001).

Wavelength (nm)	Bond vibration	Structure
1143	C−H second overtone	Aromatic
1160	C=O stretch fourth overtone	C=O
1170	C−H second overtone	-HC=CH
1195	C−H second overtone	$-CH_3$
1215	C−H second overtone	$-CH_2$
Wavelength (nm)	**Bond vibration**	**Structure**
1225	C−H second overtone	-CH
1360	C−H combination	$-CH_3$
1395	C−H combination	$-CH_2$
1410	O−H first overtone	ROH, oil
1415	C−H combination	$-CH_2$
1417	C−H combination	Aromatic
1420	O−H first overtone	ArOH
1440	C−H combination	$-CH_2$
1446	C−H combination	Aromatic
1450	O−H stretch first overtone	Starch; H_2O
1450	C=O stretch third overtone	C=O
1460	Sym N−H stretch first overtone	Urea
1463	N−H stretch first overtone	$-CONH_2$
1471	N−H stretch first overtone	-CONHR
1483	N−H stretch first overtone	$-CONH_2$
1490	N−H stretch first overtone	-CONHR
1490	O−H stretch first overtone	Cellulose
1490	Sym N−H stretch first overtone	Urea
1492	N−H stretch first overtone	$ArNH_2$
1500	N−H stretch first overtone	-NH
1510	N−H stretch first overtone	Protein
1520	N−H stretch first overtone	Urea
1530	N−H stretch first overtone	RNH_2
1540	O−H stretch first overtone	Starch
1570	N−H stretch first overtone	CONH
1620	C−H stretch first overtone	$=CH_2$
1685	C−H stretch first overtone	Aromatic
1695	C−H stretch first overtone	$-CH_3$
1705	C−H stretch first overtone	$-CH_3$
1725	C−H stretch first overtone	$-CH_2$
1740	S−H stretch first overtone	−SH
1765	C−H stretch first overtone	CH_2
1780	C− stretch first overtone	Cellulose
1780	C−H stretch/HOH deformation combination	Cellulose
1790	O−H combination	Water
1820	O−H stretch/C−O stretch second overtone combination	Cellulose
1860	C−C1 stretch sixth overtone	$C-C_1$
1900	C=O stretch second overtone	$-CO_2H$

Table 2.1 (*continued*)		
1908	O−H stretch first overtone	P−OH
1920	C=O stretch second overtone	-CONH
1930	O−H stretch/HOH deformation combination	Starch; cellulose
1940	O−H bend second overtone	H_2O
1950	C=O stretch second overtone	$-CO_2R$
1960	O−H stretch/O−H bend combination	Starch
1980	Asym N−H stretch/amide II[a] combination	$-CONH_2$
Wavelength (nm)	**Bond vibration**	**Structure**
1990	N−H stretch/N−H bend combination	Urea
2030	C=O stretch second overtone	Urea
2050	N−H/Amide II[a] or N−H/Amide III[a] or combination	-CONH; $CONH_2$
2055	Sym N−H stretch/amide I[a] combination	Protein
2060	N−H bend second overtone or N−H bend/N−H str. comb.	Starch
2070	N−H deformation overtone	Urea
2070	O−H combination	Oil
2090	O−H combination	-OH
2100	O−H bend/C−O stretch combination	Starch
2100	Asym C−O−O stretch third overtone	Cellulose
2140	C−H stretch/C=O stretch combination or sym.	?
	C−H deformation	Oil; HC=CH
2170	Asym C−H stretch/C−H deformation combination	HC=CH
2180	N−H bend second overtone	Protein
	C−H stretch/C=O stretch combination	Protein
	C=O stretch/amide III[a] combination	Protein
2200	C−H stretch/C=O stretch combination	−CHO
2270	O−H stretch/C−O stretch combination	Cellulose
2280	C−H stretch/CH_2 deformation	Starch
2300	C−H bend second overtone	Protein
2310	C−H bend second overtone	Oil
2322	C−H stretch/CH_2 deformation combination	Starch
2330	C−H stretch/CH_2 deformation combination	Starch
2335	C−H stretch/C−H deformation	Cellulose
2352	CH_2 bend second overtone	Cellulose; protein
2380	C−H stretch/C−C stretch combination	Oil
2470	C−H combination	$-CH_2$
2470	Sym C−N−C stretch first overtone	Protein
2488	C−H stretch/C−C stretch combination	Cellulose
2500	C−H stretch/C−C and C−O−C stretch	Starch
2530	Asym C−N−C stretch first overtone	Protein

[a]Amide I: C=O stretch. Amide II: N-H in-plane bend; C-N stretch. Amide III: N-H in-plane blend; C-N stretch.

The path length of NIR radiation is usually a few millimetres in food samples or even up to a few centimetres depending on the physical properties of the sample, but in any case it is longer than

that of MIR. This effect is beneficial for the analysis of big samples as multiple scattering of the light inside the material is possible. MIR and NIR spectra follow the Beer-Lambert law in the absence of scattering, while diffuse scattering is governed by Kubelka Munk theory. The analysis of food samples using NIR gives the advantage of less or no sample preparation in comparison to the MIR region, but more extensive application of data analysis is required. Particle size, hardness and sample density are the most important factors driving the depth of radiation penetration (Ferrari, Foca, & Ulrici, 2013). The penetration length tends to be smaller at longer wavelengths and also depends on the ratio of the refractive indices of the sample and the angle of incidence (Osborne, Fearn, & Hindle, 1993). The pathway of a photon is known to depend on the number of scattering centres and the scattering properties of the material under analysis (Boldrini, Kessler, Rebner, & Kessler, 2012). Qin and Lu (2009) reported that the light penetration depth in many fruits and vegetables was between 0.43 to 8.67 cm, in the spectral region 500-1000 nm, however the majority of these materials often show a penetration of just a few millimetres (Qin & Lu, 2009). Depending on the food material, the penetration depth of NIR light has been reported up to 4 mm in the region 700-900 nm, while it was 2-3 mm in the range 900-1900 nm (Lammertyn, Peirs, De Baerdemaeker, & Nicolaı, 2000). Other authors reported a penetration depth of 13 mm in fish tissue (Hampton, Cavinato, & Mayes, 2003). Using diffuse NIR hyperspectral imaging for fruit and vegetables, the light penetration depth was between 0.97 and 6.52 cm in the NIR region 500-1000 nm (Qin & Lu, 2008).

In addition, it has been reported that, for samples with complex composition, the absorption of specific groups of compounds can be slightly different from their theoretical absorbance if a pure compound or standard is used. For example, absorbance bands appear at ~1450 and ~1930 nm for pure water, while for water in complex samples these wavelengths consist of several overlapping bands, and the apparent location of these bands might change from one sample to another. It has been also been reported that the spectrum profile can be altered by changing sample temperature, as at higher temperature the band at 1900 nm reduces and the one at 1928 nm increases (Shenk et al., 2001). The critical role of temperature is explained by its influence on the anharmonicity of absorbing groups (Pelletier & Pelletier, 2010).

2.2. NIRS AND HSI IN AGRICULTURE AND FOOD RESEARCH

The first applications of NIR spectroscopy (NIRS) reported in the literature date back to the 1940s and 1950s, while the first commercial applications for moisture detection were developed in the 60s by Delwiche at the United States Department of Agriculture (USDA). At the beginning of the 1960s, NIR instruments used a limited number of selected wavelengths to monitor some food components such as protein, fat and moisture in grain. Some works on forage quality assessment using NIRS were reported in the late 70s, followed by the spread of commercial solutions, also due to the development of chemometrics and computers, both in terms of computational capacity and new software (Afseth & Böker, 2011; Sasic et al., 2011; Shenk et al., 2001).

The advances in optics, computers and chemometric methods for the analysis of spectral data allowed NIR spectroscopy to overcome the issues related to the traditional domain of using it only as a laboratory tool. Moreover, the lowering in the costs enhanced its feasibility for real time, on-line measurements or for the monitoring and inspection of processed food products or unprocessed, raw ingredients. NIR spectroscopy is currently largely applied at the agricultural and industrial levels for the analysis of bulk, average properties (Burns & Ciurczak, 2007). A further advance was provided by techniques enabling the measurement of spatial variations in the properties of food products, which can be beneficial to obtain effective inspection. The term "hyperspectral imaging" was formulated in the field of remote sensing. During the 1970s and 1980s HSI was used for airborne mineral mapping, while the use of CCD cameras allowed further development of the technology (Park & Lu, 2015). In 1983, NASA's laboratories developed the Airborne Visible/Infrared Imaging Spectrometer (AVIRIS), while it was in 1987 that the first hyperspectral image was acquired in the NIR region 400-2500 nm at a 10 nm spectral resolution (ElMasry, Kamruzzaman, Sun, & Allen, 2012). Hyperspectral imaging was firstly used in satellite remote sensing for environmental monitoring, mineral mapping, atmosphere composition analysis and monitoring, military reconnaissance or target detection, and crop yield or growing condition monitoring or prediction (Park & Lu, 2015). References to NIR chemical imaging in books focused on NIR spectroscopy only appeared after 1992, which indicates that this technique

is relatively new (Lewis & Kidder, 2010). Spatially resolved NIR instruments appeared after 2001, when several companies started to commercialise these, such as Malvern Instruments (Columbia, MD, USA), Perkin Elmer (Shelton, CT, USA) and Specim (Oulu, Finland) (Lewis & Kidder, 2010).

2.3. INSTRUMENTATION

2.3.1. Machine vision technology

Advantages of non-destructive methods such as machine vision technologies (that use computers connected with electrical and mechanical devices in order to avoid human intervention) in the food industry comprise reduced costs, simplification of the processing operations and provision of better final quality to the consumer. For these reasons, machine vision technologies have been applied in several fields, including precision farming, postharvest quality assessment, classification and sorting, as well as process automation. Not only the visible region can be applied, but also the ultraviolet (UV), near-infrared (NIR) and infrared (IR) (Chen, Chao & Kim, 2002). It has also been applied for grain quality evaluation to obtain rapid, accurate and reliable classification or prediction of grain properties, in a cost-effective and automatic way (Vithu & Moses, 2016).

Machine vision technologies can provide physical and structural information on food samples in a non-invasive way and ideally allow inspection of the whole production, not just a few samples that are assumed to be representative of the full batch. Thanks to imaging, machine vision allows detection of the presence of foreign material, external or internal defects, assessment of maturity degree and other sample characteristics linked to their defined quality (Guidetti, Beghi, & Giovenzana, 2012; Zheng, Sun, & Zheng, 2006). Anomalies in food products can be easily detected, so that manual methods for inspection can be replaced, and a more objective method for food evaluation is reached (Vithu & Moses, 2016). This is particularly important for grains, compared to bigger food products such as meat or some fruits (Steiner, 2011).

Many efforts have been carried out to reach fully automated quality evaluation systems by acquiring image using digital cameras (Martin, 2007; Steiner, 2011). When working with multispectral or hyperspectral imaging, the instrumentation can be classified according to the

spectral region they are able to detect, or the technology used for data acquisition, as described in the following section.

2.3.2. Hyperspectral imaging

Multispectral imaging and hyperspectral imaging (HSI) are similar technologies, the main difference is the number of spectral bands they are capable of acquiring (ElMasry et al., 2012). Another difference is related to the vicinity of the spectral bands, which can form a continuous spectrum in the case of HSI, but can just acquire some discrete, specific wavelengths in the case of multispectral systems (Figure 2.2). Thus, not only the number of bands is important but also the range covered by the system. In theory, a HSI system could cover for example 20 bands but still considered as hyperspectral when these bands are contiguous in a quite narrow spectral range (ElMasry & Sun, 2010).

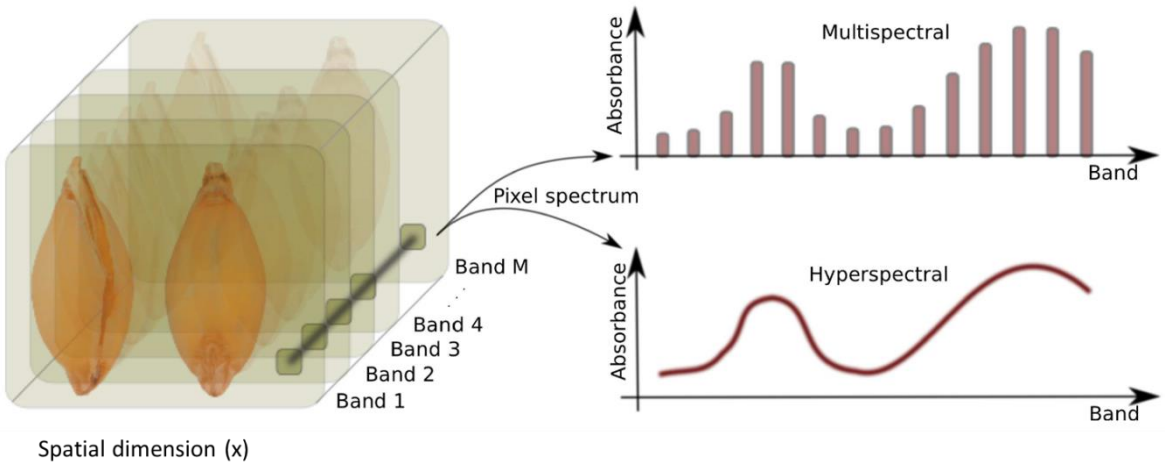


Figure 2.2. Scheme of the difference between multispectral and hyperspectral imaging (Arngren, Hansen, Eriksen, Larsen, & Larsen, 2011).

Hyperspectral imagers can use different technologies to acquire the so-called "hypercube", which is the name given to the three-dimensional dataset containing the two spatial dimensions and the spectral dimension. The size of a hypercube depends on the number of pixels acquired by the camera, and the number of spectral bands acquired. Hyperspectral imagers can be either point-by-point, line scanning or area scanning. They are named "whisk-broom", "staring" and "push-broom" imaging systems, respectively. The whisk-broom system scans the sample pixel-by-pixel

in the two spatial dimensions, and acquires the spectrum for each pixel. It is typically an off-line technique for NIR, MIR and confocal microscopy. The whisk-broom approach has the disadvantage of being time-consuming as the sample needs to be re-positioned, so is conveniently applied when the acquisition time is not a critical factor (Wu & Sun, 2013a). The "staring" approach acquires the spatial information using a camera, but the spectral information is acquired sequentially, by either using illumination at different wavelengths, or by using fixed bandpass filters. In this case, the entire field of view is illuminated, and the image is acquired simultaneously. The acquisition time depends on the spectral bands to be recorded, as higher number or very high spectral resolution results in longer times needed for the data acquisition (Lewis & Kidder, 2010). It should be also noted that a high spectral resolution is usually not required for NIR spectroscopy or HSI, as the vibrational overtone bands are quite broad at the spectral range investigated (Boldrini et al., 2012). The advantage of this setting is that there is no need to move the sample, but it is practical only when a limited number of wavelengths are analysed (ElMasry et al., 2012; Guidetti et al., 2012). Being unsuitable for moving objects means that this system is not suitable for real-time scanning or analysis (Wu & Sun, 2013a).

The "push-broom" system is the most frequently used approach, as it allows simultaneous acquisition of all spectral bands (Boldrini et al., 2012; ElMasry et al., 2012). The sensor captures a bi-dimensional array of data, i.e. one spatial and the spectral dimension of the target object. As this operation is repeated for each line, a full hypercube is constructed. It is stable and has many advantages in terms of acquisition speed and reduction of the amount of illumination needed. Only one line at a time needs to be illuminated during the image acquisition (He & Sun, 2015). Typical "push-broom" HSI systems consist of a CCD or CMOS (Complementary Metal Oxide Semiconductor) camera, a spectrograph, an illumination unit, and a computer equipped with image acquisition software. The camera is a two-dimensional detector, and the spectrograph (wavelength dispersing unit) generates a spectrum for each point on the scanned line (ElMasry et al., 2012).

Portable instruments have also been described in the literature. They are currently commercialised by several manufacturers, so that the operator can acquire spectral information of agricultural and

food products directly in the field or in the processing plant. The advances in terms of hardware and software allow improving the speed of data acquisition and treatment (Zamora-Rojas, 2013). Table 2.2 reports a schematic comparison between conventional NIR spectroscopy, imaging and multi/hyperspectral imaging. A comparison between bulk traditional NIR measurements and NIR hyperspectral imaging analysis is reported in Table 2.3.

Table 2.2. Main differences among imaging, spectroscopy, and hyperspectral imaging techniques, modified from ElMasry & Sun (2010).

Features	**HSI**	**NIR Spectr.**	**Imaging**	**Multisp. imaging**
Spectral information	Yes	Yes	No	Limited
Spatial information	Yes	No	Yes	Yes
Multi-constituent information	Yes	Yes	No	Limited
Detectability of small objects	Yes	No	Yes	Yes
Flexibility of spectral information extraction	Yes	No	No	Yes
Generation of chemical images	Yes	No	No	Limited
Possibility of rapid screening	Yes	Yes	Yes	Yes
Possibility of individually analyse grain	Yes	No	Yes	Yes
Possibility of analysing internal quality attributes	Limited	Limited	No	Limited

Table 2.3. Comparison between bulk NIR spectroscopy and NIR-HSI in terms of instrument settings (Geladi, Grahn, & Manley, 2010).

Instrument Setup Attributes	**Bulk NIR Spectroscopy**	**NIR Hyperspectral Imaging**
Sample preparation	Grinding, homogenizing	Preferably none
Sample holder	Cup, petri dish	Flat surface, dark or reflecting background
Illumination	May be heterogeneous	As homogeneous as possible
Detector	Si, InGaAs, PbS	Si, InGaAs, HgCdTe, InSb
Wavelength range	Vis-2500 nm	Vis-1000 nm, 900–1700 nm, 1000–2500nm
Penetration depth	0.1–10mm	1–2mm
Mode	Reflection	Reflection
	Transmission	Fluorescence
	Transflection	Transmission
Measurement	Integrating sphere	Focal plane (stare down)
	Rotating–moving cup	Line scan (push broom)
	Flow cell	Point scan (whisk broom)
	Liquid cell	
Desired property	Concentration	Chemical gradients, local damages, local infections, and local parasites

2.3.2.1. Components of HSI systems

A typical line mapping spectrograph for HSI uses a light source to illuminate the sample and allow the detection of the light after its interaction with the sample. The diffuse reflectance NIR signal is collected through the optics, i.e. lenses, and focused into the spectrograph (Lewis & Kidder, 2010). The specific configuration of HSI systems can vary depending on the modality of data acquisition, based on four interaction phenomena of light with the sample: transmittance, reflectance, transflectance and interactance. These arrangements differ in the way the light beam is received by the sensor, and the choice strongly depends on the optical properties of the sample and the desired acquisition conditions. The transmittance approach is limited to samples for which the light radiation can partially pass through the sample, and typically requires a high intensity of illumination. The reflectance approach is suitable for opaque samples, and has other advantages which are detailed elsewhere (Guidetti et al., 2012). Interactance mode is a combination of the two arrangements, and the light source is located in the same side close to the detector (ElMasry et al., 2012). The main application for interactance mode is for the analysis of big samples, e.g. whole fruits. It can be conveniently applied when the aim is to detect internal defects of samples, and during on-line applications it is important to put a barrier between the incident light and that returning to the sensor. Finally, the transflectance technique is suitable only for samples for which the light can penetrate easily (Guidetti et al., 2012).

Reflectance mode is the most common setting for NIRS and HSI for solid products and enables data to be obtained with samples having strong absorption, not suitable for transmittance mode (ElMasry et al., 2012; Lewis & Kidder, 2010; Sasic et al., 2011).

2.3.2.2. Illumination source

The most common light source is composed of Tungsten filament halogen lamps, which show high intensity in the NIR region. Light emitting diodes (LED) are also available, but generate narrow band light in the visible region, and are thus limited for studies in the NIR region (Guidetti et al., 2012). Fluorescent lamps, quartz halogen lamps, metal halide lamps, lasers and infrared lamps are also used (Martin, 2007; Steiner, 2011). The optimisation of sample illumination is of paramount importance to obtain good quality HSI data. Illumination should be intense enough

and relatively uniform across the field of view. Variations in signal-to-noise characteristics of data across samples can be particularly problematic, and this problem is more evident for the line mapping HSI systems (Lewis & Kidder, 2010). Correct illumination is important to reduce light scattering and spectral artefacts arising from specular reflection from samples. However, even using an ideal diffuse illumination, specular reflection may be present, depending on the scattering properties of the object, if it is not planar, i.e. in case of non-flat objects like food grains.

2.3.2.3. Optics and Detectors

Detectors are able to convert the incident light energy into a signal, which is amplified and processed. Sensors are semiconductor devices that produce an electrical signal when they absorb photon energy. They can be structured into a single line or bi-dimensional focal plane array (FPA), and the most common technology is called charge-coupled device (CCD). HSI typically uses area detectors. Details on the architecture of CCD sensors are reported elsewhere (Abdullah, 2016). An alternative to CCDs is the complementary metal oxide semiconductor (CMOS). CMOS sensors include both photodetector and readout amplifier in each pixel, so image acquisition is faster. However, they have higher noise and higher dark current than CCD sensors (Chen, Chao, & Kim, 2002; Singh, 2009). The following commercial FPAs available for multispectral or HSI are silicon, indium antimonide (InSb), platinum silicide (PtSi), indium gallium arsenide (InGaAs), germanium (Ge), mercury cadmium telluride (HgCdTe), and quantum well infrared photodetectors (QWIPs). InSb, InGaAs, HgCdTe, and QWIP are the most commonly used detectors in multispectral/hyperspectral imaging (Tran, 2003). InSb are usually applied for MIR based imaging. The InGaAs detectors are most commonly used in the 900-1700 nm wavelength band, for their sensitivity, spectral range, low noise, and fast response in the NIR region, whereas their detection is poor beyond 1700 nm (Singh, 2009). HgCdTe detectors also have high sensitivity, can be designed to operate in a very wide range of the IR region (1000-26,000 nm), and cut-off can be selected by changing the composition of the material. HgCdTe-based detectors are generally more expensive than other detectors (Manley, 2014). The quantum well infrared photodetectors (QWIPs) are used in long wave IR imaging systems (*Hyperspectral imaging for food quality analysis and control*, 2010; Tran, 2003). The cheapest detector is silicon-based, which is used

for visible imaging. For higher spectral regions, lead sulphide (PbS) or indium gallium arsenide (InGaAs) detectors are used (Agelet, 2011; Geladi, 2007; *Hyperspectral imaging for food quality analysis and control*, 2010).

For HSI instruments, the choice of the hardware depends on the size of the samples to be analysed, specifically factors such as the field of view, magnification and illumination uniformity (Polder, Van Der Heijden, Keizer, & Young, 2003; Sasic & Ozaki, 2011). There are several options for cameras: VNIR 400-1000 nm, NIR 900-1700 nm, SWIR 1000-2500 nm, MWIR 2600-5000 nm, LWIR 8000-12000 nm. The VNIR machines are sold with halogen-based fibre optical line light operating in the range 400-1700 nm, while NIR cameras use linear halogen array illumination which gives higher illumination and heat load. HSI could be applied also for fluorescence applications using UV light, but the detection is carried out in the visible range and not in the NIR spectrum (He & Sun, 2015). The quality of a spectral imager depends on several factors, including the spectral linearity, spectral resolution, signal-to-noise ratio (SNR), and image distortion; e.g. smile effect, which is a geometrical distortion of the horizontal spectral lines in the hypercubes. The optics are equally important, in terms of efficiency of the optics and diffraction efficiency of the grating, as well as the spatial resolution and presence of stray light, ghost lines or ghost image caused by reflections from defective optical surfaces (Boldrini et al., 2012). When analysing small objects like grain kernels, specular reflections can be common especially in the central region of the image, and can be influenced by the light position. This is due to the need of longer exposure time to obtain high signal intensity over the whole kernel area, while when multiple lamps are used, the kernels are properly illuminated using a shorter exposure time, which in turns avoid saturation of the signal at the central portion of the kernel.

2.3.2.4.Spatial resolution and magnification

In HSI systems, the term resolution can refer both to the spatial and spectral resolution. The spatial resolution describes the smallest sized objects that can be distinguished and is influenced by the resolving power of the optics and the magnification and detector pixel size. For practical purposes, the effective resolution is also limited by light scattering within the sample. The smallest size particle that can be clearly distinguished is ultimately determined by the system spatial

resolution and not by the magnification employed (Lewis & Kidder, 2010). On the other hand, the spectral resolution is determined partly by the optical resolution of the spectrograph, and also by the detector resolution and by the wavelength range used and the number of pixels provided in the spectral domain (Boldrini et al., 2012).

2.4. APPLICATIONS OF HSI IN FOOD SCIENCE AND TECHNOLOGY

Many research papers reporting on the application of HSI for food and agricultural products have been applied for animal product evaluation, especially meat and fish, followed by fruits and vegetables. Sasic and Ozaki (2011) described the application of HSI in food science and technology by reporting a few dozen papers published on food quality and safety for each of the food categories of meat/fish, cereals, fruits/vegetables and others (nuts, oilseeds, etc.). Since the date of publication of that book, the number of research published using HSI on food commodities has dramatically increased. For example, when the book was published, no research paper had been published on the application of InGaAs sensors in the long NIR wavelength region (1100-2500 nm) for the study of food products. Over 350 papers have since been published in the years from 2010-2018 on HSI for meat and fish quality evaluation; 40 documents reporting on its applications to cereals, and 320 papers referring to vegetables or fruits. Table 2.4 details the most recent research utilising HSI, although studies involving meat, fish or their derivatives have been excluded as they are outside the scope of this thesis. More details on the applications of HSI for muscle foods can be found in ElMasry et al. (2012) and Wu and Sun (2013b). The table also presents the approaches used for HSI acquisition, mostly applying the reflectance mode. The purpose of these studies is mostly to obtain qualitative information (e.g. for discrimination or identification purposes), with such studies representing approximately 70% of the published papers herein reviewed. A range of chemometric tools has been applied, while fewer strategies employed for the image processing, the most popular segmentation approach being thresholding. In terms of spectral range, the vast majority of the studies investigated the visible and lower NIR region, but to date very limited research has been conducted so far for these food products using the full NIR range, i.e. up to 2500 nm.

Table 2.4. Summary of recent publications (>2008) of HSI in quality evaluation of food products (excluding meat and fish products). Modified from the following sources: (Huang, Liu, & Ngadi, 2014; Liu, Zeng, & Sun, 2015; Rahman & Cho, 2016; Su, He, & Sun, 2017; Wu & Sun, 2013b).

Mode	Product	Camera	Spectral range (nm)	Type of analysis	Image processing	Chemometrics	Reference
Reflectance	Almond nut	n.a.	700-1000	Qualitative	n.a.	Band ratio	Nakariyukul & Casasent (2011)
	Almond nut	n.a.	950-1390	Qualitative	n.a.	SVM	Nakariyukul & Casasent (2011)
	Apple	CCD	600-1000	Quantitative	Thresholding	PLSR	Huang & Lu (2010)
	Apple	CCD	450-1000	Quantitative	n.a.	PLS-DA	Peng & Lu (2008)
	Apple	CCD	400-1000	Qualitative	Thresholding	Stepwise MLR	ElMasry et al., (2009)
	Apple	n.a.	600-1000	Qualitative	Locally linear embedding	SVM, PLS-DA	Huang et al., (2012)
	Apple	EMCCD	400-1000	Quantitative	Multi-resolution wavelet transform; etc.	PLSR	Mendoza et al., (2012)
	Apple	EMCCD	500-1000	Quantitative	Multi-resolution wavelet transform; etc.	PLSR	Mendoza et al., (2011)
	Apple	n.a.	400-1000	Qualitative	PCA, minimum noise fraction	SIMCA	Baronowski et al., (2012)
	Apple	n.a.	1000-2500	Qualitative	Minimum noise fraction (MNF)	LDA, SVM	Baranowski et al., (2012)
	Apple, Peach, Kikifruit, plum	CCD	500-1000	Quantitative	Thresholding	Manual analysis	Qin & Lu (2008)
	Banana	CCD	400-1000	Quantitative	n.a.	MLR, PLSR	Rajkumar et al., (2012)
	Barley	InGaAs	900-1700	Quantitative	PCA, MNF	Maximum likelihood multinomial regression classifier	Arngren et al., (2011)
	Barley, wheat, sorghum	n.a.	1000–2498	Qualitative	PCA	PCA, PLS-DA	McGoverin et al., (2011)
	Blueberry	CCD	500-1000	Quantitative	Thresholding	PLSR	Leiva-Valenzuela et al., (2013)
	Citrus	CCD	400-1100	Qualitative	Geometric factor correction	Digital elevation model	Gómez-Sanchis et al., (2008)

Table 2.4 (*continued*)

Product	Camera	Spectral range (nm)	Type of analysis	Image processing	Chemometrics	Reference
Citrus	EMCCD	450-930	Qualitative	Thresholding	Spectral information divergence mapping	Qin & Lu (2009)
Citrus	n.a.	460–1020	Qualitative	n.a.	Receiver operating characteristic (ROC)	Lorente et al., (2012)
Citrus	CCD	450–930	Qualitative	PCA	SID, Band ratio	Zhao et al., (2010)
Citrus	CCD	730, 830	Qualitative	n.a.	Band ratio	Qin et al., (2012)
Field peas	n.a.	392–889	Quantitative	Radiometric filter (band threshold)	LDA	Nansen et al., (2014)
Grape	CCD	400–1000	Quantitative	Thresholding	PLSR	Baiano et al., (2012)
Grape seed	CCD	914-1715	Quantitative	PCA, minimum noise fraction	PLSR, DA	Rodríguez-Pulido et al., (2013)
Grape skin	CCD	400-1000	Quantitative	n.a.	PCA	Fernandes et al., (2011)
Kiwifruit	CMOS	408–1117	Qualitative	PCA	SVM	Lü et al., (2011)
Maize	InGaAs & HgCdTe	960-1662 & 1000-2498	Qualitative	Thresholding	PLS-DA	Williams et al., (2009)
Maize	HgCdTe	1000-2498	Qualitative	PCA	PLSR	Williams et al., (2012)
Maize	CCD	380–1030	Qualitative	PCA	PCA, KPCA, LS-SVM, BPNN	Zhang et al., (2012)
Maize	CCD	400-1000	Qualitative	n.a.	PCA-DA	Del Fiore et al., (2010)
Maize	HgCdTe	1000–1700	Quantitative	n.a.	PLS-DA	Kandpal et al., (2015)
Maize	EMCCD	1000–2500	Qualitative	n.a.	PLS-DA	Ambrose et al., (2016)
Mandarin	CCD	320-1100	Qualitative	Geometric factor correction	LDA, classification and regression trees (CART)	Gómez-Sanchis et al., (2008)
Mung bean	InGaAs	1000-1600	Qualitative	PCA	PCA, LDA, QDA	Kaliramesh et al., (2013)
Mushroom	n.a.	880–1720	Qualitative	n.a.	Ensemble Monte Carlo variable selection (EMCVS), PLS-DA	Esquerre et al., (2012)

Table 2.4 (*continued*)

Product	Camera	Spectral range (nm)	Type of analysis	Image processing	Chemometrics	Reference
Mushroom	CCD	400-1000	Quantitative	n.a.	PLSR	Taghizadeh et al. (2011)
Mushroom	CCD	400-1001	Quantitative	Thresholding	PCA	Gaston et al. (2010)
Mushroom	n.a.	400-1002	Qualitative	Thresholding	PCA	Gowen et al. (2008)
Mushroom	n.a.	450-850	Quantitative	n.a.	MLR, PCR	Gowen et al. (2008)
Mushroom	n.a.	450-950	Qualitative	Interactive selection	PCA	Gowen et al. (2009)
Muskmelon	HgCdTe	948–2494	Qualitative	n.a.	PLS-DA	Kandpal et al. (2016)
Oat and groat	InGaAs	1000-1650	Qualitative	PCA	PLS-DA	Serranti et al. (2013)
Onion	InGaAs	1000-1600	Qualitative	Thresholding	Manual analysis	Wang et al. (2012)
Onion	InGaAs	950-1650	Qualitative	PCA	PCA, SVM	Wang et al. (2012)
Orange	CCD	400-1100	Qualitative	PCA	PCA, BR, TH	Li et al. (2011)
Peach	n.a.	400–1000	Qualitative	Band ratio	PCA	Herrero-Langreo et al. (2012)
Peach	n.a.	680-800	Qualitative	Band ratio	PCA	Kleo et al. (2011)
Peanut	CCD	400–2500	Quantitative	n.a.	PLSR	Jin et al. (2015)
Pickles	CCD	400-740	Qualitative	Thresholding	PLS-DA, K-NN	Ariana & Lu (2010)
Pickles	CCD	450-740	Qualitative	Thresholding	PLS-DA	Lu & Ariana (2013)
Pickles	CCD	400-675	Qualitative	Thresholding	PCA	Ariana & Lu (2010)
Rape	CCD	380–1030	Quantitative	n.a.	PLSR	Zhang & He (2013)
Rice	n.a.	874-1734	Qualitative	n.a.	PLS-DA, SIMCA, KNN, SVM, random forest	Kong et al. (2013)
Rice	n.a.	400–1000	Qualitative	n.a.	PCA, BPNN	Wang et al. (2015)
Rice	CCD	400–1000	Quantitative	n.a.	PLSR	Siripatrawan et al. (2011)
Rice	CCD	405-970	Qualitative	Thresholding	PCA, PLS-DA, LS-SVM, PCA-ANN	Liu et al. (2014)
Soybean	CCD	400–1000	Quantitative	n.a.	PLSR	Huang et al. (2014)
Soybean	n.a.	850–1700	Quantitative	n.a.	PLSR	Zhu et al. (2012)

Table 2.4 (*continued*)

Product	Camera	Spectral range (nm)	Type of analysis	Image processing	Chemometrics	Reference
Spinach	EMCCD	400-1000	Qualitative	Thresholding	Spectral angle mapper, PLS-DA, leafy vegetable evolution	Diezma et al. (2013)
Spinach	CCD	400-1000	Qualitative	Radiometric correction	PCA, analysis of variance	Lara et al. (2013)
Strawberry	InGaAs	1000-1600	Qualitative	Thresholding	LDA	Sugiyama et al. (2010)
Strawberry	InGaAs	1000-1600	Qualitative	Multi-band image segmentation	Multi-band multivariate classifier, uni-band univariate classifiers, multiband decision-fusion classification	Nanyam et al. (2012)
Strawberry	CCD	400–1000	Quantitative	Thresholding	PLSR, MLR	ElMasry et al. (2007)
Watermelon	n.a.	1000–2500	Qualitative	n.a.	PLS-DA	Bae et al. (2016)
Wheat	n.a.	400-1000	Qualitative	Thresholding	SAM	Bauriegel et al. (2011)
Wheat	FFT-CCD	700-1100	Qualitative	PCA	LDA, QDA	Singh et al. (2010)
Wheat	InGaAs	960-1700	Qualitative	Image cropping, feature extraction	LDA, QDA, ANN	Mahesh et al. (2008)
Wheat	InGaAs	1000-1600	Qualitative	PCA	LDA, QDA	Singh et al. (2009)
Wheat	n.a.	400–1000 (& 1000–2500)	Quantitative	Thresholding	PLSR	Shahin et al. (2014)
Wheat (durum)	CCD (Liquid crystal tunable filter)	650–1100	Qualitative	n.a.	DA	Gorretta et al. (2006)
Wheat	Lextel	950–2450	Qualitative	n.a.	Smoothing, visual spectral inspection	Shahin et al. (2008)
Wheat	InGaAs	950–1700	Qualitative	n.a.	PCA, PLS, visual inspection	Smail et al. (2006)

Table 2.4 (*continued*)

Mode	Product	Camera	Spectral range (nm)	Type of analysis	Image processing	Chemometrics	Reference
	Wheat	ASD spectro meter	420–2500	Qualitative	n.a.	Penalized Discriminant Analysis	Berman et al. (2007)
	Wheat	HgCdTe	1000–2500	Quantitative	n.a.	PLSR	Xing et al. (2011)
	Wheat	HgCdTe	1255–2300	Quantitative	n.a.	PCA, PLSR	Xing et al. (2009)
Transmittance	Pickles	CCD	740-1000	Qualitative	Thresholding	PLS-DA, KNN	Ariana & Lu (2010)
	Pickling cucumbers	CCD	740-1000	Qualitative	Thresholding	PLS-DA	Lu & Ariana (2013)
	Soybean	CCD	400-1000	Qualitative	n.a.	Support vector data description classifier	Huang et al. (2013)
	Pickles	CCD	675-1000	Qualitative	Thresholding	PCA	Ariana & Lu (2010)
	Maize	CCD	750-1090	Quantitative	SNV, de-trending, MSC	PLSR	Cogdill et al. (2004)
	Almond nut	InGaAs	700-1400	Qualitative	n.a.	Band ratio, SVM	Nakariyakul & Casasent (2011)
Fluorescence	Tomato	EMCCD	400-700	Qualitative	PCA	PCA	Cho et al. (2013)
	Maize	CCD	400-700	Qualitative	Thresholding	Discriminant analysis	Yao et al. (2013)
	Maize	CCD	425-775	Qualitative	n.a.	PCA, SVM	Jiang et al. (2007)
	Maize	n.a.	399–701	Qualitative	PCA	Least squares-SVM, KNN	Zhu et al. (2016)
	Orange, Peach	CCD	700-1000	Quantitative	n.a.	MLR	Liu and Sun (2015)
	Tomato	EMCCD	400-700	Qualitative	Thresholding	PCA	Cho et al. (2013)
	Peanut	n.a.	400-900	Qualitative	LDA, QDA	MAV (Multivariate analysis of variance)	Xing et al. (2017)

EMCCD: electron multiplying CCD sensors (usually gives higher signal-to-noise ratio and they are applied for fluorescence and Raman imaging). MFN: minimum noise fraction (it is transformation procedure to remove noise caused by the detector). Other pre-processing and transformation techniques are explained in detail by Yao et al. (2010). N.a. = not available or unclear.

HSI has also been applied for contaminant detection, for both macroscopic and microscopic contaminants such as extraneous materials, microbes or hazardous chemicals. Foreign body identification has been reported by Bhuvaneswari et al. (2011) in semolina to detect fragments of insects. Fernández-Pierna et al. (2012) applied segmentation techniques to identify several materials/objects within a hypercube, i.e. straw, seeds from weeds, stones, insects, fragments of plastic, wood, etc.; Support Vector Machine (SVM) allowed classification accuracy above 95%. Adulteration or contamination can be detected at surface or subsurface level, and even internal defects have been successfully detected, the latter being more easily obtained by transmittance measurement (Wu & Sun, 2013b).

Several calibrations have been reported using HSI systems in evaluating meat and seafood products. ElMasry et al. (2012) reported a detailed review on the applications of HSI for meat quality evaluation, including its use for chemical composition, detection of faeces and parasites, etc. Silversten (2011) reported an example demonstrating the possibility of implementing HSI (450-700 nm) at the industrial level for the detection of cod fillet freshness, the discrimination of frozen and fresh fish, and detection of nematodes. The system was applied using a conveyor belt working at a speed of 0.3-0.4 m/s as typically used for fish processing. For fruits and vegetables, research has focused on the assessment of internal quality attributes as well as external defects such as the presence of bruises or injuries that are difficult to be identified visually (Wu & Sun, 2013b).

More limited research has been carried out using HSI on grains (Liu et al., 2015). Efforts have been reported on the use of non-destructive techniques for seed evaluation in terms of insect damage and diseases, which have been recently reviewed by Rahman and Cho (2016) describing the most recent applications for seed damage, variety identification and seed viability.

Cheewapramong (2007) showed that it is possible to detect internal damage in wheat kernels caused by insect infestation using reflectance NIR spectroscopy. Six groups of wheat kernels were analysed on a single seed basis and were all placed in a consistent orientation, i.e. crease down.

The classification model accuracy was approximately 90%, depending on the type of larvae, but it was poor for kernels containing younger larvae, i.e. 50% for 3-week-old insects.

Even properties not directly related to the chemical composition or directly detectable from the NIR/HSI spectra have been predicted by some authors, e.g. seed weight of rapeseed (Velasco, Möllers, & Becker, 1999), or rice weight (Wu & Shi, 2004). HSI in the NIR range offers the advantage for obtaining more information than physical parameters such as shape, colour and other visible characteristics. When information on the chemical composition or chemically-related properties is acquired using HSI on individual grain basis, segregation of single kernels is possible, with consequent economic and technological benefits of obtaining different production streams.

2.4.1. Quality inspection of granular food commodities

The food industry is faced with a number of challenges, including maintenance of high-quality standards and assurance of food safety (Huang et al., 2014). Quality and safety of food are usually defined by physical attributes (e.g., texture, colour, marbling, tenderness), chemical attributes (e.g., fat content, moisture, protein content, pH, drip loss), and biological attributes (e.g., total bacterial count). Traditionally, assessment of quality and safety involves human visual inspection by trained inspectors or more often using instrumental analytical techniques. Both approaches are tedious, laborious, time-consuming and costly, and human inspection can also lead to human error and inconsistency. The traditional methods used for chemical or biological analyses can be environmentally unfriendly, and also destructive in their nature and often time-consuming (Huang et al., 2014). Automation of quality assessment operation can optimize quality inspection and remove human subjectivity and inconsistency (ElMasry et al., 2012; Wu & Sun, 2013b).

Granular materials can be readily evaluated by imaging techniques using the visible range, but some internal properties or chemical composition such as moisture, fat, and protein content cannot be detected. In this case, the advantages of hyperspectral imaging become evident. Many studies have been conducted for grain analysis using HSI for almost two decades, e.g. colour classification of grain, vitreousness determination of wheat kernel, identification of sound or problematic grains, and discrimination models (Wu & Sun, 2013b).

Table 2.5 summarises the literature on the application of non-destructive methods based on infrared measurement for the compositional analysis of seeds, and seed classification/discrimination using these techniques.

Table 2.5. Application of HSI for quantitative prediction of seed composition, with examples of classification methods (modified from the following sources (Liu et al., 2015; Rahman & Cho, 2016; Su et al., 2017).

Seed	Chemical composition	Method	Spectral range (nm)	Chemometrics	Result	References
Corn	Oil, oleic acid	HSI	950–1700	PLSR	RMSEP = 0.74%, 14%	Janni et al. (2008)
Maize	Moisture, oil content	HSI	750–1090	PLSR	R_p^2= 0.87, 0.75	Cogdill et al. (2004)
Maize	Oil, oleic acid	HSI	950-1700	PLSR	RMSEP = 0.74%, 14%	Weinstock et al. (2006)
Maize	Moisture, oil content	HSI	750-1090	PLSR	R_p^2 = 0.87, 0.75	Codgill et al. (2004)
Soybean	Colour, moisture	HSI	400–1000	PLSR	R_p^2= 0.83, 0.97	Huang et al. (2014)
Soybean	Protein, fat	HSI	850–1700	PLSR	R_c^2 = 0.9, 0.97	Zhu et al. (2011)
Soybean	Sweetness, amino acid	HSI	400–1000	ANNR	R^2 = 0.61, 0.60–0.74	Monteiro et al. (2007)
Soybean	Colour, moisture	HSI	400-1000	PLSR	R_p^2 = 0.83, 0.97	Huang et al. (2004)
Soybean	Moisture, fat, ash, protein	NIRS	1250–2500	PLSR	R^2=0.72 (moisture), R^2=0.73 (ash), R^2=0.88 (protein), R^2=0.81 (lipid)	Ferreira et al. (2014)
Sunflower	Fatty acid	Spectroscopy	400–2500	MPLSR	R_c^2= 0.94	Moschner & Biskupek-Korell (2006)
Wheat	α-amylase activity	Spectroscopy	1000–2500	PLSR	R_p^2= 0.63–0.82	Xing et al. (2011)
Wheat	Protein	HSI	960–1700	PLSR, PCR	R_p^2= 0.68, 0.82	Mahesh et al. (2015)
Wheat	α-amylase activity	HSI	1000-2500	PLSR	R_c^2 = 0.72-0.88	Xing et al. (2011)
Wheat	Protein	HSI	960-1700	PLSR, PCR	R_p^2 = 0.68, 0.82	Mahesh et al. (2011)
Wheat	α-amylase activity	HSI	1255-2300	PCA, PLSR	R_p^2 = 0.54, 0.73	Xing et al. (2009)
Cocoa	Fat content	FT-NIR	1000-2500	PLSR, SVMR, iPLS	R_c^2=0.93-0.98; R_p^2=0.92-0.97	
Cocoa	pH, fermentation index	FT-NIR	1000-2500	PLSR, iPLS	R_c^2=0.93-0.98; R_p^2=0.92-0.97	Teye et al. (2015)

Table 2.5 (*continued*)

Seed	Chemical composition	Method	Spectral range (nm)	Chemometrics	Result	References
Coffee	Ash and lipid content	NIRS	1100–2200	PLSR	R_c^2=0.77-0.97 (ash); R_c^2=0.76-0.99 (lipids)	Pizarro et al. (2004)
Coffee	Roasting degree	NIRS	1100–2200	PLSR	R_c^2=0.98-0.99; R^2_{cv}=0.97-0.98	Shan et al. (2015)
Walnut	Classification	HSI	425-775	SVM	90.30%	Jiang et al. (2007)
Wheat	Moisture	HSI	960–1700	PCA, LDA, QDA	61–100%	Mahesh et al. (2011)
Maize	Species identification	HSI	380–1030	PCA, KPCA, LS-SVM, BPNN	98.89%	Zhang et al. (2012)
Wheat	Hardness (glassy-floury)	HSI	960-1662 & 1000-2498	PLS-DA	84.9-98%	Williams et al. (2009)
Wheat	Classification	HSI	960-1700	LDA, QDA, ANN	95%, 93%, 90%	Mahesh et al. (2008)
Wheat	Classification	HSI	960-1700	LDA, QDA, ANN	99.10%	Choudhary et al. (2009)
Wheat	Classification	HSI	1000-1600	MVI	85-100%	Singh et al. (2009)
Wheat	Classification	HSI	700-1100	MVA	95.9-99.3%	Singh et al. (2010)
Wheat	Classification	HSI	1006-1650	PLS-DA	100%	Serranti et al. (2013)
Wheat	Geographical origin	NIRS	950–1650	PCA, LDA, DPLS	92.50%	Zhao et al. (2013)
Cocoa	Ghana bean differentiation	FT-NIR	1000-2500	LDA, KNN, BP-ANN, SVM	72-100%	Teye et al. (2013)

2.4.2. Single grain analysis

Compared to bulk analysis, the measurement of grain properties on a single seed basis has been scarcely reported (Agelet, 2011). A summary of the research on single seed analysis using NIR spectroscopy is reported in Table 2.6. The analysis of single seeds implies a more limited sample size, and the great advantage to obtain information on single seed variability. This can be useful to breeders in terms of the uniformity of a sample regarding a particular quality trait (Osborne, 2006). Previous studies anticipated that single kernel applications for grain quality assessment would be applied for sorting processes in cereal breeding programmes and processing industries. In fact, the rapid non-destructive analysis of single grains in breeding programmes reduces the costs, while application at the primary production level can lead to benefit in terms of quality optimisation for specific quality traits. In addition, the processing industry can benefit from a more consistent raw product, or even sort grains into specific streams for different applications (Fox & Manley, 2014).

Breeding programmes are very time consuming and require important investments, especially for self-fertilising plants, for which four or five generations need to be segregated. Screening of plant material requires testing of large number of samples, even thousands per year (Osborne, 2006). Thus, the use of NIRS-based methods to assess the functionality of grains and seeds would be beneficial for plant breeders to lower the cost and to perform screening of thousands of genetic lines in a more efficient way (Ozaki, McClure, & Christy, 2006). Previous studies have highlighted that high speed discrimination of single kernels is of interest in cereal breeding programmes, for farmers and processing industries to improve the quality of the product and gain higher added value (Fox & Manley, 2014).

Some authors suggested that the best approach for the study of small grains is to set homogeneous illumination, and to scan whole kernels on both sides (Agelet, 2011; Janni, Weinstock, Hagen, & Wright, 2008). For quantification purposes, an issue could be related to the way the response (reference measurement) is expressed, i.e. the absolute value or the relative units. For instance, three different ways can be also used to express the moisture basis: i) wet basis, which is at the moisture content within the sample at the moment of analysis; ii) on a dry matter basis (dmb),

which requires drying the sample to assess its moisture; iii) calculated on a defined moisture level (Agelet, 2011).

Previous work highlighted the risk of non-uniform illumination, especially at the seed edges, when working with NIRS measurement of single seeds. In addition, kernel size has been also shown to influence spectral response and prediction of chemical constituents in single grains (Agelet & Hurburgh, 2014). A possible limitation of single seed analysis is related to the reference analysis by traditional laboratory testing. Many protocols require a sample size above the amount of a single kernel. Even when kernels can be analysed individually, replicates are not possible and thus the random error coming from the technique cannot be reduced by averaging replicated measurements (Agelet & Hurburgh, 2014).

Differences exist in food grain composition depending on genetic and environmental factors. For example, plant nutrition, rain conditions and other climatic factors can influence the final composition of fruits and seeds, but differences related to the plant physiology also exist, even within the same plant (Agelet & Hurburgh, 2014). Differences in protein content within the same spikelet of wheat plants have been recognised, when analysing individual kernels (Levi & Anderson, 1950). The study of single kernel prediction using NIR spectroscopy is not new in food science and technology. The first calibration reported for wheat protein at a single kernel level using NIR spectroscopy was described by Delwiche (1995), using transmittance measurement. The prediction error was between 0.4 and 0.9%, and later research reported RMSEP values of 0.48% (Nielsen, Pedersen, & Munck, 2003). Other studies have demonstrated that single kernel NIRS analysis leads to higher prediction error compared to the average spectra from several kernels (n= 10, 30, 50 or 100). The SECV decreased from 0.63% for the single kernel, to 0.38%, 0.22%, 0.18% and 0.16%, respectively (Delwiche & Hruschka, 2000)

Cogdill et al. (2001) applied transmittance NIR spectroscopy for single maize seed measurement of moisture and fat prediction. The SECV for moisture model built by PLS regression was 1.20% (R^2=0.87), while worse results were obtained for fat prediction, with SECV of 1.38% and R^2=0.54. Armstrong (2006) reported the use of reflectance NIR spectroscopy for single soybean prediction of moisture and protein contents. The PLS regression model had SECV=0.32% for moisture

prediction (R^2=0.99) and SECV=0.99% for protein (R^2=0.96). Calibrations for total protein and inorganic phosphorus content in single soybean kernels were reported by Delwiche et al. (2006), who tested reflectance and transmittance NIRS. The single-seed performance was lower for protein content, whose cross-validation R^2 value was 0.32 and RMSEP=13.9 g kg^{-1}. The prediction improved using the average spectra from 24 beans, showing R^2=0.77 and RMSEP=6.7 g kg^{-1}.

For single rapeseed, calibrations for protein prediction generally had R^2 values of 0.94-0.96 and a prediction error of 0.74-0.77% (Hom, Becker, & Möllers, 2007; Velasco & Möllers, 2002).

Lipid content in oilseeds is another parameter that has been investigated by several researchers, including in single seeds (Velasco et al., 1999). Hom et al. (2007) applied NIR spectroscopy and tested the possibility of using NIR calibrations developed for batches on the same amount of a single oilseed kernel. The prediction of oil, protein and glucosinolate content was reported for 20 samples at a reduced sample size (mass of kernels sampled, starting from ~3 grams). The prediction performance decreased but was still acceptable when sample size was in range of 100-450 mg. Other parameters were not predicted as accurately, including some fatty acids, moisture and aromatic compounds. Single seed analysis had R^2 values of 0.79 for protein and 0.72 for oil prediction, while it was 0.29 for glucosinolate content, thus NIR spectroscopy was suggested for rough estimation of oil and protein content.

Other commodities for which NIRS has been applied for single kernel or single beans were husked sunflower achenes (Velasco, Pérez-Vich, & Fernandez-Martinez, 2004), for the purpose of predicting fatty acid composition. Fat content and composition is of particular interest for oilseeds, as their market is based on the lipid content, but indication of the fat composition might be also suitable for defining their quality, specifically their susceptibility to auto-oxidation process. For this reason, several authors have reported NIR-based prediction on oil, in addition to other attributes.

NIRS has been used in the literature for evaluating several types of cereal grains including barley, oats and triticale. Fox et al. (2011) used NIR spectroscopy to predict single kernel protein in barley and malt, using 180 barley kernels (160 for the calibration and 20 as validation set) from breeding

lines and commercial varieties. Then, a commercial malting variety was used to have a considerably higher number of kernels to study the natural compositional variability. The R^2 obtained from the calibration model was 0.903, and a wide variability of protein content in individual barley grain was obtained from the results, ranging from 7.3 to 16.6%. Within the same batch from the same variety, the range of protein content was between 5.0 and 14.5% (wet basis).

Table 2.6. Application of NIRS for single seed quantitative analysis, modified from Agelet & Hurburgh (2014), where the full reference list can be found.

Seed	Attribute	SEP	R^2	Suggested use
Barley	Protein	0.80%	0.84	Usable
Common beans	Mass	41.2 mg	0.74	Screening
	Protein	1.60%	0.82	Quality control
	Starch	4.90%	0.56	Rough screening
Maize	Energy	183–93.9 cal/g	n.a.	Rough screening
	Ergosterol	1.74 mg/kg	0.81	Quality control
	Fumonisin	1.33	0.78	Usable
	Fungal infection	6.3–9.6%	0.80	Usable
	Mass	27.6–30.0 mg	0.87	Screening
	Moisture	0.76–1.2%	0.87–95	Quality control
	Oil (%), Oil (mg)	0.6–1.4%, 2.7 mg	0.55–95; 0.85	Usable, Screening
	Palmitic, Oleic, Linoleic fatty acids	2.2% (palmitic) - 13.3 (linoleic) mg	0.38 (palmitic)- 0.89 (oleic)	Rough Screening/ Screening
	Protein (%)	0.3–1.7%	0.75–95	Usable
	Protein (mg)	2.3–3.8 mg	0.77–89	Screening
	Starch (%)	0.7%–11.5% 17.8–	0.66–88	Screening
	Starch (mg)	18.2 mg	0.85	Screening
Meadow-foam seed	Oil	3.00%	0.95	Usable
Rapeseeds	7 Fatty acids	0.42-8.9%	0.14-97(oleic)	Rough screening
	Glucosinates	10.3 mmol/g	0.86	Screening
	Indole	1.4 mmol/g	0.86	Screening
	Mass	0.51 mg	0.85	Usable
	Oil	1.14%	0.74–97	Quality control
	Protein	0.74–0.77%	0.94–96	Quality control
Rice	Amylose	2.3–3.6%	0.67–85	Screening
	Mass	1.09–1.30 mg	0.67–71	Screening
	Moisture	0.24–0.29%	0.98	Quality control

Table 2.6 (*continued*)

Seed	Attribute	SEP	R^2	Suggested use
Rice	Protein	0.39–0.52%	0.93–94	Usable
Sesame	Moisture	0.40%	0.87	Usable
	Oil	1.50%	0.82	Screening
	Palmitic, stearic, oleic, linoleic fatty acids	0.8%-1.5%	0.0-63	Unusable/rough screening
Soybean pods	Protein	1.00%	0.78	Screening
	Sucrose	0.37%	0.75	Screening
	Free aminoacids	0.21%	0.69	Screening
Soybeans	Isoflavones	0.02%	0.99	Quality control
	Mass	10–16 mg	0.78–91	Quality control
	Moisture	0.32–0.88%	0.98–99	Quality control
	Oil	0.2–1.44%	0.96–98	Quality control
	Protein	0.3–1.57%	0.87–98	Quality control
Sunflower seeds	Palmitic, stearic, oleic, linoleic fatty acids	27.7-84.3 g kg^{-1}	0.52-91	Rough screening/screening
Wheat	Amylose	0.4–0.9%	0.90	Usable
	DON and Vomitoxin	40–60.8 ppm	0.64–87	Screening
	Ergosterol	100 ppm	0.64	Rough screening
	Hardness	7.6–15 h.u.	0.71–91	Usable
	Mass	2.4–2.9 mg	0.37–79	Screening
	Moisture	0.3–1.0%	0.81–98	Quality control
	Oil	0.10%	0.69	Rough screening
	Protein	0.4–1.37%	0.84–99	Quality control

2.4.3. On-line application of NIR and HSI

NIRS and HSI can be implemented off-line, at-line, on-line and in-line for the measurement of food components. The definition of "on-line" measurement implies that the sample is taken from the production flow/process line to be analysed, even using an automated sampling system, while the term "in-line" means that the analysis is done directly on the production flow/line (*in situ*). However, the two terms are often used as synonyms (Porep, Kammerer, & Carle, 2015). Among on-line applications of traditional NIR spectroscopy at industrial level, a few examples have been reported in the literature, e.g. for the analysis of fat content in pork trimmings or intact beef trimmings, or screening of fatty acid composition in intramuscular fat of beef, beef tenderness and several other quality characteristics of meat. Beyond the meat industry, some online applications of NIRS have been reported within the dairy industry in automatic milking systems to evaluate fat, protein and lactose content of milk (Huang, Yu, Xu, & Ying, 2008; Porep et al.,

2015). In the wheat industry, Long et al. (2008) described an online application of NIRS (600-1100 nm) for monitoring wheat protein content directly on a harvester system. Despite the few references in the literature on NIRS for industrial application, this technology is widely spread in the food industry in commercial use. At-line NIR measurements at higher speed for the food industry include determination of moisture, fat, protein, degree of bake and are implemented in a variety of food products including coffee, flour and grain industry, nuts and seeds (http://www.ndc.com/Products/On-Line-NIR-Gauges.aspx). Similarly, NIR/VIS spectroscopy was used for on-line analysis of grapes at a winery intake, with good prediction ability for sugar and acidity, but poor prediction of tartaric acid. Good performance was achieved for the prediction of total grape quality, despite the inaccurate prediction of individual attributes (Porep et al., 2015).

Table 2.7. Main source of variance in NIR spectroscopy, modified from Burns & Ciurczak (2007).

Variance source	**Suggested solution**
Non-homogeneity of sample	Improve grinding and mixing procedures Average replicated measurements Rotate sample cup and obtain multiple readings
Analytical error	Suggest improvements on analytical procedures Retrain analysts on procedures Check reagents and equipment
Physical variation in sample	Improve sample mixing Improve light conditions (diffuse light desired) Obtain a fine powder of the sample Average multiple scans Rotate sample cup and obtain multiple readings
Chemical variation in sample over time	Freeze-drying of sample(s) Short time between sample preparation and analysis Identification of kinetics of chemical change
Population sampling error	Review calibration set selection criteria Use sample selection techniques
Non-linearity	Use small concentration ranges Use baseline correction techniques Use one or more indicator variables
Spectroscopy does not equal wet chemistry	Check dynamic range of the instrument Use different chemical procedures Redefine analytical requirements
Instrument noise	Check instrument noise (gain, lamp voltage, warm-up time, etc.) Determine signal-to-noise Check precision with standard sample replicate measurements

Table 2.6 (*continued*)

Variable sample presentation	Improve sample presentation methods Investigate wide variety of commercially available presentation equipment
Incorrect calibration models	Carefully selection of test calibration model Re-calculate calibration model
Poor calibration transfer	Select calibration with lowest noise, wavelength shift sensitivity and offset sensitivity Identify and transfer actual wavelength and corresponding regression coefficients

The implementation of HSI at the industrial level is not straightforward, as several issues must be addressed (Sivertsen, 2011), for example height differences among samples (which can be overcome by using remote detection), or the presence of dust, high humidity, temperatures and the presence of vibration and noise can adversely affect the measurements. A description of the possible sources of variation in NIR spectroscopy measurements is reported in Table 2.7.

2.4.4. Limitations

Despite the numerous advantages of non-destructive techniques based on vibrational spectroscopy (e.g. NIRS and HSI), there are currently some limitations affecting their practical application. NIRS and HSI are secondary analytical methods (indirect methods) which require accurate reference analysis to build robust predictions. In addition, the equipment is still relatively expensive (especially HSI) and the method strongly relies on chemometric models, which requires the building of robust calibrations. A large enough number of samples is required, to include all possible variation that is likely to be observed in future measurements. The calibration should be also frequently updated to include new variability, such as that associated with new registered varieties (Blanco & Villarroya, 2002; Ozaki et al., 2006). In addition, some compounds/analytes do not absorb in the infrared region so they cannot be detected by NIR/HSI (Lohumi, Lee, Lee, & Cho, 2015), and generally NIR is not very sensitive to compounds at low concentrations in complex samples (Blanco & Villarroya, 2002).

Detection limit is a major drawback for NIR spectroscopy, as usually compounds present in trace amounts cannot be detected, and those below 0.1% are analysed with limited accuracy. When compounds found at very low levels, such as mycotoxins, that have been reported to be predicted

by NIR spectroscopy, the measurement is likely due to indirect detection of other properties/compounds correlated to the analyte (Agelet & Hurburgh, 2014).

The spectral data obtained by NIR and HSI is difficult to interpret, and the assignment of chemical groups to specific spectral bands is not straightforward. For quantification purposes by HSI, the attribution of a reference measurement to the spectrum of each single pixel is of little significance. Thus, averaging the pixels within a region of interest is often the preferred strategy (Moore, 2015; Wu & Sun, 2013a). With particular reference to grains, HSI has been reported to be sensitive to grain topography, particularly kernel curvature, which might affect the prediction performance (Wu and Sun, 2013b). In addition, many fruits and vegetables usually possess a surface layer (skin) that can exhibit different optical properties than their internal material (Qin & Lu, 2008). However, despite the fact that not all food properties or compounds can be analysed by NIR-based methods, there are examples of successful prediction models even for inorganic compounds or properties that are not detectable in the NIR region, often explained by indirect measurements, e.g. determination of minerals (Manley, 2014). Finally, HSI offers no advantage for the analysis of liquid samples or very homogenous samples, as one-point scanning can be used instead (ElMasry & Sun, 2010).

2.4.5. Advantages of HSI

The advantages of HSI are associated with the limited or (more frequently) absence of required sample preparation, thus samples can be directly scanned with no conditioning, grinding, extraction procedures. This avoids the use of chemicals and solvents that is often required in analytical chemistry, which are often unsafe for the operator and are environmental pollutants. Due to the non-destructive nature of the HSI analysis, samples can be used for any further analyses or application, as there is no sample manipulation involved (Gowen, O'Donnell, Cullen, Downey, & Frias, 2007). Once a prediction calibration is built, it is relatively simple to apply and to run routine analysis, and even to automate the analysis. As it does not require any chemicals/reagents or consumables, the cost of each analysis is reduced, with the only significant cost being represented by the initial purchase of the instrumentation itself (ElMasry et al., 2012; Wu & Sun, 2013a).

HSI provides both qualitative and quantitative information, which can be used for classification models or quantitative purposes. From one hypercube, several constituents can be simultaneously predicted, using one scan. In addition, it is possible to select just a region of interest (ROI) instead of the full image, to be able to quantify/classify particular regions within the sample. The application of HSI calibrations also allows visualisation of compound/property distribution across the sample, which is impossible for conventional NIRS (Manley, 2014; Su et al., 2017; Yao, Lewis, & Sun, 2010). The inability of traditional NIR spectroscopy for measuring the spatial distribution of compounds within a sample has been thus overcome by HSI (Du Toit, 2009). Besides having the capability to map chemical components, HSI offers the possibility of high throughput screening (Boldrini et al., 2012; ElMasry et al., 2012).

2.5. DATA HANDLING

The huge amount of information recorded by HSI might represent a drawback in terms of computation time and processing when building prediction models. Similarly to NIRS, HSI is an indirect technique and therefore reference analyses are required to build calibrations. Thus chemometrics is of paramount importance to obtain reliable predictive models (Guidetti et al., 2012; Sonka, Hlavac, & Boyle, 2014).

Correct data processing and data reduction are important to extract relevant chemical information from HSI. The high co-linearity among close wavelengths causes high redundancy of some spectral data in the hypercube. However, there is a risk of losing discrimination power or prediction accuracy when data reduction is not carried out properly (ElMasry et al., 2012). A scheme showing the steps required to extract useful information from HSI data for supervised and unsupervised prediction is shown in Figure 2.3. Reference measurements are required to build supervised predictions, in particular quantitative models. To build these models, it is necessary to use appropriate (and often destructive) analytical methods, whose error and repeatability can affect the prediction of the HSI method. Once the spectral data and the reference measurement for a set of samples are obtained, quantitative prediction can be obtained using regression models, often PLS regression being regarded as the statistical method bringing the best performance.

2.5.1. Structure of the data cube (hypercube)

As mentioned earlier, a hypercube is a three-dimensional dataset, a matrix that includes the spatial dimension (***x*** and ***y***) and the spectral information (***λ***). The spectra extracted from the hypercubes can be treated mathematically in a similar way to the classical spectroscopy datasets, thus some chemometric tools previously applied for NIR spectroscopy can be directly applied to HSI data (Prats-Montalbán, De Juan, & Ferrer, 2011). Several software packages are commercially available for data handling of the hypercubes. IDL and ENVI (Environment for Visualizing Images) are widely applied in the remote sensing community, and can be readily applied to hyperspectral imaging.

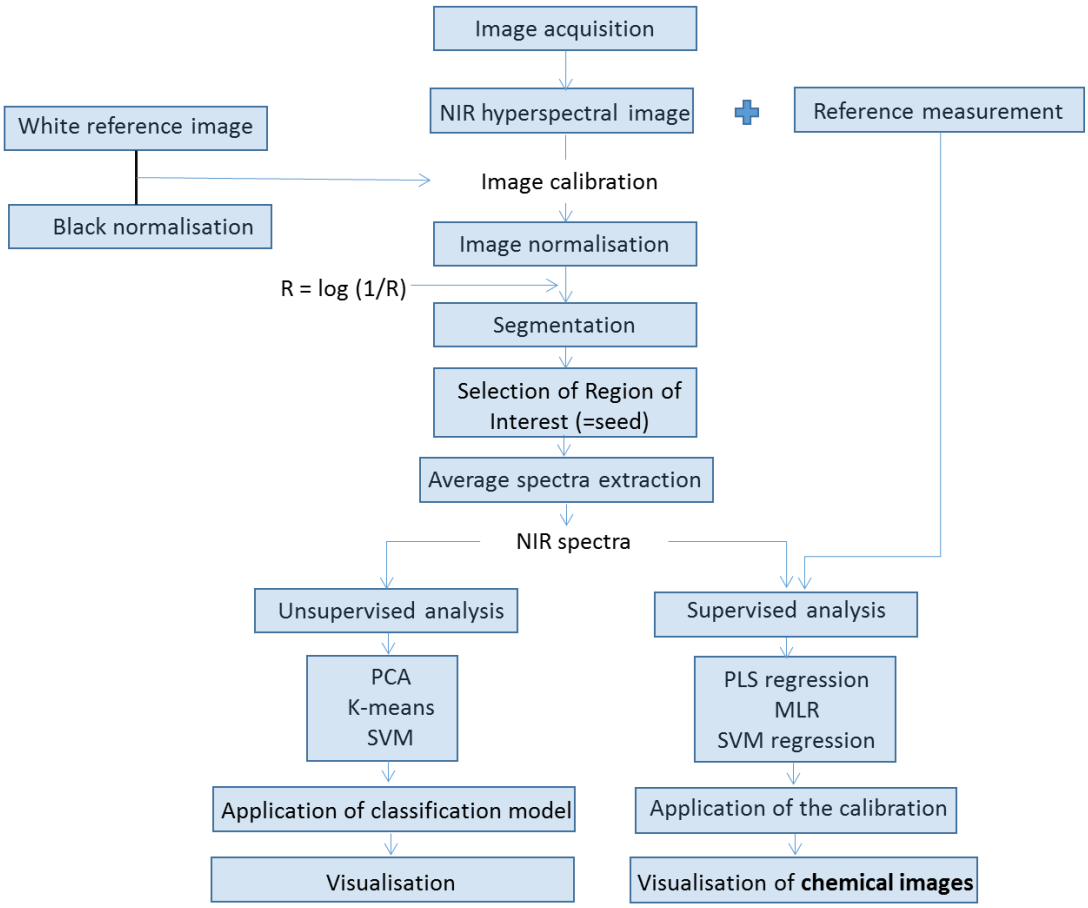


Figure 2.3. Simplified scheme of hyperspectral imaging processing steps and analyses.

MATLAB is another commonly used software, especially since add-ons have been developed to address specific characteristics of the hypercubes, e.g. PLS Toolbox (Eigenvector Research, Inc., WA, USA). Other software tools have been described for hyperspectral imaging data processing

or packages that can be adapted to work with hypercubes, including Evince chemometric software, ImageJ and Visualization Toolkit (VTK) (Burger & Gowen, 2011).

2.5.2. Image analysis

2.5.2.1.Image calibration

Using diffuse reflectance NIRS, the spectral information is recorded in reflectance mode, thus calculation of the absorbance is commonly applied (ElMasry & Nakauchi, 2016; Geladi et al., 2010). The reflectance calculation is needed to remove noise and compensate for offset and spatial non-uniformity, but it also corrects for possible temperature variation on the sample caused by the illumination source (Brown, Tauler, & Walczak, 2009). Raw reflectance (R) is converted into absorbance (A) using the formula: $A = -\log_{10}(R)$; or equivalently $\log(1/R)$. Absorbance is accepted by spectroscopic standardisation, while the arbitrary intensity is not an accepted spectroscopic unit (Geladi, 2007).

The use of absorbance data is useful for quantitative studies, because it removes some non-linearities due to scatter (Ghamisi, 2015). The NIR absolute reflectance might not always have a linear relationship with the analyte concentration, thus relative reflectance data can instead be used. The latter is calculated using a stable material with constant reflectance value. No standard reference material is universally accepted or suggested for HSI systems: it has been suggested that standards used for NIR instruments such as NIST 2036 can be also applied for HSI. Reference materials used include Spectralon, Teflon, NIST standard reference material 2035A (Burger & Geladi, 2007), Halon, and a special ceramic (Marten, Shenk, & Barton, 1989).

HSI data handling includes the use of the dark current data and white reference data to normalise and transform the raw signal intensity into absorbance. In other terms, it is a two-point calibration using the 0% and 100% reflectance. This gives an approximation and assumes linearity. A three-point calibration has been also reported in the literature to deal with possible non-linearities. The reference material can be moved during image acquisition, or by averaging several spectra within the ROI of the reference material (Burger & Geladi, 2005; ElMasry & Nakauchi, 2016).

Several steps are needed for HSI data processing before applying any statistical methods such as cleaning, background removal and object segmentation. This is followed by exploratory analysis, to remove pixels that are not useful, as well as redundant information (Geladi et al., 2010).

Image cleaning is a paramount step involved in the analysis of hypercubes and the selection of important and relevant information. HSI cameras have a certain number of pixels that do not work correctly originated from sensors elements that can be dead or respond erroneously (Boldrini et al., 2012). These pixels are called "dead pixels", or "bad pixels", and give a negative, infinity, zero or one response. They should be removed before building any chemometric model, as they can have a great influence on the response unrelated to sample properties (Du Toit, 2009; Grahn & Geladi, 2007). Erroneous pixels can be removed by replacing the spectrum with the median values of the surrounding pixels, or using a neighbourhood region of interest, however one of the most practical and effective ways is to set a threshold, as bad pixels present values that are far from "normal" ones obtained by other pixels (Vidal & Amigo, 2012).

Image processing can be performed directly on the hypercube, whether this includes all the variation expected, e.g. due to the presence of multiple samples within the same image, or using a "mosaic image", which is built by adding several images together. Another very advantageous approach is to select Regions of Interest (ROI) and perform feature extraction (ElMasry & Nakauchi, 2016).

Background can be even removed manually, by selecting one spectral band at which differentiation in terms of spectral absorption is obtained (Burger & Gowen, 2011; Geladi, 2007). The type of background is an important aspect in HSI, and a segmentation step is required to remove any region not belonging to the object under investigation (Steiner, 2011). Image segmentation is the separation between the region of interest (ROI) and the unwanted or non-relevant portion of the image, specifically the hypercube in the case of HSI analysis. Segmentation in digital image analysis has the aim to find the different objects/parts within an image, and/or to extract the desired information and separate it from the background. Several algorithms can be applied to perform it automatically (e.g. thresholding, morphological processing, edge-based segmentation and spectral image segmentation). Thresholding is the most commonly used

approach, using either a global thresholding approach or an adaptive thresholding. In the latter case, instead of setting a fixed threshold, it can change depending on different regions in the image (Prats-Montalbán et al., 2011; Wu & Sun, 2013a). Thresholding is especially effective when there is high contrast between the object and the background. Several other segmentation methods exist, which are detailed in He et al. (2016).

2.5.3. Chemometrics and multivariate analysis

The term chemometrics is often used to refer to the methods used to extract information and create statistical models for chemical systems. In the case of samples being comprised of components with well-separated spectral features, it is possible to use a univariate approach (single wavelength/marker band). However, spectral overlap is typically significant and therefore the univariate approach can only use a fraction of the available data. Accordingly, a multivariate data analysis is a better approach as more data can be included. The construction of a multivariate model for NIR instruments includes the collection of several spectra from samples to cover the range of analyte expected in the unknown samples. Multivariate techniques are classified into unsupervised and supervised methods (Figure 2.3). Unsupervised techniques do not require previous knowledge about sample properties, while supervised techniques are built on reference information previously given to build the model. In the first case, no previous knowledge on the sample structure is required and the samples are classified according to their similarity. Principal Component Analysis (PCA) is an example of the most common unsupervised technique, used to reduce the spectral information into loadings that contain the maximum variance observed in the dataset. On the other hand, the most common supervised classification method is Linear Discriminant Analysis (LDA), which finds the optimum boundaries among classes by maximising the ratio between inter-class variance, while minimising the intra-class variance (ElMasry et al., 2012).

For HSI, the application of supervised methods is becoming predominant, despite the efforts required to construct reliable models, because reference analysis of a high number of samples is required, compared to classification models or unsupervised methods that are only based on differences in the spectra.

Other methods include the projection pursuit (PP), random projection, independent component analysis and multivariate curve resolution (MCR). However, details on these methods are not reported herein as they were not applied in the present thesis, but the reader can refer to reviews reporting information on these methods in detail (Burger & Gowen, 2011).

2.5.3.1. *Principal Component Analysis (PCA)*

Principal Component Analysis can be used to understand the variance and covariance of the spectral bands, thus reducing the dimensionality of the data in order to explain the biggest source of variance. PCA is the most used unsupervised method in chemometrics for exploratory analysis, bringing to considerable data reduction by decomposing the data matrix to give score vectors and loading vectors (or weights). The score vectors can be reorganised to produce score images (Ferrari et al., 2013; Ghamisi, 2015). The use of score and loading plots from the PCA is very useful for the data interpretation and exploration of its structure. Despite the loss of spatial information when PCA is applied, it is still a predominant tool in HSI analysis, as it gives a good overview of the source of variance (Amigo, Martí, & Gowen, 2013). Positive examples are present in the literature on the use of PCA for the analysis of hyperspectral images, however unsupervised classification methods are difficult to interpret and to apply to new samples. In constrast, supervised methods for classification and quantification purposes have been successfully applied (Guidetti et al., 2012).

2.5.3.2. *Quantitative models*

For quantitative predictions, several methods can be used: multiple linear regression (MLR), principal component regression (PCR), and partial least squares (PLS). MLR gives a linear regression prediction using several explanatory variables, but resulting in co-linearity and overfitting issues. PCR is a regression technique based on PCA, where the model is built using MLR on the selected principal components. The disadvantage of this technique is that the first PCs are often not the most informative for the target compound or property. PLS regression is more widely used for its characteristics of robustness and reliability. It first extracts a series of orthogonal factors called Latent Variables (LV), or factors (ElMasry et al., 2012). Strictly speaking,

PLS latent variables are not principal components (PC), but they are rotations of the PCA principal components using a slightly different optimisation criterion (Burns & Ciurczak, 2007). Other statistical techniques exist for building quantitative models, including Multivariate Image Regression, Discriminant regression and Multiple Linear Regression, but they are not described in this thesis as PLS regression was the main tool applied for the majority of experiments.

Partial Least Squares (PLS) Regression. PLS is a regression method based on estimated latent variables similar to PCR and MLR, but it differs from PCR because it considers the responses and not just the spectral matrix when calculating the new orthogonal variables. In this way, the new variables, i.e. "latent variables" (LV), maximise the explained variance of the spectral data (Osborne et al., 1993). Optimisation of the number of LVs is critical to obtaining a robust model and low prediction error, whilst also avoiding overfitting of the data (Gowen, Downey, Esquerre, & O'Donnell, 2011). A low number of LVs does not use all the information available to explain all the possible variance, while using too many factors can lead to use excessive noise from the dependent and independent variables (Burns & Ciurczak, 2007). The ideal number of factors can be determined based on the minimum value of the obtained R^2, and several additional strategies can be applied to avoid over-fitting. For example, previous literature suggest the use of a maximum of (n-10)/10 factors (latent variables), where n is the number of samples (Osborne et al., 1993; Millar and Hall, 2004). The optimal LV would be the one leading to the lowest prediction error before the increase in prediction error due to overfitting. In some cases, when the prediction error decreases in a very little extent by increasing the LV, it is suggested to choose a smaller factor (Lewis & Kidder, 2010; Martens & Naes, 1992). Generally, the use of excessively large numbers of variables should be avoided but not using enough variables leads to underfitted models, not describing the whole observed variance (Roberts & Cozzolino, 2016).

Non-linear algorithms. Non-linear methods include Artificial Neural Networks (ANN), local regressions and Support Vector Machine (SVM). PLS and ANNs are among the most known supervised techniques to analyse HSI data, with SVM being described as a new chemometric tool (Brown et al., 2009).

Qualitative models (classification). Qualitative models are statistical methods used to find qualitative differences among the samples, i.e. classification based on spectral differences. Unsupervised classification methods include cluster analysis, unsupervised ANN and minimal spanning tree. Supervised methods include Soft Independent Modelling of class analogies (SIMCA), PLS-Discriminant Analysis (PLS-DA) and supervised ANN. In supervised clustering, in most cases it is necessary to reduce the variables to a smaller number of variables using PCA, MRC or other techniques such as SVM and radial basis function (RBF) (Geladi et al., 2010). Classification methods based on spectral features include PLS-Discriminant Analysis (PLS-DA) and ANN (Agelet & Hurburgh Jr, 2010).

2.5.3.3.Sample size

HSI, similarly to NIR spectroscopy, requires calibration for quantitative prediction. This is done by building multivariate statistical models against reference samples. For a correct statistical analysis and building robust models, the composition of the calibration set is of paramount importance. Samples in the calibration set should ideally cover the full range of compounds under investigation, in terms of chemical composition, spectral and physical characteristics, so that new samples will be predicted adequately (Fearn, 2005). A universally accepted "rule" to select the most appropriate number of samples does not exist, and it greatly depends upon the objective of the study. The same is true for the range of the target compounds, but a uniform distribution within this range is desired. In terms of sample number, it has been suggested that it should be at least bigger than the number of factors used in the regression model (Ciurczak & Igne, 2014).

Generally, two approaches have been described in the literature to overcome the issue of obtaining representative samples when building NIR-based calibrations. The first one is the accumulation of a sufficiently large number of samples and then to analyse all of them by the reference method to build the prediction model. An alternative approach is to select only samples that differ in their spectra, i.e. the biggest variance, and run the reference analyses only on those samples (spectral method) (Williams, 2001). Spectral sample selection reduces the amount of samples to be analysed, however there are several limitations including the fact that all sources of variance must still be identified. More importantly, when the focus is the analysis of minor

constituents, the spectra do not vary in appreciable extent as a result of these compounds, thus chemometric models are needed to establish whether significant correlations exist between the spectral variation and the target compounds or properties (Williams, 2001). It is important to choose correct sampling procedures, including the sample size, randomisation and the inclusion of representative samples when developing a calibration. In theory, the calibration should include all possible variation that is likely to be obtained when analysing new samples (Martens & Dardenne, 1998).

2.5.3.4.Spectral pre-treatment

Chemometrics can be applied directly on the absorbance spectra, i.e. log(1/R) values, however it is of great advantage to remove variations that are uninformative and due to sample presentation, morphology or light effects such as scattering. Three major groups of techniques for spectral pre-processing exist: (i) de-noising techniques, which are smoothing techniques, through several algorithms such as moving average or more frequently Savitzky-Golay smoothing; (ii) scatter correction techniques, e.g. standard normal variate (SNV) or multiplicative scatter correction (MSC); (iii) derivatives, which reduce additive effects as spectral baseline offsets and slopes. First derivative removes the additive baseline, while second derivatives remove linear baseline (Vidal and Amigo, 2012). Other spectral pre-treatments include mean centring, MSC and orthogonal signal correction (OSC)(Burns & Ciurczak, 2007). Savitzky-Golay smoothing is a filtering technique that uses a convolution approach, using a defined number of smoothing points, to then fit a polynomial equation. This method is more rapid compared to other techniques, but has the disadvantage of truncating the points at both ends, which a drawback when working with a limited number of bands (Yao et al., 2010). Normalisation and SNV have similarities with MSC, except that they do not require a common reference signal, and each observation is processed independently (Rinnan et al., 2009). The application of derivative treatments of spectra from hypercubes reduces the variance due to the scattering effect, but it is not able to eliminate the particle size effects. Not all spectral pre-treatments give better quality spectra, as some corrections to remove physical effects might not completely remove them independently from absorption information, or sometimes the physical features of the sample such as particle size might be useful

to build a better calibration (Burns & Ciurczak, 2007). The choice of the best pre-processing method is case-specific usually relies on trial and error user experience, and no universal rule exists for the choice of the most appropriate treatment (Agelet, 2011).

2.5.4. Outlier identification and removal

The correct identification and removal of outliers is another aspect that can influence the quality of prediction models. Several approaches have been reported in the literature, for example by considering the Leverage or Hotelling's T^2 statistics and the model residuals. However, removing the most extreme sample might also represent a risk of removing samples bringing a genuine difference, which would be of interest to include as much observed variability as possible (Næs, Isaksson, Fearn, & Davies, 2002). Outliers can be classified as X-outliers or Y-outliers. The first type represents anomalies in the predictors, with respect to the response, and can arise as a consequence of sample deterioration between the reference measurement and the HSI data acquisition, but also resulting from issues during the HSI scan of a particular sample. The second is caused by anomalies in the reference method or transcription errors. Outliers can be identified by several means, e.g. PCA, leverage, scores of the PLS latent variables or residual variance. High leverage samples (leverage being defined as the measure of how far away the independent variable values of an observation are from those of the other observations), i.e. those with values of 3-4 times higher than the mean leverage, might be considered as outliers, but they are not necessarily outliers. An alternative to the use of leverage is represented by the use of the T^2 value, which is based on Mahalanobis distance from the mean (Forina, Lanteri, & Casale, 2007).

2.5.5. Model validation and independence of the datasets

Classification or quantification models require estimation of the prediction accuracy, thus validation is needed. There are several ways one can apply to validate a calibration, cross-validation being one of the most used methods (Roberts & Cozzolino, 2016). Cross-validation evaluates the predictive model by excluding a subset of samples from the dataset and then use this subset as the validation data. A full cross-validation removes one sample at a time, while the segment cross-validation randomly select several samples to be used for the model evaluation. The use of cross-

validation is common in NIR spectroscopy applied to food and agricultural products (Kempeneers, 2007). However, it has been suggested that an independent validation avoids the risk of over-optimistic predictions caused by some interdependence (Fearn, 2014). The spectra and reference values can first be visually inspected to remove the ones that are obvious outliers, especially the bad spectra. The dataset is then segregated into calibration and validation data sets (Fearn, 2014; Roberts & Cozzolino, 2016). Further outliers may be removed from the calibration dataset once the equation is created, but no outliers should be removed from the validation dataset (Fearn, 2014).

Several statistics can be used to evaluate quantitative prediction models, the regression coefficient (R^2) being the most common used one is (Fearn, 2002). The Standard Error of Prediction (SEP) or Standard Error of Cross-Validation (SECV) can be also used to evaluate the performance of PLSR models. The root mean square error (RMSE) is the measurement of the differences between predicted values in the regression model and the values obtained by the reference method. The RMSE of calibration (RMSEC) applies the calibration equation directly on the calibration dataset, and it can lead to overestimation of the model performance. For this reason, prediction is carried out using a cross-validation, so that the RMSE of cross-validation (RMSECV) is used, or even an external validation, leading to RMSE of prediction (RMSEP). The RMSEP or RMSECV also include information about the bias, thus in this case the information on the bias can be avoided when reporting the results of a prediction model. Briefly, the most applied statistics are the following ones:

- Bias: systematic error that can be obtained due to very different samples present in the calibration dataset, different instruments used, differences during the acquisition of the reference measurement or different sample preparation;
- Standard error: it estimates the performance of the predictive model for an unknown dataset by calculating the average difference, corrected by the bias, between the predicted and reference values. RMSEC, RMSECV or RMSEP can be used, depending on the dataset.

- Ratio of Performance to Deviation (RPD): it is defined as the ratio between the standard deviation of the reference measurements dataset and the RMSECV or RMSEP (Fearn, 2002). The RPD has been suggested as a good indicator for NIRS prediction, with a value above 3 is desired when this technique is proposed to substitute the reference measurements (Ozaki et al., 2006). Other researchers suggested that RPD values above 5 can be used for estimating absolute contents, while values ranging from 2.5 to 4.9 are suitable for comparison purposes and screening (Scholz et al., 2014; Williams & Sobering, 1993).

The coefficient of determination (R^2) is a more indicative than the correlation itself (r), as it represents the proportion of explained variance (Fearn, 2002; Roberts & Cozzolino, 2016; Williams, 2001). It has been suggested that a correlation coefficient value of at least 0.65 can be used for sorting agricultural products into at least two grades, i.e. above and below the acceptable value, with approximately 80% accuracy (Shenk et al., 2001).

Despite the statistics used to evaluate prediction models, especially in NIR and HSI applications, it has been suggested that food scientists should interpret the models in the overall context of their application (Dardenne, 2010; Roberts & Cozzolino, 2016).

2.5.6. Application of calibrations

Calibration models can be applied to either map the distribution of a compound or property, at a single pixel level or to predict the average composition within the region of interest. This latter is done by averaging the spectral information within the ROI and applying the calibration on the average spectrum. The different approaches might bring differences in the computational speed, as the latter strategy is likely to be quicker as it requires application of a calibration on a single spectra instead of thousands spectra.

The application on a single pixel basis produces classification maps or "chemical images", which are images showing the distribution of a predicted compound or property on a single pixel basis (ElMasry et al., 2012). The "chemical image" is an image built by applying multivariate statistical models in a pixel-wise manner in order to visualise the distribution of a property or compound in a hypercube. It can be visualised as grescale image, colour or indexed image, where the estimated

concentration of food constituent is shown for each pixel (ElMasry & Nakauchi, 2016). The term is thus used when referring to the visualisation of compound distribution using HSI, combining the chemical characterisation of a sample, its physical properties and its visualisation (imaging) (Boldrini et al., 2012). Once a calibration model is built, its coefficients can be applied on a single pixel basis on the unfolded hypercube, i.e. on the data deconstructed into their spatial and spectral dimensions. An hypercube where a prediction model is applied on each pixel is referred as chemical image (Amigo et al., 2013).

2.6. WHEAT QUALITY

Wheat (*T. aestivum*) is one of the oldest and most extensively cultivated crops, and is nowadays considered as a staple food. World wheat production is above 729 million tons, second just to sugar cane and maize, whose production is 1884 and 1037 million tons, respectively (FAO, 2017). Botanically, common wheat is named *Triticum aestivum*, to distinguish it from the wheat used for pasta making, i.e. *Triticum durum*, whose name refers to its harder texture. The first one is genetically a hexaploid, while the second one is tetraploid, which originated from domestication of a wild tetraploid progenitor. A distinction among wheat is defined by hardness into hard and soft classes, and according to sowing period, into winter or spring wheats. A further classification can be done based on the kernel colour, into red and white varieties, the latter less suitable for wet climates.

Grain quality means, in a general sense with the suitability for a particular purpose, and criteria of quality are ease of processing and yield and quality of the end product (flour, bread, pasta and other baked goods). This can include endosperm texture, milling quality (flour yield, freedom of flour from bran specks), flour water absorption, bread and biscuit baking quality, moisture, protein content and Hagberg Falling Number (HFN). The kernel weight is routinely tested, in addition to screenings (contamination with foreign material and broken seeds), presence of sprouted kernels, moisture content, and the dough-quality related attributes that define the suitability of the wheat for the final product (Wrigley, 2009).

Among wheat quality criteria, the weight of a thousand kernels, or the hectolitre weight are traditionally used as possible indicators of potential flour yield. Hardness is also often measured to aid classification of varieties and because this parameter affects milling performance. A universally accepted definition of wheat hardness does not exist and this value depends on the method used for the measurement, however an instrument named Single Kernel Characterisation System (SKCS) is widely utilised by the industry. It measures the force required to crush single kernels between two surfaces. The SKCS results are expressed as the hardness index, which is calculated based on the crush force profile. This can differentiate hard samples with values above 50 from soft kernels, showing hardness index values below 50. Calibrations based on NIR spectroscopy for the prediction of wheat hardness are nowadays widely applied, including calibrations against SKCS measurements.

Protein content is a critical quality parameter for wheat, and is often used to define the price of this commodity. Measurement of protein content can be carried out using digestion or combustion methods to analyse the Nitrogen content, and thus estimate the protein content based on a conversion that considers the average amino acid profile of wheat. NIR-based methods have been demonstrated to be valid and accurate to predict protein content in wheat, and they are nowadays commonly applied at the industrial and laboratory level (Sissons, Osborne, & Sissons, 2006).

The functional properties of wheat flour are mainly attributed to its protein characteristics. Initial classification of wheat proteins was based on their solubility ("Osborne fractions"), by grouping them as albumin (soluble in water), globulin (soluble in saline solution), gliadin (soluble in 70% ethanol) and glutenin (soluble in alkali or diluted acids). The first two classes of proteins represent 20% of the protein mass, and they are more abundant in the external parts of the kernel, aleuronic cells and germ, but less abundant in the endosperm (Shewry & Halford, 2002).

Quality is influenced by environmental conditions such as agronomic practices, soil, climate, etc., but a major role is played by the genotypes. The current quality and yield of wheat reached in recent years is due to improvement in the agronomic conditions such as fertilisation, but mostly attributed to improvement in wheat breeding over the last decades. Long-term breeding

programmes led to the development of semi-dwarf varieties and improvement in the "flag leaf", which is particular importance during the grain filling period. Wheat grains are contained on a spike, which brings 15-18 spikelets at maturity. Variability of wheat composition has been described over several decades; e.g. Ali et al. (1969) reported the lowest third of the spike had the highest protein content. The kernel weight is also reported to vary according to the position on the plant and on the spikelet. Difference in kernel hardness is also strong between spikes, with up to 25% of the total variation (Miller, 2008).

Table 2.8 summarises the most important quality requirements for wheat, as applied to the UK market. All milling wheat should be free of pest infestation, ergot and other contaminant, should have a moisture content of 15% or below, and a level of impurities less than 2% by weight; it should also comply with the limits referred to agrochemicals, and with the specific weight required, which is usually above 76 kg/hl. The so-called "milling quality", i.e. the separation of white flour (endosperm) from germ and bran, is dependent on the wheat type, specific wheat and on the hardness (hard/soft), which is a genetically defined characteristic. The yield (amount of flour obtained per mass of wheat kernels processed) is an important aspect of wheat milling (Finch, Samuel, & Lane, 2014).

Table 2.8. Typical wheat quality requirements (Finch et al., 2014).

Market	Max moisture content (%)	Min specific weight (kg/hl)	Max impurities (% w/w)	Protein content (%)	Hagberg Falling Number (s)	W value	P/L value
Bread making	15	76	2	13	>250	-	-
Biscuit making	15	74	2	11.5	>220	-	-
Export (bread making wheat)	15	76	2	11-13	>250	>170	<0.9
Export (soft wheat)	15	75	2	10.5-11.5	>220	<120	<0.55
Feed	15	72	2	-	-	-	-

W and P/L values are from Chopin Alveograph Tests. W indicates the strength of the dough, P is the resistance to pressure and L is the elasticity value.

Additional properties can be used to evaluate grain quality in addition to the ones reported above, for example in barley seed germinability and viability are relevant quality parameters (Rahman &

Cho, 2016). Beyond protein content, gluten quality is also a relevant parameter in determining the bread baking quality of wheat, and it is largely a variety characteristic.

Rapid methods for the assessment of bread making quality would be of invaluable assistance to wheat breeders. Since the 80's, studies have been carried out using NIR for the assistance in wheat-breeding programs. The first attempts were made on protein and moisture content, as well as on grain texture (hardness) (Williams & Norris, 1987).

NIRS has been applied for wheat classification according to several quality indicators. Not all quality characteristics can be measured with sufficient accuracy, and the advantage of speed must be weighed against the error that can be tolerated, which depends to the application (Osborne, Fearn, & Stevenson, 1987; Williams & Norris, 1987).

2.6.1. HSI for wheat quality inspection

Wheat being the most economically relevant cereal worldwide, it is unsurprising that most of the scientific literature focuses on this commodity, for assessing quality parameters of cereals by NIR spectroscopy. The first applications of NIRS in the cereal industry was for the analysis of ground wheat and flour, while the possibility of scanning whole kernels without the need of grinding was demonstrated and prediction of whole kernel composition it is now routinely carried out.

HSI has been applied to detect artificially sprouted wheat kernels (Koç, Smail, & Wetzel, 2008; Smail, Fritz, & Wetzel, 2006), or for vitreousness evaluation of durum wheat (Gorretta et al., 2006; Shahin & Symons, 2008). Prediction of chemical compounds has been reported in maize kernels for moisture and lipid content (Cogdill et al., 2004), while the detection of mould damage in wheat or other cereal grains has been also studied, with some trials to estimate the content of mycotoxins such as *Fusarium spp.* or *A. flavus* (Wu and Sun, 2013b). The classification of wheat classes is another common application of HSI (Mahesh et al. 2008). This technology was applied for the determination of cereal grains viability. Sorghum, barley and wheat from different varieties were incubated in Petri dishes in a wet environment. Samples were taken up to 72 h and frozen at -80 ºC. They were then freeze-dried and analysed by HSI in the range of 1000-2500 nm. The authors reported that the region 1920-1940 nm was mainly associated with a loss of kernel viability. PLS-

DA was applied to differentiate between viable and non-viable proportions of the image and the model was able to explain 61% of the variance (McGoverin et al., 2011).

Variety identification by HSI has been also applied for grains other than wheat (Choudhary, Mahesh, Paliwal, & Jayas, 2009; Mahesh, Manickavasagan, Jayas, Paliwal, & White, 2008; Zhu et al., 2012), such as maize seed (Huang, Tang, Yang, & Zhu, 2016; Zhang et al., 2012) and rice (Kong et al., 2013). It has been also applied to differentiate between conventional and genetically modified soybean (Agelet, Ellis, et al., 2012) or rice (Liu et al., 2014).

Generally, the majority of HSI applications for food products use two spectral regions, around the visible region (400-1000 nm) or the NIR range 1000-1700 nm. Also, diffuse reflectance is predominantly used, due to the opaque nature of most solid foods (Wu and Sun, 2013b). A few applications of HSI have been reported in transmission mode, such as the estimation of oil and moisture content in maize kernels (Cogdill et al., 2004). This approach was successful for moisture but not satisfactory for fat prediction.

HSI has been applied to classify oat and groat kernels, which is of industrial interest for the rapid measurement of the amount of hull-less oat kernels, which is a key quality parameters for oats (Serranti, Cesare, Marini, & Bonifazi, 2013). The authors used a HSI system working in the NIR range of 1000-1700 nm and applied PLS-DA to discriminate between oat and groat samples. The discriminant model achieved an accuracy above 99%. Using fewer selected wavelengths (1132, 1195 and 1608 nm), the model was 97.1% and 99.0% for groat and oat, respectively. Pierna et al. (2012) reported a classification model for cereal grains using HSI in the reflectance NIR region 1100-2400 nm, to detect extraneous materials such as animal contaminants, botanical impurities, cellulose and other contaminants. The model was based on PCA and SVM using the quadratic model.

NIR hyperspectral imaging has been also applied to whole maize kernels to classify glassy or floury endosperm texture. The authors used two systems acquiring in the range 960-1662 and 1000-2498 nm, and applied PCA or PLS-DA for classification. PCA was effective in classifying pixels belonging to the two types of endosperm, while PLS-DA was effectively used to discriminate

fungal infected kernels, with classification accuracy of 96 and 99%, depending on the spectral system used (Kempeneers, 2007).

Robert et al. (2004) applied HSI for the single kernel analysis of maize kernels to predict moisture and fat content in the NIR region 750-1150 nm. The best model for predicting moisture had SECV of 1.20%, and a RPD of 2.74, while the best fat prediction model had RSMECV of 1.38% and RPD of just 1.45. In addition, a comparison between PLS regression and PCR indicated that PLS regression resulted in better prediction performance.

In many countries, protein content is a critical factor affecting the grain price, particularly wheat (Huang et al., 2008). The first attempts of applying NIRS as a rapid technique for protein analysis of cereals were done in the 1980s, when NIRS was compared with dye-binding and the reference method Kjeldahl for the quantification of protein in oats. The accuracy obtained by NIRS was satisfactory, whereas the authors highlighted that NIRS measurement tended to overestimate protein content at concentrations below 19.4%, and underestimate the higher ones (Biston & Clamot, 1982; Norris, 1982). Nowadays NIR spectroscopy is a well-recognised technique in the wheat and cereal-processing industry for routine quality assessment. Typical applications include ground wheat, while it was demonstrated that reliable prediction of wheat composition is possible using NIR directly on the whole kernels, which represented a great advance with benefits in terms of sample preparation, cost and applicability (Williams & Sobering, 1993).

Delwiche (1998) applied NIR reflectance spectroscopy to assess protein variability in single wheat kernels from five USA wheat classes, by using >300 samples and scanning 10 individual kernels of each in the spectral region 1100-2498 nm after drying of the kernels. PLS and MLR models gave satisfactory results (R^2=0.90-0.97).

2.6.2. Prediction of wheat enzymatic activity

α-amylase is an enzyme that hydrolyses alpha bonds of large, alpha-linked polysaccharides, such as starch and glycogen, yielding glucose and maltose. It is present in seeds containing starch as a food reserve. In germinated grain, α-amylase is synthesized by the scutellum and later by the adjacent aleurone layer. It is also located in the seed coat in a lower concentration (Barrero et al., 2013).

The α-amylase activity is known to be as affected by germination time and environmental temperature (Reddy, Ching, & Metzger, 1984). A pre-maturity α-amylase activity can exist also in absence of germination (Kettlewell & Cashman, 1997). Excess α-amylase activity is deleterious in wheat, as it negatively influences the rheological behaviour of the obtained dough, and is measured by Hagberg Falling Number (HFN). HFN is the industrial reference method applied for the evaluation of wheat quality, based on measurement of the time for a plunger to fall through a whole-meal paste in hot water after mixing (Major, Kettlewell, & Scott, 2001).

A small portion of sprouted grains may be sufficient to drop the HFN below the acceptable quality limits (Mares & Mrva, 2014). Sprout damage is often analysed by visual methods, however biochemical measurement can be also applied, but these approaches are still laborious and time consuming (Dencic, DePauw, Kobiljski, & Momcilovic, 2013).

With the aim of detecting problematic grains for possible segregation, HSI has been applied for the prediction of α-amylase activity in single kernels. Xing et al. (2009) used the spectral region of 1255-2300 nm, with 7 nm increments for assessing the level of translucency and amylase activity in two wheat classes. Low R^2 values of 0.54 and 0.73 were obtained for the two wheat classes analysed. Despite the poor performance, this might still be sufficient for classification purposes, as the authors reported a discriminant analysis accuracy up to 94% for high α-amylase content, and 88% for low α-amylase samples was achieved (Xing et al., 2009). In another study, the visible region (400-1000 nm) was used to detect pre-germination in wheat (Xing, Symons, Shahin, & Hatcher, 2010). The ratio between absorbance at 878 and 728 nm was suggested as a possible indicator to discriminate between sound and sprouted kernels. The authors also selected the germ end of wheat kernels as the Region of Interest (ROI) when predicting for α-amylase activity, to minimise the influence of other parts of the kernels.

Xing et al. (2011) applied hyperspectral imaging in the NIR region (1000-2500 nm) to evaluate individual kernels of Canadian Western Red Spring wheat. Two sets of 144 and 120 wheat kernels were artificially sprouted or field germinated respectively. The spectral intensities across the entire wavelength region were directly related to the enzymatic activity. In addition, the performances of SWIR and Fourier Transform NIR (FT-NIR) instruments were assessed. The PLS regression

model had R^2 values of 0.80-0.86 depending on the spectral pre-treatments and the instrumentation used. However, FT-NIR spectrometer always gave slightly better performance. The log transformation of the reference enzymatic activity led to improved prediction performance, compared to the original values. In this case, the SWIR-HSI system had slightly better performance, with the best prediction model showing R_c^2=0.86 and R_v^2=0.82, using the raw spectra. All the models applied tended to overestimate enzyme activity at lower values and underestimate at high values.

Koç et al. (2008) applied HSI for pre-sprouting damage identification using an InGaAs detector (1000-1700 nm). Six wheat varieties were tested at different levels of sprouting produced artificially by using increasing time of moisture exposure up to 36 h, building a classification model according to the level of sprouting. A similar experiment was reported by Chen et al. (2013), who forced wheat germination until 48h. The authors reported that the reflectivity in the spectral region of 870-1300 nm increased with increasing soaking time. A stronger absorbance at 1400 nm is related to increased water uptake from germinated kernels.

Singh (2009) used three imaging systems working in the range of 1000-1600 nm, 700-1100 nm and 400-700 nm range to classify wheat kernels affected by fungal damage or sprouted kernels. Wheat kernels were soaked for ~48 h to promote germination and freeze-drying was used to standardise the moisture content to 14%. However, this operation might have influenced the physical structure of the kernels and consequently their reflectance spectra. In addition, the analysed kernels had visible sprouts which were manually removed before imaging, suggesting a very intense sprout damage. These conditions are not applicable at industrial level as they do not reflect realistic conditions, in which i) the moisture content naturally varies among and within batches, ii) the sprouted kernels can be clearly identified by visible cameras so that more complex technology is not required, iii) the main issue related to wheat processing industry is the pre-sprouting increase of α-amylase, i.e. the negative consequence of enzymatic activity on HFN without visible changes on the wheat kernels.

2.7. COCOA QUALITY

Cocoa is a major agricultural product for several countries, especially in West and Central Africa, e.g. Cote d'Ivoire, Ghana, Nigeria and Cameroon. West Africa produces up to 70% of the world cocoa (Kongor et al., 2016). Ivory Coast, Ghana, Indonesia, Nigeria, Cameroon, Brazil and Ecuador are the major producing countries worldwide (Fowler & Coutel, 2017) (Figure 2.4). The world cocoa production is localised mostly in 6 major producing countries, Ivory Coast being the major producer with approximately 1.4 million tons per year (FAO, 2017); Indonesia and Ghana produce slightly above 0.8 and 0.7 million tons respectively. Nigeria production decreased from approximately 0.4 million tons reported on 2011 to 0.25 in 2014, while Cameroon and Brazil each produce above 0.25 million tons of cocoa beans per year.

The cocoa plant is a small tree that can be reproduced sexually or asexually (cutting, grafting, etc.). It requires warm, humid climates with temperatures between 20 and 30 ºC, and well-distributed rainfall of 1500-3000 mm/year. Its cultivation requires the use of other trees that can partially protect cocoa plants from excessive sun exposure. The cocoa fruit is a drupe, named cocoa pod, weight approximately 500 grams and contains 20-60 cocoa beans, embedded in a white pulp (Ferrari, 2014).

Criollo, Trinitario and Forastero are the three major classes of cocoa. Each type gives particular flavours, and has different agro-climatic conditions for cultivations (Owusu, 2010). Criollo belongs to *cacao* subsp. *cacao* and is mostly cultivated in Mexico, Colombia and Venezuela. Its cultivation is very limited (~3% world production) due to the plant's susceptibility to diseases. It gives an aromatic product with low bitterness characteristic and delicate flavour. Forastero, which name means "from abroad", is the most cultivated species in the world (~85%). Its success is due more to the easy cultivation and high plant resistance, rather than excellent sensory characteristics. Some products within this group show, however, very good quality, e.g. Arriba produced in Ecuador. Trinitario is cultivated for 6-8% the world production, and gives a product with fruity and persistent sensory notes. There is a common way to classify cocoa as "ordinary" or "bulk", and "fine" or "flavour". The first group represents 96% the world production, while the fine

cocoa comprises only 4%. However, Fowler and Coutel (2017) highlighted that there is no agreed definition of fine cocoas except that they have higher price based on flavour or colour.

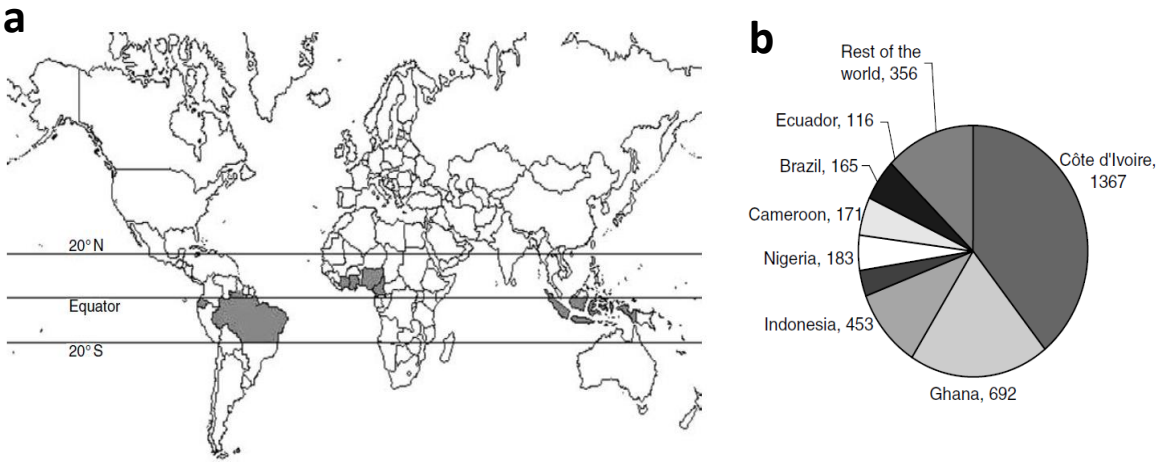


Figure 2.4. **a)** Main growing countries for cocoa production and **b)** average production of cocoa beans per country (1000 tonnes; years 2003-2006; taken from Fowler and Coutel, 2017).

Botanically, the cocoa bean consists of a shell (testa) and the kernel or cotyledon, which represents 86-90% of the total weight (Afoakwa, 2017). Cocoa bean genotype influences protein content and quality, carbohydrates and polyphenols (Afoakwa, Paterson, Fowler, & Ryan, 2008).

Cocoa processing includes a fermentation step. Fermentation is necessary to give good flavour and to remove the mucilaginous material, as well as to remove excessive bitterness and astringency. This is one of the most critical steps for flavour development (Afoakwa, 2017). The way this process is carried out depends on the location, climatic conditions and the facilities available. The most common process is using the "heap" fermentation or "box" fermentation. In heap fermentation, cocoa beans are piled on the ground and covered with leaves. Fermentation can be also carried out in wooden boxes, usually for 3 days to approximately one week. Fermentation leads to high temperatures of the seeds, up to 50 °C, and several compounds diffuse into the beans, e.g. acids, amino acids, peptides and reducing sugars (Nielsen et al., 2007).

During cocoa fermentation, indigenous yeasts act on the material in a sequential way. During the first anaerobic phase, predominated by yeast, pulp is degraded through pectinolysis, releasing the

viscous pulp. Yeasts produce ethanol and organic acids such as acetic acid and succinic acid, as well as a series of volatile compounds. Lactic acid bacteria and acetic acid bacteria start their activity, as the temperature, pH and substrate conditions change. Optimal fermentation should not exceed 4 days, to avoid the risk of bacilli and filamentous fungi development, or even entobacteriaceae (De Vuyst & Weckx, 2016).

The overall quality of cocoa bean is evaluated in terms of the presence of desirable flavours, absence of off-flavour and some physical properties such as cocoa butter hardness. Cocoa beans are firstly classified by weight, then the level of defective beans using the "cut test" to verify mould or insect infested, unfermented, germinated or flat seeds (Fowler & Coutel, 2017). Cocoa quality is related to several factors including the genotype, i.e. the cocoa variety, and the prevailing agro-climatic conditions (Kongor et al., 2016). Consistency of cocoa bean quality is an important parameter for growers, importers and the industry (Dand, 1997). The final quality of cocoa beans depends also on the ripening degree at which they are harvested. Unripe cocoa beans can reduce the yield of dry cocoa, while over-ripe beans might rot or germinate. After harvest, the cocoa pods are split open and the seeds are separated from the placenta, so fermentation can follow.

During fermentation, acetic and lactic acids are produced. Excessive levels of lactic acid can negatively influence cocoa flavour. Poorly fermented (slaty) beans as little as 3% can be deleterious for the quality of the whole batch (Dand, 1997). After fermentation, cocoa beans must be dried to usually 7-8% moisture content starting from an initial moisture content of ~55%. In general, higher moisture should be avoided to reduce mould development. Also, lower moisture can result in fragile beans so that the processing becomes more difficult. Usually, cocoa beans are sundried by placing them on the ground in layers of a few centimetres, or they can be dried using warm air or mechanical dryers. The method generally depends on the country where cocoa is produced (Gutiérrez & Pérez, 2015; Owusu, 2010). Artificial drying might be carried out too quickly, thus resulting in very acidic beans, or it might cause smoke to enter in contact with the beans (Fowler & Coutel, 2017).

Drying causes a further oxidation of polyphenols, catalysed by polyphenol oxidase, resulting in new flavour development and formation of brown colouring. After drying, roasting is necessary

to modify and fully develop the flavour of cocoa beans, which are bitter, acidic, astringent and nutty. Roasting causes a decreasing in acidity and the development of a range of odour-impact volatile compounds, mostly arising from Maillard reaction (Afoakwa et al., 2008). Dry cocoa beans are finally stored and typically transported in jute bags of approximately 60 kg. Further details on chocolate manufacturing are not reported here, but they can be found elsewhere (Beckett, 2011).

2.7.1. Cocoa composition

The cocoa bean consists of a cotyledon which is 86-90% of the total weight of the dry seed, and a shell (testa), with approximately 10-14% total weight (Table 2.9). The testa is permeable to water, ethanol, some acids and some volatile compounds. The cotyledon (nib) contains approximately 30% of water in the fresh state, with ~30% fat, while phenolic compounds, starch, sugars and other components are found at lower concentrations. The level of phenolic compounds, also referred to as polyphenols, in unfermented dried beans of Forastero cocoa has been reported to be above 7.5%, and above 17% when expressed on fat-free material (Kongor et al., 2016). Dramatic compositional changes are observed not only due to the drying but also for the fermentation, leading to a rapid decrease of the polyphenol content due to oxidation, and other important biochemical changes affecting cocoa quality and flavour (Afoakwa, 2017; Fowler & Coutel, 2017).

Polyphenols are found at relatively high concentrations in cocoa beans, compared to other food products, being up to 14-20%. The major groups of phenolic compounds are represented by catechins or flavan-3-ols (~37%), procyanidins (~4%) and proanthocyanidins (~58%) (Kongor et al., 2016). The amount of fat-soluble polyphenols decreases from 15-20% in fresh seeds to approximately 5% after fermentation. Polyphenols confer deep purple colour to fresh Forastero cocoa beans, with anthocyanins being the main responsible for the purple colour. Epicatechin, a compound found at relatively high abundance and possessing strong bitter notes, tends to polymerise due to oxidation, which reduces the astringency of the cocoa (Kongor et al., 2016).

Fermentation index is another important quality parameter for cocoa beans. It is assessed by visual evaluation of colour of a cut bean, by grouping each bean into fully brown (fully fermented), partly brown and partly purple, fully purple, slaty beans (Ilangantileke, Wahyudi, & Bailon, 1991). An

alternative to this time-consuming method has been described in the literature, using a solid-liquid extraction under acidic conditions, filtration and spectrophotometric measurement at 460 and 530 nm. The fermentation index has thus been defined as the ratio between 460 and 530 nm absorbance (Ilangantileke et al., 1991).

Cocoa butter is a major product of cocoa beans, also affecting its price. Once the fat is partially removed, the cocoa powder is the other product obtained from cocoa beans, used for chocolate production. Cocoa powder can differ in the fat content, colour, degree of alkalinisation, with speciality powders showing some peculiarities. Two types of cells are found in cocoa beans, storage cells containing fat and proteins, and the pigment cells containing phenolic compounds, theobromine and caffeine.

Table 2.9. Composition of cocoa beans, modified from (Fowler & Coutel, 2017).

	Whole dried cocoa beans (as traded)			
	%	**Range (%)**		
Water	7.5	5-8		
Shell (dry basis)	12.5	10-16		
Nib (dry basis)	80	78-82		
	Unfermented beans (dry, fat-free)	**Fermented beans (dry, fat-free)**		
	mg/g	**mg/g**		
Total polyphenols	150-200	40-150		
Procyanidins	61	23		
Epicatechin	-	3-16		
	Nib		**Shell**	
	Mean (%)	**Range (%)**	**Mean (%)**	**Range (%)**
Water	3.7	2-5	7.0	4-11
Fat	53.5	48-57	2.8	2-6
Protein	12.7	11-16	14.7	13-20
Starch	6.7	6-9	8.1	6.5-9
Fibre (crude)	2.5	2.1-3.2	16.6	13-19
Ash	2.9	2.6-4.2	8.2	6.5-20.7
Theobromine	1.30	0.8-1.4	0.87	0.2-1.3
Caffeine	0.22	0.1-0.7	0.13	0.04-0.3

Note: Values depend on type of beans and method of analysis. They also vary according to storage conditions and the degree of drying or roasting.

Theobromine and caffeine are methylxanthines, and contribute to the typical bitterness of cocoa beans, and it has been suggested that they probably diffuse from the cotyledons during fermentation. Cocoa butter hardness is a quality parameter; it depends on the fatty acid composition, which is influenced by the variety and growing conditions, as well as fermentation and drying. The presence of off-flavour is usually assessed by sensory analysis, carried out by trained panels (Fowler & Coutel, 2017).

2.7.2. NIR and HSI applied for cocoa analysis

NIR-based methods have been applied for cocoa bean or chocolate quality assessment or composition analysis mostly by analysing ground cocoa or liquor. However, HSI has not been applied so far for evaluating the quality of this product. The first study investigating chocolate quality using NIRS was conducted by Davies et al. (1991) who used NIRS of raw and roasted cocoa beans, as well as chocolate to predict the sensory properties of the products. Ground cocoa beans were analysed at room temperature, while chocolate was previously heated to 50 °C to melt it. Spectra were acquired in the range of 1100-2500 nm and PCA was applied to predict sensory parameters. The model had limited performance, showing a correlation among spectral and sensory data of r=0.813. It has been argued that this lack of strong prediction ability is due to the fact that sensory properties of cocoa and chocolate depend on compounds present at very low concentrations, which are not detectable or hardly detectable by NIRS (Davies et al., 1991). Teye et al. (2013) applied NIRS for discrimination of cocoa beans from Ghana. Several chemometric methods were used, including KNN, LDA and SVM. SVM had good classification performance in predicting the geographical origin within Ghana. Ten grams of ground cocoa beans were scanned in the reflectance mode and spectral range 1000-2500 nm.

In another study, cocoa beans were ground mixed with water, and the obtained liquor was filtered and analysed by reflectance NIRS (1000-2500 nm) to build classification models using PCA and SVM on 5 varieties. The classification rate was from 80 to 93% (Teye, Huang, Takrama, & Haiyang, 2014). Classification models have also been developed (Jentzsch et al., 2016) using Raman spectroscopy on 20 samples of fermented cocoa beans from Ecuador. This work was one

of the very few ones in which IR methods have been used on unground cocoa beans. The classification accuracy for geographical origin was 91.8%.

Also, NIRS has been successfully used for fat quantification, as well as nitrogen and moisture content in cocoa powder (Veselá et al., 2007). FT-NIR (1000-2500 nm) has been used to predict total fat content in ground cocoa bean samples (Teye & Huang, 2015). The fat content ranged from 51.3 to 68.0; the R^2 values were 0.93-0.98 and 0.92-0.97 for the calibration and prediction datasets, respectively. The prediction error for fat content prediction was RMSECV=0.01-0.02%, with RMSEP of ~0.02%. Fifty samples were used for the calibration dataset and 30 for the external prediction.

Veselá et al. (2007) compared NIR and FT-IR (spectral regions, i.e. 1100-2500 nm and 1670-2500 nm) to predict fat, nitrogen and moisture content in powdered cocoa. Fat content exhibited a wide range, 2.4-22.0%. The NIR prediction model for this constituent had R^2=0.96 and RMSECV=7.0%. When using FT-IR, the model had R^2=0.94 and RMSECV=10.4%.

Moreover, Álvarez et al. (2012) applied reflectance spectroscopy in the region of 780-2500 nm to predict fat, caffeine, theobromine and epicatechin content. For fat content ranging from 46 to 64%, the R^2 value was 0.94, RMSECV=0.89%, and RPD=3.4.

Other properties of cocoa beans were estimated using FT-IR, in particular pH and fermentation index (Teye et al., 2015). The range of fermentation index was from 0.37 to 1.37. The regression coefficients of PLS regression models were 0.97 and 0.96 for calibration and validation datasets, respectively. The RMSECV was 0.07 and RMSEP of 0.08. Good performances were also reported for pH prediction. Other chemometric models had slightly better performances, for example using an efficient variable selection and neural network regression.

Phenolic compounds, particularly procyanidins, have been investigated in cocoa liquor using NIRS (Whitacre et al., 2003). The spectral region used was 700-2500 nm and the reference analysis was carried out using HPLC analysis. Excellent prediction was reported, with R^2 value of 0.98 for total procyanidin oligomers.

Similarly, only one research paper has been found in the literature using IR methods on whole cocoa beans for quantification purposes. Sunoj et al. (2016) fermented six batches of cocoa pods

at four fermentation times up to 21 days. FT-IR spectra were acquired in the range 800-2778 nm, and PLS regression was used to build calibrations for total polyphenols, pH and fermentation index. Total phenolics ranged from 7.0 to 16.2 mg g^{-1}. The best PLS regression prediction model had R^2=0.84 and RMSECV=0.93 mg g^{-1} using vector normalisation. The prediction model for fermentation index had R^2=0.83-0.86 and RMSECV=0.06-0.09 mg g^{-1}, depending on the spectral pre-treatments, suggesting adequate performance for screening (Sunoj et al., 2016).

2.8. COFFEE QUALITY

Coffee is the second most traded commodity in the world, being second in value only to petroleum and is described as the most popular beverage worldwide (de Azeredo, 2011; Van Hilten, Fisher, & Wheeler, 2011). World coffee production is estimated above 130 million bags (of 60 kg), with a consumption of above 8 million tons. Brazil, Vietnam and Colombia are the major producing countries, with Brazil comprising 32-34% (Van Hilten et al., 2011). The two main cultivated species of coffee are Arabica (*Coffeea Arabica* L.) and Robusta (*Coffeea canephora P.*). Coffee originates from Africa: Arabica is indigenous from Ethiopia and Robusta from the Atlantic coast. Arabica represents 60% of the world production, while Robusta almost 40%.

Grading and classification of green coffee can be carried out using several criteria, including altitude or region, variety, post-harvest processing, bean size, amount of defects, bean density and cup quality. The global market consists of three quality segments, named "exemplary quality", "high/premium quality" and "mainstream quality". The first category is defined to possess "unique cup quality", the second category is "good tasting coffee", while the last one has "average quality" (Van Hilten et al., 2011). The international regulations state that Arabica coffees having over 86 defective beans per 300 g sample, or Robusta coffees with more than 150 defects per 300 g should not be exported. To be exported, green coffee beans should contain moisture content between 8% and 12.5%. However, it has also been highlighted that of the total coffee exported, about 10% of the coffees were outside the accepted limits, the vast majority being Robusta (Van Hilten et al., 2011).

Identification of the coffee species can be done by trained inspectors, by looking at the colour and size, which is relatively easy for green coffee but might be difficult for roasted coffee beans (Barbin, Felicio, Sun, Nixdorf, & Hirooka, 2014). Traditionally, coffee quality assessment is performed by the "cup testing", which has been developed by the International Coffee Organisation (ICO). It uses a 100-points scale to evaluate coffee brew quality, based on the attributes of fragrance, flavour, aftertaste, acidity, body, uniformity, balance, clean up, sweetness and overall flavour. The method involves roasting, grinding and brewing 10 grams of ground coffee with 230 g boiling water. Coffee cupping involves the use of small cups into which ground coffee is placed and nearly boiling water is poured, and then a large spoon is used to slurp the brew. Certain differences in coffee aroma have been attributed to the post-harvest processing, as the beverage obtained from wet-processed beans lead to a pleasant acidity, while the dry-processed ones typically give a full body (Poisson, Blank, Dunkel, & Hofmann, 2016; Van Hilten et al., 2011).

Coffee harvesting is carried out by picking, stripping or mechanical harvest. The first method generally produces better quality coffee, while stripping causes immature cherries to be harvested together with fully mature ones and leaves. The detection of defects such as immature, black, sour, black-immature, broken or insect-damaged seeds is often assessed as they can bring unwanted flavours or strong off-flavours. The cherries are processed to remove the cherry pulp that is rich in water, sugars, fibre and mucilaginous material. Wet or dry processing can be carried out on the fresh coffee cherries: the first method implies soaking the cherries in rotation tanks with water to better separate the pulp and skin from the seed. The dry process is carried out by drying the cherries in the sun to 10-12% moisture content. The coffee is then de-hulled to remove the pulp but leaving the mucilaginous material (silver skin). Wet processed coffees are commonly seen as higher quality. An intermediate process called "natural processing" is also used especially in Brazil, and it has intermediate characteristics between wet- and dry-processing (Van Hilten et al., 2011).

Robusta coffees are mostly dry-processed in the sun, although "washed" (wet-processed) Robustas exist, which are appreciated for the body and neutral taste. Wet-processed Arabicas are

commonly described as well balanced in terms of body and acidity compared to dry-processed beans (Van Hilten et al., 2011).

2.8.1. Coffee composition

As shown in Table 2.10, polysaccharides are major constituents of green coffee, with 34-44% in Arabica and 48-55% in Robusta. Sucrose ranges from 6 to 9% in Arabica, while it ranges from 0.9 to 4% in Robusta coffee. Nitrogenous compounds are generally present at concentrations of 10-15%, while fat is also present at similar concentrations (Farah, 2012). Robusta and Arabica green coffee beans have been reported to possess significantly different fat content, from 15-17% in Arabica to 7-10% in Robusta (Illy & Viani, 2005).

Chlorogenic acids and other compounds affecting the final flavour of coffee are also found at lower concentrations. In particular, caffeine range is reported to be 0.9-1.3% in Arabica and 1.5-2.5% in Robusta coffee, while trigonelline is 0.6-2.0% in Arabica and 0.6-0.7% in Robusta (Farah, 2012). Among non-volatile compounds that are relevant for coffee overall flavour, caffeine, trigonelline, acids, lipids and minerals play a role in coffee quality (Buffo & Cardelli-Freire, 2004). Some of these compounds possess bitter, astringent or sour notes, which are key indicators of coffee quality. Caffeine and trigonelline are nitrogen-containing molecules that exert a marked bitter note. Their behaviour during coffee roasting is different, as caffeine content remains fairly constant, but trigonelline dramatically degrades (Farah, 2012; Perrone, Donangelo, Donangelo, & Farah, 2010).

The study of coffee components such as trigonelline, nicotinic acid and caffeine is commonly carried out based on High Performance Liquid Chromatography (HPLC) methods. For example, Casal et al. (1998) investigated the effect of roasting conditions, i.e. temperature 140-240 ºC for 5-20 minutes, on the concentration of these components in Arabica and Robusta coffees. Other researchers investigated the natural variability of caffeine, trigonelline, chlorogenic acid and sucrose in green coffee beans depending on the botanical and geographical origins. Sucrose in Arabica coffee was shown to vary from 7.4 to 11.1%, caffeine from 0.96 to 1.62% while

trigonelline ranged from 0.88 to 1.77%. Robusta coffee had sucrose range from 4.1 to 7.1%, caffeine 1.5-3.3% and trigonelline 0.8-1.2% (Ky et al., 2001).

Table 2.10. Chemical composition of green and roasted coffee beans (modified from Farah, 2012).

Parameter	**Green**		**Roasted**	
	Coffea Arabica	***Coffea canephora***	***Coffea Arabica***	***Coffea canephora***
Carbohydrates/fibre				
Sucrose	6.0–9.0	0.9–4.0	4.2-tr	1.6-tr
Reducing sugars	0.1	0.4	0.3	0.3
Polysaccharides (arabinogalactan, mannan, glucan)	34–44	48–55	31–33	37
Lignin	3.0	3.0	3.0	3.0
Pectins	2.0	2.0	2.0	2.0
Nitrogenous compounds				
Protein/Peptides	10.0–11.0	11.0–15.0	7.5–10	7.5–10
Free amino acids	0.5	0.8–1.0	-	-
Caffeine	0.9–1.3	1.5–2.5	1.1–1.3	2.4–2.5
Trigonelline	0.6–2.0	0.6–0.7	1.2–0.2	0.7–0.3
Nicotinic acid	-	-	0.016–0.026	0.014–0.025
Lipids				
Coffee oil (triglycerides with unsaponifiables)	15.0–17.0	7.0–10.0	17	11
Diterpene (free and esterified)	0.5–1.2	0.2–0.8	0.9	0.2
Minerals	3.0–4.2	4.4–4.5	4.5	4.7
Acids and esters				
Chlorogenic acids	4.1–7.9	6.1–11.3	1.9–2.5	3.3–3.8
Aliphatic acids	1.0	1.0	1.6	1.6
Quinic acid	0.4	0.4	0.8	1
Melanoidins	-	-	25	25

Concentrations are expressed as wt %.

2.8.2. Coffee roasting

Coffee is consumed after roasting, which is carried out to fully develop its flavour. This is an important operation, as it strongly influences coffee final quality. Roasting is based on continuous heating of the green beans, causing a series of complex physical and chemical reactions. There are two major types of roasters - drum and fluidized-bed roasters. In the former, the seeds are in contact with fire or a hot surface, while the second type is newer and coffee beans are in contact

with hot air or gases. This system transfers heat using hot air and is characterised by high homogeneity, guaranteed by the fact that beans are not static but continuously floating in the air flow. It allows achieving the desired level of roasting in a few minutes, typically 3-6 minutes. Fluidised-bed roasters have several advantages, particularly the time needed to roast, the temperature control and the production of a more homogeneous colour. Rotating cylinder equipment is the most traditional method used for coffee roasting, which uses a gas heater and rotating drums. The cylindrical shape of the chamber allows its use in continuous operation. The heating is achieved using convective flow of hot air. The time and temperature are chosen according to the roasting degree wanted, the temperature usually varying in the range 210-240 °C. The roasting degree can be controlled by setting a defined time for roasting, or by continuous checking of the colour or other indicators such as weight loss, which can help in obtaining a more objective measurement (Farah, 2012).

When the internal temperature of the coffee beans increases, caramelisation starts (at ~130 °C) with a visual change of the colour. At 160 °C, there is an increase in seed volume and aroma formation. Higher temperatures, up to 190 °C, bring full flavour development due to the Maillard reaction, Strecker degradation and pyrolysis. At this stage, the colour changes from a light brown to black. The roasting degree is often assessed in the industry by trained operators who visually evaluate the beans and define the roasting degree by hearing the crack (first and second cracks, which is the sound emitted by the beans during the roasting; Figure A.3 in Appendix).

Moisture decreases dramatically during roasting, together with changes in many other compounds. Objective methods include the determination of weight loss, density and moisture, as well as colour measurement due to the ease of analysis (Santos et al., 2016). Obtaining a uniform degree of roasting is difficult, and currently no universally accepted method to define roasting degree exists (Baggenstoss, Poisson, Kaegi, Perren, & Escher, 2008). However, the definition of roasting degree should be independent of variations in the raw material. Colour assessment has been described as not reliable for evaluation of coffee roasting degree, as different quality coffees can reach the same reflectance value, or coffees treated under the same time/temperature profile can present different colour values. Thus, visual assessment and cracking parameters can give

inaccurate determination as they depend on the subjectivity of the operator (Shan, Suzuki, Ogawa, & Kondo, 2015). In addition to colour measurement, Franca et al. (2009) pointed out that also weight loss measurement alone is not a good and reliable indicator of coffee roasting degree.

Typical roasting conditions using traditional industrial drum roasters vary from 180 to 240 ºC for a period of 8-15 minutes. Medium roasted coffee is often reported as the best roasting degree to maximise the production of aroma compounds and flavour complexity of the final product.

Some green coffee constituents, such as caffeine and lipids, are scarcely affected by the roasting, while others dramatically decrease, e.g. chlorogenic acids and trigonelline. Trigonelline gives volatile compounds and methyl nicotinate, other compounds are relatively heat stable, for example caffeine (Farah, 2012). The loss of these compounds after roasting has also been linked to the maturity stage at which the coffee cherries are collected. Carbohydrates are another important class of compounds that undergo changes over roasting. Phenomena such as caramelisation of low molecular weight carbohydrates give important flavour compounds, and they are also precursors of several aliphatic acids (Poisson et al., 2016).

Lipids are another important class of compounds in green and roasted coffee beans, as coffee fat gives the characteristic mouth impact of "body", also acting as a solvent and carrier for hydrophobic aroma compounds (Poisson et al., 2016). Similarly, chlorogenic acids are degraded to as little as 1% their initial content depending on the time-temperature conditions. Degradation of these products yields most of the volatile compounds contributing to the characteristic aroma of roasted coffee beans.

2.8.3. Coffee flavour generation

Many green coffee constituents are precursors of flavour compounds formed during roasting, particularly sugars, proteins, trigonelline and other nitrogen-containing compounds, as well as chlorogenic acids (Figure 2.5). Despite hundreds of volatile compounds reported in roasted coffee, only approximately 25-30 molecules are key odorants, which strongly contribute to the overall coffee aroma (Blank, 2002; Grosch, 1998, 2001b; Mayer, Czerny, & Grosch, 1999; Schenker et al., 2002; Semmelroch & Grosch, 1996). Volatiles such as guaiacol, 4-vinylguaiacol,

4-ethylguaiacol, 4-hydroxy-2,5-dimethyl-3(2H)-furanone, 3-hydroxy-4.5-dimethyl-2(5H)-furanone, 2,3-butanedione, 2,3-pentanedione and 3-methylbutanal have been described as potent odorants in coffee brews in both Arabica and Robusta coffees (Semmelroch & Grosch, 1996).

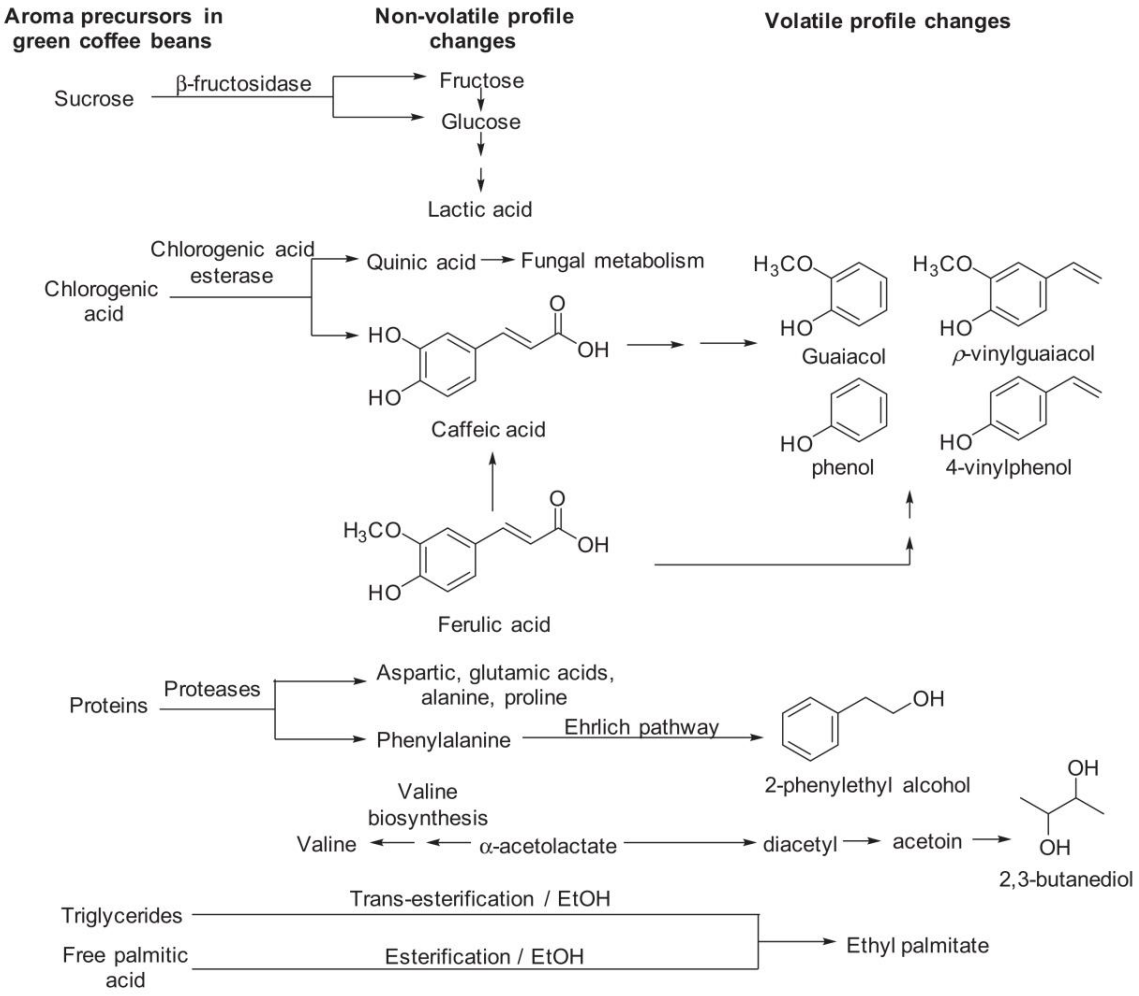


Figure 2.5. Link between green coffee composition and aroma generated after coffee roasting (Lee, Cheong, Curran, Yu, & Liu, 2016).

The Maillard reaction exerts a critical role in coffee flavour formation. The following phenomena take place leading to aroma compound generation (Buffo & Cardelli-Freire, 2004) during roasting:

- Water loss, carbon dioxide formation, lipid migration on the bean surface;
- Maillard reaction between nitrogen-containing compounds and reducing carbohydrates yielding aminoaldoses and aminoketones by condensation;

- Strecker degradation, between amino acids and dicarbonyl yielding aminoketones, that form nitrogen heterocyclic compounds or oxazoles;
- Sulphur amino acid degradation, which gives mercaptans, thiophenes and thiazoles;
- Hydroxy-amino acid breakdown, which react with sucrose to give alkylpyrazines;
- Proline and hydroxyproline, which interact with Maillard intermediates, and give pyrrolyzines, alkyl-, acyl- and furfurylpyrroles;
- Trigonelline degradation, that gives alkyl-pyridines and pyrroles;
- Quinic acid moiety degradation, that produce volatile phenols;
- Pigment degradation (carotenoids);
- Lipid degradation (mainly diterpenes);
- Interactions among intermediate products (mostly unknown).

The pathway of reactions starts from condensation of amino groups and reducing sugars, giving so-called Amadori products, which further degrade into sugar fragmentation products, by releasing the amino group. Reactions of dehydration, fragmentation, cyclization and polymerization follow (Van Boekel, 2006). Furfural generation arises from Amadori rearrangement products, in particular from deoxyosones, when the sugar is a pentose. In the case of hexoses, hydroxymethylfurfural has been described to originate from this reaction. Pyrroles, pyranones and furanones are generated from sugar fragmentation of deoxyosones, with a further action of reductions. When other amino acids participate in the reaction, the Strecker reaction of aldehydes with aminoketones, followed by heterocyization gives a series of aroma-active volatile compounds, such as pyridines, pyrazines, thiazoles and pyrroles. Pyrroles reaction involves heterocyclization with acetoin, which is therefore a particularly interesting compound in aroma formation.

Whilst the Maillard reaction is still not fully understood, however kinetic models have been proposed in the literature to explain the formation of volatile compounds. Strecker aldehydes such as 3-methylbutanal are known to be generated from amino acid decarboxylation, followed by a breakdown into aminoacetone and finally the aldehyde (Grosch, 2001a). Baggenstoss et al. (2008) reported that these aldehydes increase especially in the initial roasting, and a decrease is observed

at longer roasting time. Despite several mechanisms proposed in the literature for α-diketones, such as 2,3-butanedione and 2,3-pentanedione, no clear mechanism is accepted, but it is clear that the formation pathway involves glucose, or an intermediate product of sucrose degradation (Baggenstoss et al., 2008). High energy at the beginning of the roasting process seems to lead to increased levels of 2,3-butanedione, while generation of 2,3-pentanedione was reported to be less influenced by the roasting profile. Previous studies proposed the hypothesis that 2,3-pentanedione arises from 2,3-butanedione degradation (Weenen & Apeldoorn, 1996), whereas Baggenstoss et al. (2008) suggested an independent generation.

Pyridines can arise from trigonelline degradation, protein pyrolysis, Strecker degradation and Maillard reaction (De Maria, Trugo, Neto, Moreira, & Alviano, 1996). Their concentration is influenced by the species, Arabica being richer in these compounds, and by the roasting degree (Franca et al., 2009). Other compounds that are strictly dependent upon the roasting degree, in this case in a negative correlation, are furan and furanyl compounds, as they are synthesized by the thermal degradation of carbohydrates upon pyrolysis. On the contrary, other compounds such as 4-vinylguaiacol have been described as unaffected by the roasting degree (Franca et al., 2009). Pyridine content is strongly related to the roasting time, as initial high concentration of this compound is observed at the initial roasting, followed by continuous decrease over roasting (Baggenstoss et al., 2008).

Degradation of chlorogenic acids causes the appearance of a series of neo-formation products (Kamiyama, Moon, Jang, & Shibamoto, 2015). Phenol and 2,5-dimethylfuran were reported to be formed from 5-caffeoylquinic acid degradation over roasting. Some acids, including formic acid and acetic acid, increase their concentration during roasting, and their maximum concentration has been reported for medium roasted coffee (Ginz, Balzer, Bradbury, & Maier, 2000). Volatile compounds such as guaiacol and 4-vinylguaiacol are formed from degradation of chlorogenic acid during roasting. 4-Vinylguaiacol generation at high concentration is temperature-dependent at initial stage of roasting, while very low concentrations are obtained at when the temperature is increased. This effect has been explained by the initial quick degradation of 5-feruloylquinic acid, which requires low activation energy, but at higher roasting condition 4-vinylguaiacol can degrade

to give guaiacol (Dorfner, Ferge, Kettrup, Zimmermann, & Yeretzian, 2003; Kamiyama et al., 2015). Similarly, furaneol, also named 4-hydroxy-2,5-dimethyl-3(2H)-furanone, has been reported in green and roasted coffee (Scheidig, Czerny, & Schieberle, 2007; Yeretzian, Jordan, Badoud, & Lindinger, 2002). Under certain conditions, 4-vinylguiacol can also give guaiacol and phenol (Hertz-Schünemann, Dorfner, Yeretzian, Streibel, & Zimmermann, 2013). The concentration of certain volatile compounds is strictly inter-related, for example ferulic acid degradation gives 4-vinylguaiacol, which can give guaiacol and phenol when some of its functional groups are lost during roasting (Dorfner et al., 2003).

Trigonelline is an important aroma precursor as it gives pyridine and derivative compounds. Vanillin and guaiacols are generated from caffeic and ferulic acids, which are derivatives of chlorogenic acids (Yeretzian et al., 2002).

Furfural is formed by decomposition of pentosane or glucose and also by oxidation of furfuryl alcohol, whereas the furfurylalcohol is a product of the reaction of (deoxy)ribose or sucrose with cystein/methionine (Hertz-Schünemann et al., 2013).

Table 2.11 summarises the typical contents of coffee aroma precursors in the green coffee and the corresponding volatile compounds obtained after roasting, for Arabica and Robusta.

Table 2.11. Precursors of coffee aroma compounds found in green coffee beans.

Precursor compound	**Arabica**	**Robusta**	**Corresponding volatile compounds (incomplete)**
Chlorogenic acids	Low (0.55-6.69 %)	High (0.81-7.74 %)	Volatile phenols
Trigonelline	High (0.19-1.35 %)	Low (0.02-0.79 %)	Pyridine
Caffeine	Low (0.98-1.27 %)	High (2.15-2.22 %)	Caffeine (non-volatile)
Carbohydrates (sucrose)	High (4.20-9.65%)	Low (1.66-3.53 %)	Furan derivatives
Lipids	High (12.8-16.2 %)	Low (6.70-8.70 %)	Fatty acids, oxidation prod.
Sulphur compounds	Low	High	Methanethiol
α-Dicarbonyls	High	Low	Carboxylic compounds
Cafestol	Presence	Presence	Anhydrous cafestol
Kahweol	Presence	Absence	Anhydrous kahweol

Modified from Hertz-Schünemann et al., (2013), and Fischer et al., (2014).

2.8.4. Variability of coffee aroma compounds

Coffee aroma is known to vary in relation to several factors such as roasting, the coffee species and post-harvest treatment (Franca et al., 2009; Gonzalez-Rios et al., 2007). Gloess et al. (2014) reported that the aroma profile of coffees from different origins and those treated using different time-temperature profiles vary dramatically, and the roasting conditions affect the intensity of volatile compounds as well as their relative composition. Some compounds are found to be more dependent upon the roasting intensity compared to others. For instance, pyridine is greatly influenced by the roasting time, as shorter roasting causes over 6-fold higher presence of this volatile (Yang et al., 2016). In addition, shorter roasting time causes significant and dramatic difference in the majority of volatile compounds in the resulting coffee brew. Some of the compounds previously correlated with the roasting degree were 2,5-dimethylpyrazine, 2-ethylpyrazine, 2,3-dimethylpyrazine, 2,5-dimethyl-3-ethylpyrazine, guaiacol, 2-ethylguaicol, and 4-vinyl-guaiacol (Toci & Farah, 2014).

Some of these compounds are also linked to coffee storage, including 2,3-butanedione, 2,3-pentanedione, hexanal, 2-methylbutanal, 5-methylfurfural, furfural, several thiols and carboxylic acids, but also 2,3-diethylpyrazine (Toledo, Pezza, Pezza, & Toci, 2016). In relation to the botanical origin, Arabica is often characterised by 2,3-pentanedione and furaneol, while Robusta coffees have higher content of several pyrazines, as well as 2-methylbutanal, 4-vinylguaiacol, guaiacol and pyridine, as well as some pyrroles. The post-harvest processing is also known to influence the volatile composition of the resulting roasted coffee (Gonzalez-Rios et al., 2007).

Some agronomical conditions can influence coffee aroma, for example the environmental conditions of the plant during the seed development (Bertrand et al., 2012). This might for example be due to the influence of sunlight radiation exposure on sugar biosynthesis in green coffee beans (Geromel et al., 2008), as well as the post-harvest processing. Compounds such as fructose and glucose have been reported to be affected, while sucrose content seems not to be significantly affected (Poisson et al., 2016). Acetic acid and 2-phenylethanol are highly correlated with the average temperature of the growing location, while 2,3-Butanediol and 1-butan-3-diol are

reported to be associated with solar radiation. In addition, pyrrole was correlated with the temperature during wet processing (Bertrand et al., 2012).

Coffee price varies widely, with prices up to 65 US dollars per kg for niche coffees, and as low as 2 dollars per kg for low quality products. Thus, the industry could take advantage of consumers' willingness to pay a premium for specific growing regions, thus investigations into possible volatile markers of specific geographical regions have been conducted. Some compounds such as 2,3-butanediol, 2,3-pentanediol, 4-vinylguaiacol, 4-ethylguaiacol and others have been previously related to the coffee origin, while 4-ethylguaiacol, propanal, 2(5)-ethyl-4-hydroxy-5(2)-methyl-3(2H)-furanone and others have been described as affected by roasting (Mayer et al., 1999).

The understanding of the extent of natural variability of coffee aroma compounds is an interesting aspect of coffee flavour chemistry. Tran et al. (2017) reported on a wide study on coffee aroma variability in terms of morphology and chemical composition. Using Solid-Phrase Micro-extraction (SPME) coupled with GC-MS, they analysed the variation of 18 volatile compounds from small batches of coffee roasted under constant conditions. The coefficient of variation (CV) varied from 14% (4-vinylguaiacol) to 62% (geraniol), demonstrating high variability even at batch level. Despite previous studies into the variation of coffee volatile compounds during roasting for different roasting profiles and applying methods for on-line measurement of volatile compounds (Gloess et al., 2014), very little is still known about single coffee bean variability. Experiments have been proposed in the literature to analyse single bean volatile compounds using proton transfer reaction MS (PTR-MS) methods, often by adopting an untargeted approaches, by which a tentative assignment of molecules can be obtained so no clear identification of volatile compounds is given. In addition, it is important to mention that these methods analyse the headspace of the whole coffee bean, and not the resulting ground material, which might have a different odour impact. Hertz-Schünemann et al. (2013) studied single coffee bean volatile compounds using resonant laser ionisation time-of-flight mass spectrometry (TOF-MS) for single coffee bean analysis, and tentative assignment of compounds was based on the molecular mass (m/z values). However, the coffee beans were not roasted in order to mimic/reproduce industrial roasting conditions.

2.8.5. NIRS and HSI applied for coffee quality evaluation

The need for rapid, low-cost and reliable methods for the evaluation of coffee quality has been highlighted previously. Thus, spectral-based methods have been developed for applications in the coffee industry and research laboratories. Specifically, NIRS has been widely applied for coffee analysis over the last decade, both for classification purposes and for prediction of coffee composition. Table 2.12 summarises the research carried out on coffee using infrared-based techniques.

Major constituents of coffee such as moisture content have been successfully measured by NIRS in batches of raw coffee, for example moisture was predicted with a regression coefficient (R^2) of 0.818 and prediction error of 0.298% (Morgano, Gomes Faria, Flores Ferrâo, Bragagnolo, & Miguel de Castro Ferreira, 2008). Measurement of caffeine, theobromine and theophylline in roasted and ground coffee, and in liquid extracts has been also obtained using NIRS. The R^2 values for caffeine and theobromine prediction were 0.86 and 0.85, respectively, while the prediction error was 0.40 and 0.10% (Huck, Guggenbichler, & Bonn, 2005). The RPD value for caffeine was 1.47 while it was 1.2 for theobromine, thus showing relatively poor performance for quantitative purposes but still applicable for rapid screening.

Other authors reported lower prediction ability for caffeine prediction in ground coffee at different roasting degrees. Despite the use of a broad NIR range (1250-2500 nm), the calibration models had R^2 values from 0.653 to 0.793, depending on the spectral pre-treatments. RMSECV ranged from 0.56 to 0.67 mg g^{-1}, on a reference caffeine content ranging from 12 to 15.5 mg g^{-1} (Zhang et al., 2013). Dos Santos Scholz et al. (2014) evaluated several coffee constituents by NIRS, reporting a caffeine range from 0.66 to 1.57%. Lipid content ranged from 10.15 to 16.69%, and sucrose from 4.72 to 10.58% (dry matter basis, dmb). The regression coefficients for the caffeine, lipid and sucrose calibrations were 0.83, 0.0.86 and 0.90, respectively. Protein prediction exhibited the best performance (R^2=0.97). However, batches of ground green coffee were analysed, thus no indication was reported for whole seeds or single beans (dos Santos Scholz et al., 2014).

Ash and lipid content have also been predicted by NIR spectroscopy in roasted and ground coffee. The best PLS regression model for ash content had R^2=0.968 and RMSEP=3.1%, while a lipid

prediction model had R^2=0.987 and RMSEP=2.2% (Pizarro, Esteban-Díez, Nistal, & González-Sáiz, 2004).

Also, NIR spectroscopy has been used to predict the sensory properties of coffee brew starting from the roasting coffee data (Ribeiro, Ferreira, & Salva, 2011). Similar work has been reported by Tolessa et al. (2016), who tested the use of NIRS for prediction of "coffee cup" (brew) quality and showed variable prediction ability depending on the parameter evaluated. Poor prediction was obtained for total cup quality or aroma, while acceptable prediction ability was obtained for acidity and body.

A recent paper described a real-time in situ monitoring of parameters such as antioxidant activity and total phenolic compounds in coffee during roasting, based on diffuse NIR spectroscopy (1100-2500 nm). Fifty-six samples belonging to 4 batches were taken and analysed at intervals of 3 minutes, and PLS regression was used to build quantitative models. The PLSR prediction models had good performance for antioxidant capacity and total polyphenols, showing promising results for quantification of polyphenols and antioxidant capacity (Catelani et al., 2017).

Despite the amount of work carried out on this commodity, very limited research has been reported to describe coffee distribution at a single seed level. Fox et al. (2013) applied an FT-NIRS calibration for caffeine in ground and whole green coffee beans, on both bulk and single coffee beans. The authors reported a caffeine concentration in single bean range from 7 to 17 mg g^{-1}, but they also included some decaffeinated samples. The prediction performance of the PLS regression model was very promising, with R^2=0.93, SECV=1.6 mg g^{-1} and RPD=2.75.

El-Abassy et al. (2011) applied Raman spectroscopy on single green coffee beans to discriminate between Arabica and Robusta coffee beans, selecting one bean per batch on 30 samples and manually cutting them into slices for analysis in the spectral range 4800-20,000 nm. PCA resulted in good clustering, which was mostly explained by the different amount of chlorogenic acids, as well as lower lipid content. Despite the good grouping of the samples by PCA, Raman spectroscopy is not a rapid technique and the spectra acquisition requires prior sample manipulation, with consequent destruction of the sample itself. Other studies on NIRS and other spectroscopy-based methods for coffee evaluation have focused on authentication or

classification of coffee variety, as well as for the discrimination of defective coffee beans and evaluation of roasting degree (Barbin et al., 2014).

The use of NIR spectroscopy for on-line and in-line monitoring of coffee quality has been described as a challenge for the future (Barbin et al., 2014). In this context, it is obvious that HSI can offer further benefits and advances over conventional NIRS instruments, so that bean-by-bean differences can be detected. For instance, Calvini et al. (2017) used HSI for classification purposes of Arabica and Robusta green coffee beans. The spectra were not acquired on single beans but on bulk, and the data were treated at a single pixel level. PLS-DA was used to discriminate pixels belonging to the coffee species, and a multispectral imaging model was additionally proposed for a more rapid differentiation of each pixel, by describing a sparse PLS-DA model for a more rapid computation. A classification model to verify the consistency of roasted coffee constituents by HSI was reported by Nansen et al. (2016). Fifteen samples were ground and analysed by HSI in the spectral range 400-1000 nm. Extractable protein and reducing sugar content were predicted by PLS regression, resulting in acceptable performance for screening of protein content but poor prediction for sugars. The model based on LDA demonstrated good classification accuracy for the roasting degree.

Zhang et al. (2017) predicted caffeine content in four cultivars of Chinese roasted coffee by HSI by selecting 20 beans per batch, using an InGaAs sensor with a spectral range of 874–1734 nm. However, no information was reported at a single bean level. Ground coffee was used for reference analysis based on UV spectrophotometric absorbance. It should be noted that the authors reported a caffeine content that is ten times lower than the expected concentration for coffee. Cho et al. (2017) recently investigated the prediction of roasting degree by HSI (1100-1700 nm), referred to as roasting defects. One batch of Indian Arabica green coffee was roasted at five roasting degrees and then scanned by HSI. PLS-DA was then used to classify for the roasting degree, with a validation accuracy of 86.7%. From the beta-coefficient plot, it was obvious that the wavelength at 1420 nm (related to water absorbance) explained the majority of observed variance. Also in this case, no information is reported on a single coffee bean level nor green coffee beans, and no quantitative model was proposed for coffee constituents.

Table 2.12. Spectral-based researches applied to coffee, modified from Barbin et al. (2014).

Application	Aim	Coffee status	Tech.	Spectral range	Chemometrics	Reference
Adulteration	Glucose, starch, chicory detection (presence)	Soluble coffee	FT-IR	2500–12500 nm	LDA, PCA, PLS, ANN	Briandet et al. (1996)
	Presence of barley	Ground & Roasted	FT-IR	1000–2500 nm	PLS and PLS–GA	Ebrahimi-Najafabadi (2012)
	Robusta content in roasted coffee	Ground & Roasted	NIRS	1100–2500 nm	PLS	Pizarro et al. (2007)
	Authentication of Kona coffee	Ground & Roasted blends	FT-NIR	2500–25,000 nm	PLS and PCR	Wang et al. (2009)
Classification /discrimination	Classify batches/producers	Ground & Roasted	NIRS	800–2500 nm	PLS-DA and SIMCA	Santos et al. (2012)
	Identifying Arabica and Robusta	Ground & Roasted blends	NIRS	1100–2500 nm	Potential functions	Esteban-Díez et al. (2004)
	Arabica/Robusta classification	Ground & Roasted blends	NIRS	1100–2500 nm	Potential functions	Esteban-Díez et al. (2007)
	Arabica/Robusta classification	Ground & Roasted	NIRS	400–2498 nm	PCA and FDA	Downey et al. (1996)
	Arabica/Robusta classification	Ground & Roasted	NIRS	400–2498 nm	FDA and PLS	Downey et al. (1996)
	Arabica/Robusta classification	Ground & Roasted	FT-IR	2500–12,500 nm	PCA and DA	Kemsley et al. (1995)
	Geographic and genotypic origin	Ground Arabica (green)	NIR	1100–2498 nm	PLS-DA	Marquetti et al., (2016)
	Defective/non-defective beans	Arabica green coffee (ground)	FT-IR	2500–14,285 nm	PCA, clusters	Craig et al. (2012a)
	Defective/non-defective beans	Arabica green coffee (ground)	FT-IR	2500–25,000 nm	PCA and LDA	Craig et al. (2012b)
	Defective beans	Arabica & Robusta; green, whole	FT-IR	1000–2500 nm	PCA and PLS	Santos et al. (2012)
Composition	Caffeine content	Ground & Roasted	FT-IR	2500–12,500 nm	Linear regression	Garrigues et al. (2000)
	Caffeine, theobromine and theophylline	Liquid coffee extracts (roasted Arabica & Robusta)	FT-IR	1000–2495 nm	PLS	Huck et al. (2005)
	Moisture content	Arabica green coffee (ground)	NIRS	1000–2222 nm	PLS	Morgano et al. (2008)
	Ash and lipid content	Ground & Roasted (Ar. & Ro.)	NIRS	1100–2500 nm	PLS	Pizarro et al. (2004)
	Caffeine content and colour	Ground & Roasted (Ar. & Ro.)	NIRS	1100–2500 nm	PLS	Pizarro et al. (2007)
	Caffeine content	Ground & Roasted (Arabica)	NIRS	1000–2500 nm	PLS	Zhang et al. (2013)
	Sucrose and colour prediction	Roasted Ar. & Ro. (whole)	FT-NIR	1000-2500 nm	PCA and PLS	Santos et al. (2016)
	Prediction of ochratoxin	Green Arabica beans (whole)	FT-NIR	800–2500 nm	PLS	Taradolsirithitikul et al. (2017)
	Moisture content	Green A. & R. beans (whole)	FT-NIR	1000-2500 nm	PLS	Adnan, Hörsten, and Pawelzik (2017)

Table 2.12 (*continued*)

Application	Aim	Coffee status	Tech.	Spectral range	Chemometrics	Reference
	Prediction of antioxidant properties	Roasted Arabica and Robusta (whole)	FT-NIR	1000-2500 nm	PLS	Catelani et al. (2017)
Sensory prediction	Sensory attributes	Ground & Roasted	FT-IR	2500–25,000 nm	PCA and PLS-DA	Ribeiro et al. (2010)
	Sensory attributes	Coffee brew	NIRS	1100–2500 nm	PLS	Ribeiro et al. (2011)
	Sensory attributes	Coffee brew	NIRS	1100–2500 nm	PLS (& IPW–PLS)	Esteban-Díez et al. (2004c)
	Prediction of coffee cup quality	Green Arabica beans (whole)	FT-NIR	870-2500 nm	PLS	Tolessa et al. (2016)
Roasting degree	Prediction of roasting degree	Ground Arabica & Robusta coffee (green & roasted)	FT-NIR	830–2500 nm	PLS	Alessandrini et al. (2008)
	Effect on roasting conditions	Coffee brew	FT-IR	2500–14,285 nm	-	Lyman et al. (2003)
	Determination of roasting degree	Ground & Roasted (Arabica/Robusta blends)	FT-NIR	800-2857 nm	PLS	Bertone et al. (2016)

3. WHEAT PROTEIN PREDICTION IN SINGLE KERNELS

3.1. INTRODUCTION

Rapid measurement of protein content in wheat is traditionally based on NIRS by scanning batches of ground wheat or flours (Osborne, 1984). The feasibility of NIR prediction in batches of whole kernels without the need of grinding has been also demonstrated (Williams & Norris, 1987). Whole-grain applications became attractive to breeding programmes and industry due to the non-destructive scanning of samples and the speed of analysis, with the possibility of on-line or in-line data acquisition (Osborne, 1987; Williams & Sobering, 1993). Total protein prediction models based on NIR and visible spectroscopy of batches of whole wheat have high correlation coefficients (Cozzolino, Delucchi, Kholi, & Vázquez, 2006). However, the traditional NIR spectroscopy approach is based on bulk grains, and thus no indication of the protein variability among kernels is given (Bramble, Dowell, & Herrman, 2006). Some authors have tested single kernel by using NIR analysis, and applied it successfully to measure wheat protein content in transmittance mode (Delwiche, 1995). More recently, reflectance NIR spectroscopy has been also applied, due to its better applicability at the industrial level, and even tested for single kernels (Bramble et al., 2006).

The potential of single kernel NIR analysis strongly depends on the quality parameter studied. For example, it has limited potential to identify wheat varieties in breeding programmes, while it is more successful for determining physical grain quality, moisture, protein, kernel hardness and loss of viability (Fox & Manley, 2014). Protein variability among wheat kernels was reported for some USA wheat classes using NIR reflectance spectroscopy on a single kernel basis (Delwiche, 1998), and it was demonstrated that protein prediction of the batch can be improved by averaging a few hundred kernels from single kernel measurements (Delwiche & Hruschka, 2000). A single kernel characterisation of some European wheats was also performed by NIR transmittance spectroscopy (Nielsen et al., 2003). The possibility of high speed classification of single kernels for quality attributes is relevant in cereal breeding programmes, and to improve product quality.

Whilst single kernel protein calibrations have been demonstrated, presentation of kernels individually results in practical difficulties for rapid analysis of bulk samples. Hyperspectral imaging (HSI) provides a potential approach to enable single kernel data to be acquired for larger numbers of kernels, with the advantage of NIR spectrometry being contactless and rapid.

Despite the large information available on NIRS applied for the prediction of wheat composition, limited information is reported in the literature by using HSI, as described in detailed in Chapter 2. Few research papers have focused on single kernels and specifically to predict protein content of wheat, or similar grains (Cogdill et al., 2001 and 2006; Fox and Manley, 2014; Delwiche et al., 2013).

Therefore, the first aim of the present study was to develop a HSI calibration model for predicting total protein content in whole wheat kernels on a single grain basis, and to apply this calibration model to visualise the protein distribution within single kernels.

3.2. MATERIAL AND METHODS

3.2.1. Wheat samples

Samples were obtained from a wide range of suppliers, mainly millers and breeders from the UK. Examples of Canadian, French, Italian, German and Eastern European wheat samples were also included. Samples came from the 2013 and 2014 harvests. They were selected to obtain a wide variation in terms of cultivars, environmental and agronomic conditions besides some genotypes from breeding trials and not yet registered or under registration. A total of approximately 190 wheat samples were used for the present experiment. From each sample, 10-12 kernels were randomly selected to be used for the analyses. Each kernel was presented for HSI measurement in both crease-up and crease-down orientations, resulting in a total of ~4200 kernel spectra. Each kernel was then analysed by the Dumas method to determine its protein content. The spectra and reference protein values were used for development and validation of the calibration models.

3.2.2. Hyperspectral imaging

Data was acquired using a laboratory-scale hyperspectral imaging system described by Millar, Whitworth, Chau & Gilchrist (2008) and Caporaso et al. (2016). Pictures of the instrument, with indication of its components, are shown in Figure 3.1.

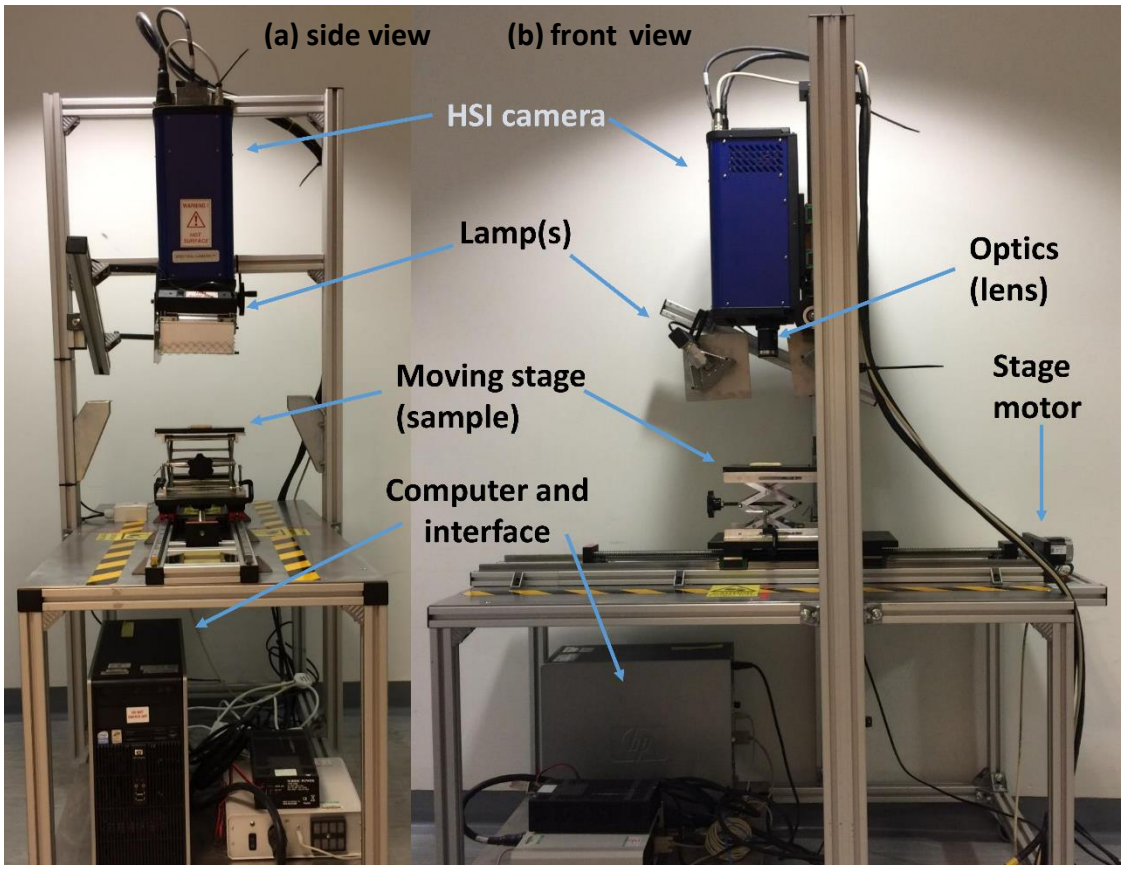


Figure 3.1. Hyperspectral imaging system used in the present thesis, with indication of some of its components.

The instrument was supplied by Gilden Photonics Ltd. (Glasgow, U.K.) and includes a SWIR spectral camera (Specim Ltd., Oulu, Finland) containing a cooled 14 bit 320×256 pixel HgCdTe detector and N25E spectrograph providing 256 spectral bands over a wavelength range of ~980-2500 nm with a spectral resolution of about 6 nm. Samples were presented on a moveable sample stage and imaged using a push-broom acquisition mode. The camera was mounted above the stage at a distance of 220 mm and a 31 mm focal length lens was used, resulting in a swathe of 35 mm and a pixel size of 0.109 mm for 320 spatial pixels. Images were acquired at a rate of 100 fps, using a stage translation speed of 10.9 mm s^{-1}, providing the same spatial resolution parallel and perpendicular to the scan direction. A single 500 W incandescent illumination source was

used for the first ~1000 kernels, and 2 lamps were used for the remaining samples. The additional lamp was added in order to use more uniform lighting conditions and avoiding shading in the images, however no difference was found in the overall prediction ability depending on the number of lamps. SpectralCube 3.0041 software (Specim) was used to control the camera and translation stage. The camera shutter was automatically closed for 1 s at the end of each scan and ~100 frames were recorded to establish the baseline signal of the detector (black reference). Separate scans of approximately 100 frames were also recorded for a white PTFE reference material with approximately 100% reflectance across the entire measured spectral range (white reference). Wheat samples were presented with grains arranged in two rows on a black, NIR-absorbent plastic tray, and the hypercubes were obtained in diffuse reflectance mode. Images were first acquired for the dorsal side of the kernels, and the kernels were then manually rotated and a second image acquired for the ventral side. To minimise heating of the sample, the lamps were only turned on for the duration of the scan. The general flowchart used for the image analysis and chemometrics for the present experiment and for the other experiments presented in further chapters is reported in Figure 3.2.

3.2.3. Analysis of hyperspectral data

Hyperspectral images were analysed using ENVI-IDL 5.2 software (Harris Geospatial Solutions, Virginia, USA). The following operations were carried out to obtain NIR spectra for each kernel from the hypercubes (Figure 3.3):

1. Calculation of reflectance data from the raw image by subtraction of the black reference and normalisation by the white reference. Reflectance values, $R(x,y,\lambda)$ were calculated for each pixel (spatial coordinates x,y, wavelength λ) by subtracting the black reference value for the corresponding detector pixel (x,λ) and normalising by the corresponding white reference value and by the ratio of exposure times (when different exposure times are used for the sample and white reference), assuming a linear response. Absorbance values were then calculated as $A=\log_{10}(1/R)$, where R is the reflectance for each pixel. It should be noted that in push-broom mode, the x dimension is defined by the HSI system, with 320 pixels in the

present case, while the *y* dimension can be varied depending on the length of the sample, or the operator choice during the acquisition.

2. Removal of spikes from absorbance data. These are caused by factors such as bad pixels in the detector. They were identified as single pixel outliers by comparing with the median absorbance of neighbouring pixels;
3. Segmentation of kernel images from the background tray using a binary threshold criterion of absorbance at 1186 nm > 0.9;
4. Identification of kernels as the Region of Interest (ROI), one for each kernel, and indexing according to their position on the tray;
5. Calculation of the mean absorbance spectrum for each kernel, and export for statistical analysis. After these operations, chemometrics is applied to build multivariate statistical models.

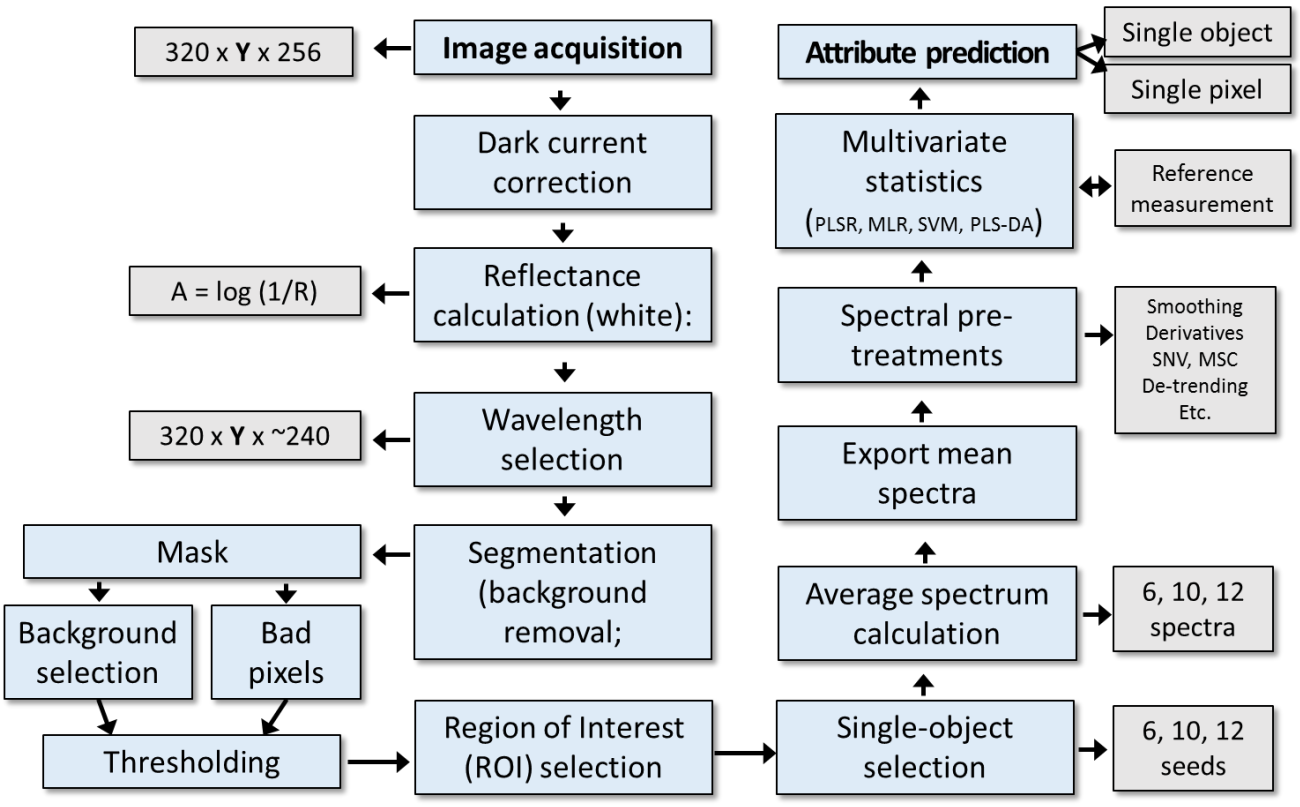


Figure 3.2. Flowchart of image pre-processing steps applied to hypercubes.

An example of hypercube visualised at a particular spectral band is shown in Figure 3.3. Three steps of the image processing are shown, i.e. raw image with indication of the spectrum belonging to one pixel, absorbance image calculated as reported above, and the same image treated using 2nd derivative calculation of the spectra, aiming to remove some light scattering.

The next step of HSI analysis was removal of spikes, which can be caused by bad pixels in the detector, and can include both high and low signal values (Burger, 2009; Vidal & Amigo, 2012). Appropriate threshold selection is crucial to effectively identify spikes, sometimes using basic statistics as spikes have usually larger deviation from the normal mean spectrum. The spike removal can be then applied by substituting the specific point by the median of the neighbouring spectra (Vidal & Amigo, 2012). In this study, an enhancement of this approach was used, in which each image pixel was compared with the median of neighbouring pixels, and a weighted average was calculated, with greater weighting towards the median value if the difference is large.

Following spike removal, images were segmented to identify the grains. Figure 3.4 shows an example. Figure 3.4 shows a reflectance image for the 1186 nm band after spike removal, as well as the log(1/R) image for the same band. To segment grains, a binary threshold was first applied to this band to select pixels with $\log(1/R_{1186}) < 1$ equivalent to reflectance, $R_{1186} > 0.1$. A binary opening operation was then applied with a circular kernel with a radius of 10 pixels (1.09 mm) to remove noise and small projections, including sprouts. The resulting image, shown in Figure 3.4d was used to segment kernels for spectral analysis. A flat uniform background, both spatially and spectrally, is generally recommended to aid segmentation of samples from the background (Dorrepaal, Malegori, & Gowen, 2016). Figure 3.5 shows example single pixel absorbance spectra for a grain and for the tray. The chosen tray material has high log(1/R) values over the entire NIR spectral range, providing good contrast, and a binary threshold is therefore sufficient to achieve good segmentation (Millar et al., 2008). The wavelength 1186 nm was chosen for segmentation, as it resulted in low log(1/R) values for the grain regions, with good contrast and low noise. The effect of the spike removal procedure is also shown. The method is effective in removing spikes due to bad pixels, while preserving spectral bands. According to the normalisation procedure, the

spectrum for the white reference material is defined to have a log(1/R) of 0 at all wavelengths, to within noise.

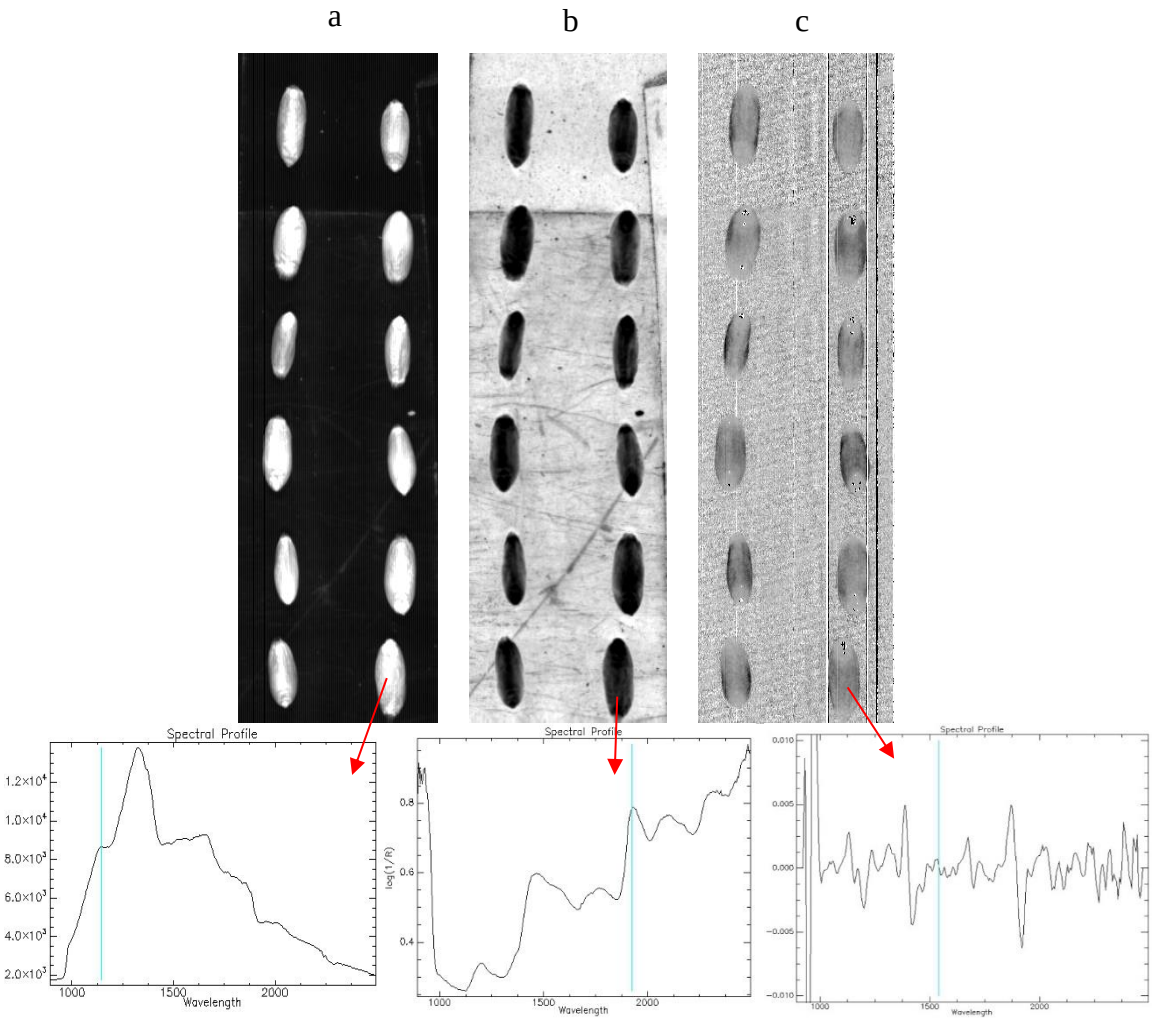


Figure 3.3. Example of image processing procedure on wheat kernels to illustrate the hyperspectral images at a particular spectral band (top) and the spectral profile when selecting one pixel of a wheat kernel (bottom). **a**) raw signal of wheat kernels before dark and white correction; **b**) Absorbance image (log(1/R)); **c**) Second derivative calculation.

Mean spectra were calculated for each segmented kernel and exported for separate development of calibration models in comparison with reference measurements. For the camera system used, the initial 16 spectral bands did not contain useful data and only bands from ~1100 to 2500nm were used for spectral analysis, due to ineffective measurement of the detector in the lower spectral range.

Visualisation of chemical images.

Once calibration equations had been created, they could be applied for rapid prediction of the target property (protein content in this case) of test samples, using another ENVI-IDL program previously developed for this purpose (not commercially available).

Hyperspectral images of wheat were acquired in the same manner, but with no restriction on the orientation, position or number of kernels and using a higher number of kernels for each batch (100-200 kernels per samples). Absorbance values were calculated for each pixel as above and kernel images were segmented from the pixels belonging to the tray. The program applied the chosen spectral pre-treatments and applied the calibration coefficients to calculate a protein value for each pixel in the kernels. This enabled the spatial variation of predicted protein content to be visualised within a single grain or average protein values to be calculated for each kernel or sample.

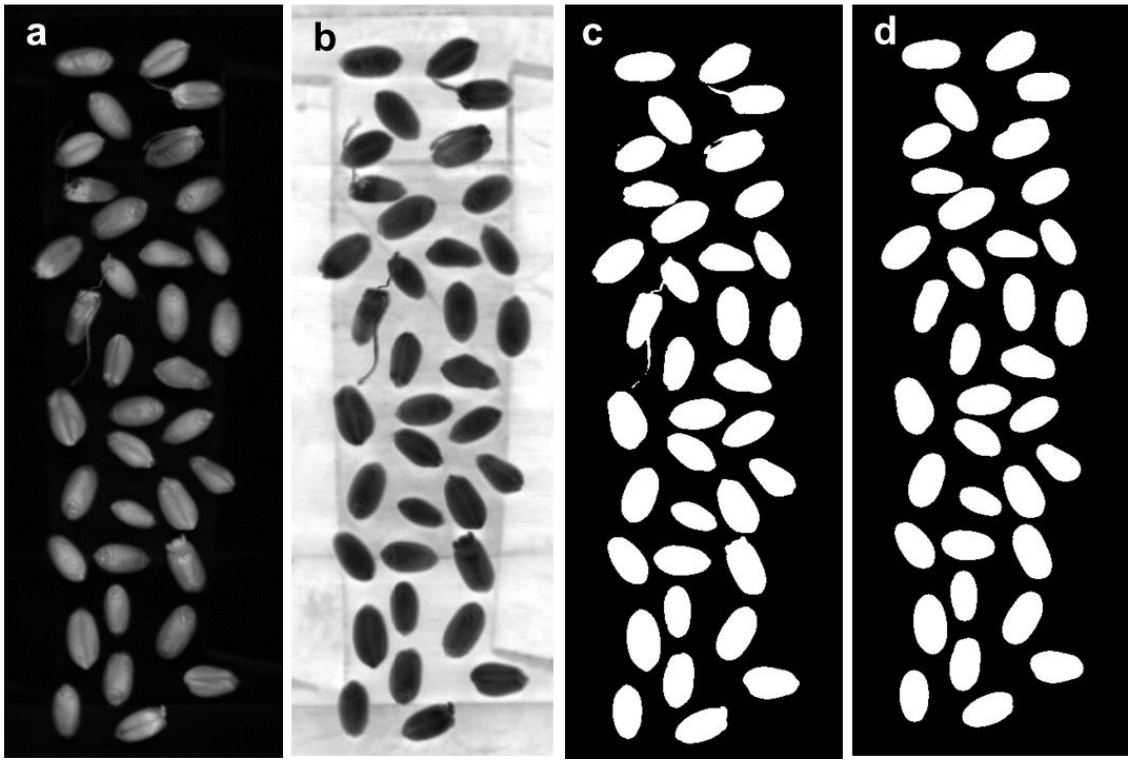


Figure 3.4. Images of wheat kernels obtained by HSI, showing the hypercube at a specific wavelength. The picture is for illustrative purposes and includes sprouted examples. a) reflectance image at 1186 nm; b) log(1/R); c) binary thresholding; d) morphological processing for kernel segmentation.

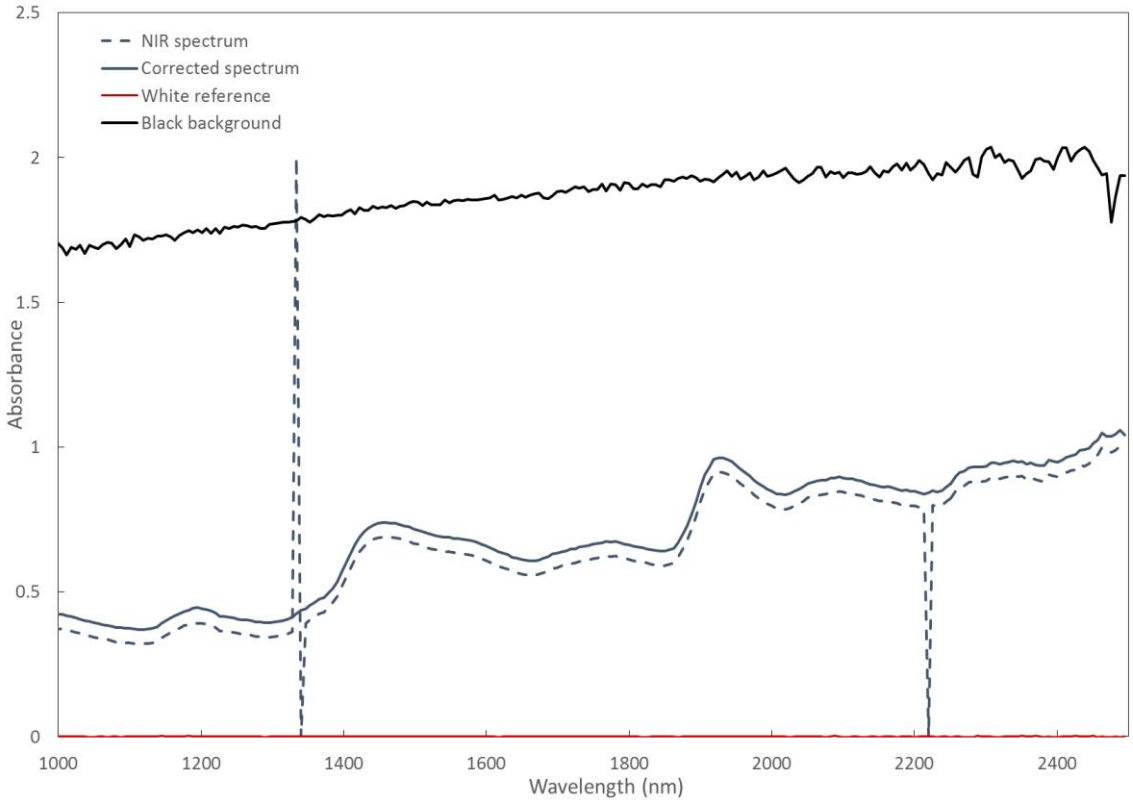


Figure 3.5. Example log(1/R) spectra for a pixels corresponding to a wheat kernel before and after spike removal, and the black tray used as a background, showing good contrast at all wavelengths. An additive constant was added to the corrected spectrum for illustration purposes

3.2.4. Reference analysis for protein analysis

Dumas combustion was used to determine the protein content of each wheat kernel. As a part of this determination, the mass of each kernel was also measured. Dumas protein values were measured on wet basis (N x 5.7) according to TES-CM-119 based on CCAT method no. 19 and conforming to ISO/TS 16634-2 (2009). For the measurement, each grain is digested through oxidative combustion at temperatures between 850 and 1100 ºC to produce oxides of nitrogen that are catalytically reduced to nitrogen gas. Interfering combustion products such as carbon dioxide and water and other components e.g. sulphur compounds and hydrogen halides are removed by selective absorption. The nitrogen remaining in the carrier gas (helium, 99.995% purity) is measured using a thermal conductivity detector. Total nitrogen is calculated from the detector response that has been calibrated by the use of a standard nitrogen compound. Crude protein content is then calculated by multiplying the nitrogen content by a standard conversion facto (5.70 for wheat). A Leco FP-628 (LECO, Stockport, UK) instrument was used to perform the analysis. To minimise moisture changes between HSI and Dumas measurements, the samples

were analysed on the same day and exposure to high temperature was avoided. Two samples of flour with low (10.2%) and high (12.4%) protein values were systematically used to check for possible drift during the analysis. The repeatability of the method was below 0.1 %, while the reproducibility (method standard deviation) was 0.6% for the low protein and 0.7% for the high protein check sample.

3.2.5. Data analysis and PLS calibration

The NIR reflectance spectra extracted from each single kernel and the corresponding Dumas protein measurements were processed using The Unscrambler X 10.3 (Camo, Norway) to develop calibrations for protein content based on PLS regression analysis. Approximately 2100 individual wheat kernels were scanned both dorsally and ventrally, resulting in a dataset of ~4200 mean spectra. From these, spectra for approximately 80% randomly selected grains were used as the calibration set, while the remaining 20% constituted the independent validation set. Spectral outliers were detected by considering the residual versus leverage plots and residual variance once the PLS model was developed, while some outliers from reference measurements were removed in case of error during the Dumas measurement. The optimal number of latent variables for the model was determined according to the RMSECV (using a 20-segment random cross validation algorithm), and leaving the software to choose the best latent variable, or principal component. The model was then validated using the selected number of LVs by testing the calibration on an external validation set, randomly selected from the full dataset (1000 samples). The following spectral pre-treatments and combinations of these were tested to assess their effect on the calibration performance. Scatter correction pre-treatments including standard normal variate (SNV), de-trending and multiplicative scatter correction (MSC) were used to minimize the non-linear effect of light scatter due to particle size differences among samples (Barnes, Dhanoa, & Lister, 1989). Different orders of derivative were also tested, mainly applying first and second derivatives using 5-point Savitzky-Golay smoothing. The coefficient of determination (R^2), slope, bias, ratio of performance deviation (RPD) and root mean square error of calibration (RMSEC) and prediction (RMSEP) were used to describe the fitness of models generated.

3.2.6. Manual sorting of wheat kernels

As a further validation of the concept that the application of single wheat kernel prediction models are able to give practical benefits to the industry, for rapid grain measurement, a manual sorting experiment was performed based on the predicted protein content. A relatively large number of kernels (above 150 kernels per batch) was scanned by HSI and the protein prediction calibration was applied, so that kernels with very high and very low predicted protein within the batch were visualised. Kernels were manually sorted into three classes, named "high", "medium" and "low" protein content, by selecting approximately the top 10% and bottom 10% of the total sample. Four batches were used of the varieties Scout, DNS, Viscount and Solstice. Each sub-sample was ground using a Buhler MIAG system to avoid loss of material and analysed for several parameters, to assess whether other changes other than protein content were significantly different among these. The following analyses were carried out: Dumas combustion method for protein content determination (duplicate analysis of 0.3 g samples as per the official method); SE-HPLC; SKCS.

Size-exclusion chromatography

Size Exclusion chromatography (SE-HPLC) was applied to characterise the different protein fractions of the sorted wheat. The method is based on total extraction of wheat flour proteins in phosphate buffer using elevated temperature and sonication prior to separation by Size Exclusion High Performance Chromatography (SE-HPLC) using a silica gel column (TSK gel SW). About 160±0.5mg ground wheat were weighed and 20 mL extraction solution was added and mixed with the sample, which is shaken in an oven at 60 °C for 80 min. The sample was then allowed to cool and then sonicated using a Microson ultrasonic cell disruptor for 3 min. Samples were then centrifuged for 10 min at 2000 rpm at room temperature, using a MIKRO 22 centrifuge. Finally, the samples were filtrated using a 0.2 μm filter. The extracted sample was analysed using a Jasco PU-980-02 HPLC system, quipped with a UV-975 UV/VIS detector and AS-950 sampler, using a TSKgel G4000 SW 30cm x 7.5mm (Sigma 805790) column. For HPLC analysis, the run length was 25min and flow rate 0.7 ml min^{-1}. Each sample was analysed in duplicate in 2 different extraction sets. Chromatographic peak integration was performed as reported by Millar et al. (2003). The chromatogram is treated to selected 4 areas (named F1-F5), belonging to different

protein fractions, e.g. glutenins and gliadins, etc. The uncertainty associated with the results was comprised between 0.5% for F3 to 1.4% for F2.

Single Kernel Characterisation System (SKCS)

A Perten Single Kernel Characterisation System 4100 was used to obtain distribution measurements from 6 small batches of ~50 grains. The SKCS system provides weight, diameter, hardness and moisture values from samples of whole grains. By means of a rotating pickup wheel (Singulator) with vacuum ports, individual kernels are dropped into a bucket in which the weight is measured. The kernel then falls into a narrowing crushing gap where crush force (hardness) and diameter are measured. Kernel moisture content is measured by conductivity during the crushing step. The final hardness value is calculated with inclusion of the weight and moisture measurements.

3.3. RESULTS AND DISCUSSION

3.3.1. Single kernel protein variability

To build HSI predictions for single wheat kernel composition, samples were analysed by reference measurement using Dumas combustion method. Thus, single kernel measurement of above 2100 individual seeds was obtained and data were analysed to understand the variability of protein content within and between batches. The descriptive statistics of the samples used in the present study is reported in Table 3.1. The statistics for the validation and calibration datasets are shown separately, reporting the protein content and single kernel weight. Figure 3.6 shows the distribution of single kernel protein content measured by the Dumas method for the samples used in this study.

Figure 3.6b describes the distribution of reference protein content in single kernels by also displaying the kernels belonging to the same batch, and the average protein content for each batch. In this way, the total protein content is shown, alongside the within-batch variability. The minimum protein value was slightly above 6.1%, while the maximum was 19.8%. From the protein distribution plot, 42% of kernels had a protein content in the range 8-10%, which is generally

considered as medium-low protein content for wheat batches, while in the present case it is shown at single kernel level. Moreover, in certain countries such as the UK, a wheat batch cannot be classified in the superior category when its batch average protein content is below a certain value, e.g. 13% in the case of Group 1 wheats according to the nabim scheme.

Samples used in this experiment also included some batches of Durum wheat and several batches of Canadian hard red wheat, which are especially grown for their high protein content, thus this is likely to be the reason for the non-Gaussian distribution observed for the whole dataset, with a few kernels showing a protein content above 16%, while the mean value of the batches did not reach 16% protein. This irregular distribution was expected, as several samples of hard wheat used as improvers of protein content were analysed, e.g. Canadian or other hard wheats with high protein content, which in general are used in addition to UK wheat with moderate protein content.

Table 3.1. Statistical analysis for the parameters used in this thesis, separately showing the **a**) calibration and **b**) validation datasets. SD = standard deviation. CV = coefficient of variation.

a) Calibration dataset	**Mean**	**Range**	**Min**	**Max**	**SD**	**CV (%)**
Protein content (%)	10.59	13.62	6.15	19.77	2.07	19.55
Kernel weight (mg)	49.6	72.2	15.5	87.7	12.1	24.47
b) Validation dataset						
Protein content (%)	10.45	12.66	6.6	19.26	2.06	19.67
Kernel weight (mg)	49.5	65.5	17.4	82.9	12.0	24.30

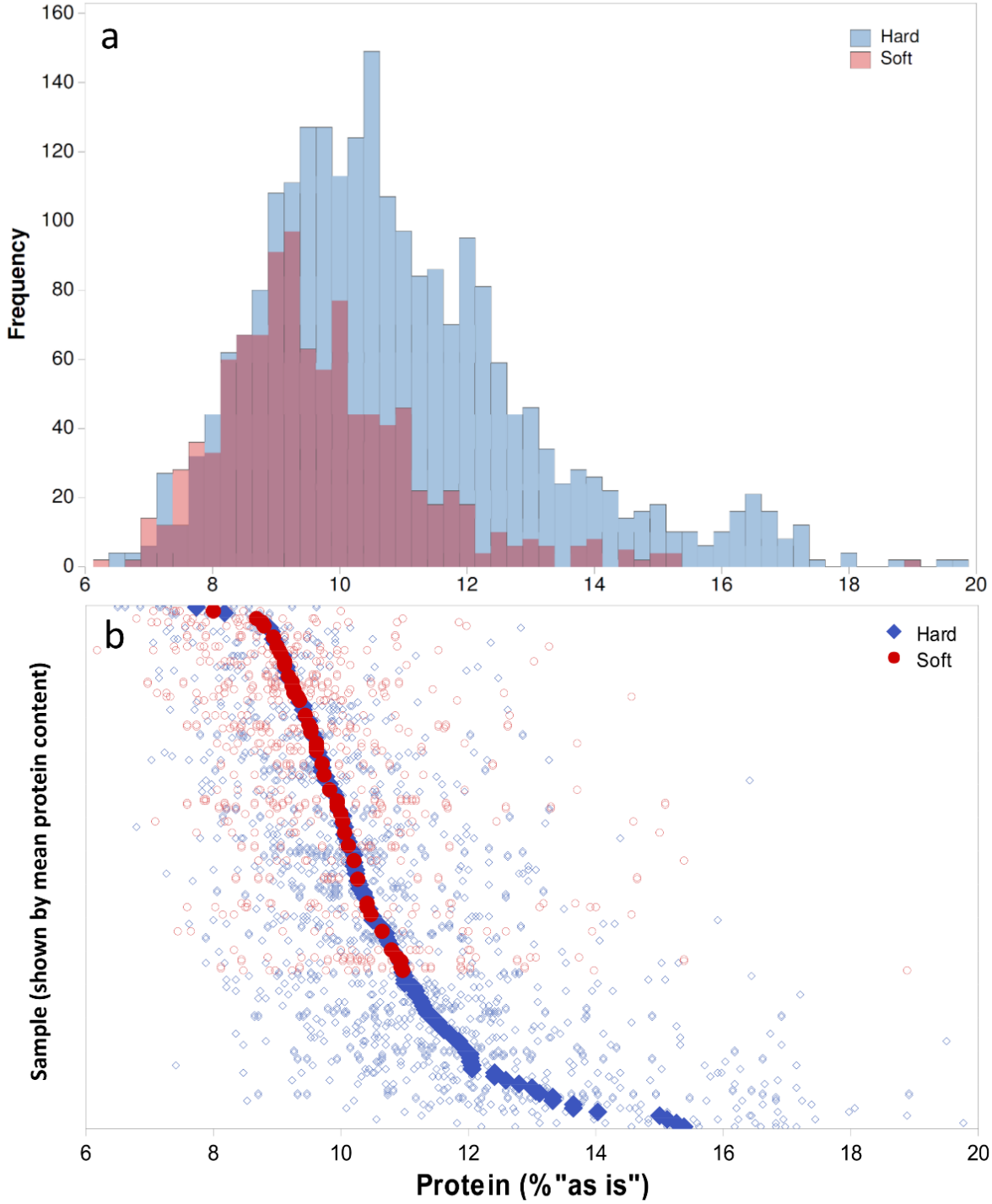


Figure 3.6. **a**) Distribution of total protein content in single wheat kernels, on the full dataset used in the present experiments, by separately showing the hard and soft wheats (according to their variety, as traded). **b**) Dispersion of protein content on a single kernel basis (empty symbols) and average of the batches (filled symbols).

The average protein content of the whole dataset was 10.59%, with a standard deviation of 2.07, and a range from 6.15 to 19.77%. When discriminating according to the hardness class, hard wheats had higher average protein content of 10.5%, compared to 9.5% in soft wheat. This difference was expected as hard wheat cultivars include those produced for bread-making for which higher protein content is desirable. On the contrary, soft wheat cultivars generally present lower protein content and include those favoured for biscuit production (Payne, 1987).

Although wheat kernels were collected from bigger datasets than those previously reported in the literature, including several hard and soft wheats, several harvesting years and geographical origin, a high correlation is not apparent between protein content and kernel size as shown in Figure 3.7. The Pearson correlation coefficient was -0.131 ($p<0.001$), thus showing a very weak negative relationship, which was however statistically significant. Therefore, the use of kernel mass as an indication of protein content would be ineffective.

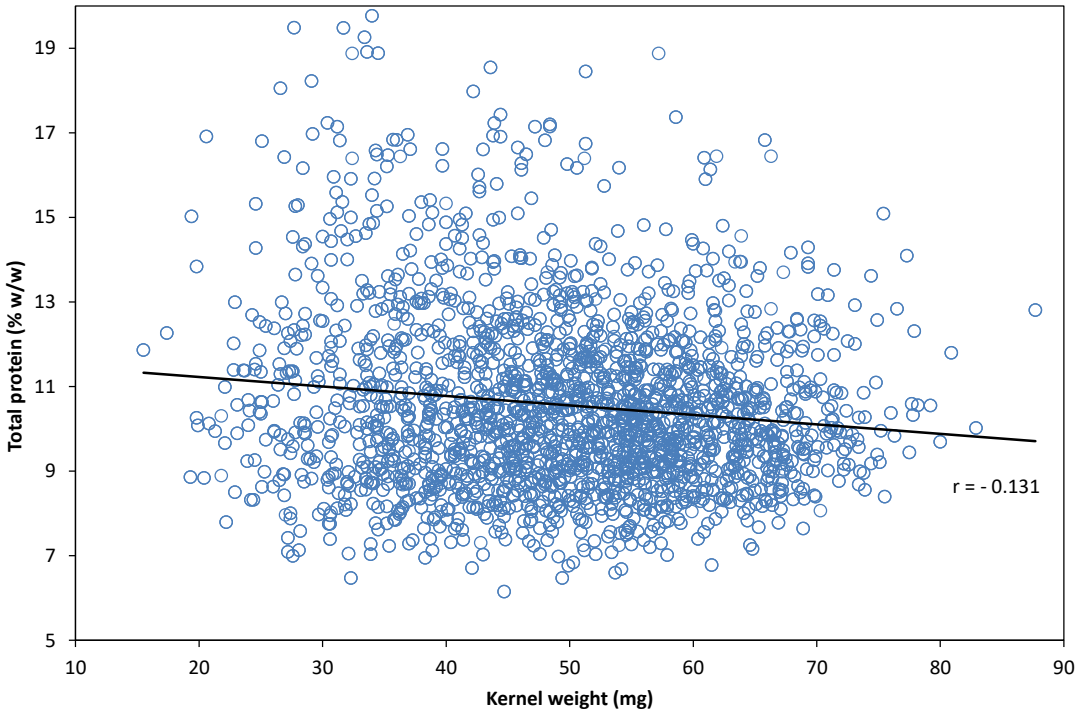


Figure 3.7. Relationship between single wheat kernel weight and total protein content, in the dataset used in the present study (n=2069). Samples include soft and hard wheats mostly from the UK, but examples of imported wheats and Durum wheats. The result of Pearson correlation analysis is shown.

3.3.2. Protein prediction by HSI and application of the calibration

Table 3.2 reports the performances of the developed PLS models for predicting protein content from the spectra (spectral region: 1060-2500 nm) of >2000 individual wheat kernels, considering several spectral pre-treatments. As each kernel was scanned on the dorsal and ventral side, two average spectra were acquired for each sample, thus giving more than 4000 spectra. From the average reflectance spectra obtained, it was possible to build PLS models for single kernel protein content with a root mean square error (RMSE) lower than 1%, both for the calibration and validation datasets, and a R^2 of 0.79 and 0.76, respectively. The best performance was achieved for standard normal variate (SNV) treatment followed by first derivative calculation, resulting in R^2 of 0.824 and 0.790 and a RMSE of 0.857 and 0.944%, for the calibration and validation datasets respectively. The result for this model is shown in Figure 3.8. However, the selection of the best prediction model should also take into account the number of LVs, by preferring the one using the lowest number to avoid overfitting.

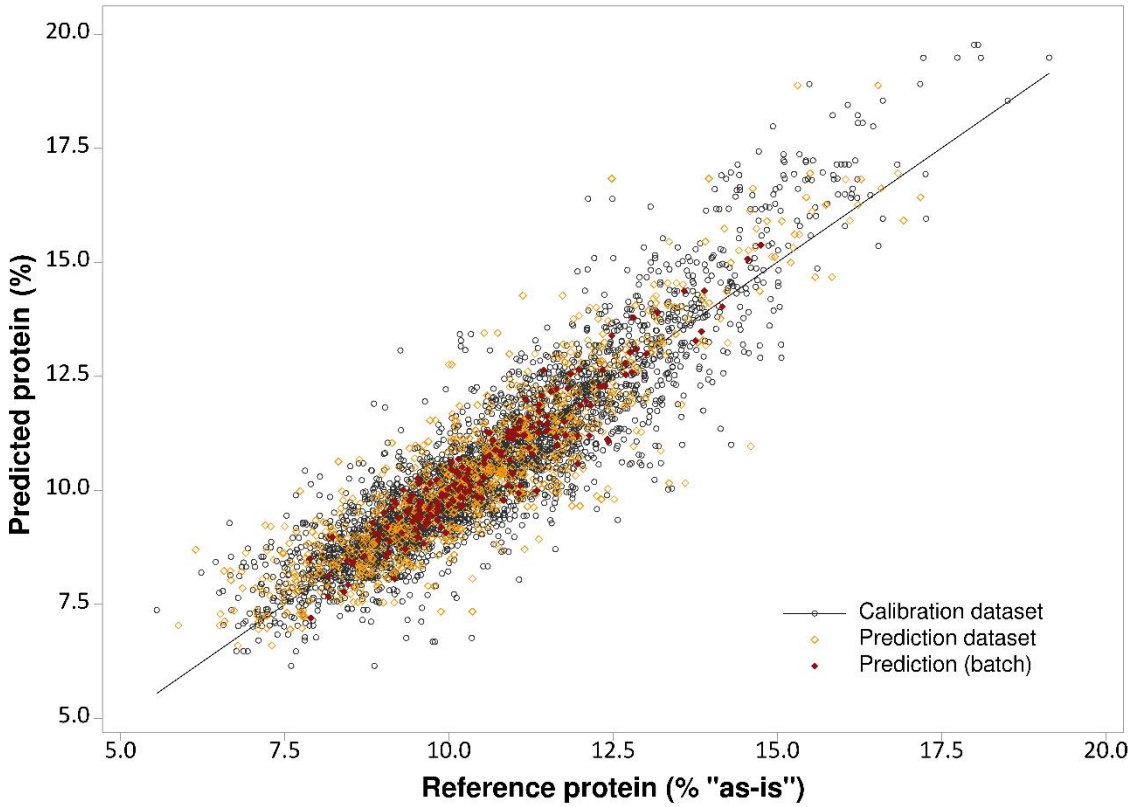


Figure 3.8. Predicted vs Reference value for total protein content in single wheat kernels, obtained using PLS regression built on NIR HSI spectral region ~1060-2500 nm (pre-treatments used: SNV and first derivative calculated using Savitzky-Golay smoothing). Black: calibration dataset; orange: validation dataset; red: prediction on batch.

This performance for single kernels compares slightly better with typical results for bulk samples when the model is calculated for the 10-12 grains in a batch (filled symbols in the figure), by averaging the spectra and the reference protein value. In this case, the model shown gives R^2=0.916 for the calibration dataset, with RMSEC=0.376% and RMSECV=0.507%.

The models reported in Table 3.2 were built using an external validation dataset and not a cross-validation, which leads to the risk of overfitting calibration models (Martens & Dardenne, 1998). Some authors have overcome this issue by using a leave-one-out cross-validation (Schulmerich et al., 2012), but an independent validation offers more confidence in the prediction ability.

Table 3.2. Performance summary of hyperspectral imaging PLS regression models based on the raw and pre-treated near-infrared reflectance spectral data for protein content prediction in single wheat kernels.

Pre-processing	**Calibration (n=3250)**				**Validation (n=868)**				**PC**	**RPD**
	Slope	**Bias**	**RMSEC**	**R_c^2**	**Slope**	**Bias**	**RMSEP**	**R_p^2**		
Raw data	0.786	-0.004	0.949	0.786	0.799	-0.030	1.005	0.762	18	2.06
Normalisation	0.769	0.000	0.984	0.769	0.779	-0.050	0.990	0.768	16	2.09
MSC	0.810	0.000	0.897	0.810	0.800	-0.067	0.968	0.779	15	2.14
SNV	0.800	0.000	0.920	0.800	0.791	-0.066	0.973	0.777	15	2.13
SNV + 1st der.	0.824	0.000	0.857	0.824	0.819	-0.030	0.944	0.790	12	2.19
SNV + de-trend	0.802	0.000	0.915	0.802	0.792	-0.072	0.983	0.772	13	2.11
2nd derivative	0.750	-0.007	1.025	0.750	0.777	0.012	1.075	0.728	10	1.93

Both first and second derivatives were calculated by also applying the Savitzky-Golay smoothing. RMSEC and RMSEP are expressed in % (wet basis).

From the obtained hypercubes, spectral pre-treatments are required to reduce scattering effects and the influence of the light source and sample presentation (Figure 3.9). In the present case the SNV+1st derivative treatment resulted in the best model performance compared to the other treatments tested. Previous work investigated the effectiveness of spectral pre-treatment for NIR and HSI. For example, Agelet et al. (2012) discussed that, whereas SNV has been shown to minimise scattering effects, the combination and interaction of several factors producing scattering cannot be successfully addressed by SNV, as their calibration quality did not improve with SNV pre-treatment for single seed NIR measurements on soybean. However, here SNV appeared to be one of the most effective spectral pre-treatments, which can be attributed to

differences in the shape and surface properties of the wheat kernels regarding the light scattering during the analysis. A generalisation on the spectral pre-treatment cannot be made as usually each study tested several pre-treatments and compared the performance of the models obtained, which strictly depends on the instrumentation used and sample presentation.

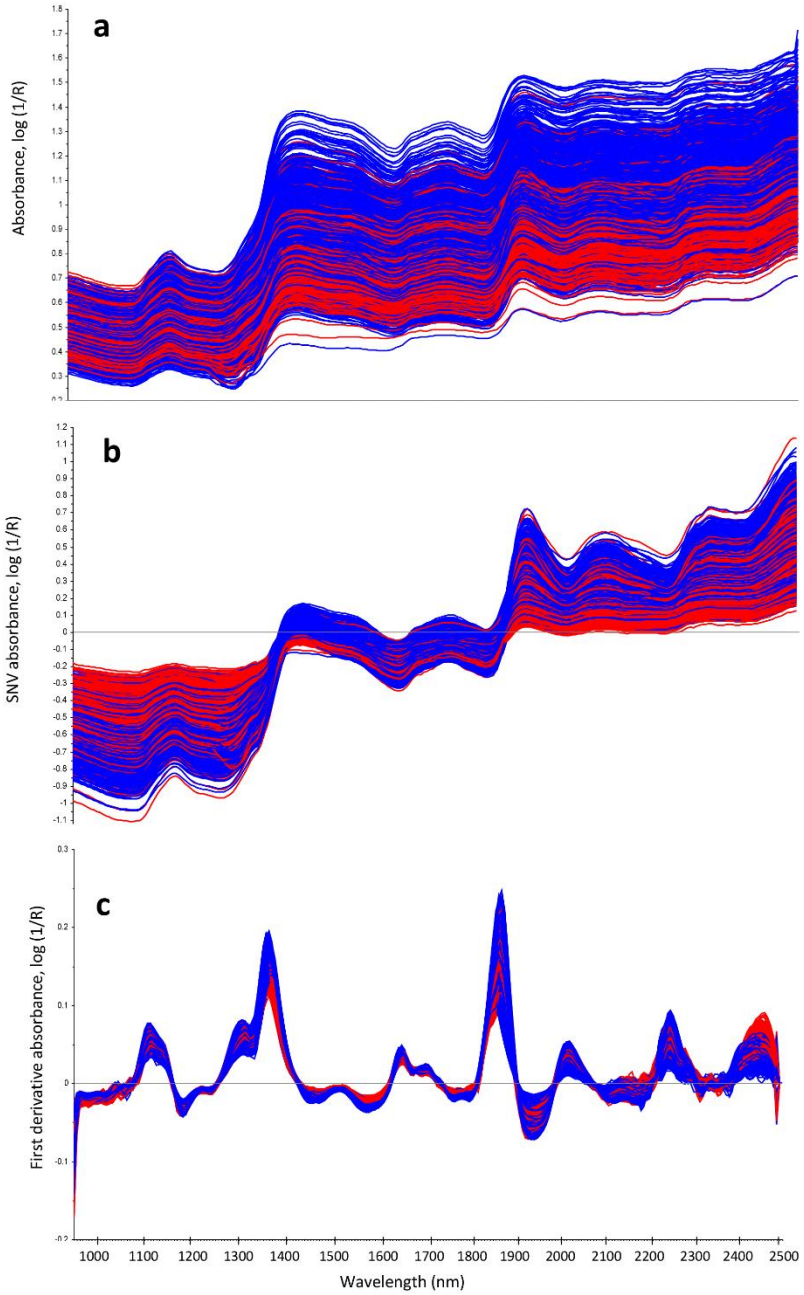


Figure 3.9. Mean NIR spectra for all wheat kernels: a) absorbance spectra; b) SNV-corrected spectra; c) spectra after SNV+first derivative calculation. Red: dorsal kernel side; blue: ventral side.

The calibration and prediction errors obtained in the present study are in line with previous literature on whole wheat kernels analysed by NIR instrumentation, and even with some papers dealing with protein in single wheat kernels. For example, Delwiche (1998) reported an SEC value of 0.494% for PLS calibration models based on reflectance NIR spectroscopy of different wheat classes, Cozzolino et al. (2006) reported SECV=0.54% for bulk whole wheat and Bramble et al. (2006) reported errors of 0.32 to 0.51% for four wheat varieties with weight correction and 0.93 to 1.52%.

Many authors, however, used traditional NIR instruments and not a hyperspectral imager, where there is also an interference of the sample presentation, e.g. moving tray, possible shadows and light position effects. Thus, whereas a different technique was applied, thus implying a worse sample presentation, the prediction ability of the HSI calibration shown in the present chapter is comparable to previous models. The results herein presented are also in accordance with Bramble et al. (2006) regarding the observed apparent departure from the ideal slope at high protein content, which should be considered for samples with very high protein content.

The protein prediction models were previously reported to show differences in both the SECV and R^2 values depending on the wheat cultivar tested. For instance, Bramble et al. (2006) reported a comparison of single-kernel prediction by reflectance NIR spectroscopy in four cultivars of hard red winter wheat, for which the R^2 ranged between 0.79 and 0.93 with weight correction, and SECV values of 0.93-1.52% (protein range: 7.2-13.8%). Therefore, despite the fact that the authors did not apply HSI but just NIR, and they used only one wheat class, the model herein obtained compared favourably. Using NIR in transmittance mode in the narrower spectral region 850-1050 nm, Delwiche (1995) reported a value of the coefficient of determination for protein prediction in wheat of 0.89, and a SEP of 0.45 (with a range of 0.4-0.9%), by analysing 94 samples of Northern American wheats.

The general lower prediction ability for single kernel HSI models compared to the conventional spectroscopy methods was previously highlighted by Delwiche et al. (2013), for three quality parameters of wheat, i.e. flour yield, softness equivalent and sucrose solvent retention capacity. For example, the authors reported that the coefficient of determination for softness equivalent

was approximately 0.5 with HSI, and 0.6 for traditional NIR instruments. This may be due to additional random error coming from the single kernel determination, and for single kernel reference measurement, and potentially due to differences in detector performance. However, a calibration equation should be evaluated not just on the basis of equation performance itself, but also taking into consideration the advantages that NIR spectroscopy and particularly HSI brings over other analytical methods and even compared to bulk NIR spectrometers.

Possible sources of error in protein prediction by NIR spectroscopy can be attributed to the uncorrectable spectral differences unrelated to the chemical composition and caused by kernel size and shape, analytical error for the reference measurement and the different wheat varieties used (Delwiche, 1998). Delwiche (1998) suggested that the region between 1100 and 1400 nm is most important spectral one for protein prediction, and that the accuracy of the model was lower when higher spectral regions were investigated. However, in the present case the performance of the model improved when using more spectral bands. In this experiment, the HSI system used had a push-broom configuration that can have advantages in terms of sample scanning, as individual measurements for a high number of wheat kernels can be acquired on-line. In addition to the rapid and non-destructive analysis, HSI gives the possibility to visualise the composition of a food product on a single grain basis up to a single pixel distribution (Fox & Manley, 2014). The compensatory advantage of HSI is thus the possibility of parallel on-line scanning of samples on a single object basis, which is impossible with other NIR technologies. However, the cost of HSI instrumentation and its added complexity should also be taken into consideration for practical applications.

A potential benefit of HSI is the ability to study protein variation within wheat kernels. Figure 3.10 gives an example of the application of the best PLS model to a hyperspectral image on a single pixel basis, showing the predicted distribution of protein content for one of the sample batches (cultivar JB Diego, hard winter UK wheat).

The predicted protein values are non-uniform within each grain, visualised by applying the calibration on each pixel of the hypercube. In particular, a consistently higher protein is predicted for the ends of the grain, particularly those where the germ is located. The effect was consistent

for images of the same kernels taken in multiple orientations, and implies that this is a genuine non-uniformity in protein content, within the grains and not an artefact of the illumination or imaging conditions. Previous literature investigated the distribution of protein within cereal kernels, but focusing on the seed development physiology of protein accumulation.

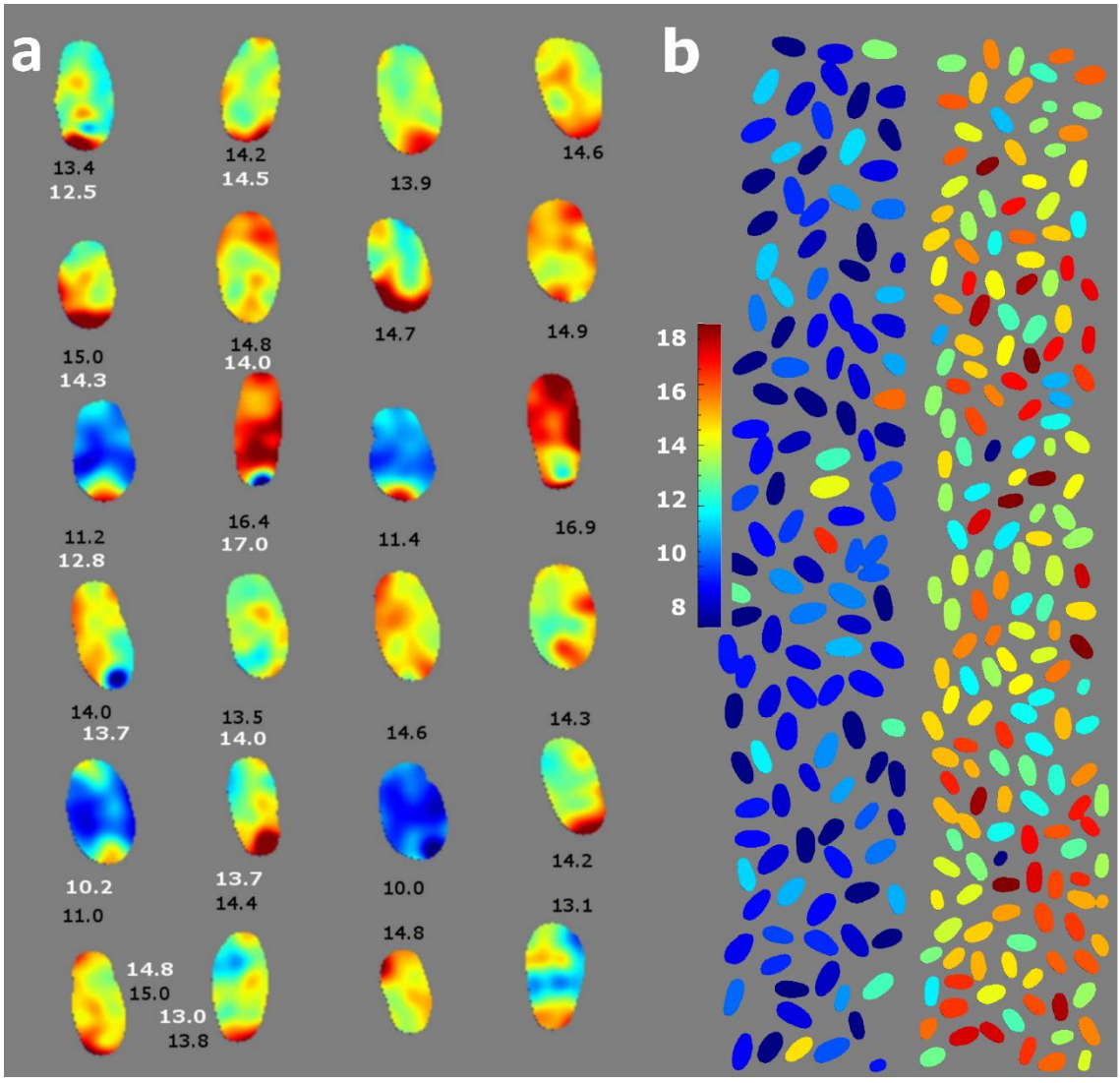


Figure 3.10. Application of the PLS regression protein calibration. a) Application at single pixel level, showing the dorsal (left; average: 12.7%) and ventral (right; average: 13.5%) sides of the same kernels. Reference protein measurement for the batch: 13.1%. b) Application by averaging the spectra for each kernel; Left: low protein sample, Viscount, reference protein content = 10.2%; predicted value = 9.7%. Right: high protein batch, DNS, reference protein content = 15.1%, predicted value = 14.6%. Black text; predicted values; white text: reference values (% wet basis).

Sub-aleurone cells have been reported to contain few starch granules and high proportion of proteins; in addition, these cells contain variable amount of total protein content across the wheat endosperm (Shewry & Halford, 2002).

Through the application of the calibration on a HSI machine, it is possible to rapidly scan a considerable number of samples and predict the protein content on the average spectra from each kernel, as exemplified in Figure 3.10b for two wheat samples.

This aspect has been verified in the present research, by applying the best protein calibration for four independent wheat batches, and obtaining hypercubes of over 100 kernels per batch, for which bulk reference protein measurements were taken by Dumas analysis. The average predicted error for the batches was 0.1-0.8% of the reference measurement of the batch.

3.3.3. Bulk HSI protein prediction

Protein prediction was also performed on a bulk basis, to test whether the prediction ability of HSI can be improved when a calibration is built using multiple kernels in a batch, instead of single kernels. As SNV+1st derivative pre-treatment resulted in the best one for wheat kernels, it was applied to build a PLSR model based on the spectra averaged for each wheat batch, against the average protein content measured by the Dumas method. The performance of the calibration is shown in Figure 3.11.

The calibration R^2 value was 0.916, with prediction error of 0.389%, while the cross-validation error was 0.507% and R^2=0.859. Thus, the calibration error (RMSEC) using batches (averaged kernel data) was lower than half the error obtained for the single kernel model, i.e. 0.389 % for multiple kernels while the single kernel model had RMSEC of 0.857 %. Similarly, the RMSEP value was approximately half of the single kernel prediction (0.51 vs 0.94 %). The prediction error of 0.5 % protein in the present case would be probably lower in the case of replicated measurements of the reference analysis, due to larger sample size. To build this model, reference data from single kernels analysed by Dumas method were averaged, but single kernels were still analysed individually.

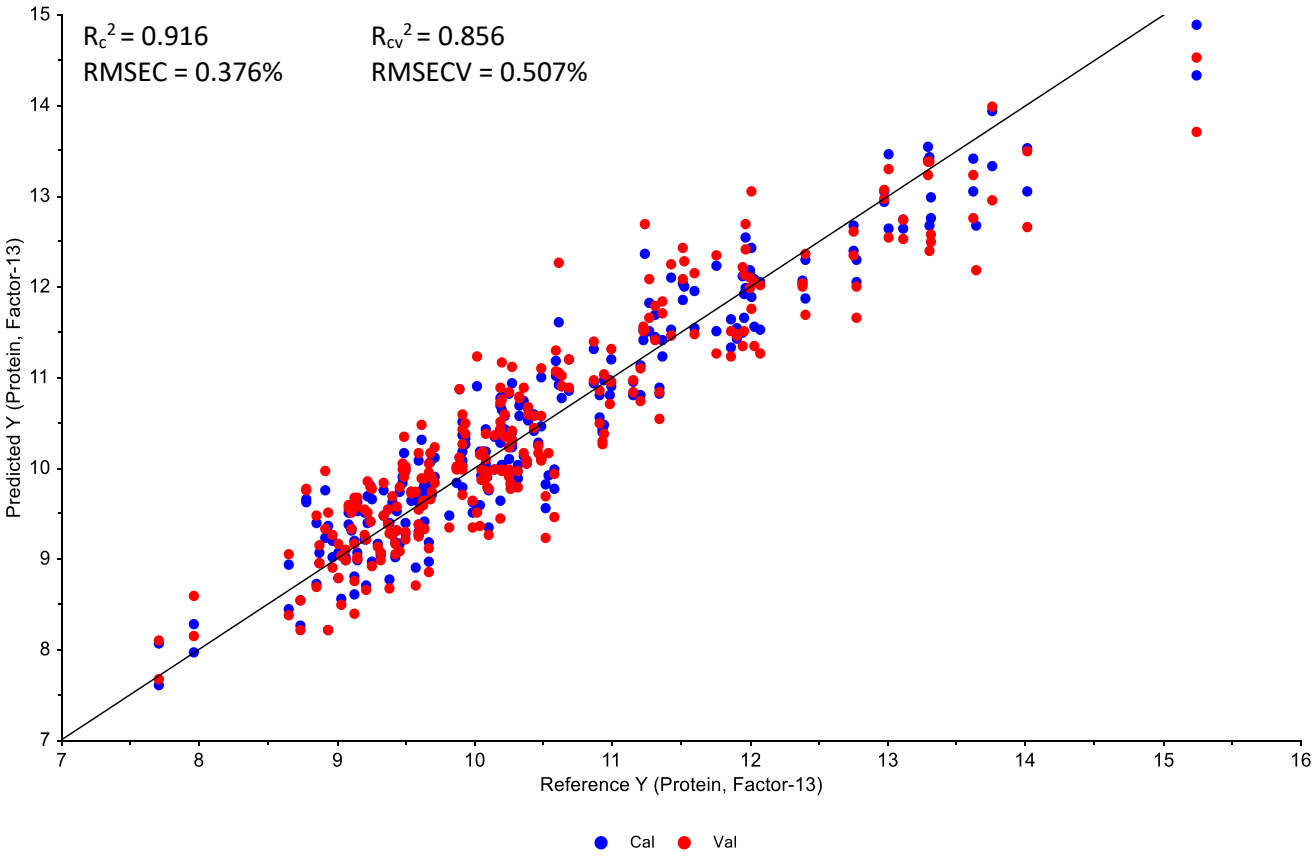


Figure 3.11. HSI prediction of total protein content in whole wheat kernels as bulk (10-12 kernels per batch; averaged spectra and averaged reference measurement): predicted vs reference plot. Black line indicates ideal prediction. Pre-treatment: SNV+1st derivative. LVs = 13 for both calibration and cross-validation models.

Figure 3.12 shows the calibration and cross-validation errors depending on the number of LVs, also showing the β-regression coefficients plot is also indicated. As shown in the figure, the LV chosen for the model was selected based on the minimisation of cross-validation error, but without using an excessive number of factors. The figure also reports the regression coefficients of the PLS regression model. The most intense peaks were observed around 1700-1750 nm, while less intense coefficients were obtained around 1200-1250 nm and 2150-2200 nm. These peaks correspond to the 2nd overtone and 1st overtone region (up to ~2000 nm), while the longer wavelengths correspond to the combination bands (Section 2.1). Despite the strong absorbance expected at 2000-2200 nm for protein, it was noted that the major coefficients were not in this spectral range. This is possibly due to the difference between theoretical absorbers for pure compounds than those in complex food systems.

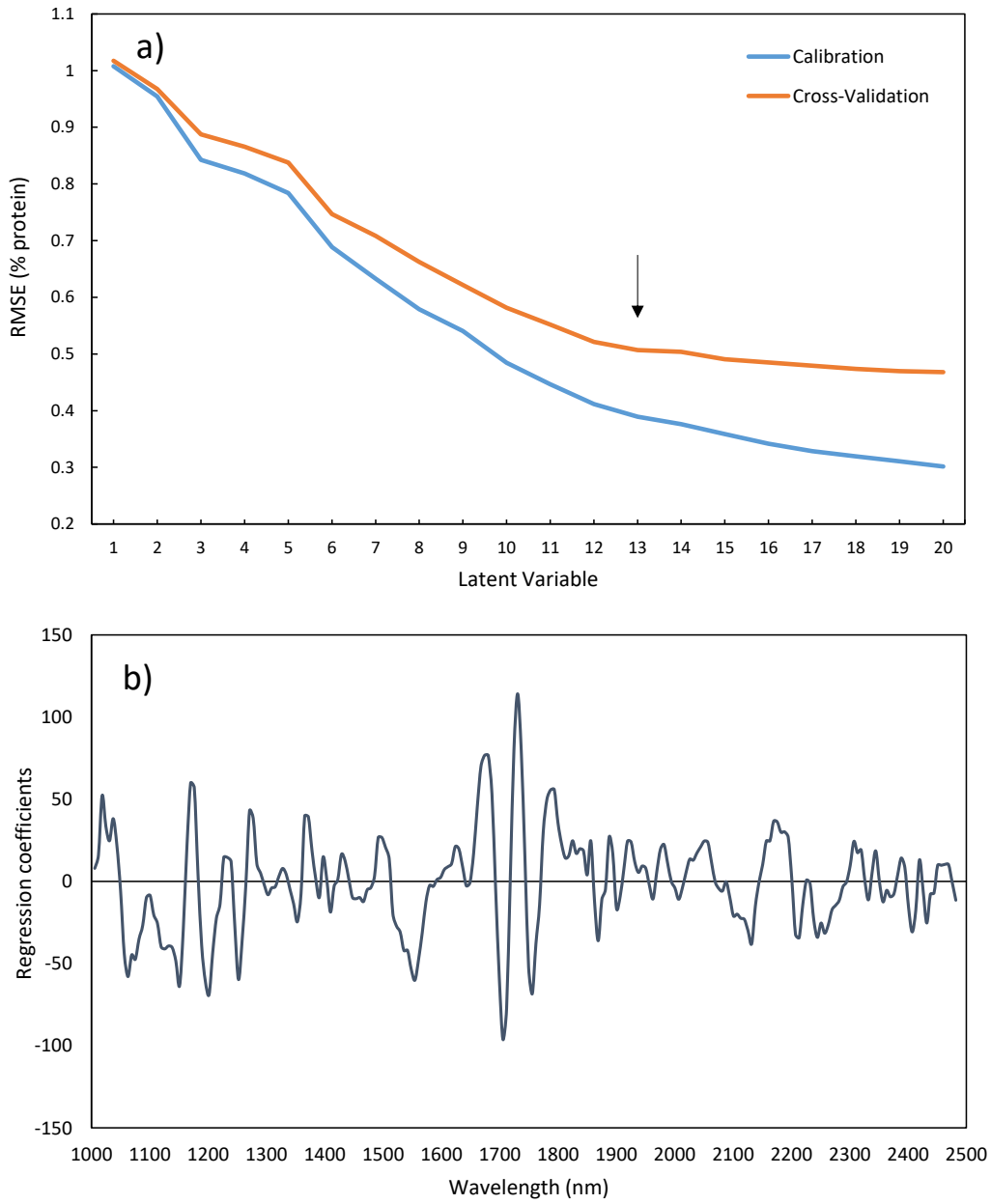


Figure 3.12. PLSR model prediction of protein content in wheat kernels as bulk; **a**) prediction error (calibration and cross-validation) plot for the identification of the best number of latent variables; **b**) β-regression coefficients for the regression model.

3.3.4. Effect of kernel presentation, hardness and spectral range

As the dataset included a wide range of both hard and soft wheat varieties, it was of interest to study whether the sample presentation and hardness class influenced the performance of HSI for protein prediction. In addition, the effect of longer wavelengths has been assessed by excluding the higher spectral region to build a new model in the region 1000-1700 nm only, which is of interest for lower cost detectors. Table 3.3 shows the performances of the PLS models obtained

by considering the effect of sample orientation, wheat classes and lower spectral region. As reported in Table 3.3a, the kernel position did not significantly influence the models' performance. A slightly lower prediction error was observed when the kernels were placed crease-down, i.e. the dorsal side was analysed. However, the R^2 values were similar and sample orientation had little effect on calibration performance and thus no improvement was obtained when building separate PLS models for the kernel position (RMSEP of 0.95-0.96%, while the best general model had RMSEP of 0.94%). This indicates that a unique calibration can be applied to wheat kernels with no need to place them in the same orientation. A similar comparison (Table 3.3b) was seen for soft and hard wheat classes. In both cases, the best prediction model was obtained by applying SNV+1st derivative treatment. The RMSE was 0.61% for the soft wheat class and 0.85% for hard wheat, for the calibration dataset, and the R^2 values were similar for both calibration and validation datasets. However, as the performance is not much better for separate calibrations, a general model applicable to several wheat classes is recommended. In general, the grain processing industry would prefer a comprehensive PLS model that includes both hard and soft wheat classes, instead of having two separate calibrations.

The performance was also tested for a model using only the 1000 to 1700 nm spectral region, to simulate detectors operating in a shorter spectral range and compare the improvement obtained in protein prediction when using HgCdTe detectors. Detectors such as InGaAs operating in this band are available at lower cost than those operating at longer wavelengths. Fox and Manley (2014) reported that it is interesting especially for protein to use sensors which are capable of detecting higher wavelengths, up to 2500 nm.

Table 3.3. Performances of the PLS models for protein prediction in single wheat kernels, by creating separate models depending on (**a**) the orientation, (**b**) the hardness class and (**c**) for a restricted spectral range.

	Pre-processing	Variable	Calibration				Validation				PC	RPD	Sample n.	
			Slope	Bias	RMSEC	R_c^2	Slope	Bias	RMSEP	R_p^2			Cal.	Val.
a)	Raw data	Crease-up	0.774	0.008	0.990	0.774	0.743	0.029	1.048	0.728	15	1.97	1647	522
	SNV + 1st derivative		0.824	0.000	0.868	0.824	0.803	0.024	0.958	0.773	13	2.15		
	2nd derivative		0.757	0.026	1.028	0.757	0.775	0.010	1.091	0.705	10	1.89		
	Raw data	Crease-down	0.841	0.000	0.796	0.841	0.792	-0.062	0.958	0.768	18	2.15	1490	473
	SNV + 1st derivative		0.834	0.000	0.817	0.834	0.804	-0.080	0.947	0.773	9	2.18		
	2nd derivative		0.794	-0.002	0.885	0.794	0.751	-0.045	1.082	0.704	9	1.90		
b)	Raw data	Soft wheat	0.773	-0.004	0.703	0.773	0.711	-0.070	0.838	0.733	14	2.46	708	223
	SNV + 1st derivative		0.812	-0.025	0.611	0.819	0.721	-0.059	0.790	0.764	11	2.61		
	2nd derivative		0.790	-0.001	0.670	0.790	0.705	-0.052	0.841	0.731	11	2.45		
	Raw data	Hard wheat	0.791	0.022	0.923	0.791	0.766	0.107	0.996	0.763	17	2.07	1626	511
	SNV + 1st derivative		0.824	0.000	0.852	0.824	0.826	0.032	0.901	0.806	12	2.29		
	2nd derivative		0.744	-0.009	1.026	0.074	0.769	0.003	1.114	0.704	10	1.85		
c)	Raw data	<1700 nm	0.675	-0.009	1.192	0.675	0.668	0.013	1.185	0.648	14	1.74	3138	992
	SNV		0.732	0.012	1.063	0.732	0.711	0.007	1.129	0.681	14	1.83		
	MSC		0.747	0.013	1.034	0.747	0.728	-0.545	1.233	0.620	14	1.67		
	SNV + 1st derivative		0.688	0.000	1.159	0.688	0.702	-0.018	1.173	0.655	10	1.76		
	2nd derivative		0.703	-0.153	1.128	0.703	0.721	-0.008	1.187	0.647	10	1.74		

Number of spectral bands selected: 240 for **a**) and **b**); 107 for **c**). RMSEC and RMSEP are expressed in % (wet basis). The same number of PCs (LV) were used for the calibration and validation models.

As shown in Table 3.3c, the PLS regression model built on NIR data with limited spectral range resulted in lower R^2 and higher RMSE values. The RMSEC ranged from 1.03 to 1.19%, while RMSEP values were 1.13-1.23%. The best model was achieved with SNV treatment. Although the R^2 for the restricted spectral region was reduced from 0.82 to 0.73 for the calibration and from 0.72 to 0.68 for validation, this performance could still be useful at practical level for the rapid screening of kernel protein content, using a lower cost detector working in the spectral region 1000-1700 nm.

A comparison has been made of the PLS loading weights for the models using the full spectral region and the reduced one (Figure 3.13).

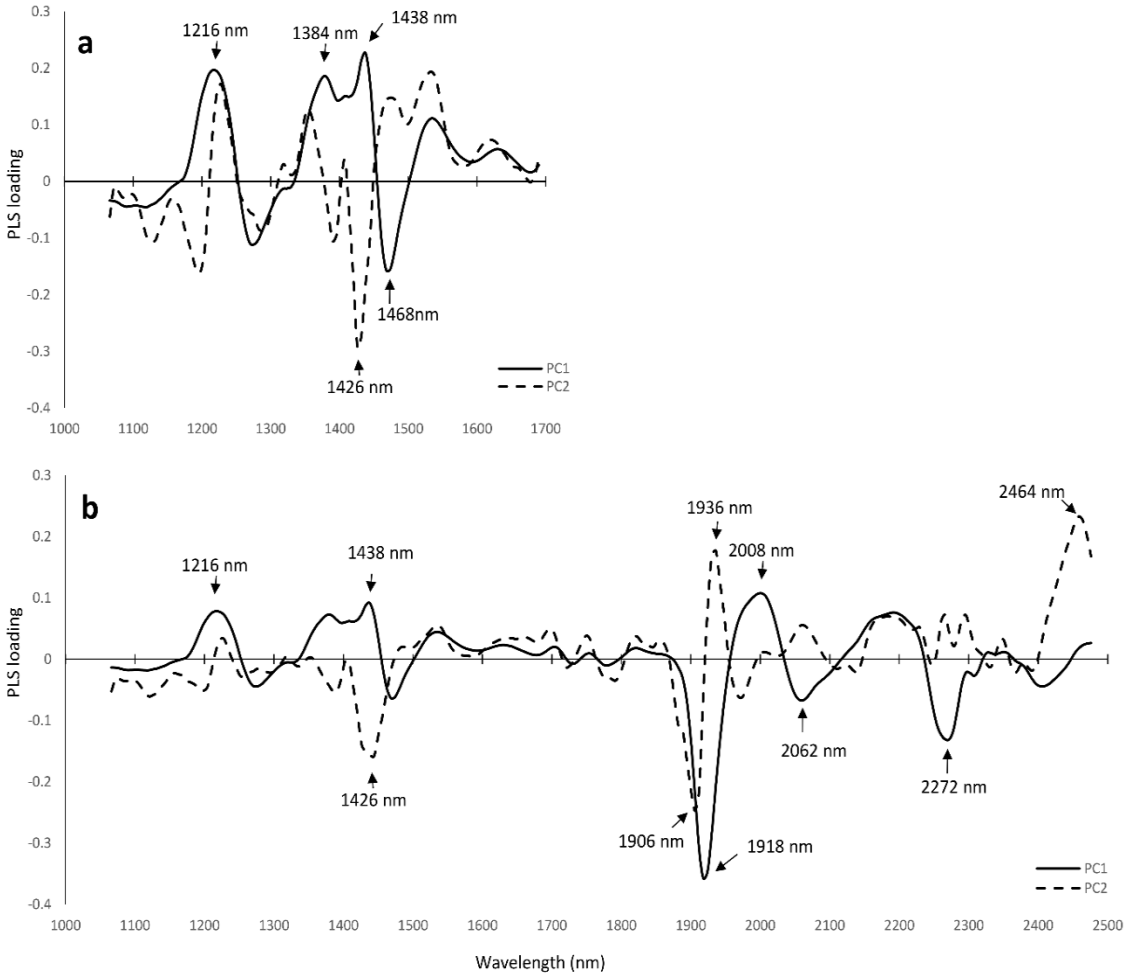


Figure 3.13. Loading weights of the first two factors for PLS model in the region 1000-1700 (**a**) and 1000-2500 nm (**b**), for the PLS models applying SNV+1st derivative pre-processing calculation.

The main wavelengths contributing to PC1 are 1216, 1384, 1438 and 1468 nm. When the full spectrum is taken, a marked influence of the following wavelengths was also obtained: 1918, 2008, 2062 and 2272 nm. The most prominent feature was found at 1918 nm, which is attributed to a C=O second overtone, –CONH structure, indicating protein (Osborne et al., 1993). In the case of PC2, the main influencing wavelengths were those at 1426, 1906, 1936 and 2464 nm. The 1936 nm wavelength has one of the highest scores, and this region represents the O-H combination of stretch and deformation, which is attributed to moisture. It is known that the C-H combination bands are mainly shown in the regions 1000-1100 nm and 2000-2500 nm, while the N-H combination bands absorb predominantly around 2000 nm (Osborne et al., 1993). For this reason, and considering the fact that the HSI detector used gives more noisy spectra in the region 970-1060 nm, the most interesting region was above 1700 nm. In the overtone region, the N-H bond absorbs in the spectral range around 1500 nm. In the combination region, the N-H bond is mainly detected slightly below 2100 nm and around 2250 nm, and thus the main peaks at 2062 and 2272 nm were attributed to N-H vibration. The other peaks were mostly attributed to C-H combination bands (Shenk et al., 2001).

In conclusion, the study recommends that the spectral region above 1700 nm should be used to obtain better protein prediction performance, and lower the prediction error, as shown in this chapter by comparing the full NIR spectrum with the restricted one below 1700 nm. However, practical considerations regarding price differences of the detectors should be taken into consideration.

3.3.5. Validation of single-kernel sorting

The wheat industry needs reliable grain composition data for many purposes, e.g. trade, the definition of the final use of the grains and of their price. Grain analytics is an active area of research and emerging technologies may lead to industrial innovations for grain compositional analysis (Schulmerich et al., 2012). Protein content has a significant impact on the final price of the commodity, and sometimes, a premium is given for higher protein content is obtained (Wrigley, 2009). The feasibility of applying a sorting operation on whole wheat kernels was tested

after the application of HSI calibration for protein content. The result of wheat batches manually sorting is reported in Table 3.4.

The choice of the four varieties investigated was driven by their wide spread in the UK wheat market. Viscount is a soft wheat characterised by excellent agronomics, especially recommended in Northern regions (Scotland). It has good yield and is especially cultivated for distillers. Solstice is a nabim group 1 wheat (hard wheat), popular for its milling behaviour, gluten properties and baking performance. Its lower yields are compensated by the higher selling price for premium sector. The average protein content reported by the breeder for this variety is 11.9% (http://www.lgseeds.co.uk/products/cereals/solstice/), which is slightly above the protein content found in the batch analysed in the present experiment (11.14-11.26%). However, the high protein sub-batch led to protein content of 13.25%, statistically significant higher than the initial (unsorted) batch, with an increase of 2.1% compared to the initial sample.

Table 3.4. Result of total protein content analysed by Dumas in wheat fractions sorted according to the HSI calibration model for single kernel protein content. Values are followed by the standard deviation (SD), and different letters for each variety indicate a statistically significant difference ($p<0.05$) by ANOVA. Unsorted is the fraction that has not been scanned by HSI, while "batch" (intermediate) is the remaining wheat after removing of the top ("high") and bottom ("low") fractions.

Variety	Sub-sample	Protein (%)	SD	
Viscount	Unsorted	8.43	0.03	a,b
	Batch	8.72	0.05	a
	High	9.70	0.38	a
	Low	8.16	0.01	b
Scout	Unsorted	8.17	0.08	a,b
	Batch	8.47	0.21	b
	High	9.65	0.03	c
	Low	7.77	0.03	a
Solstice	Unsorted	11.14	0.10	b
	Batch	11.26	0.22	b
	High	13.25	0.47	a
	Low	10.32	0.60	b
DNS	Unsorted	13.94	0.02	a, c
	Batch	14.11	0.06	a
	High	14.48	0.11	a
	Low	13.67	0.01	b, c

Fractions were sorted by applying the predicted protein content on single kernels and manually selecting the kernels with the predicted highest and lowest protein content. These fractions were then analysed as batches by the reference method (Dumas protein determination).

Scout is a winter wheat mainly grown for biscuits. It is more cultivated for its yield, adaptability to different environments and soils and resistance to diseases rather than for the flour quality. Its protein content was comparable to Viscount sample, and manual sorting led to approximately 2% increase, with the high protein batch showing almost 10% protein content. DNS, whose full name is Dark Northern Spring - is a US wheat class belonging to the wider group of "Hard Red Spring" wheats, bread wheats with the highest protein content that deliver excellent milling and baking characteristics. They are usually imported into the UK to adjust flours with low protein content. From the present data, it was shown that a statistically significant increase in the protein content was not reached. The low-protein fraction had significantly lower protein content than the unsorted fraction and the remaining batch, however for DNS data suggest consistency of protein content, as the difference between the low- and high-fractions was only 0.8% protein content.

Single kernel characterisation system (SKCS)

Figure 3.14 shows the results of SKCS analysis. The moisture in DNS sample was significantly ($p<0.001$) lower than the other samples. However, no difference was observed among the sub-fractions within each sample, nor among Solstice, Crusoe and Viscount. Lower moisture in DNS sample is likely to be due to the possible drier weather at harvesting or to the fact that this is an imported wheat that can partially dehydrate during shipment and storage. The results of hardness analysis clearly showed the presence of two groups which were significantly different ($p<0.001$), i.e. DNS and Solstice, and Crusoe with Viscount. This result was expected, as these samples belong to hard and soft wheat classes, respectively. However, among the sub-samples, no statistically significant difference was observed, as the spread of hardness at single kernel level was relatively high, especially for the soft wheat samples. Similarly, no significant difference was obtained in terms of diameter among all samples, as the SD was very high in all samples, showing wide range in terms of dimensions. DNS resulted significantly different from the other 3 samples in terms of kernel weight, but also in this case no significant difference was appreciated among the sorted fractions.

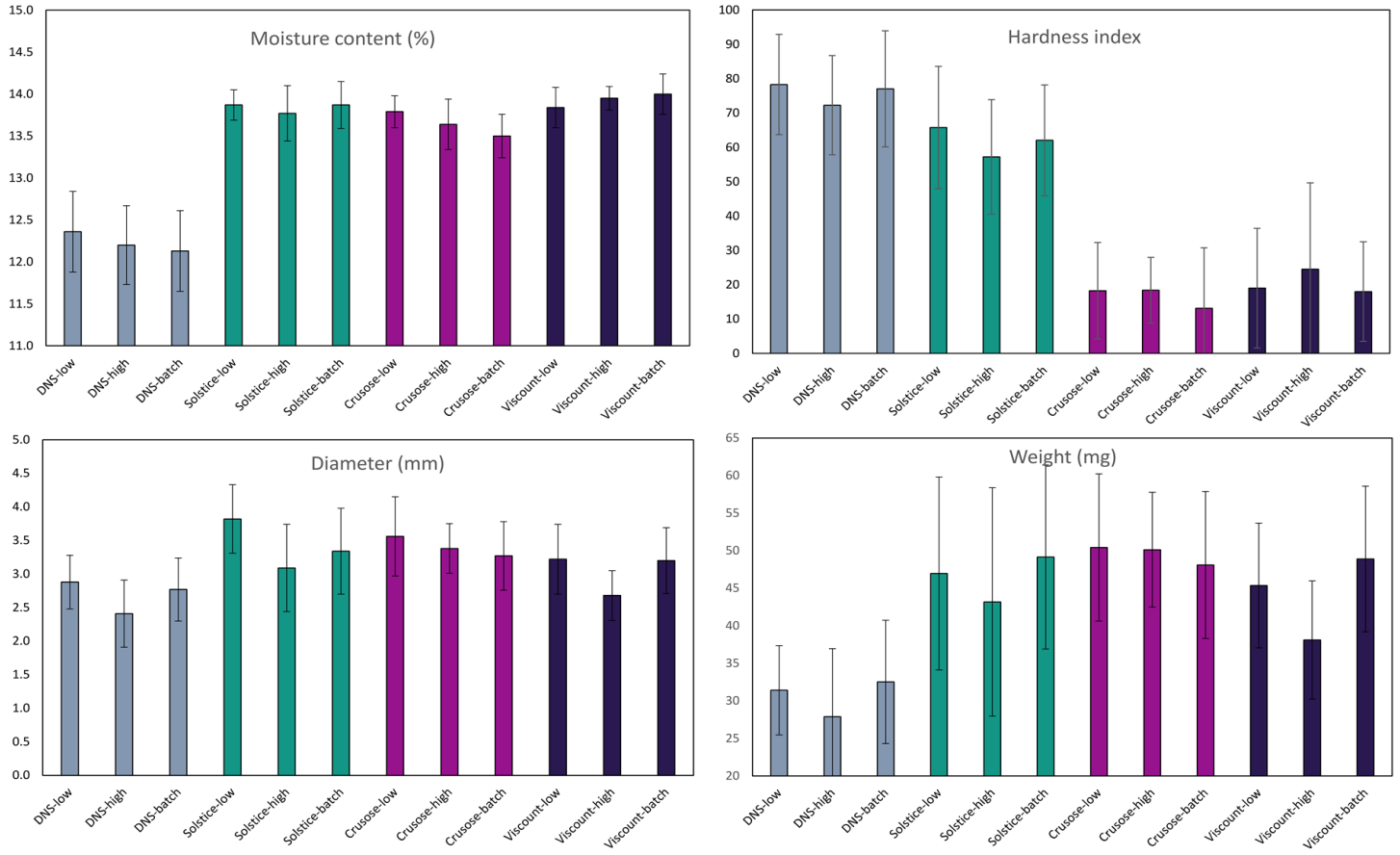


Figure 3.14. Results of the Single-Kernel Characterisation System (SKCS) of sorted wheat sub-samples using the HSI-based calibration for protein content. The system gives single kernel estimation of moisture content, hardness, diameter and weight. Batches consisted of approximately 100 kernels, while selected fractions (high and low protein content) consisted of approximately 15 kernels each.

This result indicates that no other significant changes are observed when sorting wheat kernels by HSI according to their total protein content. In addition, it suggests that the prediction is genuinely done on total protein content and not based on an indirect influence of some other physical property.

SE-HPLC

Proteins separate into several fractions according to their solubility, and wheat also includes insoluble proteins, which are polymeric and dominated by the glutenin fraction, a high molecular weight (MW) material. Size-exclusion chromatography (SE-HPLC) is an indicative technique that offers the potential to characterise the different protein fractions of wheats and flour, according to their molecular weights. Due to the way the column works, larger compounds are eluted earlier than smaller ones. In flour, the following fractions are described: F1, high MW glutenins, F2, low MW glutenins, F3 and F4, gliadins, and F5, albumin and globulins.

As shown in Figure 3.15, in all cases for the four varieties studied, no significant statistical difference ($p<0.05$) was found among the different sub-fractions of all the batches analysed. Similar results were obtained for another useful index, defined as the ratio between the sum of F3 and F4, divided by F1, i.e. [(F3+F4)/F1]. This indicator has been used to classify flours into bread-making and non-bread-making classes, while the ratio F1/F2 has been used as indicator of "extra strong bread" (Millar, 2003).

In the results herein reported, no significant difference was obtained in the sorted fractions for all four batches analyses, in relation to the F1/F2 ratio. However, it was noticed that the two soft wheats tended to show similar low F1/F2 values for the "low-protein" fractions.

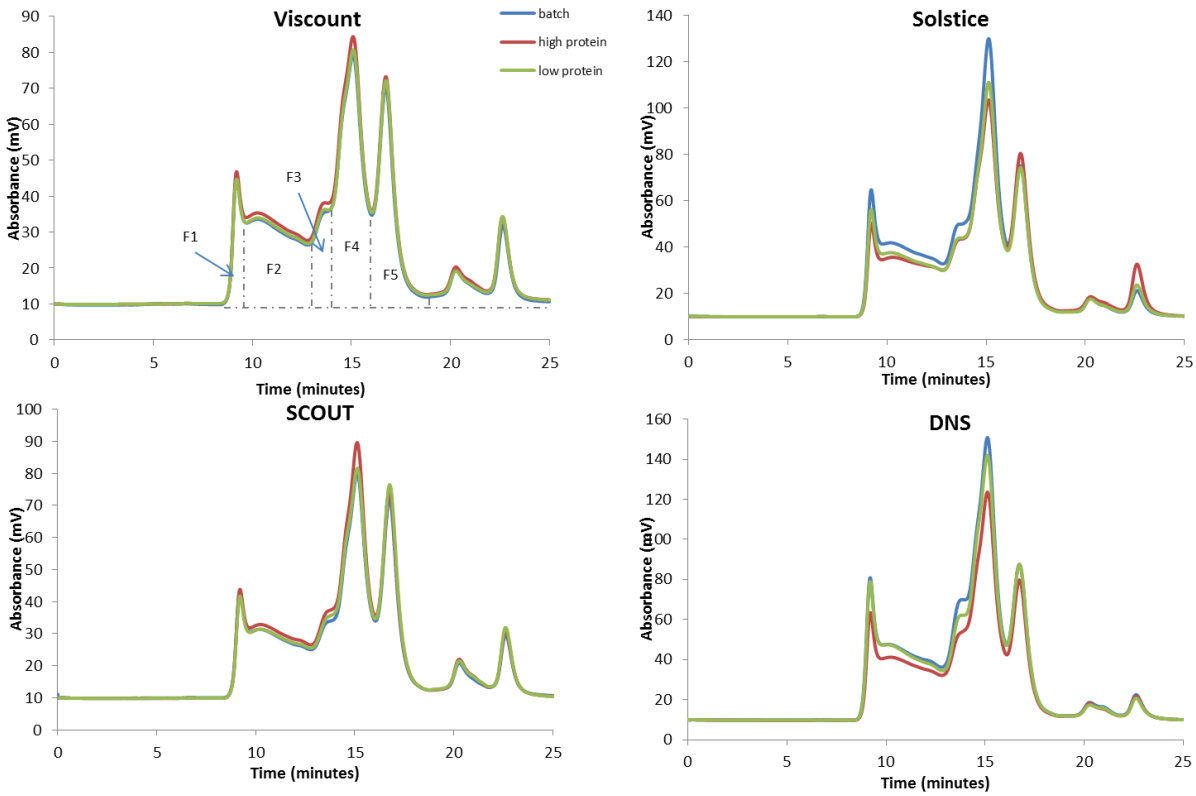


Figure 3.15. HPLC profiles of size-exclusion chromatography analysis of wheat sorted according to the predicted protein content by HSI. Four batches (2 hard and 2 soft wheat varieties) were sorted into high-protein and low-protein fractions (~10% kernels), while "batch" is the unsorted wheat.

On the contrary, the two hard wheats had lower F1/F2 values in both low- and high-protein fraction, compared to the remaining batch. The (F3+F4)/F1 value was generally higher in the high- and low-fractions of soft wheats, while different behaviour was observed for the hard wheats. In the latter group, the value remained constant for the low-protein fraction, but it was higher in the high-protein fraction, compared to the control (unsorted batch). Therefore, there was no significant change in the protein quality when samples are sorted according to their total protein content.

Higher F1/F2 ratio indicates better bread-making capacity, when the (F3+F4)/F1 value is lower, because of the higher MW fractions that confer elasticity.

Hard and soft wheats showed some differences in the different fractions analysed by SE-HPLC; the high-protein fraction in soft wheat always had higher levels of all fractions, while the opposite was found for hard wheats.

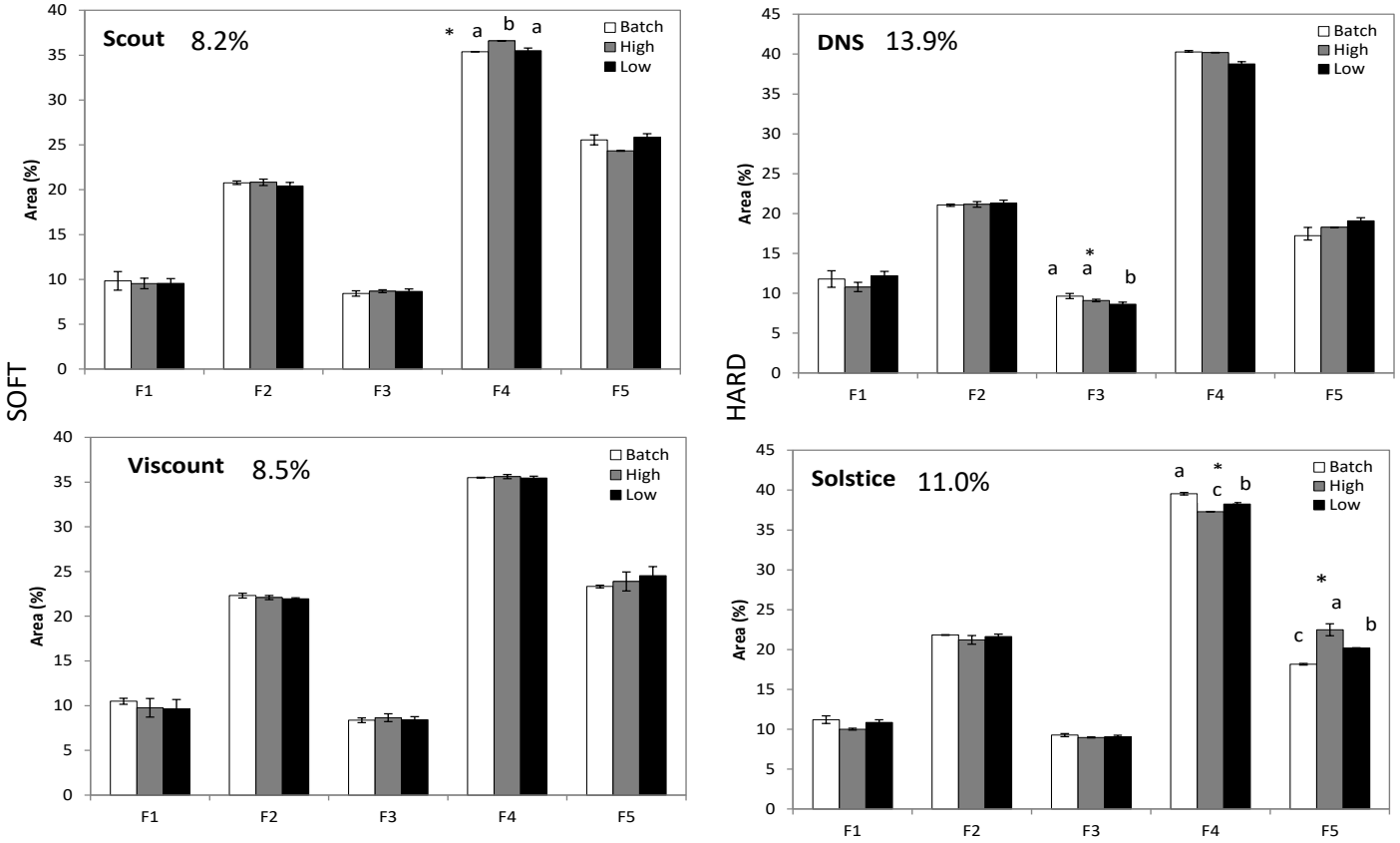


Figure 3.16. Results of SE-HPLC analysis of protein component of wheat batches (four varieties) sorted according their total protein content using HSI calibration. Batch, "high" and "low" indicate the unsorted wheat batch, the fraction with the highest and lowest protein content, respectively. Different letters and asterisk indicate a statistically significant difference ($p<0.05$) for each fraction. The fractions were segregated according to single kernel predicted total content by HSI.

The low-protein fraction resulted to have levels of protein fraction similar to the batch, except for F4 and F5 in soft wheat, where it was slightly higher than the remaining batch. Looking at F1 to F2 ratio (high/low molecular weight gluten), the general trend was a higher ratio for the remaining batch compared to the sorted sub-batches. Generally low values were observed for the high-protein fraction, indicating this fraction is more abundant in low-MW gluten. The value of F3+F4/F1 indicated that the sorted wheat had higher gliadins over glutenin ratio, with particularly high values for the high-protein fraction. The ratio gliadins/high MW glutenins was always higher in the high-protein fraction. No clear trend was observed in term of high/low MW glutenins ratio, thus suggesting that no significant glutenin content are obtained in the sub-fractions when sorting wheat kernels for their total protein content.

3.4. CONCLUSIONS

The present chapter reported a study on a wide range of wheat genotypes and cultivation locations from commercial samples, in contrast to previous research published so far on wheat quality variability which report on samples in field trials, where typically attempts were made to maintain the soil characteristics, soaking rate and agronomic practices in general as consistent and possible. A wide spread of protein content has been found on over 2000 kernels individually analysed, from approximately 6 to 20%, with a standard deviation in protein content above 1.5% (range 0.5-3%) between kernels in each wheat batch. HSI has been successfully applied for the visualisation of protein content in single wheat kernels, obtaining a statistical model with R^2 above 0.8 and a prediction error below 1%. The model included samples sourced from a variety of genotypes and locations, and the obtained calibration was applied on both hard and soft wheats, including differences in the kernel orientation.

The spectral range of 1000-2500 nm was used for the general model, which gave a noteworthy improvement over the prediction achievable using shorter spectral range (1000-1700 nm), simulating InGaAs sensors. The prediction error for single kernel protein is greater than that typically achieved for the protein content of bulk samples by traditional NIR instruments, but is comparable with previous studies for single kernels. This provides additional information on

sample uniformity, and the HSI approach provides the potential for rapid analysis of large numbers of kernels. The calibration error would be suitable for segregation of wheat kernels.

While the single kernel approach is likely not to substitute bulk analysis for protein determination in wheat trading, it can bring several advantages for researchers, as it allows a faster and non-destructive method for single kernel protein analysis. The measurement of protein by HSI also has potential application to wheat breeding to select kernels according to their protein content. These results could be also useful for agronomists to understand the best factor to optimise when aiming to obtain more uniform yields in terms of protein content, as well as for breeders and researchers to deep into the variability obtained from real field condition under the common agronomic practices applied by farmers.

In addition, the ability to select wheat fractions with substantially higher or lower protein content than the original bulk sample was demonstrated, and this was independent of physical properties such as grain weight, diameter or hardness.

4. PREDICTION OF PRE-GERMINATED WHEAT KERNELS INFLUENCING HAGBERG FALLING NUMBER

4.1. INTRODUCTION

Wheat quality criteria include protein content and Hagberg Falling Number (HFN), which is a measurement of the α-amylase activity influencing the technological quality of flour. This enzyme hydrolyses alpha bonds of polysaccharides yielding glucose and maltose. In germinated grain, α-amylase is synthesized by the scutellum and later by the adjacent aleurone (Barrero et al., 2013). Its activity is known as affected by germination time and environmental temperature (Reddy et al., 1984).

HFN is an indirect measurement of the α-amylase activity, which is very relevant for flour functionality in terms of the dough rheology and quality of baked products, especially bread (Kent & Evers, 1994). Especially in wet conditions before the harvesting period or in problematic years, the α-amylase may be activated prematurely and has deleterious effects on the functional properties of the resulting flour. Pre-harvest sprouting has been reported as one of the most important factors for wheat quality, because it can lead to significant economic losses in a short time just before the wheat harvest (Mares & Mrva, 2014). The intensity of the damage depends on the climatic conditions and on the susceptibility of particular cultivars to sprout damage. Direct or indirect methods for α-amylase measurement are commonly applied, usually limited to bulk measurements only. HFN is the officially accepted method to assess the quality of wheat and flour related to the α-amylase activity (ICC standard method no. 107/1, 1968)(ICC, 1968).

The HFN method is based on measurement of the time for a plunger to fall through a wholemeal paste immersed in boiling water after mixing. High α-amylase activity causes starch to break down under the conditions of the test, reducing the viscosity of the paste and reducing the time for the plunger to fall. The minimum HFN value is 60 s, this being the initial mixing time, while good bread-making wheats can have values higher than 400 s. HFN values above 250, 300 or in

some cases 350 s are required for high-quality grading depending on the receival standards set by the wheat industries in different countries (Mares & Mrva, 2008). A small portion of sprouted grains may be sufficient to drop the HFN below the acceptable quality limits. Therefore, the selection and screening of the best lines resistant to specific environmental conditions is of paramount importance for breeding programmes (Mares & Mrva, 2014). It has been highlighted that the use of tools to rapidly analyse sprouted and unsprouted kernels would be beneficial in breeding programmes (Smail et al., 2006).

HFN is relatively time-consuming and requires preparation of a ground sample, an accompanying analysis of moisture content, and duplicate analyses. Alternative analytical methods have been investigated, e.g. enzymatic kits for α-amylase activity measurement (McCleary & Sturgeon, 2002), antibody tests (Verity, Hac, & Skerritt, 1999), and spectroscopic methods (McGoverin et al., 2011; Osborne, 1984; Xing et al., 2010). Despite the development of antibody-based tests for the measurement of α-amylase activity, the traditional HFN method is still regarded as the preferred one because it combines ease of use, reliability of results and its wide use throughout the wheat and milling industry, especially for quality control and screening purposes.

HFN requires analysis of ground samples and cannot give information on single wheat kernels. This might be useful as a small portion of sprouted grains may be sufficient to drop the HFN below the acceptable quality limits. It has also been reported that screening technologies are needed to identify cases of late maturity α-amylase, which causes low HFN in wheat in absence of preharvest sprouting, and different genotypes show different degrees of sprout resistance (Dencic et al., 2013; Mares & Mrva, 2014).

The application of NIR spectroscopy has been previously applied to estimate sprouting problems in wheat (Osborne, 1984; Xing et al., 2011), even reporting a screening system to evaluate wheat quality parameters on bulk by NIR reflectance spectroscopy (Risius, Hahn, Huth, Tölle, & Korte, 2015).

HSI has also been recently applied. Koc et al. (2008) used HSI to understand sprout damage in wheat, using six wheat varieties with artificially induced sprouting achieved by exposing kernels

to high moisture up to 36 h. A classification model was reported according to the level of sprouting, and kernels were analysed by PCA on a single pixel level. Better correlations with germination time were achieved for the embryo region of the kernel than for other regions, but no clear classification of sprouted/unsprouted grains was possible. HSI was also applied to predict α-amylase activity in single wheat kernels, using enzymatic kits as the reference method (Xing et al., 2011; Xing et al., 2009). However, all the models reported tended to overestimate the enzyme activity at low values and underestimate at high values. The prediction models for enzymatic activity using PLS regression had R^2 values of 0.54 and 0.73 for Canada Western Amber Durum and Canada Western Red Spring, respectively (Xing et al., 2009). Developing accurate single kernel calibrations for wheat quality parameters is challenging, due to the difficulty of obtaining reference data for single kernels, as many analytical methods require larger amounts of sample. For this reason, a potential approach is to develop calibrations using reference measurements for bulk samples, and to apply them to single kernels, even if this approach might "dilute" the spectral information of problematic kernels. In addition, when applying HSI predictions, it is relevant to define the approach for data treatment, in particular whether the hypercube should be treated on a single pixel basis or whether the ROI should be previously selected.

Therefore, the aim of the present chapter was to build a PLS calibration model for the estimation of HFN in intact wheat kernels using HSI in the NIR region, or classification according to the reference HFN. In addition, two approaches for the application of calibrations to HSI images of wheat kernels were compared.

4.2. MATERIALS AND METHODS

4.2.1. Wheat samples

Wheat samples cultivated in the United Kingdom were used in the present experiment, including examples of a wide range of varieties (>30) and from multiple growing areas within the UK. The total number of samples was 425, as described in Table 4.1. These were composed of two sets of samples. The first set comprised 309 samples from a field test involving late harvesting to

assess HFN problems, using two bread wheat varieties (Crusoe and Skyfall) grown in six locations across the UK. The second set comprised 116 samples from thirty wheat batches including the most common UK varieties (e.g. Chilton, Claire, Cordial, Crusoe, Einsten, Gallant, Invicta, JB Diego, Mulika, Panorama, Solstice), and examples of a German and a French wheat. These samples were treated in the laboratory to reach a pre-germination step, which increased the α-amylase activity, but avoiding visible sprouting. This was achieved by soaking the samples in distilled water for 30 min and subsequently spreading them on plastic trays, covered with wet paper tissue to maintain high relative humidity and stored at 20 °C. Sub-samples of circa 500 g were taken at discrete intervals (typically 3, 9, 12 h) during this period up to ~30 h, and finally dried at 30 °C in an oven to remove excess moisture (Mitchell dryers, UK), which took approximately 6-8 h. The moisture content of the samples was periodically checked using a SINAR moisture analyser until it was below 12-13%. An aliquot of each sample was analysed for HFN as described below. Previous workers have applied freeze-drying to samples to stop the germination process. However, it was considered that freezing the wet grains may affect the internal microstructure of the kernels and could affect the NIR spectra, thus oven drying at mild temperature conditions was therefore used in the present study (Figure A.1 in Appendix shows a wheat kernel microstructure). This is more similar to the approach used to process commercial wheat samples with excess moisture content.

Table 4.1. Descriptive statistics of reference HFN in the wheat samples used to develop PLS models.

	Calibration set						**Validation set**					
	Mean	**Median**	**SD**	**Min**	**Max**	**n**	**Mean**	**Median**	**SD**	**Min**	**Max**	**n**
Field wheat experiment	265.75	293	84.1	62	418	213	269.72	295	89.4	64	404	96
Laboratory germination	257.74	258	86.1	62	404	87	281.31	279	84.6	62	405	29
Complete dataset	263.43	283	84.6	62	418	300	272.41	295	88.1	62	405	125

Data were obtained from duplicate analysis by the HFN method. SD: standard deviation. Mean, Median, SD, min and max are expressed in seconds. n = number of wheat batches.

4.2.2. Hagberg Falling Number measurement

HFN was used as the reference method, according to the international standardised method (ICC, 1968). 300 g of each sample was milled using a Laboratory Mill LM 3100 (Perten instruments, Hägersten, Sweden) with a 0.8 mm sieve to obtain a consistent particle size. The moisture content of ground wheat was checked using a PerCon Inframatic 8611 NIR spectrometer (Perten Instruments) before the HFN measurement to define the amount of water to be added. 7±0.05 g ground wheat were put into a viscometer tube and 25±0.2 mL of distilled water was added, in relation to the previous determined value of moisture content. A Perten FN1700 instrument was used for the analysis, which was done in duplicate. The method is based on mixing a defined amount of water according to the initial moisture content of the ground wheat in glass tubes, which are then placed in a bath of boiling water. The machine mixes the slurry for 60 seconds, and then a timer starts in order to measure the time needed for the metallic mixer to fall. The concept that a relatively low amount of sprouted kernels in a batch can affect the rheological properties of the obtained flour was tested by adding increasing amount of sprouted (HFN=84 s) and severely sprouted kernels (HFN=62 s) in a batch of sound kernels (HFN=308 s) (Figure 4.1). A dramatic decrease of the HFN was observed, and the value dropped below 250 s using only 2.5-5% (w/w) wheat kernels with sprouting issues.

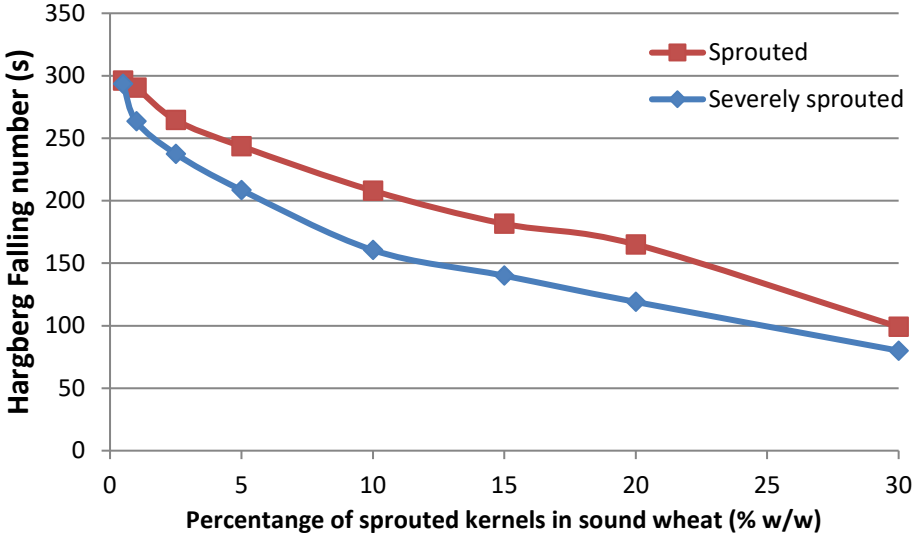


Figure 4.1. Effect of adding sprouted and severely sprouted wheat kernels in sound kernels on the Hagberg Falling Number (HFN). The first three points are at 0.5%, 1% and 2.5% (w/w).

4.2.3. HSI data acquisition and treatment

The hyperspectral imaging system and the acquisition parameters were the same as reported in Section 3.2, with the only exception related to the number of kernels scanned within each hypercube for each sample. In addition, no replicate scans were done on the two surfaces of the wheat kernels, but they were randomly oriented on the scanning platform. Similarly, the data processing steps applied in the present research are detailed in Section 3.2.

4.2.4. Statistical treatment of the data

The exported mean spectra were statistically treated using The Unscrambler X 10.3 software package (CAMO, Norway). Calibrations were developed using Partial Least Squares (PLS) regression on 240 spectral bands against the reference HFN, to build quantitative prediction models for HFN. The algorithm used was Non-linear Iterative Partial Least Squares (NIPALS). The PLS regression models were validated using an independent validation dataset and the number of Latent Variables (LV) was chosen in order to minimise the RMSECV, leaving the software to choose the best LV. An initial approach was tested using the full set of single-kernel spectra and attributing them the HFN reference value for the corresponding bulk, but this approach was then avoided as the calibration performance was inadequate. Instead, the spectra from each batch (scanned sample of bulk wheat) were averaged, and the average spectra were then used for the statistical model. Several spectral pre-treatments were tested, including standard normal variate (SNV), second derivative using Savitzky-Golay smoothing (5 points smoothing, second order derivative), baseline correction, de-trending and multiplicative scatter correction (MSC) (Rinnan, van den Berg, & Engelsen, 2009). In addition, Linear Discriminant Analysis (LDA) was used as a classification method to discriminate samples into classes, i.e. high and low HFN value. LDA was calculated using PCA with 20 principal components, and a quadratic method.

4.3. RESULTS AND DISCUSSION

4.3.1. Distribution of HFN in wheat samples

Table 4.1 shows the statistical description for the reference HFN measurement of wheat samples used in the present experiment. The total number of sample (complete dataset) was 425, comprised of field wheat where no further treatment was applied, and a laboratory-treated dataset; the complete dataset was randomly split into a calibration and a validation dataset for the PLS regression analysis. The results of the two groups used indicate that the range of HFN values was similar between the field wheat experiment and the laboratory germination dataset, 62 s being the minimum value and 418 and 404 s the maximum values for the first and second group, respectively. The average HFN for the dataset was slightly above 250 s, which is considered as the minimum limit for high quality bread-making wheats by the industry.

Figure 4.2 shows the distribution of reference HFN values for the test samples. A bimodal distribution was obtained, with 53 samples having values below 150 s and 372 samples above this threshold. The samples in the lower range are those with high α-amylase activity indicating sprouting problems, and they are desired in the dataset because the aim was to identify problematic samples, especially those with average HFN below 150 s.

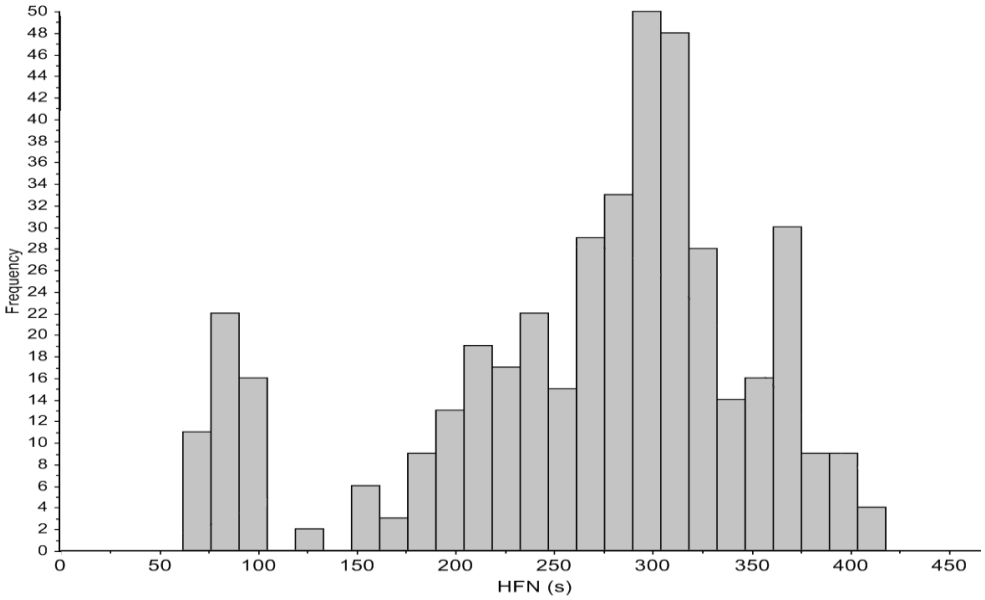


Figure 4.2. Distribution plot of HFN measured in the whole dataset of wheat samples (n=425).

4.3.2. PLS calibration for HFN prediction

Table 4.2 reports the performance of the PLS models for HFN prediction in the NIR region (~1100-2500 nm) by testing several spectral pre-treatments. The spectral pre-treatments provided improved calibration performance. The best performance was achieved for the second derivative treatment, with R^2 of 0.60 and RMSEP of 50 s. The R^2 values for the external validation dataset were between 0.41-0.47, with little improvement depending on the spectral pre-processing applied. The error was slightly above 60 s, which compares favourably with a repeatability of the reference HFN method of 8.5% for ground wheat (from 5 to 35 s with the HFN range found in the present experiment). The calibration with SNV pre-processing gave slightly poorer calibration performance, but has also been used herein for comparison purposes to evaluate different methods when applying HSI calibrations. Therefore, taking into consideration the robustness and performance of this model, the chemical images shown from these models are for illustration purpose only.

Table 4.2. Performance of the PLS models for HFN prediction by HSI, by testing several spectral pre-treatment methods.

Pre-treatments	**Calibration (n=300)**				**Validation (n=125)**				**LV**
	Slope	**R_c^2**	**RMSEC**	**Offset**	**Slope**	**R_p^2**	**RMSEP**	**Offset**	
Raw	0.397	0.40	62.6	161.7	0.383	0.42	67.0	170.4	8
2nd derivative	0.599	0.60	50.4	110.8	0.508	0.43	62.7	130.2	11
SNV	0.513	0.51	56.7	128.9	0.490	0.47	63.9	139.6	11
Baseline+detrend	0.424	0.42	61.6	153.3	0.409	0.41	67.5	161.5	9
MSC	0.415	0.41	61.9	156.7	0.408	0.42	66.8	159.9	7

The calibration performance compares favourably with the value of 73 s reported by Osborne (1984) for an NIR spectroscopy method, with a tested range of 62 to 377 s, and a R^2 value of 0.56. The author applied NIR spectroscopy on ground wheat and therefore only a bulk measurement was done.

Previous papers have reported a quite poor correlation when trying to predict HFN by NIR spectroscopy. Xing et al. (2009) reported the prediction of α-amylase activity by HSI in Canadian wheats, a hard red spring and a durum variety, with R^2 of 0.73 and 0.54 respectively, although creation of a single calibration model for both classes was not successful. This could be sufficient

for classification purposes, as the authors reported discriminant analysis accuracy up to 94% for high α-amylase content and 88% for low level samples. More recently, the same authors grouped Canadian West Red Spring wheat samples into three categories, namely low, medium and high α-amylase activity. They reported higher coefficients of correlations for FT-NIR spectrometer (R^2=0.82), while it was 0.79 for the best model using HSI. While the log transformation of the reference α-amylase activity helped in improving the model performance, the group with high enzymatic activity had visible sprouting, which could have affected NIR response. Xing et al. (2011) highlighted that the spectral intensities across the entire wavelength region, i.e. the raw spectra from the short-wavelength infrared (SWIR), were directly related to the enzymatic activity. The performances of SWIR and Fourier Transform NIR (FT-NIR) instruments were also assessed, and the first method resulted in better performances. The log transform improved the prediction value of the model, with a R^2 of 0.86 vs 0.80 when using the original α-amylase activity values.

An earlier study predicted α-amylase activity in two Canadian wheat classes using PCA and PLS, but the authors reported poor results with similar R^2 values compared to this research (Xing et al., 2009). Another study investigating HSI pre-sprouting damages in wheat used the spectral range 1000-1700 nm, on six wheat varieties at different levels of sprouting, artificially produced, reporting comparable results (Koç et al., 2008). Also, other works even using NIR spectroscopy to flour for the prediction or estimation of HFN reported similar or poorer results than those obtained in the current study. Millar (2003) used 300 samples of UK and French wheats, and applied traditional NIRS using the range 1000-2500 nm for flour, ground wheat and whole wheat kernels. Flour prediction using PLS regression had R^2=0.51 (SEC=36.2 s and SECV=42.0 s). Slightly poorer predictions were reported for ground wheat, with R^2=0.43, SEC=39.6 and SECV=44.4 s. The poorest prediction was obtained using whole wheat kernels, with R^2 of 0.26, SEC of 44.2 and SECV 46.3 s (mean value 326 s, SD 51.3 s) (Millar, 2003). Prediction of α-amylase activity using NIR spectroscopy or HSI is generally expected not to be particularly accurate, as this enzyme is found at very low concentrations in wheat, and its activity is more important than the sole concentration. For this reason, attempts to predict α-amylase using

alternative methods have been generally unsuccessful (Barnard, Van Deventer, & Maartens, 2005).

4.3.3. Methods to apply calibrations to hyperspectral images

Two different methods were tested to apply calibrations to hyperspectral images of test samples for predicting HFN. By applying the calibration to each pixel, HSI provides the capability to map the distribution of a chemical compound within a sample, for example across a single kernel. For assessment of average properties for whole kernels or for bulk samples, potential approaches include application of a calibration to an average spectrum for the region of interest (equivalent to bulk spectroscopic methods), or alternatively to calculate the distribution of the property of interest at single pixel and then to calculate the average value for the sample. The effects of these approaches have been compared for the HFN prediction model.

In either case, it is advisable to apply any required spike removal procedures prior to further processing to avoid their effect on the spectra. The spike removal processing on the hypercube was done in both cases at the beginning, since any bad pixels in the spectral band used for segmentation appear as vertical lines in the segmentation image, making segmentation more complex.

Method 1. ***Application of the calibrations at single pixel level, followed by averaging the output within each object***. A program was written in IDL to apply the relevant spectral pre-treatment to each pixel in the hypercube and then to apply the PLS calibration coefficients for each spectral band to assess the spatial distribution of predicted HFN values for each pixel within the kernels. The mean of these values was then calculated to predict the HFN for each kernel.

Method 2. Averaging the spectra within each object (ROI) followed by application of the calibration on the mean spectra. The alternative approach was to calculate mean spectra for each object (wheat kernel), followed by the application of the calibration, including any spectral pre-treatment, to this average spectrum to give the predicted HFN for the kernel. In the present study, a lower computational capacity is typically needed, since calculations at the single pixel level involve only calculation of mean spectra rather than application of calibrations, and the

latter is a more computationally demanding operation, particularly if spectral pre-treatments are included.

In cases where no spectral pre-treatment is applied, the two methods are equivalent, as shown by the following equations (previously shown in Caporaso et al., 2016). For absorbance values A_{ij} for spectral bands i=1 to n and spatial pixels j=1 to m within a chosen object, the value of a property Y, such as HFN, can be predicted for each pixel using an equation of the form:

$$Y_j = a_0 + \sum_{i=1}^{n} a_i A_{ij} \quad (1)$$

where a_i are the calibration constants derived from the PLS regression.

The mean value of Y for the object (method 1) is given by:

$$\overline{Y} = \frac{1}{m}\sum_{j=1}^{m} Y_j = a_0 + \frac{1}{m}\sum_{j=1}^{m}\sum_{i=1}^{n} a_i A_{ij} \quad (2)$$

Alternatively, the mean spectrum for the object may be calculated as:

$$\overline{A_i} = \frac{1}{m}\sum_{j=1}^{m} A_{ij} \quad (3)$$

Applying the calibration to this mean spectrum yields a predicted measurement (method 2) for the object of:

$$\overline{Y} = a_0 + \sum_{i=1}^{n} a_i \overline{A_i} = a_0 + \frac{1}{m}\sum_{i=1}^{n} a_i \sum_{j=1}^{m} A_{ij} \quad (4)$$

which is equivalent to the result in (2).

For spectral pretreatments, this is not necessarily the case, depending on the pretreatment. For convolution filters, the approaches are also equivalent as shown by equations 5-8. If a convolution pretreatment is applied to spectra to yield treated spectra:

$$A'_{ij} = \sum_{k=p}^{q} w_k A_{i+k,j} \quad (5)$$

or a treated mean spectrum

$$\overline{A'_i} = \sum_{k=p}^{q} w_k \frac{1}{m}\sum_{j=1}^{m} A_{i+k,j} \quad (6)$$

where w_k are the convolution weights, and for values $1 \leq i+k \leq n$, then the predicted value for the object, using alternative calibration constants b_i derived for the pretreated spectra, is

$$\bar{Y} = b_0 + \frac{1}{m}\sum_{j=1}^{m}\sum_{i=1}^{n} b_i \sum_{k=p}^{q} w_k A'_{i+k,j} \qquad (7)$$

by the first method, and

$$\bar{Y} = b_0 + \frac{1}{m}\sum_{i=1}^{n} b_i \sum_{k=p}^{q} w_k \sum_{j=1}^{m} A'_{i+k,j} \qquad (8)$$

by the second method, which are equivalent.

An example is the Savitzky Golay second derivative pretreatment, which gave the best calibration performance for the HFN calibration reported here. Figure 4.3 shows the effect of the two approaches, using this calibration. Grains from a poor quality sample, i.e. low reference HFN value, were compared to a sample with a high HFN value, and it is shown that the two approaches are equivalent in predicting the HFN for single kernels. Moreover, the predicted mean HFN values for the batches tested were very close to the reference HFN values, i.e. 117 vs 103 s for predicted and reference, respectively, in a low-quality wheat batch, and 404 vs 370 s in the case of good quality wheat. It should be noted that these predictions are made on a new dataset and not the one used for building the calibration, so the kernels shown in the figures are new batches. The first method is useful to visualise differences within a single grain, which is not possible with the second method. In the samples used in the present experiment, a distinctive distribution of HFN values was obtained within each grain, with lower values at the ends. This is independent of grain orientation, suggesting that it represents a genuine non-uniformity within the grains and not an artefact of the imaging and illumination conditions. Potentially, the distribution relates to the differential production of α-amylase activity in different regions of the grain. It should be noted that lower values are typically seen at both ends of the grain, and are therefore not only associated with the germ and scutellum. These results are in line with previous papers dealing with HSI estimation of germination in wheat, where it was suggested to use the size at the ends of the kernels as a parameter to recognise sprouted kernels, due to the swelling of the embryo during germination (Xing et al., 2010). It was also previously reported that other

regions within the wheat kernels are more useful for other predictions, e.g. HSI prediction of flour yield, while the germ tip of the kernel was the worst region for softness prediction (Delwiche, Souza, & Kim, 2013).

Previous studies applying HSI for HFN estimation observed a non-uniform distribution within the kernel: Smail *et al.* (2006) reported that the developed embryos in wheat can be recognised by HSI, as they were observed in the hypercubes of germinated kernels. The authors reported that much of change in activity during early sprouting occurs in the outer kernel layers, i.e. aleurone and germ. Here, the grains were placed in random positions in terms of crease up and crease down, and in the same hypercube, kernels in both positions were present at the same time.

Although the two methods for calculating mean HFN values for kernels are equivalent for spectral pretreatments based on convolution, the results may differ for other pretreatment methods. To test the magnitude of this effect, the SNV pretreatment reported in Table 4.2 was applied, and the PLS model using this pretreatment was used to predict unknown samples. As shown in Figure 4.3 and Figure 4.4, obvious differences in the predicted HFN values were obtained depending on the method used. When the second method was applied, generally the HFN prediction was quite similar between the two equations, i.e. the kernels with very low HFN values were identified. It should be noted that this method corresponds most closely to that used to calculate reference spectra for development of the calibration. However, differences were observed for the first method.

The kernels with the lowest HFN in the batch were still predicted successfully, but the absolute value was much higher. The first method led to a systematic overestimation of the HFN in comparison with the second method. In this example, the best prediction of the batch HFN was obtained by using the second method. Also, when the first calibration was applied (Figure 4.3), the lowest predicted HFN within a single kernel was always localised at the distal portion of the grains, while when the second equation was applied, only the germ portion had obviously lower HFN predicted values (Figure 4.4). The chemical images herein presented are derived from a quite poor model, therefore they are for illustrative purpose only.

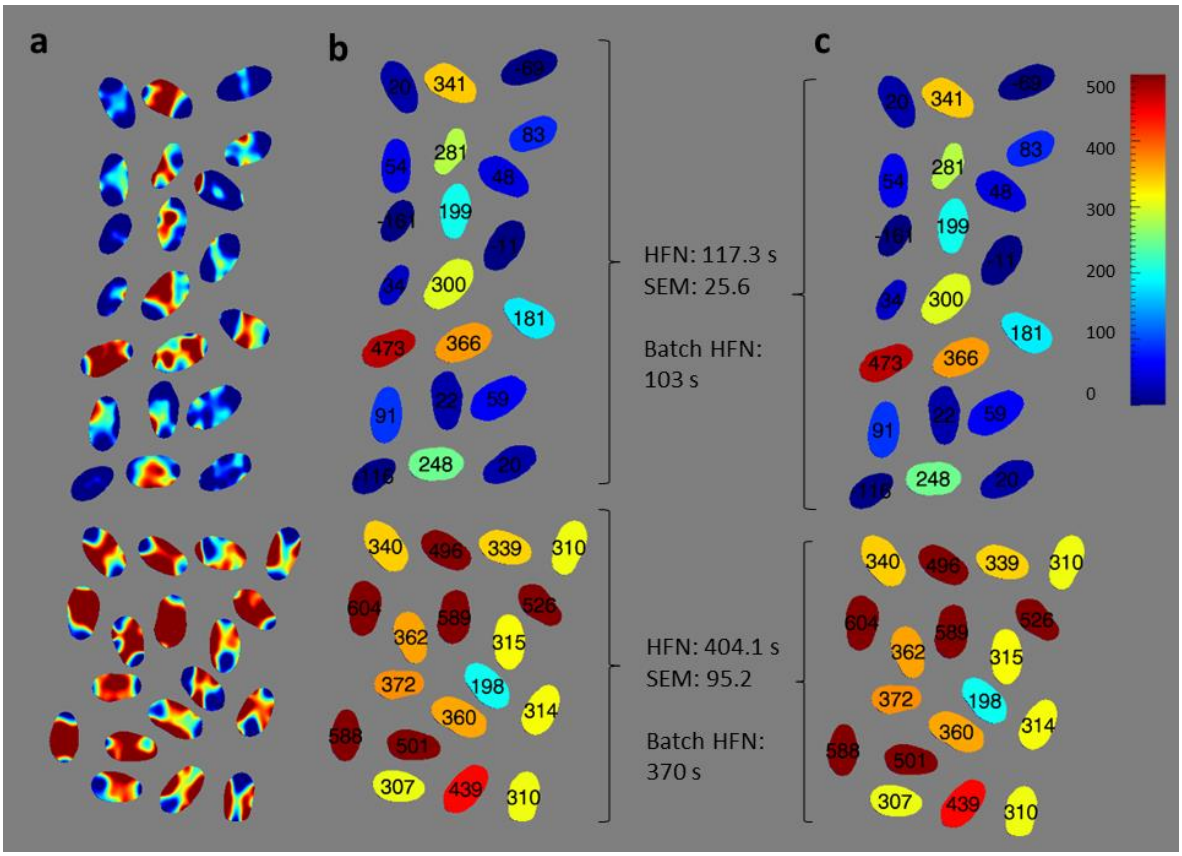


Figure 4.3. Application of a PLS models using second derivative pre-processing for HFN prediction on wheat kernels by HSI, by using two methods: a) pixel-by-pixel application of the calibration, and b) average calculation of the predicted HFN; c) application of the calibration on the mean NIR spectrum for each kernel. HFN: predicted value for the batch; SEP: Standard Error of Prediction; Batch HFN: reference measurement value. Numbers on wheat kernels indicate the predicted HFN (s). This chemical image is for illustrative purpose only.

The application of calibrations for bulk NIR instrumentation follows a different approach. Typically, a single spectrum is measured for a sample presented to the acquisition window, corresponding to a mean spectrum for that region of the sample, and is therefore closest to the second method in which calibrations are applied to mean spectra.

Therefore, the sequence of spectral processing should be taken into consideration when applying a PLS calibration on hypercubes, as it can have influence on the final predicted values. This influence depends on the spectral pre-treatments applied when building the calibration: in fact, linear methods such as convolutions do not lead to differences in the prediction, while differences were observed when the SNV pre-treatment was applied.

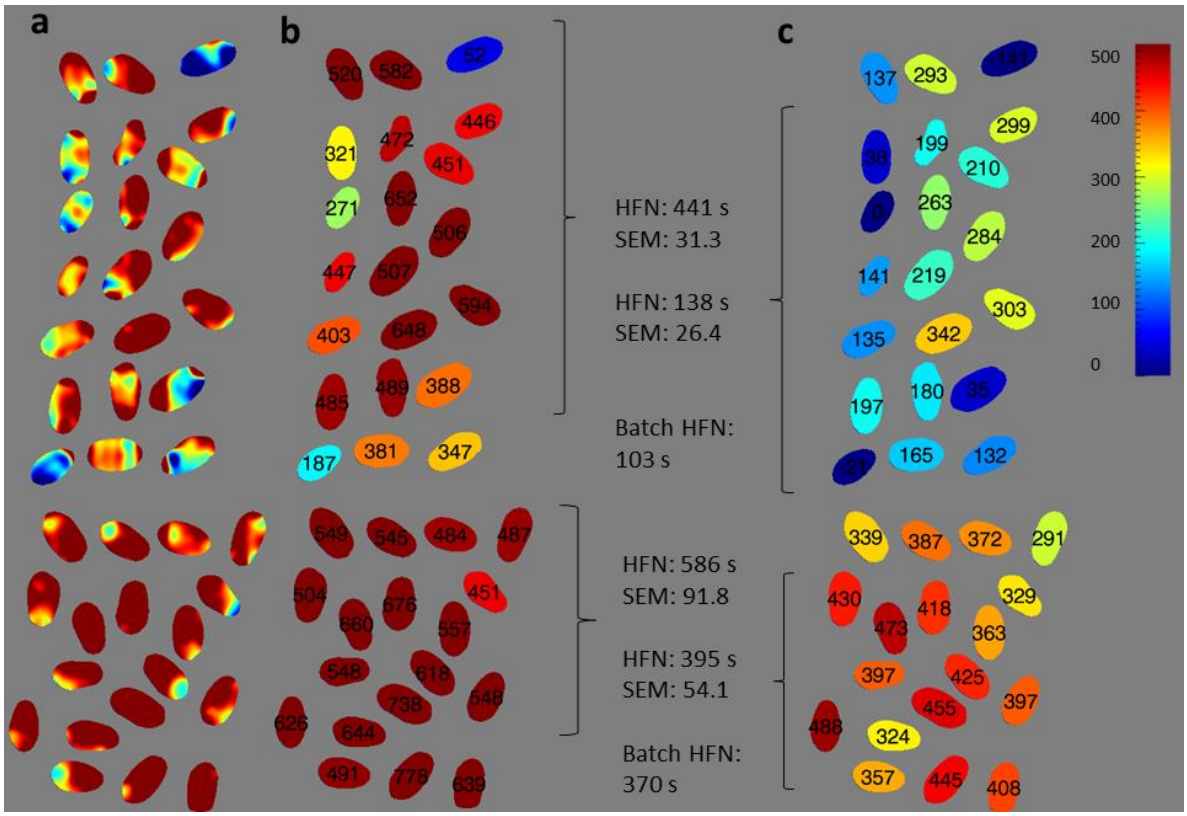


Figure 4.4. Application of a PLS calibration for HFN prediction on wheat kernels by HSI, using the two methods previously described, and a calibration where the SNV pre-processing was applied to two wheat batches with different HFN values; a) Pixel-by-pixel application of the calibration coefficients; b) second part of the method, average predicted HFN for each kernel (method 1); c) average spectrum calculation followed by application of the calibration coefficients (method 2). This chemical image is for illustrative purpose only.

The SNV method involves treating each spectrum by subtracting the mean log(1/R) over all bands and normalising by their standard deviation, resulting in a pretreated spectrum with mean of 0 and standard deviation of 1:

$$A'_i = \frac{A_i - \overline{A}}{\sigma} \qquad (9)$$

where A'_i is the corrected value, $\overline{A}$ is the mean of the band absorbances, and σ is their standard deviation. The effect of subtracting the mean is equivalent for both methods, but normalisation of each spectrum by its own standard deviation is not equivalent to normalisation by the overall standard deviation for all kernel pixels and bands. Being sensitive to noise, modifications of SNV have been proposed, e.g. using the median instead of the mean, or using the inner interquartile for mean and standard deviation calculations (Rinnan et al., 2009). This effect might be also

tested on other pre-processing techniques, e.g. multiplicative scatter correction (MSC) which is similar to SNV up to a simple rotation and offset correction. However, this is outside the scope of the present thesis. Further work is therefore needed for better understating of the optimal approach for application of PLS calibrations to hypercubes for prediction of the chemical composition of granular food commodities, and the effects for different pretreatments.

4.3.4. LDA for wheat classification related to sprouting problems

Linear Discriminant Analysis (LDA) was applied as a supervised method to classify between samples with high or acceptable HFN and those with excessively low HFN. As the PLS regression model did not result in particularly high performance for prediction of HFN values, this approach can be an alternative way to classify wheat samples for suitability for flour production.

The threshold to classify the dataset into two groups was set at a HFN value of 250 s, corresponding to the typical commercial specification for quality wheat, while also a lower threshold limit was set for grouping into "high" and "low" HFN, i.e. 150 s, which may be more relevant for identification of individual kernels that could contribute to an unacceptably low average value for a bulk sample. As shown in Figure 4.5, the LDA classification accuracy for the best models was 86.4% when the limit was 250 s, while it was 97.9% for the samples with very low HFN values (Table 4.3 reports the confusion matrix for these classification models). The plot shows Linear Discriminant values for each of the samples, with the axes representing the two categorical variables, i.e. high and low HFN. The classification was done by assigning the higher value to one of the two categories, and when a point is presented by two colours it indicates a misclassified sample.

Assuming that a low average value may be caused by a very limited number of damaged kernels, identification of these at a lower threshold may be useful for practical applications. Interestingly, the better classification performances were obtained in both cases using untreated spectra, and spectral pre-treatments did not result in better scores (data not shown). The performance of this classification might be accurate enough for practical applications in the food industry, and LDA classification might be an alternative to the PLS regression model, when the main aim is not to

predict the exact HFN value or α-amylase activity but to segregate kernels according to the quality set in terms of estimated HFN.

Several methods have been reported in the literature with the aim to classify cereal grains from NIR spectroscopy data. An alternative PLS-Discriminant Analysis (PLS-DA) model was reported by McGoverin et al. (2011) to distinguish between viable and non-viable proportions of the image and 61% of the variability in the viable/non-viable classifier was explained using six factors. The classification method was applied on each pixel of the kernels. The authors also used PLS regression as an alternative to PLS-DA, to predict the proportion of viable kernels or incubation time, in which case the obtained model was not sufficiently reliable, consistent with the results herein obtained.

Xing *et al.* (2009; 2010) applied alternative methods to predict α-amylase activity in wheat kernels, grouping samples into low, medium and high α-amylase activity. The ratio between log(1/R) at 878 and 728 nm was used to discriminate between sound and sprouted kernels, but the risk of misclassification is high. The authors applied a PCA on the hypercube and obtained a classification accuracy of 87.9% for severely sprouted kernels, whereas 64.5% of sprouted kernels were misclassified as sound (Xing, *et al.*, 2010).

Table 4.3. Confusion matrix for the LDA models built to classify sound wheat kernels from those with **(a)** low, or **(b)** very low HFN values.

a) 250 s as threshold		
	High	Low
High	254	28
Low	30	113
b) 150 s as threshold		
	High	Low
High	366	3
Low	6	50

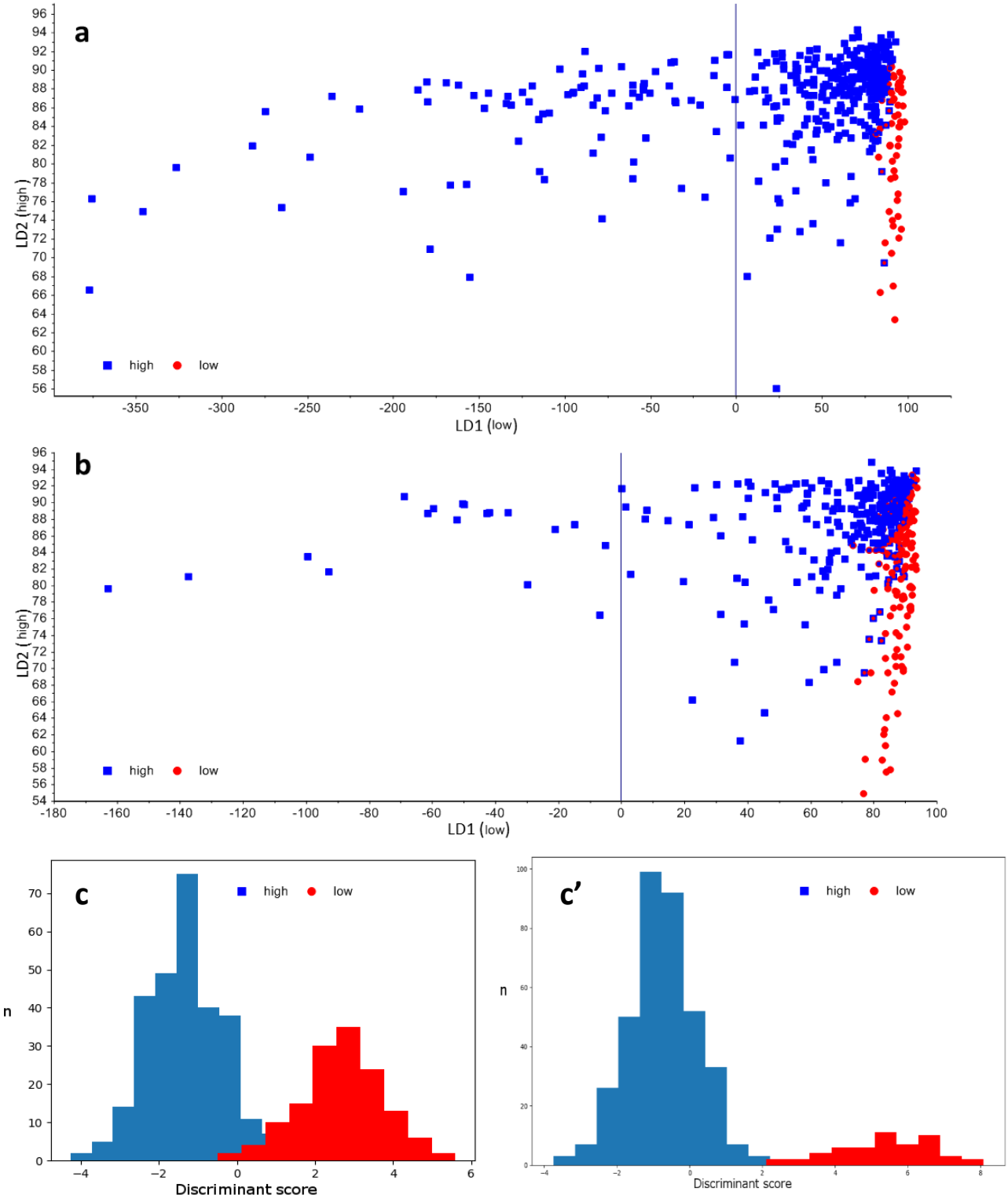


Figure 4.5. Linear Discriminant Analysis (LDA) plot for HFN classification of whole wheat kernels by HSI, setting a threshold of 250 s (a) and 150 s (b) to group into low- and high-HFN. Central colour of each point indicates reference classification, position and border colour indicate predicted NIR classification. LDA classification ability: 86.4% (a) and 97.9% (b). Histograms on transform scores are shown for the models built using (c) 250 and (c') 150 s.

In the present experiment, LDA was applied in order to classify the problematic kernels, i.e. those with low HFN values, from those with higher values. Whereas there might be a kernel-to-kernel variation, there is a strong effect of sprouted kernels on the average HFN value, and therefore the application of this classification method might help the food industry and breeders with non-destructive classification of whole wheat kernels.

4.4. CONCLUSIONS

The present chapter reported on the application of HSI for classification of pre-sprouted grains with excessive enzymatic activity, by directly scanning whole wheat kernels. An HSI calibration was built against the industry-standard HFN method, and it showed a calibration performance of R^2=0.60 (error ~50 s) and validation R^2=0.43 (error ~63 s) with samples showing HFN values in the range 62-318 s. These results compares favourably with previous studies using destructive bulk NIR analysis. Even better performance was obtained using classification models based on LDA instead of a PLS calibration. This suggests that an HSI method could be used to provide an effective, rapid, non-destructive assessment of the suitability of wheat sample HFN for flour production using a novel single kernel classification approach. A further application would be for classification of individual kernels for selection of breeding lines for sprout resistance.

Two approaches for application of calibrations were tested. It was shown that application of calibrations on a single pixel basis followed by calculation of mean values is equivalent to application of calibrations to mean kernel spectra when linear spectral pre-treatments are used for calibration development, while non-linear treatments such as SNV lead to obvious differences between these approaches.

5. COCOA COMPOSITION: LIPID CONTENT PREDICTION

5.1. INTRODUCTION

One of the most prominent quality factor for cocoa is its lipid content. Fat represents approximately half of the cocoa bean's weight and it is used to produce cocoa butter, which is one of the most valuable parts of the bean and therefore a strong influencer of its market price. Several methods are available for the analysis of fat content in food products. The Soxhlet extraction method is one of the most common, and is based on determination of crude fat gravimetrically, followed by solvent extraction. This method has been often reported to give lower results compared to other methods, such as those where digestion or hydrolysis is used. Indeed, bound fats or those naturally emulsified are not measured by Soxhlet. On the contrary, methods based on ether extraction tend to overestimate fat content. Other methods for fat analysis are based on acid hydrolysis, followed by saponification of the fats and esterification to give methyl esters of the fatty acids, which can be analysed by gas-chromatography. Despite the accuracy of this method, it is very time consuming, and involves the use of hazardous chemicals.

Rapid non-destructive techniques for the analysis of major food constituents include the use of Near-Infrared (NIR) spectroscopy, mid-infrared (MID) spectroscopy and Raman spectroscopy. However, these techniques do not give information on the spatial distribution of chemical constituents of the food. NIR spectroscopy has been proven to be effective for fat quantification in several food products including cocoa materials (Veselá et al., 2007; Vines, Kays, & Koehler, 2005). Kays et al. (2000) analysed a diverse set of cereal products by NIR spectroscopy, reporting a SECV=1.16% and R^2=0.98, using petroleum ether extraction as the reference method.

Previous literature using NIRS for the analysis of total fat in cocoa beans scanned the samples as ground material, thus only the average fat content was predicted. For example, Fourier-Transform NIR (FT-NIR) has been successfully applied in the spectral region 10,000-4,000 cm^{-1} to predict the total fat content in ground shelled cocoa beans (i.e. ground cocoa nibs) (Teye & Huang, 2015). The fat content ranged from 51.3 to 68.0%; the calibration and prediction R^2 values were 0.93-

0.98 and 0.92-0.97, respectively, depending on the different PLS regression models used. The prediction error was RMSECV=0.01-0.02% and RMSEP~0.02%. Fifty samples were used for the calibration dataset and 30 for the prediction (Teye & Huang, 2015). Despite the good calibration performance, no information on the bean-to-bean variability was reported, and more importantly, it should be noticed that this method still requires the removal of the cocoa bean shell and grinding of the resulting nibs to the required dimensions.

Other researchers compared NIR and FT-IR (1100-2500 nm and 2500-160,000 nm, respectively) for the prediction of fat, nitrogen and moisture content in cocoa powder. Fat content exhibits a wide range, i.e. 2.4-22.0% as expected, as cocoa powder is made by grinding cocoa nibs and removing some of the fat. The NIR prediction model for this constituent achieved R^2=0.96 and RMSECV=7.0%. By FT-IR, the prediction model had R^2=0.94 and RMSECV=10.4% (Veselá et al., 2007).

NIRS has also been reported to predict total fat content in shelled cocoa beans by Álvarez et al. (2012). The authors applied reflectance spectroscopy in the region 780-2500 nm to evaluate fat, caffeine, theobromine and epicatechin content. On a fat content ranging from 46 to 64%, the R^2 value was 0.94, SECV=0.89%, and RPD=3.4. Additionally, the fat content of Criollo types was generally reported to be lower than other cocoa types like Forastero and Trinitario (Álvarez et al., 2012).

The only paper found in the literature on whole cocoa beans analysis using FT-NIR has been reported by Sunoj et al. (2016). FT-NIR (800-2778 nm) was used to scan whole cocoa beans obtained from one batch fermented at different fermentation times, from 1 to 6 days. Prediction models were built for polyphenol content, pH and fermentation index using PLS regression. However, no indication on fat content was reported.

Despite the efforts on building prediction models for important quality attributes of cocoa, the traditional NIR instruments and the approach used so far are not capable of investigating single cocoa bean variability and rapidly predicting fat content in a non-destructive way. Moreover, and

more importantly, the existing NIR approach requires cocoa beans to be unshelled and ground, which is a time consuming manual process.

The use of HSI for fat prediction in grains, nuts or seeds (and especially for single objects) has received little attention to date. In a recent study, Jin et al. (2016) applied HSI using two detectors, working at 400-1000 and 1000-2500 nm spectral ranges, for quantification of oil content in single peanuts. The authors used five varieties, sampling 30 beans per batch. The performance of the PLS regression models had prediction R^2 values of 0.696-0.923, depending on the spectral pre-treatment. The prediction error (RMSEP) was between 0.416 and 0.208 %.

No previous studies have been conducted on the use of HSI for non-destructive prediction of whole cocoa bean composition. Furthermore, there are currently no reports in using HSI-based methods for determining the distribution of fat content within single cocoa beans. Therefore, the aim of the present work was to investigate the feasibility of HSI to non-destructively analyse unshelled and shelled cocoa beans on a single bean basis in order to predict total fat content and its intra-bean distribution.

5.2. MATERIALS AND METHODS

5.2.1. Samples and reagents

Seventeen samples of commercial cocoa beans were obtained, which represented all the major and some minor cocoa producers. Ten beans were randomly selected from each of the 17 batches, and analysed by HSI without any further treatment. The full experimental design is illustrated in Figure 5.1, while the list of samples is reported in Table 5.1.

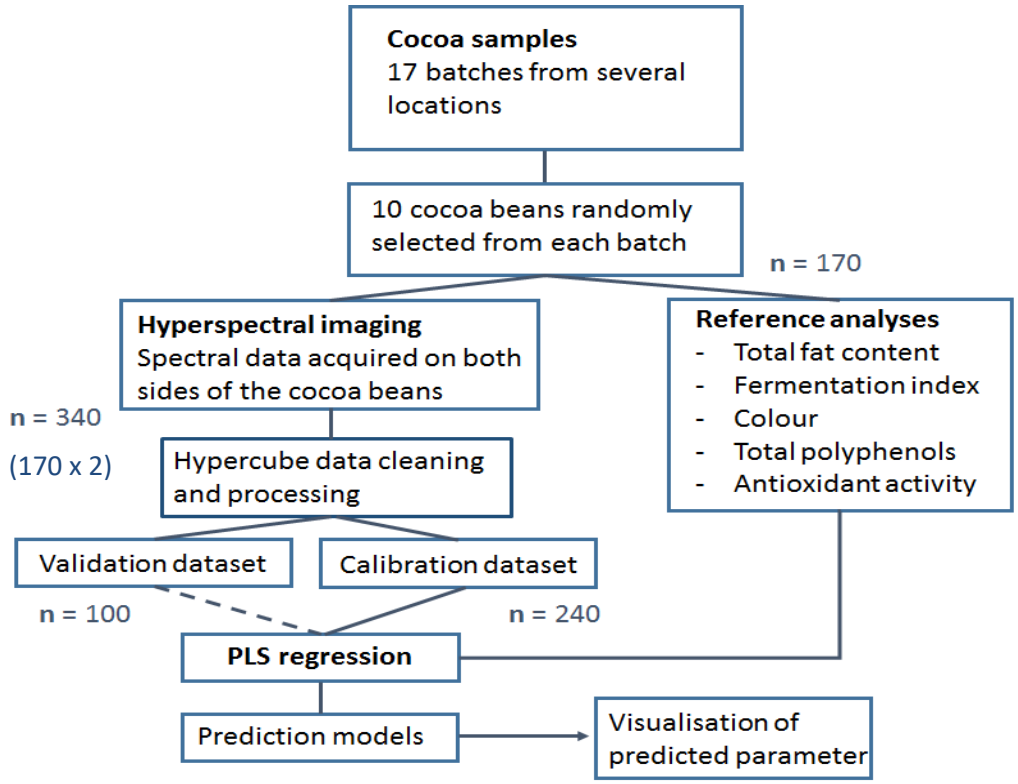


Figure 5.1. Flow chart of the experimental design used for the non-destructive prediction of cocoa bean quality. n=170 refers to the number of beans, while the other numbers indicate the mean spectra (2 spectra per bean).

Table 5.1. List of commercial cocoa samples used in the present Chapter and in Chapter 6.

Sample	Country	Continent	Type / origin of cocoa
1	Unknown		
2	Ghana	Africa	Forastero (Amazon hybrids / Amelonado)
3	Indonesia	Asia	Forastero / Trinitario
4	Ivory Coast	Africa	Forastero (Amazon hybrids / Amelonado)
5	Nigeria	Africa	Forastero (Amazon hybrids / Amelonado)
6	Ecuador	America	Trinitario (also some Arriba Nacional original types)
7	Cameroon	Africa	Trinitario
8	Ivory Coast	Africa	Forastero (Amazon hybrids / Amelonado)
9	Ghana	Africa	Forastero (Amazon hybrids / Amelonado)
10	Brazil	America	Forastero / Amelonado
11	Ecuador *	America	Trinitario (also some Arriba Nacional original types)
12	Ivory Coast	Africa	Forastero (Amazon hybrids / Amelonado)
13	Venezuela	America	Trinitario, possibly some Criollo
14	Mexico	America	Trintario?, possibly some Criollo
15	Ghana	Africa	Forastero (Amazon hybrids / Amelonado)
16	Ecuador	America	Trinitario (and possiblt Arriba Nacional)
17	Nigeria	Africa	Forastero (Amazon hybrids / Amelonado)

(*) Batch of under-fermented beans.

5.2.2. Hyperspectral imaging analysis

A SWIR HSI system described in Section 3.3 was used, by mapping the final 240 detector bands (the first 15 bands were excluded). Samples of single cocoa beans were analysed by HSI unshelled (i.e. whole, as received) or shelled unground beans (i.e. cotyledons or nibs; please refer to the figure A.2 in the Appendix showing the cocoa bean microstructure). Ten cocoa beans at a time were placed on a movable plastic stage and scanned using the push-broom approach. Details on the instrument, image acquisition, processing and hypercube data management have been previously described in this thesis (Section 3.2). Each cocoa bean was scanned on both sides, so that the final number of average spectra for the prediction models was 340. Cocoa beans were manually de-shelled and scanned again by HSI. They were then individually ground using a manual mortal, yielding approximately 1 g material for each bean. The samples were then stored at -20 °C, in readiness for reference analyses. The average spectra for each cocoa bean were exported for statistical analysis.

5.2.3. Total fat analysis

Fat content was assessed using an NMR-based system, which is routinely used to analyse food products. Single cocoa beans were manually shelled and stored at -20 ºC at least one hour to obtain fat crystallisation. The ground material was analysed by a CEM Smart Trac II Moisture and Fat analyzer (CEM Microwave Technology Ltd., Buckingham, UK). The instrument has a resolution of 0.01%, a fat range from 0.01% to 99.99% and a balance with 0.1 mg readability. Fat content was either expressed on wet basis, or on a dry matter basis (dmb), by calculating it through the CEM microwave moisture analyser.

To verify the accuracy and repeatability of the method, one batch of ground cocoa bean was analysed in 10 replicates. The analytical error, expressed as standard deviation for 10 replicated measurements (SD) was 0.81% (wet), with a coefficient of variation (CV) of 1.19%.

5.2.4. Colour measurement

The colour of individual unshelled cocoa beans and of ground cocoa nibs was determined using the DigiEye (VeriVide, Leicester, UK). Colour of in-shell cocoa beans and cocoa nibs (as ground)

was assessed for each seed within the CIE L* a* b* colour space. Samples were placed in the DigiEye chamber under constant light conditions and colour measurements were analysed using the provided software. The instrument was calibrated for white balance and uniformity, as well as for the colour using a calibrated colour chart. The images were acquired on both sides of the in-shell beans and the average colour was calculated, while one picture was taken for the ground material (Figure 5.2).

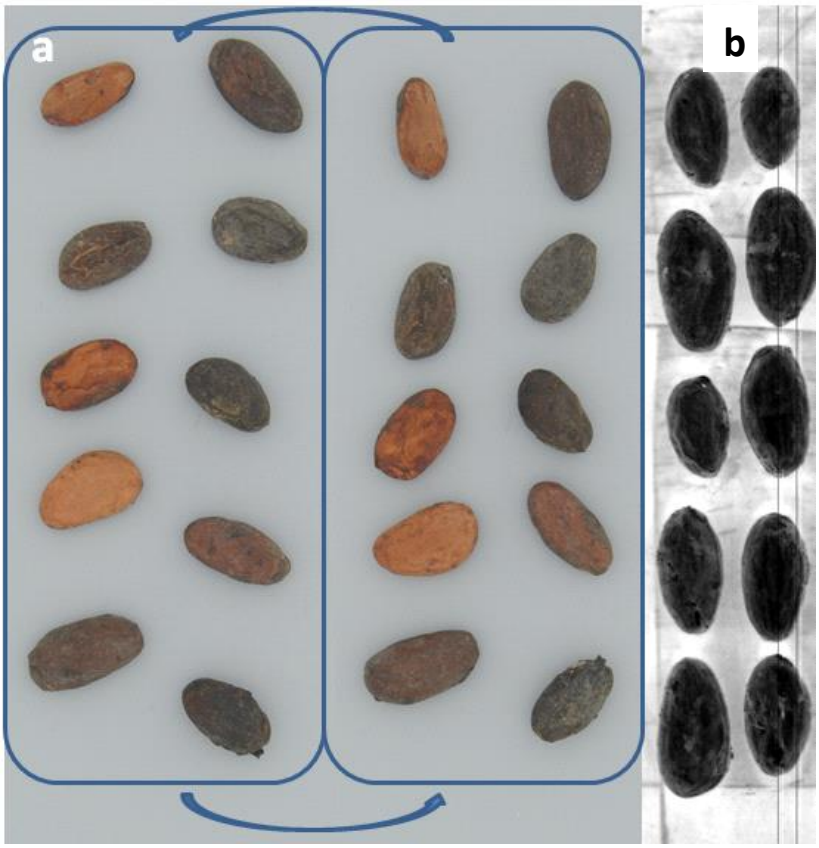


Figure 5.2. Example of **a**) pictures acquired by DigiEye for cocoa bean (in-shell) obtained on both sides and **b**) reflectance image for the same cocoa beans scanned by HSI (showing at band 40, ~1200 nm).

5.2.5. Data treatment and statistical analysis

The spectral data exported for single cocoa beans (whole, i.e. 'in-shell' and shelled) were analysed using the Unscrambler 10.3 software (CAMO, Norway). Spectra acquired from two sides of each cocoa bean (whole and shelled) were randomly split into calibration and validation datasets, using a 70:30 ratio, and making sure that spectra from the same bean were all included in either the calibration or validation set. PLS regression calibrations were evaluated based on the coefficient

of determination (R^2) and the root mean square error of calibration (RMSEC), cross validation (RMSECV) and prediction (RMSEP), as well as using the Ratio to Performance Deviation (RPD), which is defined as the ratio between the measured standard deviation and the prediction error.

5.2.6. Visualisation of chemical images

Once established, the best PLS regression prediction model was applied to the hypercubes, by exporting and using the weighted beta-coefficients. The calibration was applied in two ways; at single pixel level, by multiplying the beta-coefficients for each spectral band of each pixel, and at single bean level, by applying the regression coefficients to the average spectrum of each cocoa bean. In this way, visualisation of fat distribution across the bean can be obtained, and also a predicted average fat content. The second strategy is likely to be more convenient for practical application, while the first one is more of scientific interest because it gives understanding of the possible accumulation of a cocoa constituent across the beans, thus allowing also plant physiology and biochemical studies. The obtained images are termed "chemical images", which are graded colour images in which the colour indicates the abundance of an attribute, i.e., fat content in the present case.

5.3. RESULTS AND DISCUSSION

5.3.1. Reference analysis of fat content analysis

A preliminary objective was to investigate the natural variability of fat found in single fermented dried cocoa beans. A wide range of lipid content value was found in the whole dataset, but also an interesting wide variation of fat content was observed within batches, for which 10 beans were analysed (Figure 5.3). In rare cases, the fat content was very consistent within batches, e.g. for the batch of Mexican cocoa the fat range was below 40% (wet), while in the majority of batches the variability was wide, with the maximum variability observed in one batch from Ivory Coast, attaining approximately 25% of the overall range. The observed variability is likely to be due to the interaction between genetics and environment, and great influence is likely to be attributed to the post-harvest conditions, particularly the fermentation and drying steps. Even batches from the same origin, for example from Ivory Coast, had different fat distribution. The median of fat

content among the three batches of Ivory Coast was almost identical, with very similar average fat content, while their range varied dramatically. This could be due to the different handling of the fermentation process in the three farms, or the use of different agronomical conditions that might lead to higher or lower variability in terms of lipid accumulation in the beans. It should also be recognised that these are commercial samples and, especially in the case of Ivory Coast beans, it is likely that mixing or blending has occurred within the supply chain. Table 5.2 shows the descriptive statistics of all the parameters analysed, i.e. fat content expressed on web basis and on a dry matter basis (dmb), as well as the colour parameters assessed on the in-shell and the shelled ground nibs.

Table 5.2. Descriptive statistics for fat content and colour parameters in single cocoa bean levels.

Calibration dataset (n=119 beans)								
	Fat (% wb)	Fat (% dmb)	Unshelled			Shelled		
			L*	a*	b*	L*	a*	b*
Average	55.38	57.94	40.92	10.95	10.46	37.18	10.96	8.89
SD	6.06	6.07	5.43	5.32	5.96	4.55	2.03	3.42
Max	67.54	69.1	54.1	22.83	27.67	51.59	15.88	16.74
Min	40.26	42.33	27.98	0.89	2.06	24.77	5.28	-0.73
Validation dataset (n=51 beans)								
	Fat (% wb)	Fat (% dmb)	Unshelled			Shelled		
			L*	a*	b*	L*	a*	b*
Average	55.14	57.73	41.07	11.03	10.32	36.06	11.58	8.98
SD	5.72	5.7	5.55	5.11	6.02	4.65	2.51	4.04
Max	66.87	69.96	54.05	22.72	27.65	51.48	17.77	22.61
Min	34.62	36.71	31.87	1.26	2.12	28.68	5.46	1.62

The calibration and independent validation datasets are shown separately, and a similar range and standard deviation was observed between the two groups, with slightly higher SD for fat content for the calibration dataset, but no statistical significant difference was obtained from t-test (data not shown). The fact that the range of fat content for the validation dataset is within the calibration range is desired, and theoretically this should happen also for new samples that will be scanned in the future from new sources, new harvesting years, etc. However, generally, from a practical point

of view, NIR and HSI calibrations are intended to be periodically updated with new samples so that new varieties or unexpected samples are correctly classified or quantified.

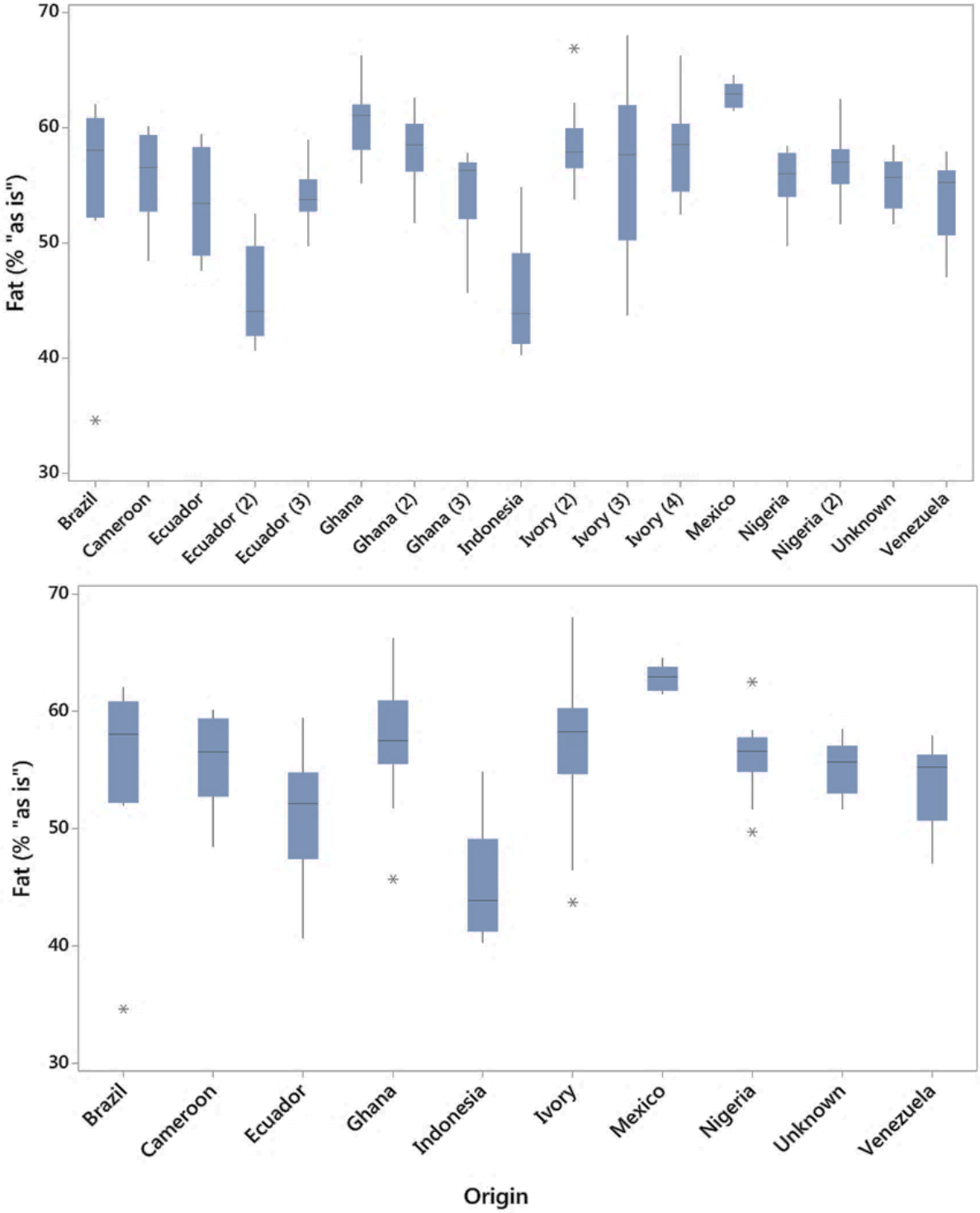


Figure 5.3. Variability of total fat in single dry cocoa nibs, expressed on wet basis for 1) each batch (n=10), or 2) grouped by geographical origin.

5.3.2. HSI for fat content prediction

PLS regression models for total fat content were built both from whole, "in-shell", beans and from whole nibs, after appropriate treatment of the information in the hypercubes. The results of these prediction models for whole cocoa nibs are reported in Table 5.3 and Table 5.4. When the model was built on reference data wet, the use of spectral pre-treatment caused very slight improvement in the prediction models, from R^2=0.81 to 0.83. However, a larger difference was observed for the cross-validation and the external validation datasets, where the use of log(1/R) spectra showed worse results in terms of R^2 and prediction errors. Multiple scatter correction (MSC) and standard normal variate (SNV) had similar prediction performance, as expected, as both are intended to remove light scattering effects. Derivatives also showed good performance, with the first derivative treatment model resulting in a slightly lower prediction error. However, MSC treatment led to the model with the best performance and the highest ratio to performance deviation (RPD), with both cross-validation and prediction R^2=0.843-0.841. Both RMSECV and RMSEP were below 2.3% (wb). Considering the range of natural variability observed even within the same batch, often being 10-20%, an error of approximately 2% for a single bean fat determination is acceptable for screening purposes and sorting of higher/lower fraction.

Similarly, the prediction on dry matter basis (dmb) achieved a good level of performance, with slightly worse R^2 values and slightly higher calibration and prediction errors than the prediction made on fat content expressed on a wet basis. This difference might be due to the incomplete drying of samples using the CEM instrument, which is based on microwave drying. While the fat analysis is based on NMR, which is very accurate in analysing fats, moisture is obtained gravimetrically and the error was likely to be higher as the sample size was very small.

The SNV spectral treatment gave the best prediction model for fat content expressed as dmb, with calibration and prediction R^2 of both 0.829.

This demonstrates robustness of the model and reliability for future applications on unknown samples. The cross-validation and prediction errors were approximately 2.5 and 2.4% (dmb), respectively. Generally, this performance allows the application of the calibration for screening purposes and to estimate single-bean fat content. In some cases, this prediction error is

comparable to traditional methods for fat content analysis. For example, the AOAC method 922.06 for fat content through acid hydrolysis has SD ranging from 0.7 to 7.5%, depending on the type of food analysed. Therefore, the method presented here is perfectly acceptable even for quantification purposes, especially given its advantages for 1) single bean analysis; 2) non-destructive measurement; 3) rapidity and 4) operator skill levels with no hazardous chemicals.

The performance of total fat content in unshelled cocoa beans is reported in Table 5.4. For this model, the whole beans were scanned before any treatment. Poor performance was observed compared to the shelled beans. The best model was the one using the 2nd derivative pre-treatment, and it showed R^2=0.62 and 0.52 for the calibration and prediction datasets, respectively. The prediction RPD value was 1.41, thus indicating poor quality for using this model for quantification purposes. However, it could still be potentially applied for general screening purposes. The calibration error was 3.6%, while the external prediction error was 4.0%. This value might appear relatively high when compared to traditional methods for fat content analysis, but the HSI model herein presented has practical applicability. Even 4% of prediction error might be acceptable considering that in many of the batches, the single bean variability was above 15%. Thus, using HSI would allow identification of seeds with the highest and lowest fat content in a rapid inexpensive way at the reception before any processing step.

Figure 5.4 shows the predicted fat content in shelled and unshelled cocoa beans for the best prediction models, while Figure 5.5 reports the β-coefficients for these fat quantification models for the shelled beans and Figure 5.6 shows the models for in-shell beans. The best models using whole cocoa nibs used SNV as the spectral pre-treatment, while the model built on unshelled cocoa beans used 2nd derivative treatment. The wavelengths at 1107, 1212, 1302, 2057, 2145 and 2295 nm were among the most influential ones for the whole cocoa nib models. The beta-coefficients were very similar when the models built on wet basis or on dry matter basis. Slight differences were observed around 1940 nm, where the O-H bond absorbs strongly. On the contrary, fat prediction model from whole unshelled cocoa beans had major peaks at 1390, 1900-1994, and 2270-2326 nm.

Table 5.3. Performance of PLS regression models for total fat content in shelled single cocoa beans (nibs). RMSE = root mean square error of calibration, cross-validation or prediction. RPD = ratio to performance deviation, calculated as the ratio between the reference standard deviation and the RMSECV or RMSEP. MSC = multiplicative scatter correction. SNV = standard normal variate. Values for the error are indicated as percentage (%, on wb or dmb). 238 samples (average spectra) used for calibration, 102 for validation. The same LV was used for calibration, cross-validation and validation models.

a) Wet Basis	**LV**	**Calibration**		**Cross-Validation**		**Validation**		**RPD_{CV}**	**RPD_P**
		R_c^2	**RMSEC**	**R_{cv}^2**	**RMSECV**	**R_p^2**	**RMSEP**		
Log(1/R)	6	0.810	2.639	0.781	2.780	0.769	2.785	2.18	2.05
Normalisation	7	0.809	2.710	0.798	2.718	0.824	2.385	2.23	2.40
MSC	6	0.829	2.505	0.842	2.286	0.841	2.273	2.65	2.52
1st derivative	5	0.814	2.609	0.814	2.425	0.809	2.486	2.50	2.30
2nd derivative	6	0.813	2.620	0.811	2.573	0.799	2.552	2.35	2.24
Standard Normal Variate	6	0.829	2.503	0.843	2.313	0.841	2.274	2.62	2.51
SNV+1st derivative	6	0.840	2.440	0.806	2.680	0.827	2.359	2.26	2.42
b) Dry Matter Basis	**LV**	**Calibration**		**Cross-Validation**		**Validation**		**RPD_{CV}**	**RPD_P**
		R_c^2	**RMSEC**	**R_{cv}^2**	**RMSECV**	**R_p^2**	**RMSEP**		
Log(1/R)	5	0.821	2.563	0.773	2.833	0.800	2.543	2.14	2.24
Normalisation	7	0.822	2.579	0.840	2.316	0.795	2.534	2.62	2.25
MSC	5	0.825	2.555	0.801	2.686	0.828	2.353	2.26	2.42
1st derivative	5	0.810	2.651	0.791	2.602	0.791	2.594	2.33	2.20
2nd derivative	6	0.811	2.657	0.785	2.826	0.782	2.653	2.15	2.15
Standard Normal Variate	6	0.825	2.553	0.816	2.452	0.828	2.355	2.47	2.42
SNV+1st derivative	5	0.840	2.440	0.813	2.617	0.827	2.359	2.32	2.42

Table 5.4. Results of PLS regression models for **a**) total lipid content in unshelled single cocoa beans (calibration, n=238; validation, n=102), as well as colour prediction in **b**) shelled and **c**) unshelled cocoa beans.

A - Fat in unshelled bean (% wet basis)										
			Calibration		**Cross-Validation**		**Validation**			
	Pre-treatment	**LV**	**R_c^2**	**RMSEC**	**R_{cv}^2**	**RMSECV**	**R_p^2**	**RMSEP**	**RPD_{CV}**	**RPD_P**
	Log(1/R)	9	0.525	4.006	0.446	4.340	0.247	4.940	1.40	1.16
	MSC	4	0.388	4.738	0.324	5.001	0.169	5.187	1.21	1.10
	1st derivative	8	0.652	3.441	0.504	4.098	0.299	4.801	1.48	1.19
	2nd derivative	6	0.623	3.581	0.491	4.182	0.519	4.060	1.45	1.41
	SNV+1st derivative	6	0.540	3.753	0.421	4.224	0.195	5.110	1.43	1.12
B - shelled beans for internal colour										
			Calibration		**Cross-Validation**		**Validation**			
Parameter	**Pre-treatment**	**LV**	**R_c^2**	**RMSEC**	**R_{cv}^2**	**RMSECV**	**R_p^2**	**RMSEP**	**RPD_{CV}**	**RPD_P**
	Log(1/R)	11	0.512	3.126	0.464	3.287	0.418	3.660	1.38	1.27
L*	1st derivative	9	0.437	3.453	0.382	3.598	0.375	3.778	1.26	1.23
	2nd derivative	12	0.516	3.147	0.418	3.435	0.361	3.806	1.32	1.22
	Log(1/R)	11	0.276	1.885	0.200	1.987	0.286	2.171	1.02	1.15
a*	1st derivative	9	0.303	1.841	0.231	1.939	0.356	2.062	1.05	1.22
	2nd derivative	12	0.260	1.876	0.113	2.060	0.423	1.952	0.99	1.28
	Log(1/R)	11	0.436	2.513	0.344	2.695	0.254	3.470	1.27	1.16
b*	1st derivative	9	0.429	2.686	0.348	2.889	0.377	3.173	1.18	1.27
	2nd derivative	12	0.344	2.804	0.195	3.119	0.447	2.988	1.10	1.35

Table 5.4 (*continued*)

C - unshelled beans for external colour

Parameter	Pre-treatment	LV	Calibration (n=238)		Cross-Validation		Validation (n=102)		RPD_{CV}	RPD_P
			R_c^2	RMSEC	R_{cv}^2	RMSECV	R_p^2	RMSEP		
L*	Log(1/R)	9	0.336	4.440	0.203	4.895	0.389	4.319	1.11	1.29
	SNV	14	0.512	3.765	0.385	4.249	0.491	3.928	1.28	1.41
	1st derivative	12	0.577	2.527	0.498	3.857	0.417	4.221	1.41	1.32
	2nd derivative	11	0.563	3.602	0.464	4.004	0.403	4.272	1.36	1.30
a*	Log(1/R)	9	0.694	2.937	0.581	3.413	0.678	2.886	1.56	1.77
	SNV	14	0.752	2.589	0.693	2.906	0.524	3.419	1.83	1.50
	1st derivative	**12**	**0.770**	**2.517**	**0.732**	**2.728**	**0.720**	**2.693**	**1.95**	**1.90**
	2nd derivative	11	0.734	2.703	0.680	2.975	0.631	3.094	1.79	1.65
b*	Log(1/R)	9	0.673	3.400	0.505	4.217	0.63	3.641	1.41	1.65
	SNV	14	0.716	3.174	0.651	3.538	0.552	3.986	1.68	1.51
	1st derivative	**12**	**0.757**	**2.945**	**0.710**	**3.226**	**0.678**	**3.399**	**1.85**	**1.77**
	2nd derivative	11	0.742	3.029	0.672	3.423	0.617	2.704	1.74	2.22

The most important absorption wavelengths resulting from the regression equation reported by Vaselá et al. (2007) for fat prediction in cocoa powder by traditional NIRS were those at 1728-1744, 2308-2322, 2334-2348 nm. The results herein presented are thus in agreement with previous literature, as observed here some influence of the bands around 1700 and 2300 nm; however, they are not the most intense one for the fat prediction model. The calibration herein presented cannot be directly compared to previous literature, as they used cocoa powder, with fat content ranging from to 5 to~23% rather than cocoa nibs. In addition, despite the good R^2 value (0.96), the cross-validation error was 7.0%. Literature is very scarce or non-existent in relation to the application on HSI for qualitative or quantitative prediction of cocoa bean quality of composition, chocolate or other cocoa products. Conventional NIRS has been applied in previous studies to evaluate other parameters in this product, for example sucrose content in chocolate mass (da Costa Filho, 2009). Whitacre et al. (2003) successfully predicted the procyanidins content in cocoa liquor by using NIR spectroscopy in the range 700-2500 nm. Other authors applied FT-NIR spectroscopy for classification purposes, so that differentiation of ground cocoa beans from different regions within Ghana was possible (Teye et al., 2013). FT-NIR spectroscopy has also been reported more recently for fat quantification in cocoa beans, also acquired as ground samples, showing excellent prediction performance (Teye et al., 2013). A similar technique was applied by Sunoj et al. (2016), and Teye et al. (2015) for the prediction of fermentation index, pH and polyphenols in cocoa beans, scanned as ground material.

Previous authors using HSI for fat measurement in single peanut kernels scanned samples individually by placing only one kernel at a time on the mobile platform (Jin et al., 2016), while in this study a program was written in IDL+ENVI to manage hypercube processing in a more efficient manner. In this way, several kernels can be scanned together and contained in the same hypercube. Based on the kernel position in the image, the program was able to attribute a sample number in order to track them individually and export the mean spectra automatically. Previous fat calibration for single peanut kernels demonstrated that the use of spectral range 1000-2500 nm over the region 400-1000 nm leads to dramatic improvements in the prediction. Indeed, using the

visible region led to R^2 values of 0.536-0.696, depending on the spectral pre-treatment. Using the longer wavelength region, the prediction models had R^2 values of 0.536-923 (Jin et al., 2016).

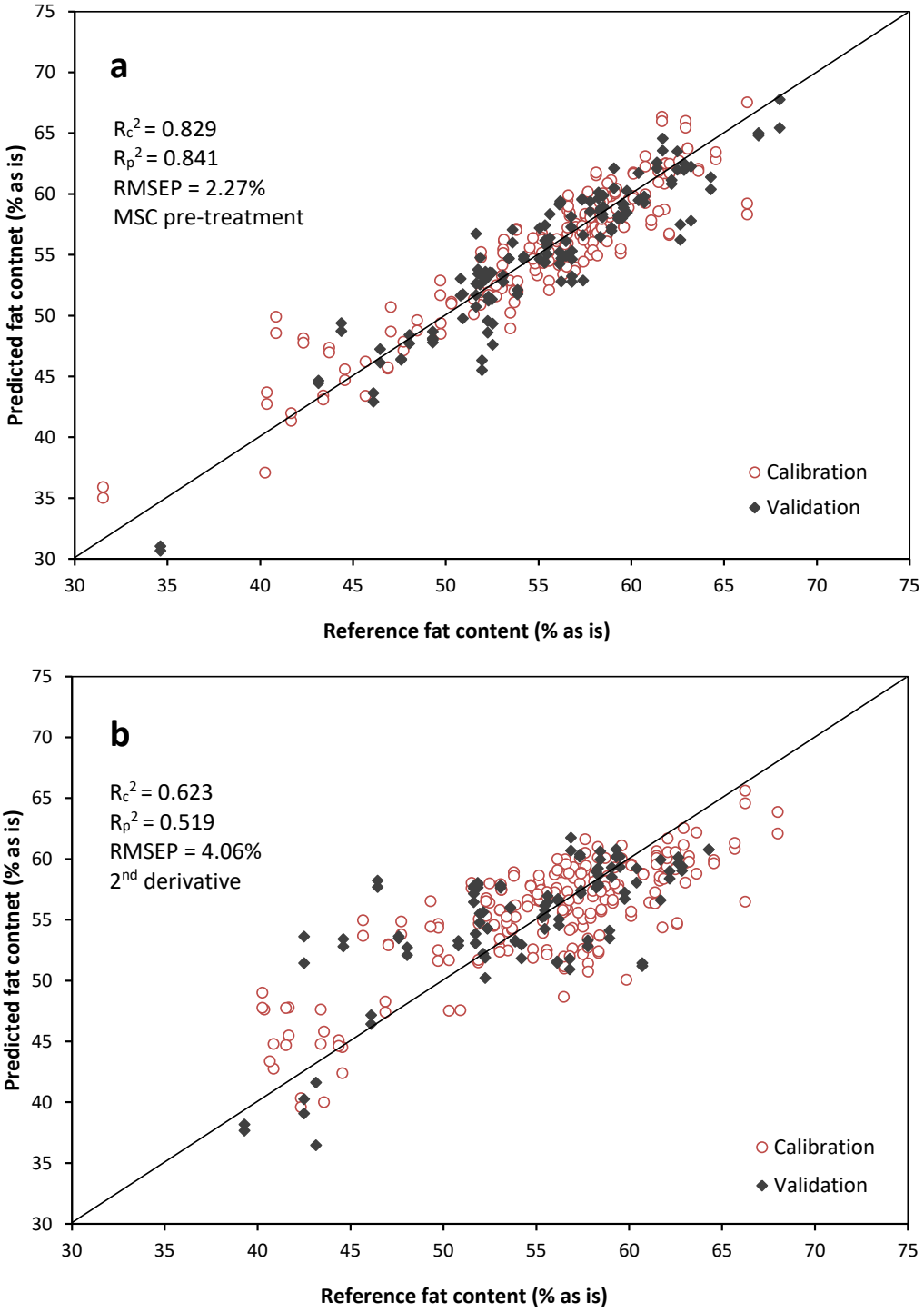


Figure 5.4. Predicted vs Reference values of fat content in **a**) whole shelled cocoa beans (nibs), and **b**) unshelled cocoa beans, using the best HSI prediction models.

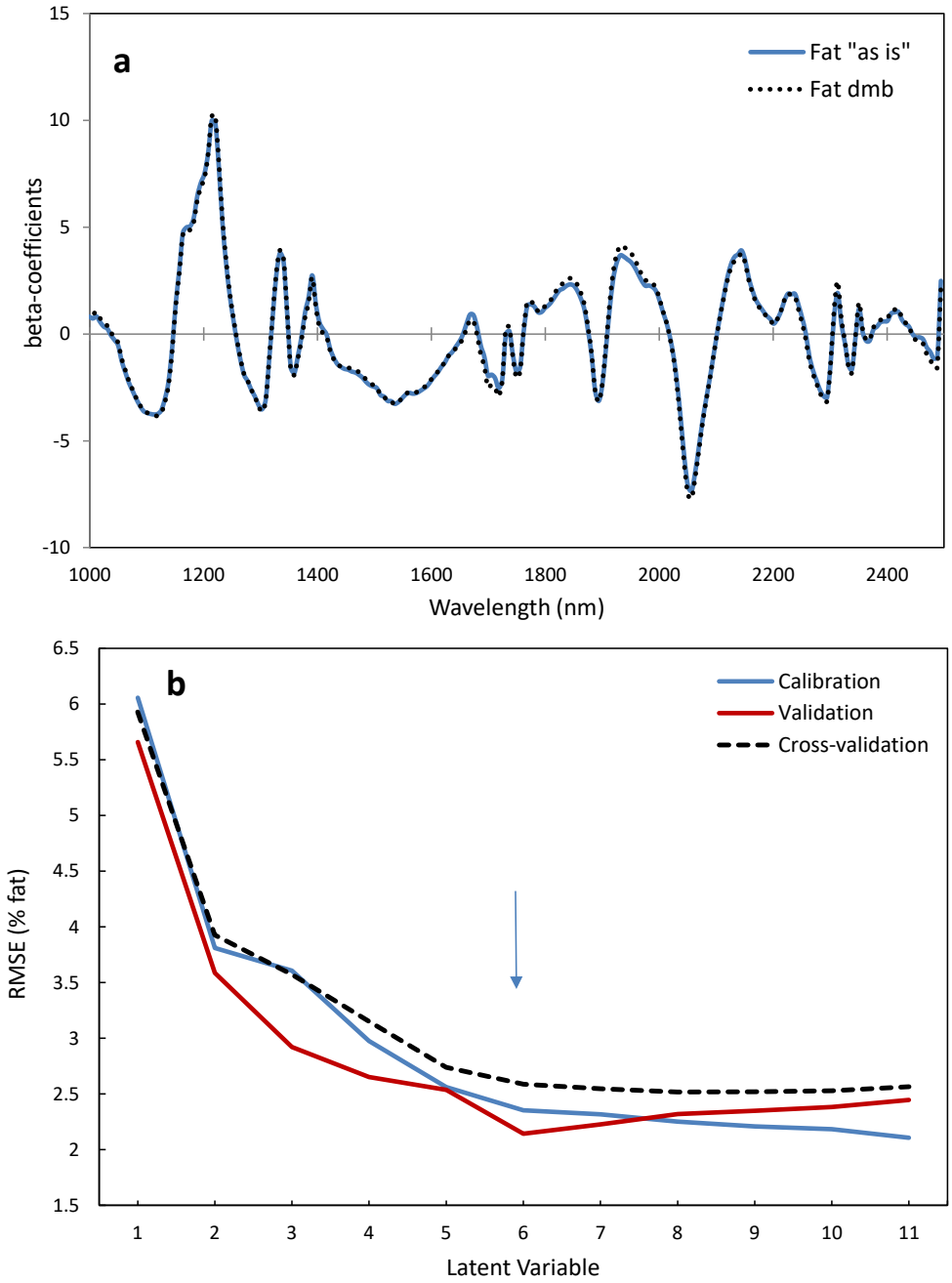


Figure 5.5. PLS regression model for fat prediction by HSI in single shelled cocoa beans. **a**) Regression coefficients for fat expressed on wet or dry matter basis. **b**) Latent Variable plot to express the calibration, cross-validation and external prediction error (RMSE). Models use MSC spectral pre-treatment.

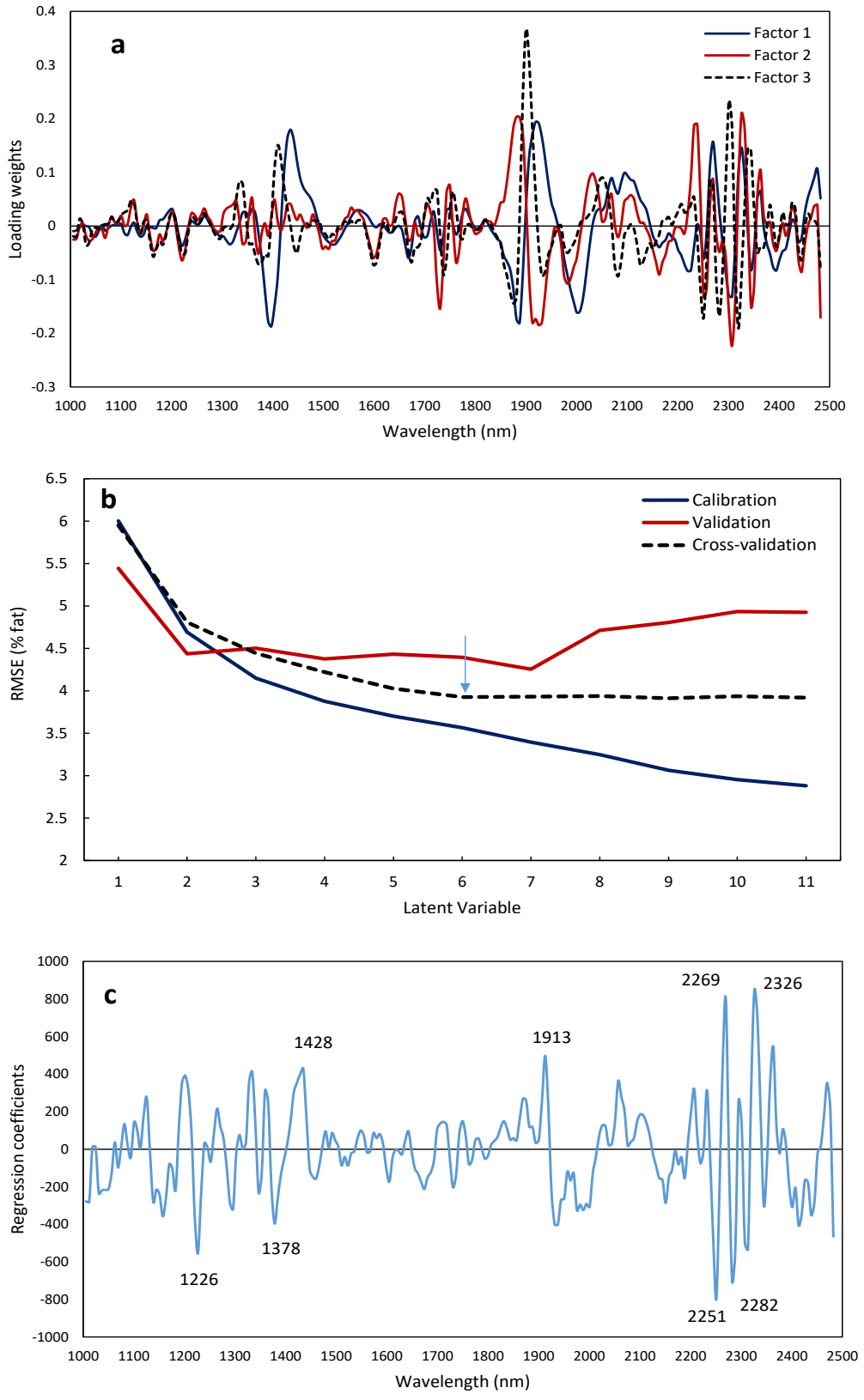


Figure 5.6. HSI fat prediction model on in-shell single cocoa bean, with indication if the (a) loading plot of the first 3 Principal Components, (b) prediction error (RMSE) depending on the Latent Variable showing the selected LV, and (c) regression coefficient plot. Numbers indicate the wavelength in nm.

5.3.3. Wavelength selection for multi-spectral imaging systems

For applications especially at the industrial level, a multispectral imaging system could be preferred due to the lower price and higher computational speed required. Thus, starting from the full spectrum PLS regression model presented above, a selection of the most important wavelengths was carried out. Selection was made based on the weighted regression coefficients of the PLS regression model. The results of these models are reported in Table 5.5. For the unshelled beans, the R^2 value was above 0.5 when using just 5 spectral bands. In the case of shelled cocoa (cotyledons), the performance was much better, with R^2 values above 0.8. The validation R^2 value was also above 0.8, when using either 16 bands or 4 bands. Lowering the number of bands did not result in poorer prediction and 4 wavelengths even gave better validation performance (R^2=0.85, RMSEP=2.2%). This is possibly explained by the strong absorbance bands of lipids, and the removal of uninformative bands that bring certain noise in the model. However, it should be pointed out that these models were built on the spectra treated using the second derivative or MSC pre-treatments, which are obviously applicable only when full spectra are available. When a multispectral imaging system capable of acquiring just those spectral bands, no spectral pre-treatment is possible, thus the absorbance data, i.e. log(1/R) can only be used. This is likely to bring lower prediction performance due to scattering effects.

Table 5.5. PLS regression performance of fat prediction model using a reduced number of spectral bands, on unshelled or shelled single cocoa beans.

Sample presentation	**Pre-treatment**	**LV**	**Calibration**		**Cross-validation**		**Validation**		**N. bands**
			R_c^2	**RMSEC**	**R_{cv}^2**	**RMSECV**	**R_p^2**	**RMSEP**	
Unshelled	2nd deriv.	3	0.524	4.102	0.492	4.267	0.358	4.692	5
Shelled	MSC	5	0.838	2.350	0.834	2.388	0.825	2.382	16
Shelled	MSC	3	0.816	2.506	0.812	2.541	0.849	2.214	4
Sample presentation	**Selected wavelengths**								
Unshelled	1428, 2259, 2269, 2282, 2326								
Shelled	1107, 1214, 1302, 1371, 1700, 1736, 1749, 1768, 1938, 2057, 2145, 2295, etc.								
Shelled	1220, 2057, 2145, 2295								

Fat expressed on wet basis. Validation was carried out on 102 samples (51 beans, by randomly taken 2 beans from each batch).

5.3.4. Application of HSI calibration

The best prediction models based on PLS regression for fat prediction were applied by HSI on a larger number of cocoa beans (for unshelled beans, the model performance reported in Table 5.3 for wet basis prediction; for shelled beans, the performance is reported in Table 5.4). Once the β-regression coefficients were exported and applied to the hypercubes, it was possible to predict the property of interest even at the single pixel level, within a ROI belonging to one cocoa bean, thus visualising the distribution across the seed. As shown in Figure 5.7, the prediction on single pixel allowed visualisation of fat distribution across the beans, as shelled unground beans. Images were acquired on both sides of the beans, by overturning them on the vertical axis. Application of the prediction on wet basis and on dry matter basis agrees with the expected bias due to the moisture content. For practicality, it is useful to obtain visualisation of the predicted average fat content for each cocoa bean, thus images were also produced in this sense. This can allow rapid detection of beans with high or low fat content, which can be selected for specific applications, e.g. segregation of beans with low fat content and thus higher non-fat solids, which could be used for dark chocolate manufacture.

To prove the concept of selecting the top and bottom fractions of the cocoa beans based on HSI predicted fat content, a manual sorting experiment was carried out on an independent set of beans, as shown in Figure 5.8. Three cocoa beans were picked for the "high fat" fraction, 3 for the "low fraction" batch and 3 belonging to the remaining beans with average fat content. The beans were manually ground and analysed by the reference method. The results demonstrated that the high and low fractions had statistically significant differences in fat content, with $P<0.01$. The high fraction had also higher fat content than the "average" (batch) fraction, whereas the latter did not show significant difference with the "low" fat fraction, due to the large standard deviation. Therefore, the results showed that it is possible to sort whole cocoa beans into sub-batches, which can be further included into different streams according to the industrial or scientific needs.

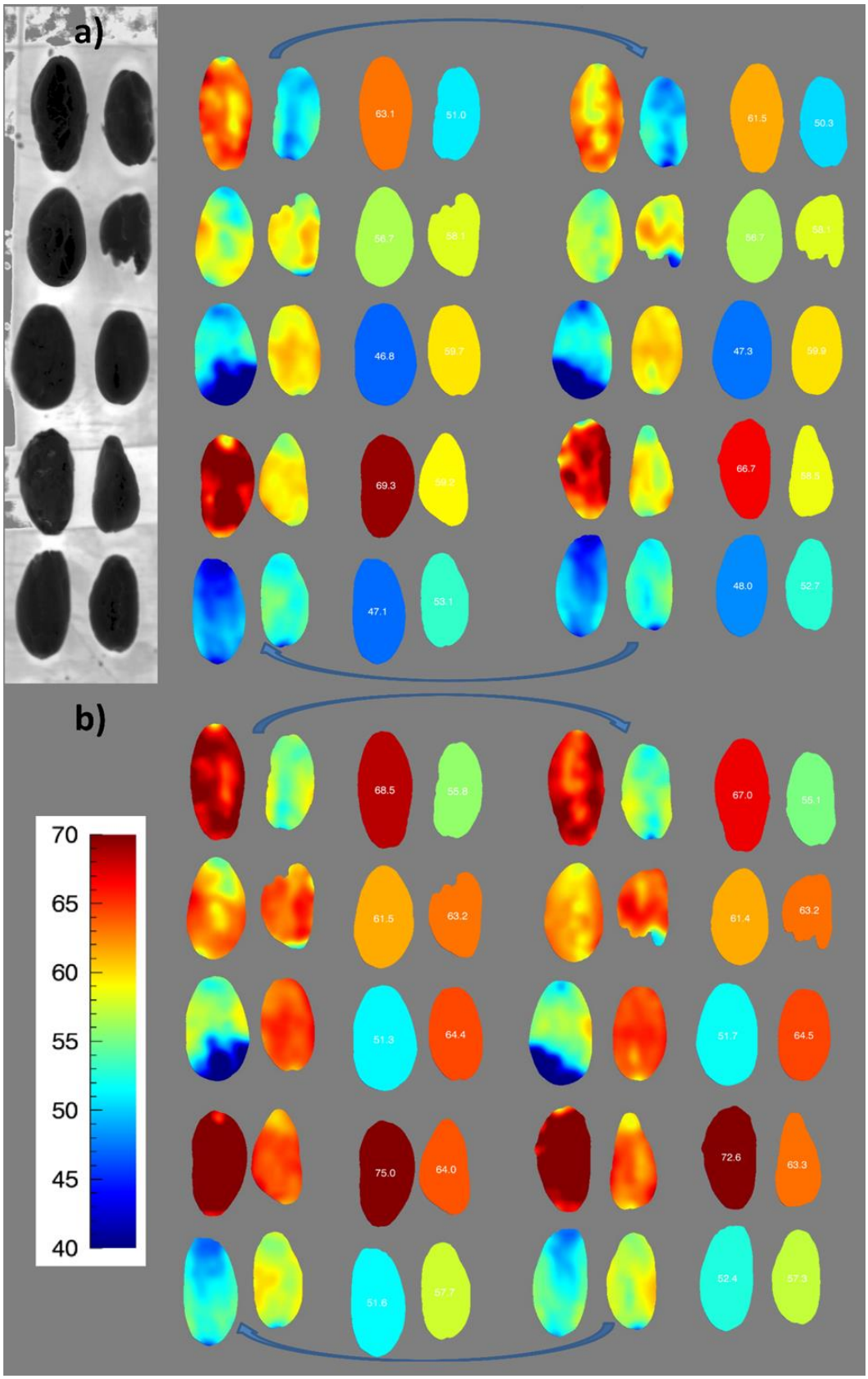


Figure 5.7. Applied calibration models for total fat content visualisation in unroasted whole cocoa beans (unshelled) at a single pixel level, predicted on (**a**) wet or (**b**) dry matter basis. Beans are shown on both orientation, numbers indicate the predicted average value for each seed (batch of Ivory Coast).

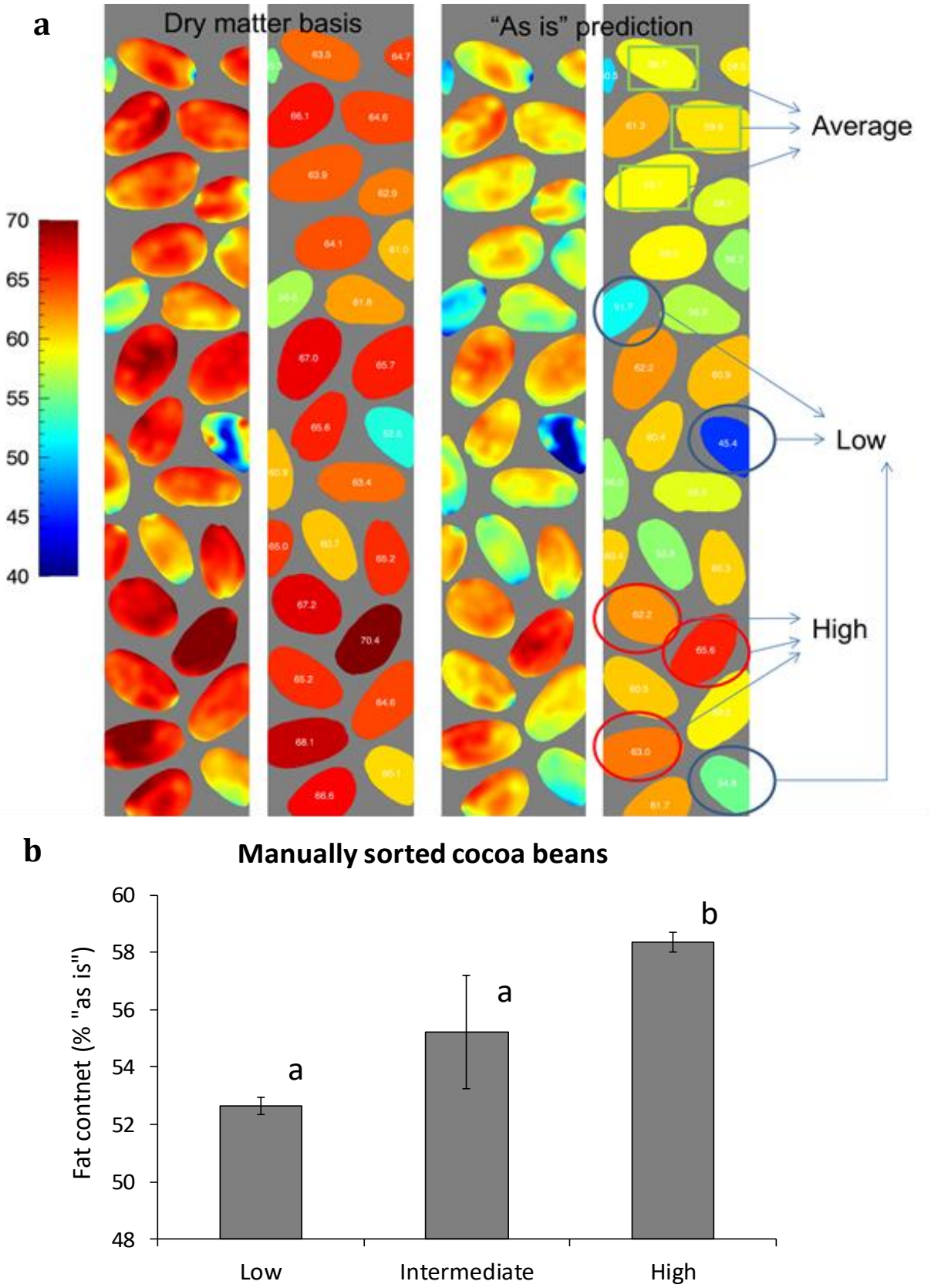


Figure 5.8. Results of manual sorting of whole cacao nibs for total fat content. **a**) Chemical images of the scanned beans. **b**) Mean fat content in the three sub-batches, analysed by the reference method (3 beans picked per each batch selected). Bars indicate the standard deviation, and different letters indicate statistically significant differences among the fractions ($p<0.05$).

5.3.5. HSI for colour prediction models

A PLS regression model was evaluated for predicting colour parameters, in particular the L*, a* and b* values. Table 5.4b and c reports the colour prediction for unshelled cocoa beans and the shelled beans, i.e. whole nibs (colour of the unshelled seeds or the ground powder).

Using spectra from unshelled beans, the external colour was predicted with sufficient accuracy for a* and b* parameters, while L* value was poorly predicted. The best model for a* prediction had R^2=0.770 and 0.720 for calibration and validation, respectively. R^2 for b* prediction was 0.757 and 0.678 for calibration and validation. The RPD values were 1.90 and 2.22 for a* and b*, thus showing fairly acceptable performance.

When the prediction was done on the whole shelled nibs against reference colour measurement of the ground cocoa, poorer performance was obtained for predicting colour attributes. The best model was for L* value prediction, showing calibration R^2=0.512 and validation R^2=0.418. This result was unexpected, but it might be due to the poor correlation between the internal and external colour of the cocoa beans, even when the shell is removed. In fact, some of the colour differences that can be visually appreciated are obvious when the beans are ground, while they appear similar when they are whole due to similar shell colours. This is also the reason why some traditional visual tests are carried out by cutting the cocoa beans to see the internal colour.

5.4. CONCLUSIONS

Whilst a few studies previously reported total fat prediction using conventional NIR instruments, previous calibrations were done on ground samples and nothing was reported on a single cocoa bean level. The current research established:

i) the possibility of predicting fat content at a single cocoa bean level;

ii) that an HSI-based rough prediction of fat content is possible on the raw cocoa bean without the need to remove the shell, and is sufficient to sort samples, resulting in differences of up to 6% in the fat content of the nibs for sorted fractions;

iii) a wide range of fat content is obtained at a single cocoa bean level, possibly due to the combination of physiological and processing effects.

Accordingly, the use of HSI can allow a more efficient screening based on the assessment of individual cocoa beans, and can be implemented in an on-line scale. Further research is required to investigate the reason for such a good prediction ability for fat despite the presence of the shell. For instance, whether there are physiological reasons such as similar ratio of fat accumulation in the shell, or technological factors including fat migration during the fermentation or drying, as the light penetration through the shell is insufficient to obtain a direct measurement.

6. COCOA BEANS: FERMENTATION INDEX, ANTIOXIDANT ACTIVITY AND TOTAL POLYPHENOL PREDICTION

6.1. INTRODUCTION

Fermentation index (FI) is an important parameter related to cocoa bean quality, as it can affect the final flavour of the cocoa powder and chocolate. An indication of the fermentation level can be obtained by visual assessment, using the cut test: unfermented beans are grey (slaty), under-fermented beans are violet or purple and fully fermented beans are brown in colour. However, this method is time consuming and subjective. Alternatively, a FI can be obtained using a method that involves grinding the cocoa beans, pigment extraction using methanol:HCl and spectrophotometric readings at 520 and 460 nm. Despite the more objective measurement, this method is still time-consuming (overnight extraction) and involves the use of harmful reagents. Non-destructive and rapid methods to predict fermentation index of cocoa, potentially on a single bean basis, would be of great practical interest.

Polyphenols received attention because of their physiological effects including their antioxidant activity, i.e. the capacity to retard lipid oxidation. Fresh cocoa beans are more abundant in polyphenols than the fermented dried product, with over 5-6% total phenolics (dmb) reported. Further polyphenol degradation can be observed when alkalisation is applied to produce cocoa powder, together with dramatic changes in the colour of the nibs (cotyledons) (Fowler & Coutel, 2017). Niemenak et al. (2006) reported that the polyphenol content of cocoa beans varies from 67 to 149 mg g^{-1} (dmb) expressed as epicatechin equivalent in the freshly harvested product, with variation further depending on the botanical variety, geographical origin and postharvest processing.

The antioxidant capacity of foods is also another important aspect related to the quality of several food products. It can be assessed by using several methods, the most common being 2,2'-azino-bis(3-ethylbenzothiazoline-6-sulphonic acid) (ABTS) and DPPH assays. Foods have complex composition and contain both hydrophilic and lipophilic compounds, present both in free or

bound states, which can represent an issue during their extraction. In addition, polyphenols have different polarity, which further complicates the measurement of total antioxidant capacity. A new approach has been recently proposed to overcome this issue, named QUENCHER (from "QUick, Easy, New, CHEap, and Reproducible"), which involves the direct addition of free radicals to the solid food (Gökmen, Serpen, & Fogliano, 2009). ABTS or DPPH can be used to run the QUENCHER approach, and a comparison between the two methods on several foods showed that ABTS is more sensitive to phenolic compounds while DPPH is more dependent upon Maillard reaction products. In addition, ABTS generally gives a slightly lower analytical error (Serpen, Capuano, Fogliano, & Gökmen, 2007). The antioxidant activity of cocoa beans is known to vary also depending on the origin of cocoa beans (Othman, Ismail, Ghani, & Adenan, 2007), however information on variation at a single cocoa bean level is not available.

Despite no work being published on within-batch cocoa bean variation, a large variability is expected, similar to that found in other seeds or nuts. The post-harvest processing (fermentation and drying) can further exacerbate natural differences, giving a wide range of properties within the same batch. For these reasons, the study of natural distribution of cocoa quality-relevant parameters such as phenolic compounds can be useful for the industry, especially when non-destructive and rapid techniques are applied. Quantification of cocoa constituents by non-destructive techniques has been scarcely investigated, and previous research used conventional NIR spectroscopy for the prediction of fat content in ground cocoa (Álvarez et al., 2012; Teye & Huang, 2015; Veselá et al., 2007), as well as nitrogen compounds and moisture (Veselá et al., 2007), or other compounds such as caffeine and theobromine (Álvarez et al., 2012). Phenolic compounds, and particularly procyanidins, have been investigated in cocoa mass (liquor) using NIRS (Whitacre et al., 2003). The spectral region used was 700-2500 nm and the reference analysis was carried out using HPLC analysis of phenolic compounds. Very good prediction was reported, with R^2 value of 0.98, for total procyanidin oligomers.

Only one research paper used IR-based methods on whole cocoa beans for quantification purposes. Sunoj et al. (2016) applied FT-IR (800-2778 nm) to build PLS regression models to predict total polyphenols (TP), pH and FI. The best PLS prediction model for polyphenol content

had R^2=0.84 and RMSECV=0.93 mg g^{-1} using vector normalisation, while first derivative pre-treatment led to worse performance, i.e. R^2=0.79 and RMSECV=1.06 mg g^{-1}. Similarly good prediction was obtained for fermentation index, with the best model showing R^2=0.88 and RMSECV=0.06 (Sunoj et al., 2016).

No information has been published using HSI or even traditional NIR spectroscopy for single cocoa beans. Therefore, the aim of the present work was to use HSI (1000-2500 nm) to predict fermentation index, total polyphenols and antioxidant activity of individual dry fermented cocoa beans scanned on a single bean basis. In addition, the distribution of these compounds has been reported in a wide range of samples showing single-seed variability.

6.2. MATERIALS AND METHODS

6.2.1. Samples and reagents

All reagents used were of pure laboratory grade. HPLC-grade methanol and ethanol, and HCl were supplied by VWR (Poole, UK). ABTS was supplied by Roche (Penzberg, Germany). Folin-Ciocalteu reagent, Ferulic acid (99% purity), (±)-6-Hydroxy-2,5,7,8-tetramethylchromane-2-carboxylic acid (Trolox; 97% purity) and potassium persulphate (99.99%) were supplied by Sigma-Aldrich (St. Louis, Missouri, USA).

Seventeen batches of fermented, unroasted, unshelled cocoa beans were obtained from importers representing a range of producing countries including Ivory Coast, Ghana, Cameroon, Nigeria, Ecuador, Indonesia, Brazil, Mexico and Venezuela. Ten beans were randomly selected from each batch, thus obtaining 170 single beans (see Chapter 5.2 and Table 5.1), which were analysed individually (single cocoa beans) by HSI and for reference measurements.

6.2.2. Hyperspectral imaging

The acquisition parameters for HSI are reported in Chapter 5, with similar experimental design and sample size.

6.2.3. Fermentation index

Fermentation index (FI) was measured in each bean according to the method of Sunoj et al. (2016). About 10 mg of ground shelled cocoa beans were placed in glass tubes and 5 mL of a methanol:HCl (97:3 v/v) solution was added, and then stored at 10 ºC for 20 h. The mixture was then filtered using a Whatman filter no. 1 and spectrophotometric readings were made at 460 and 530 nm using an Evolution 201 spectrophotometer (Thermo Fisher scientific, Waltham, WA, USA). The fermentation index is defined as the ratio between these absorbances, with values above 1 indicating a well fermented sample and values below 1 indicating under-fermented beans.

6.2.4. Total polyphenols

Total polyphenols (TP) were analysed according to the Folin-Ciocalteu method (Singleton and Rossi, 1965), as described by Othman et al.(2007), slightly modifying the volumes. The extraction conditions were chosen according to Sunoj et al. (2016) for cocoa bean phenolic analysis. In particular, the total polyphenols were analysed directly on the ground cocoa material. 1 mL of an ethanol:water solution (70:30 v/v) was added to 100 mg sample of ground cocoa. The dispersion was shaken for 30 seconds and centrifuged for 5 minutes at 1500 g using a Mikro 22 centrifuge (Hettich, Tuttlingen, Germany). 100 μL of the supernatant was taken and 750 μL of Folin-Ciocalteu reagent were added. After exactly 5 minutes, 750 μL of a 0.45 M sodium hydrogen carbonate solution was added to stop the reaction. After 90 minutes, the absorbance was read at 725 nm using an Evolution 201 spectrophotometer. A 7-point calibration curve was built using pure ferulic acid in the range 0-0.20 mg mL^{-1}, with R^2=0.998 (Figure 6.1). The standard error of laboratory (SEL) can be calculated as the ratio between the standard deviation (SD) of the measurements and the square root of the number of replicates. The SEL for total polyphenol reference analysis was 3.23 mg Ferulic acid g^{-1} cocoa. A second indicator of the repeatability of the reference measurement is given by the coefficient of variation (CV), which was 3.68% for polyphenol content.

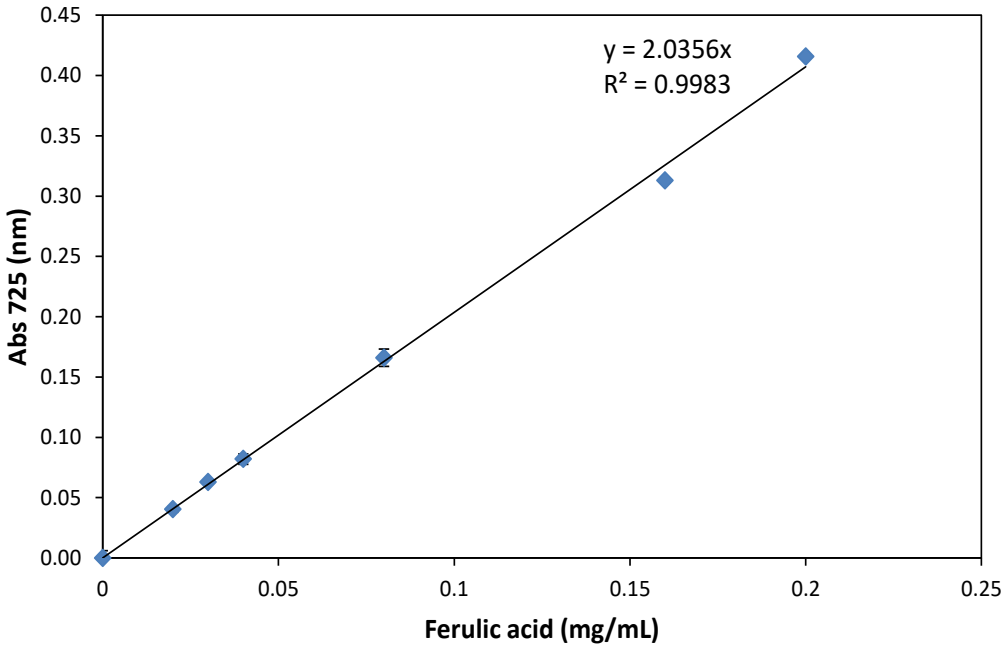


Figure 6.1. Calibration curve built for total polyphenol analysis in cocoa by the Folin-Ciocalteu method, expressed as ferulic acid. Bars indicate the standard deviation of three replicates of analysis.

6.2.5. Antioxidant activity

The antioxidant activity (AA) was evaluated using the QUENCHER approach, according to Serpen et al., (2007). This method is particularly useful to assess the antioxidant capacity of solid foods, particularly for those compounds that are bound in the food matrix and are insoluble, yet exert AA (Gökmen et al., 2009). The ABTS working solution was prepared by mixing a 0.7 mM aqueous solution ABTS and 2.45 mM potassium persulphate. The mixture was kept in the dark at room temperature for 12–16 h to obtain a stable ABTS solution. ABTS working solution was prepared by diluting (~1:88) ABTS standard solution with 50:50 ethanol:water (v/v). Ten mg of ground cocoa beans were added to 1.7 mL ABTS working solution. After vortexing the samples for 2 min, they were placed in an orbital shaker and centrifuged at 9200 g for 2 min. The supernatant was taken and absorbance at 734 nm was read using an Evolution 201 spectrophotometer. The reading was performed at exactly 6 min after mixing the ABTS reagent with the sample. Trolox was used to build a calibration curve to express the antioxidant capacity as Trolox equivalent antioxidant capacity (TEAC), i.e. mmol Trolox equivalent per kg sample. A 5-point calibration curve was built in the range 20-120 mmol Trolox equivalent, showing

R^2=0.985 (Figure 6.2). The SEL for this method was 21.02 mmol Trolox equivalent kg^{-1} cocoa, with CV value of 14.78%.

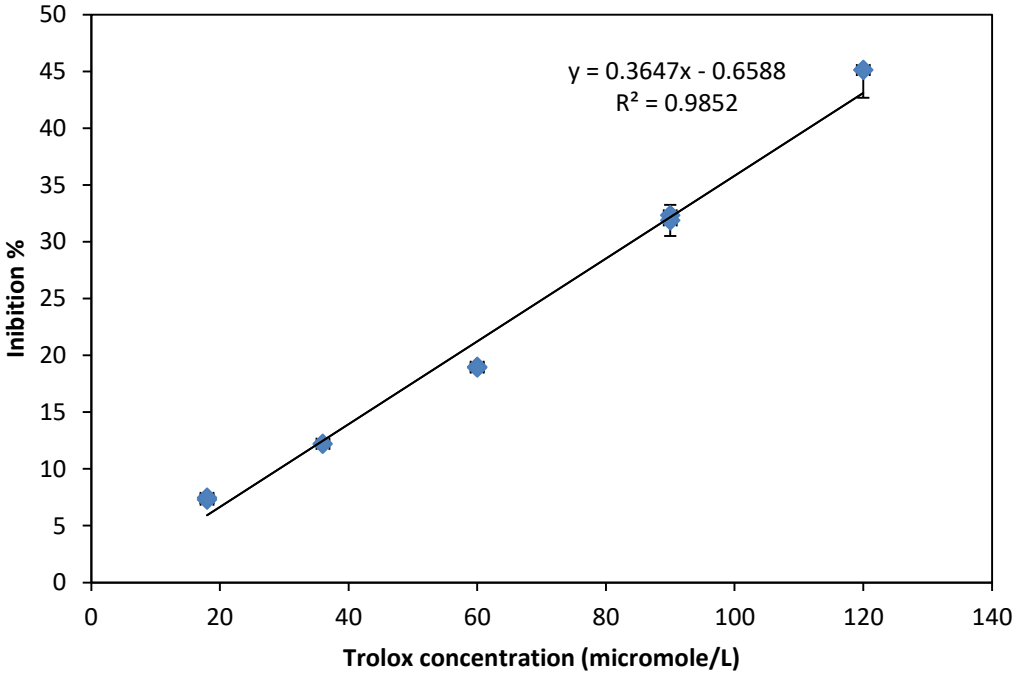


Figure 6.2. Calibration curve built for antioxidant activity in cocoa by the ABTS method, expressed as Trolox concentration. Bars indicate the standard deviation of three replicates of analysis.

6.2.6. Statistical analysis

The spectral data exported for each cocoa bean were treated in The Unscrambler 10.3 (CAMO, Norway), and treated as detailed in Section 5.2. As an alternative to PLS regression, Support Vector Machine Regression (SVM-R) model was used to test whether a non-linear algorithm was able to predict the target compounds in a more effective way. The epsilon SVR type was used, with radial basis function as the kernel type, and the following parameters: C value=1, epsilon=1, gamma=0.01. A 10-segment cross validation was performed. The statistical analysis was performed using The Unscrambler 10.3 (CAMO, Norway).

6.3. RESULTS AND DISCUSSION

6.3.1. Reference measurements of TP, AA and FI

Reference measurements for total phenolic compounds, antioxidant activity and fermentation index for single shelled cocoa beans are shown in Table 6.1. For the calibration set, fermentation index ranged from 0.38 to 2.13, with an average FI of 0.98 and standard deviation of 0.34. Antioxidant activity ranged from 13.8 to 462.7 mmol Trolox equivalent kg^{-1} cocoa, mean 186.1 and standard deviation (SD) of 116.1 mmol Trolox equivalent per kg sample. Average polyphenol content was 68.4 mg ferulic acid equivalent g^{-1} cocoa, with a standard deviation of 54.5, with a minimum 2.9 and maximum 204.5 mg ferulic acid equivalent g^{-1} cocoa. The reference methods used in the present study are well established procedures, and the parameters analysed are accepted by the industry as cocoa quality indicators. The direct measurement of total polyphenols on cocoa beans was previously reported by Sunoj et al. (2016) and it was suggested as a valid approach.

Table 6.1. Descriptive statistics for the parameters evaluated in single cocoa beans. Fermentation index are expressed in absolute values, while polyphenols are expressed as mg ferulic acid equivalent per g cocoa; antioxidant activity is expressed as mmol Trolox equivalent per kg cocoa.

Parameter	Calibration (n=119)				Validation (n=51)			
	Min	Max	Mean	SD	Min	Max	Mean	SD
Fermentation index	0.38	2.13	0.98	0.34	0.39	2.21	1.00	0.38
Total polyphenols	2.87	204.46	68.41	54.47	6.43	213.87	85.45	60.53
Antioxidant activity	13.75	462.71	186.13	116.13	20.88	472.26	208.77	114.94

In this case, cocoa bean composition was analysed on a single bean basis, thus giving further information on the possible natural variability within a batch. Figure 6.3 shows the intra- and inter-batch variability of the three parameters studied, where each batch consists of 10 single cocoa beans.

A wide variability within and between batches was obtained for the three parameters evaluated, and in several cases one single batch almost covered the full range for the total samples. The

within-batch distribution strongly depended upon the batch, for example in three batches (7, 13 and 15) the fermentation index was very broad, suggesting little uniformity during fermentation, or mixtures of well-fermented beans with poorly fermented ones. On the other hand, one batch (11) had a very low range of fermentation indices, as this batch consisted of under-fermented Ecuadorian beans. This batch also showed the highest values of AA and TP. These results are relevant for practical applications, as obtaining a consistent and uniform quality of the raw material is important for the production of high quality end-products. Sample 7 originates from Cameroon and showed particularly high range of FI, as well as one of the lowest concentration of TP. This different might be attributed to the different plant material, as this country is characterised by plants of Trinitario origin. Similarities among samples from Ivory Coast, Ghana and Nigeria were expected, due to origin of plant material, geography and cultural practices. However, no clear pattern was observed and compositional differences were also observed in batches from the same country.

Correlations between the parameters analysed were tested (Figure 6.4). TP and AA had a quite strong statistical correlation with Pearson $r=0.876$ (with a statistical significance, $P<0.001$). Similarly, a moderate negative correlation was observed between polyphenols and fermentation index, with $r=-0.570$, and between FI and AA, $r=-0.443$. These results were expected, as polyphenols are known to be a major source of antioxidant activity in many food products. In addition, a strong decrease of polyphenols is expected to occur during the cocoa bean fermentation, from an initial content of 150-200 mg g^{-1} cocoa (fat free) in fresh beans (Fowler & Coutel, 2017), to 60-100 mg g^{-1} expressed as ferulic acid equivalent, in fully fermented beans (Jonfia-Essien, West, Alderson, & Tucker, 2008).

FI is a parameter commonly assessed in research laboratories and at the industrial level, as the degree of fermentation is related to differences in composition. For example, fermentation causes dramatic changes in the phenolic profile and bitterness impact.

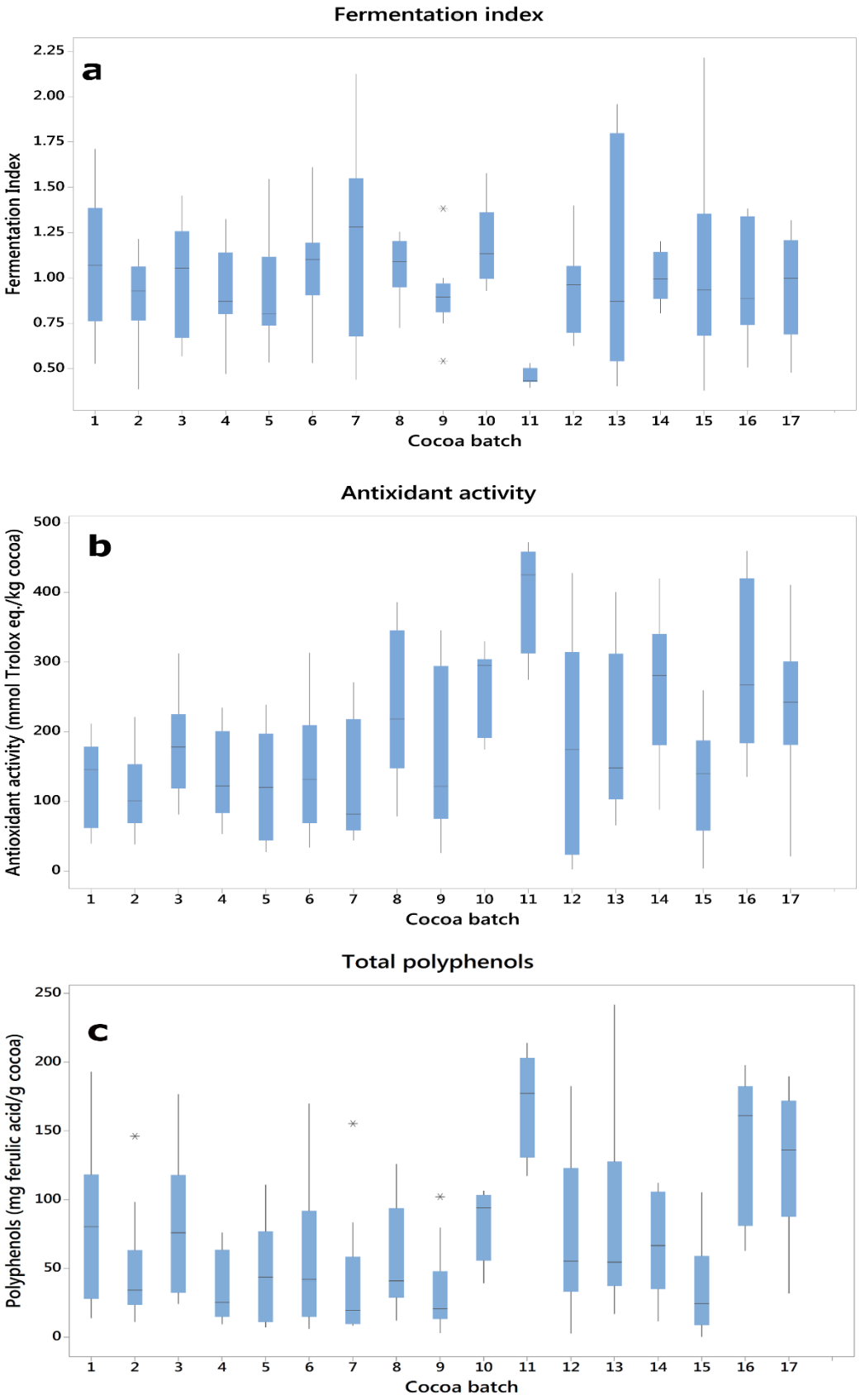


Figure 6.3. Box-plot distribution of (**a**) fermentation index, (**b**) antioxidant activity and (**c**) total polyphenols in fermented cocoa beans assessed on a single cotyledon basis (n=10 per batch).

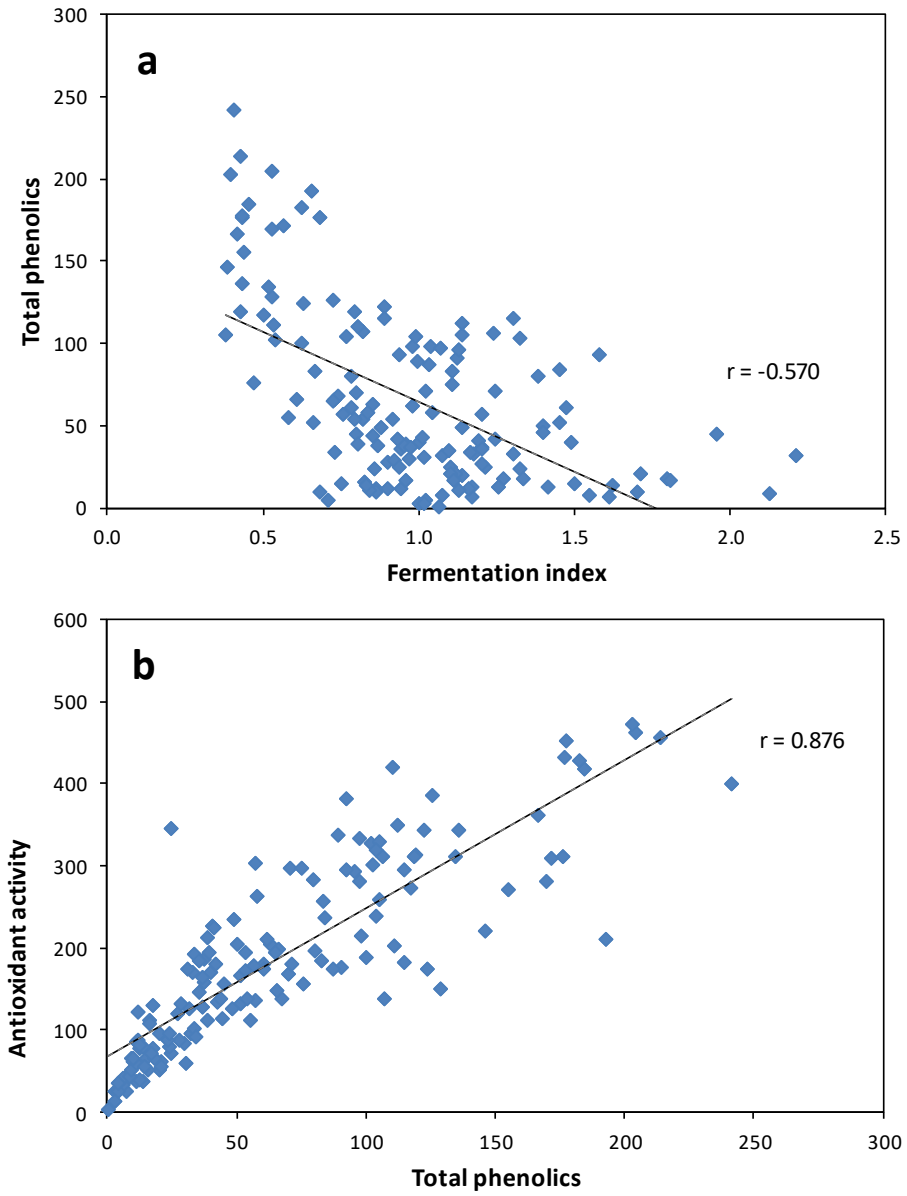


Figure 6.4. Correlations between **a**) fermentation index and total polyphenols; and **b**) total polyphenols and antioxidant activity in single unroasted cocoa beans, using reference methods. r indicates the Pearson correlation coefficient.

Estimation of the degree of fermentation is commonly carried out by assessing the colour changes inside the cocoa bean, or by the use of phenolic compounds as an analytical parameter to derive the fermentation index (León-Roque, Abderrahim, Nuñez-Alejos, Arribas, & Condezo-Hoyos, 2016; Romero-Cortes et al., 2013). Anthocyanins exhibit a maximum absorbance at 500-550 nm and their concentration decreases during fermentation. The ratio 460/530 nm of a cocoa methanolic acid extract has been shown to be a reliable indicator of fermentation, demonstrating a non-linear relationship with the visual "cut-test" (León-Roque et al., 2016). The FI of cocoa

beans has been previously correlated with total polyphenol content, which significantly decreases over fermentation, while FI continuously increases over fermentation time (Romero-Cortes et al., 2013).

Polyphenol content in cocoa is an important quality parameter, as it affects the bitterness and astringency of the final product, as well as its health properties. Despite the inconsistency often found in the literature about the polyphenol content of cocoa beans, a recent review reported on the information published so far by several sources, and described the content as ranging from 40 to about 150 mg g^{-1} cocoa (Oracz, Zyzelewicz, & Nebesny, 2015). Previous works demonstrated that the level of TP decreases as a function of fermentation times, e.g. Bonvehi and Coll (1997) reported a decrease from approximately 150 mg g^{-1} cocoa to less than 50 mg g^{-1} cocoa.

The mean results are in agreement with these findings, in terms of average TP. The cocoa batch with the minimum phenolic content (9) had 33.1 mg polyphenol g^{-1} cocoa, while the highest value of 166.7 mg g^{-1} cocoa was observed for batch 11, which related to the under-fermented beans. When looking at single bean variability, a large variation was observed, reaching very low values in several cases, while the highest value was approximately 200 mg g^{-1} cocoa.

Ortega et al. (2008) investigated different fractions of phenolic compounds and TP content in whole cocoa beans (including the shell), nibs (i.e. broken cotyledons), cocoa mass and powder. They reported concentrations of ~140 mg g^{-1} in the cocoa powder, and ~250-300 mg g^{-1} in the other sources. The highest value was observed for cocoa nibs (rather than the beans due to the dilution effect of the shell). Lower levels were found in the cocoa mass and powder probably due to degradation during the further processing. Previous literature also suggested the absence of qualitative differences among different cocoa genotypes or fermentation processes, but dramatic quantitative differences are often observed, as a result of growing and fermentation conditions (Niemenak et al., 2006). The authors investigated individual phenolic compounds and total polyphenols in several cocoa clones under two fermentation-like conditions. The total polyphenols ranged from ~80 to 140 mg g^{-1}, with some compounds showing interesting larger variability, e.g. 2.4-44.6 mg g^{-1} for catechin and 0.15-2.8 mg g^{-1} for cyanidin-3-galactoside.

Unfermented dried beans have very high phenolic content, up to 20%, which are mainly represented by proanthocyanidins, flavan-3-ols and anthocyanins (Afoakwa, 2017). However, during fermentation, oxidation and polymerisation (condensation) reactions take place, and there is some diffusion of phenolic compounds out of the beans into the fermentation sweatings (Wollgast & Anklam, 2000).

6.3.2. HSI calibrations for whole cocoa beans

The spectra of cocoa beans were acquired by HSI as unshelled beans and shelled individual cotyledons, and are reported in Figure 6.5 and Figure 6.6**.** The first 16 spectral bands were excluded from the prediction model due to the high noise in the HSI detector. Spectral pre-treatments were then applied to remove non-chemical effects such as baseline and slope variation. Figure 6.5b shows the 2nd derivative treated spectra. Spectra of beans obtained on the whole beans without removing the shell (in-shell seeds) showed a higher variability, especially in the region below 1400 nm. Strong absorbance bands are seen at 1208, 1340, 1397-1437, 1724-1743, 1919 and 2307-2326 nm, for the shelled beans. From the unshelled beans, the wavelengths 1208, 1340, 1397-1437, 1881-1913 and 2232 nm were the most absorbing ones.

The absorption band at 1208 nm is probably due to the C-H stretching second overtone (-CH_3), attributed to carbohydrates and in particular to fibre (Esteban-Diez, González-Sáiz, & Pizarro, 2004). Absorbance at 1397 nm has been previously assigned to second C-H stretching and end C-H deformation. The same chemical group also absorbs around 1440 nm, where the C-H combination is exhibited. The wavelength 1919 nm has been attributed to the C=O stretching second overtone in the carbonyl groups (-CO_2H) (Esteban-Diez et al., 2004).

However, this absorption band is very close to 1923 nm, which is assigned to O-H group of molecular water (Workman & Weyer, 2012), and therefore it might be influenced by this chemical group. The HSI absorbances at 1724-1743 and 2307-2326 nm are characteristics of lipids, due to the high fat content of the cocoa beans. Absorption around 2230 nm is also known to be characteristic of lipids (Burns & Ciurczak, 2007). The assignment of absorption band at 1744 nm has been previously done to lipids, as C-H stretch first overtone (CH_2) absorbs at this wavelength.

The CH_2 group also absorbs at 1725 nm, due to the C-H stretch first overtone (Burns & Ciurczak, 2007).

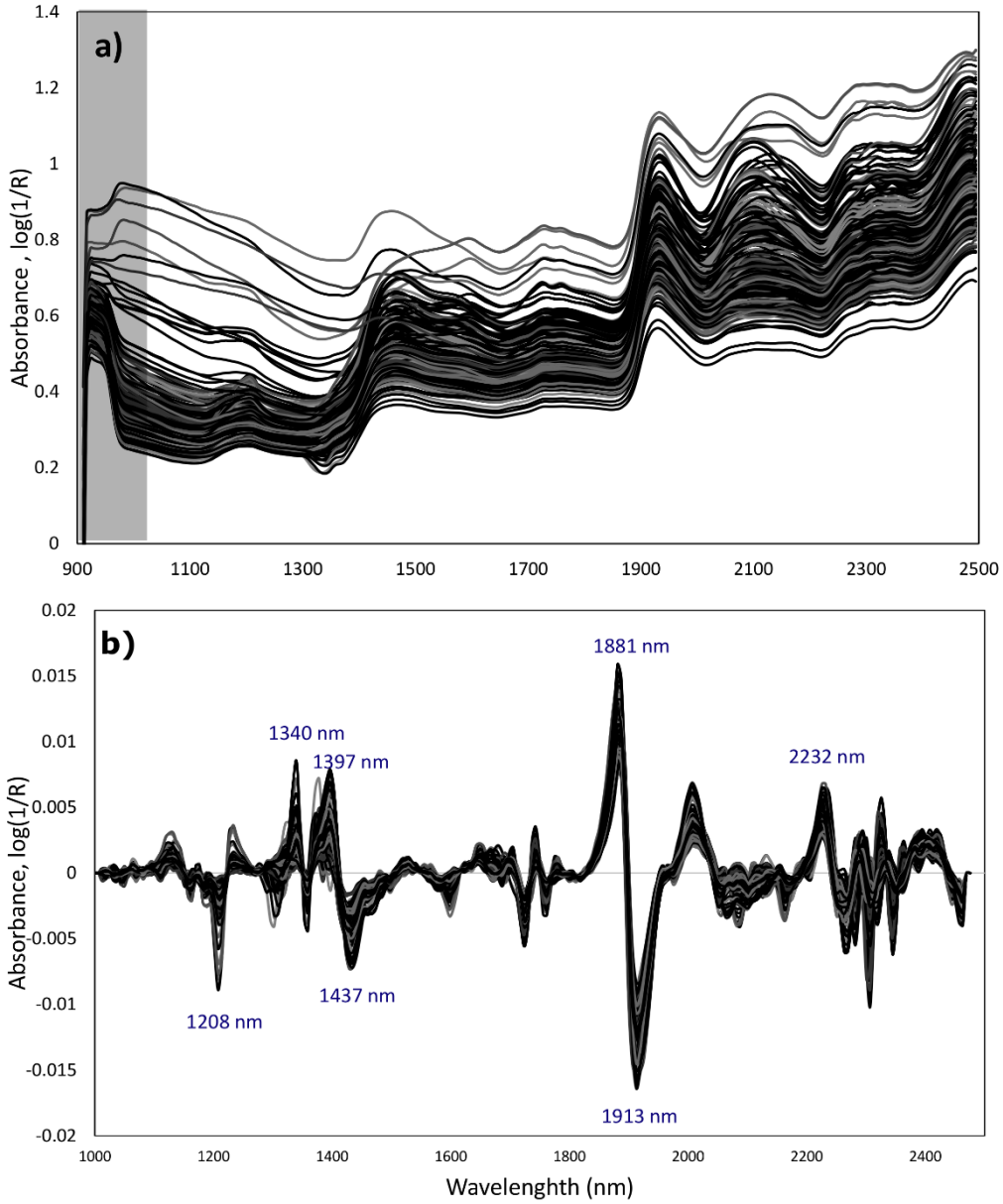


Figure 6.5. Average spectra of single whole cocoa beans, i.e. with shell (testa), (a) showing the absorbance without spectral pre-treatments and (b) treated by applying second derivative calculation. The region in grey does not contain useful spectral data for this camera and was excluded.

The wavelength 1914 nm has been attributed to the C=O stretching second overtone (-CO_2H) (Esteban-Diez et al., 2004), while absorption around 1881 has been similarly attributed to C=O stretching second overtone (Burns & Ciurczak, 2007).

In the case of shelled seeds (nibs), the HSI spectra showed strong characteristics absorbances at 1724-1743 and 2307-2326 nm, also attributed to lipids.

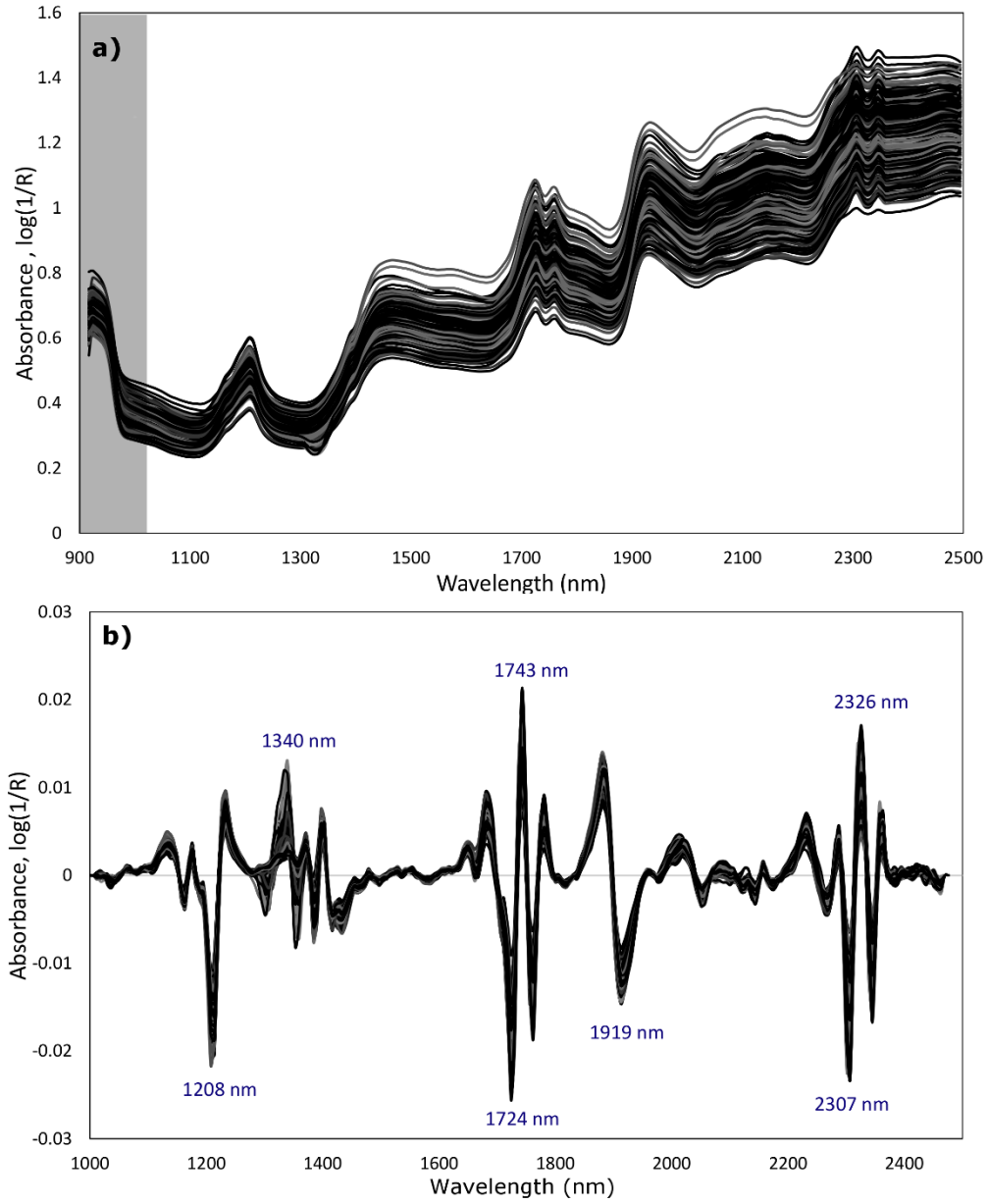


Figure 6.6. Average spectra of single shelled cocoa beans (cotyledons), (a) showing the absorbance without spectral pre-treatments and (b) treated by applying second derivative calculation. The lower wavelength region indicated in grey does not contain useful spectral data for this camera and was excluded.

The absorption at 1744 nm has been previously assigned to carbohydrates and amino acids, as C-H stretch first overtone (CH_2) absorb at this wavelength. CH_2 group absorbs at 1725 nm, due to the C-H stretch first overtone (Burns & Ciurczak, 2007).

PLS regression was used to build prediction models in whole unshelled cocoa beans and in the shelled seeds (whole unground nibs) based on HSI data from unshelled and shelled beans. The performance of the predictive models is shown in Table 6.2, depending on the spectral pre-treatment applied. HSI prediction of cocoa composition using unshelled beans had poor performance. The best calibration coefficient of regression (R^2) for fermentation index was 0.561, and prediction R^2=0.350. The RMSEC and RMSEP were 0.207 and 0.350, respectively. Total polyphenol prediction was slightly better, R_c^2=0.625 and R_p^2=0.413. The prediction error was 32.9 mg ferulic acid equivalent g^{-1} cocoa for the calibration set, and 48.2 for the independent validation set. The first derivative treatment resulted in the best models for all the parameters analysed. The low prediction ability is, however, compensated by the fact that prediction can be made on the untouched beans, in a rapid manner, so that indication of beans with very high or very low content can be detected and segregated.

Better prediction was achieved on shelled cocoa beans. However, the model for FI was poorer, although it could be acceptable for separating high and low FI samples (validation being R^2=0.498 and RMSEP=0.272, with RPD of 1.40). Better performance was achieved for TP and AA. Normalisation pre-treatment gave the best performance for TP, with R_c^2=0.817 and R_p^2=0.700; the prediction error was RMSEC=23.4 and RMSEP=34.1 mg g^{-1}. The best performances were achieved for AA, using second derivative pre-treatment, which gave R_c^2=0.764 and R_p^2=0.735. The calibration error was 55.3 and the prediction error was 60.0 mg ferulic acid equivalent g^{-1} cocoa. The performance of PLS model in predicting TP and AA is sufficient for practical use, as the RPD values (1.77 and 1.91) are almost comparable to previous work using traditional bulk NIR spectroscopy techniques for whole cocoa beans. However, as expected for whole beans the models herein presented are poorer than those previously published for ground cocoa or cocoa mass, however it compensates for the additional applicability of HSI. Figure 6.7 shows the predicted vs reference FI, TP and AA, in unshelled and shelled cocoa beans. The best calibration models are shown, by separately reporting the calibration and the external validation datasets, as well as the PLS regression coefficients for these predictions, with indication of the most important wavelengths.

Table 6.2. **a**) Unshelled (whole, including testa) and **b**) shelled single cocoa beans quantitative predictions. Performance of the PLS regression models for fermentation index, total polyphenols and antioxidant activity obtained by HSI.

a)	**LV**	**Calibration**		**Cross-validation**			**Prediction**		
		R_c^2	**RMSEC**	R_{cv}^2	**RMSECV**	RPD_{cv}	R_p^2	**RMSEP**	RPD_p
Fermentation index									
Log(1/R)	9	0.344	0.270	0.237	0.296	1.15	0.244	0.334	1.14
SNV	6	0.305	0.279	0.256	0.292	1.16	0.228	0.337	1.13
1st derivative	15	0.561	0.207	0.369	0.280	1.21	0.350	0.310	1.23
2nd derivative	6	0.403	0.248	0.249	0.305	1.11	0.293	0.323	1.18
Total polyphenols									
Log(1/R)	5	0.316	43.99	0.256	47.94	1.14	0.393	48.89	1.24
SNV	8	0.433	39.02	0.323	44.77	1.22	0.364	50.63	1.20
1st derivative	13	0.625	32.93	0.451	42.66	1.28	0.413	48.16	1.26
2nd derivative	14	0.714	27.58	0.498	40.78	1.34	0.390	49.48	1.22
Antioxidant activity									
Log(1/R)	3	0.296	93.06	0.239	102.82	1.13	0.310	97.26	1.18
SNV	6	0.355	87.70	0.297	94.70	1.23	0.253	101.34	1.13
1st derivative	7	0.430	85.83	0.373	92.36	1.26	0.410	89.67	1.28
2nd derivative	6	0.458	85.33	0.424	88.60	1.31	0.353	93.85	1.22

b)	**LV**	**Calibration**		**Cross-validation**			**Prediction**		
		R_c^2	**RMSEC**	R_{cv}^2	**RMSECV**	RPD_{cv}	R_p^2	**RMSEP**	RPD_p
Fermentation index									
Log(1/R)	15	0.534	0.230	0.502	0.249	1.37	0.489	0.275	1.38
Normalisation	16	0.570	0.223	0.523	0.243	1.40	0.498	0.272	1.40
SNV	14	0.536	0.232	0.516	0.234	1.45	0.454	0.283	1.34
1st derivative	11	0.492	0.242	0.475	0.255	1.33	0.355	0.308	1.23
2nd derivative	8	0.470	0.243	0.360	0.282	1.21	0.300	0.321	1.18
Total polyphenols									
Log(1/R)	15	0.809	23.96	0.727	29.74	1.83	0.660	36.39	1.66
Normalisation	16	0.817	23.35	0.757	28.09	1.94	0.700	34.13	1.77
SNV	14	0.812	23.66	0.660	36.49	1.49	0.680	35.21	1.72
1st derivative	11	0.820	22.98	0.744	28.81	1.89	0.551	41.84	1.45
2nd derivative	8	0.810	23.39	0.697	31.36	1.74	0.573	41.04	1.47
Antioxidant activity									
Log(1/R)	15	0.818	49.37	0.710	62.72	1.85	0.625	71.15	1.62
Normalisation	16	0.825	48.25	0.738	59.55	1.95	0.680	65.88	1.74
SNV	14	0.804	51.11	0.664	67.37	1.72	0.652	68.44	1.68
1st derivative	11	0.831	46.97	0.747	58.52	1.98	0.646	69.10	1.66
2nd derivative	8	0.764	55.25	0.741	59.23	1.96	0.735	60.04	1.91

LV = latent variables. R^2= coefficient of regression. RMSEC, RMSECV and RMSEP= root mean square error or calibration, or cross-validation and of prediction, respectively.
RPD = ratio to performance deviation.

The models obtained on unshelled beans, had wavelengths at 1119, 1988 and 2364 nm among the most important ones for prediction of fermentation index. 1145 and 1340 nm were the most influential bands for TP prediction, while AA prediction was influenced by wavelengths at 1056, 1126, 1321, 1680, 1894 and 2245 nm.

In the case of shelled beans, some wavelengths had strong influence on several models, for example those at 1132, 1492, 1661, 2057 and 2313 nm. In addition, FI was also influenced by the wavelength at 1094 nm; AA was also influenced by the wavelength at 1403, 1441, 1687, 1875 and 2145 nm. The absorbance at 1132 nm was strong for the 3 models, while a strong peak at 1492 nm was found for the FI and TP models, as well as absorbances at 1661, 2057, 2257 and 2313 nm.

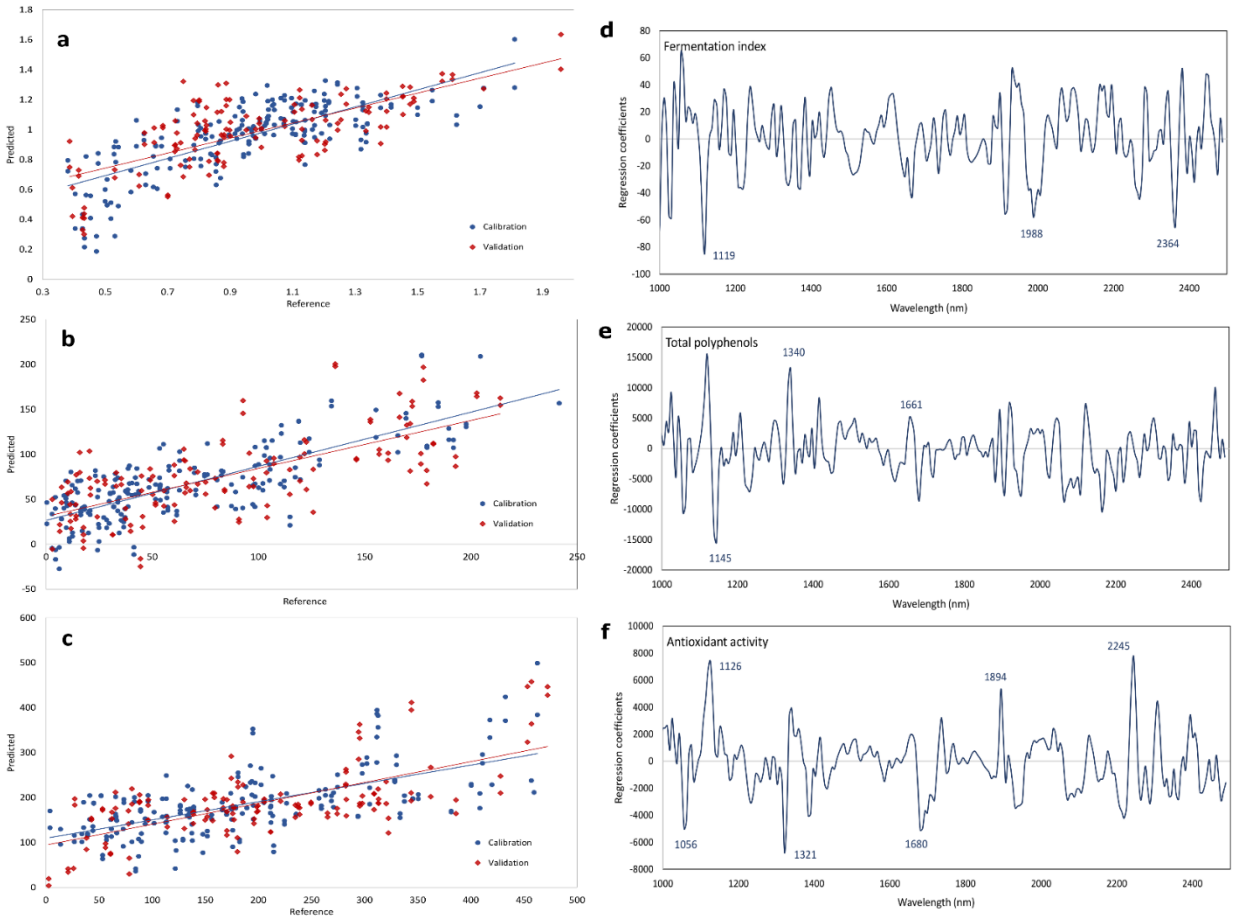


Figure 6.7. Prediction models for unshelled (whole) cocoa beans. Left: Predicted vs reference (**a**) fermentation index, (**b**) total polyphenols, and (**c**) antioxidant activity in single shelled cocoa beans, by applying the best PLS calibration from HSI. Right: Regression coefficients of the best PLS models for quantitative prediction of fermentation index, total polyphenols and total antioxidant activity, in single cocoa beans by HSI.

In the case of AA, the strongest absorbances were observed at 1441, 1668, 2057 and 2145 nm. Absorbance around 1490 nm has been attributed in the literature to several possible chemical bond vibrations, including N-H stretch first overtone and O-H stretch first overtone, thus indicating amides or compounds such as cellulose. The absorbance around 1400 nm is caused by C-H combination bond, thus indicating a $–HC_2$ structure. However, absorbance around 1450 nm has been attributed to the carbonyl group (C=O, e.g. ketones and aldehydes) as well as O-H polymeric groups, which can be due to starch and/or polymeric alcohol (Burns & Ciurczak, 2007). Interestingly, the region 1400-1440 nm was important for all the 3 models, and this region has been also attributed to aliphatic alcohols and to phenols, even monomeric phenols (which absorb at 1420 nm) (Workman & Weyer, 2012). The absorbance at 2057 nm observed for all the models indicates N-H stretch/amide 1st combination band, which has been attributed to protein. The peaks at 2145 and 2313 nm have been tentatively attributed to C-H deformation and C-H deformation and C-H bend second overtone, respectively, both indicating lipids (Burns & Ciurczak, 2007). The influence of lipid absorbances in the models for TP and AA might be explained by their possible negative influence on these parameters due to the fact that beans with relative higher fat content have lower non-fat solids, where polyphenols are concentrated.

The most absorbing bands for the unshelled cocoa beans were found at 1145 nm, attributed to the C-H second overtone (aromatic structure). Similarly, absorbance around 1680 nm was associated to aromatic groups, due to the C-H stretch first overtone. It is interesting to note that the aromatic groups are the most common structure found in polyphenols. For the whole unshelled beans, the compounds that were expected to contribute to the spectra were cellulose, hemicelluloses, pectins and lignin, these compounds being the most abundant ones in the cocoa shell. In both cases, i.e. in the presence of shell or on unshelled cotyledons, prediction of chemically-related properties has been shown to be possible, despite the relatively low concentrations of chemical compounds (TP) or the complexity of the properties investigated (AA and FI). Previous works successfully reported prediction of complex properties in cocoa and chocolate by NIRS, including sensory properties. However, some authors argued on the reason for this positive result. The question is not trivial as compounds present at very low concentrations

are not likely to be detected in the NIR region, especially when complex materials such as food products are analysed. However, Davies et al. (1991) suggested that the successful prediction of these properties is likely to be due to the fact that flavour compounds arise from many precursors which are found in larger concentrations.

Previous research reporting on cocoa composition analysed by NIR spectroscopy, described the absorbance bands at 1730-1744 nm and those at 2308-2348 nm as the most intense regression coefficients for fat prediction in cocoa (Veselá et al., 2007). Similarly, the bands at 1414-1444 nm were important absorbers for moisture prediction in cocoa powder, together with those around 1930 nm and 2040 nm (Veselá et al., 2007).

Limited information has been found in the literature regarding the prediction of polyphenol content using NIR-based techniques, and HSI has not been tested for cocoa bean analysis. Nogales-Bueno et al. (2015) applied HSI to predict extractable polyphenols in red grape skins, using the spectral range 900-1700 nm to scan two grape varieties, collecting 100 single berries per variety which were used for three different reference analyses, so the final calibrations consisted of 33 samples. The PLS prediction model built using the Folin-Ciocalteu quantification had R^2=0.82 and SECV=0.92 mg g^{-1} (range: 1.4-4.2 mg g^{-1}).

The results herein presented are comparable with previous reports where NIRS was used for the prediction of polyphenol content and antioxidant activity. For example, Catelani et al. (2017) recently reported NIRS calibrations for roasted coffee beans, with validation R^2=0.927 and 0.909 for polyphenol content and antioxidant activity, respectively. The RMSEP was 1.97 (range: 25-50) g gallic acid kg^{-1} coffee, and 95 (400-1250) mmol Trolox kg^{-1} of coffee, respectively.

The possibility of predicting fermentation index in cocoa beans using colour measurement has been recently reported by León-Roque et al. (2016). Two cocoa varieties were fermented in three different regions of Peru and sun-dried, before 40 beans per batch were sampled and manually shelled. The colour analysis was carried out using a mobile phone, "under constant conditions of light". It has been reported that colour measurement by itself is not a useful way to predict fermentation index, and even the application of complex statistical models such as Artificial Neural Network (ANN) did not lead to very good prediction of FI based on colour.

Other authors have proposed different indicators of fermentation degree, in particular the amount of nitrogen compounds, and some authors also proposed a traditional NIR spectroscopy approach to estimate the concentration of NH_3. Very good performance was shown for this parameter, with R^2=0.97, SECV=24 ppm (range 25-441) and RPD=3.9, however the NIR spectra were acquired from bulk ground samples of cocoa beans (Hue et al., 2014). Therefore, no indication has been reported so far on single bean variability, especially predictions that avoid the grinding step of the beans.

6.3.3. Use of non-linear algorithms (SVM-R)

The results of the SVM-R prediction of FI, TP and AA are reported in Table 6.3. The prediction was calculated for the shelled cocoa beans. This non-linear model led to generally similar performances to PLS regression, with fermentation index showing a very slight improvement in terms of prediction error, i.e. 0.252 vs 0.272 for SVM-R and PLSR, respectively. The other two parameters were predicted with slightly lower performance.

Table 6.3. Results of Support Vector Machine Regression (SVM-R) for the three parameters predicted in single cocoa nibs (shelled beans) by HSI.

Parameter	Calibration		Prediction	
	R_c^2	RMSE	R_p^2	RMSE
Fermentation index	0.575	0.237	0.511	0.252
Total polyphenols	0.738	31.59	0.678	34.76
Antioxidant activity	0.729	64.65	0.688	69.01

6.3.4. Visualisation of cocoa constituents at single bean level

Once calibrations had been developed for cocoa constituents, they were applied by HSI so that indication of TP, AA and FI was visualised for single cocoa beans in a rapid way. In addition, HSI allows visualising the composition of a target compound or property within single beans, by applying the calibration on a single pixel level, as shown in Figure 6.8. From the unshelled cocoa beans, a relatively poor prediction was expected, however it was still possible to detect the beans with the highest and lowest values, especially for TP prediction. In the case of AA, for many beans in the batch the predicted absolute values were approximately double the reference value, but

relative differences were still successfully observed, so there could be potential of segregating the seeds with the highest and lowest AA and TP. Much better prediction was obtained on shelled beans, as shown in Figure 6.9, where the best HSI calibrations allowed accurate visualisation of the three parameters studied. Seeds with very low FI also showed the highest TP content and AA, while the opposite was not observed. Thus, by applying the proposed method, classification of cocoa bean quality can be made at single seed level, but also visualisation of internal properties and distribution of chemical composition might aid prediction of poor quality or damage.

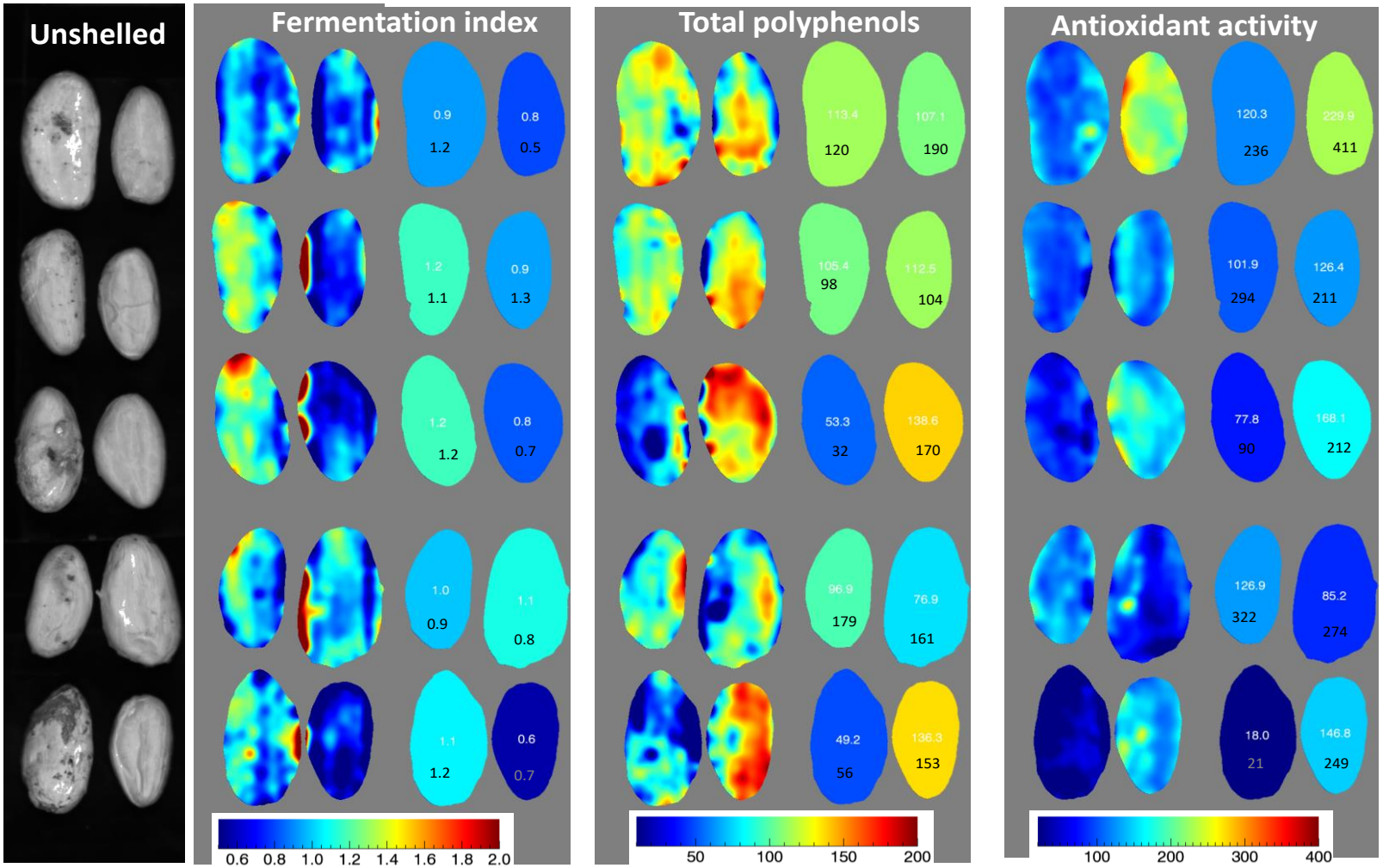


Figure 6.8. Applied calibrations on unshelled cocoa beans, for fermentation index, total polyphenols and antioxidant activity estimation. Calibrations are shown at a single pixel level (pictures on the left), or averaging the predicted values to obtain single-bean values. Numbers in white show the predicted average, while those in black indicate the reference measurement. Values for FI values are dimensionless, TP are expressed as mg ferulic acid equivalent g^{-1} cocoa, while AA is expressed as mmol Trolox equivalent kg^{-1} cocoa. Due to the performance of the models built on unshelled beans, these chemical images are intended for demonstrative purposes only.

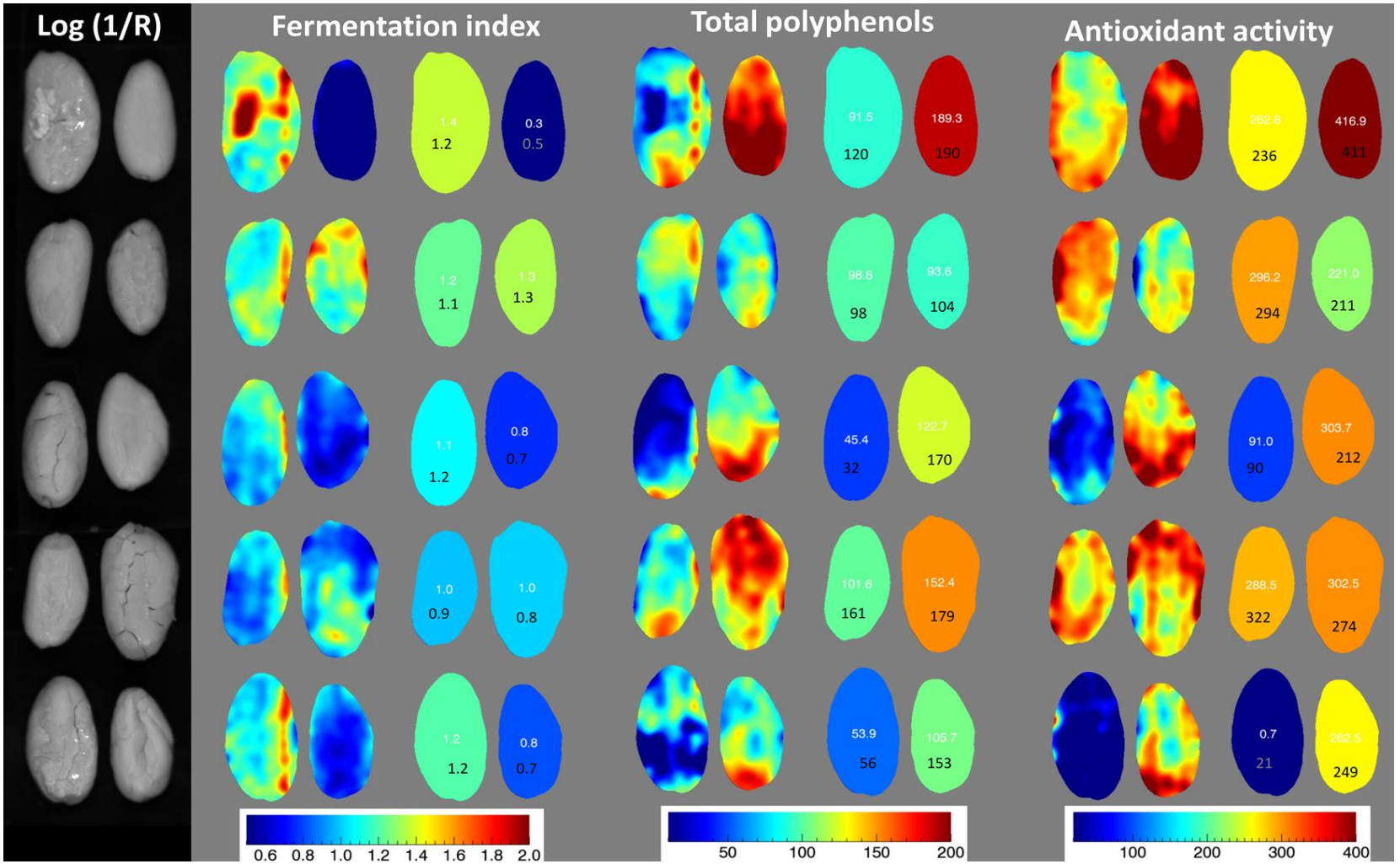


Figure 6.9. Applied calibrations for FI, TP and AA in shelled cocoa beans. Calibrations are shown at a single pixel level (pictures on the left), or averaging the predicted values to obtain single-bean values Numbers in white show the predicted average, while those in black indicate the reference measurement. Values for FI values are dimensionless, TP are expressed as mg ferulic acid equivalent g^{-1} cocoa, while AA is expressed as mmol Trolox equivalent kg^{-1} cocoa.

6.4. CONCLUSIONS

Quantitative predictions based on HSI for shelled cocoa beans were reported on a single bean basis. Cocoa composition predictions were also tested without removing the shell or testa of the bean. Despite the lower prediction ability found for the un-shelled seeds, the results would still be considered as acceptable due to the advantages of HSI scanning of untreated beans. Thus, applications of these prediction models to define the chemical composition of cocoa nibs without expensive and time-consuming analyses is of interest for screening, also enabling single beans to be analysed separately.

It was shown that HSI in the NIR region is able to give information on the distribution of polyphenols, antioxidant activity and fermentation index on single shelled cocoa beans within a batch. This variability was shown to be particularly wide, possibly due to the natural variability within and among plants due to environmental conditions, but also to the post-harvest practice. This approach can be also interesting for the scientific community, as it can used to further elucidate the natural variability and the consistency of the fermentation/drying process to obtain higher quality product. In addition, it can be used to segregate cocoa nibs with particularly high or low polyphenol content or antioxidant activity in a non-destructive manner. In turn, this can lead to the production of functional foods with increased health properties, and improving product consistency.

7. COFFEE BEANS: PREDICTION OF MOISTURE AND FAT CONTENT ON SINGLE BEANS

7.1. INTRODUCTION

Coffee quality is defined by several factors, mostly depending on the green bean composition including moisture and fat (Illy & Viani, 2005). Moisture, in particular, is a critical quality parameter because it affects coffee bean shelf life. The determination of coffee bean moisture content is very important to ensure safe transport and storage and to avoid the risk of mould development (fungal growth during storage), since an excessively dry or excessively wet green coffee bean will not maintain its quality (Wintgens, 2009). Lipids are another important component of green coffee beans, with fat content ranging from 7–10% in Robusta coffee and up to 15–17% in Arabica (Farah, 2012). The lipid fraction of coffee is relevant for its sensory impact in the final coffee brew, as well as for the shelf life and storage of the beans.

Several methods are available for the measurement of moisture in coffee, including the oven drying method, Karl-Fischer titration, conductivity meters and water activity measurement (Reh, Gerber, Prodolliet, & Vuataz, 2006). Conductivity meters are relatively rapid and easy to use but cannot measure a single coffee bean, and so alternative methods should be applied when focusing on individual coffee beans. On the other hand, the traditional solvent extraction techniques applied for fat analysis (e.g. Soxhlet method) are hazardous and time consuming and can take over 16h (Speer & Kölling-Speer, 2006). Rapid analytical techniques are therefore needed for the quantification of total lipids in foods.

Previous authors reported moisture prediction on single peanuts using two spectral ranges (400–1000 and 1000–2500 nm) (Jin et al., 2015). Both peanut models return calibration and prediction coefficients of determination (R^2) of about 0.9, with RMSEC and RMSECV of 0.06%, for a moisture content ranging from 3.5 to 4.5%. A higher error was reported by Codgill et al. (2004) for moisture prediction in maize seed kernels by HSI. Utilizing the 750–1100 nm spectral region,

the reported calibration had R^2=0.87 and prediction errors slightly above 1% for maize kernels with a moisture content between 9.7% and 30.5% and lipid content of 0.3–12.2% (wet basis).

There is a complete absence of literature relating to single beans or green coffee bean quantitative models by HSI. Only a single study investigating moisture determination by HSI on instant granulated coffee has been published (Achata et al., 2015). The coffee moisture content was artificially changed at defined levels in the laboratory and scanned by HSI in the spectral region 880–1720 nm, showing excellent performance.

Coffee species classification (i.e. Arabica and Robusta) is another interesting aspect for the coffee industry because it affects coffee price, Arabica being considered higher quality and more expensive than Robusta coffee (Rubayiza & Meurens, 2005). While coffee bean species identification is a relatively easy task for experts based on visual inspection of the green coffee, discrimination between Arabica and Robusta on roasted samples is a more challenging task (Keidel, von Stetten, Rodrigues, Máguas, & Hildebrandt, 2010). Even for green coffee there is a need to assess individual beans within a whole batch, due to the variability expected within the population, caused by genetic, environmental and post-harvest factors. However, this is impractical to undertake through visual inspection and so rapid, objective methods are required.

Common analytical methods to discriminate the coffee species, e.g. gas-chromatography of volatile compounds, matrix-assisted laser desorption/ionization mass spectrometry or gas-chromatography-mass spectrometry, are time-consuming, and they require grinding and extraction or the samples (Myles, Zimmerman, & Brown, 2006). They are also relatively complex, expensive and are not applicable online (Buratti et al., 2015).

To address this, several authors used non-destructive techniques for coffee bean discrimination, including NIRS (Downey, Boussion, & Beauchêne, 1995; Myles et al., 2006). Good performance of NIRS for authenticity purposes of ground coffee has been demonstrated, e.g. for the quantification of other ground coffees in Kona coffee blends (Wang, Jun, Bittenbender, Gautz, & Li, 2009), the addition of barley in roasted coffee (Ebrahimi-Najafabadi et al., 2012), as well as extraneous materials intentionally added for fraudulent purposes (Barbin et al., 2014). Rubayiza and Meurens (2005) successfully classified coffee species using FT-Raman spectroscopy in the

mid-infrared region based on green and roasted ground coffee beans. Reflectance NIRS in the region 1100–2500 nm was also successfully applied on ground and roasted coffees for the same purpose (Esteban-Diez, Gonzalez-Saiz, Sáenz-González, & Pizarro, 2007). However, for unground coffee only a single example has been found in the literature for classification, which used reflectance NIRS in the spectral region 1100–1800 nm in conjunction with Linear Discriminant Analysis (LDA), resulting in prediction errors of 5% to 15% depending on the spectral pre-treatment applied (Myles et al., 2006). The only existing study reporting HSI (955–1700 nm) for the discrimination of Arabica and Robusta green coffee beans was recently published by Calvini et al. (2015), who tested several classification methods and obtained accuracy of 97%.

From the above, it is clear that there has been very little attention on analysing coffee beans without prior grinding, and no previous research dealing with quantitative prediction models of composition for green coffee based on HSI. In addition, HSI calibrations for single coffee beans have not been previously reported for any coffee constituent, including moisture and fat. This can be of interest for breeders and the industry, to obtain information on the distribution of these constituents within the population via a non-destructive approach.

Therefore, the primary aim of the present study was to assess the applicability of HSI for predicting total lipid content and moisture content on green coffee beans on an individual seed basis by HSI. Moreover, a classification exercise was applied to demonstrate a single-object classification for Arabica-Robusta species discrimination based on unsupervised methods.

7.2. MATERIALS AND METHODS

7.2.1. Coffee samples

A total of 27 batches of green coffee beans were used for the experiment, and from each batch several coffee beans were randomly selected and individually analysed, so that the inter- and intra-batch variability was included. The samples were obtained from several producing countries, comprising Brazil, Colombia, Costa Rica, Ethiopia, India, Mexico, Honduras, Kenya, Nicaragua, Uganda, Rwanda and Vietnam (Figure 7.1). Both post-harvesting processing techniques were

included, with approximately 60% wet processed and 40% dry processed. Twenty batches belonged to the Arabica species, while 7 were Robusta. Approximately six beans were randomly selected from each batch for moisture and fat determination, while ten were selected for the species classification experiment. As the observed moisture range was relatively narrow, an extended moisture content range was also created artificially by treating two sub-batches of a Mexican Arabica coffee to obtain more dry and wet coffee beans. One sub-batch was placed in an oven at 50 °C, while a second one was placed in a chamber at saturated humidity, for 3 to 12 hours.

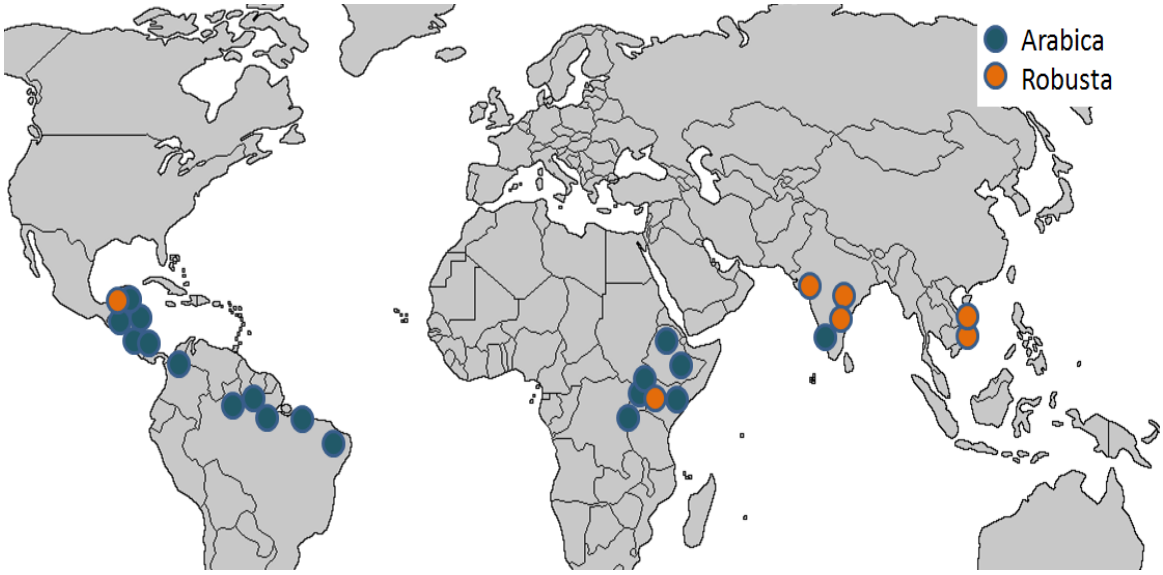


Figure 7.1. Geographical origin of the green coffee batches using in the present study, with indication of the species.

The full list of coffee batches used in the present experiment, as well as in the experiments reported in Chapters 8 and 9 is shown in Table 7.1.

To build Arabica-Robusta classification models, hyperspectral images were acquired on both sides of beans both before and after roasting. The coffee beans were roasted using a Roastilino (Fracino, Birmingham, UK) roaster at 210 °C for 3 minutes, which resulted in a medium-high roasting degree. Figure 7.2 shows a scheme of the experiments carried out for green coffee bean experiment, reported in the present chapter and in the following one.

Table 7.1. Description of the batches of green coffees used for the experiment, with indication of the coffee species and their post-harvest treatments.

N.	Origin	Species	Post-harvest treatment
1	Costa Rica	Arabica	Wet
2	Vietnam	Robusta	Wet
3	Kenya	Arabica	Wet
4	Nicaragua	Arabica	Wet
5	Arabica - Guatemala	Arabica	Wet
6	Ethiopia	Heirloom*	Dry
7	Arabica - Uganda	Arabica	Dry
8	Arabica - Uganda	Arabica	Dry
9	Arabica - Guatemala	Arabica	Wet
10	Arabica - Brazil	Arabica	Dry
11	Arabica - Brazil	Arabica	Dry
12	Brazil	Arabica	Dry
13	India	Robusta	Wet
14	India	Robusta	Wet
15	Guatemala	Robusta	Wet
16	Vietnam	Robusta	Wet
17	Uganda	Robusta	Dry
18	India	Robusta	Dry
19	India Monsoon Malabar	Arabica	Wet
20	Mexico	Arabica	Wet
21	Java Lington	Arabica	Dry
22	Rwandan	Arabica	Wet
23	Ethiopia Sidamo	Arabica	Dry
24	Colombian Supremo	Arabica	Wet
25	Brazil	Arabica	Wet
26	Kenyan 100% Bourbon	Arabica	Wet
27	Honduras Liquidambar	Arabica	Wet

* Heirloom is a particular Ethiopian coffee that is descendent from Arabica coffee but has intermediate characteristics between Arabica and Robusta.

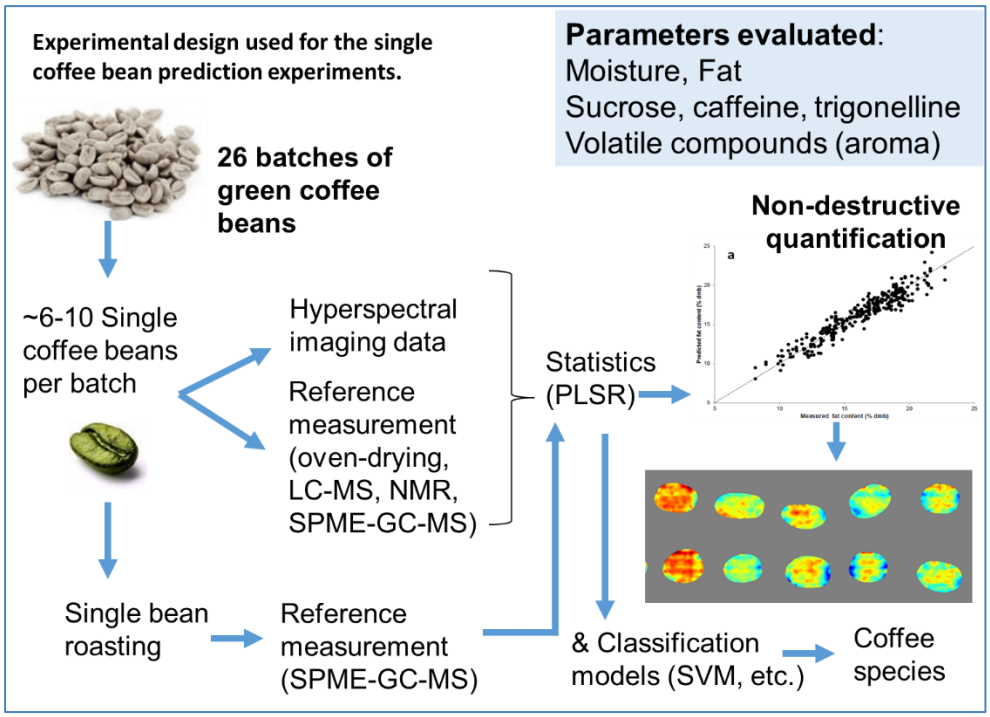


Figure 7.2. Experimental design used for the single coffee bean prediction experiments.

7.2.2. Reference analyses for moisture and fat

Moisture content was analysed by oven drying using an adaption of the method ISO 11294 (1994) which involved using a slightly lower temperature and longer time to avoid excessive sample degradation. This is because the analysis of moisture content through the official ISO method could result in a partial degradation of the product when analysing the coffee beans, which will influence the overall weight loss (Reh et al., 2006). The individual samples of green coffee beans were placed on an aluminium tray and dried in a Sanyo 112-F (San Diego, CA, USA) oven at 95 °C for about 24h. The water content was then expressed as percentage of coffee bean weight. An instrument based on Nuclear Magnetic Resonance (NMR) was used for reference lipid analysis, due to its advantages in terms of rapidity and accuracy, and because the required sample size makes it feasible to analyse the single coffee beans. The single coffee beans were ground using a Retsch PM 200 Planetary Ball Mill grinder (Retsch, GmbH, Germany), by first cooling the sample using liquid nitrogen (cryomilling) and then grinding for 30 s at 25 min^{-1}. The NMR-based fat analysis includes a complete drying of the sample ground material, followed by measurement of total lipid content using a CEM Smart Trac II Moisture and Fat analyzer (CEM Microwave

Technology Ltd., Buckingham, UK). The instrument contains calibrations for total fat for several food products, and the measurement was adjusted for bias using two batches of green coffee. A Mexican Arabica coffee and a Robusta coffee from Vietnam were used for the calibration and reference analysis for fat content. The bias for the fat calibration was 0.76%, which was obtained by comparing the results from NMR determination and those obtained from a standard method with acid hydrolysis. The instrument has a resolution of 0.01%, a fat range from 0.01% to 99.99% and a balance with 0.1 mg readability. The method repeatability was 0.24%.

7.2.3. Hyperspectral imaging and data treatment

Data were acquired as described in Section 3.2 and in previous publications (Caporaso, Whitworth, & Fisk, 2017; Millar et al., 2008). Both sides of the coffee beans were scanned, and analysed using ENVI 5.2-IDL 8.4 (Harris Geospatial Solutions). Average absorbance spectra for each coffee bean were computed from the component pixel spectra and exported for subsequent statistical analysis.

7.2.4. Statistical analysis

Moisture and fat prediction in green coffee beans was carried out by PLS regression using The Unscrambler X 10.3 software (Camo, Norway). Species classification models for green and roasted coffee beans were built using Linear Discriminant Analysis (LDA) and Support Vector Machine (SVM). LDA is a powerful tool that performs dimensionality reduction and automatic object classification. It is based on finding the optimal boundaries among classes, by maximising the between-class variance while minimizing the within-class variance. SVM is a non-linear modelling technique that finds the optimal hyperplane as a surface able to separate the largest fraction of data points, and it maximises the margins among classes. A detailed explanation of SVM classifiers, with examples applied to HIS, is provided by Jiang et al. (2007). In the present case, LDA was performed using linear method, assuming equal prior probability and applying a previous PCA. SVM classification was performed using a C-SVC type classifier, with a radial basis kernel function, and C and gamma values chosen according to the previously computed probabilities. The C-CSV SVM type was used for the classification, with several kernel types

tested, including radial basis function and polynomial. To choose the best gamma and C values, a grid search was performed before calculating the SVM model, and a cross-validation was applied using 10 random segments. The evaluation of PLS models for moisture and fat determination was performed by considering the coefficient of determination (R^2), and root mean square error for the calibration (RMSEC) and cross-validation (RMSECV) datasets. In addition, the Ratio of Performance to Deviation (RPD) was used to give an indication of the goodness of fit. This parameter is defined as the ratio between the standard deviation of the reference values and the RMSECV. The sample outliers were identified and removed according to the sample residuals and leverage, as well as on the Hotelling's T^2 values (Fearn, 2002).

7.3. RESULTS AND DISCUSSION

7.3.1. Descriptive statistics for reference measurements

The average moisture content for green coffee beans at their natural moisture range was 10.8%, while the average total fat content was 14.7% and 16.4%, expressed on wet and dry matter basis (dmb), respectively (Table 7.2). The values in Table 7.2a are derived from a single set of samples, whereas Table 7.2b reports the moisture content assessed by oven drying for samples in a "natural state" as well as for the batch of samples that was treated to consider a wider range of moisture content.

Table 7.2. Descriptive statistics for reference measurements on green coffee beans for (**a**) fat prediction model and for (**b**) moisture models.

	Parameter	Mean	SD	Max	Min	No.
a	Moisture by NMR (%)	10.28	1.33	17.23	7.35	352
	Fat (% wet basis)	14.66	2.64	20.32	7.91	
	Fat (% dry basis)	16.41	3.10	22.74	8.13	
	Weight (mg)	119.00	37.10	252.40	32.60	
b	Moisture (oven drying) - natural	10.80	0.79	12.10	7.20	320
	Moisture (oven drying) - lab. treated	14.86	10.77	52.10	4.50	480

As mentioned above, this was done to build a calibration with a moisture content extended beyond the narrow range of the samples received (SD=0.8%). This is particularly important to include cases where batches of coffee beans are stored in improper humidity conditions that can result in lower quality, and even be at risk from mould development.

Generally, a moisture content of between 8.0% and 12.5% is regarded as suitable for the storage of green coffee beans in order to avoid microbial growth and altered sensory quality.

The average total fat content in green coffee beans of Arabica and Robusta species was 17.51±2.21% (average content dmb ± standard deviation) and 12.63±1.85%, respectively. There was a statistically significant difference ($p<0.01$, Student's t-test) between the two groups. The intra-batch and inter-batch variability of moisture and fat content is shown in Figure 7.3, where each group represents a batch, while the distributions are shown in Figure 7.4.

Literature data for bulk measurements of green coffee report a fat content range from 7% to 17% dmb, with strong differences depending on the species, i.e. 15% on average for Arabica and 10% for Robusta coffee (Speer & Kölling-Speer, 2006).

As expected, for the reference measurements, no statistically significant difference was observed in moisture content of Arabica coffee batches compared to Robusta ones, despite obvious and statistically significant differences for total lipids, with Robusta having lower fat content than Arabica samples. The distribution of reference measurement for moisture and fat in single green coffee beans is reported in Figure 7.4, showing the moisture distribution in the un-treated and artificially-wet beans (Figure 7.4a) and the fat content showing separately Arabica and Robusta samples (Figure 7.4b,c).

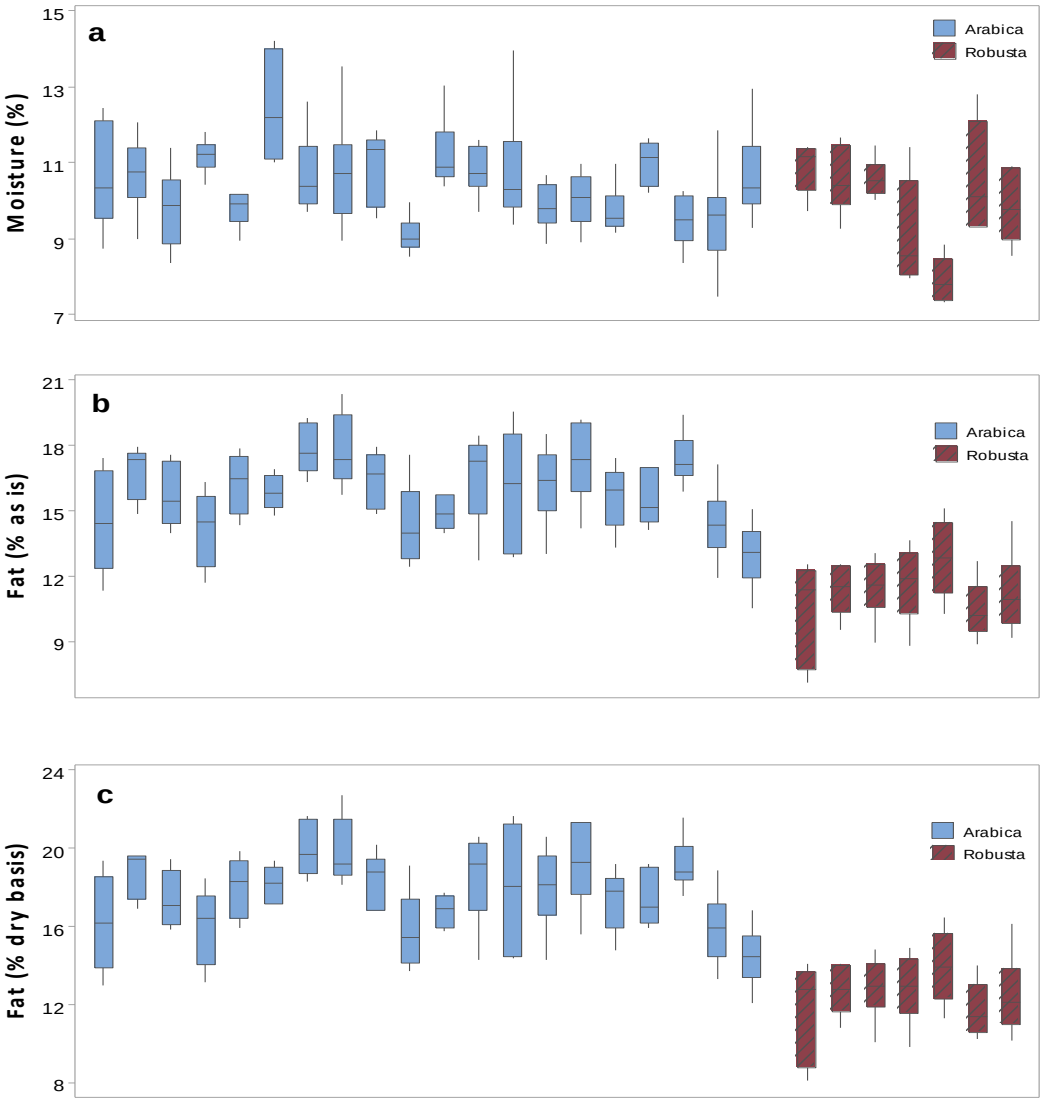


Figure 7.3. Distribution of the reference data for moisture and fat content in green beans, from independently sourced batches sourced from a range of suppliers, classified as Arabica or Robusta. a) Moisture content obtained by the fat analyzer; b) fat content (wet basis); c) fat content on a dry basis. Each batch comprises 6 individual coffee beans. Values within the box represent the range between the lower and upper quartile, the horizontal bar represents the median and the vertical bars represent the scores outsides the middle quartiles.

7.3.2. Moisture and fat prediction in single green coffee beans

The average reflectance spectra obtained for each coffee bean and the second derivative of these spectra are shown in Figure 7.5, indicating the most characteristic spectral features.

The performance of the PLS regression models for moisture prediction by HSI built on individual green coffee beans was calculated using several spectral pre-treatment methods, which slightly influenced the final prediction error (Table 7.3). The first derivative treatment resulted in the best

calibration performance for both sets of samples, with a calibration R_c^2=0.90 and cross-validation R^2 (R_{cv}^2)=0.86 in the case of natural moisture content, and R_c^2=0.97 and R_{cv}^2=0.96 for the laboratory treated beans.

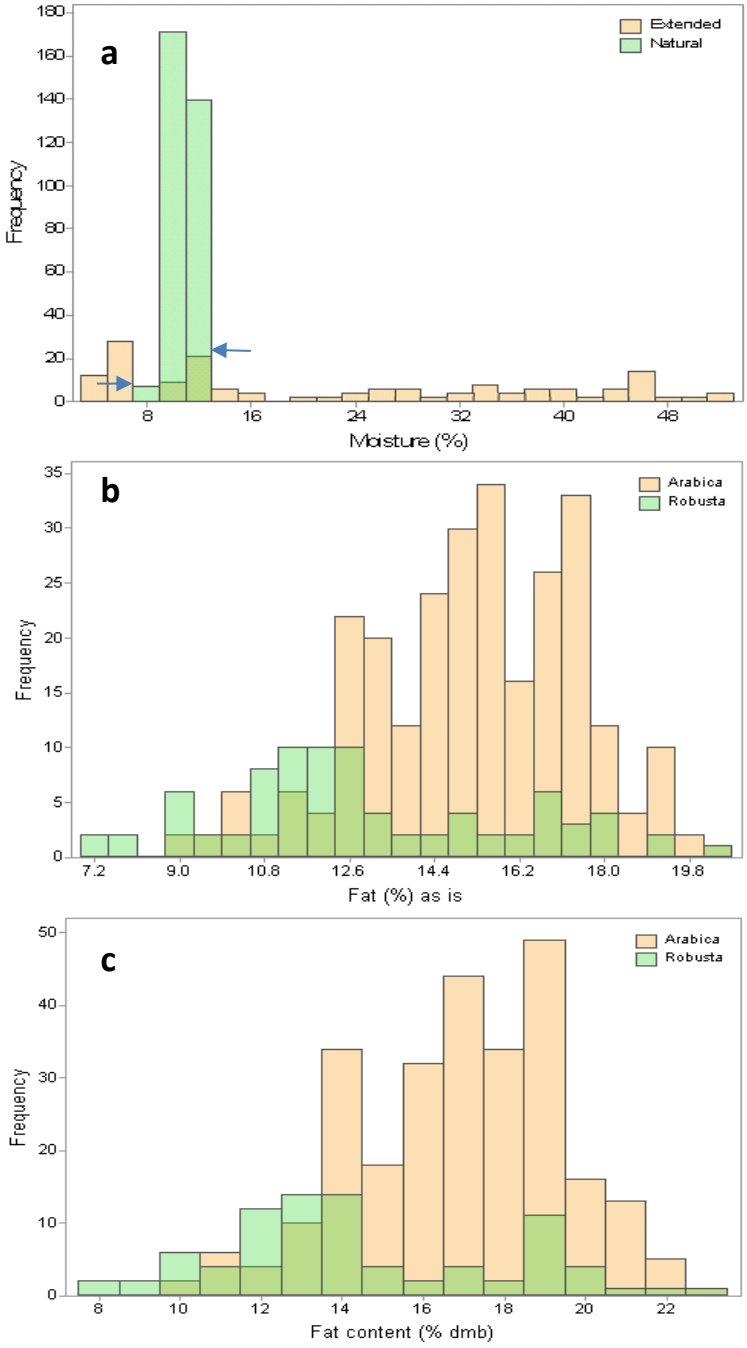


Figure 7.4. Distribution of **a**) moisture (natural moisture and extended moisture based on laboratory-treated beans), **b**) fat content expressed on wet basis, and **c**) fat expressed on dry matter basis (dmb).

Considering the range of moisture content in both models, the obtained prediction errors are acceptable for quantification purposes, depending on the desired application: for natural moisture the prediction error was always much below 0.3% for a range of 4.2%, whereas for laboratory treated beans the cross-validation error was 2.0% for a moisture range of 47.6%. Plots of the four calibrations obtained are shown in Figure 7.6.

The capability of NIRS for moisture analysis in foodstuffs is widely known to be due to water molecules corresponding to strong absorbance of water at specific wavelengths in the near-infrared region. The application of NIRS has been reported by Osborne (1987) for moisture determination in flour, ground wheat and whole wheat, demonstrating a good performance of a multiple regression calibration built on the wavelengths of 1940 nm and 2310 nm.

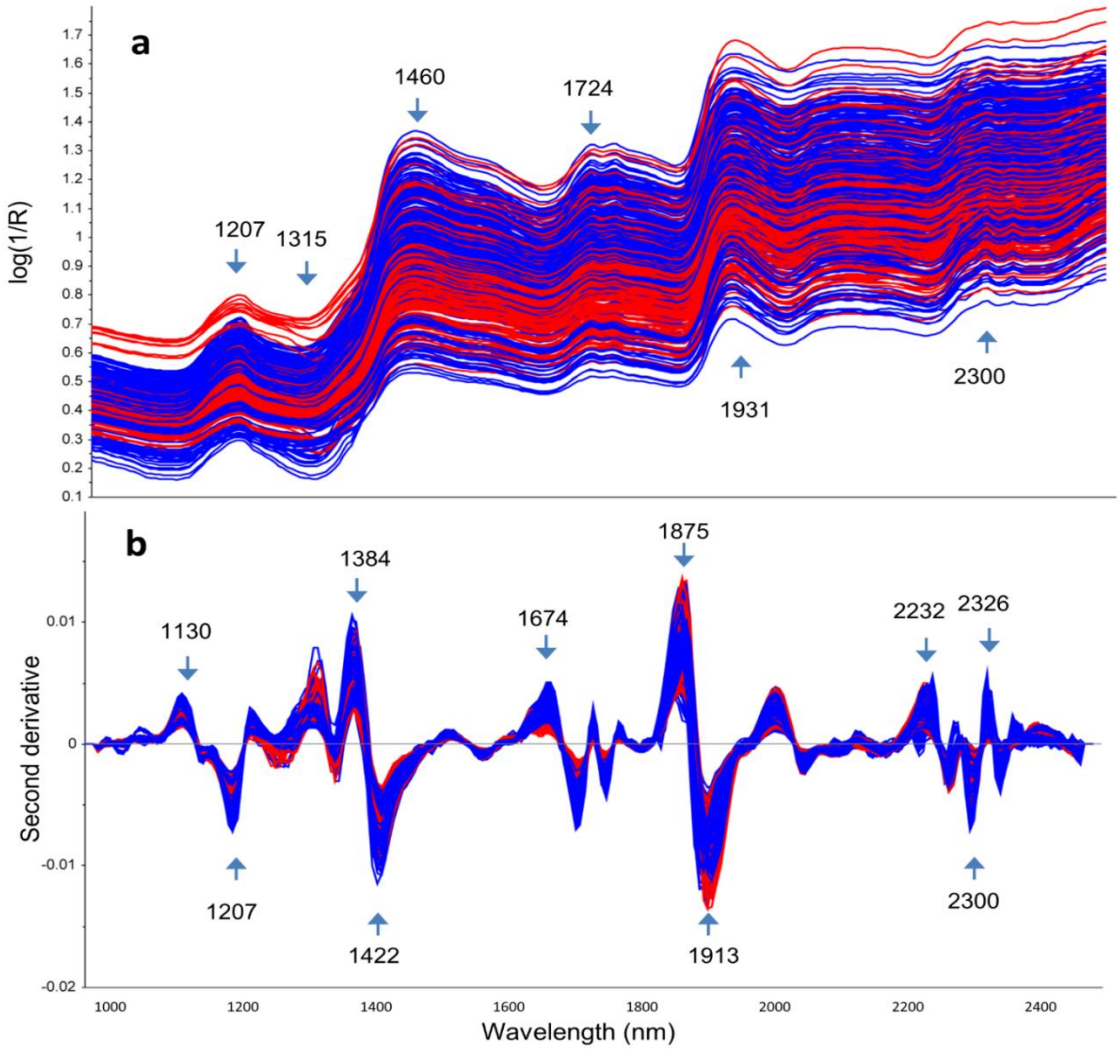


Figure 7.5. Mean reflectance spectra obtained from single green coffee beans: a) log(1/R); b) second derivative treatment. Red lines: Robusta; blue: Arabica. Numbers indicate the wavelength as nm.

Table 7.3. Performance of the PLS regression model for moisture content in single green coffee beans.

Parameter	Pre-processing	LV	R_c^2	RMSEC	Slope	R_{cv}^2	RMSECV	Slope	RPD
Natural moisture content	Log(1/R)	8	0.842	0.291	0.815	0.819	0.312	0.828	2.53
	Mean centred	8	0.844	0.289	0.844	0.825	0.307	0.834	2.57
	1st derivative	11	0.899	0.233	0.899	0.858	0.276	0.879	2.86
	2nd derivative	12	0.898	0.237	0.898	0.813	0.322	0.852	2.45
	SNV	12	0.897	0.235	0.897	0.850	0.285	0.872	2.77
Laboratory-treated beans	Log(1/R)	5	0.951	2.234	0.951	0.950	2.279	0.949	4.73
	Mean centred	5	0.947	2.314	0.947	0.947	2.372	0.946	4.54
	1st derivative	5	0.966	1.916	0.966	0.963	1.999	0.965	5.39
	2nd derivative	4	0.957	2.209	0.957	0.955	2.266	0.955	4.75
	SNV	3	0.962	2.041	0.963	0.912	2.074	0.962	5.19

Sample size (n): 320. Error is indicated as %. R_c^2, R_{cv}^2 = R^2 of calibration and cross-validation, respectively. The same number of LVs was use for the calibration and cross-validation models.

It was noted that whole kernels showed worse performance than ground material, with 0.29% prediction error in a moisture range 12.3–17.8%. The performance of this HSI calibration for moisture content is consistent with previous studies reporting similar calibrations, when taking into consideration the prediction error and the range of reference moisture analysed (Cogdill et al., 2004; Jin et al., 2015). However, a direct comparison with these studies is not possible as they involve different granular foods and not coffee.

The results for total fat calibration in intact single green coffee beans are reported in Table 7.4. The second derivative pre-treatment gave the best model performance on wet basis, obtaining a R^2 value of 0.89 and 0.88 for the calibration and cross-validation datasets. When the lipid content was expressed on a dry matter basis, the R^2 value was slightly better, being 0.90 and 0.89 for the calibration and validation datasets.

The prediction error was approximately 1% in all cases, whether expressed on wet or dry matter basis. In both cases, the cross validation error was below 1.0%, and thus perfectly suitable for quantitative purposes, considering the range of total fat (13.2% on wet basis).

The second derivative treatment has also been successfully applied by other authors to analyse fat content and oxidation in food products through NIRS (Khodabux, L'Omelette, Jhaumeer-Laulloo, Ramasami, & Rondeau, 2007).

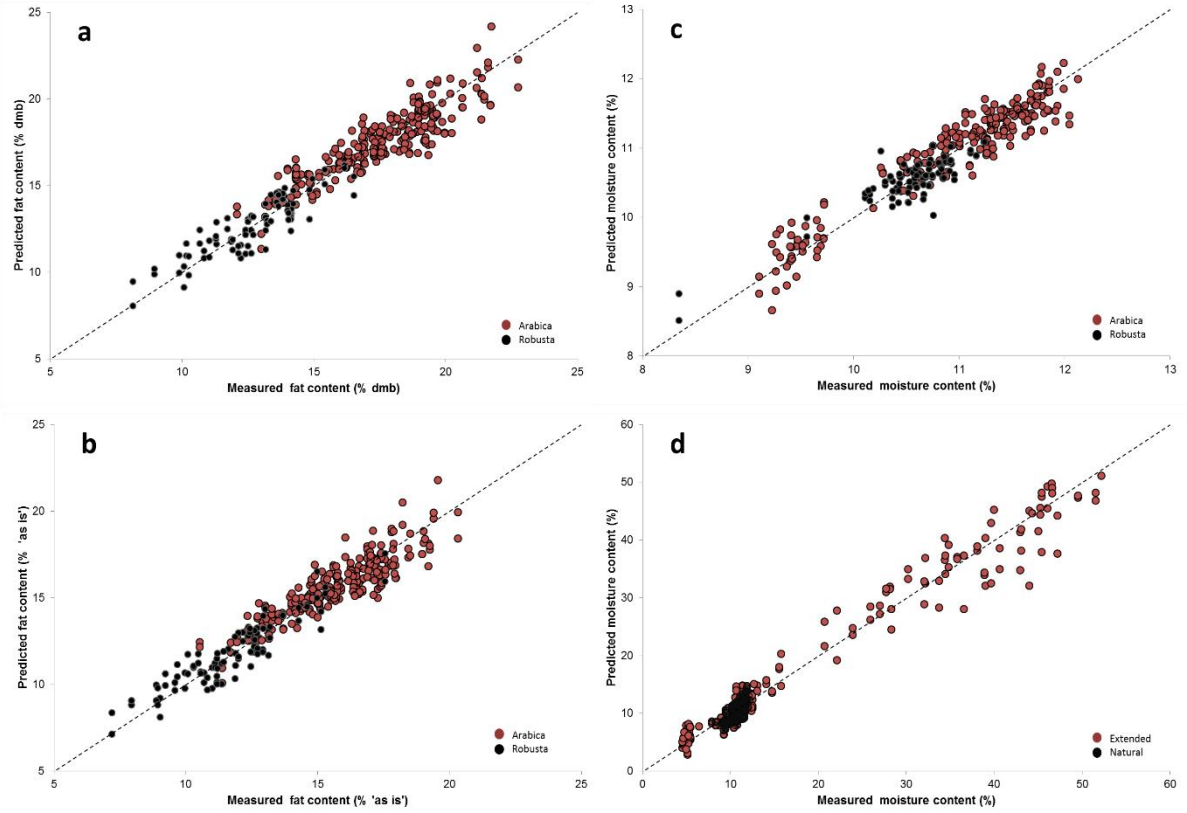


Figure 7.6. Prediction of coffee constituents in single green coffee beans using PLSR models based on HSI. **a**) Total fat content expressed as dry matter basis (dmb) (n=345); **b**) Fat content expressed on wet basis (n=345); **c**) Moisture content at the natural moisture range (n=314); **d**) Moisture content on the extended moisture range (laboratory treated beans and natural moisture beans) (n=463). The dotted line shows the ideal prediction.

Table 7.4. Performance of the PLS regression model for total lipid content in green coffee beans expressed on an wet (wb) or dry matter basis (dmb).

	Pre-processing	**LV**	**R_c^2**	**RMSEC**	**Slope**	**R_{cv}^2**	**RMSECV**	**Slope**	**RPD**
Wb	Log(1/R)	6	0.850	1.019	0.850	0.837	1.062	0.843	2.49
	1st derivative	4	0.866	0.961	0.866	0.860	0.985	0.857	2.68
	2nd derivative	6	0.893	0.861	0.893	0.883	0.904	0.885	2.92
	SNV	5	0.859	0.990	0.859	0.849	1.028	0.857	2.57
	Baseline	6	0.852	1.010	0.852	0.841	1.050	0.847	2.51
Dmb	Log(1/R)	6	0.864	1.087	0.864	0.855	1.125	0.862	2.76
	1st derivative	4	0.871	1.062	0.871	0.866	1.091	0.864	2.84
	2nd derivative	6	0.900	0.935	0.900	0.890	0.985	0.890	3.15
	SNV	5	0.864	1.081	0.864	0.855	1.117	0.860	2.78
	Baseline	6	0.857	1.116	0.857	0.845	1.169	0.853	2.65

Sample size (n): 350. Error is indicated as % (either on wet or dmb). R_c^2, R_{cv}^2 = R^2 of calibration and cross-validation, respectively. The same number of LVs was use for the calibration and cross-validation models.

The loading plots for the best PLS regression models for moisture and total fat content are shown in Figure 7.7.

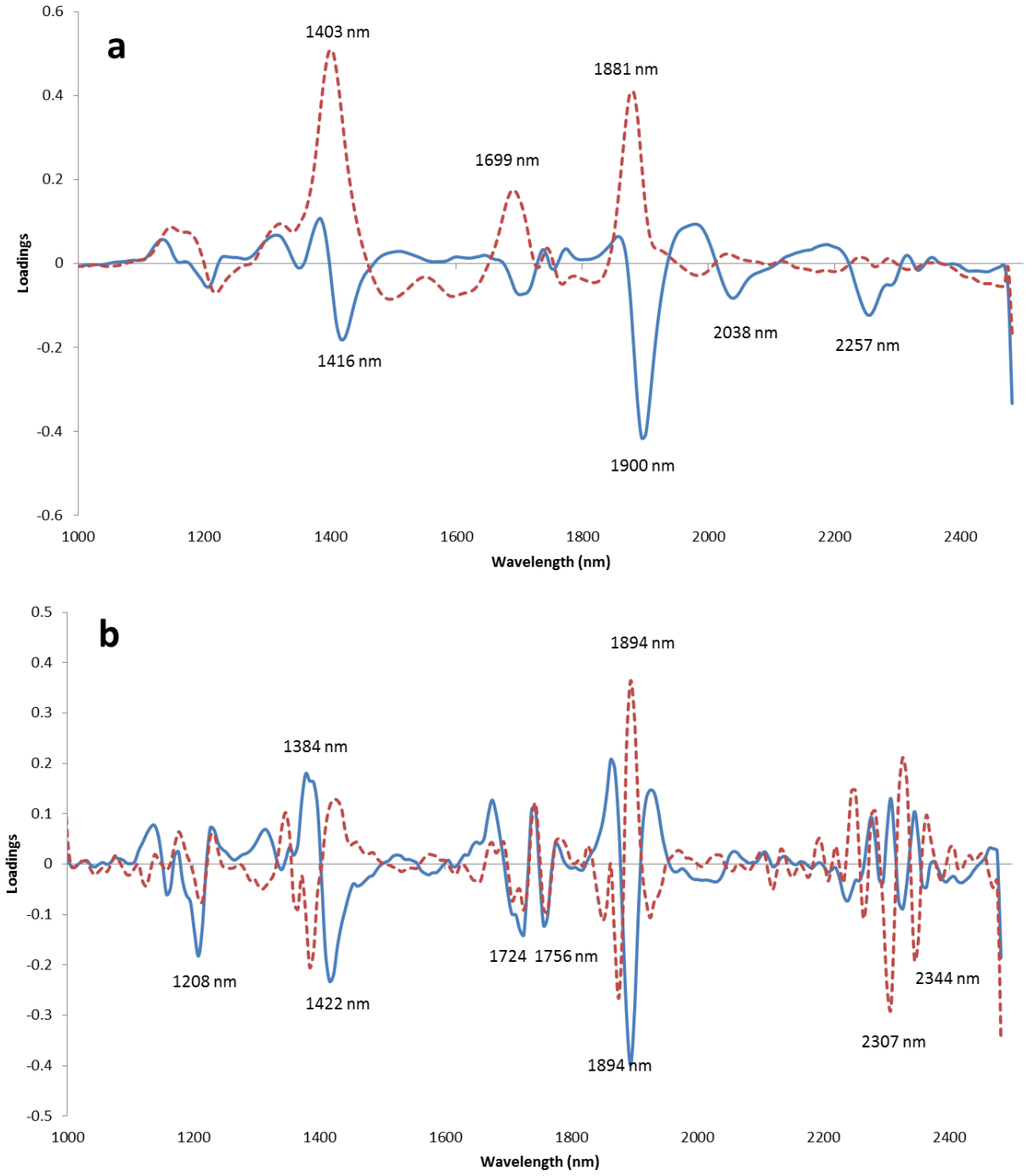


Figure 7.7. Loading of the first two PLS components for the (a) moisture (natural water content) and (b) fat (wet basis) PLS models showing the best performances for average spectra on a single green coffee bean basis obtained by HSI. The first (a) and second (b) derivatives were applied, respectively. Continuous blue line: PC1; dotted red line: PC2.

The strongest features observed for the moisture model were at 1416, 1900, 2038 and 2257 nm for PC1, and 1403, 1699 and 1881 nm for PC2 (Figure 7.7b). For total fat, the highest loadings were for 1208, 1384, 1422, 1724, 1756, 1894, 2307 and 2344 nm. Previous research on water loss of green coffee under drying conditions described a major peak at 1940 nm (Reh et al., 2006), which is related to the 2nd overtone of O-H (Esteban-Diez et al., 2004). Morgano et al. (2008) reported that the most important wavelengths for NIR moisture prediction in green coffee were 1975, 1852, 2040 and 2150 nm, and their regression model allowed moisture quantification with a validation R^2 of 0.818 and RMSECV 0.298%. The results herein presented show comparable, but even better performance (R_{cv}^2=0.858 and RMSECV=0.276%) despite employing a HSI system on intact coffee beans, as opposed to using a NIR instrument on ground coffee material as in Morgano et al. (2008). The number of LVs was similar when using the reference data on the wet basis or the predicted dmb, however the use of spectral pre-treatments generally allowed the use of lower number of LVs, the first derivative allowing building a good prediction model using only 4 LVs.

The low number of LVs suggest robustness of the model, and the successful detection of lipids in the NIR region was expected, also due to their relatively high abundance in coffee beans.

In comparison, Cogdill et al. (2004) reported a poorer performance for moisture prediction model, with their best PLS regression model having R^2 of 0.56 and a prediction error above 1%. The authors commented that this poor performance might be attributed to error both in the HSI instrument during acquisition and the higher error obtained for the reference measurement, because when single kernels/beans are analysed they are destroyed with no possibility of averaging repeated measurements to decrease noise and to detect anomalies.

The peaks at 1210, 1360, 1700–1760 and 2275–2300 nm have been reported to arise from the first and second overtone of C-H, and stretching of the -CH_2 groups. Absorption peaks around 1160 and 2130 nm were attributed to -HC=CH-, while the bands around 1200, 1400, 1750, 2310 and 2340 nm are usually associated to the C-H bond. The region between 2083 and 2222 nm is considered to be the combination of C-H stretching related to cis double bonds in the molecules, which exist due to the unsaturation of fatty acids (Khodabux et al., 2007).

A scheme of the main wavelengths absorbing in the NIR range, previously reported in the literature, is shown in Figure 7.8, by also showing some important coffee constituents.

Previous works attributed the absorbances at 1748 nm to carbohydrates (first overtone C-H stretching) and chlorogenic acids (Páscoa, Magalhães, & Lopes, 2013; Pizarro, Esteban-Díez, González-Sáiz, & Forina, 2007), while 1865 nm has been related to fibre content (O-H content and C-H stretching combination band; please refer to the Table A.1 in Appendix for further data on band assignment in coffee) (Esteban-Diez et al., 2004). Absorbances at 1862 and 1667 nm have associated to caffeine, being related to the C-H stretching first overtone (Pizarro et al., 2007). Absorbance at 1627 nm has been attributed to aromatic group, while 1748 nm to compounds containing the thiol group (Poisson, Schmalzried, Davidek, Blank, & Kerler, 2009).

The Ratio of Performance to Deviation (RPD) provides an indication of the quality of calibration equations for PLS regression models. Values above 2 have been described to give excellent models, while RPD values of between 1.4 and 2 is fair, and values below 1.4 indicative of non-reliable models (Ncama, Opara, Tesfay, Fawole, & Magwaza, 2017). In the present case, the RPD was 2.9 for moisture with the natural content and 5.4 for the model with extended moisture range. This dramatic improvement for the laboratory treated beans was attributed to the very large range of moisture content, although the performance of the natural moisture content model suggests that it can be used for standardisation of the batch in order to detect single beans with excessive or very low moisture content.

The RPD value was 2.92 for lipids expressed on an wet basis, but the dry matter basis (dmb) model was more accurate with an RPD of 3.15. The performance of the model herein presented is comparable to other calibrations built using traditional NIR instruments, even for ground coffee beans.

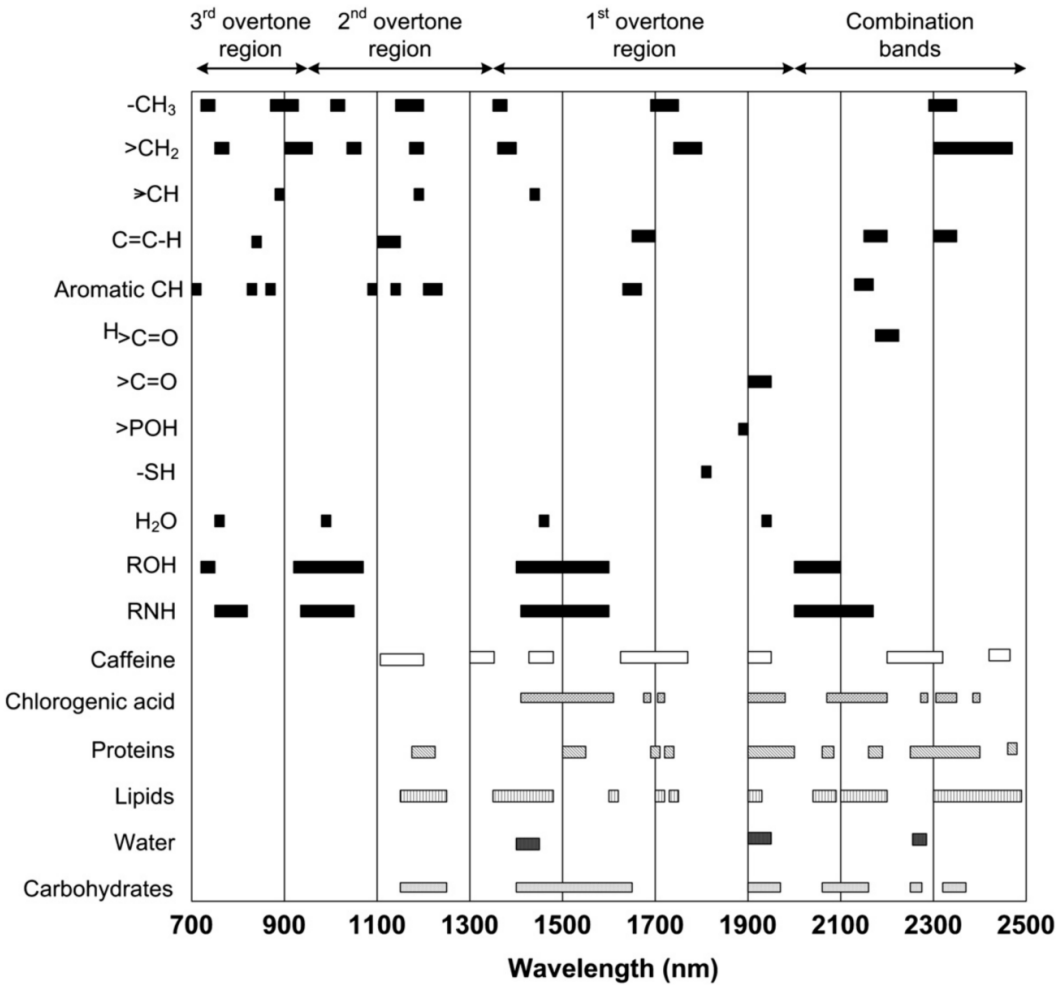


Figure 7.8. Schematisation of the main absorption bands for chemical groups or compounds found in coffee (Barbin et al., 2014).

For instance, Pizarro et al. (2004) reported calibration R^2 values of 0.763–0.987 for a PLS regression calibration for total fat in roasted and ground coffee using NIR data in the region 1100–2500 nm for a variety of spectral pre-treatments. However, it should be noted that roasted and green coffees have very different spectra, with also a dramatic change of the lipid content. The two species overlap in terms of fat content in the middle region of the distribution (Figure 7.3), for this reason a general model was proposed, which can be usefully applied to any coffee species. In addition, multivariate prediction models were separately built for the Arabica and the Robusta samples, obtaining a general improvement of the prediction error of approximately 0.15%. However, this slightly better prediction might not compensate for the disadvantage to have separate models, especially when blends are analysed.

7.3.3. Wavelength selection

As illustrated in Figure 7.9, the regression coefficient plot for HSI fat prediction showed a few strong absorbance wavelengths. This suggests that the decrease of the number of spectral variables might be effective in predicting fat content while using a multispectral imaging system rather than a full spectral band system.

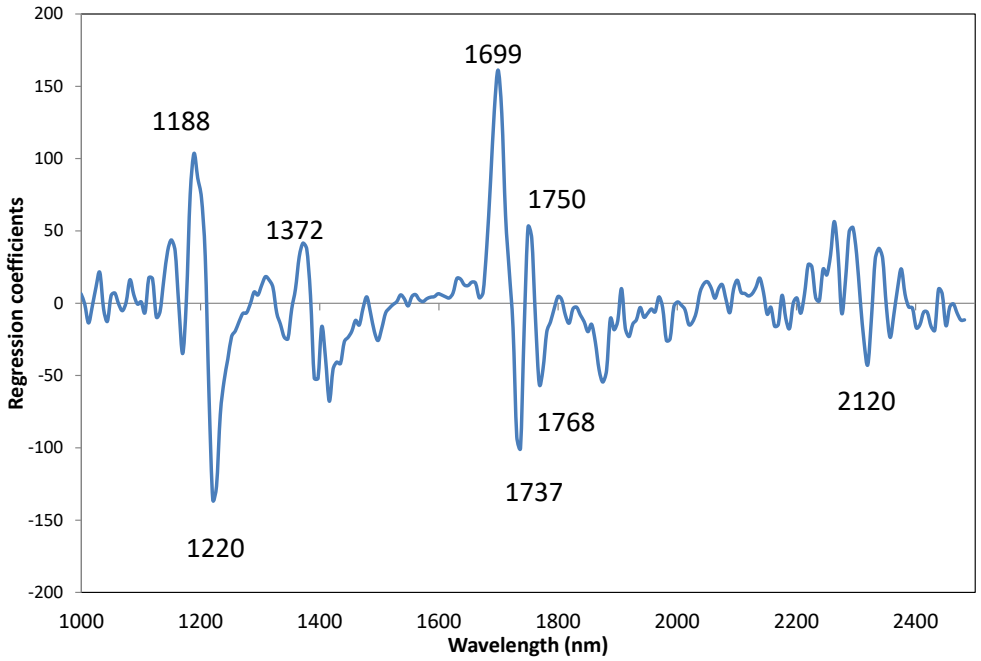


Figure 7.9. Regression coefficients of the PLSR model for total fat prediction in single green coffee beans by HSI.

For practical applications, data reduction strategies are of interest as they may enable cheaper multispectral sensors to be used to target fewer specific diagnostic wavelengths. To evaluate this, a wavelength reduction strategy was applied to the best models for moisture and fat prediction, according to strategies previously published in the literature (Mehmood, Liland, Snipen, & Sæbø, 2012; Osborne, 1987).

The wavelength selection methods that start from the whole PLSR model and remove the less useful bands are based on the assumption that only those wavelengths with large β-coefficients are useful for the prediction. Therefore, by setting a cutting off value, those bands with the highest value in absolute terms are taken to build a new model with reduced number of spectral variables.

The selection of the most important wavelengths was carried out based on the regression coefficients for these PLSR models. Table 7.5 shows the performance of Multiple Linear Regression (MLR) models built using the selected wavelengths.

Table 7.5. Multiple Linear Regression (MLR) models for moisture and fat content (% wet basis) in green coffee beans obtained by selecting the most important variables using log(1/R) values with no spectral pre-treatment.

Parameter	**Variable**	**Calibration**		**Cross-validation**		**Validation**
	no.	**R_c^2**	**RMSE**	**R_{cv}^2**	**RMSECV**	**Offset**
Moisture	6*	0.615	0.459	0.596	0.471	0.61
	42	0.887	0.242	0.842	0.286	0.29
Fat	6*	0.693	1.464	0.676	1.503	4.57
	6§	0.841	1.053	0.834	1.078	2.36
	22	0.860	0.988	0.832	1.081	2.17

Parameter	**Validation Offset**
Moisture	980, 1283, **1384, 1391,** 1756, 2151 1384, 1441, 1755, 1975, **2150,** 2270, **2276,** etc.
Fat	1208, 1372, 1711, 1749, **1881,** 2295 1182, **1208,** 1302, 1429, 1542, 2244 1170, **1182,** 1208, **1214,** 1843, 1850, 2120, 2270, etc.

*Variable selection was performed based on the β-coefficients of the PLS model (filter method).
§Model built by PLS regression (LV=6). The only treatment done on the spectra was noise removal and absorbance calculation [log(1/R)]. Numbers in bold indicate the most intense wavelengths.

The use of 42 bands led to a good performance compared to the PLSR model reported in the previous section for moisture using the full spectra range. In fact, it had a RMSE of 0.242% and RMSECV of 0.286%, which is comparable to the PLS regression model. A further reduction of the number of selected wavelengths down to 6 still led to R^2 values of 0.615 and 0.596 for calibration and cross-validation, respectively, along with a marked increase in prediction error.
It should be noted that this prediction is made on the reflectance data with no spectral pre-treatment, as derivatives cannot be applied in such circumstances, which brings a larger prediction error when using filter instruments with few selected wavelengths. The selected wavelengths for the fat and moisture prediction models are shown in Figure 7.10.

The use of multispectral imaging systems instead of full range HSI might be of interest for the industry for its practicality, particularly for the advantages in terms of computational capacity required and the possible use of lower-cost sensors. Thus, the multi-spectral model herein obtained could be considered as acceptable for some practical applications for rapid screening or higher or lower moisture beans, especially when lower cost sensors are needed.

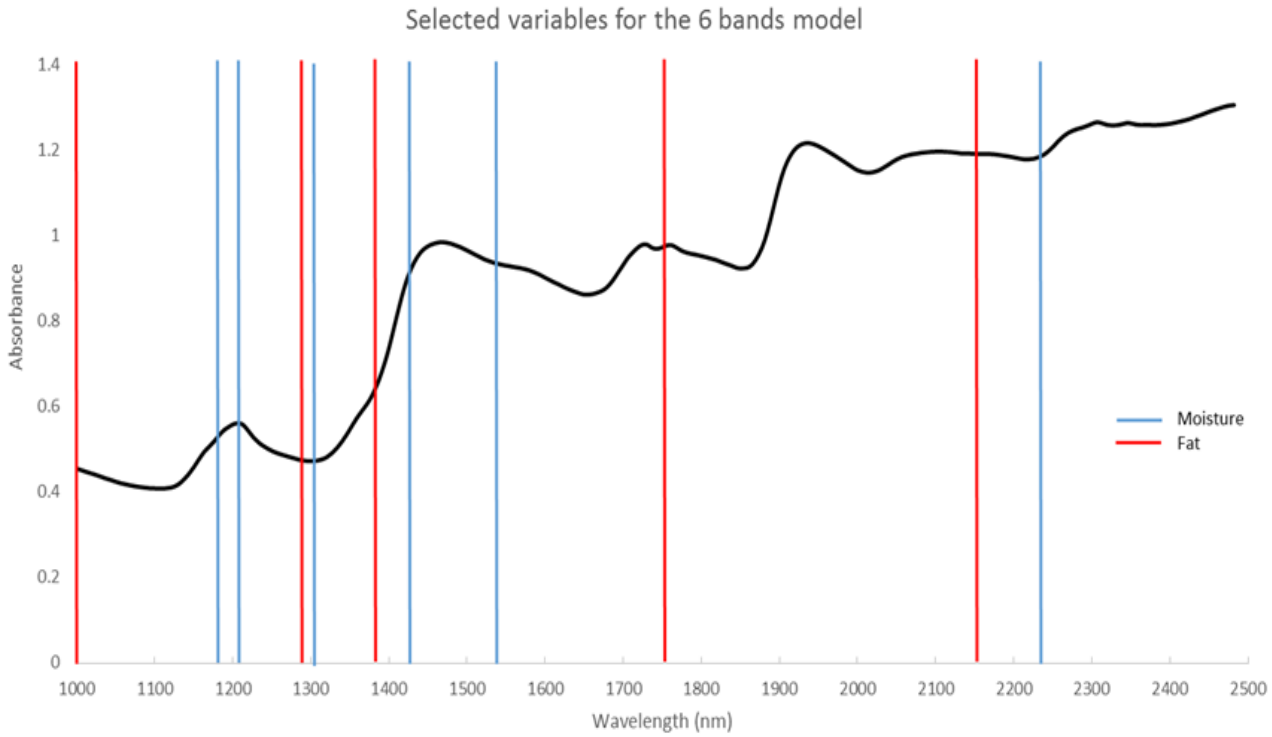


Figure 7.10. Most important spectral bands selected for the HSI moisture and fat prediction model, to build a multi-spectral imaging prediction.

The fat prediction models were similarly affected by the number of variables selected, and the statistics applied. The use of 22 wavelength variables resulted in a performance almost identical to the PLSR model built using the full spectral range. This finding is in agreement with other studies (Xu, Riccioli, & Sun, 2016), and suggests that most bands exhibit redundant information due to collinearity, and that waveband reduction techniques could be advantageous for the implementation of HSI technology for practical applications, e.g. screening of fat content in the food industry. Reduced bands resulted in similar prediction error when using PLS regression, while the poorest performance was obtained using 6 wavelengths and a MRL model. However, even in this case, the cross-validation error was 1.5%, which might be acceptable for some

practical application and screening. These results are in agreement with previous literature on HSI variable reduction applied to food, which reported that some practical application and screening optimized models show comparable performances with PLSR models where the whole spectra are used (Xu et al., 2016). Also, it should be noticed that despite the fact that water is known to absorb in defined regions of the NIR spectrum, mostly where the O-H water bands absorb, the sole use of those bands do not lead to a good predictive model, and many other bands are needed. This is in agreement with previous literature dealing with moisture prediction in food products: Zhao et al. (2017) recently applied HSI to predict total fat and moisture in ground beef, and they selected a higher number of variables for the moisture model, i.e. from 11 to 43, than the one to describe the fat content, from 7 to 40, depending on the spectral pre-treatment applied.

Despite water having characteristic absorption features in specific regions of the NIR spectrum, the sole use of those wavelengths does not lead to good predictive models and so additional wavelengths are required. This is in agreement with the findings of Zhao et al. (2017).

7.3.4. Application of PLS calibrations (chemical mapping)

The developed PLS regression models for the prediction of moisture and total fat in green coffee beans were applied to HSI hypercubes to visualize the moisture and lipid distribution and content both between coffee beans and within individual beans, with the models using the full NIR spectrum available. Figure 7.11 shows the distribution and content of moisture in a batch of Mexican Arabica green coffee beans.

By applying the calibration coefficients at a single pixel level, it was possible to both predict the average moisture content for a single coffee bean, and even visualize the water content within the beans. For some beans, the distribution of moisture appears to vary somewhat throughout. However, there are practical difficulties in validating such differences at a single pixel level with the aid of analytical reference measurements.

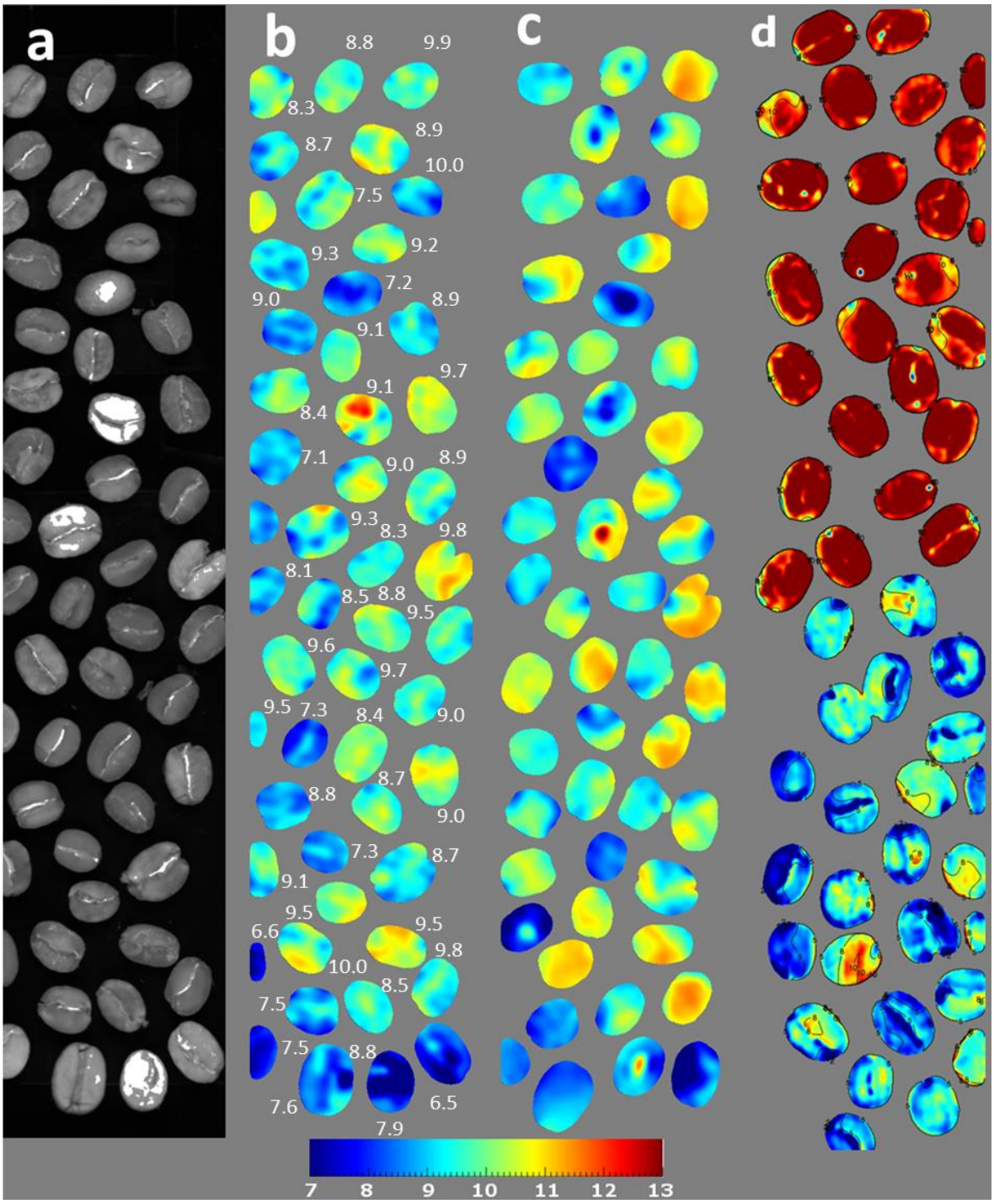


Figure 7.11. HSI calibration applied for moisture content in green coffee beans on a batch of Mexican Arabica. **a**) grayscale images showing the reflectance hypercube obtained from a continuous moving stage, at one spectral band (1150 nm); **b**) reconstructed image showing predicted moisture content visualized at single pixel level; **c**) predicted moisture obtained after the rotation of the coffee beans on the other face; **d**) batch subdivided into an aliquot placed under humid conditions (upper beans) or partially dried in an oven (lower). Numbers indicate the average predicted moisture expressed as %.

Figure 7.12 shows two batches of coffee beans, one Arabica and one Robusta, which clearly reveals the interspecies variation when visualizing the lipid distribution on a single pixel level. As expected, the Arabica and Robusta coffee batches had significant differences in their lipid content; the latter containing much lower fat content. Minimal effects of coffee bean orientation were found during imaging. The six coffee beans belonging to the Arabica batch had lipid content ranging from approximately 17% to more than 22% (dmb).

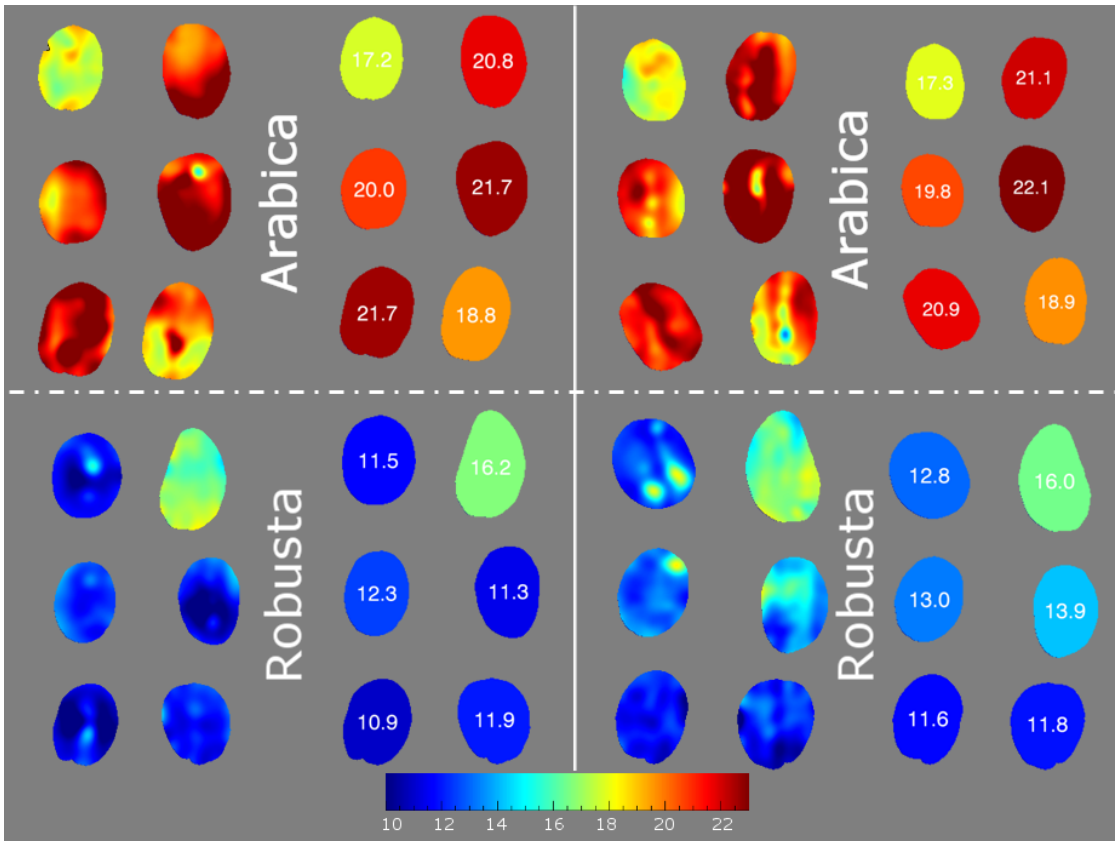


Figure 7.12. Application of HSI calibration (chemical imaging) for total lipid content visualisation in green coffee beans: example for Arabica (top) and Robusta (bottom) batches. The left and right halves of the figure show the same coffee beans placed on the opposite surface (inverted 180° about the y-axis). The numbers shown are the predicted average lipid content calculated from the single pixel shown for each bean, expressed as % (dmb).

The Robusta batch ranged from approximately 11% to 16%. A calibration for fat such as this would be interesting not just for visualising the distribution within individual coffee beans, but also for application to botanical and plant physiology studies related to lipid accumulation and especially the changes of lipid content at the outer layer in the post-harvest processing.

7.3.5. Coffee bean species classification

In addition to quantitative models, HSI is also applicable for rapid classification of intact granular food commodities, through the building of classification models. Both green and roasted beans (treated using the same time-temperature profile during roasting) were analysed individually. Figure 7.13 shows the HSI spectra of the coffee beans, to demonstrate the absence of clear difference in any particular NIR range between the two coffee species.

As reported in Table 7.6, Linear Discriminant Analysis (LDA) for green coffee produced better performances than Support Vector Machine (SVM), achieving up to 100% classification accuracy. The highest SVM classification accuracy for green coffee beans was just over 97%. For the roasted coffee beans, SVM achieved validation accuracies of 91.8 and 97.1% depending on the function applied, with SNV pre-treatment resulting in the best performance.

For roasted coffee, LDA produced the best results with a linear function, achieving 100% correct classification accuracy for log(1/R), first and second derivative pre-treatment.

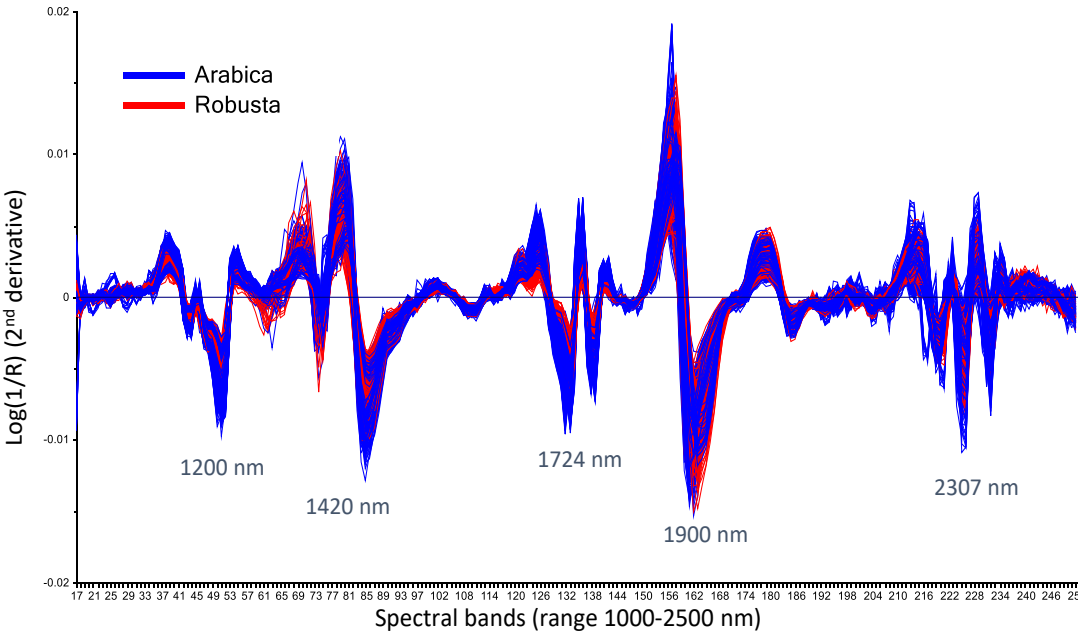


Figure 7.13. Average NIR spectra of single green coffee beans belonging to Arabica or Robusta species, after second derivative spectral pre-treatment using Savitzky-Golay smoothing.

Table 7.6. Coffee bean classification models for species identification (Arabica-Robusta) based on Linear Discriminant Analysis (LDA) and Support Vector Machine (SVM) for green and roasted whole coffee beans. Sample size: 510 for green; 340 for roasted beans.

Method	Function	Pre-treatment	Green		Roasted	
			Correct (%)	Incorrect (%)	Correct (%)	Incorrect (%)
LDA	Linear	Log(1/R)	98.39	1.61	98.53	1.47
		1st derivative	99.29	0.71	100.00	0.00
		SNV	98.57	1.43	98.53	1.47
		MSC	98.75	1.25	98.53	1.47
		2nd derivative	99.61	0.39	100.00	0.00
	Quadratic	Log(1/R)	100.00	0.00	100.00	0.00
		1st derivative	99.80	0.20	99.12	0.88
		SNV	99.80	0.20	99.71	0.29
		MSC	100.00	0.00	99.41	0.59
		2nd derivative	99.80	0.20	98.82	1.18
Method	**Function**	**Pre-treatment**	**Training accuracy (%)**	**Validation accuracy (%)**	**Training accuracy (%)**	**Validation accuracy (%)**
SVM	Polynomial	Log(1/R)	74.90	74.12	87.06	84.42
		1st derivative	72.55	72.55	64.71	64.71
		SNV	88.43	87.06	94.12	91.76
		MSC	82.75	82.16	95.00	88.24
		2nd derivative	72.55	72.55	64.71	64.71
	Radial basis function	Log(1/R)	84.90	83.92	90.29	88.24
		1st derivative	91.18	91.18	88.24	88.24
		SNV	97.45	97.25	98.23	97.06
		MSC	94.51	94.12	95.00	94.12
		2nd derivative	89.02	88.82	84.71	84.42

SVM is a classification algorithm that is part of the family of statistical learning methods, and it works in a way that minimises the risk of overfitting. The method finds the maximal margin hyperplanes in data subsets between different classes (Sun, 2016). However, in the present case it resulted in similar or slightly poorer results compared to LDA.

This is the first reported attempt of Arabica-Robusta classification based on HSI using the full NIR spectral range, i.e. above 1700 nm. Previous publications reported on the possibility to group Arabica-Robusta beans by applying Principal Component Analysis (PCA) and to separate the two sets using the first two PCs (Esteban-Diez et al., 2007; Rubayiza & Meurens, 2005).

7.4. CONCLUSIONS

HSI has been applied for the first time for the prediction of coffee constituents on a single coffee bean basis. The devised approach uses averaged spectral data from the hypercube to enable PLS calibrations to be built on a single object (bean) basis. The wide distribution of lipid content has been herein demonstrated, within the same batch and between batches, and developed a moisture calibration that is capable of detecting problematic seeds within the population. The prediction of lipid content on single coffee beans could be of practical interest for the industry, for example for the production of soluble coffee one can use the beans with the lowest fat content as it does not influence the yield or quality, while it has a critical importance for espresso-like preparations due to the formation of "crema". Applying the calibration at a single pixel level provided the means to visualise compound distribution within individual coffee beans.

This approach showed excellent prediction capabilities for both moisture and total fat content analysed through HSI, which is a technique showing potential for rapid and non-destructive screening, to obtain accurate indication on the coffee bean composition and uniformity in a whole bean dataset. The application of these calibrations would allow detecting beans with unacceptably high moisture content (storage issues) or very dry beans (risk of burning during roasting), as well as analysing their fat content with implication on coffee quality, e.g. "crema" and body in espresso-like preparations.

8. PREDICTION OF SUCROSE, CAFFEINE AND TRIGONELLINE IN SINGLE GREEN COFFEE BEANS.

8.1. INTRODUCTION

Sucrose and alkaloids are known to directly influence the final drinking quality of coffee (Joët et al., 2010). However, existing published literature on the variability of green coffee constituents is limited. For this reason, the study of the composition and the variability of single green coffee beans is relevant in terms of quality control and for product standardisation.

The sucrose content is reported to have a wide range between batches of green coffee beans, from 3.8 to 10.7% (dry weight basis), depending on the botanical and geographical origins (Campa et al., 2004). Green Arabica coffee beans have sucrose contents ranging from 6.25 to 8.45%, whereas in Robusta it ranges from 0.9% to 4.85%, with Robusta containing more reducing sugars (Clarke & Vitzthum, 2008). Other researchers reported sucrose content for Robusta coffee of 4.05–7.05% (dwb) (Ky et al., 2001). The post-harvest processing of coffee beans can also affect their composition; for example, ranges of 2.60–3.02% and 6.60–7.02% have been reported for sucrose in dry-processed and wet-processed green coffee, respectively (Clarke & Vitzthum, 2008). Acids and alkaloids both play a critical role in terms of coffee quality, as they influence the flavour of the beverage. Caffeine content in Arabica coffee beans is in the range of 0.9–1.3% (Farah, 2012), while it ranges from 1.51 to 3.33% (dwb) for Robusta (Ky et al., 2001). Trigonelline is an alkaloid whose synthesis is carried out by enzymatic methylation of nicotinic acid. Its importance in coffee is mainly related to its degradation during roasting to give several volatile compounds, mainly pyrroles and pyridines. Its concentration in Robusta varies from 0.75 to 1.24% (dwb) (Ky et al., 2001), which is considerably higher than Arabica (Farah, 2012). The natural variability of these compounds in green coffee beans has been studied in relation to the coffee accessions (Ky et al., 2001). Trigonelline and sucrose content depends on the coffee genotype (Campa et al., 2004), but not significantly affected by the country of origin, nor the genetic groups (Ky et al., 2001).

The analysis of coffee constituents is usually performed by wet chemistry, particularly high-resolution liquid chromatography (HPLC). HPLC with Diode-Array Detector (DAD) has been applied for the simultaneous analysis of trigonelline, nicotinic acid and caffeine in coffee (Casal et al., 1998). More recently, Perrone et al. (2008) described a method which also allowed the identification and quantification of sucrose, based on HPLC-MS analysis. However, despite the advances in analytical speed and the possibility of simultaneously analysing sucrose, caffeine and trigonelline with a single coffee extraction, the destructive nature of the testing and the considerable time required for the grinding, extraction and analysis is impractical for industrial settings. For this reason, the development of fast, non-destructive techniques for green coffee composition is of great research and commercial interest. Moreover, the study of single beans without grinding offers the possibility of understanding variability on a single coffee bean basis. This would offer the potential for the selection of breeding lines with desired characteristics.

NIR spectroscopy (NIRS) has potential to analyse bulk coffee properties, by prediction of caffeine (Fox et al., 2013; Pizarro et al., 2007), chlorogenic acids (Martín, Pablos, & González, 1998) and total sugars (dos Santos Scholz et al., 2014). Other research demonstrated even certain prediction of the final cup quality based on NIR scanning of bulk roasted coffee beans, as a ground material (Esteban-Diez et al., 2004; Ribeiro et al., 2011). Pizarro et al. (2007) reported a prediction model based on reflectance NIR in the region 1100–2500 nm for caffeine content in ground and roasted coffee using PLS regression. Most NIR studies used ground material, so information on the natural variability among coffee beans is absent and no indication of the spatial distribution of chemical compounds within individual beans can be obtained. However, there is very little information available on the use of HSI for coffee evaluation. Nansen et al. (2016) used HSI to characterise commercial roasted and ground coffee batches from the market to assess the consistency of their quality. Calvini et al. (2015) presented a case study of HSI on coffee beans to demonstrate a new sparse method for pixel classification within the hypercube. Cho et al. (2017) reported on the use of HSI to investigate the qualitative properties of defective roasted coffee beans, which can be considered as different degrees of roast. The authors used one batch only, which was split into five sub-samples and treated under different time-temperature profiles. The

classification model built on the spectral region 1000–1700 nm produced accuracies of 85.7% and 86.7% for the calibration and validation datasets, respectively. Even where HSI has been applied to whole coffee beans, the majority of these cases are for classification without reference measurement and not for quantification purposes. Moreover, the analysis was limited to the NIR region below 1700 nm.

Therefore, the aim of this study was to explore the feasibility of HSI, in the range 1000–2500 nm, for the prediction of sucrose, caffeine and trigonelline contents in individual green coffee beans, whilst visualising their distribution at a single pixel level.

8.2. MATERIALS AND METHODS

8.2.1. Coffee samples, chemicals and reagents

Green coffee samples were sourced from several producing locations worldwide, comprising Brazil, Colombia, Costa Rica, Ethiopia, Guatemala, Honduras, India, Kenya, Mexico, Nicaragua, Rwanda, Uganda and Vietnam. These included batches treated using both the washed post-harvest system and the drying system ("natural"), as well as a semi-washed sample from Rwanda and a Monsoon Malabar treated batch from India. Reference standards of sucrose, trigonelline and methanoic acid (purity >95%) were supplied by Sigma-Aldrich (St. Louis, MO, USA), and caffeine (98.5% purity) was supplied by Acros organics (New Jersey, USA). Lead (II) acetate basic solution was supplied by VWR International Ltd (Lutterworth, UK) and HPLC grade methanol was supplied by Fisher scientific (Loughborough, UK). All other chemical and reagents used were of analytical grade.

8.2.2. HSI analysis

Single green coffee beans were scanned on both sides using an HSI system as described in Sections 7.2 and 3.2.

8.2.3. Caffeine, sucrose and trigonelline extraction

The reference analysis of caffeine, sucrose and trigonelline was performed according to Perrone et al. (2008). Green coffee beans previously scanned by HSI were individually ground using a

Perten 3100 electric grinder (Perten, Hägersten, Sweden). Approximately 0.1 g of the recovered material was accurately weighed; 20 mL boiling distilled water was added, and immediately shaken in a Stuart Orbital incubator SI500 at 250 rpm for 15 min. After cooling the flask under running water, 0.1 mL of a saturated lead acetate solution was added to clarify the extract. Samples were then centrifuged for 5 min at 3000 rpm using a Rotina 380R centrifuge (Hettich, Tuttlingen, Germany). The supernatant, excluding the upper lipid phase, was recovered and filtered through a 0.45 μm Millex MF-Millipore membrane. The final extract was diluted 1:5 with distilled water for HPLC/MS analysis.

8.2.4. HPLC/MS analysis

The coffee extract was analysed using an Agilent 1100 HPLC coupled with a Quattro Ultima MS/MS system, according to Perrone et al. (2008), with slight modifications. Chromatography separation was performed using a Phenomenex Kromasil 5ODS (C18) column (250 mm x 3.2 mm i.d. x 5 μm particle size, Waters, Milford, USA). Eluent A comprised water with 0.3% methanoic acid, while eluent B was methanol. The HPLC program started with 25% B, increased to 65% B after the injection, and was held for 7 min. The ratio was then altered to 25% B at 7 min and held for another 4 min to equilibrate the column. The electrospray ionization source operated in negative ion mode during the first 4 min, while the positive ion mode was used from 0 to 7 min. The source temperature was 100 °C, and the desolvation temperature was held at 400 °C. The cone gas flow was 100 L h^{-1} while the desolvation flow was 500 L h^{-1}. The capillary voltage was set at 2.0 V for ES^+, and 2.5 V for ES^-, with a cone voltage of 40 V and 50 V, respectively. The multiplier was set at 500 for ES^+, and 650 for ES^-. The detector was operated in Selective Ion Mode using the following m/z for the three compounds: 387 (sucrose), 195 (caffeine) and 138 (trigonelline). Identification was performed by comparing retention time and mass spectra with pure reference compounds, and the quantification was performed using calibrations established with pure compounds (Figure 8.1). The extracts were analysed in duplicate. The data were processed in MassLynx 4.0 (Waters, Milford, USA) and Microsoft Excel, and exported for the statistical analysis.

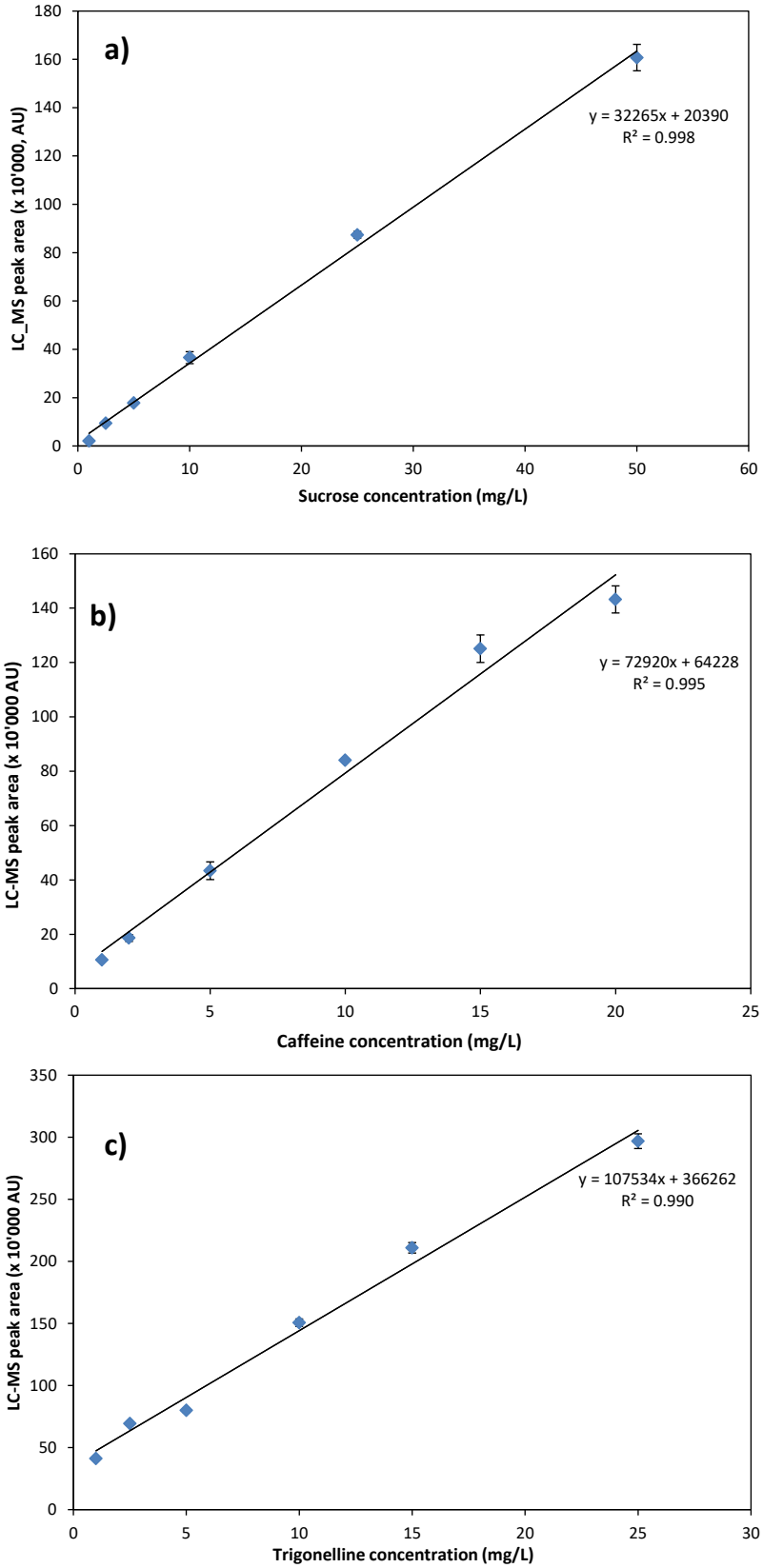


Figure 8.1. LC-MS calibration curves for pure **a**) sucrose, **b**) caffeine and **c**) trigonelline. Bars indicate standard deviation from triplicate analysis.

8.2.5. Recovery experiment, limits of detection and quantification

A recovery experiment was performed using a green Mexican Arabica sample as a blank for spiking with the standard compounds. Three different levels of spiking were applied. Triplicate analyses were performed for each level and for the unspiked sample. The limits of detection (LOD) and quantification (LOQ) were calculated as three times and ten times the signal-to-noise ratio (S/N), respectively (Perrone et al., 2008). Examples of the HPLC-MS traces for each of the analyte are shown in Figure 8.2.

8.2.6. Data processing and statistical analysis

Hypercube data normalisation and spectral pre-treatments were applied as previously described (Section 3.2). Two PLS regression models were built for each target compound, i.e. sucrose, caffeine and trigonelline. One was to express the concentration on wet basis (as it was analysed, with no moisture adjustment or drying of the beans). However, to test whether the use of dry matter basis reference data could give better prediction performance, a previously established moisture calibration model (Chapter 7) was applied on the hypercubes so that the predicted moisture content was calculated, and the reference measurements were also expressed on a predicted "dry matter basis" (dmb). The models were validated using the cross-validation method, using a 20-segment random cross-validation technique. In addition, a non-linear prediction model named Support Vector Machine Regression (SVM-R) was tested as an alternative to linear regression. The SVM type was the epsilon SVR, with radial basis function kernel type, and the following parameters: C value=10; Epsilon=0.1; Gamma=0.01. 10-segments cross validation.

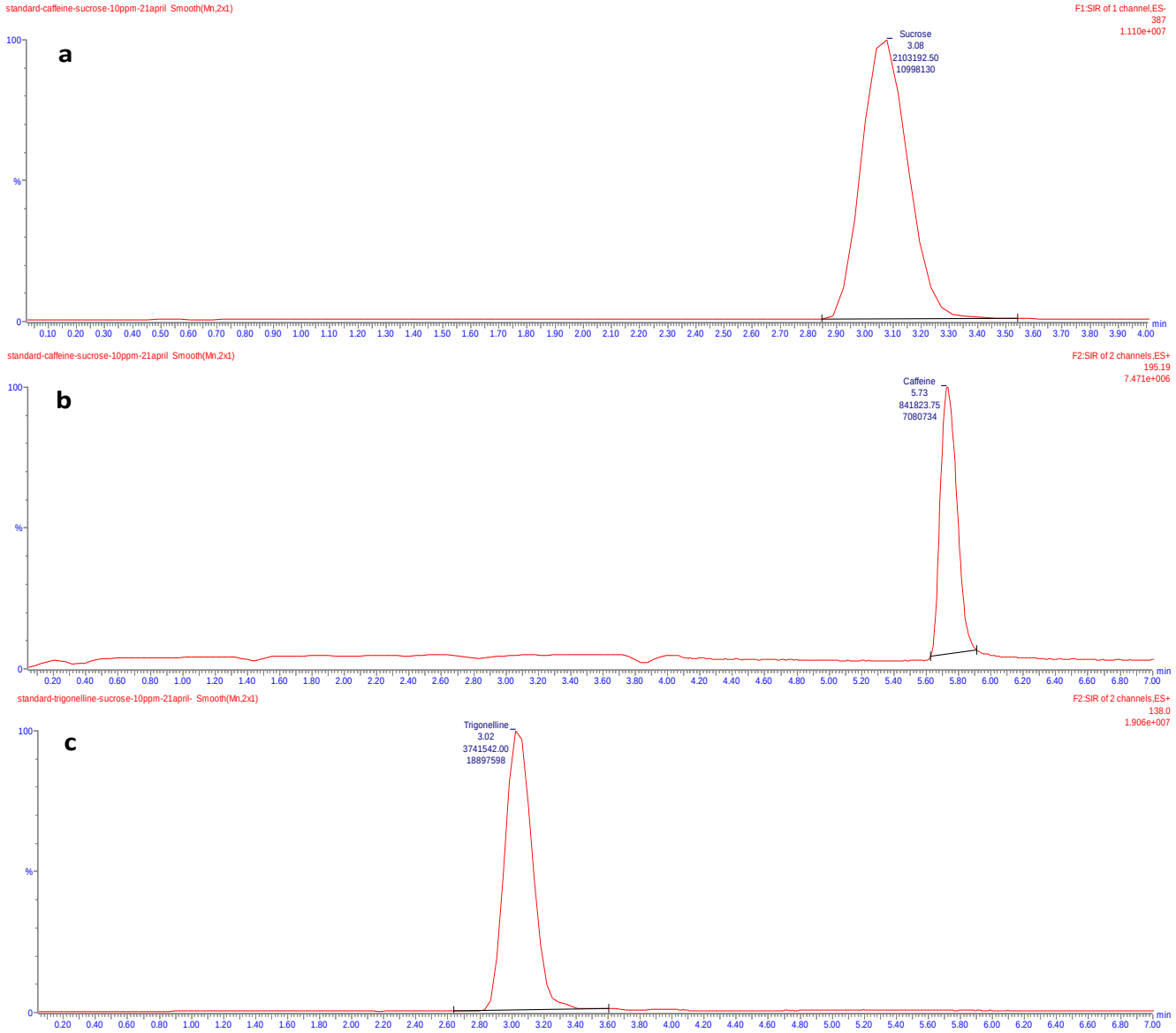


Figure 8.2. High-Performance Liquid Chromatography (HPLC) / Mass-Spectroscopy (MS) profiles of **a**) sucrose, **b**) caffeine and **c**) trigonelline in a green coffee extract.

8.3. RESULTS AND DISCUSSION

8.3.1. Coffee constituent variation and accuracy of reference measurement

The descriptive statistics for the reference measurements, the results for the recovery experiment and the limits of detection (LOD) and quantification (LOQ) are reported in Table 8.1. To understand and minimise analytical errors, duplicate HPLC-MS analysis was performed on each extract, on a total of 277 coffee beans analysed. The LOD and LOQ of the method were very

low with respect to the concentrations of coffee constituents found in the analytes; the LOQ being 26.3, 81.7 and 56.5 mg kg^{-1} for caffeine, sucrose and trigonelline, respectively.

The recovery experiment resulted in an excellent recovery (≥95%) for caffeine and sucrose, and ≥80% recovery for trigonelline. The recovery ranged from 112% for samples spiked with 10 mg g^{-1} caffeine, to 71% for trigonelline at 20 mg g^{-1} spiking. These results are in line with previous findings, also regarding the fact that the recovery of some coffee compounds was lower at the higher levels of spiking (Perrone et al., 2008). The results for the reference measurements were acceptable in terms of accuracy of determination and repeatability (average repeatability for sucrose=3.7%, caffeine=2.4%, trigonelline=2.5%).

Table 8.1. Reference measurements on single green coffee beans: **a**) descriptive statistics, expressed on wet basis and on dry weight basis (n=277); **b**) recovery and repeatability of pure reference compounds; **c**) the limit of detection (LOD) and limit of quantification (LOQ) obtained by LC/MS analysis.

a	**Compound**	**Mean (mg/g)**	**SD (mg/g)**	**Min (mg/g)**	**Max (mg/g)**
wet basis	Sucrose	43.3	10.2	5.3	70.8
	Caffeine	18.1	4.7	9.2	31.9
	Trigonelline	8.3	2.0	3.9	15.0
dwb	Sucrose	47.8	11.5	5.8	80.0
	Caffeine	19.9	5.1	10.2	34.8
	Trigonelline	9.1	2.2	4.3	17.0

b	**Compound**	**Spike level (mg/g)**	**Recovery (%)**	**Repeatability (%)**
	Sucrose	10	80.6 ± 1.6	5.8
		40	111.6 ± 0.2	1.8
		80	94.4 ± 0.2	3.6
	Caffeine	10	112.0 ± 5.3	4.7
		20	104.0 ± 2.8	1.7
		30	91.8 ± 1.9	0.9
	Trigonelline	5	84.9 ± 0.3	1.0
		10	84.0 ± 0.3	1.7
		20	71.0 ± 0.5	4.7

c	**Compound**	**LOD (mg/g)**	**LOQ (mg/g)**
	Sucrose	7.9×10^{-3}	26.3×10^{-3}
	Caffeine	24.5×10^{-3}	81.7×10^{-3}
	Trigonelline	17.0×10^{-3}	56.5×10^{-3}

Values for **a**) are expressed as mg/g of ground coffee material. Values for the recovery are the mean of triplicate analysis, followed by the standard deviation (SD). The recovery experiment was performed on a batch of ground Arabica green coffee beans from Mexico. Repeatability is expressed as relative SD. The LOD and LOQ were calculated according to Perrone et al. (2008).

The ranges of sucrose, caffeine and trigonelline concentration in single green coffee beans are reported in Table 8.1a. The reference measurements are shown on wet basis, which was the actual analysis performed, as well as on a predicted dry weight basis. All the compounds analysed showed a broad range of concentrations. For example, the maximum sucrose level was over ten times higher than the lowest and in the case of caffeine and trigonelline, the maximum concentrations were three or four times higher than the minimum. As expected, the concentrations of sucrose and trigonelline were significantly higher in Arabica than Robusta coffee beans, while caffeine content was higher in Robusta than Arabica coffee. The average sucrose content was 46.7±7.5 mg g^{-1} for Arabica and 33.6±9.1 mg g^{-1} for Robusta, while the average caffeine content was 15.7±2.3 and 19.9±4.9 mg g^{-1} (wet basis), respectively. For trigonelline, an opposite trend was found, with Arabica richer in trigonelline than Robusta, i.e. 8.6±1.8 vs 7.3±1.7 mg g^{-1} (wet basis), respectively. A statistically significant difference was observed for all the compounds between Arabica and Robusta ($p<0.001$), but some overlap was observed in the middle region for all three compounds (Figure 8.3). These results are in agreement with the literature, and demonstrate similar overlapping between these species (Campa et al., 2004).

Despite some difference observable among different batches, particularly the expected differences among Robusta and Arabica species, intra-batch variability was noticeably high. This large variability makes it interesting to apply HSI as a rapid non-destructive method to obtain predictions on the single-bean variability, so that beans with the highest and/or lowest concentration of certain compounds of interest can be selected.

Previous studies investigating the natural variability of sucrose, caffeine and trigonelline in green coffee reported similar average values as the present experiment (Campa et al., 2004; Casal et al., 1998; Dessalegn, Labuscagne, Osthoff, & Herselman, 2007; Ky et al., 2001). However, the standard deviation and range previously reported in the literature were usually more narrow, e.g. Dessalegn et al. (2007) studied 42 accessions of Ethiopian Arabica coffees, and reported a standard deviation of 8.2, 1.0 and 1.3 mg kg^{-1} for sucrose, caffeine and trigonelline, respectively. This might be due to the absence of investigation on single coffee compositional variation.

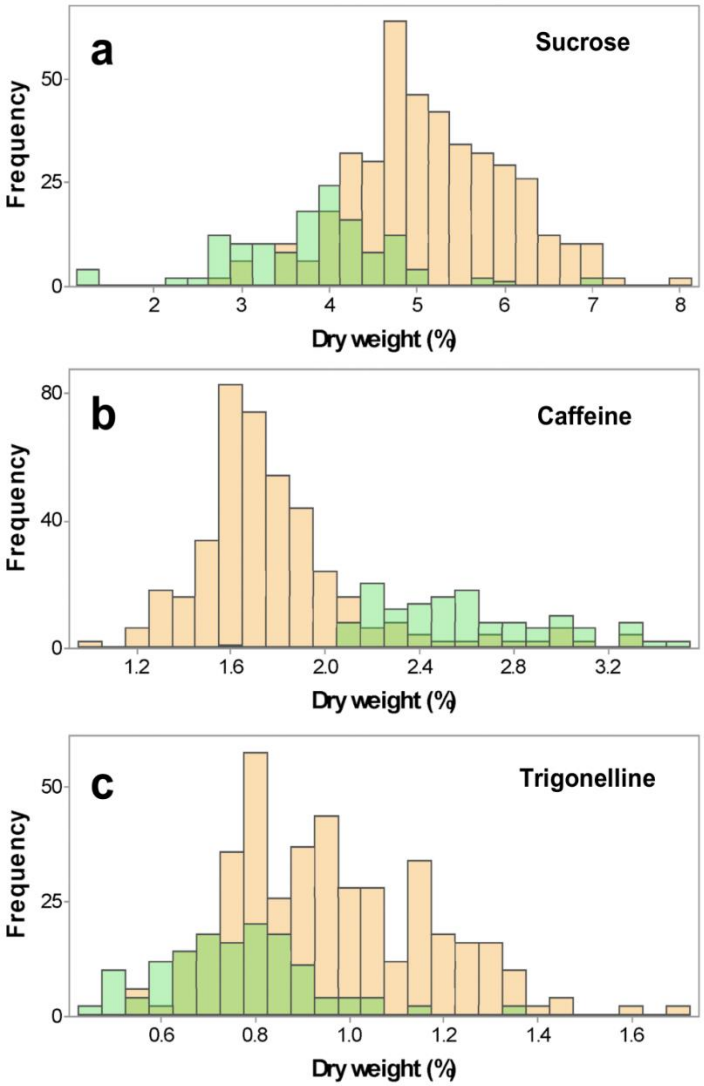


Figure 8.3. Distribution plots of (a) sucrose, (b) caffeine and (c) trigonelline in single green coffee beans analysed by HPLC/MS, by discriminating Arabica (orange) and Robusta samples (green).

A smaller variation would be expected for batch measurements compared to single coffee beans and due to the small sample range. In this thesis, the average sucrose content was 4.67±0.75 % for Arabica and 3.36±0.91 for robusta, caffeine content was 1.57±0.23 % for Arabica and 1.99±0.49 % for robusta; trigonelline content was 0.86±0.18 % for Arabica and 0.73±0.17 % for robusta. The values reported by Ky et al. (2001) for Arabica were 9.23, 1.22 and 1.19 % (dmb) for sucrose, caffeine and trigonelline. These compounds were reported to be 5.45, 2.54 and 1.01 % (dmb), respectively, on average for robusta coffees using 38 genotypes. The slight difference observed for sucrose content could be due to the different growing conditions, as the authors

used accessions collected from experimental fields, under ideal growing conditions and not using commercial samples. The variation of sucrose content in green coffee beans is attributed to several factors as discussed previously, including the post-harvest processing and the coffee species, as well as agronomic factors.

The presence of correlations among the three coffee constituents analysed was investigated, and statistically significant differences were found among the compounds when expressing the data on wet basis (Figure 8.4a) and on a dry matter basis (Figure 8.4b). Most of the observed difference was attributed to differences between Arabica and robusta, and minimal correlation was observed among each species.

The observed difference was statistically significant ($p<0.01$) in every case, with a positive Pearson correlation coefficient obtained for sucrose and trigonelline, i.e. 0.395. Sucrose vs. caffeine had $r=-0.445$, while caffeine vs. trigonelline correlate with low Pearson values of -0.185.

Previous research reported a high negative correlation between caffeine and trigonelline in roasted coffee beans (Casal, Oliveira, Alves, & Ferreira, 2000), for bulk coffee and it was not investigated on single bean basis. In addition, trigonelline content dramatically changes due to roasting, as a function of the intensity of the roasting degree, thus a valid comparison cannot easily be made based on original sample properties. The correlation among the three constituents analysed might be also influenced by the presence of different levels of moisture which can naturally fluctuate between the green coffee beans, especially when considering single coffee beans instead of batches.

However this was not the case, as when concentrations were expressed on a dry matter basis, a slight negative but significant correlation was found between caffeine and trigonelline ($r=-0.194$). Similarly, a moderate negative correlation was observed between sucrose and caffeine ($r=-0.424$), while a moderate positive correlation was observed between sucrose and trigonelline ($r=0.419$, $n=277$), with statistical significance. These results are in partial contrast with Leroy et al. (2011), who described the absence of any significant correlation among these two coffee constituents on a wide range of coffee genotypes, over several years. However, the authors only investigated Robusta coffee accessions for breeding programmes.

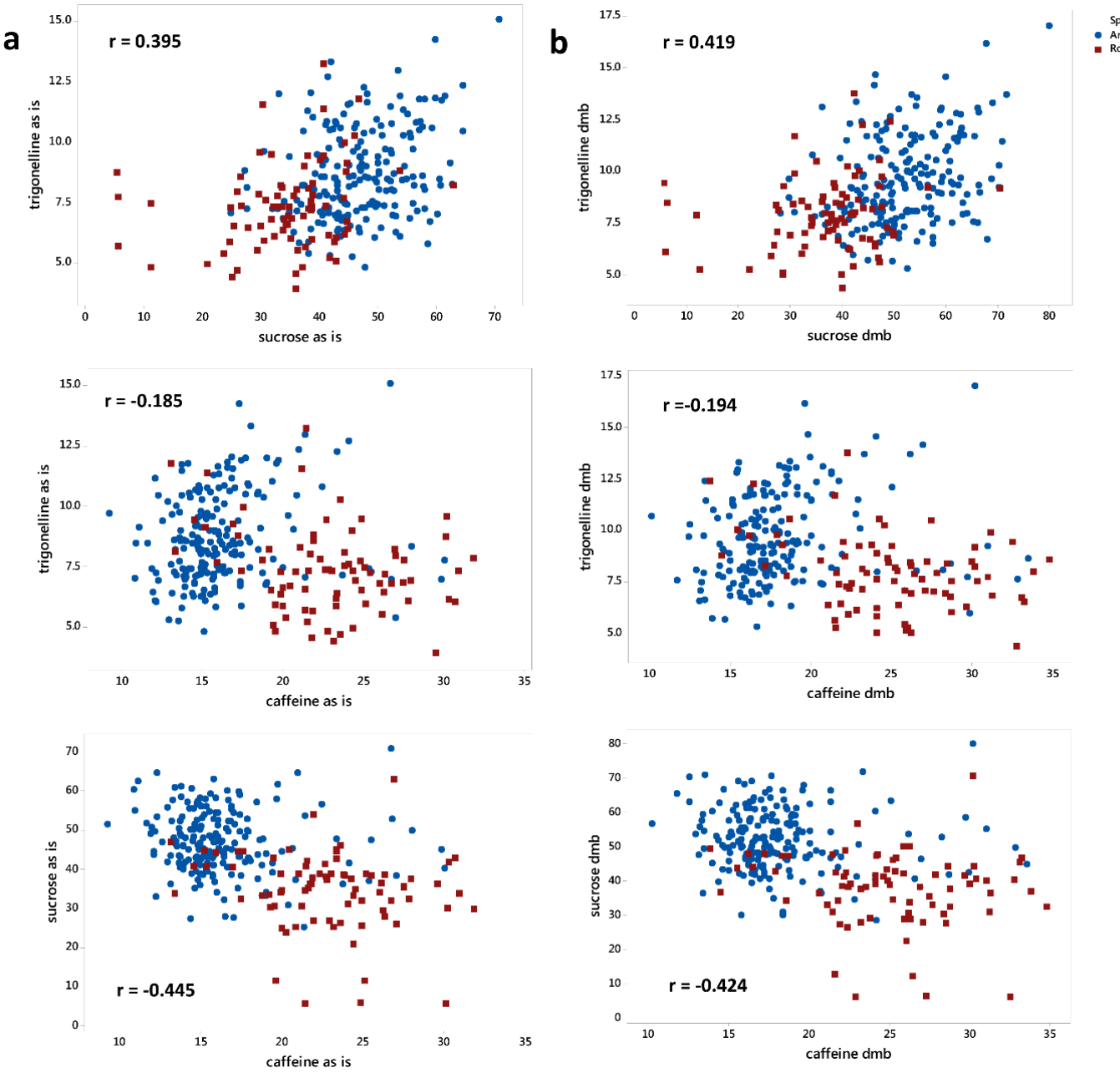


Figure 8.4. Correlation plots among sucrose, caffeine and trigonelline in single green coffee beans including Arabica and Robusta species. **a**) Values expressed on wet basis or **b**) dry matter basis (dmb). Pearson correlation coefficients (r) are indicated in the graphs ($p<0.001$ in all cases, thus indicating that a statistical significance was found).

8.3.2. PLS regression for prediction of coffee constituents

Trigonelline, sucrose and caffeine show characteristic absorption features in the NIR region (Figure 8.5). Whilst sucrose has significantly higher log(1/R) values, trigonelline and caffeine showed similar absorption bands. Caffeine main absorption peaks were at 1668, 2250 and 2425 nm. Trigonelline had similar absorption peaks at 1668 and 2269 nm. Sucrose had a characteristic

absorption in the region 1460–1700 nm, and a second major peak observed around 2070 nm. The reflectance spectra of whole coffee beans show strong absorption features around 1430 nm, followed by two peaks at 1730 and 1760 nm, and another major peak at 1930 nm. Although the spectra are noisier in the upper wavelength region, another major absorption peak was observed around 2250 nm. The peak around 1430 nm is related to the C-H stretch and C-H deformation vibration, whereas the region around 1800–1900 nm indicates the vibration of the second overtone of the carbonyl group, and the peak observed at 2250 nm relates to the –OH vibration. The absorptions at 1730 and 1760 nm are related to lipids, as they are attributed to the $–CH_3$ and $–CH_2$ overtone, respectively (Huck et al., 2005).

Previous publication attributed specific regions in the NIR region to green coffee compounds, as shown in Figure 8.6. However, these assignments should be taken as tentative, due to the overlap of different chemical bonds in such a complex system such as coffee beans, where a variety of major and minor compounds is found.

Table 8.2 reports the performance of PLS regression models for the prediction of sucrose, caffeine and trigonelline in single green coffee beans using several pre-processing techniques.

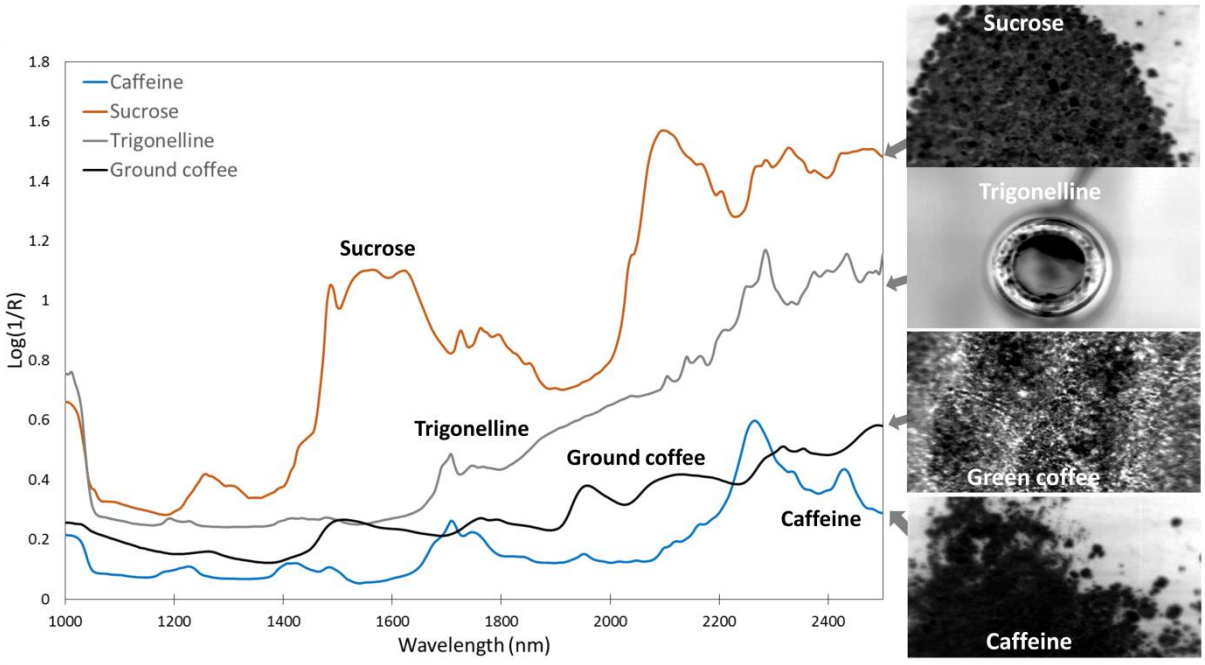


Figure 8.5. Average spectra obtained by HSI on samples of pure reference caffeine, sucrose and trigonelline, and example of a ground green coffee bean, showing also the absorbance images obtained from the hypercube at one spectral band ~1400 nm (right).

Two separate models were built: one on wet basis and a second built on a predicted dry weight basis. Generally, the two approaches resulted in a similar prediction performance, with slightly higher errors for the dry matter basis groups. The best caffeine and trigonelline models produced R^2 values of R_c^2=0.851 and 0.823, respectively. The cross-validation R_2 values were 0.793 and 0.703, with prediction error of 1.929 and respectively. However, the choice of the best model should also consider the number of LVs used, in order to minimise them but still use enough information.

The RMSECV value for caffeine was 1.9 mg g^{-1}, and 1.0 mg g^{-1} for trigonelline. Sucrose models performed considerably worse, with the best calibration accuracy of R_c^2=0.65, and R_{cv}^2 of 0.65-0.51, and RMSECV of 7.07 mg g^{-1} on an wet basis. On the whole, the model built on the second derivative pre-treatment was deemed to be the best sucrose model because it uses the fewest latent variables (LVs) with little effect on the overall performance, thus this model is most robust and avoids overfitting, whilst also helping to reduce the effect of scattering relative to the untreated log(1/R) data.

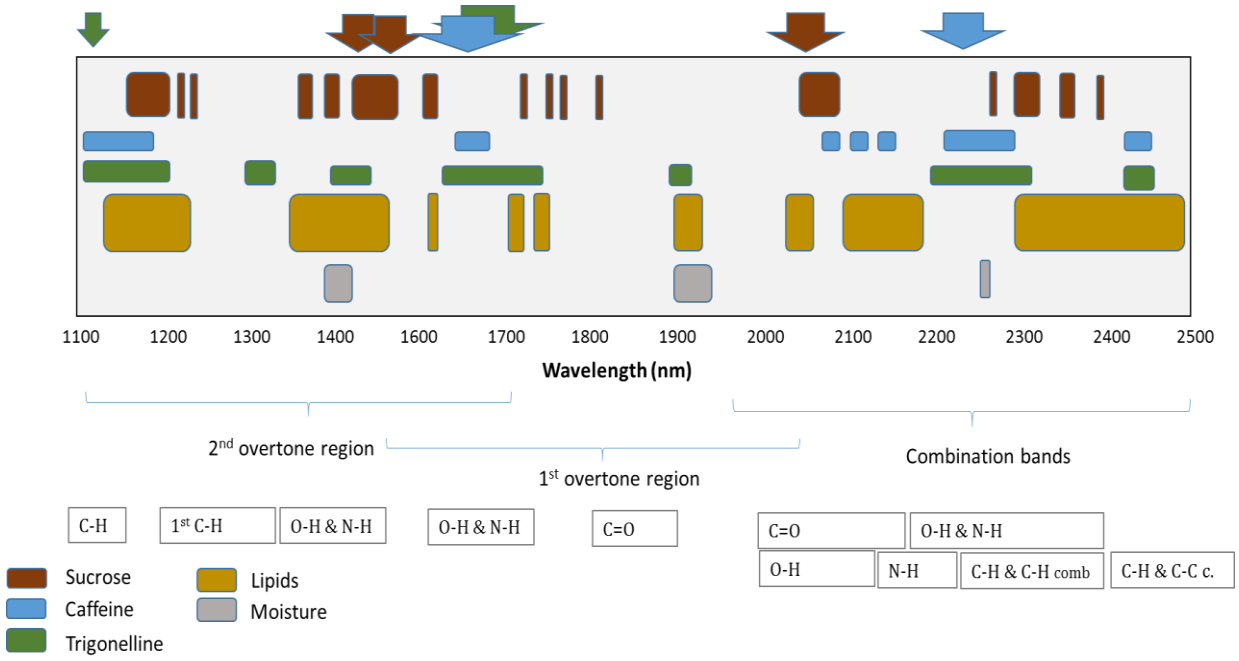


Figure 8.6. Proposed assignment of NIR absorption wavelengths to chemical compounds in green coffee suggested by previous authors (modified from (Ribeiro et al., 2011). Arrows indicate the most important absorption bands in the PLS regression models experimentally obtained in this thesis. The magnitude indicates the content in green coffee beans.

Table 8.2. Performance of the PLS regression models for sucrose, caffeine and trigonelline, for HSI quantification on single green coffee beans, with coffee constituents expressed on (**a**) wet basis or (**b**) dry matter basis (dmb).

a. Content expressed on wet basis

Compound	Treatment	LV	Calibration		Cross-Validation	
			R_c^2	RMSEC	R_{cv}^2	RMSECV
Sucrose	log(1/R)	20	0.651	5.931	0.506	7.071
	SNV+1st der	16	0.652	5.894	0.476	7.254
	2nd der	12	0.647	5.912	0.462	7.250
Caffeine	log(1/R)	13	0.666	2.647	0.628	2.799
	SNV+1st der	16	0.851	1.635	0.793	1.929
	2nd der	10	0.782	2.068	0.724	2.333
Trigonelline	log(1/R)	23	0.761	0.958	0.665	1.135
	SNV+1st der	25	0.820	0.809	0.713	1.022
	2nd der	17	0.823	0.794	0.703	1.034

b. Content expressed on dmb

Compound	Treatment	LV	Calibration		Cross-Validation	
			R_c^2	RMSEC	R_{cv}^2	RMSECV
Sucrose	log(1/R)	20	0.653	6.489	0.509	7.751
	SNV+1st der	16	0.564	7.485	0.482	8.181
	2nd der	15	0.701	6.119	0.526	7.722
Caffeine	log(1/R)	20	0.799	2.107	0.729	2.451
	SNV+1st der	16	0.851	1.843	0.792	2.177
	2nd der	11	0.797	2.159	0.726	2.513
Trigonelline	log(1/R)	25	0.795	0.979	0.689	1.208
	SNV+1st der	25	0.833	0.860	0.733	1.090
	2nd der	19	0.842	0.843	0.709	1.146

LV = Latent Variable, or Principal Component. RMSEC = root mean square error of calibration. RMSECV = root mean square error of cross-validation. The errors are expressed as mg g^{-1} coffee beans. The same number of LVs were used for calibration and cross-validation.

According to Shenk & Westerhaus (1996), calibrations with R^2 values between 0.50 and 0.69 can be used to separate into low, medium and high values, while R^2 of 0.70–0.89 can be considered as good enough for quantification purposes. According to the obtained RMSECV values, the models can be considered as good for caffeine and trigonelline, but poor for sucrose quantification, although this model could still be used for screening purposes. As a proportion of the range, the cross-validation error was 11.8, 8.5 and 9.2% for sucrose, caffeine and trigonelline (wet basis), respectively. When expressing the values on a dry matter basis, this proportion was 10.4, 8.8 and 8.6%, respectively.

An explanation on the choice of the optimal LV is reported in Figure 8.7 (more detailed plots are presented in Appendix in Figure A.5). The graphs shows the explained variance of models built in the coffee constituents expressed on wet basis, and using the second derivative spectral pre-treatment calculation. To build models that are more robust and to avoid overfitting, the preference was to avoid an excessively large number of LVs, so in some occasions the lowest prediction error was not chosen when no big improvement on the prediction was obtained.

The quality of the calibrations presented can be evaluated using the Ratio of Performance to Deviation (RPD), which is calculated as the ratio between the standard deviation and the standard error of cross-validation (Fearn, 2002; Williams & Sobering, 1993). RPD is dimensionless and higher values indicate better analytical performance, however it has some limitations and generally the R^2 value should be preferred to evaluate the quality of prediction models. In the present experiment, the lowest performance was obtained for sucrose, with RPD of 1.4 (wet basis) and 1.5 (dwb). For caffeine and trigonelline, the RPD values were very similar between the wet basis and dry matter basis; caffeine had RPD=2.7 and trigonelline RPD=2.0. For trigonelline, despite the significantly lower prediction error (i.e. almost half the RMSECV of caffeine), the higher RPD value was explained by the more limited range observed for trigonelline content. Despite the low prediction ability of such calibration, previous literature for other products still suggested the application of PLS calibrations with RPD values of 1.3–1.6 for in-line analysis, as it might be useful for breeding programs to select particularly higher or lower values in a population (De Marchi, Riovanto, Penasa, & Cassandro, 2012).

Figure 8.8 shows the predicted versus measured plots of the best PLS models for sucrose, caffeine and trigonelline prediction in single green coffee beans, while Figure 8.9 also reports the loading weights of the first two Principal Components for each of the predicted compounds. It is shown that the models do not overfit as a relatively low number of LVs was used, even lower than the suggested one by cross-validation. The loading plots show that the models were quite similar comparing the wet and dry matter basis, especially for sucrose and caffeine. All the models had a strong common absorbance at 1900 nm, with a second one at 1400 nm and in the region 22500-2344 nm. Figure 8.10 shows the regression coefficient plots for the three coffee constituents.

Caffeine and trigonelline models were less noisy than sucrose, with clear peaks around 1700 nm. However, except this strong absorbance, the strong coefficients were not observed, probably due to the complexity of the predicted compounds (low concentration compared to major coffee constituents).

A previous study reported that the second derivative pre-treatment was less effective than the first derivative in terms of PLS regression models for chemical components such as caffeine, theobromine and theophylline (Huck et al., 2005). The PLS regression model based on NIRS reported by these authors for caffeine had R_c^2 value of 0.86 and R_{cv}^2=0.82. However, the authors predicted caffeine content on liquid coffee extracts having caffeine concentrations from 0.1 to 4.1%, thereby enhancing the capability of NIRS by removing the influence of other non-extractable compounds. Despite this, the prediction error was 3.4 and 4 mg g^{-1} for the calibration and validation datasets, respectively.

The literature reporting on HSI applied to coffee is very limited, for example Zhang, Jiang, Liu & He (2017) recently used HSI for coffee bean prediction of caffeine content. The authors worked in the NIR region 874–1734 nm, but instead of using single coffee beans the reference caffeine analysis was carried out on a small batch of 20 coffee beans, ground and analysed by a spectrophotometric method. Despite 10 times lower caffeine concentrations compared to the literature and this thesis (ranges 4-11 mg g^{-1}, 12-15 mg g^{-1} and 10-23.5 mg g^{-1} reported in previous works), the authors claimed a good prediction performance for caffeine, i.e. R_C^2=0.897 and R_{CV}^2=0.834, and prediction errors of RMSEC=111.3 and RMSECV=142.1 μg g^{-1}.

Generally, larger prediction errors are expected for calibrations obtained by HSI compared to traditional NIRS instruments, and particularly with ground material and liquid coffee extract or coffee brew. This is attributed to the following factors: (1) the sample is less homogenous than ground coffee; (2) the sample presentation is less uniform and the illumination conditions are different; (3) the sample size is typically smaller for HSI, which influences both the spectral acquisition and (4) the reference analytical methods.

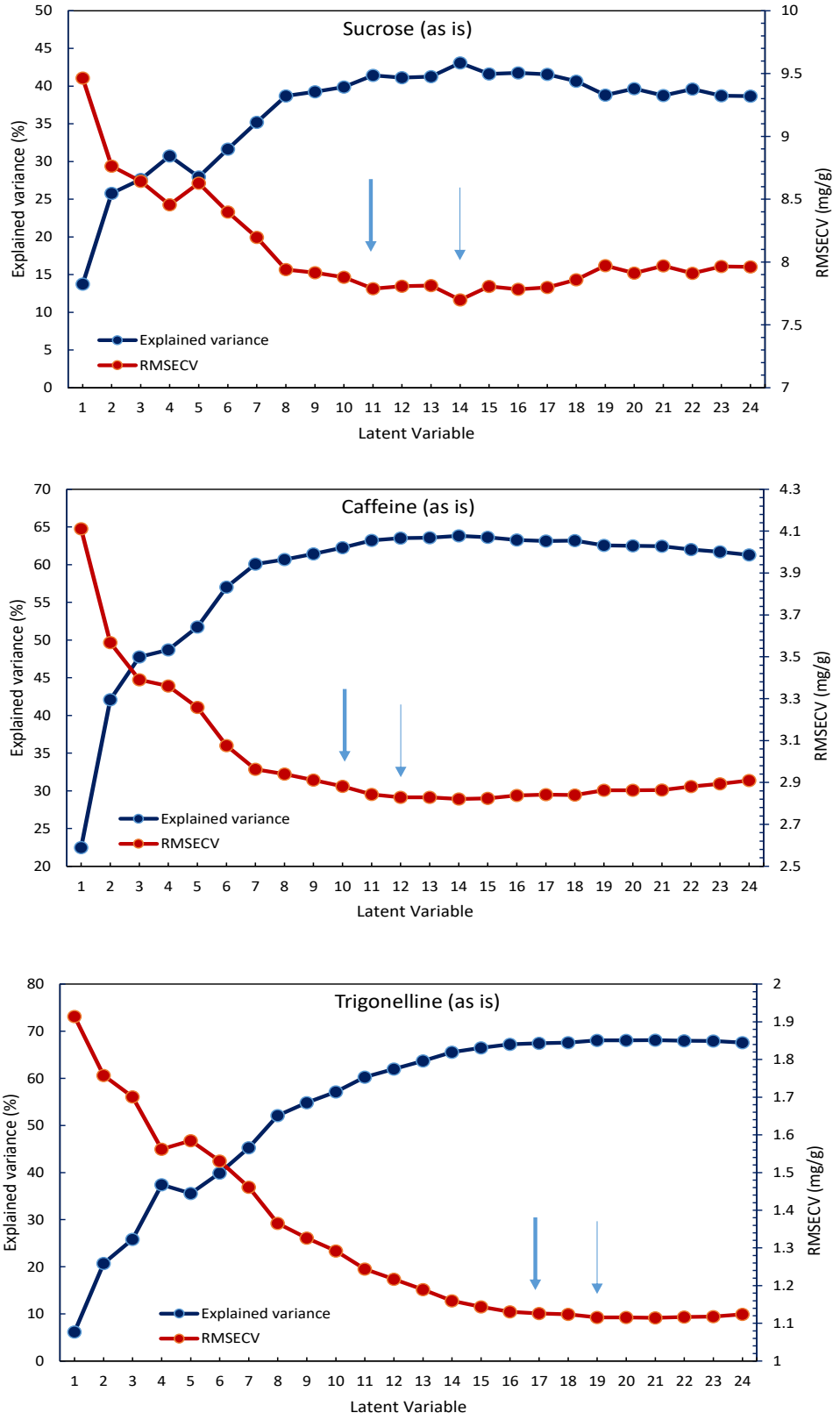


Figure 8.7. Selection of the optimal Latent Variable for HSI single coffee bean prediction of sucrose, caffeine and trigonelline (wet basis spectra treated using the 2nd derivative). The thinner arrows indicate the LV giving the lowest prediction error, while the thicker one was selected to avoid the risk of overfitting.

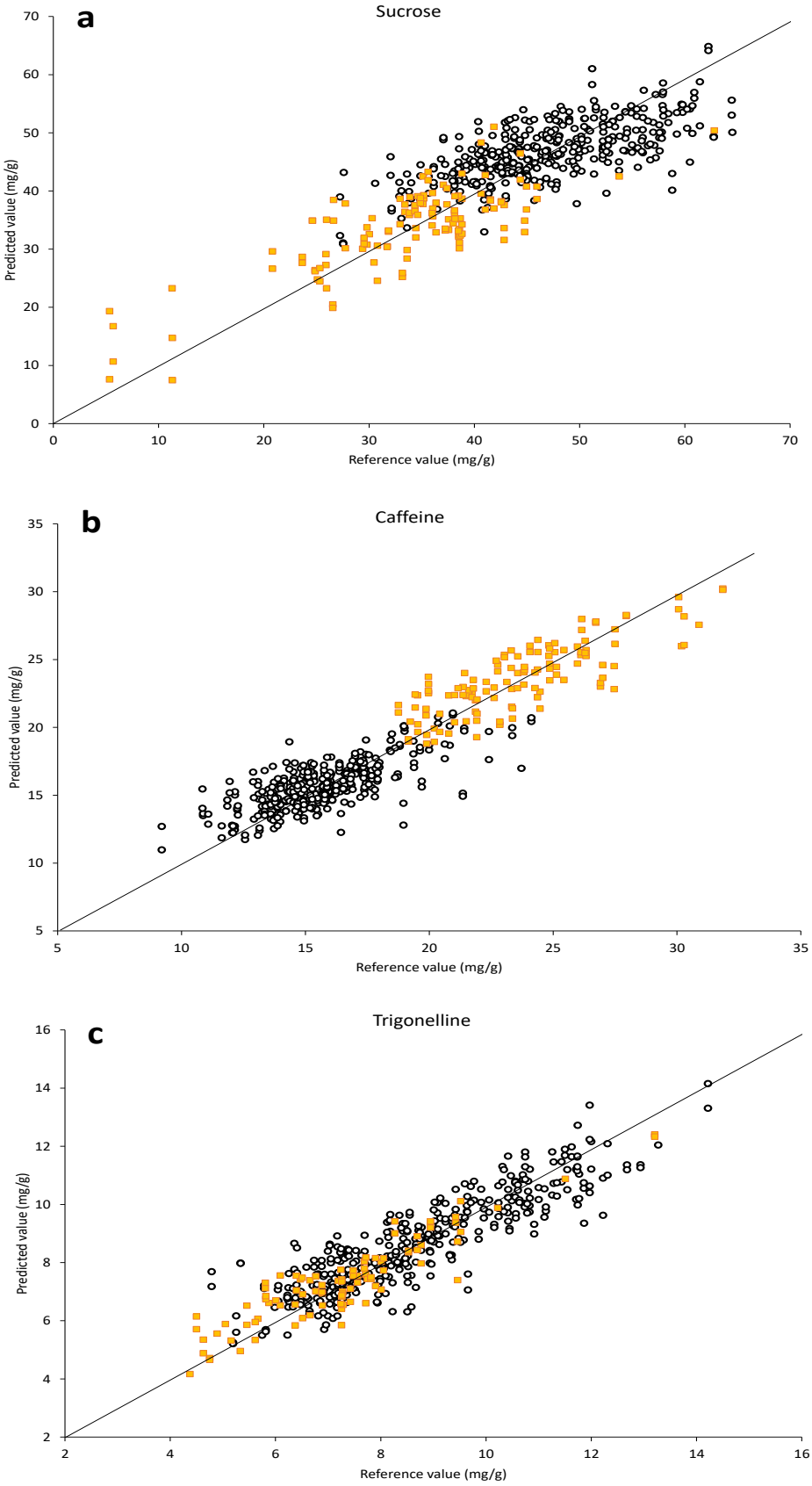


Figure 8.8. Predicted versus measured values of (**a**) sucrose, (**b**) caffeine and (**c**) trigonelline in single green coffee beans for the best PLSR models, expressing the compound concentration as mg/g coffee (wet basis). Black circles: Arabica; orange squares: Robusta.

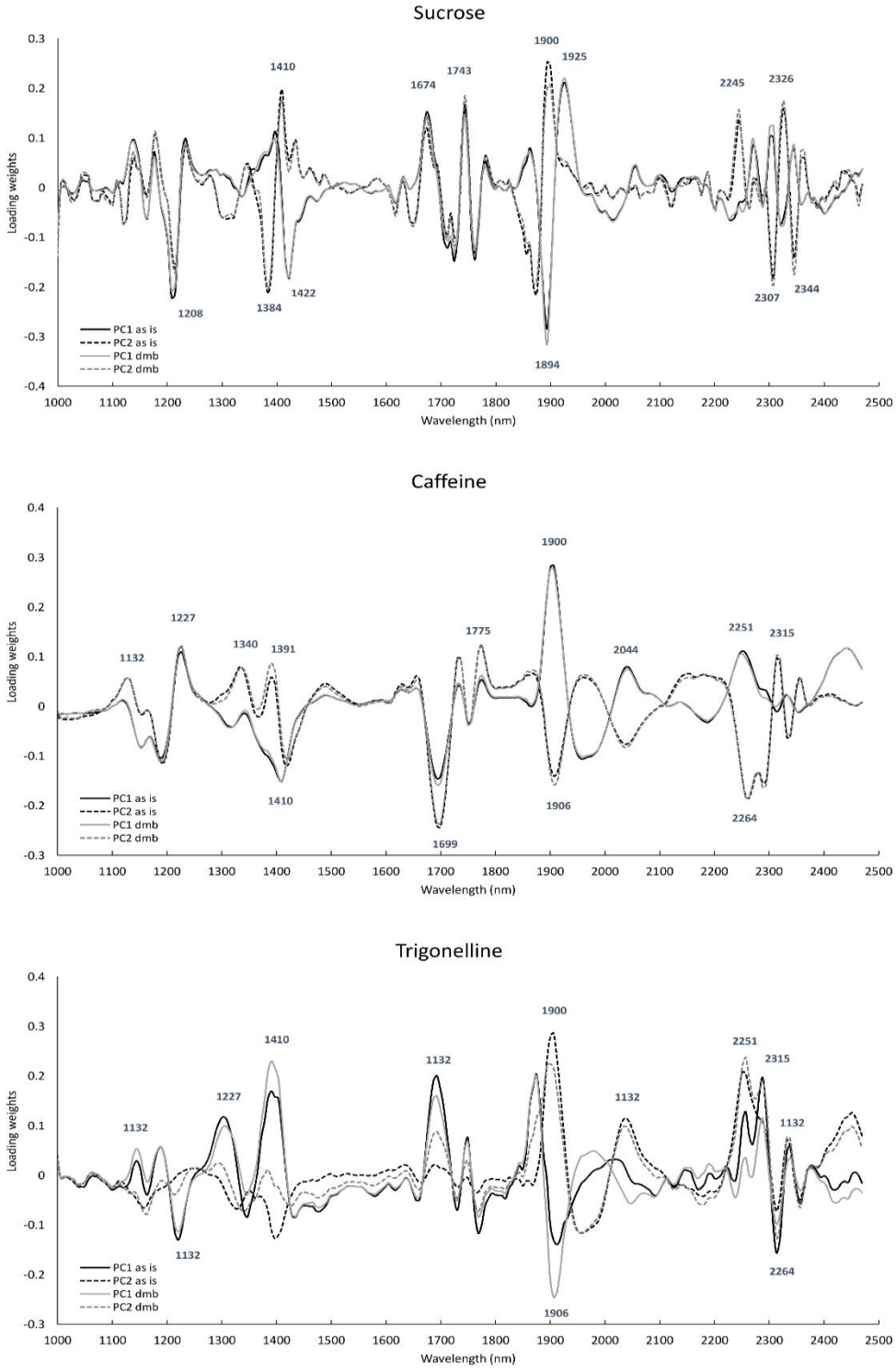


Figure 8.9. Loading weights of the PLS regression models for sucrose, caffeine and trigonelline in single green coffee beans, showing the reference measurements expressed on wet basis or on a predicted dry weight basis, for the first 2 Principal Components (PC).

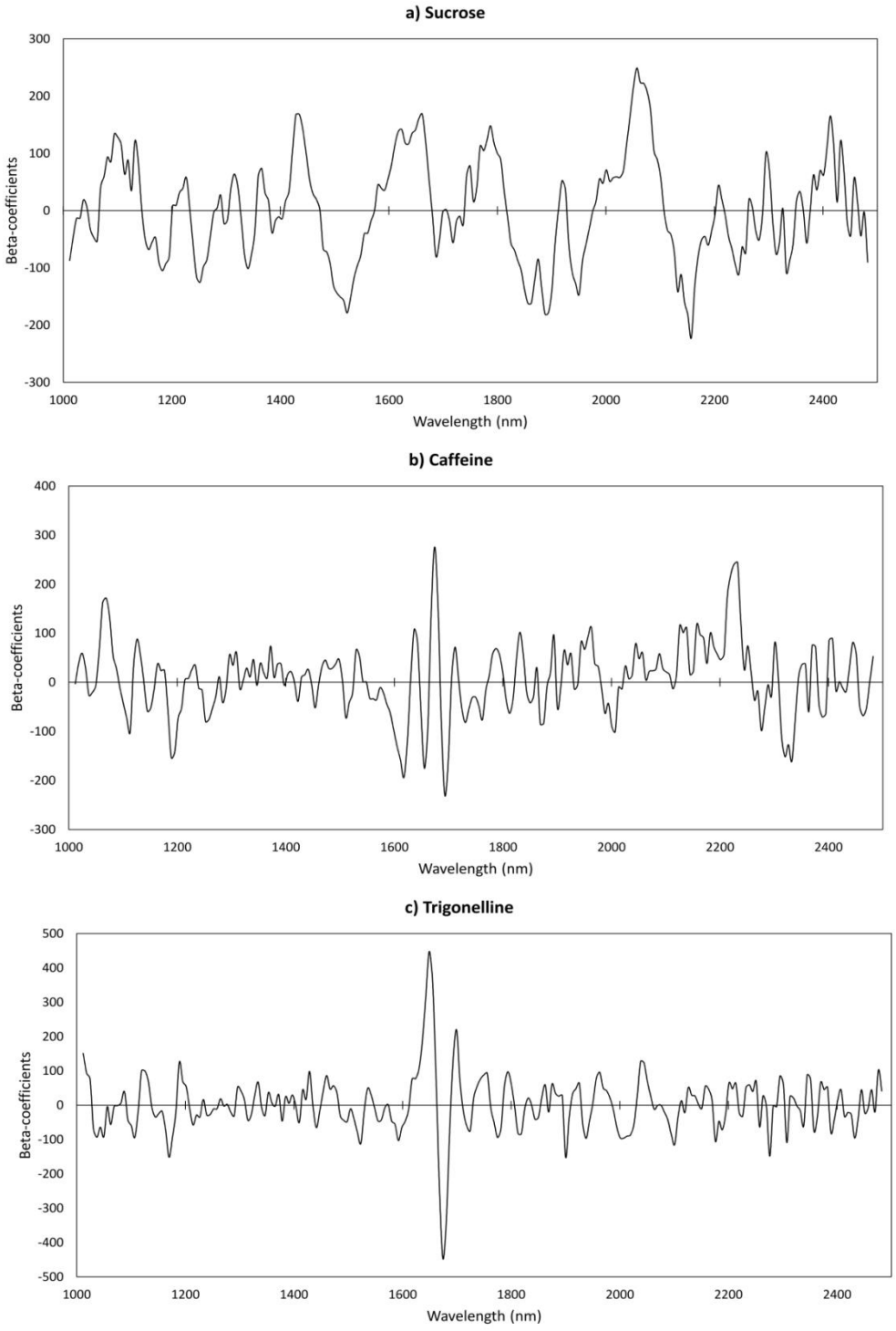


Figure 8.10. Regression coefficients for the PLSR models built on single green coffee beans, for the prediction of the three coffee constituents. Pre-treatments applied: sucrose, 2nd derivative; caffeine and trigonelline, SNV+1st derivative.

Despite these considerations, the performance of the models favourably compares with the existing literature. Previous research on NIRS caffeine quantification in coffee generally reported better performances for the calibration models, but acquisition is typically done on roasted and ground coffee, or even coffee beverage. For instance, Pizarro et al. (2007) reported an R^2 above 0.99 for caffeine calibration in roast and ground coffee. Fox et al. (2013) investigated the use of FT-NIRS (~830–2500 nm) for caffeine quantification in whole and ground coffee, also testing single coffee beans, taking 25 beans from five batches. The prediction performances reported by the authors were generally better than the calibrations shown in the present chapter, but Fox et al. (2013) also included a decaffeinated batch in their samples, which could have greatly influenced the model. In addition, it should be noted that their instrument has different sample presentation and illumination. There are also limitations related to the capability to implement it on an industrial scale for rapid and on-line measurement of single coffee beans. The R^2 reported for single beans without considering decaffeinated samples (i.e. using 4 batches of roasted coffee) was 0.93, with a cross-validation R^2 of 0.86. The RMSEC and RMSECV were 1.2 and 1.6 mg g^{-1}, respectively (Fox et al., 2013).

Despite the slightly worse calibration performance found herein using HSI, there are advantages in using HSI compared to NIRS for two main reasons. Using traditional NIR instruments, even if the construction of a single coffee bean calibration is technically possible, the application of such calibration on a considerable number of beans would be time-consuming and therefore of limited applicative interest.

Here, prediction models were also built on the datasets for Arabica or Robusta alone, as reported in Table 8.3. The sucrose prediction performance was slightly better for Robusta coffee, even showing R^2 value of 0.82 for the calibration dataset. However, the validation R^2 were dramatically lower, thus no providing actual improvement over the general model and suggesting a high risk of misprediction when applying the model on new independent samples. Therefore, it is not recommended to use these models and the use of the comprehensive model would bring better prediction and other benefits in terms of practical applicability.

Table 8.3. HSI prediction models for sucrose, caffeine and trigonelline in single green coffee beans using PLS regression models separately built according to the coffee species. Models are built on (**a**) dry basis or (**b**) dry matter basis (dmb).

a. Reference data on wet basis

Compound	Species	Treatment	LV*	Calibration		Validation	
				R_c^2	RMSEC	R_{cv}^2	RMSECV
Sucrose	Arabica	log(1/R)	19	0.52	5.87	0.30	7.06
	Robusta	log(1/R)	20	0.82	4.56	0.45	8.16
	Arabica	2nd der	8	0.36	5.80	0.17	6.59
	Robusta	2nd der	5	0.53	5.62	0.36	6.72
Caffeine	Arabica	log(1/R)	9	0.40	2.20	0.34	3.00
	Robusta	log(1/R)	10	0.65	1.91	0.54	2.23
	Arabica	2nd der	8	0.45	2.09	0.29	2.40
	Robusta	2nd der	9	0.83	1.31	0.56	2.12
Trigonelline	Arabica	log(1/R)	23	0.80	0.84	0.65	1.10
	Robusta	log(1/R)	7	0.63	0.88	0.55	0.98
	Arabica	2nd der	14	0.80	0.80	0.65	1.07
	Robusta	2nd der	5	0.69	0.78	0.57	0.95

b. Reference data on dry matter basis

Compound	Species	Treatment	LV	Calibration		Validation	
				R_c^2	RMSEC	R_{cv}^2	RMSECV
Sucrose	Arabica	log(1/R)	15	0.41	6.46	0.27	7.18
	Robusta	log(1/R)	11	0.61	5.85	0.43	7.12
	Arabica	2nd der	8	0.52	1.88	0.35	2.19
	Robusta	2nd der	4	0.48	7.47	0.34	8.46
Caffeine	Arabica	log(1/R)	10	0.45	1.92	0.39	2.03
	Robusta	log(1/R)	10	0.64	2.09	0.50	2.49
	Arabica	2nd der	8	0.48	2.00	0.30	2.33
	Robusta	2nd der	8	0.80	1.53	0.58	2.26
Trigonelline	Arabica	log(1/R)	20	0.76	1.00	0.63	1.24
	Robusta	log(1/R)	7	0.56	0.93	0.46	1.04
	Arabica	2nd der	15	0.83	0.85	0.69	0.85
	Robusta	2nd der	6	0.70	0.77	0.49	1.02

* The same number of LVs were used for both the calibration and cross-validation models. These models were not applied for the visualisation of chemical images, but the general model was preferred (Table 8.2).

Prediction of caffeine content was better in Robusta coffee compared to Arabica, however the R^2 value and the prediction error were always lower compared to the general model. These results could be partially attributed to the different number of samples belonging to the two species, and the particularly lower number of robusta samples used. Robusta had in fact much smaller sample number (n=140) than Arabica (n=410). Opposite results were obtained for trigonelline, for which

Arabica had better prediction performance. The improvement however, was not dramatic and the validation error was similar, e.g. 0.85 vs 1.02% for Arabica and robusta, respectively, using the second derivative treatment. The better performance obtained from a unique model employing the whole dataset is likely due to the larger variation observed, i.e. larger concentration range.

This result could be used for both Arabica and Robusta species as it would allow the prediction of the coffee constituents studied, without the need to discriminate the coffee species and apply separate calibrations for screening the raw material.

Unsupervised methods have been previously applied using HSI for coffee species classification (Calvini et al., 2015). More limited research has been reported using HSI for quantitative prediction of food chemical composition. In this case, the prediction performance strongly depends on the compound investigated. Caffeine has been recently predicted by NIR HSI in the spectral range 874–1734 nm, showing good prediction performance on bulk coffee beans, with prediction R^2=0.84 (Zhang et al., 2017).

Despite the slightly lower prediction performance frequently obtained by HSI compared to NIRS, and the expected lower prediction error when analysing single seeds, the HSI calibrations herein reported offer the advantage of screening single coffee beans without any preparation step, and detecting or segregating beans with extreme values in a rapid manner.

As an alternative to PLS regression, a non-linear model named SVM-R was tested to predict green coffee constituents. The second derivative pre-treatment was used to build the models as it generally leads to the best prediction performances, probably because it removes scattering and other unwanted effects in a more effective way compared to other pre-treatments. The results are reported in Table 8.4 (graph representing the predicted versus reference values is reported in Appendix Figure A.6). In comparison to PLSR models, SVR-R led to generally better calibration R^2 values, while the validation R^2 values were similar to PLSR models. For example, despite a calibration R^2=0.852 for sucrose prediction (for both wb or dmb), the validation was approximately 0.50-0.51. In terms of prediction error, the validation error was almost double the calibration error, with 7.2 and 8.0 mg g^{-1} for the wb or dmb models. This error is very similar or slightly better than the one obtained by PLS regression. Caffeine and trigonelline had high

calibration R^2 values, much above 0.85, and validation regression coefficients generally above 0.7. The prediction error was very similar to the models built by PLSR, with trigonelline showing the best performance in terms of validation error.

Considering the similar results obtained in terms of performance, this non-linear model was not further implemented due to the difficulties in applying such a model on HSI data, in particular in ENVI+IDL. In addition, using SVM it is impossible to get more information on the influence of each spectral variable on the model.

Table 8.4. Results of SVM-R (Support Vector Machine Regression) prediction of sucrose, caffeine and trigonelline in single green coffee beans. Compounds are expressed on (**a**) wet or (**b**) dry matter basis.

a)	**Calibration**		**Cross-validation**	
	R_c^2	**RMSECV**	**R_{cv}^2**	**RMSECV**
Sucrose	0.852	4.023	0.501	7.284
Caffeine	0.876	1.658	0.709	2.519
Trigonelline	0.915	0.586	0.738	1.002
b)	**Calibration**		**Cross-validation**	
	R_c^2	**RMSECV**	**R_{cv}^2**	**RMSECV**
Sucrose	0.858	4.445	0.518	8.060
Caffeine	0.867	1.864	0.699	2.781
Trigonelline	0.919	0.637	0.745	1.101

8.3.3. Application of the calibrations (chemical images)

The best prediction models for the three compounds analysed were selected and the beta-regression coefficients were applied to the treated hypercubes after applying image segmentation and spectral pre-processing, so that a "chemical image" was generated to reveal the distribution of compounds at a single pixel level. The model are those presented in Table 8.2 expressed on wet basis and using the full spectrum available.

The application of the best PLS calibrations for sucrose, caffeine and trigonelline are shown in Figure 8.11, using a batch of Robusta coffee from Vietnam and an Arabica coffee sample from Kenya. Each sample was scanned twice to acquire both sides of the coffee bean, and they are shown separately; very few differences were observed depending on the coffee bean position. Some minor effects observed within single coffee beans can be attributed to both actual chemical

differences across the sample, but also to topographical differences, e.g. the midline crease that corresponds to the mesenteric root. This portion of the bean was excluded from the calibration stage as the absorbance values might have influenced the computation of a representative average spectrum for each bean.

Once the calibration is applied, obvious differences in the sucrose and caffeine content are visible between Arabica and Robusta coffee beans. Arabica coffee beans had significantly lower caffeine content, with a more uniform distribution compared to the Robusta beans. For Robusta, variability was observed within and between coffee beans (please refer to supplementary material for further information), which is possibly due to differences in the total caffeine as affected by the maturity degree at collection or uneven post-harvest processing and drying. When visualising the predicted trigonelline content, little difference between the species was apparent. Robusta samples generally had lower predicted trigonelline levels, with a few samples showing higher content. Arabica samples show interesting differences within the same coffee beans, without a clear general pattern. This effect might be due to physiological reasons, possibly related to the migration during the post-harvest process over the external layers of the beans. There is also the possibility that some of the observed variability across a single coffee bean might be due to noise in the spectra.

Either way, further research is needed to verify whether genuine spatial differences do exist. This would primarily be dependent on the availability of analytical techniques that would enable the acquisition of reference data for specific locations on individual beans.

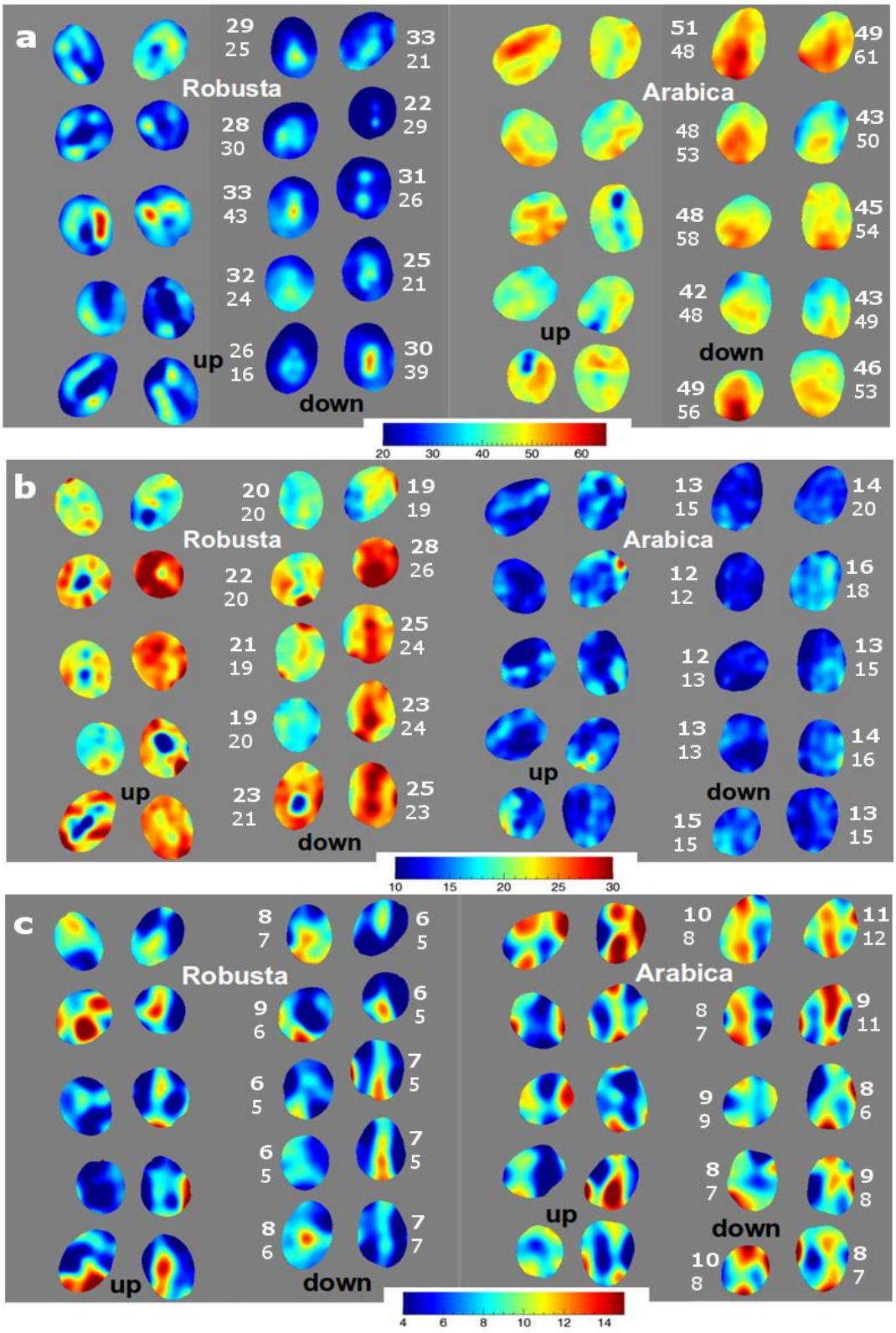


Figure 8.11. Application of the calibrations to visualise (a) sucrose, (b) caffeine and (c) trigonelline in a batch of Robusta and Arabica green coffee beans, at a single pixel. Numbers indicate the concentration of each compounds, expressed as mg g^{-1} coffee (predicted and actual). For each bean, numbers in bold (the number on the top for each coffee bean) indicate the predicted compound concentration, while the numbers of the bottom indicate the reference measurement.

8.4. CONCLUSIONS

HSI was applied to single green coffee beans to explore the potential to quantify chemical constituents present at relatively low levels, and reveal their concentrations on a single coffee bean basis. It was shown that HSI is effective for the non-destructive and rapid analysis of sucrose, caffeine and trigonelline in green coffee beans. The devised method allows the rapid prediction of coffee constituents not just for batch measurements, which could be performed with traditional NIR spectroscopy, but simultaneously on multiple individual coffee beans. This is the first reported application of HSI for the prediction of sucrose, caffeine and trigonelline on a single coffee bean basis.

Despite lower prediction accuracy compared to traditional analytical techniques, the advantages offered by HSI are of particular interest for practical applications, as such prediction of chemical compounds influencing coffee quality on a single bean basis is of industrial and scientific interest. Furthermore, the spatial distribution of the compounds was revealed across individual beans, which may be of interest to roasters, breeders or biologists.

9. COFFEE AROMA GENERATION PREDICTION FROM GREEN AND ROASTED SINGLE COFFEE BEANS

9.1. INTRODUCTION

The volatile composition of roasted coffee is complex, with more than 800 compounds identified. Many attempts have been made to link the complex pattern of volatile compounds to the sensory impact of coffee, thus selecting the so-called key aroma compounds (Sunarharum, Williams, & Smyth, 2014).

The typical aroma of coffee is generated during roasting, which causes a complicated pathway of reactions (Farah, Monteiro, Calado, Franca, & Trugo, 2006). A complex series of chemical reactions involved in the generation of coffee aroma include the Maillard and Strecker reaction, degradation of proteins, sugars, trigonelline and chlorogenic acid (De Maria et al., 1996). Different coffees can lead to different aromas, even when roasted under identical conditions.

The flavour of roasted coffee is influenced by the composition of the green beans, which in turn depends upon the species, environmental conditions and post-harvest processing (Sunarharum et al., 2014). Major differences exist between Arabica and Robusta coffees, but compositional differences are also observed among the same type of coffee, and even a considerable natural variability has been reported within the same batch (Chapters 7 and 8). This in turn affects the quality and consistency of the final roasted coffee, leading to over-roasted and under-roasted coffees, or possibly to generation of a different profile of volatile aroma compounds, which could include off-flavour formation.

It is generally accepted that a medium roasted coffee contains the highest amount of volatile compounds (Yeretzian et al., 2002), while a light roasted coffee gives rise to stronger notes of sweet, cocoa and nutty aromas, and a darker roasting causes more intense notes of burnt, sour, pungent and roasted (Bhumiratana, Adhikari, & Chambers, 2011). In this study, the key compounds for roasted and ground coffee were 2-ethyl-3,5-dimethylpyrazine, 3-mercapto-3-

methylbutyl-formate, 2-furfurylthiol and beta-damascenone, while other compounds were reported to be key odorants in the obtained coffee brew.

In addition to the analysis of variability of volatile compounds at batch level, it is also relevant to look at possible variation within batches, i.e. for individual coffee beans. This aspect has been reported by only a few studies. Fischer et al. (2014) used a time-of-flight mass spectrometer to collect information on the volatile release in a time-resolved manner during roasting. In this way, the authors were able to tentatively link the volatile compounds generated to the possible source; pyridines were reported to be generated from trigonelline, phenols from chlorogenic acids, furfuryl alcohol from carbohydrates, 1,2-benzenediol, guaiacol, vinylguaiacol and ethylguaiacol from chlorogenic acids. However, further research is still required in order to fully understand volatile compound formation in coffee, and to link their presence to precursors in the green coffee (Dorfner et al., 2003).

Despite the numerous analytical techniques available to measure the volatile composition of coffee beans, most are time-consuming and some of them use harmful chemicals. Near-Infrared (NIR) spectroscopy has been utilised for the evaluation of coffee brew quality, by trying to correlate the spectral information to the sensory response of a panel of consumers, so that some descriptors can be predicted without the need of sensory assessors (Esteban-Diez et al., 2004). NIRS shows promising results in terms of predicting the sensory impact of espresso coffee brew, as good performances have been reported for the prediction of several sensory attributes, such as the perceived acidity, which showed the best performance, i.e. R^2=0.9 (Esteban-Diez et al., 2004). Other studies applied NIRS to assess coffee roasting degree (Shan et al., 2015), and the changes in moisture, density and weight loss during roasting (Alessandrini, Romani, Pinnavaia, & Dalla Rosa, 2008), however, samples were scanned as ground material. Prediction of the coffee roasting degree has also shown to be promising, although the authors of this study analysed only one Arabica coffee batch at increasing roasting time (Shan et al., 2015). The PLS regression had high R^2 values, of 0.99 and 0.97 for the calibration and validation datasets, with RMSECV of 0.81% (range: 2–18%). The band at 1940 nm was described as the most important in the regression model, thus demonstrating the dramatic influence of the water absorption band (Shan et al., 2015).

When different roasting conditions are applied, the prediction of the roasting degree using PLS regression was successfully demonstrated, and the bands at 1450 and 1943 nm were the most influencing on the model, indicating the first overtone of O-H stretching and the combination band of O-H stretching and O-H deformation, respectively (Alessandrini et al., 2008; Barbin et al., 2014).

NIRS was proposed by Santos et al. (2016) for the measurement of titratable acidity over roasting, reporting good prediction ability on bulk (R_p^2=0.89 and RMSEP=0.16 ml NaOH 0.1 mol L^{-1} per g of coffee). Coffee cup quality has been also predicted by NIRS by scanning the green coffee (Tolessa et al., 2016). The authors used PLS regression to predict several sensory attributes such as total cup quality, acidity, body, aroma, flavour and aftertaste. FT-NIR in the spectral range 870–2500 nm was used to scan 15 grams of ground Arabica coffee from 86 batches from Ethiopia, while 100 grams from the same sample were roasted under the same time-temperature conditions, ground and analysed as coffee brew by three assessors for the cupping test. The PLS regression models had R_{cv}^2 values of 0.48 for total quality, and up to 0.89 for overall cup preference. Aroma was one of the attributes with the lowest prediction performance, showing RPD values of 1.57 (cross-validation) and 0.74 (prediction). Other attributes such as acidity and body were shown to give promising results. However, the authors analysed ground coffee as bulk and no information was reported on within-batch variability. In addition, they used coffee samples which were similar in terms of growing location and genetics. This can potentially produce good performing models but does not take into consideration the variability expected from other samples. This is particularly important for the coffee market, as blending is often carried out using different origins to obtain consistent results in terms of final quality.

HSI has been scarcely applied to study coffee beans. Fiore et al. (2008) used four roasting times, mixed Arabica and Robusta at various ratios, and scanned ground coffee using HSI in the region 400–1000 nm. The results of the PCA showed good clustering between Arabica and Robusta green coffees, while medium and dark roasted samples could not be clearly differentiated. Linear Discriminant Analysis (LDA) was applied and 75–95% correct classification was achieved on ground roast coffee to both differentiate the coffee species and the amount of Arabica in the

blend (Fiore et al., 2008). Only a single study on the application of HSI for the assessment of whole roasted coffee beans has been published, by Nansen et al. (2016), who used one batch of coffee only, roasted it under different conditions and then applied a classification model to discriminate these roasting conditions (named "roasting defects" in the paper). No quantitative prediction was undertaken in the study.

Therefore, the aim of this Chapter is to determine, for the first time, the feasibility of HSI to predict aroma generation potential of coffee beans – both green and roasted beans – on an individual seed basis. The approach to verify the differences in the aroma profile of roasted coffee based on a single bean involves roasting green coffees under the same time/temperature profile and analysing the resulting volatile compounds. The hypothesis tested in this Chapter is that, despite the low levels at which volatile compounds are present, it is possible to estimate their presence in single roasted coffee beans, and that their generation can be predicted by scanning single green coffee beans by HSI.

9.2. MATERIALS AND METHODS

9.2.1. Coffee samples and chemicals

Samples of commercial green coffee were sourced from UK and European importers with the aim to obtain a wide geographical and botanical distribution of batches. A total of 25 coffee batches were used, by randomly taking 10 beans per batch. Reference chemical compounds for the volatiles analysed were obtained from Sigma-Aldrich (Steinheim, Germany), and Fluka (Buchs, Switzerland).

9.2.2. Sample preparation and roasting

Samples were roasted using a Fracino Roastilino (Fracino, Birmingham, UK) roaster. This roaster is a fluid-bed type and was chosen as it gives the most uniform roasting conditions and it allows roasting of single beans in a rapid manner (Table 9.1). Preliminary tests were conducted to identify the best time-temperature profile to give a medium-high roasting level to all beans. This comprised running experiments in the time range 2–6 minutes and at 160–230 ºC, always in isothermal conditions. Individual coffee beans were placed in the roaster and thermally treated at constant

temperature of 210 ºC for 3 min. As a result, all the samples were treated using the same time/temperature profile to standardise the process. After roasting, colour measurement taken using a DigiEye instrument, and the roasted coffee beans were stored frozen at -20 ºC until the moment of grinding and analysis. The beans were then ground using a manual grinder (Devo, Holland) and stored in 1.5 mL Eppendorf tubes at -80 ºC until the moment of SPME-GC-MS analysis. Green coffee beans were individually weighed before and after the roasting process to calculate the weight loss, as an indication of the roasting degree in addition to the colour measurement.

Table 9.1. Scheme of the characteristics of different coffee roasting systems available.

	Oven roasting	**Fluidized bed roasted**	**Gas flame**
Advantages	Roasting done in batches (speed);	Relatively quick Good temperature control;	Might better replicate industrial conditions;
Disadvantages	Hot and cold spots in the oven;	Need accurate time control;	Very slow Inaccurate temperature control;

9.2.3. SPME-GC/MS analysis

Coffee volatile compound sampling conditions were chosen according to Ribeiro et al. (Ribeiro, Teófilo, Augusto, & Ferreira, 2010), where optimal conditions for pre-equilibrium time and temperature, extraction and injection was reported. The fibre was a 1 cm 50/30 μm DVB/Carboxen/PDMS StableFlex (Supelco, Sigma Aldrich, UK). This fibre was chosen because it was described as the most efficient for coffee aroma volatile compounds (Franca et al., 2009; Rojas Monroy, 2005). Ten minute pre-equilibrium at 40 ºC, 20 min fibre exposure and 5 min injection times were applied.

A trace 1300 series Gas-Chromatograph coupled with the Single-Quadrupole Mass Spectrometer (Thermo Fisher Scientific, Hemel Hemptead, UK) was used for the GC-MS analysis. The GC conditions were chosen as per Akiyama et al. (2007), slightly adapted to the type of column available. The column used was a 30 m length Zebron ZB-WAX capillary column, with 0.25 mm internal diameter and 1.00 μm film thickness (Phenomenex, Macclesfield, UK). The initial column

temperature was set at 40 ºC for 5 min, with an increase of 3 ºC min^{-1} up to 180 ºC, followed by an increase to 250 ºC with a rate of 10 ºC min^{-1}, and 250 ºC was then maintained for 5 min. A constant flow of 1.6 ml min^{-1} was applied and the Selective Ion Mode was used. Mass spectra were acquired in the electron impact mode at 70 eV, using a m/z range of 50–350 and 2 s scan time. Compound identification was conducted using reference compounds, where available, and by comparing their mass spectra with database (NIST). In addition, the identification was carried out by comparing the linear retention indices (LRI) of volatiles under the experimental conditions reported above, with literature data. LRI were built using a commercial mixture of n-alkanes analysed under the same GC-MS conditions in order to calculate the value for each volatile identified, on the basis of the difference of retention times between the previous and the following alkane. The concentration of volatile compounds was expressed as the relative concentration to the total GC-MS peak areas. An internal standard was also used to be able to express volatile compounds in absolute values, i.e. mg kg^{-1} ground coffee. An example of GC-MS trace of roasted coffee beans analysed in the present study is shown in Figure 9.1.

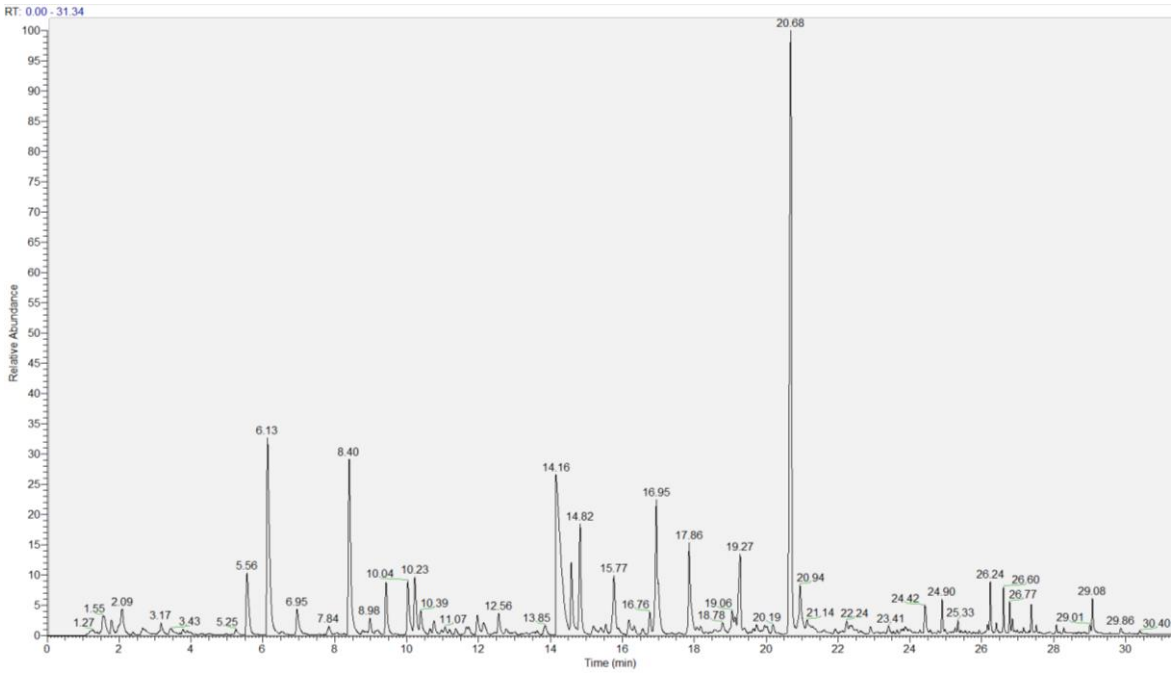


Figure 9.1. Example of chromatogram obtained by SPME-GC-MS analysis of volatile compounds in single ground and roasted coffee beans, for illustrative purpose only. Numbers indicate the retention times (min). The full list of compounds is reported in Table 9.2.

9.2.4. Colour measurement

As mentioned above, the colour of single roasted coffee beans was assessed using a DigiEye imaging system. Coffee was illuminated under D65 daylight conditions and the system was calibrated using a reference chart with 240 known colours, using CIELAB (L*, a*, b*) space. Images were acquired on both sides of the bean, and average measurements of L*, a* and b* were calculated. L* represents the lightness, a* the contribution of green or red, and b* the blue or yellow (an example of pictures is reported in Appendix in Figure A.7). Correlations among the colour parameters and the weight loss of roasted coffee are shown in Figure 9.2 (other plots on correlation among colour parameters are reported in Appendix in Figure A.15). More consistent results were generally obtained when taking the bean in the crease-down position, possibly due to the interference of the crease colour, where the outlier layer is not removed during the roasting and it has a slightly different colour. Previous studies reported the use of L* parameter to predict coffee roasting degree (Bicho, Leitão, Ramalho, & Lidon, 2012; Wei & Tanokura, 2015). However, as shown in Figure 9.2 the regression coefficient between L* value and the weight loss in single beans was very poor, probably due to the narrow range. Thus, coffee colour data were not further considered, and they were used as an additional indication when identifying possible outliers.

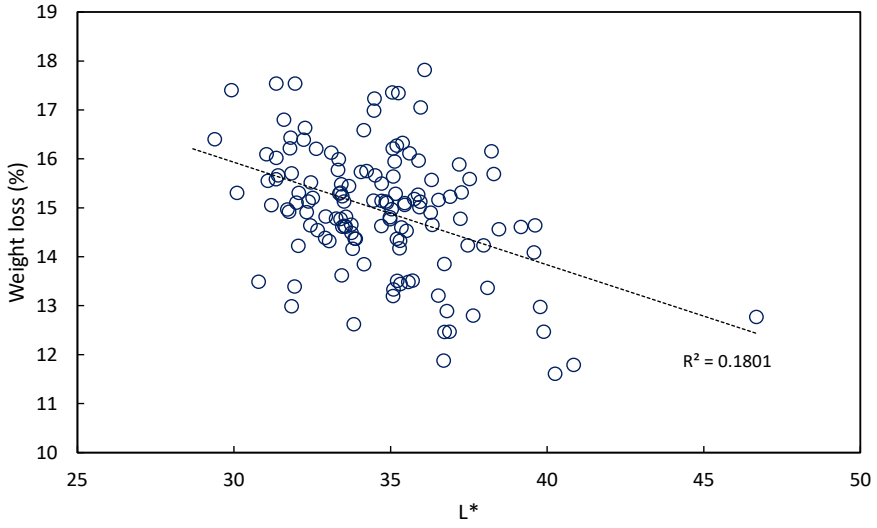


Figure 9.2. Correlation between L* value and the weight loss of roasted single beans, showing the poor correlation found.

9.2.5. HSI acquisition, data treatment and statistical analysis

Green coffee beans were scanned on both sides using the HSI instrument that was previously described in Section 3.2. Beans belonging to each batch were acquired in the same hypercube and treated as previously described (Sections 3.2 and 4.2). The beans were also scanned as whole single beans after roasting, before grinding and reference analyses.

The single bean spectra were treated by statistical analysis using The Unscrambler (CAMO, Norway). PLS regression models were built; specifically, PLS2 was used, so that more response variables could be modelled (one for each volatile compound). In order to reduce the number of responses, volatile compounds were grouped according to either their chemical groups or their sensory descriptors described in the literature. Minitab 18 (Pennsylvania, USA) was also used for analysing the data of volatile compounds by PCA to understand possible grouping of samples, and to perform correlation analysis by using Pearson correlation, at a significance level of $p<0.05$.

9.2.6. GC-MS analysis of sorted coffee beans

A trial of manual sorting was carried out to determine whether application of the calibrations for predicting volatile compounds in single coffee beans can enable creating sub-batches with distinctive characteristics. To do this, the calibrations for predicting coffee aroma generation from green and roasted coffee beans were applied to one batch of Arabica and Robusta coffees, and a few beans were manually selected according to the predicted aroma. The manually sorted beans were roasted as small batches under the same conditions (3 minutes at 210 ºC). The batches were ground using a manual grinder and one gram of sample was weighted and analysed by SPME-GC-MS as reported in section 9.2.3, using the same analytical conditions, including the same sample presentation.

9.2.7. Sensory analysis of sorted coffee beans

Over 250 green coffee beans were scanned by HSI by evenly spreading the beans on the tray in random positions and orientations, for each coffee species. The established calibrations for predicted sensory impact were applied; the four sensory descriptors with the best predictions were nutty, roasted, sweet and spicy. However, the first 2 and the last 2 are strongly correlated among

them, while negative correlation is observed between nutty/roasted and sweet/spicy. Thus, beans were selected based on predicted nuttiness, which was negatively correlated with "sweet". The top ~10% and bottom 10% of the total number of beans were manually selected. The sorted top and bottom fractions were roasted at 210 ºC for 3 minutes, manually ground and placed in amber glass vials (1 g per vial).

The method chosen for the sensory test was the triangle test, which is useful to determine whether a perceptible difference exists. The British Standard method for sensory analysis using Triangle test (BS EN ISO 4120:2007) was followed to assess whether statistically significant differences exist between the top and lower fraction of coffee beans manually sorted by applying the HSI prediction of expected aroma. Samples were placed in amber glass vials to avoid any visual cues that might have influenced the assessors.

Sensory assessors recruited were predominantly employees at Campden BRI, who were informed about the nature of the sample, the general aim of the project and were briefly instructed on how to assess the samples. They were also asked to complete and sign a "participant consent form" according to the regulations of the University of Nottingham (School of Biosciences). Approval to run the sensory test was previously obtained from the school, in accordance with the ethical guidelines. The ethical approval code for this experiment is SBREC160141A (SB1617/46 PGR Caporaso/Fisk). The number of assessors was chosen according to the ISO method for triangle test (EN ISO 4120:2007), which comprised 30 assessors (age range: 24-52). Panellists were presented with three samples, of which two were identical, and were then asked to sniff the vials and identify which one was the different sample, based exclusively on the odour. Specifically, assessors were asked to sniff the vials and identify which sample was different, based on the odour; in addition, optional open questions were asked to understand "why is it different" and give a preference (Figure 9.3). The number of correct responses was used to calculate the statistical significance. For the test of difference, when using an alpha-level of 0.05, using 30 assessors, the minimum number of correct responses should be 15, while α of 0.01 would be obtained with 17 correct responses.

Participant Consent Form

Project Title:
Sensory evaluation of the odour of coffee brews for Arabica and Robusta coffees.

In signing this consent form I confirm that:

I have read the Participant Information Sheet and the nature and purpose of the research project has been explained to me.	Yes ☐	No ☐
I have had the opportunity to ask questions.	Yes ☐	No ☐
I understand the purpose of the research project and my involvement in it.	Yes ☐	No ☐
I understand that my participation is voluntary and I may withdraw from the research project at any stage, without having to give any reason and withdrawing will not penalise or disadvantaged me in any way.	Yes ☐	No ☐
I understand that while information gained during the study may be published, any information I provide is confidential (with one exception – see below), and that no information that could lead to the identification of any individual will be disclosed in any reports on the project, or to any other party. No identifiable personal data will be published.	Yes ☐	No ☐
I understand that data will be securely stored	Yes ☐	No ☐
I understand that the information provided can be used in other research projects which have ethics approval, but that my name and contact information will be removed before it is made available to other researchers.	Yes ☐	No ☐
I understand that I may contact the researcher if I require further information about the research, and that I may contact the Research Ethics Officer of the School of Biosciences, University of Nottingham, if I wish to make a complaint relating to my involvement in the research.	Yes ☐	No ☐
I agree to take part in the above research project.	Yes ☐	No ☐

Two samples are the same and one is different. Smell the samples from left to right and identify the DIFFERENT one.

☐ ☐ ☐

934 462 548

Why is it different?

Which one do you prefer and why?

Two samples are the same and one is different. Smell the samples from left to right and identify the DIFFERENT one.

☐ ☐ ☐

514 754 568

Why is it different?

Which one do you prefer and why?

Figure 9.3. Copy of the Participant Consent Form submitted to each sensory assessor, and example of the form used during the triangle test.

9.3. RESULTS AND DISCUSSION

9.3.1. Reference analysis of volatile compounds

A total of 50 volatile compounds were identified in roasted and ground coffee samples on a single bean basis, these are shown in Table 9.2, with an indication of the Linear Retention Index, sensory descriptors and odour threshold from the literature. Five compounds were tentatively identified as furaneol (LRI 1485), ethyl propanoate (1520), N-acetyl-4(H)-pyridine (1705), 3-Hydroxy-4.5-dimethyl-2(5H)-furanone (1728) and 3-methoxy-5-methyl-2-cyclopenten-1-one (1745). This was because these compounds had low similarity with the MS spectra from database. All the compounds have been previously reported in food materials and especially in coffee. The compounds shown in bold are potent odorants, i.e. they have a strong impact in coffee aroma. In terms of chemical classes, the most represented groups were ketones and pyrazines, with 12 compounds for each class. Five aldehydes, 4 phenols and 4 acids were also identified, while fewer compounds were identified for other classes.

Figure 9.4 shows the distribution of each volatile compound in all the samples analysed, comparing Arabica and Robusta coffees. A few compounds had concentrations higher than 10-20% total peak areas, while the majority of volatiles were found at lower concentrations. Generally, Robusta had a higher content of pyrazines, and a lower aldehydes content. However, it should be noted that there are factors other than solely the concentration of volatile compounds that influences their odour impact, as compounds found at very low concentration might be potent odorants in coffee due to the their low detection threshold (Caporaso, Genovese, Canela, Civitella, & Sacchi, 2014; Genovese, Caporaso, Civitella, & Sacchi, 2014; Grosch, 1998, 2001a; Semmelroch & Grosch, 1996).

The correlation among volatile compounds was investigated by using the Pearson statistics, and results are reported in Table 9.3, with values in bold indicating the strongest correlations. Generally, compounds from the same chemical group are positively correlated, probably due to their common chemical origin, or similar biochemical pathway of their precursors.

Table 9.2. Identification of volatile compounds in roasted Arabica and Robusta coffee samples analysed by SPME-GC-MS for single beans.

n.	RT	LRI	Compound*	Sensory descriptors	Literature LRI	Odour thr. (ppb)	IM	Chemical group
1	1.29	<1040	**acetaldehyde**	Pungent, fruity	690	80	MS	Aldehyde
2	1.79	<1040	2-methylfuran	Pungent, fruity	838-866	4000	MS, L	Furan
3	2.09	<1040	**3-methylbutanal**	Fruity, malty	906-914	1.2	MS	Aldehyde
4	2.65	<1040	**2,3-butanedione**	Buttery	955	15	MS, L	Ketone
5	3.77	1046	**2,3-pentanedione**	Buttery, oily, caramel-like	1053-1056	30	MS, ST, L	Ketone
6	4.12	1069	**hexanal**	Green, grassy, fruity	1024-1087	5	MS, ST	Aldehyde
7	5.24	1128	**1-methyl-1H-pyrrole**	Smoky, woody, herbal	1123	37	MS, ST	Heterocyclic N
	5.56	*1142*	*3-heptanone (Internal Standard)*	*Fruit, green, fatty, sweet*	*1162-1185*		*MS, ST*	*Ketone*
8	6.13	1166	pyridine	Sour, putrid, fishy, amine, bitter, roasted	1195-1183	2000	MS, L	Heterocyclic N
9	6.95	1201	pyrazine	Cooked spinach, rancid peanuts, strong	1192-1214	177000	MS, L	Pyrazine
10	8.4	1252	**2-methyl-pyrazine**	Nutty	1260-1282	60	MS, ST	Pyrazine
11	8.98	1272	**acetoin (=3-hydroxy-2-butanone)**	Sweet, buttery, creamy	1265	800	MS, ST, L	Ketone
12	9.42	1287	1-hydroxy-2-propanone (=acetol)	Sweet, caramellic	1294, 1208	100000	MS	Ketone
13	10.03	1308	**2,5-dimethylpyrazine**	Nutty, roasted, grassy	1316	2600	MS, ST, L	Pyrazine
14	10.22	1314	**2,6-dimethylpyrazine**	Chocolate, cocoa, roasted nuts, fried	1319	3100	MS, ST, L	Pyrazine
15	10.39	1319	ethylpyrazine	Nutty, peanut, butter	1323-1325	6000	MS, ST	Pyrazine
16	10.8	1333	**2,3-dimethylpyrazine**	Nutty, roasted	1335	250	MS, ST, L	Pyrazine
17	11.66	1361	1-hydroxy-2-butanone	Sweet, coffee	1368		MS	Ketone
18	11.72	1362	3-ethylpyridine	Tobacco, oak, moss, leather	1376, 1397		MS	Heterocyclic N
19	11.99	1371	**2-ethyl-6-methylpyrazine**	Flowery, fruity, hazelnut-like	1363-1381, 1387-1388	30	MS, ST, L	Pyrazine
20	12.12	1375	**2-ethyl-5-methylpyrazine**	Coffee-like	1393-1395	100	MS, ST, L	Pyrazine
21	12.58	1390	**2-ethyl-3-methylpyrazine**	Nutty, peanut	1405-1407	130	MS, ST, L	Pyrazine
22	13.57	1422	2,3-diethylpyrazine	Raw, nutty, green pepper	1454 , 1444		MS, L	Pyrazine

Table 9.2 (*continued*)

n.	RT	LRI	Compound*	Sensory descriptors	Literature LRI	Odour thr.	IM	Chemical group
23	13.85	1431	**3-ethyl-2,5-dimethylpyrazine**	Earthy, roasted	1435-1470, 1439	1	MS	Pyrazine
24	14.17	1441	acetic acid	Pungent, vinegar	1435-1459	34000	MS, ST, L	Acid
25	14.58	1454	furfural	Sweet, woody, almond	1447-1466	3000	MS, ST, L	Aldehyde
26	14.84	1462	1-(acetyloxy)-2-propanone (=acetoxyacetone)	Fruity, buttery, dairy	1454		MS	Ketone
27	15.21	1474	furfurylmethyl sulphide	Onion, garlic, sulphuraceous	1476-1480		MS	Sulphide
28	15.38	1479	2-ethyl-3,5-dimethylpyrazine	Earthy, roasted	1450-1466-1469	1	MS, ST	Pyrazine
29	15.55	1485	furaneol (=4-Hydroxy-2,5-dimethyl-3(2H)-furanone)	Caramel, sweet		31	TI	Ketone
30	15.7	1490	2-acetylfuran	Sweet, balsam, almond, cocoa	1483, 1499	10000	MS, L	Furan
31	16.76	1520	**ethyl propanoate**	Sweet, fruity, rum, juicy		10	TI	Ester
32	16.96	1527	**2-furanmethanol acetate**	Ethereal-floral, herbal-spicy	1514	100	MS	Acetate
33	16.99	1528	propanoic acid	Pungent, acidic, cheesy, vinegar	1531	20000	MS	Acid
34	17.86	1557	**5-methyl-2-furancarboxaldehyde (=5-methylfurfural)**	Spice, caramel, maple	1551, 1570	6	MS, ST	Aldehyde
35	18.19	1569	2,3-butanediol	Fruity, creamy, buttery	1580	75000	MS	Alcohol
36	19.13	1600	2-formyl-1-methylpyrrole	Roasted, nutty	1610-1620-1626, 1618	40	MS	Pyrrole
37	19.25	1604	γ-butyrolactone (=dihydrofuran-2(3H)-one)	Creamy, oily, fatty, caramel	1602-1615-1643, 1614	1000	MS,	Ketone
38	20.7	1653	2-furanmethanol	Caramellic, burnt, smoky	1573-1667	2000	MS, ST, L	Alcohol
39	20.96	1662	3-methyl-butanoic acid	Cheesy, dairy, creamy, fermented	1670-1678-1683	400	MS, ST	Acid
40	22.23	1705	N-acetyl-4(H)-pyridine			20	TI	Heterocyclic N

Table 9.2 (*continued*)

n.	RT	LRI	Compound*	Sensory descriptors	Literature LRI	Odour thr.	IM	Chemical group
41	22.91	1728	3-Hydroxy-4.5-dimethyl-2(5H)-furanone	Buttery, seasoning-like	1726 - 2203	50	TI	Ketone
42	23.41	1745	3-methoxy-5-methyl-2-cyclopenten-1-one				TI	Ketone
43	23.98	1764	3-methyl-2-butenoic acid	Green, phenolic, dairy	1776	14000	MS	Acid
44	24.43	1815	3-methyl-1,2-cyclopentanedione	Spice, caramellic, maple, sweet, burnt	1822	300	MS	Ketone
45	24.89	1848	**guaiacol (=2-methoxyphenol)**	Phenolic, burnt, smoky	1850-1859	3	MS, ST, L	Phenolic
46	26.25	1961	2-(1H-pyrrol-2-yl)-ethanone	Smoky, spicy	1952	170000	MS	Ketone
47	26.6	1994	phenol	Phenolic, plastic, rubber, smoky	1996-2051	2400	MS	Phenolic
48	26.77	2012	1H-pyrrole-2-carboxaldehyde (=2-Formylpyrrole)	Musty, beefy, coffee	2028-2030		MS	Heterocyclic N
49	26.86	2022	**4-ethylguaiacol**	Spicy, phenolic, sweet	2020-2024, 2032-2036	50	MS, ST, L	Phenolic
50	28.28	2186	**4-vinylguaiacol**	Clove	2151-2187-2205-2210	3	MS, ST, L	Phenolic

* Compounds in bold are considered as potent odorants in roasted coffee, based on literature data. Sensory descriptors and odour thresholds are taken from the literature (Akiyama et al., 2007; Caporaso et al., 2014; Czerny & Grosch, 2000; Maeztu et al., 2001; Piccino, Boulanger, Descroix, & Sing, 2014; Puvipirom & Chaiseri, 2012; Semmelroch & Grosch, 1996). RT = retention time; LRI = linear retention index; IM = identification method (MS = experimental mass spectra compared to database, or L = literature; ST = standard compound, i.e. pure reference compound; TI = tentative identification).

Table 9.3. Pearson correlation among volatile compounds in single roasted coffee beans, analysed by SPME-GC-MS. Only compounds showing highly significant ($p<0.001$) correlations are shown, using Pearson correlation statistics. Bold values indicate the strongest correlations.

	pyrazine	**2-methyl pyrazine**	**acetoin**	**1-hydroxy-2-propanone**	**acetaldehyde**
2-methyl-pyrazine	**0.806**				
1-hydroxy-2-propanone	-0.292	-0.328	**0.899**		
2,5-dimethylpyrazine	0.633	**0.932**	-0.229	-0.198	
2,6-dimethylpyrazine	0.683	**0.944**	-0.408	-0.376	
ethylpyrazine	0.774	**0.974**	-0.338	-0.347	
2,3-dimethylpyrazine	0.672	**0.858**	-0.080	-0.140	
1-hydroxy-2-butanone	-0.386	-0.412	**0.867**	**0.913**	
2-ethyl-6-methylpyrazine	0.685	**0.925**	-0.418	-0.397	
2-ethyl-5-methylpyrazine	0.645	**0.910**	-0.336	-0.309	
2-ethyl-3-methylpyrazine	0.652	**0.896**	-0.420	-0.404	
furfural	-0.509	-0.437	0.709	**0.829**	
acetaldehyde	0.110	-0.068	0.694	**0.834**	
2,3-butanedione	-0.120	-0.380	**0.827**	**0.882**	**0.859**

	2,5-dimethyl pyrazine	**2,6-dimethyl pyrazine**	**ethylpyrazine**	**2,3-dimethyl pyrazine**	**2-ethyl-3-methyl pyrazine**
2,6-dimethylpyrazine	**0.973**				
ethylpyrazine	**0.942**	**0.948**			
2,3-dimethylpyrazine	**0.843**	**0.803**	**0.887**		
2-ethyl-6-methylpyrazine	**0.939**	**0.951**	**0.975**	**0.867**	
2-ethyl-5-methylpyrazine	**0.937**	**0.921**	**0.969**	**0.873**	
2-ethyl-3-methylpyrazine	**0.888**	**0.894**	**0.948**	**0.877**	
3-ethyl-2,5-dimethylpyrazine	**0.807**	**0.808**	**0.863**	**0.789**	**0.968**

	1-hydroxy-2-butanone	**3-ethylpyridine**	**2-ethyl-6-methyl**	**2-ethyl-5-methylpyrazine**
2-ethyl-5-methylpyrazine	-0.429	-0.373	**0.984**	
2-ethyl-3-methylpyrazine	-0.523	-0.244	**0.979**	**0.966**

Table 9.3 (*continued*)

	1-hydroxy-2-butanone	**3-ethylpyridine**	**2-ethyl-6-methyl**	**2-ethyl-5-methylpyrazine**
2,3-diethylpyrazine	-0.749	0.225	**0.826**	0.794
3-ethyl-2,5-dimethylpyrazine	-0.535	-0.15	**0.934**	**0.928**
furfural	**0.893**	-0.555	-0.494	-0.434
furaneol	**0.871**	-0.168	-0.726	-0.673
1H-pyrrole-2-carboxaldehyde	-0.559	**0.943**	-0.191	-0.232
1-methyl-1H-pyrrole	-0.456	**0.930**	-0.271	-0.299
pyridine	-0.476	**0.983**	-0.315	-0.364

	furaneol	**2-acetylfuran**	**ethyl propanoate**	**2-furanmethanol**
propanoic acid	0.523	**0.809**	-0.063	0.511
5-methyl-2-furancarboxaldehyde	**0.891**	0.546	-0.293	0.496
2,3-pentanedione	**0.837**	0.016	-0.056	0.189
propanoic acid	0.526	0.757	**0.828**	0.578

	γ-butyrolactone	**2-furan methanol**	**3-methyl-butanoic acid**	**N-acetyl-4(H)-pyrrole**	**2-(1H-pyrrol-2-yl)-ethanone**	**phenol**	**2-formyl pyrrole**	**guaiacol**
1H-pyrrole-2-carboxaldehyde	**0.878**	0.442	-0.116	0.760	0.509	-0.462		**0.803**
2-methylfuran	**0.875**	0.541	-0.038	0.603	0.422	-0.601	**0.912**	0.713
1-methyl-1H-pyrrole	**0.844**	0.614	-0.038	0.770	0.446	-0.518	**0.878**	0.624
pyridine	**0.893**	0.595	-0.086	0.716	0.442	-0.564	**0.951**	0.693

Numbers in bold indicate the highest correlation coefficients.

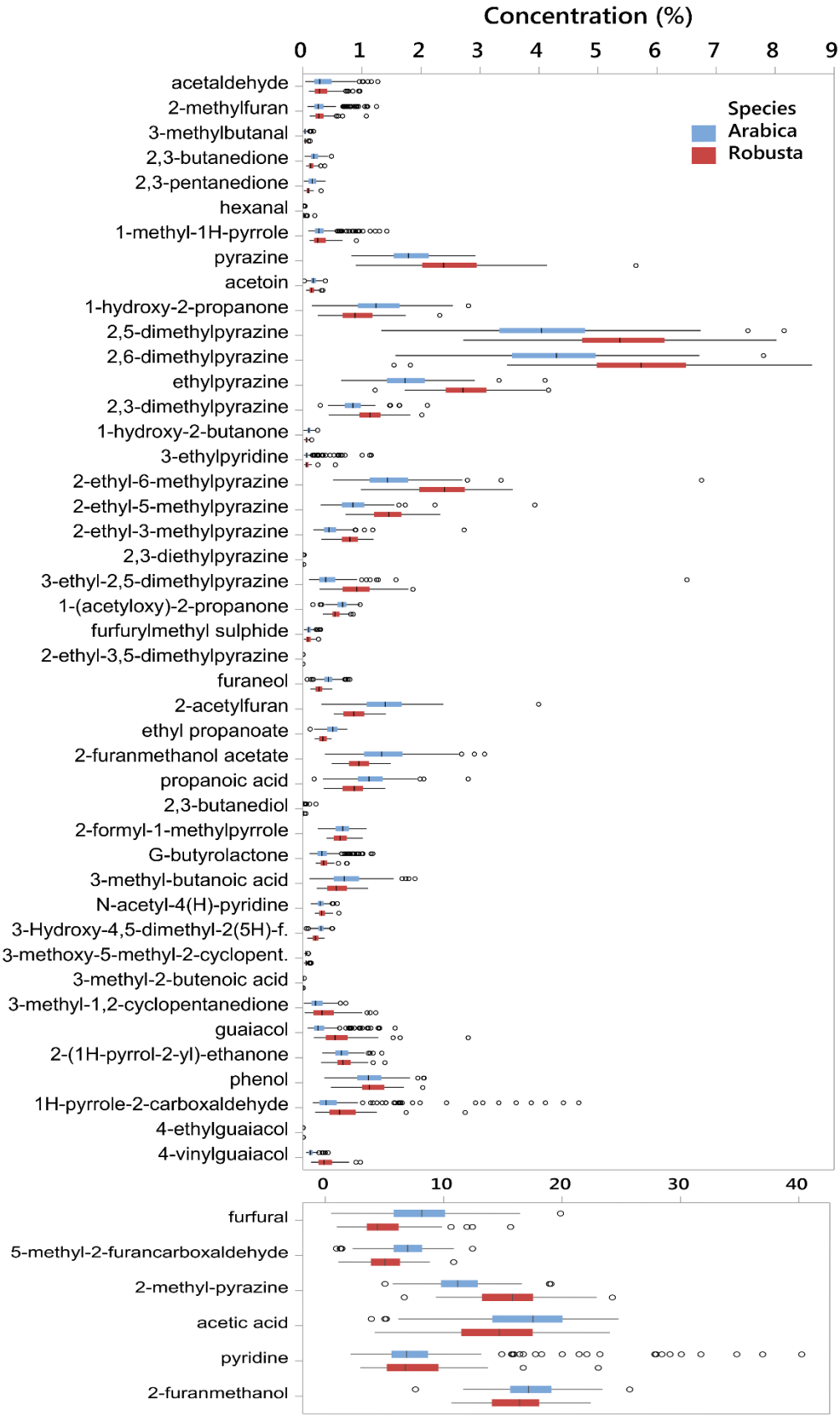


Figure 9.4. Boxplot distribution of the relative concentration of volatile compounds in single roasted coffee beans, by separately showing Arabica and Robusta species. The bottom plot shows the highest concentrated compounds.

9.3.2. Roasted coffee: HSI prediction of volatile compounds

Two approaches were tested to build the prediction models with the aim to describe the possible relationship between the spectral information from HSI of single green and roasted coffee beans, and the reference volatile compounds of the roasted beans. Firstly, prediction models were built on all volatile compounds individually, while a second approach utilised a data reduction strategy to cluster compounds according to their chemical groups (aldehydes, ketones, pyrazines, acids, etc.), or according their odour impact (i.e. sensory descriptors).

Table 9.4 reports the prediction performance of single volatile compounds in roasted coffee beans scanned by HSI. Ethylpyrazine, ethylpropanoate, 5-mehtylfurfural, acetoxyacetone, 2-ethyl-5-methylpyrazine and 2-ethyl-5-methylpyrazine were the compounds showing the highest cross-validation R^2 values. The lowest RMSECV values were obtained for 2-ethyl-3,5-dimethylpyrazine, 4-ethylguaiacol, 2,3-diethylpyrazine and 3-methyl-2-butenoic acid. The prediction error by itself, however, is not a good indicator of which compound was predicted with the best performance, as the range of concentrations at which each compound was found should be also taken into consideration.

Table 9.4. Performance of PLS2 regression model to predict individual volatile compounds in single coffee beans, by HSI scanning of roasted coffee beans.

Compound	Calibration		Cross-validation		RPD
	R^2	RMSE	R^2	RMSE	
acetaldehyde	0.22	0.16	0.12	0.17	1.37
2-methylfuran	0.313	0.092	0.249	0.097	1.13
3-methylbutanal	*0.08*	*0.02*	*0*	*0.02*	*1.22*
2,3-butanedione	0.285	0.065	0.188	0.070	1.16
2,3-pentanedione	0.384	0.057	0.299	0.061	1.31
hexanal	0.197	0.017	0.046	0.019	0.84
1-methyl-1H-pyrrole	0.331	0.0957	0.164	0.1078	1.57
pyridine	0.417	1.906	0.236	2.193	1.72
pyrazine	0.608	0.416	0.479	0.482	1.27
2-methyl-pyrazine	**0.689**	**1.841**	**0.552**	**2.222**	**1.48**
acetoin	0.367	0.049	0.257	0.054	1.09
acetol	0.427	0.346	0.319	0.379	1.27
2,5-dimethylpyrazine	0.606	0.790	0.441	0.951	1.47
2,6-dimethylpyrazine	**0.646**	**0.843**	**0.512**	**0.992**	**1.43**
ethylpyrazine	**0.755**	**0.339**	**0.631**	**0.418**	**1.62**
2,3-dimethylpyrazine	0.378	0.235	0.229	0.263	1.08

Table 9.4 (*continued*)

Compound	**Calibration**		**Validation**		**RPD**
1-hydroxy-2-butanone	0.484	0.028	0.378	0.031	1.34
3-ethylpyridine	0.362	0.040	0.160	0.046	1.85
2-ethyl-6-methylpyrazine	**0.645**	**0.414**	**0.538**	**0.478**	**1.51**
2-ethyl-5-methylpyrazine	**0.666**	**0.259**	**0.534**	**0.308**	**1.46**
2-ethyl-3-methylpyrazine	0.602	0.182	0.459	0.214	1.26
2,3-diethylpyrazine	0.657	0.0014	0.509	0.0017	1.36
3-ethyl-2,5-dimethylpyrazine	0.438	0.366	0.321	0.405	1.27
acetic acid	0.386	3.618	0.146	4.299	1.04
furfural	**0.642**	**1.928**	**0.520**	**2.242**	**1.59**
acetoxyacetone	0.630	0.081	0.542	0.091	1.53
furfurylmethyl sulphide	0.39	0.036	0.32	0.038	1.39
2-ethyl-3,5-dimethylpyrazine	*0.09*	*0.0001*	*0.01*	*0.0001*	*1.82*
furaneol	0.572	0.085	0.481	0.094	1.38
2-acetylfuran	0.584	0.282	0.505	0.309	1.54
ethyl propanoate	**0.651**	**0.074**	**0.58**	**0.082**	**1.54**
2-furanmethanol acetate	0.565	0.262	0.518	0.276	1.74
propanoic acid	0.576	0.241	0.47	0.27	1.34
5-methylfurfural	**0.690**	**1.038**	**0.578**	**1.226**	**1.67**
2,3-butanediol	*0.12*	*0.02*	*0.04*	*0.02*	*0.91*
2-formyl-1-methylpyrrole	*0.18*	*0.12*	*0.09*	*0.12*	*1.29*
γ-butyrolactone	*0.2*	*0.08*	*0.1*	*0.09*	*1.13*
2-furanmethanol	0.21	2.19	0.19	2.39	1.11
3-methyl-butanoic acid	0.284	0.257	0.210	0.271	1.16
N-acetyl-4(H)-pyridine	0.32	0.054	0.238	0.058	1.35
3-Hydroxy-4.5-dimethyl-2(5H)-furanone	0.598	0.053	0.529	0.057	1.43
3-methoxy-5-methyl-2-cyclopenten-1-one	0.362	0.015	0.255	0.017	1.07
3-methyl-2-butenoic acid	0.443	0.0021	0.333	0.0024	1.26
3-methyl-1,2-cyclopentanedione	*0.09*	*0.18*	*0*	*0.19*	*1.03*
guaiacol	0.559	0.161	0.486	0.175	1.87
2-(1H-pyrrol-2-yl)-ethanone	0.501	0.13	0.441	0.138	1.34
2-formylpyrrole	0.446	0.213	0.352	0.231	1.30
phenol	0.273	0.225	0.307	0.237	1.70
4-ethylguaiacol	0.507	0.00045	0.434	0.00049	1.36
4-vinylguaiacol	0.483	0.118	0.423	0.126	1.25

Compounds in bold indicate the best models, while the ones in Italics indicate the poorest model performances. The PLS2 regression model was built on the HSI spectra pre-treated using 2nd derivative treatment.

For example, despite the low prediction error of hexanal, this compound was poorly predicted as it had R^2 value of almost zero and RPD value of 0.84. The RPD value may therefore be a better indicator of the model performance, but it should still be considered alongside the calibration and prediction R^2 values. For example, despite the high RPD values obtained for 3-ethylpyridine and 2-ethyl-3,5-dimethylpyrazine, these compounds were in fact poorly predicted (validation R^2 of 0.16 and 0.01, respectively). The pyrazine compounds, with exceptions (2,3-dimethyl pyrazine and 2-ethyl-3,5-dimethylpyrazine), showed the best prediction performances. In addition, good prediction was obtained for guaiacol (RPD=1.87), 2-furanmethanol acetate (RPD=1.74), 5-methylfurfural (RPD=1.67) and furfural (RPD=1.59).

Figure 9.5 shows the plot of cross-validation error (RMSECV) in relation to the number of LVs, for all single volatile compounds. This graph is useful to show the expected prediction error and was used by the software to suggest the optimal LV, which was 11 in this case. The big difference in the prediction error among volatile compounds is due to the different concentrations at which they are found in coffee headspace, as some of them are present at 10-20%, while others are much below 1% (Figure 9.4).

Some of the volatiles showing the best performances are shown in Figure 9.6 to present the predicted versus reference plots. Generally, a very good spread of volatile compounds was observed, as the range of variation observed was fully covered. Compounds belonging to the pyrazine group had good prediction performance, with 2-methylpyrazine, ethylpyrazine, 2,6-dimethylpyrazine, 3-ethyl-2,5-dimethylpyrazine demonstrating good performance in both roasted and green coffee beans. Similarly, furaneol, a ketone described with sweet and caramel odour notes, was successfully predicted. Figure A.10 reports the regression coefficients for the prediction of some volatile compounds in roasted coffee beans. As expected, some compounds with very similar chemical structure had similar regression coefficient plots, i.e. the absorbance bands were the same, despite differences observed in terms of intensity. An example of this is provided by 2-ethyl-6-methylpyrazine and 2-ethyl-5-methylpyrazine. There was some similarity between furaneol and ethyl propanoate to some extent.

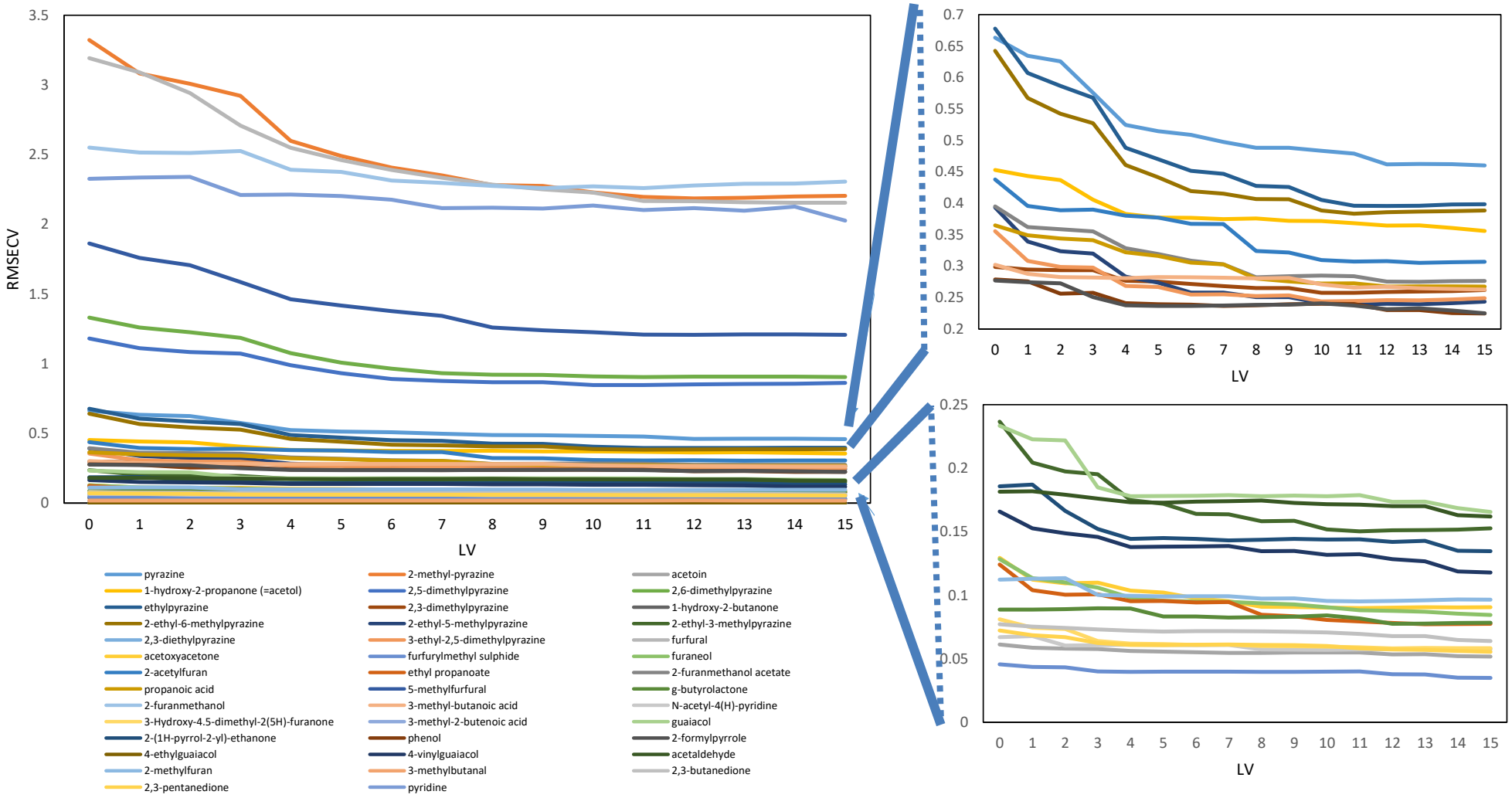


Figure 9.5. Prediction error (RMSECV) plot depending on the number of Latent Variables (LV) in PLS2 models to predict specific volatile compounds in single roasted coffee beans using HSI (roasted beans scanned). The optimal LV identified for the general model was LV=11. The figures on the right reproduce the one on a different abscissa in order to better visualise lower concentred compounds.

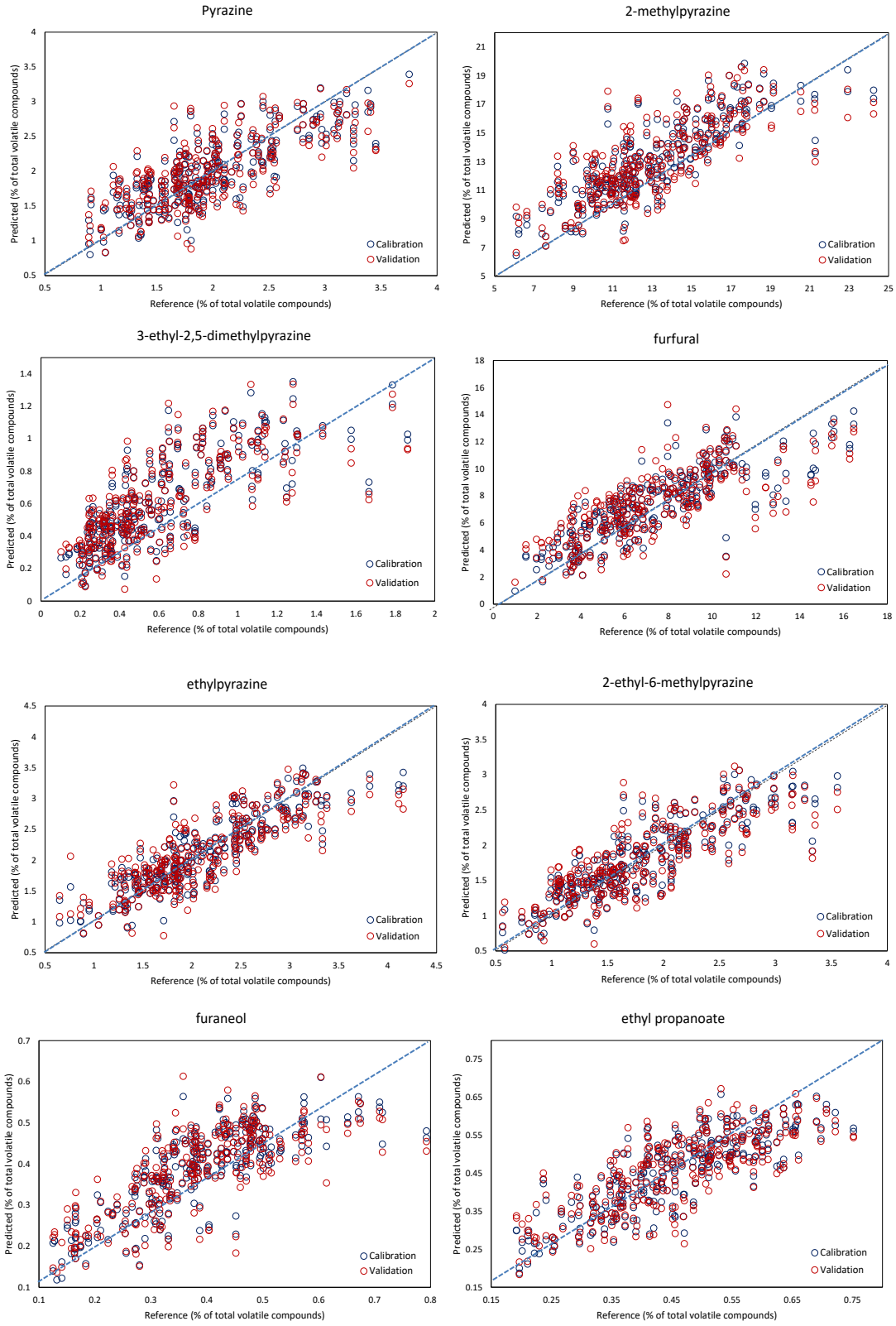


Figure 9.6. Predicted versus reference concentration of single volatile compounds (odour impact compounds) in single roasted coffee beans by using HSI, and PLS2 as the chemometric method. Compounds are expressed as % of each compound compared to the total GC-MS peak areas (n~300).

9.3.3. Green coffee: HSI prediction of volatile compounds

Table 9.5 reports the results of the prediction models built on single green coffee beans, for individual volatile compounds in roasted coffee (the general plot of explained variance is reported in Appendix in Figure A.9). The prediction performance is strongly dependent on the compound, as for many volatiles it can be concluded that no prediction can be made, while others showed good performance. A total of 12 compounds had cross-validation R^2 values greater than 0.5; they mostly belong to pyrazines, with also furanol, 2,3-pentanedione, 2,3-butanedione and furfural resulting in good prediction ability. A total of 14 compounds had cross-validation R^2 below 0.2, indicating very poor prediction ability: volatile phenolic compounds, aldehydes, heterocyclic nitrogen compounds, alcohols, a sulphide compound and even a pyrazine (2-ethyl-3,5-dimethylpyrazine).

Despite the chemical similarity of 2-ethyl-3,5-dimethylpyrazine with 3-ethyl-2,5-dimethylpyrazine, different prediction ability was observed for these two compounds. Very good prediction was obtained for the latter compound, giving the highest RPD value observed among all the volatiles studied (2.13). Other pyrazines had relatively high RPD values, between 1.74 and 1.84 (2-ethyl-6-methylpyrazine, 2-ethyl-3-methylpyrazine, ethylpyrazine and 2-ethyl-5-methylpyrazine). Other pyrazines also showed good performance. In addition, furaneol had RPD value of 1.69, while potent odorants such furfural, 2,3-pentandione and 2,3-butanedione had RPD values above 1.5, thus still usable for screening purposes.

Table 9.5. Performance of PLS2 prediction model for single volatile compounds in single coffee beans, using green coffee beans scanned by HSI.

Compound	Calibration		Cross-Validation		RPD
	R^2	RMSE	R^2	RMSE	
acetaldehyde	0.497	0.163	0.480	0.170	1.37
2-methylfuran	0.218	0.166	0.250	0.174	1.15
3-methylbutanal	*0.140*	*0.022*	*0.083*	*0.023*	1.06
2,3-butanedione	**0.543**	**0.054**	**0.523**	**0.056**	1.45
2,3-pentanedione	**0.589**	**0.050**	**0.555**	**0.053**	1.50
hexanal	*0.12*	*0.013*	*0.05*	*0.013*	1.23
1-methyl-1H-pyrrole	*0.189*	*0.158*	*0.090*	*0.170*	1.23
pyridine	*0.172*	*4.383*	*0.063*	*4.697*	1.23
pyrazine	0.564	0.401	0.473	0.438	1.40

Table 9.5 (*Continued*)

Compound	Calibration		Validation		RPD
2-methyl-pyrazine	**0.693**	**1.782**	**0.610**	**2.000**	1.64
acetoin	0.398	0.044	0.348	0.046	1.28
acetol	0.525	0.322	0.481	0.342	1.41
2,5-dimethylpyrazine	0.535	0.859	0.455	0.932	1.50
2,6-dimethylpyrazine	0.590	0.848	0.508	0.927	1.53
ethylpyrazine	**0.748**	**0.333**	**0.671**	**0.380**	1.78
2,3-dimethylpyrazine	0.514	0.198	0.431	0.215	1.32
1-hydroxy-2-butanone	0.548	0.027	0.493	0.029	1.43
3-ethylpyridine	*0.18*	*0.103*	*0.080*	*0.110*	1.44
2-ethyl-6-methylpyrazine	**0.700**	**0.354**	**0.627**	**0.393**	1.84
2-ethyl-5-methylpyrazine	**0.656**	**0.238**	**0.600**	**0.257**	1.74
2-ethyl-3-methylpyrazine	0.642	0.138	0.582	0.149	1.81
2,3-diethylpyrazine	0.600	0.0013	0.532	0.0014	1.65
3-ethyl-2,5-dimethylpyrazine	0.577	0.228	0.524	0.242	2.13
acetic acid	*0.21*	*3.79*	*0.12*	*4.04*	1.11
furfural	**0.600**	**2.139**	**0.516**	**2.370**	1.51
acetoxyacetone	0.387	0.104	0.323	0.110	1.27
furfurylmethyl sulphide	0.164	0.047	0.105	0.049	1.08
2-ethyl-3,5-dimethylpyrazine	*0.13*	*0.0003*	*0.07*	*0.0003*	0.61
furaneol	**0.670**	**0.072**	**0.620**	**0.077**	1.68
2-acetylfuran	0.484	0.317	0.429	0.334	1.43
ethyl propanoate	0.481	0.088	0.428	0.092	1.37
2-furanmethanol acetate	0.424	0.348	0.374	0.367	1.31
propanoic acid	0.408	0.261	0.318	0.280	1.30
5-methylfurfural	0.461	1.400	0.353	1.533	1.34
2,3-butanediol	*0.1*	*0.017*	*0.04*	*0.018*	1.01
2-formyl-1-methylpyrrole	0.264	0.132	0.234	0.138	1.12
g-butyrolactone	0.263	0.145	0.189	0.154	1.18
2-furanmethanol	0.332	2.089	0.253	2.208	1.21
3-methyl-butanoic acid	0.279	0.255	0.237	0.265	1.18
N-acetyl-4(H)-pyridine	0.322	0.062	0.267	0.065	1.20
3-Hydroxy-4.5-dimethyl-2(5H)-furanone	0.432	0.0586	0.351	0.0628	1.30
3-methoxy-5-methyl-2-cyclopenten-1-one	0.452	0.013	0.394	0.014	1.30
3-methyl-2-butenoic acid	0.536	0.0022	0.376	0.0024	1.26
3-methyl-1,2-cyclopentanedione	*0.08*	*0.18*	*0.03*	*0.20*	0.98
guaiacol	*0.23*	*0.28*	*0.14*	*0.30*	1.09
2-(1H-pyrrol-2-yl)-ethanone	0.390	0.14	0.350	0.15	1.23
2-formylpyrrole	0.27	0.24	0.21	0.25	1.21
phenol	*0.16*	*0.54*	*0.07*	*0.58*	1.19
4-ethylguaiacol	*0.19*	*0.00058*	*0.11*	*0.00061*	1.08
4-vinylguaiacol	0.377	0.125	0.329	0.130	1.21

In bold: models with the best prediction performance; in Italics: poorest models.

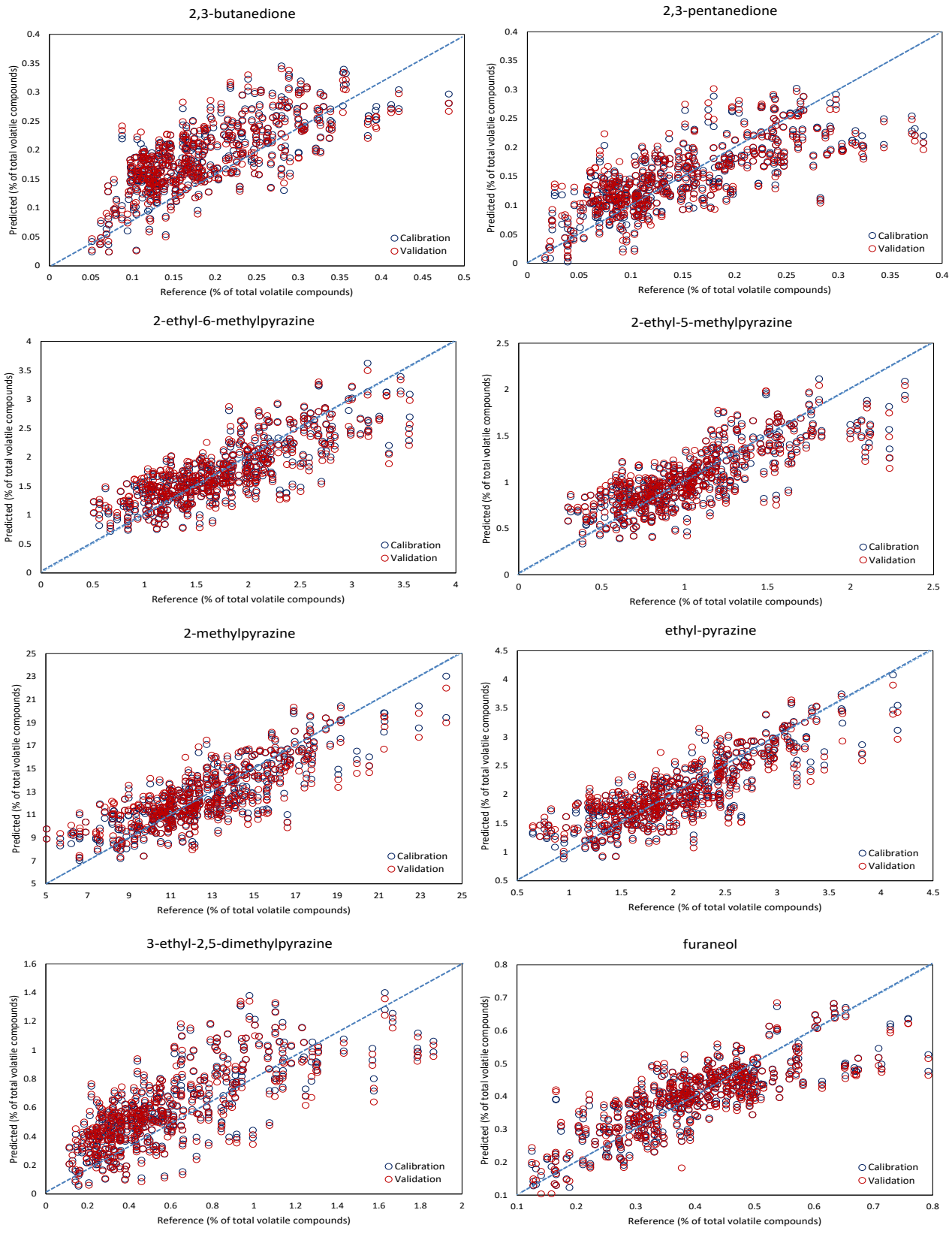


Figure 9.7. Predicted versus reference concentration of single volatile compounds (odour impact compounds) from single green coffee beans using HSI, and PLS2 as the chemometric method. Compounds are expressed as % of each compound to the total GC-MS peak areas (n~490).

Figure 9.7 shows some of the best prediction models for individual volatile compounds from green coffee beans (please refer to the Appendix for additional figures related to the PLS regression coefficients for several models reported in this chapter; Figures A.10-A.14). As expected, pyrazines had very similar plots, as they share the most important wavelengths. For furfural and furaneol, despite the obvious difference in absolute value, these two compounds have many wavelengths in common.

It is apparent that the concentration of volatile compounds seemed not to be a factor influencing the HSI predictions. In fact, 3-ethyl-2,5-dimethylpyrazine and furaneol are found at very low concentrations compared to 2-methylpyrazine or furfural, and a similar good prediction was obtained despite their low concentration. 2,3-Butanedione and 2,3-pentanedione are found at even lower concentrations, but they were successfully predicted in green coffee beans. This result suggests that other factors are likely to be involved. In roasted coffee beans, it could depend on the chemical structure or the predicted volatile(s), while for green coffee it is hypothesized to depend upon the chemical precursors of volatile compounds, i.e. whether they directly originate from a precursor found in the green coffee or whether they are interdependent upon many precursors, as well as influenced by intermediates formed during roasting.

The prediction of aroma generation from the green coffee HSI data is likely to be possible from the detection of coffee constituents that are flavour precursors. In particular, sugar degradation in caramelisation gives furaneol, while phenomena such as the Maillard reaction and Strecker degradation, also involve amino acids, forming diketones, aldehydes, pyrazines, 2-furfurylthiol and other compounds. Trigonelline degradation through pyrolysis gives pyridine and other derivatives, while chlorogenic acid degradation can result in the generation of a series of volatile and non-volatile compounds including vanillin and guaiacol.

The different generation pathway for different classes of volatile compounds, or some specific aroma compounds, can explain the resulting different performances herein obtained using HSI. For example, it is likely that pyrazines and aldehydes were better predicted because they are generated from sugar and amino acid degradation, which are abundant compounds in green coffee, and detectable in the NIR region. Other compounds might be predicted with lower

performance as they originate from precursors found at low concentrations, e.g. below 0.1%, or are generated from more complex reactions.

Coffee constituents found at high concentrations in the green beans can potentially be flavour precursors, e.g. sugars, proteins, trigonelline, chlorogenic acids and lipids, thus their presence might be the reason for the promising good prediction of volatile compound generation based on HSI spectral information. A scheme of the volatile compounds found in roasted coffee bean and their origin, i.e. precursors in the green coffee, is reported in Figure 9.8.

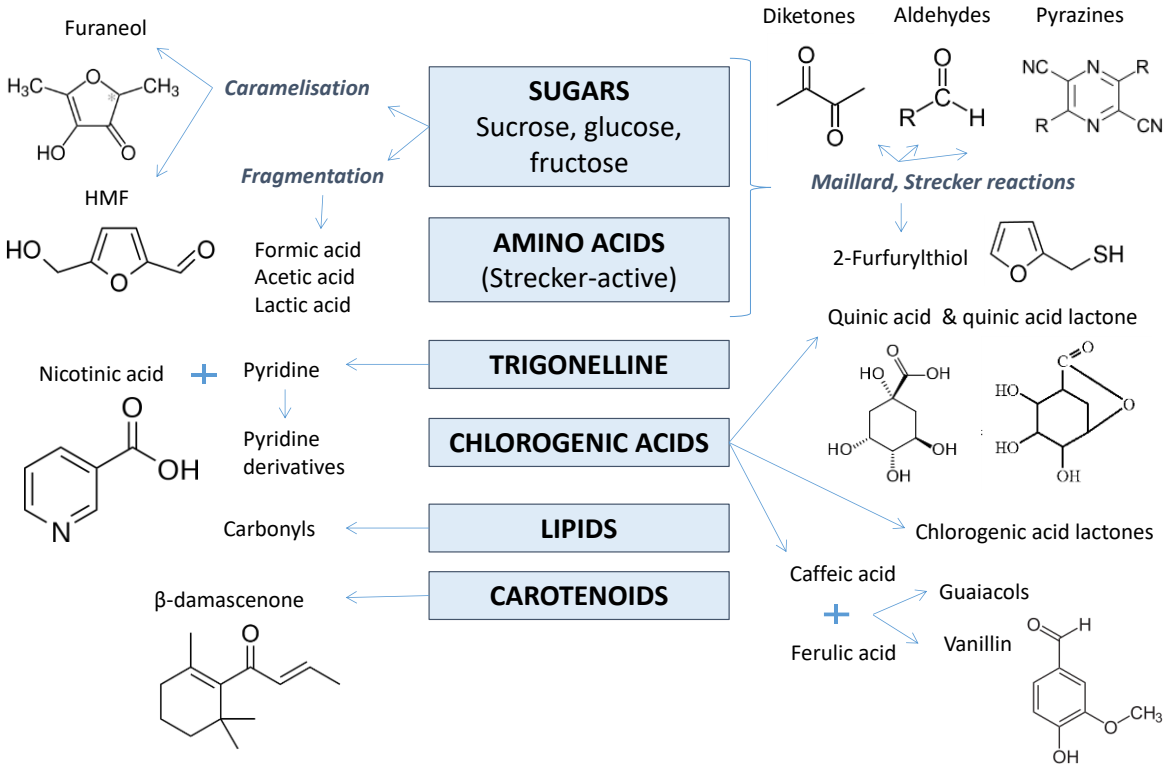


Figure 9.8. Precursors of coffee aroma, modified from Yeretzian et al. (2002).

9.3.4. Roasted coffee: prediction of chemical groups and aroma impact

Grouping the volatile compounds according to their chemical groups is a valid strategy to reduce the number of responses in the statistical model. It is also useful to build a more comprehensive model that has more applicative potential, as it can synthetically describe the aroma quality of coffee beans using only few parameters. A first reduction was made by grouping the compounds according to their chemical class, while a second approach was to group them by taking the odour descriptors of each aroma compound. The plots of explained variance in relation to the number

Latent Variables (LVs) for the two models are shown in Figure 9.9. Table 9.6 reports the results for prediction of chemical groups of volatile compounds in single coffee beans scanned by HSI as roasted.

Table 9.6. Results of PLS2 prediction of volatile compounds as chemical groups, using different spectral pre-treatment, on HSI spectra acquired on single roasted coffee beans.

Spectra pre-treatment	LV	Parameter	Calibration		Validation		RPD
			R^2	RMSE	R^2	RMSE	
Log(1/R)	17	**Aldehydes**	**0.717**	**2.83**	**0.633**	**3.22**	**1.61**
		Pyrazines	**0.774**	**4.28**	**0.662**	**5.30**	**1.56**
		Ketones	0.562	0.59	0.452	0.66	1.32
		Phenols	0.509	0.30	0.381	0.34	1.37
		Acids	0.375	3.83	0.208	4.36	1.10
		Heterocyclic N	0.385	2.58	0.221	2.93	1.26
		Aldehydes/Pyrazines	**0.693**	**0.19**	**0.596**	**0.22**	**1.50**
SNV	17	**Aldehydes**	**0.793**	**2.33**	**0.701**	**2.77**	**1.87**
		Pyrazines	**0.807**	**3.61**	**0.726**	**4.39**	**1.88**
		Ketones	0.600	0.55	0.497	0.60	1.45
		Phenols	0.544	0.26	0.439	0.29	1.61
		Acids	0.368	3.73	0.208	4.24	1.13
		Heterocyclic N	0.396	2.14	0.198	2.49	1.48
		Aldehydes/Pyrazines	**0.750**	**0.17**	**0.666**	**0.19**	**1.74**
2nd derivative	11	**Aldehydes**	**0.776**	**2.42**	**0.676**	**2.85**	**1.82**
		Pyrazines	**0.808**	**3.65**	**0.699**	**4.65**	**1.78**
		Ketones	0.556	0.57	0.433	0.64	1.37
		Phenols	**0.589**	**0.23**	**0.542**	**0.25**	**1.87**
		Acids	0.361	3.69	0.182	4.26	1.12
		Heterocyclic N	0.376	1.79	0.263	1.95	1.89
		Aldehydes/Pyrazines	**0.769**	**0.16**	**0.669**	**0.19**	**1.74**

The 2nd derivative and SNV treatments gave similar results, with the former resulting in slightly better prediction of phenols and heterocyclic nitrogen compounds. Although the prediction accuracy being lower than SNV treatment in some cases, it uses a fewer lower number of LVs, and thus it might be preferred. Aldehydes and pyrazines were predicted with the highest accuracy among all chemical groups, showing R^2 values of approximately 0.8 for calibration and 0.7 for cross-validation set. The ratio between aldehydes and pyrazines groups was also successfully predicted, with RPD value of 1.7. The RPD values for aldehydes and pyrazines was 1.7-1.8, thus indicating sufficient accuracy for screening purposes.

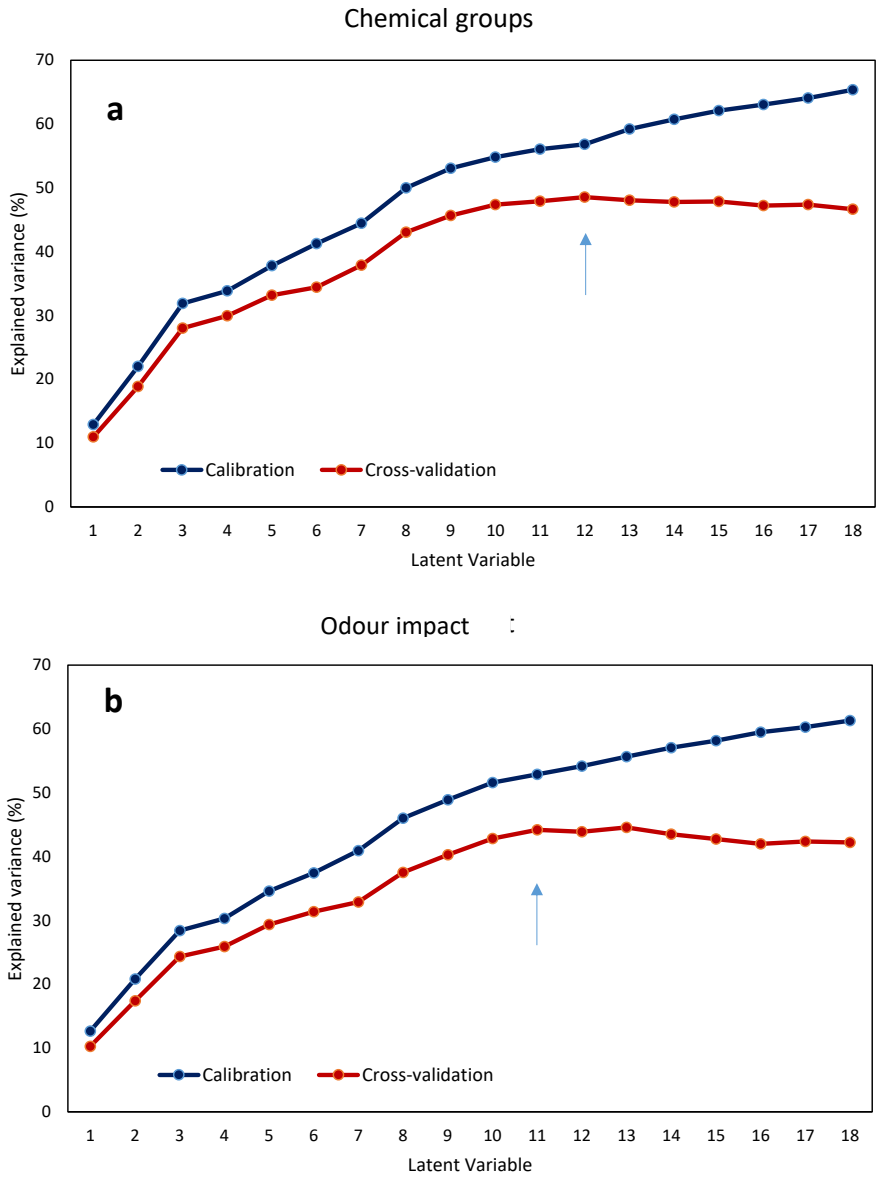


Figure 9.9. Explained variance plots depending on the number of Latent Variables, for PLS2 regression models to predict volatile compounds as (**a**) chemical groups or (**b**) odour impact in terms of sensory descriptors.

The RPD value for chemical groups was above 1.5 for pyrazines, ketones and the ratio aldehydes/pyrazines. Previous authors suggested that RPD values between 1.4 and 2 could be considered as fairly reliable, while for proper quantification, values above 2 are desired (Bellon-Maurel, Fernandez-Ahumada, Palagos, Roger, & McBratney, 2010; Davey et al., 2009; Ncama et al., 2017). The predicted versus reference plots for aldehydes, pyrazines, phenols and aldehydes/pyrazines are shown in Figure 9.10.

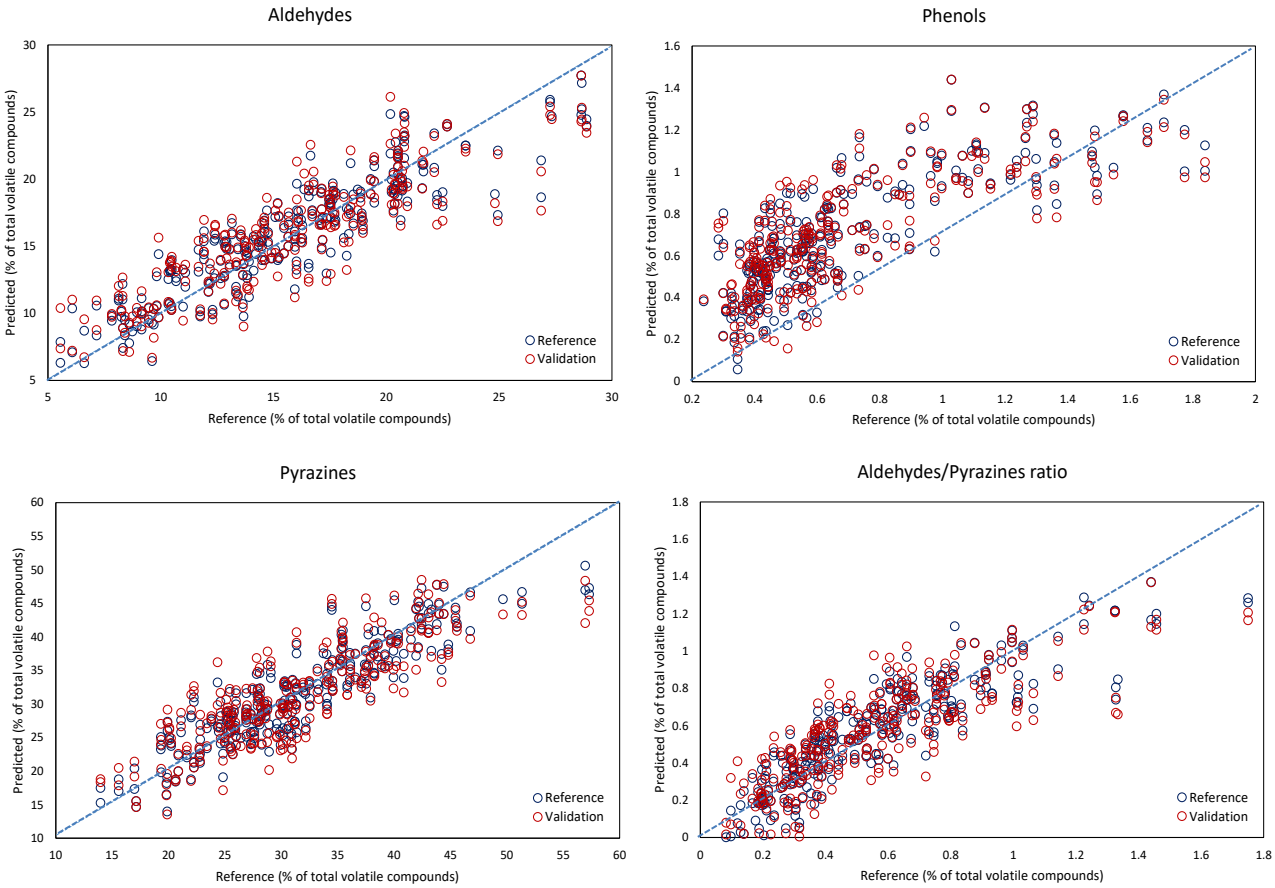


Figure 9.10. Predicted versus reference plots of some chemical groups predicted by HSI on single roasted coffee beans. Pre-treatment: 2nd derivative (LV-11).

A similar approach for data reduction was used by grouping the volatile compounds into "sensory groups", according to the main odour descriptor for each compound. In this way, an indication of the possible sensory impact in terms of expected odour is obtained.

The performance of the prediction models is reported in Table 9.7. The application of spectral pre-treatment gave improvement for all the models, except "fruity" and "musty", where very little improvement was obtained. The descriptors predicted with the highest accuracy were those of "nutty", "sweet" and "spicy", which had calibration R^2 values above 0.7, and even 0.799 for nutty. The cross-validation R^2 was 0.717 for nutty, and 0.63-0.64 for sweet and spicy. The poorest performance was obtained for fruity, for which the RPD value was below 1.0. Generally, lower performances were obtained for the prediction of odour impact in roasted coffee beans, compared to the use of chemical groups. The RPD values for sweet and spicy suggest the model applicability for screening purposes (1.6 and 1.8, respectively). As observed in the case of chemical groups, the

2nd derivative pre-treatment gave similar performance to SNV, while it made use of 11 LVs instead of 16. It should be noted that large number of LVs were used, however these models are not in the overfitting region, as verified by plotting the prediction error versus the number of LV (Fig. A.9). In addition, the model using the lowest number of LVs was preferentially used, i.e. the one using the 2nd derivative treatment in this case. The predicted versus reference plots for nutty, roasted, sweet and spicy are shown in Figure 9.11.

Table 9.7. Results of PLS2 prediction of volatile compounds as odour impact in terms of sensory odour descriptors, using different spectral pre-treatment, by HSI acquired on single roasted coffee beans.

Spectra pre-treatment	LV	Parameter	Calibration		Validation		RPD
			R^2	RMSE	R^2	RMSE	
Log(1/R)	19	Fruity	0.410	0.426	0.212	0.496	0.90
		Nutty	**0.725**	**2.949**	**0.573**	**3.690**	**1.47**
		Roasted	0.549	2.168	0.368	2.583	1.23
		Sweet	**0.721**	**2.200**	**0.589**	**2.692**	**1.50**
		Sour	0.390	3.523	0.216	4.020	0.95
		Spicy	**0.724**	**1.069**	**0.588**	**1.314**	**1.40**
		Musty	0.647	2.698	0.513	3.192	0.68
		Positive/Negative	0.504	0.241	0.335	0.280	1.05
SNV	16	Fruity	0.380	0.350	0.206	0.390	1.15
		Nutty	**0.799**	**2.432**	**0.707**	**2.998**	**1.81**
		Roasted	0.604	2.000	0.448	2.245	1.42
		Sweet	**0.757**	**1.983**	**0.648**	**2.334**	**1.73**
		Sour	0.28	3.240	0.13	3.650	1.05
		Spicy	**0.762**	**0.895**	**0.686**	**1.042**	**1.76**
		Musty	0.466	1.590	0.329	1.783	1.22
		Positive/Negative	0.467	0.214	0.323	0.246	1.19
2nd derivative	11	Fruity	0.268	0.458	0.091	0.509	0.88
		Nutty	**0.812**	**2.433**	**0.717**	**3.060**	**1.78**
		Roasted	0.575	2.077	0.426	2.433	1.31
		Sweet	**0.743**	**2.033**	**0.632**	**2.374**	**1.70**
		Sour	0.335	3.250	0.130	3.768	1.02
		Spicy	**0.729**	**0.984**	**0.637**	**1.155**	**1.59**
		Musty	0.358	1.900	0.225	2.084	1.05
		Positive/Negative	0.490	0.220	0.319	0.259	1.14

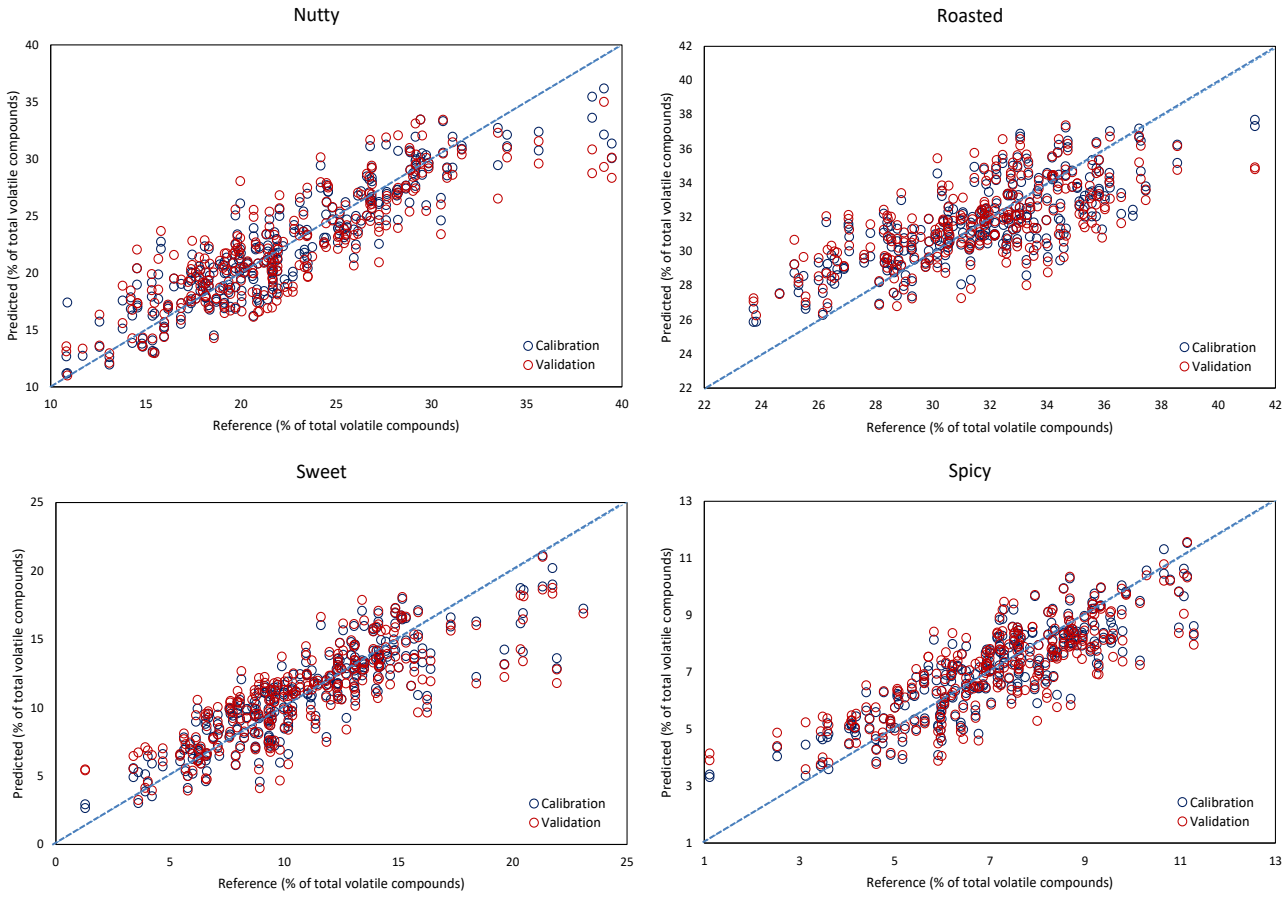


Figure 9.11. Predicted versus reference plots of some odour predictions by HSI on single roasted coffee beans. The spectral pre-treatment applied was 2nd derivative (LV-11).

9.3.5. Green coffee: prediction of chemical groups and odour impact

The prediction of single volatile compounds, despite effective for some compounds, would not be of great applicability when the aim is to obtain information on the complete aroma profile. Thus, a reduction strategy was applied on the response variables (volatile compounds) to group them in order to test new prediction models able to describe single coffee bean aroma in a more comprehensive and synthetic manner.

Table 9.8 reports the performance of HSI models for volatile compounds grouped by chemical classes, predicted from green coffee beans. Slightly poorer predictions were obtained compared to roasted coffee. The SNV and 2nd derivative pre-treatment gave similar prediction performance, with the latter treatment resulting in slightly higher RPD values. The best prediction was obtained for pyrazines, with cross-validation R^2=0.696. Aldehydes, ketones and the ratio

aldehyde/pyrazines had cross-validation R^2 values between 0.55 and 0.62, still indicating good prediction.

In terms of RPD value, the performance of green coffee prediction was lower than the roasted coffee, with the exception for pyrazines, acids and the ratio aldehydes/pyrazines. For these three responses, the RPD values were generally comparable to the prediction from roasted coffee. In contrast, aldehyde, phenol and heterocyclic nitrogen compound predictions were dramatically lower, with poor predictions obtained especially for phenols and acids (RPD of ~0.8). Ketones and aldehydes/pyrazines had RPD values above 1.6, while pyrazines had RPD=1.8. These results suggest that successful prediction of these three parameters, which can be predicted with enough accuracy for screening purposes. Some of the best models are presented in Figure 9.12.

Table 9.8. Results of PLS2 prediction of volatile compounds as chemical groups, using different spectral pre-treatment, on HSI spectra acquired on single green coffee beans.

Spectra pre-treatment	LV	Parameter	Calibration		Validation		RPD
			R^2	RMSE	R^2	RMSE	
Log(1/R)	12	Aldehydes	0.563	3.689	0.511	3.922	1.32
		Pyrazines	**0.669**	**5.142**	**0.617**	**5.533**	1.49
		Ketones	0.581	0.539	0.533	0.570	1.53
		Phenols	0.156	0.650	0.071	0.686	0.68
		Acids	0.247	4.081	0.176	4.289	1.12
		Heterocyclic N	0.155	5.492	0.065	5.809	0.63
		Aldehydes/ Pyrazines (ratio)	0.597	0.219	0.535	0.236	1.40
SNV	11	**Aldehydes**	**0.597**	**3.503**	**0.553**	**3.706**	1.40
		Pyrazines	**0.731**	**4.435**	**0.696**	**4.733**	1.75
		Ketones	**0.598**	**0.521**	**0.566**	**0.544**	1.60
		Phenols	0.134	0.632	0.065	0.658	0.71
		Acids	0.241	4.027	0.186	4.185	1.14
		Heterocyclic N	0.169	5.193	0.094	5.433	0.68
		Aldehydes/ Pyrazines (ratio)	**0.666**	**0.196**	**0.623**	**0.209**	1.58
2nd derivative	11	**Aldehydes**	**0.606**	**3.300**	**0.536**	**3.550**	1.46
		Pyrazines	**0.774**	**3.985**	**0.687**	**4.558**	1.81
		Ketones	**0.614**	**0.500**	**0.565**	**0.530**	1.64
		Phenols	0.212	0.562	0.124	0.600	0.78
		Acids	0.258	3.827	0.177	4.033	1.19
		Heterocyclic N	0.189	4.461	0.102	4.742	0.78
		Aldehydes/ Pyrazines (ratio)	**0.687**	**0.18**	**0.605**	**0.199**	1.66

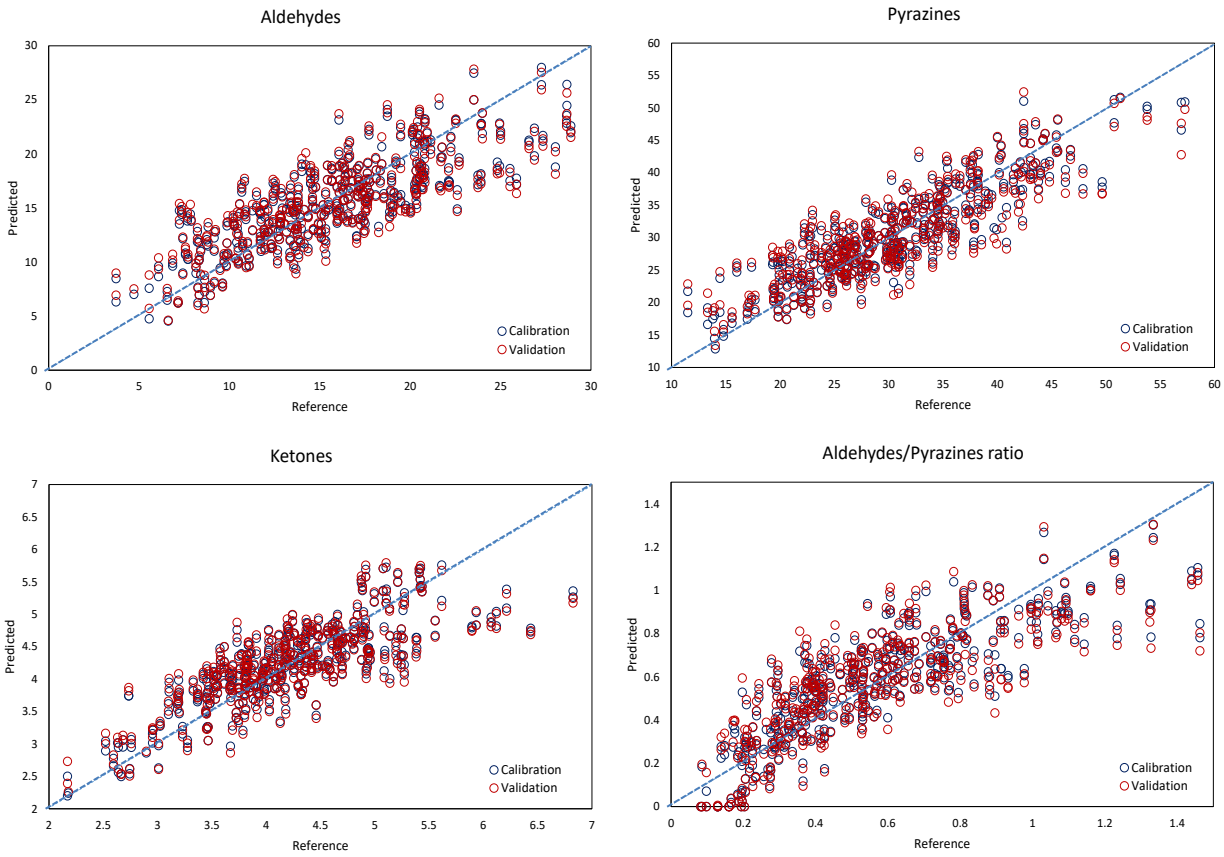


Figure 9.12. HSI prediction of chemical groups of volatile compounds (as a percentage of total volatile compounds) generated in single green coffee beans. Predicted versus references value plots of the best models (2nd derivative spectra pre-treatment).

HSI prediction of the odour impact is reported in Table 9.9. Good prediction of the attributes "nutty" and "sweet" was obtained even using the absorbance data without spectral pre-treatment. However, spectral pre-treatments gave predictive improvement, especially the 2nd derivative treatment. The cross-validation R^2 values obtained for nutty and sweet were 0.65 and 0.60, respectively. Other attributes were predicted with limited performance, while the other acceptable models are for "roasted" and "spicy" prediction, which had cross-validation R^2 values slightly above 0.4. The RPD values for nutty and sweet were 1.76 and 1.58, respectively, indicating good prediction ability.

Compared to the roasted models, the sensory prediction from green coffee was generally poorer. However, the prediction was almost comparable to the one with roasted coffee for certain attributes, especially for "nutty" prediction. The plots of predicted versus reference aroma attributes are shown in Figure 9.13.

Table 9.9. Results of PLS2 prediction of volatile compounds as odour impact in terms of sensory odour descriptors, using different spectral pre-treatment, by HSI acquired on single green coffee beans.

Spectra pre-treatment	LV	Parameter	Calibration		Validation		RPD
			R^2	RMSE	R^2	RMSE	
Log(1/R)	16	Fruity	0.230	0.474	0.162	0.497	0.90
		Nutty	**0.710**	**3.014**	**0.668**	**3.230**	**1.68**
		Roasted	0.459	2.452	0.392	2.614	1.22
		Sweet	**0.630**	**2.675**	**0.582**	**2.850**	**1.41**
		Sour	0.291	4.305	0.184	4.628	0.83
		Spicy	0.459	1.536	0.394	1.630	1.13
		Musty	0.233	5.185	0.129	5.545	0.39
		Positive/Negative	0.365	0.296	0.267	0.318	0.92
SNV	10	Fruity	0.218	0.448	0.172	0.463	0.97
		Nutty	**0.638**	**3.251**	**0.597**	**3.424**	**1.59**
		Roasted	0.441	2.397	0.395	2.510	1.27
		Sweet	**0.591**	**2.760**	**0.549**	**2.923**	**1.38**
		Sour	0.204	4.218	0.136	4.395	0.87
		Spicy	0.427	1.506	0.367	1.586	1.16
		Musty	0.179	4.713	0.121	4.911	0.44
		Positive/Negative	0.292	0.293	0.230	0.306	0.96
2^{nd} derivative	11	Fruity	0.289	0.424	0.222	0.444	1.01
		Nutty	**0.743**	**2.687**	**0.645**	**3.086**	**1.76**
		Roasted	0.537	2.179	0.461	2.336	1.36
		Sweet	**0.673**	**2.317**	**0.605**	**2.547**	**1.58**
		Sour	0.285	3.435	0.183	3.664	1.05
		Spicy	0.522	1.248	0.413	1.353	1.36
		Musty	0.213	3.291	0.140	3.476	0.63
		Positive/Negative	0.409	0.246	0.299	0.265	1.11

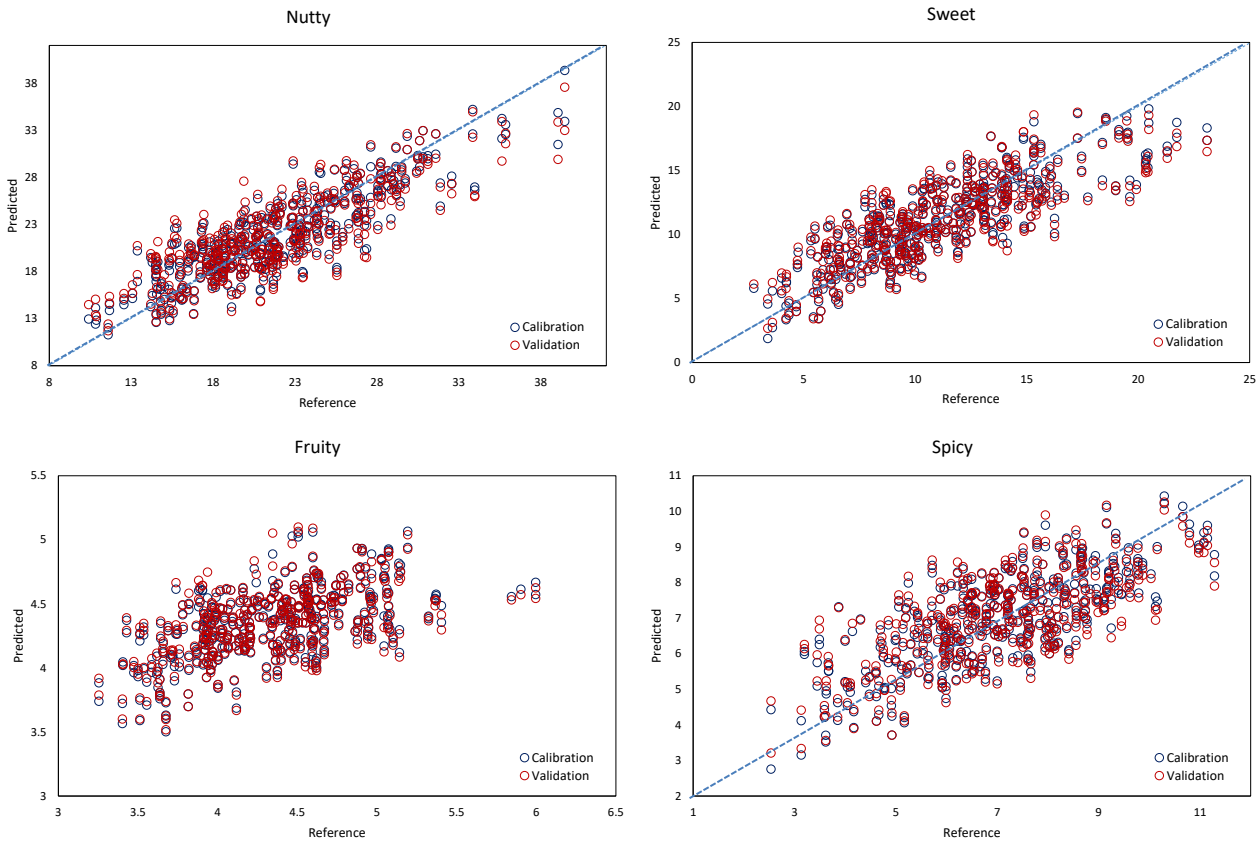


Figure 9.13. Prediction of odour impact of volatile compounds generated in single green coffee beans by HSI. Predicted versus references value plots of the best models (2nd derivative pre-treatment).

9.3.6. Application of calibrations (chemical images)

The PLS calibrations built for the prediction of aroma generation potential can be applied on new hypercubes, allowing visualisation of the volatile compounds that can be potentially generated from the green coffee beans, or estimating the amount of volatiles in the roasted beans. Figure 9.14 shows the application of some of the best calibrations on green coffee beans, with indication of the predicted values for each bean. In the example shown, pyrazines were the most abundant chemical groups among the three predicted, with relatively consistent values of 30-50% stability in 8 of the 10 beans. Two beans had much lower pyrazine values, of 8-16% of total volatiles. These beans were also those showing high predicted aldehyde concentration. The variation of predicted aldehydes content was large, with the lowest values of 0.4-1.9 and the highest ones being 18.3-14.6%.

The calibrations for "nutty" and "sweet" are also shown, the latter being correlated with the observations for aldehydes, i.e. beans with high sweet prediction gave also the highest predicted aldehydes. The prediction of nutty was similar to pyrazines, as the bean with dramatically lower nutty prediction also had the lowest value for pyrazines. However, in this case two beans with high nutty odour impact had average values of pyrazines. This could potentially be explained by the fact that not just pyrazines exert sensory notes described with "nutty".

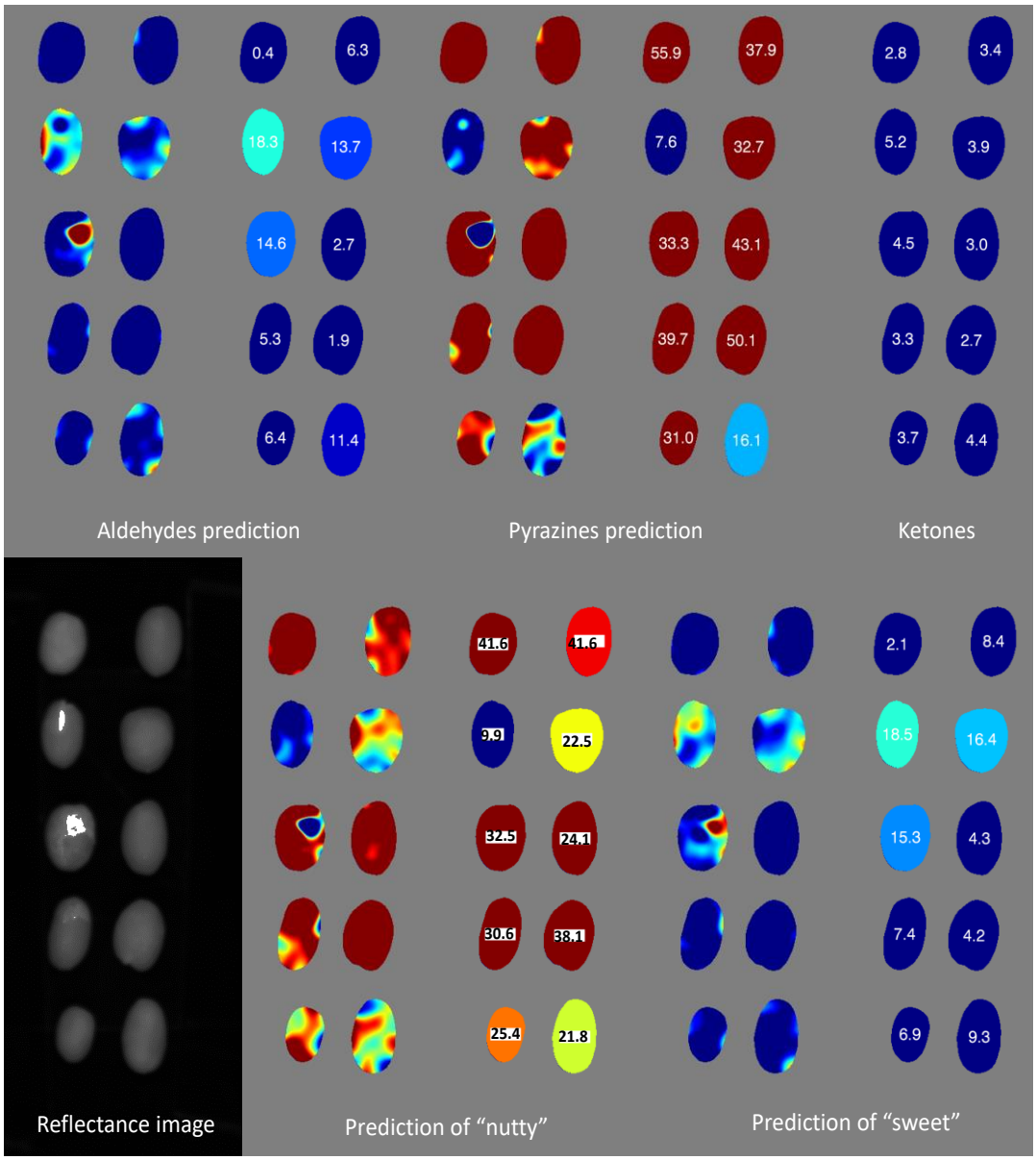


Figure 9.14. Prediction of odour impact from green coffee beans. Example on a batch of Java Lington Arabica coffee from Indonesia. Upper pictures: prediction of chemical classes as a percentage of total volatiles. Lower pictures: prediction of expected odour impact after roasting. Numbers represent the predicted % of volatiles belonging to each chemical class, or described with "nutty" or "sweet" characteristics, of the total peak areas of volatiles.

9.3.7. Manual sorting of coffee batches: GC-MS

A validation of the HSI approach to predict volatile chemical groups and aroma impact was carried by sorting sub-fractions of coffee beans, and analysing their volatile composition after batch roasting. The analysis was done by SPME-GC-MS from the beans roasted together and treated similarly to those used for the calibration. An experiment was carried out by scanning green coffee, while a second one was performed by scanning roasted beans.

Roasted beans.

The roasted beans were scanned by HSI, and ~10% of the bean with the predicted higher and lower values of pyrazine concentration were manually sorted, to be analysed in triplicate as bulk by GC-MS in comparison to the remaining fraction ("batch"). As shown in Figure 9.15**,** the application of pyrazine calibration was effective in obtaining a batch with significantly ($p<0.05$) higher pyrazine content, while the low pyrazine group did not show a significant difference compared to the unsorted batch. A statistically significant higher pyrazine concentration was obtained in the High Pyrazine (HP) fraction, and it was lower in the LP fraction, but in this case a statistically significance was not reached, compared to the control. From the same hypercubes, it was possible to predict several attributed, thus the odour impact was also predicted. The HP fraction also had significantly lower concentration of ketones, but slightly higher predicted "fruitiness". In terms of predicted sensory "nuttiness", the two fractions showed some trend, but they were not statistically significant from the unsorted batch. In addition, the pyrazine content and the predicted nuttiness were correlated. It was also noted that heterocyclic nitrogen compounds has a similar trend to pyrazines. The predicted sensory note of "nuttiness" measured from the volatile compounds was significantly higher in the "high pyrazine" fraction and lower in the "low pyrazine" fraction, which demonstrates the effectiveness of the proposed approach. As pyrazines and "nutty" sensory note are positively correlated, the results obtained when the calibration for "nutty" applied were similar to those obtained for pyrazines.

Figure 9.16 shows the results of volatile compounds grouped according to the expected sensory impact, in these sorted fractions of roasted beans. Only the batch sorted by applying the pyrazine

calibration resulted in significantly higher scores of "sour", while no statistically significant difference was obtained for the "roasted" character.

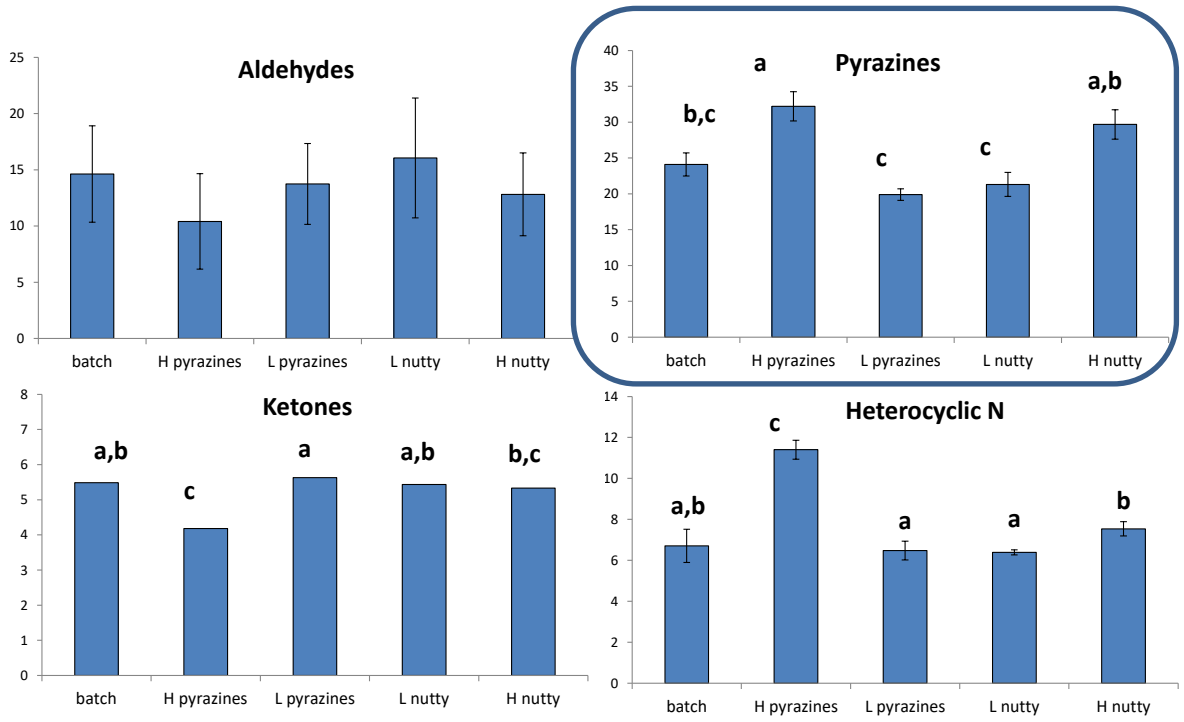


Figure 9.15. Concentration of volatile compounds grouped according to their chemical groups (pyrazines, %), in roasted single coffee beans analysed by SPME-GC-MS and manually sorted after roasting, by applying HSI calibrations for predicted pyrazine content or predicted sensory "nutty" character. L=low; H=high. Different letters indicate a statistical significant difference among the samples by ANOVA, with $p<0.05$. Aldehydes did not show any statistical significant difference. The top and bottom 10% of the beans were selected to obtain the "high pyrazine" and "low pyrazine" fractions, while "batch" represents the remaining fraction. "Batch" indicates the remaining beans after sorting the High and Low fractions.

Green beans.

A similar sorting experiment was carried out by scanning green beans. Figure 9.17 shows the results using the calibration for yield of pyrazines after roasting. The pyrazine content analysed by the reference method in the sorted high-pyrazine fraction was significantly higher than the batch (unsorted beans). The predicted low pyrazine fraction had a slightly lower actual pyrazine concentration than the remaining batch but it did not show a statistical significance. A similar trend was observed for heterocyclic nitrogen compounds. On the contrary, alcohols in both sorted fractions were significantly higher than the batch, while no statistically significant difference was observed for aldehydes in these fractions.

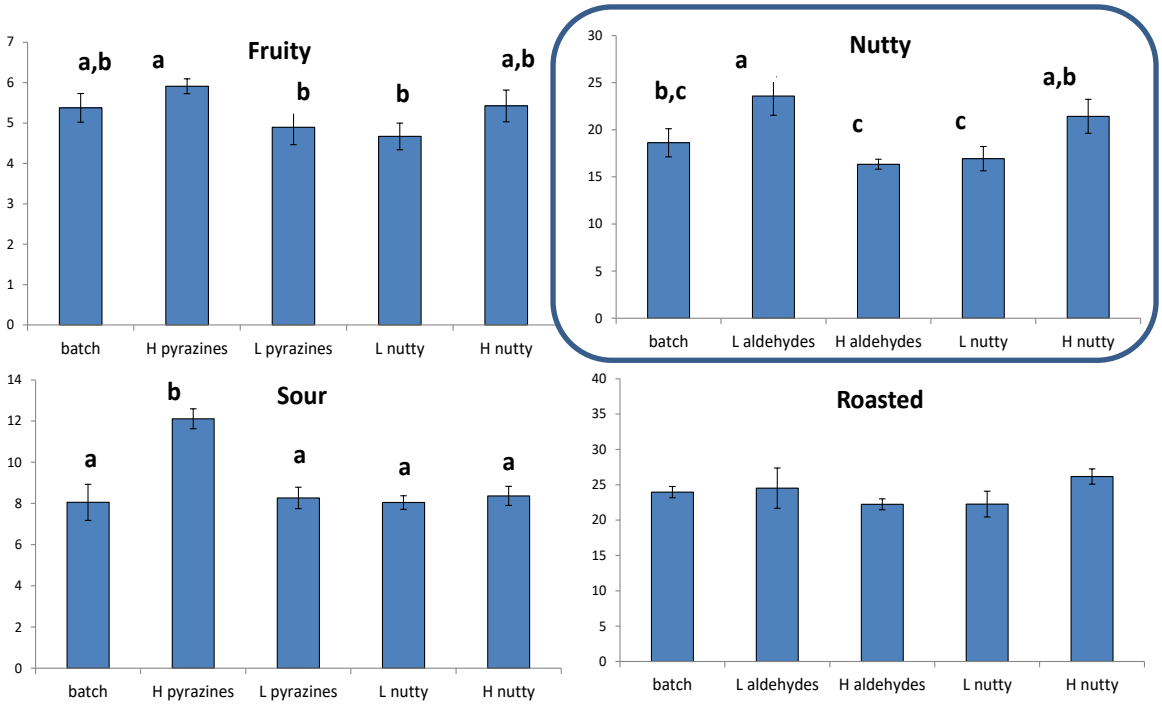


Figure 9.16. Predicted sensory impact of single roasted coffee beans, obtained through the analysis of volatile compounds by SPME-GC-MS, and by clustering them according to their sensory descriptors (% of total GC peak areas). The different samples were obtained by manually sorting single beans after roasting, after the application of HSI calibrations to predict pyrazine content or "nutty" character. L=low; H=high. Different letters indicate a statistical significant difference among the samples by ANOVA, with $p<0.05$. "Roasted" did not show any statistical significant difference.

As expected, the sorted fractions showed also differences in terms of predicted odour impact, with the high-pyrazine fraction also showing higher scores for "nutty" and "roasted". The PLS regression coefficients for the odour predictions are reported in the appendix (Figures A.10-A.14). From the model, a lack of strong absorbing bands was observed, in contrast to other compounds found at higher concentrations or with a clear absorbance plot, e.g. water or lipids. Generally, the four models built on odour prediction had stronger absorbances at similar spectral bands, with some differences mostly observed between nutty/roasted and sweet/spicy, which were in opposite directions (positive/negative). However, no clear predominance of some specific wavelengths was obtained, due to the complexity of the parameter evaluated.

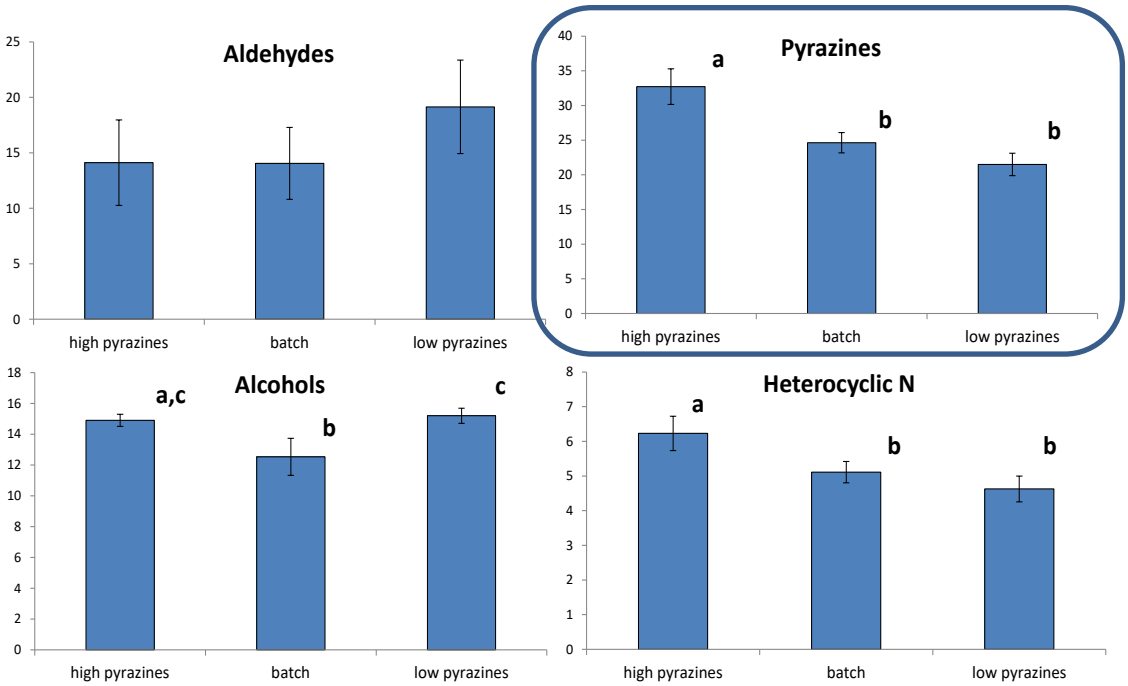


Figure 9.17. Results of manual sorting of a batch of green Arabica coffee beans according to the predicted pyrazine concentration in the roasted coffee using a HSI calibration. Different letters indicate statistical significant differences among the samples by ANOVA ($p<0.05$).

9.3.8. Manual sorting of green coffee batches: sensory analysis

In addition to the GC-MS analysis of volatile compounds, a sorting experiment was carried out by applying the HSI predictions on green coffee beans, then roasting them and analysing them by sensory analysis. Similarly to the previous experiment, ~10% of the coffee beans were manually sorted to select the highest/lowest predicted beans, as shown in Figure 9.18. The result of the triangle test is shown in Table 9.10. For Arabica, the number of correct responses from the 30 assessors was 16, which was above the number required to obtain a statistically significant effect at $\alpha=0.05$ (15 correct responses from panellists; BS EN ISO 4120:2007). For robusta coffee, 17 correct responses were obtained, giving a statistical significance difference at $\alpha=0.01$.

Thus, it was concluded that the two fractions of roasted and ground coffee had perceivable odour differences in both coffee species (Table 9.10). These results were obtained on untrained assessors, i.e. individuals with no specific training on coffee flavour or no expertise on coffee odour evaluation, thus this is an evidence that fractionation of single green coffee beans using HSI is effective in giving roasted and ground coffee showing different odour profiles.

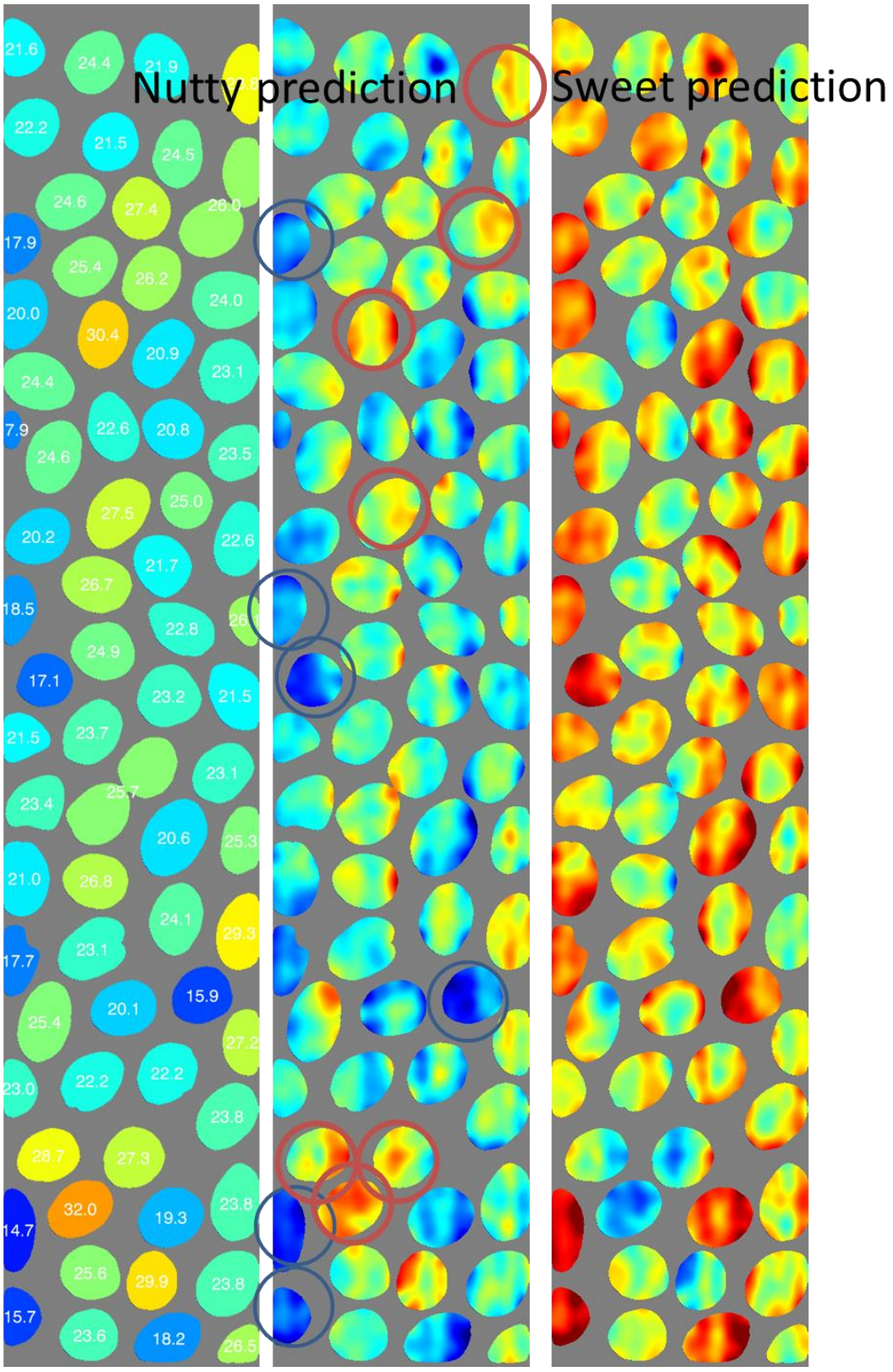


Figure 9.18. Example of green coffee bean sorting according to the predicted sensory characteristics of “nutty” and “sweet” after roasting. The first left and central columns show the nutty prediction as single-bean average and single-pixel, respectively. The right column shows the single-pixel prediction of “sweet” odour. The blue and red circles indicate the beans selected for the “low” and “high” fractions for nuttiness, respectively.

Table 9.10. Result of discriminant sensory test (triangle test) for roasted and ground coffee obtained by HSI manual sorting according to the predicted sensory impact. Number of assessors = 30. Two independent experiments were carried out for one batch of Arabica (origin: Mexico) and one batch of Robusta (origin: Vietnam).

Sample	Correct	Incorrect	Significance (p)
Arabica	16	14	<0.05
Robusta	17	13	<0.01

In addition to identifying the different sample, assessors were asked "Why is it different" and "Which one do you prefer and why". For the Arabica coffee batch, the low nutty/high sweet fraction was mostly described as "lighter", "sweeter", "less intense", "less bitter"; in contrast, the high nutty/low sweet fraction was "stronger", "more intense", "more toasted", "more nutty", "burnt", "more pleasant roasted". In terms of preferences, of the 16 assessors that correctly identified the different sample, 12 preferred the "high nutty" sample, thus representing 75% of the assessors. The panellists who preferred the less nutty sample, justified their choice because they desire a milder, sweeter and "less strong" or "less burnt" coffee.

For Robusta coffee, the low nutty/high sweet fraction was described as "milder", "more smoky", "less floral/fruity", "less intense", "weaker", "less bitter", "less oaty smell", "sweeter"; the high nutty fraction was described as "stronger", "more intense", "bitter", "sharp smelling", "deeper/earther". Assessors' preference was slightly higher for the high nutty fraction, with 8 assessors expressing their preference, while 6 assessors preferred the low nutty sample. The remaining assessors did not express any preference, and these results are just related to assessors who correctly identify the different sample.

These results indicate that sorting green coffee beans according to the HSI calibrations is effective in providing two sub-fractions with distinctive odour characteristics, and that the predicted descriptors were also appreciated by untrained panellists, even using terms that were applied in the construction of the predictive models ("roasted"/"smoky", "sweet"/"fruity", etc.), in the same direction as the basis of sorting. In terms of general preference, these results indicate that panellists generally tend toward a more roasted/nutty coffee, where the distinctive notes are stronger. This might be due to the consumer habit of associating coffee with roasted/burnt/nutty odour notes. However, an appreciable number of panellists did express their preference toward

the sweeter/fruity coffees, which might be due to either their habit of "milder coffee" consumption, or due to an actual knowledge of the Arabica coffee odour notes, described as sweet, floral, fruity, etc. However, in conclusion, consumer preference cannot be generalised and this result could in turn be beneficial for the industry, which can take advantage of the market segmentation to reach consumer expectations in terms of final coffee aroma.

9.3.9. Discussion

The results shown in this chapter demonstrate that it is possible to predict the concentration of volatile compounds from single coffee beans by HSI. The models built to predict individual volatile compounds (from either roasted beans or green beans) indicates that some compounds are predicted with sufficient accuracy for screening purposes, while others are poorly predicted. Differences in the prediction ability have been noted even for compounds with very similar chemical structure. In contrast, the relative concentration by itself was not shown to be a critical factor in terms of prediction ability, e.g. some compounds found at high concentrations were poorly predicted, while compounds found at much lower concentration were better predicted. This is explained not only by the chemical structure of the molecules, but it is more likely linked to the biochemical origin of these volatile compounds. Generally, compounds belonging to the pyrazine class showed better prediction. Pyrazines are heterocyclic aromatic compounds that are generally described as nutty, roasted, peanut, coffee-like and earthy, and many pyrazines have been described as potent odorants in roasted coffee (Czerny & Grosch, 2000; Grosch, 2001b; Scheidig et al., 2007).

A lower prediction ability of roast properties by HSI measurement of green coffee beans compared to the roasted beans was expected. However, for certain compounds, similar or even better prediction was achieved, e.g. acetaldehyde, 2,3-butanedione, 2,3-pentanedione and furaneol. Acetaldehyde is naturally occurring in coffee due to plant metabolism, while the presence of 2,3-butanedione and 2,3-pentanedione in coffee is thought to originate from the roasting. Several mechanisms have been proposed in the literature to explain the generation of α-diketones, such as 2,3-butanedione and 2,3-pentanedione, but no clear explanation is accepted, however it is

known that their formation pathway involves glucose, or an intermediate product of sucrose degradation (Baggenstoss et al., 2008).

Due to the common origin of several compounds from a limited number of precursors, and the strong correlations observed among volatiles, it is not surprising that the PLS regression loading plots showed similar patterns for many compounds. This fact might explain the better predictions obtained by PLSR models built by grouping compounds belonging to the same chemical class (Sections 1.1.4 and 1.1.5).

The models built on roasted coffee beans for prediction of odour impact showed important absorbance wavelengths at 1043, 1982, ~1416-1460, ~1670-1680, 1956-1975, 2276, 2257 and 2357 nm (Figure A.12). Some of these wavelengths were also important for the pyrazine prediction model, e.g. 1416 nm, 1862 nm and 2276 nm. The band at 1416 nm was also one of the most important wavelengths for ketone prediction, in addition to 1435, 1680, and 2088 nm. Absorption at 1416 nm is attributed to the 1st overtone of O-H and N-H, and has been previously reported to be an important absorbance wavelength for the prediction of "bitterness" assessed by sensory analysis in coffee (Ribeiro et al., 2011). Similarly, absorptions around 1128 and at 2050 nm were linked to the perceived "flavour", while ~2270 nm was linked to "acidity" and "body". Absorption wavelengths previously associated with "flavour" were those at 1975 and ~1435, while those at 2276 and 2088 nm were important for acidity and bitterness, respectively (Ribeiro et al., 2011). Bands at 2050 nm show the absorbance of 1st overtone of C=O and O–H combination; those around 2270 nm can be either due to N–H and O–H combination or C–H+C–H combination. 1680 nm, represents the 1st overtone of C–H, while the region 1944-1982 nm shows the 2nd overtone of C=O stretching. The absorption at 2088 nm is due to 1st overtone of C=O and O–H combination bands, while the region 1412-1444 nm shows the 1st overtone of O–H and N–H.

It is known that acidity decreases over roasting, while compounds such as pyrazines and ketones are more intensively generated at longer roasting, which might explain the common presence of strong absorptions at these wavelengths, particularly for nutty/roasted and pyrazines/ketones.

The β-regression plots of the models built from green beans showed different absorptions compared to roasted beans, which is explained by the different composition of the green beans compared to the roasted ones. However, it also suggests that the predictions are based – in some cases – not on the same absorption bands, as the volatile compounds could not be directly detected in the green beans. The wavelengths at 1182, 1724 and 2056 nm were important for the prediction of sensory impact (Figure A.13). Absorption around 1725 nm is associated to the 1st overtone of C–H, while 2056 nm showed the 1st overtone of C=O and O–H combination bands; they have both been previously reported in NIR prediction models for "flavour" (Ribeiro et al., 2011). Absorption bands at ~1110-1120, ~1950 and 2066-2096 nm were previously assigned to chlorogenic acids by Esteban-Diez et al. (2004), and were important in the regression models presented here. The wavelength at 1113 nm has been also attributed to caffeine and carbohydrates, while the region at ~1724 nm has been attributed to fatty acids. Similarly, absorption at ~2150 nm has been attributed to either caffeine or fatty acids (cis-unsaturations) (Esteban-Diez et al., 2004). However, it should be noted that these assignments are tentative due to the typical overlap observed in the NIR region when analysing material of heterogeneous composition.

The understanding of coffee quality using NIR-based methods is challenging due to the low concentrations of compounds that exert a sensory impact, in terms of both aroma and taste. However, some taste-active compounds are found at much higher content compared to volatile compounds, e.g. acids and caffeine in ground and roasted coffee are found in appreciable quantity (Farah, 2012), suggesting possible detection in the NIR region. In contrast, the concentration of volatile compounds is unlikely to be directly predicted, especially in food matrices where many other constituents are found. Due to the complexity of coffee composition, other authors have previously tried to build quantitative models to predict the sensory impact of the coffee beverage by NIR spectroscopy. Ribeiro et al. (2011) scanned 52 samples of ground and roasted coffee (medium roasted) by NIRS (1100-2500 nm) and performed a cup testing on the bulk, to predict sensory parameters such as acidity, bitterness, flavour, cleanliness, body and "overall quality". All PLS regression models had R_{cv}^2 values above 0.7, with flavour, cleanliness and overall quality showing the highest R^2 values (0.83-0.86). However, this experiment was carried out on roasted

and ground coffee, and no indication on the bean-to-bean variability can be obtained using this method. A similar approach was previously applied to espresso coffee, for the prediction of sensory attributes by NIRS, scanning roasted and ground coffees (Esteban-Diez et al., 2004). Five batches of green coffees were roasted under different conditions to obtain 35 final samples, scanned in the range 1100-2200 nm to build PLSR models for body, acidity, bitterness and appearance. Acidity had the highest R_{cv}^2 values, of 0.92-0.94; good prediction ability was also shown for bitterness, R_{cv}^2=0.84-0.94.

More recently, Tolessa et al. (2016) applied FT-NIR spectroscopy (900-2500 nm) on 86 samples of green Arabica coffee beans to predict the final cup quality of the beverage. The samples were scanned as bulk, and PLS regression was used to predict sensory scores. Models for overall cup preference and acidity had good performance (R_{cv}^2=0.81 and 0.83, respectively), while other parameters such as flavour and aroma were poorly predicted, the R_{cv}^2 values being 0.66 and 0.59, respectively. Despite the considerably large sample number, however, the authors investigated only Arabica coffees from one country only (Ethiopia). Consequently, the models cannot be generalised as botanical or geographical differences can influence coffee composition, their absorbance spectra and thus leading to less optimistic predictions.

Thus, the research so far on coffee flavour prediction using NIRS was only based on conventional NIR spectroscopy from bulk, and more commonly from ground and roasted samples, which does not allow estimation of the resulting quality of the coffee before any processing step (roasting, grinding, etc.). Due to the nature of sensory analysis, it is also impossible to generate data on a single coffee bean, thus the approach herein presented might provide a solution for this issue and give information on the expected variation on a single coffee bean basis.

Green coffee beans show a relatively complex composition, as carbohydrates, lipids, proteins, acids and a series of other minor compounds are found. Even in the roasted coffee beans, volatile compounds are found at low concentrations, typically a few hundreds of mg kg^{-1} ground coffee beans; it is very likely that a direct detection of these molecules is not possible in the NIR region. The successful correlation of green coffee bean spectra and the volatile compounds obtained in the roasted coffee was thus not attributed to a direct detection of these volatiles. However, it was

attributed to the presence of other major compounds that are detectable by NIR/HSI. Flavour precursors are very likely the reason of the successful detection of volatile compounds. It is known that the level of volatile precursors in the green coffee bean has a dramatic role in the final generation of aroma compounds (De Maria et al., 1996). Polysaccharides, proteins, trigonelline, sucrose and chlorogenic acids are all - at different extents - responsible for the production of volatile compounds in coffee upon roasting. For example, pyridine and pyrroles are known to be generated from trigonelline degradation (Chapter 8).

The majority of existing studies on the application of NIRS or HSI methods for quantification purposes of agricultural or food products focused on one or a few specific target compounds, while little information has been found on the prediction of many reference compounds. In the present research, PLS2 has been applied to predict several dependent variables using the spectral information obtained by HSI.

However, the aim of the present research was not to quantify accurately the concentration of volatile compounds by HSI, but to verify whether a correlation exists and whether estimation of the generated volatile compounds is possible. Once a correlation has been found, it is therefore possible to predict the level of some volatile compounds, or at least to describe the potential aroma formation, for example creating categories of high, medium or low volatile generation. Such a model is particularly useful at an applicative level. Modern processing coffee roasters tend to control the roasting conditions in the most accurate way, but it is known that different coffee beans react differently to the same thermal treatment and therefore the volatile compounds formed can be significantly different, thus bringing differences in terms of aroma and flavour. The application of a rapid and non-destructive method to predict the potential aroma generated from single coffee beans, would allow better standardisation of the final quality, and even selection of the most distinctive coffee beans to create higher quality coffee for special target markets, or removal beans that would cause unwanted odours and lower the quality of the batch.

9.4. CONCLUSIONS

The present Chapter reports HSI prediction of aroma generation from green coffee beans on a single bean basis. This is the first study carried out to predict volatile compound generation by HSI, and the first using any NIR-based techniques. Whilst prediction models have been reported by traditional NIR spectroscopy from ground beans compared to the sensory quality of brewed coffees, no previous work started from green coffee beans and used single coffee beans. The results indicated that a prediction is possible for some single volatile compounds, both from green and roasted coffee beans. More promising results were obtained by grouping the volatile compounds according to their chemical groups or their sensory description. In this way, calibrations models were applied more easily to give indication on the expected aroma of single coffee beans. The models gave satisfactory prediction and sorting experiments were successfully carried out in order to validate the proposal that sorting the top and bottom ~10% of the beans gave differences in both the abundance of compounds and perceived aroma of the resulting roasted and ground coffee.

The present work might be of great interest for the coffee industry but also for producers and importers, in providing new tools for quality evaluation from the first stage of processing, i.e. evaluation of the raw material.

10. GENERAL DISCUSSION AND CONCLUSIONS

This thesis aimed to explore the potential of hyperspectral imaging (HSI) for the prediction of the chemical composition of granular food commodities, focusing on quality-related properties and compounds that could give added value to the food industry. Specifically, this research has tried to overcome the limitations associated with conventional bulk prediction methods, by seeking to utilise HSI as a rapid and non-destructive alternative for compositional analysis. The focus was on single seed prediction, which is an innovative application of HSI in the food science and technology sector.

Conventional NIR spectroscopy has the limitation of only being able to provide average bulk values, instead of single seed prediction. Whilst quantitative predictions could be built even by NIR spectroscopy by scanning one seed at a time on the acquisition window, its application is limited to a few kernels. On the contrary, this thesis demonstrated that the use of hyperspectral imaging can permit the scanning of multiple seeds at a time, offering the potential for automatic and rapid scanning of food granular commodities.

From the results presented in this thesis, a wide variation in the chemical composition was found between single kernels or beans of all three commodities studied (wheat, cocoa and coffee). Some of this variation was attributed to variety or genotypes. However, the large variations observed even within the same batch suggest that agronomic and environmental conditions, as well as plant physiological factors play an important role.

This research has a wider impact with regards to achieving a more consistent product by evaluating the raw material composition and exploiting its intra-batch variability, also giving new opportunities to obtain a wider range of products starting from the same batch. This could be achieved by the sorting of higher and lower quality seeds within a batch, whether to remove seeds that could affect the whole production by possessing defects related to the chemical composition, or to obtain a high quality product aimed for "specialty" production.

Moreover, the techniques present in this thesis could ultimately help the food industry and analytical laboratories to lower the cost of the routine chemical analyses required for quality assessment, with the conventional approaches often being expensive, time consuming, and requiring expert operators. Plant breeding is another area where this thesis could have an impact, as rapid seed phenotyping can allow the selection of those with the desired characteristics, thus saving time and lowering the costs. A method that can effectively predict the characteristics of seeds would be especially useful for plants with slow growth, such as cocoa.

The calibrations presented in this thesis could be applied by the food industry at the reception or before any processing. By applying compositional predictions, HSI gives the ability to upgrade a sample that would otherwise have been outside the required specifciations, e.g. minimum protein content for wheat, especially for bread-making. In the case of cocoa, a first sorting operation could be carried out before the shell removal to differentiate the higher value beans, or a sorting machine could be used on the nibs to obtain a better indication of quality-relevant properties, in particular when the target is to develop food with increased functionality and better nutritional properties. In the case of coffee beans, HSI sorting machines could offer great potential to add value to the product, as large differences exist based on the coffee quality. Depending on the final product, the coffee industry could usefully apply HSI prediction of total lipids to select those with high fat content for espresso-like production, while using the low-fat fraction for the production of soluble coffee. Similarly, the prediction of sucrose, caffeine and trigonelline from the green beans give an indication of the expected final quality of the roasted coffee and the brew, thus it can be applied by importers or roasters to define different production streams in order to differentiate between "regular" or higher quality coffee beans. Lastly, the aroma prediction on single coffee beans (either as green or roasted) can be used by the industry for similar purposes. The implementation of HSI before and after the roasting operation could be of interest depending on the industrial choices: for example, one could choose to scan green coffee beans at the reception and sort the green beans into multiple lines having similar characteristics, to be roasted under different conditions. On the other hand, the industry could choose to roast all the

production under the same conditions, and then scan the roasted beans to sort them according to the different aroma profiles, before grinding.

Optical sorting is currently done by using the visible region only, thus separating seeds with unwanted colour, shape or visible defects, but no technology is currently capable of sorting based on the chemical composition of food. When sub-fractions are sorted from the initial raw material, they can be separated for different production lines, different markets or different final products. For example, high- and low-protein fractions can be used for bread and non-bread applications, respectively. This would allow upgrading a sample that would otherwise be outside the required specficiations. Cocoa with high- and low-polyphenol content could be used for standard chocolate manufacturing or for more "healthy" or speciality 'fine' chocolate products. Sub-fractions of cocoa beans sorted according to their fat content can be useful for process standardisation. Green coffee beans can be sorted for their composition, for example beans with higher trigonelline content are likely to give higher aroma and they are associated with good quality coffee, giving the potential of using it for high-quality niche coffees. A naturally-low caffeine coffee could be also produced by screening and sorting coffee beans. Furthermore, HSI has been shown to oreduct the potential generation of aroma compounds upon roasting. As coffee quality is mostly given by its aroma, the approach provides the potential to sort to select beans with some particular positive notes or to remove some unwanted beans that might give defective notes to the final coffee brew is highly commerically relevant.

In conclusion, this thesis demonstrates the feasibility of HSI as a useful technique to investigate the chemical composition of food granular commodities without any sample preparation or pre-treatment. The application of the proposed calibrations allowed prediction of chemical constituents of single seeds, and HSI permitted the visualisation of compound distribution across the seed so that localisation of target compounds can be obtained. In addition, this thesis reports on a large intra-batch natural variability in a wide range of food constituents when looking at the individual seed level. This gives potential for inspection of the raw material, as well as sorting to

obtain sub-fractions with more consistent composition and quality, or to sorting materials into different process streams with different commercial value.

Possible future works arising from the outcomes of this thesis could include:

- Investigation of the best settings (e.g., field of view, spectral range, scanning speed) to rapidly apply the proposed calibrations to enable high-speed screening, with potential for real time monitoring;
- Investigation of methods that are capable of providing reference measurements on single pixels or smaller areas to verify the actual distribution of chemical compounds across an individual seed;
- Investigation of other quality-related properties, especially in terms of chemical composition, that can be industrially relevant, for example contaminants such as mycotoxins or secondary quality parameters such as yield, flavour or consumer acceptability;
- Application of HSI using the current approach to other food commodities, e.g. nuts, dried fruits, grape/raisins;
- Development of instrumentation to add three-dimensional spatial information to the hypercube, potentially exploring the internal composition of food products so that a complete characterisation is obtained, useful for plant physiology investigations;
- Optimisation of the software and hardware conditions for automation of HSI data acquisition and processing.

REFERENCES

Abdullah, M. Z. (2016). Image acquisition systems *Computer Vision Technology for Food Quality Evaluation (Second Edition)* (pp. 3-43): Elsevier.

Adnan, A., Hörsten, D. v., & Pawelzik, E. (2017). Rapid Prediction of Moisture Content in Intact Green Coffee Beans Using Near Infrared Spectroscopy. *Foods, 6*(5), 38.

Afoakwa, E. O. (2017). Cocoa bean composition and chocolate flavour development. *Chocolate Science and Technology*, 80-101.

Afoakwa, E. O., Paterson, A., Fowler, M., & Ryan, A. (2008). Flavor formation and character in cocoa and chocolate: a critical review. *Critical reviews in food science and nutrition, 48*(9), 840-857.

Afseth, N. K., & Böker, U. (2011). Raman and Infrared Imaging of Foods. *Raman, Infrared, and Near-Infrared Chemical Imaging*, 227-241.

Agelet, L. E. (2011). Single seed discriminative applications using near infrared technologies. *PHD thesis, Iowa State University (USA)*.

Agelet, L. E., Armstrong, P. R., Clariana, I. R., & Hurburgh, C. R. (2012). Measurement of single soybean seed attributes by near-infrared technologies. A comparative study. *Journal of Agricultural and Food Chemistry, 60*(34), 8314-8322.

Agelet, L. E., Ellis, D. D., Duvick, S., Goggi, A. S., Hurburgh, C. R., & Gardner, C. A. (2012). Feasibility of near infrared spectroscopy for analyzing corn kernel damage and viability of soybean and corn kernels. *Journal of Cereal Science, 55*(2), 160-165.

Agelet, L. E., & Hurburgh, C. R. (2014). Limitations and current applications of Near Infrared Spectroscopy for single seed analysis. *Talanta, 121*, 288-299.

Agelet, L. E., & Hurburgh Jr, C. R. (2010). A tutorial on near infrared spectroscopy and its calibration. *Critical Reviews in Analytical Chemistry, 40*(4), 246-260.

Akiyama, M., Murakami, K., Ikeda, M., Iwatsuki, K., Wada, A., Tokuno, K., Onishi, M., & Iwabuchi, H. (2007). Analysis of the headspace volatiles of freshly brewed Arabica coffee using solid-phase microextraction. *Journal of Food Science, 72*(7).

Alessandrini, L., Romani, S., Pinnavaia, G., & Dalla Rosa, M. (2008). Near infrared spectroscopy: An analytical tool to predict coffee roasting degree. *Analytica Chimica Acta, 625*(1), 95-102.

Ali, A., Atkins, I., Rooney, L., & Porter, K. (1969). Kernel dimensions, weight, protein content and milling yield of grain from portions of the wheat spike. *Crop science, 9*(3), 329-330.

Álvarez, C., Pérez, E., Cros, E., Lares, M., Assemat, S., Boulanger, R., & Davrieux, F. (2012). The use of near infrared spectroscopy to determine the fat, caffeine, theobromine and (–)-epicatechin contents in unfermented and sun-dried beans of Criollo cocoa. *Journal of Near Infrared Spectroscopy, 20*(2), 307-315.

Ambrose, A., Kandpal, L. M., Kim, M. S., Lee, W.-H., & Cho, B.-K. (2016). High speed measurement of corn seed viability using hyperspectral imaging. *Infrared Physics & Technology, 75*, 173-179.

Amigo, J. M., Martí, I., & Gowen, A. (2013). Hyperspectral imaging and chemometrics: a perfect combination for the analysis of food structure, composition and quality *Data Handling in Science and Technology. Vol 28* (pp. 343-370).

Ariana, D. P., & Lu, R. (2010). Evaluation of internal defect and surface color of whole pickles using hyperspectral imaging. *Journal of Food Engineering, 96*(4), 583-590.

Arngren, M., Hansen, P. W., Eriksen, B., Larsen, J., & Larsen, R. (2011). Analysis of pregerminated barley using hyperspectral image analysis. *Journal of Agricultural and Food Chemistry, 59*(21), 11385-11394.

Bae, H., Seo, Y.-W., Kim, D.-Y., Lohumi, S., Park, E., & Cho, B.-K. (2016). Development of non-destructive sorting technique for viability of watermelon seed by using hyperspectral image processing. *Journal of the Korean Society for Nondestructive Testing, 36*(1), 35-44.

Baggenstoss, J., Poisson, L., Kaegi, R., Perren, R., & Escher, F. (2008). Coffee roasting and aroma formation: application of different time− temperature conditions. *Journal of Agricultural and Food Chemistry, 56*(14), 5836-5846.

Baiano, A., Terracone, C., Peri, G., & Romaniello, R. (2012). Application of hyperspectral imaging for prediction of physico-chemical and sensory characteristics of table grapes. *Computers and electronics in Agriculture, 87*, 142-151.

Baranowski, P., Mazurek, W., Wozniak, J., & Majewska, U. (2012). Detection of early bruises in apples using hyperspectral data and thermal imaging. *Journal of Food Engineering, 110*(3), 345-355.

Barbin, D. F., Felicio, A. L. d. S. M., Sun, D.-W., Nixdorf, S. L., & Hirooka, E. Y. (2014). Application of infrared spectral techniques on quality and compositional attributes of coffee: An overview. *Food Research International, 61*, 23-32.

Barnard, A., Van Deventer, C., & Maartens, H. (2005). Comparison between methods for estimating sprout damage in wheat. *South African Journal of Plant and Soil, 22*(1), 44-48.

Barnes, R., Dhanoa, M., & Lister, S. J. (1989). Standard normal variate transformation and de-trending of near-infrared diffuse reflectance spectra. *Applied spectroscopy, 43*(5), 772-777.

Barrero, J. M., Mrva, K., Talbot, M. J., White, R. G., Taylor, J., Gubler, F., & Mares, D. J. (2013). Genetic, hormonal, and physiological analysis of late maturity α-amylase in wheat. *Plant physiology, 161*(3), 1265-1277.

Bauriegel, E., Giebel, A., & Herppich, W. B. (2011). Hyperspectral and chlorophyll fluorescence imaging to analyse the impact of Fusarium culmorum on the photosynthetic integrity of infected wheat ears. *Sensors, 11*(4), 3765-3779.

Beckett, S. T. (2011). *Industrial chocolate manufacture and use*: John Wiley & Sons.

Bellon-Maurel, V., Fernandez-Ahumada, E., Palagos, B., Roger, J.-M., & McBratney, A. (2010). Critical review of chemometric indicators commonly used for assessing the quality of the prediction of soil attributes by NIR spectroscopy. *TrAC Trends in Analytical Chemistry, 29*(9), 1073-1081.

Berman, M., Connor, P., Whitbourn, L., Coward, D., Osborne, B., & Southan, M. (2007). Classification of sound and stained wheat grains using visible and near infrared hyperspectral image analysis. *Journal of Near Infrared Spectroscopy, 15*(6), 351-358.

Bertone, E., Venturello, A., Giraudo, A., Pellegrino, G., & Geobaldo, F. (2016). Simultaneous determination by NIR spectroscopy of the roasting degree and Arabica/Robusta ratio in roasted and ground coffee. *Food Control, 59*, 683-689.

Bertrand, B., Boulanger, R., Dussert, S., Ribeyre, F., Berthiot, L., Descroix, F., & Joët, T. (2012). Climatic factors directly impact the volatile organic compound fingerprint in green Arabica coffee bean as well as coffee beverage quality. *Food Chemistry, 135*(4), 2575-2583.

Bhumiratana, N., Adhikari, K., & Chambers, E. (2011). Evolution of sensory aroma attributes from coffee beans to brewed coffee. *LWT-Food Science and Technology, 44*(10), 2185-2192.

Bhuvaneswari, K., Fields, P. G., White, N. D., Sarkar, A. K., Singh, C. B., & Jayas, D. S. (2011). Image analysis for detecting insect fragments in semolina. *Journal of Stored Products Research, 47*(1), 20-24.

Bicho, N. C., Leitão, A. E., Ramalho, J. C., & Lidon, F. C. (2012). Use of colour parameters for roasted coffee assessment. *Food Science and Technology (Campinas), 32*(3), 436-442.

Biston, R., & Clamot, G. (1982). Use of Near-Infrared Reflectance Spectroscopy and Dye-Binding Techniques for Estimating Protein in Oat Groats. *Cereal Chem, 59*(5), 333-335.

Blanco, M., & Villarroya, I. (2002). NIR spectroscopy: a rapid-response analytical tool. *TrAC Trends in Analytical Chemistry, 21*(4), 240-250.

Blank, I. (2002). *Gas chromatography-olfactometry in food aroma analysis*: Dekker: New York.

Boldrini, B., Kessler, W., Rebner, K., & Kessler, R. W. (2012). Hyperspectral imaging: a review of best practice, performance and pitfalls for in-line and on-line applications. *Journal of Near Infrared Spectroscopy, 20*(5), 483-508.

Bonvehi, J. S., & Coll, F. V. (1997). Evaluation of bitterness and astringency of polyphenolic compounds in cocoa powder. *Food Chemistry, 60*(3), 365-370.

Bramble, T., Dowell, F., & Herrman, T. (2006). Single-kernel near-infrared protein prediction and the role of kernel weight in hard red winter wheat. *Applied Engineering in Agriculture, 22*(6), 945-949.

Briandet, R., Kemsley, E. K., & Wilson, R. H. (1996). Discrimination of Arabica and Robusta in instant coffee by Fourier transform infrared spectroscopy and chemometrics. *Journal of Agricultural and Food Chemistry, 44*(1), 170-174.

Brown, S. D., Tauler, R., & Walczak, B. (2009). *Comprehensive chemometrics*: Elsevier Science.

Buffo, R. A., & Cardelli-Freire, C. (2004). Coffee flavour: an overview. *Flavour and fragrance journal, 19*(2), 99-104.

Buratti, S., Sinelli, N., Bertone, E., Venturello, A., Casiraghi, E., & Geobaldo, F. (2015). Discrimination between washed Arabica, natural Arabica and Robusta coffees by using near infrared spectroscopy, electronic nose and electronic tongue analysis. *Journal of the Science of Food and Agriculture, 95*(11), 2192-2200.

Burger, J. (2009). Bad pixel detection in hyperspectral staring camera systems. *NIR news, 20*(1), 9-12.

Burger, J., & Geladi, P. (2005). Hyperspectral NIR image regression part I: calibration and correction. *Journal of chemometrics, 19*(5-7), 355-363.

Burger, J., & Geladi, P. (2007). Spectral pre-treatments of hyperspectral near infrared images: analysis of diffuse reflectance scattering. *Journal of Near Infrared Spectroscopy, 15*(1), 29.

Burger, J., & Gowen, A. (2011). Data handling in hyperspectral image analysis. *Chemometrics and intelligent laboratory systems, 108*(1), 13-22.

Burns, D. A., & Ciurczak, E. W. (2007). *Handbook of near-infrared analysis*: CRC press.

Calvini, R., Amigo, J. M., & Ulrici, A. (2017). Transferring results from NIR-hyperspectral to NIR-multispectral imaging systems: A filter-based simulation applied to the classification of Arabica and Robusta green coffee. *Analytica Chimica Acta, 967*, 33-41.

Calvini, R., Ulrici, A., & Amigo, J. M. (2015). Practical comparison of sparse methods for classification of Arabica and Robusta coffee species using near infrared hyperspectral imaging. *Chemometrics and intelligent laboratory systems, 146*, 503-511.

Campa, C., Ballester, J., Doulbeau, S., Dussert, S., Hamon, S., & Noirot, M. (2004). Trigonelline and sucrose diversity in wild Coffea species. *Food Chemistry, 88*(1), 39-43.

Caporaso, N., Genovese, A., Canela, M. D., Civitella, A., & Sacchi, R. (2014). Neapolitan coffee brew chemical analysis in comparison to espresso, moka and American brews. *Food Research International, 61*, 152-160.

Caporaso, N., Whitworth, M., & Fisk, I. (2016). Application of calibrations to hyperspectral images of food grains: example of wheat Falling Number *Journal of Spectral Imaging, 6*(a4), 1-15.

Caporaso, N., Whitworth, M. B., & Fisk, I. D. (2017). Protein content prediction in single wheat kernels using hyperspectral imaging. *Food Chemistry, 240*, 32-42.

Casal, S., Oliveira, M., Alves, M., & Ferreira, M. (2000). Discriminate analysis of roasted coffee varieties for trigonelline, nicotinic acid, and caffeine content. *Journal of Agricultural and Food Chemistry, 48*(8), 3420-3424.

Casal, S., Oliveira, M., & Ferreira, M. (1998). Development of an HPLC/diode-array detector method for simultaneous determination of trigonelline, nicotinic acid, and caffeine in coffee. *Journal of liquid chromatography & related technologies, 21*(20), 3187-3195.

Catelani, T. A., Páscoa, R. N., Santos, J. R., Pezza, L., Pezza, H. R., Lima, J. L., & Lopes, J. A. (2017). A Non-invasive Real-Time Methodology for the Quantification of Antioxidant Properties in Coffee During the Roasting Process Based on Near-Infrared Spectroscopy. *Food and Bioprocess Technology, 10*(4), 630-638.

Cheewapramong, P. (2007). *Use of near-infrared spectroscopy for qualitative and quantitative analyses of grains and cereal products*: The University of Nebraska-Lincoln.

Chen, J., Chen, H., Wang, X., Yu, C., Wang, C., & Zhu, D. (2013). *The characteristic of hyperspectral image of wheat seeds during sprouting.* Paper presented at the International Conference on Computer and Computing Technologies in Agriculture.

Chen, Y.-R., Chao, K., & Kim, M. S. (2002). Machine vision technology for agricultural applications. *Computers and electronics in Agriculture, 36*(2), 173-191.

Cho, B.-K., Kim, M. S., Baek, I.-S., Kim, D.-Y., Lee, W.-H., Kim, J., Bae, H., & Kim, Y.-S. (2013). Detection of cuticle defects on cherry tomatoes using hyperspectral fluorescence imagery. *Postharvest Biology and Technology, 76*, 40-49.

Cho, J.-S., Bae, H.-J., Cho, B.-K., & Moon, K.-D. (2017). Qualitative properties of roasting defect beans and development of its classification methods by hyperspectral imaging technology. *Food Chemistry, 220*, 505-509.

Choudhary, R., Mahesh, S., Paliwal, J., & Jayas, D. (2009). Identification of wheat classes using wavelet features from near infrared hyperspectral images of bulk samples. *biosystems engineering, 102*(2), 115-127.

Ciurczak, E. W., & Igne, B. (2014). *Pharmaceutical and medical applications of near-infrared spectroscopy*: CRC Press.

Clarke, R., & Vitzthum, O. (2008). *Coffee: recent developments*: John Wiley & Sons.

Cogdill, R. P., Hurburgh, C., Rippke, G. R., Bajic, S. J., Jones, R. W., McClelland, J. F., Jensen, T. C., & Liu, J. (2001). *Single-kernel maize analysis by near-infrared hyperspectral imaging.* Iowa State University.

Cogdill, R. P., Hurburgh, C., Rippke, G. R., Bajic, S. J., Jones, R. W., McClelland, J. F., Jensen, T. C., & Liu, J. (2004). Single-kernel maize analysis by near-infrared hyperspectral imaging. *Transactions of the ASAE, 47*(1), 311.

Cozzolino, D., Delucchi, I., Kholi, M., & Vázquez, D. (2006). Use of Near Infrared Reflectance spectroscopy to evaluate quality characteristics in whole-wheat grain. Uso de la espectroscopía de reflectancia en el infrarrojo cercano para evaluar características de calidad en trigo. *Agricultura Técnica, 66*(4), 370-375.

Czerny, M., & Grosch, W. (2000). Potent odorants of raw Arabica coffee. Their changes during roasting. *Journal of Agricultural and Food Chemistry, 48*(3), 868-872.

da Costa Filho, P. A. (2009). Rapid determination of sucrose in chocolate mass using near infrared spectroscopy. *Analytica Chimica Acta, 631*(2), 206-211.

Dand, R. (1997). *The international cocoa trade* (Vol. 1): John Wiley & Sons.

Dardenne, P. (2010). Some considerations about NIR spectroscopy: Closing speech at NIR-2009. *NIR news, 21*(1), 8-14.

Davey, M. W., Saeys, W., Hof, E., Ramon, H., Swennen, R. L., & Keulemans, J. (2009). Application of visible and near-infrared reflectance spectroscopy (Vis/NIRS) to determine carotenoid contents in banana (Musa spp.) fruit pulp. *Journal of Agricultural and Food Chemistry, 57*(5), 1742-1751.

Davies, A., Franklin, J., Grant, A., Griffiths, N., Shepherd, R., & Fenwick, G. (1991). Prediction of chocolate quality from near-infrared spectroscopic measurements of the raw cocoa beans. *Vibrational Spectroscopy, 2*(2-3), 161-172.

de Azeredo, A. M. C. (2011). *Coffee roasting: Color and aroma-active sulfur compounds*: University of Florida.

De Marchi, M., Riovanto, R., Penasa, M., & Cassandro, M. (2012). At-line prediction of fatty acid profile in chicken breast using near infrared reflectance spectroscopy. *Meat science, 90*(3), 653-657.

De Maria, C., Trugo, L., Neto, F. A., Moreira, R., & Alviano, C. (1996). Composition of green coffee water-soluble fractions and identification of volatiles formed during roasting. *Food Chemistry, 55*(3), 203-207.

De Vuyst, L., & Weckx, S. (2016). The cocoa bean fermentation process: from ecosystem analysis to starter culture development. *Journal of applied microbiology, 121*(1), 5-17.

Del Fiore, A., Reverberi, M., Ricelli, A., Pinzari, F., Serranti, S., Fabbri, A., Bonifazi, G., & Fanelli, C. (2010). Early detection of toxigenic fungi on maize by hyperspectral imaging analysis. *International Journal of Food Microbiology, 144*(1), 64-71.

Delwiche. (1995). Single wheat kernel analysis by near-infrared transmittance: Protein content. *Cereal Chemistry, 72*(1), 11-16.

Delwiche, S., & Hruschka, W. (2000). Protein content of bulk wheat from near-infrared reflectance of individual kernels. *Cereal Chemistry, 77*(1), 86-88.

Delwiche, S. R. (1998). Protein content of single kernels of wheat by near-infrared reflectance spectroscopy. *Journal of Cereal Science, 27*(3), 241-254.

Delwiche, S. R., Pordesimo, L. O., Scaboo, A. M., & Pantalone, V. R. (2006). Measurement of inorganic phosphorus in soybeans with near-infrared spectroscopy. *Journal of Agricultural and Food Chemistry, 54*(19), 6951-6956.

Delwiche, S. R., Souza, E. J., & Kim, M. S. (2013). Limitations of single kernel near-infrared hyperspectral imaging of soft wheat for milling quality. *biosystems engineering, 115*(3), 260-273.

Dencic, S., DePauw, R., Kobiljski, B., & Momcilovic, V. (2013). Hagberg Falling Number and Rheological Properties of Wheat Cultivars in Wet and Dry Preharvest Periods. *Plant Production Science, 16*(4), 342-351.

Dessalegn, Y., Labuscagne, M., Osthoff, G., & Herselman, L. (2007). Variation of green bean caffeine, chlorogenic acid, sucrose and trigolline contents among Ethiopian Arabica coffee accessories. *SINET: Ethiopian Journal of Science, 30*(1), 77-82.

Diezma, B., Lleó, L., Roger, J. M., Herrero-Langreo, A., Lunadei, L., & Ruiz-Altisent, M. (2013). Examination of the quality of spinach leaves using hyperspectral imaging. *Postharvest Biology and Technology, 85*, 8-17.

Dorfner, R., Ferge, T., Kettrup, A., Zimmermann, R., & Yeretzian, C. (2003). Real-time monitoring of 4-vinylguaiacol, guaiacol, and phenol during coffee roasting by resonant laser ionization time-of-flight mass spectrometry. *Journal of Agricultural and Food Chemistry, 51*(19), 5768-5773.

Dorrepaal, R., Malegori, C., & Gowen, A. (2016). Tutorial: Time series hyperspectral image analysis. *Journal of Near Infrared Spectroscopy, 24*(2), 89-107.

dos Santos Scholz, M. B., Kitzberger, C. S. G., Pereira, L. F. P., Davrieux, F., Pot, D., Charmetantd, P., & Leroyd, T. (2014). Application of near infrared spectroscopy

for green coffee biochemical phenotyping. *Journal of Near Infrared Spectroscopy, 22*(6), 411-421.

Downey, G., Boussion, J., & Beauchêne, D. (1995). Authentication of whole and ground coffee beans by near infrared reflectance spectroscopy. *Journal of Near Infrared Spectroscopy, 2*(2), 85-92.

Du Toit, G. (2009). *Near infrared hyperspectral imaging and chemometrics for exploration and classification of whole wheat kernels*. Stellenbosch: University of Stellenbosch.

Ebrahimi-Najafabadi, H., Leardi, R., Oliveri, P., Casolino, M. C., Jalali-Heravi, M., & Lanteri, S. (2012). Detection of addition of barley to coffee using near infrared spectroscopy and chemometric techniques. *Talanta, 99*, 175-179.

El-Abassy, R. M., Donfack, P., & Materny, A. (2011). Discrimination between Arabica and Robusta green coffee using visible micro Raman spectroscopy and chemometric analysis. *Food Chemistry, 126*(3), 1443-1448.

ElMasry, G., Kamruzzaman, M., Sun, D.-W., & Allen, P. (2012). Principles and applications of hyperspectral imaging in quality evaluation of agro-food products: a review. *Critical reviews in food science and nutrition, 52*(11), 999-1023.

ElMasry, G., & Sun, D.-W. (2010). Principles of hyperspectral imaging technology. *Hyperspectral imaging for food quality analysis and control*, 3-43.

ElMasry, G., Wang, N., & Vigneault, C. (2009). Detecting chilling injury in Red Delicious apple using hyperspectral imaging and neural networks. *Postharvest Biology and Technology, 52*(1), 1-8.

ElMasry, G. M., & Nakauchi, S. (2016). Image analysis operations applied to hyperspectral images for non-invasive sensing of food quality–A comprehensive review. *biosystems engineering, 142*, 53-82.

Esquerre, C., Gowen, A. A., Downey, G., & O'Donnell, C. P. (2012). Wavelength selection for development of a near infrared imaging system for early detection of bruise damage in mushrooms (Agaricus bisporus). *Journal of Near Infrared Spectroscopy, 20*(5), 537-546.

Esteban-Diez, I., González-Sáiz, J., & Pizarro, C. (2004). Prediction of sensory properties of espresso from roasted coffee samples by near-infrared spectroscopy. *Analytica Chimica Acta, 525*(2), 171-182.

Esteban-Diez, I., Gonzalez-Saiz, J., Sáenz-González, C., & Pizarro, C. (2007). Coffee varietal differentiation based on near infrared spectroscopy. *Talanta, 71*(1), 221-229.

FAO, F. a. A. O. (2017). Agriculture Organization Corporate Statistical Database (FAOSTAT)(2017). *Production/Crops, Food and Agriculture Organization of the United Nations: Division of Statistics. Available from: http://faostat3. fao. org/browse/Q/QC/E*.

Farah, A. (2012). Coffee constituents. *Coffee: emerging health effects and disease prevention, 1*, 22-58.

Farah, A., Monteiro, M., Calado, V., Franca, A., & Trugo, L. (2006). Correlation between cup quality and chemical attributes of Brazilian coffee. *Food Chemistry, 98*(2), 373-380.

Fearn, T. (2002). Assessing Calibrations: SEP, RPD, RER and R 2. *NIR news, 13*(6), 12-13.

Fearn, T. (2005). Chemometrics: an enabling tool for NIR. *NIR news, 16*(7), 17-19.

Fearn, T. (2014). Structuring the population. *NIR news, 25*(8), 33-34.

Fernandes, A. M., Oliveira, P., Moura, J. P., Oliveira, A. A., Falco, V., Correia, M. J., & Melo-Pinto, P. (2011). Determination of anthocyanin concentration in whole grape skins using hyperspectral imaging and adaptive boosting neural networks. *Journal of Food Engineering, 105*(2), 216-226.

Fernández-Pierna, J., Vermeulen, P., Amand, O., Tossens, A., Dardenne, P., & Baeten, V. (2012). NIR hyperspectral imaging spectroscopy and chemometrics for the detection of undesirable substances in food and feed. *Chemometrics and intelligent laboratory systems, 117*, 233-239.

Ferrari, C. (2014). Il mercato del cacao e la produzione di cioccolato: le prospettive commerciali e gli aspetti normativi.

Ferrari, C., Foca, G., & Ulrici, A. (2013). Handling large datasets of hyperspectral images: reducing data size without loss of useful information. *Analytica Chimica Acta, 802*, 29-39.

Finch, S., Samuel, A., & Lane, G. P. (2014). *Lockhart and Wiseman's Crop Husbandry Including Grassland*: Elsevier.

Fiore, A., Romaniello, R., Peri, G., & Severini, C. (2008). *Quality assessment of roasted coffee blends by hyperspectral image analysis*. Paper presented at the Proceedings of 22nd International Conference on Coffee Science, Campinas, Brazil.

Fischer, M., Wohlfahrt, S., Varga, J., Saraji-Bozorgzad, M., Matuschek, G., Denner, T., & Zimmermann, R. (2014). Evolved gas analysis by single photon ionization-mass spectrometry. *Journal of Thermal Analysis and Calorimetry, 116*(3), 1461-1469.

Forina, M., Lanteri, S., & Casale, M. (2007). Multivariate calibration. *Journal of chromatography A, 1158*(1), 61-93.

Fowler, M. S., & Coutel, F. (2017). Cocoa beans: from tree to factory. *Beckett's Industrial Chocolate Manufacture and Use*, 9-49.

Fox, & Manley, M. (2014). Applications of single kernel conventional and hyperspectral imaging near infrared spectroscopy in cereals. *Journal of the Science of Food and Agriculture, 94*(2), 174-179.

Fox, Wu, A., Yiran, L., & Force, L. (2013). Variation in caffeine concentration in single coffee beans. *Journal of Agricultural and Food Chemistry, 61*(45), 10772-10778.

Fox, G., Kelly, A., Sweeney, N., & Hocroft, D. (2011). Development of a single kernel NIR barley protein calibration and assessment of variation in protein on grain quality. *Journal of the Institute of Brewing, 117*(4), 582-586.

Franca, A. S., Oliveira, L. S., Oliveira, R. C., Agresti, P. C. M., & Augusti, R. (2009). A preliminary evaluation of the effect of processing temperature on coffee roasting degree assessment. *Journal of Food Engineering, 92*(3), 345-352.

Garrigues, J. M., Bouhsain, Z., Garrigues, S., & de la Guardia, M. (2000). Fourier transform infrared determination of caffeine in roasted coffee samples. *Fresenius' journal of analytical chemistry, 366*(3), 319-322.

Gaston, E., Frías, J. s. M., Cullen, P. J., O'Donnell, C. P., & Gowen, A. A. (2010). Prediction of polyphenol oxidase activity using visible near-infrared hyperspectral imaging on mushroom (Agaricus bisporus) caps. *Journal of Agricultural and Food Chemistry, 58*(10), 6226-6233.

Geladi, Grahn, H., & Manley, M. (2010). Data analysis and chemometrics for hyperspectral imaging. *Raman, Infrared, and Near-Infrared Chemical Imaging*, 93-107.

Geladi, P. (2007). Calibration standards and image calibration. *Techniques and applications of hyperspectral image analysis, 1*, 203-220.

Genovese, A., Caporaso, N., Civitella, A., & Sacchi, R. (2014). Effect of human saliva and sip volume of coffee brews on the release of key volatile compounds by a retronasal aroma simulator. *Food Research International, 61*, 100-111.

Geromel, C., Ferreira, L. P., Davrieux, F., Guyot, B., Ribeyre, F., dos Santos Scholz, M. B., Pereira, L. F. P., Vaast, P., Pot, D., & Leroy, T. (2008). Effects of shade on the development and sugar metabolism of coffee (Coffea arabica L.) fruits. *Plant Physiology and Biochemistry, 46*(5), 569-579.

Ghamisi, P. (2015). Spectral and spatial classification of hyperspectral data.

Ginz, M., Balzer, H. H., Bradbury, A. G., & Maier, H. G. (2000). Formation of aliphatic acids by carbohydrate degradation during roasting of coffee. *European food research and technology, 211*(6), 404-410.

Gloess, A. N., Vietri, A., Wieland, F., Smrke, S., Schönbächler, B., López, J. A. S., Petrozzi, S., Bongers, S., Koziorowski, T., & Yeretzian, C. (2014). Evidence of different flavour formation dynamics by roasting coffee from different origins: On-line analysis with PTR-ToF-MS. *International Journal of Mass Spectrometry, 365*, 324-337.

Gökmen, V., Serpen, A., & Fogliano, V. (2009). Direct measurement of the total antioxidant capacity of foods: the 'QUENCHER'approach. *Trends in Food Science & Technology, 20*(6), 278-288.

Gómez-Sanchis, J., Moltó, E., Camps-Valls, G., Gómez-Chova, L., Aleixos, N., & Blasco, J. (2008). Automatic correction of the effects of the light source on spherical objects. An application to the analysis of hyperspectral images of citrus fruits. *Journal of Food Engineering, 85*(2), 191-200.

Gonzalez-Rios, O., Suarez-Quiroz, M. L., Boulanger, R., Barel, M., Guyot, B., Guiraud, J.-P., & Schorr-Galindo, S. (2007). Impact of "ecological" post-harvest processing on coffee aroma: II. Roasted coffee. *Journal of Food Composition and Analysis, 20*(3), 297-307.

Gorretta, N., Roger, J., Aubert, M., Bellon-Maurel, V., Campan, F., & Roumet, P. (2006). Determining vitreousness of durum wheat kernels using near infrared hyperspectral imaging. *Journal of Near Infrared Spectroscopy, 14*(4), 231.

Gowen, A., Downey, G., Esquerre, C., & O'Donnell, C. (2011). Preventing over-fitting in PLS calibration models of near-infrared (NIR) spectroscopy data using regression coefficients. *Journal of chemometrics, 25*(7), 375-381.

Gowen, A., O'Donnell, C., Cullen, P., Downey, G., & Frias, J. (2007). Hyperspectral imaging–an emerging process analytical tool for food quality and safety control. *Trends in Food Science & Technology, 18*(12), 590-598.

Gowen, A., O'donnell, C., Taghizadeh, M., Cullen, P., Frias, J., & Downey, G. (2008). Hyperspectral imaging combined with principal component analysis for bruise damage detection on white mushrooms (Agaricus bisporus). *Journal of chemometrics, 22*(3-4), 259-267.

Gowen, A., O'donnell, C., Cullen, P. J., & Bell, S. (2008). Recent applications of chemical imaging to pharmaceutical process monitoring and quality control. *European journal of pharmaceutics and biopharmaceutics, 69*(1), 10-22.

Gowen, A. A., Taghizadeh, M., & O'Donnell, C. P. (2009). Identification of mushrooms subjected to freeze damage using hyperspectral imaging. *Journal of Food Engineering, 93*(1), 7-12.

Grahn, H., & Geladi, P. (2007). *Techniques and applications of hyperspectral image analysis*: John Wiley & Sons.

Grosch, W. (1998). Flavour of coffee. A review. *Molecular Nutrition & Food Research, 42*(06), 344-350.

Grosch, W. (2001a). Chemistry III: volatile compounds. *Coffee: recent developments*, 68-89.

Grosch, W. (2001b). Evaluation of the key odorants of foods by dilution experiments, aroma models and omission. *Chemical senses, 26*(5), 533-545.

Guidetti, R., Beghi, R., & Giovenzana, V. (2012). Chemometrics in food technology *Chemometrics in practical applications*: InTech.

Gutiérrez, T. J., & Pérez, E. (2015). Significant quality factors in the chocolate processing: cocoa post harvest, and in its manufacture. *Cocoa byproducts technology, rheology, styling, and nutrition.*, 1.

Hampton, K., Cavinato, A., & Mayes, D. (2003). *Characterization of optical probe light penetration depth for non invasive analysis*. Paper presented at the American Chemical Society, Washington DC, USA.

He, H.-J., & Sun, D.-W. (2015). Inspection of harmful microbial contamination occurred in edible salmon flesh using imaging technology. *Journal of Food Engineering, 150*, 82-89.

Herrero-Langreo, A., Fernández-Ahumada, E., Roger, J.-M., Palagós, B., & Lleó, L. (2012). Combination of optical and non-destructive mechanical techniques for the measurement of maturity in peach. *Journal of Food Engineering, 108*(1), 150-157.

Hertz-Schünemann, R., Streibel, T., Ehlert, S., & Zimmermann, R. (2013). Looking into individual coffee beans during the roasting process: direct micro-probe sampling on-line photo-ionisation mass spectrometric analysis of coffee roasting gases. *Analytical and Bioanalytical Chemistry, 405*(22), 7083-7096.

Hertz-Schünemann, R., Dorfner, R., Yeretzian, C., Streibel, T., & Zimmermann, R. (2013). On-line process monitoring of coffee roasting by resonant laser ionisation time-of-flight mass spectrometry: bridging the gap from industrial batch roasting to flavour formation inside an individual coffee bean. *Journal of Mass Spectrometry, 48*(12), 1253-1265.

Hom, N. H., Becker, H. C., & Möllers, C. (2007). Non-destructive analysis of rapeseed quality by NIRS of small seed samples and single seeds. *Euphytica, 153*(1), 27-34.

Huang, H., Liu, L., & Ngadi, M. O. (2014). Recent Developments in Hyperspectral Imaging for Assessment of Food Quality and Safety. *Sensors, 14*(4), 7248-7276.

Huang, H., Yu, H., Xu, H., & Ying, Y. (2008). Near infrared spectroscopy for on/in-line monitoring of quality in foods and beverages: A review. *Journal of Food Engineering, 87*(3), 303-313.

Huang, M., & Lu, R. (2010). Apple mealiness detection using hyperspectral scattering technique. *Postharvest Biology and Technology, 58*(3), 168-175.

Huang, M., Tang, J., Yang, B., & Zhu, Q. (2016). Classification of maize seeds of different years based on hyperspectral imaging and model updating. *Computers and electronics in Agriculture, 122*, 139-145.

Huang, M., Zhu, Q., Wang, B., & Lu, R. (2012). Analysis of hyperspectral scattering images using locally linear embedding algorithm for apple mealiness classification. *Computers and electronics in Agriculture, 89*, 175-181.

Huck, C., Guggenbichler, W., & Bonn, G. (2005). Analysis of caffeine, theobromine and theophylline in coffee by near infrared spectroscopy (NIRS) compared to high-performance liquid chromatography (HPLC) coupled to mass spectrometry. *Analytica Chimica Acta, 538*(1), 195-203.

Hue, C., Gunata, Z., Bergounhou, A., Assemat, S., Boulanger, R., Sauvage, F.-X., & Davrieux, F. (2014). Near infrared spectroscopy as a new tool to determine cocoa fermentation levels through ammonia nitrogen quantification. *Food Chemistry, 148*, 240-245.

ICC. (1968). International Association for Cereal Chemistry-Standard method No 107/1. (Rev. 1995).

Ilangantileke, S., Wahyudi, T., & Bailon, M. G. (1991). Assessment methodology to predict quality of cocoa beans for export. *Journal of food quality, 14*(6), 481-496.

Illy, A., & Viani, R. (2005). *Espresso coffee: the science of quality*: Academic Press.

ISO/TC.34. (1994). N. 11294 Roasted ground coffee - determination of loss in mass at 103 C (routine method). Agricultural food products, Subcommittee SC IS, Coffee.

ISO/TS (2009). Food products—Determination of the total nitrogen content by combustion according to the Dumas principle and calculation of the crude protein

content—Part 2: Cereals, pulses and milled cereal products. *Geneva: International Standard Organization (ISO), p.25*.

Janni, J., Weinstock, B. A., Hagen, L., & Wright, S. (2008). Novel near-infrared sampling apparatus for single kernel analysis of oil content in maize. *Applied spectroscopy, 62*(4), 423-426.

Jentzsch, P. V., Ciobotă, V., Salinas, W., Kampe, B., Aponte, P. M., Rösch, P., Popp, J., & Ramos, L. A. (2016). Distinction of Ecuadorian varieties of fermented cocoa beans using Raman spectroscopy. *Food Chemistry, 211*, 274-280.

Jiang, L., Zhu, B., Rao, X., Berney, G., & Tao, Y. (2007). Discrimination of black walnut shell and pulp in hyperspectral fluorescence imagery using Gaussian kernel function approach. *Journal of Food Engineering, 81*(1), 108-117.

Jin, H., Li, L., & Cheng, J. (2015). Rapid and non-destructive determination of moisture content of peanut kernels using hyperspectral imaging technique. *Food analytical methods, 8*(10), 2524-2532.

Jin, H., Ma, Y., Li, L., & Cheng, J.-H. (2016). Rapid and non-destructive determination of oil content of peanut (Arachis hypogaea L.) using hyperspectral imaging analysis. *Food Analytical Methods, 9*(7), 2060-2067.

Joët, T., Laffargue, A., Descroix, F., Doulbeau, S., Bertrand, B., & Dussert, S. (2010). Influence of environmental factors, wet processing and their interactions on the biochemical composition of green Arabica coffee beans. *Food Chemistry, 118*(3), 693-701.

Jonfia-Essien, W., West, G., Alderson, P., & Tucker, G. (2008). Phenolic content and antioxidant capacity of hybrid variety cocoa beans. *Food Chemistry, 108*(3), 1155-1159.

Kaliramesh, S., Chelladurai, V., Jayas, D., Alagusundaram, K., White, N., & Fields, P. (2013). Detection of infestation by Callosobruchus maculatus in mung bean using near-infrared hyperspectral imaging. *Journal of Stored Products Research, 52*, 107-111.

Kamiyama, M., Moon, J.-K., Jang, H. W., & Shibamoto, T. (2015). Role of degradation products of chlorogenic acid in the antioxidant activity of roasted coffee. *Journal of Agricultural and Food Chemistry, 63*(7), 1996-2005.

Kandpal, L. M., Lee, S., Kim, M. S., Bae, H., & Cho, B.-K. (2015). Short wave infrared (SWIR) hyperspectral imaging technique for examination of aflatoxin B1 (AFB1) on corn kernels. *Food Control, 51*, 171-176.

Kandpal, L. M., Lohumi, S., Kim, M. S., Kang, J.-S., & Cho, B.-K. (2016). Near-infrared hyperspectral imaging system coupled with multivariate methods to predict viability and vigor in muskmelon seeds. *Sensors and Actuators B: Chemical, 229*, 534-544.

Kays, S., & Barton, F. (2000). *II; Windham, WR Analysis of nutritional components in cereal foods with near infrared reflectance spectroscopy*. Paper presented at the Near Infrared Spectroscopy: Proceedings of the 9th International Conference.

Keidel, A., von Stetten, D., Rodrigues, C., Máguas, C., & Hildebrandt, P. (2010). Discrimination of green arabica and robusta coffee beans by Raman Spectroscopy. *Journal of Agricultural and Food Chemistry, 58*(21), 11187-11192.

Kempeneers, P. (2007). *Information Extraction from Hyperspectral Images: Applied to Vegetation*: Universiteit Antwerpen, Faculteit Wetenschappen, Departement Natuurkunde.

Kent, N. L., & Evers, A. D. (1994). *Technology of Cereals: An introduction for students of food science and agriculture, Fourth Edition*: Pergamon.

Kettlewell, P., & Cashman, M. (1997). Alpha-amylase activity of wheat grain from crops differing in grain drying rate. *The Journal of Agricultural Science, 128*(02), 127-134.

Khodabux, K., L'Omelette, M. S. S., Jhaumeer-Laulloo, S., Ramasami, P., & Rondeau, P. (2007). Chemical and near-infrared determination of moisture, fat and protein in tuna fishes. *Food Chemistry, 102*(3), 669-675.

Koç, H., Smail, V. W., & Wetzel, D. L. (2008). Reliability of InGaAs focal plane array imaging of wheat germination at early stages. *Journal of Cereal Science, 48*(2), 394-400.

Kong, W., Zhang, C., Liu, F., Nie, P., & He, Y. (2013). Rice seed cultivar identification using near-infrared hyperspectral imaging and multivariate data analysis. *Sensors, 13*(7), 8916-8927.

Kongor, J. E., Hinneh, M., Van de Walle, D., Afoakwa, E. O., Boeckx, P., & Dewettinck, K. (2016). Factors influencing quality variation in cocoa (Theobroma cacao) bean flavour profile—A review. *Food Research International, 82*, 44-52.

Ky, C.-L., Louarn, J., Dussert, S., Guyot, B., Hamon, S., & Noirot, M. (2001). Caffeine, trigonelline, chlorogenic acids and sucrose diversity in wild Coffea arabica L. and C. canephora P. accessions. *Food Chemistry, 75*(2), 223-230.

Lammertyn, J., Peirs, A., De Baerdemaeker, J., & Nicolaı, B. (2000). Light penetration properties of NIR radiation in fruit with respect to non-destructive quality assessment. *Postharvest Biology and Technology, 18*(2), 121-132.

Lara, M., Lleó, L., Diezma-Iglesias, B., Roger, J.-M., & Ruiz-Altisent, M. (2013). Monitoring spinach shelf-life with hyperspectral image through packaging films. *Journal of Food Engineering, 119*(2), 353-361.

Lee, L. W., Cheong, M. W., Curran, P., Yu, B., & Liu, S. Q. (2016). Modulation of coffee aroma via the fermentation of green coffee beans with Rhizopus oligosporus: I. Green coffee. *Food Chemistry, 211*, 916-924.

Leiva-Valenzuela, G. A., Lu, R., & Aguilera, J. M. (2013). Prediction of firmness and soluble solids content of blueberries using hyperspectral reflectance imaging. *Journal of Food Engineering, 115*(1), 91-98.

León-Roque, N., Abderrahim, M., Nuñez-Alejos, L., Arribas, S. M., & Condezo-Hoyos, L. (2016). Prediction of fermentation index of cocoa beans (Theobroma cacao L.) based on color measurement and artificial neural networks. *Talanta, 161*, 31-39.

Leroy, T., De Bellis, F., Legnate, H., Kananura, E., Gonzales, G., Pereira, L. F., Andrade, A. C., Charmetant, P., Montagnon, C., & Cubry, P. (2011). Improving the quality of African robustas: QTLs for yield-and quality-related traits in Coffea canephora. *Tree Genetics & Genomes, 7*(4), 781-798.

Levi, I., & Anderson, J. (1950). Variations in protein contens of plants, heads, spikelets, and individual kernels, of wheat. *Canadian Journal of Research, 28*(3), 71-81.

Lewis, E. N., & Kidder, L. H. (2010). Technologies and Practical Considerations for Implementing Near-Infrared Chemical Imaging. *Raman, Infrared, and Near-Infrared Chemical Imaging*, 75-91.

Li, J., Rao, X., & Ying, Y. (2011). Detection of common defects on oranges using hyperspectral reflectance imaging. *Computers and electronics in Agriculture, 78*(1), 38-48.

Liu, C., Liu, W., Lu, X., Chen, W., Yang, J., & Zheng, L. (2014). Nondestructive determination of transgenic Bacillus thuringiensis rice seeds (Oryza sativa L.) using multispectral imaging and chemometric methods. *Food Chemistry, 153*, 87-93.

Liu, D., Zeng, X.-A., & Sun, D.-W. (2015). Recent developments and applications of hyperspectral imaging for quality evaluation of agricultural products: a review. *Critical reviews in food science and nutrition, 55*(12), 1744-1757.

Lohumi, S., Lee, S., Lee, H., & Cho, B.-K. (2015). A review of vibrational spectroscopic techniques for the detection of food authenticity and adulteration. *Trends in Food Science & Technology, 46*(1), 85-98.

Long, D., Engel, R., & Siemens, M. (2008). Measuring grain protein concentration with in-line near infrared reflectance spectroscopy. *Agronomy journal, 100*(2), 247-252.

Lorente, D., Aleixos, N., Gómez-Sanchis, J., Cubero, S., García-Navarrete, O. L., & Blasco, J. (2012). Recent advances and applications of hyperspectral imaging for fruit and vegetable quality assessment. *Food and Bioprocess Technology, 5*(4), 1121-1142.

Lü, Q., Tang, M., Cai, J., Zhao, J., & ViTTayapaduNg, S. (2011). Vis/NIR hyperspectral imaging for detection of hidden bruises on kiwifruits. *Czech Journal of Food Sciences, 29*(6), 595-602.

Lu, R., & Ariana, D. P. (2013). Detection of fruit fly infestation in pickling cucumbers using a hyperspectral reflectance/transmittance imaging system. *Postharvest Biology and Technology, 81*, 44-50.

Lyman, D. J., Benck, R., Dell, S., Merle, S., & Murray-Wijelath, J. (2003). FTIR-ATR analysis of brewed coffee: effect of roasting conditions. *Journal of Agricultural and Food Chemistry, 51*(11), 3268-3272.

Maeztu, L., Sanz, C., Andueza, S., Paz de Pena, M., Bello, J., & Cid, C. (2001). Characterization of espresso coffee aroma by static headspace GC− MS and sensory flavor profile. *Journal of Agricultural and Food Chemistry, 49*(11), 5437-5444.

Mahesh, S., Jayas, D., Paliwal, J., & White, N. (2011). Identification of wheat classes at different moisture levels using near-infrared hyperspectral images of bulk samples. *Sensing and Instrumentation for Food Quality and Safety, 5*(1), 1-9.

Mahesh, S., Jayas, D., Paliwal, J., & White, N. (2015). Comparison of partial least squares regression (PLSR) and principal components regression (PCR) methods for protein and hardness predictions using the near-infrared (NIR) hyperspectral images of bulk samples of Canadian wheat. *Food and Bioprocess Technology, 8*(1), 31-40.

Mahesh, S., Manickavasagan, A., Jayas, D., Paliwal, J., & White, N. (2008). Feasibility of near-infrared hyperspectral imaging to differentiate Canadian wheat classes. *biosystems engineering, 101*(1), 50-57.

Major, B., Kettlewell, P., & Scott, R. (2001). Mechanisms leading to excess alpha-amylase activity in wheat (Triticum aestivum, L) grain in the UK. *Journal of Cereal Science, 33*(3), 313-329.

Manley, M. (2014). Near-infrared spectroscopy and hyperspectral imaging: non-destructive analysis of biological materials. *Chemical Society Reviews, 43*(24), 8200-8214.

Mares, D., & Mrva, K. (2008). Late-maturity α-amylase: Low falling number in wheat in the absence of preharvest sprouting. *Journal of Cereal Science, 47*(1), 6-17.

Mares, D., & Mrva, K. (2014). Wheat grain preharvest sprouting and late maturity alpha-amylase. *Planta, 240*(6), 1167-1178.

Marten, G. C., Shenk, J., & Barton, F. (1989). Near infrared reflectance spectroscopy (NIRS): Analysis of forage quality. *Agriculture handbook (USA).*

Martens, H., & Naes, T. (1992). *Multivariate calibration*: John Wiley & Sons.

Martens, H. A., & Dardenne, P. (1998). Validation and verification of regression in small data sets. *Chemometrics and intelligent laboratory systems, 44*(1), 99-121.

Martin, D. (2007). A practical guide to machine vision lighting. *Midwest Sales and Support Manager, Adv Illum2007*, 1-3.

Martín, M. a. J., Pablos, F., & González, A. G. (1998). Discrimination between arabica and robusta green coffee varieties according to their chemical composition. *Talanta, 46*(6), 1259-1264.

Mayer, F., Czerny, M., & Grosch, W. (1999). Influence of provenance and roast degree on the composition of potent odorants in Arabica coffees. *European food research and technology, 209*(3), 242-250.

McCleary, B., & Sturgeon, R. (2002). Measurement of alpha-amylase in cereal, food, and fermentation products. *Cereal foods world, 47*(7), 299.

McGoverin, C. M., Engelbrecht, P., Geladi, P., & Manley, M. (2011). Characterisation of non-viable whole barley, wheat and sorghum grains using near-infrared hyperspectral data and chemometrics. *Analytical and Bioanalytical Chemistry, 401*(7), 2283-2289.

Mehmood, T., Liland, K. H., Snipen, L., & Sæbø, S. (2012). A review of variable selection methods in partial least squares regression. *Chemometrics and intelligent laboratory systems, 118*, 62-69.

Mendoza, F., Lu, R., Ariana, D., Cen, H., & Bailey, B. (2011). Integrated spectral and image analysis of hyperspectral scattering data for prediction of apple fruit firmness and soluble solids content. *Postharvest Biology and Technology, 62*(2), 149-160.

Mendoza, F., Lu, R., & Cen, H. (2012). Comparison and fusion of four nondestructive sensors for predicting apple fruit firmness and soluble solids content. *Postharvest Biology and Technology, 73*, 89-98.

Millar, S. (2003). The development of near infrared (NIR) spectroscopy calibrations for the prediction of wheat and flour quality (Project report No. 310). *CCFRA, Chipping Campden, UK*.

Millar, S., Whitworth, M., Chau, A., & Gilchrist, J. (2008). Mapping food composition using NIR hyperspectral imaging. *New Food, 3*, 34-39.

Miller, C. L. (2008). *Variation in single kernel hardness within the wheat spike*. Kansas State University.

Monteiro, S. T., Minekawa, Y., Kosugi, Y., Akazawa, T., & Oda, K. (2007). Prediction of sweetness and amino acid content in soybean crops from hyperspectral imagery. *ISPRS Journal of Photogrammetry and Remote Sensing, 62*(1), 2-12.

Moore, D. S. (2015). Reiner Salzer and Heinz W. Siesler (Eds.): Infrared and Raman spectroscopic imaging. *Analytical and Bioanalytical Chemistry, 407*(19), 5551-5552.

Morgano, M. A., Gomes Faria, C., Flores Ferrâo, M., Bragagnolo, N., & Miguel de Castro Ferreira, M. (2008). Determinação de umidade em café cru usando espectroscopia NIR e regressão multivariada. *Ciência e Tecnologia de Alimentos, 28*(1).

Myles, A. J., Zimmerman, T. A., & Brown, S. D. (2006). Transfer of multivariate classification models between laboratory and process near-infrared spectrometers for the discrimination of green Arabica and Robusta coffee beans. *Applied spectroscopy, 60*(10), 1198-1203.

Næs, T., Isaksson, T., Fearn, T., & Davies, T. (2002). *A user friendly guide to multivariate calibration and classification*: NIR publications.

Nakariyakul, S., & Casasent, D. P. (2011). Classification of internally damaged almond nuts using hyperspectral imagery. *Journal of Food Engineering, 103*(1), 62-67.

Nansen, C., Singh, K., Mian, A., Allison, B. J., & Simmons, C. W. (2016). Using hyperspectral imaging to characterize consistency of coffee brands and their respective roasting classes. *Journal of Food Engineering, 190*, 34-39.

Nansen, C., Zhang, X., Aryamanesh, N., & Yan, G. (2014). Use of variogram analysis to classify field peas with and without internal defects caused by weevil infestation. *Journal of Food Engineering, 123*, 17-22.

Nanyam, Y., Choudhary, R., Gupta, L., & Paliwal, J. (2012). A decision-fusion strategy for fruit quality inspection using hyperspectral imaging. *biosystems engineering, 111*(1), 118-125.

Ncama, K., Opara, U. L., Tesfay, S. Z., Fawole, O. A., & Magwaza, L. S. (2017). Application of Vis/NIR spectroscopy for predicting sweetness and flavour parameters of 'Valencia'orange (Citrus sinensis) and 'Star Ruby'grapefruit (Citrus x paradisi Macfad). *Journal of Food Engineering, 193*, 86-94.

Nielsen, D. S., Teniola, O., Ban-Koffi, L., Owusu, M., Andersson, T., & Holzapfel, W. (2007). The microbiology of Ghanaian cocoa fermentations analysed using culture-dependent and culture-independent methods. *International Journal of Food Microbiology, 114*(2), 168-186.

Nielsen, J. P., Pedersen, D. K., & Munck, L. (2003). Development of nondestructive screening methods for single kernel characterization of wheat. *Cereal Chemistry, 80*(3), 274-280.

Niemenak, N., Rohsius, C., Elwers, S., Ndoumou, D. O., & Lieberei, R. (2006). Comparative study of different cocoa (Theobroma cacao L.) clones in terms of their phenolics and anthocyanins contents. *Journal of Food Composition and Analysis, 19*(6), 612-619.

Nogales-Bueno, J., Baca-Bocanegra, B., Rodríguez-Pulido, F. J., Heredia, F. J., & Hernández-Hierro, J. M. (2015). Use of near infrared hyperspectral tools for the screening of extractable polyphenols in red grape skins. *Food Chemistry, 172*, 559-564.

Norris, K. (1982). Use of Near-Infrared Reflectance Spectroscopy and Dye-Binding Techniques for Estimating Protein in Oat Groats. *Cereal Chem, 59*(5), 333-335.

Oracz, J., Zyzelewicz, D., & Nebesny, E. (2015). The content of polyphenolic compounds in cocoa beans (Theobroma cacao L.), depending on variety, growing region, and processing operations: A review. *Critical reviews in food science and nutrition, 55*(9), 1176-1192.

Ortega, N., Romero, M.-P., Macià, A., Reguant, J., Anglès, N., Morelló, J.-R., & Motilva, M.-J. (2008). Obtention and characterization of phenolic extracts from different cocoa sources. *Journal of Agricultural and Food Chemistry, 56*(20), 9621-9627.

Osborne, Fearn, T., & Stevenson, S. (1987). Near-infrared research in Europe: American Association of Cereal Chemists.

Osborne, B. (2006). Applications of near infrared spectroscopy in quality screening of early-generation material in cereal breeding programmes. *Journal of Near Infrared Spectroscopy, 14*(2), 93-101.

Osborne, B., Fearn, T., & Hindle, P. (1993). *Practical NIR spectroscopy with applications in food and beverage analysis*: Longman scientific and technical.

Osborne, B. G. (1984). Investigations into the use of near infrared reflectance spectroscopy for the quality assessment of wheat with respect to its potential for bread baking. *Journal of the Science of Food and Agriculture, 35*(1), 106-110.

Osborne, B. G. (1987). Determination of moisture in white flour, ground wheat and whole wheat by near infrared reflectance using a single calibration. *Journal of the Science of Food and Agriculture, 38*(4), 341-346.

Othman, A., Ismail, A., Ghani, N. A., & Adenan, I. (2007). Antioxidant capacity and phenolic content of cocoa beans. *Food Chemistry, 100*(4), 1523-1530.

Owusu, M. (2010). *Influence of raw material and processing on aroma in chocolate.*

Ozaki, Y., McClure, W. F., & Christy, A. A. (2006). *Near-infrared spectroscopy in food science and technology*: John Wiley & Sons.

Park, B., & Lu, R. (2015). *Hyperspectral imaging technology in food and agriculture*: Springer.

Páscoa, R. N., Magalhães, L. M., & Lopes, J. A. (2013). FT-NIR spectroscopy as a tool for valorization of spent coffee grounds: Application to assessment of antioxidant properties. *Food Research International, 51*(2), 579-586.

Payne, P. I. (1987). Genetics of wheat storage proteins and the effect of allelic variation on bread-making quality. *Annual Review of Plant Physiology, 38*(1), 141-153.

Pelletier, M., & Pelletier, C. (2010). Spectroscopic theory for chemical imaging. *Raman, Infrared, and Near-Infrared Chemical Imaging*, 1-20.

Peng, Y., & Lu, R. (2008). Analysis of spatially resolved hyperspectral scattering images for assessing apple fruit firmness and soluble solids content. *Postharvest Biology and Technology, 48*(1), 52-62.

Perrone, D., Donangelo, C. M., & Farah, A. (2008). Fast simultaneous analysis of caffeine, trigonelline, nicotinic acid and sucrose in coffee by liquid chromatography–mass spectrometry. *Food Chemistry, 110*(4), 1030-1035.

Perrone, D., Donangelo, R., Donangelo, C. M., & Farah, A. (2010). Modeling weight loss and chlorogenic acids content in coffee during roasting. *Journal of Agricultural and Food Chemistry, 58*(23), 12238-12243.

Piccino, S., Boulanger, R., Descroix, F., & Sing, A. S. C. (2014). Aromatic composition and potent odorants of the "specialty coffee" brew "Bourbon Pointu" correlated to its three trade classifications. *Food Research International, 61*, 264-271.

Pierna, J. F., Vermeulen, P., Amand, O., Tossens, A., Dardenne, P., & Baeten, V. (2012). NIR hyperspectral imaging spectroscopy and chemometrics for the detection of undesirable substances in food and feed. *Chemometrics and intelligent laboratory systems, 117*, 233-239.

Pizarro, C., Esteban-Díez, I., González-Sáiz, J.-M., & Forina, M. (2007). Use of near-infrared spectroscopy and feature selection techniques for predicting the caffeine content and roasting color in roasted coffees. *Journal of Agricultural and Food Chemistry, 55*(18), 7477-7488.

Pizarro, C., Esteban-Díez, I., Nistal, A.-J., & González-Sáiz, J.-M. a. (2004). Influence of data pre-processing on the quantitative determination of the ash content and lipids in roasted coffee by near infrared spectroscopy. *Analytica Chimica Acta, 509*(2), 217-227.

Poisson, L., Blank, I., Dunkel, A., & Hofmann, T. (2016). The Chemistry of RoastingdDecoding Flavor Formation. *The Craft and Science of Coffee*, 273.

Poisson, L., Schmalzried, F., Davidek, T., Blank, I., & Kerler, J. (2009). Study on the role of precursors in coffee flavor formation using in-bean experiments. *Journal of Agricultural and Food Chemistry, 57*(21), 9923-9931.

Porep, J. U., Kammerer, D. R., & Carle, R. (2015). On-line application of near infrared (NIR) spectroscopy in food production. *Trends in Food Science & Technology, 46*(2), 211-230.

Prats-Montalbán, J., De Juan, A., & Ferrer, A. (2011). Multivariate image analysis: a review with applications. *Chemometrics and intelligent laboratory systems, 107*(1), 1-23.

Puvipirom, J., & Chaiseri, S. (2012). Contribution of roasted grains and seeds in aroma of oleang (Thai coffee drink). *International Food Research Journal, 19*(2), 2231-7546.

Qin, J., Burks, T. F., Zhao, X., Niphadkar, N., & Ritenour, M. A. (2012). Development of a two-band spectral imaging system for real-time citrus canker detection. *Journal of Food Engineering, 108*(1), 87-93.

Qin, J., & Lu, R. (2008). Measurement of the optical properties of fruits and vegetables using spatially resolved hyperspectral diffuse reflectance imaging technique. *Postharvest Biology and Technology, 49*(3), 355-365.

Qin, J., & Lu, R. (2009). Monte Carlo simulation for quantification of light transport features in apples. *Computers and electronics in Agriculture, 68*(1), 44-51.

Rahman, A., & Cho, B.-K. (2016). Assessment of seed quality using non-destructive measurement techniques: a review. *Seed Science Research, 26*(4), 285-305.

Rajkumar, P., Wang, N., EImasry, G., Raghavan, G., & Gariepy, Y. (2012). Studies on banana fruit quality and maturity stages using hyperspectral imaging. *Journal of Food Engineering, 108*(1), 194-200.

Reddy, L., Ching, T., & Metzger, R. (1984). Alpha-amylase activity in wheat kernels matured and germinated under different temperature conditions. *Cereal Chemistry, 61*, 228 - 231.

Reh, C., Gerber, A., Prodolliet, J., & Vuataz, G. (2006). Water content determination in green coffee–Method comparison to study specificity and accuracy. *Food Chemistry, 96*(3), 423-430.

Ribeiro, J., Ferreira, M., & Salva, T. (2011). Chemometric models for the quantitative descriptive sensory analysis of Arabica coffee beverages using near infrared spectroscopy. *Talanta, 83*(5), 1352-1358.

Ribeiro, J., Teófilo, R., Augusto, F., & Ferreira, M. (2010). Simultaneous optimization of the microextraction of coffee volatiles using response surface methodology and principal component analysis. *Chemometrics and intelligent laboratory systems, 102*(1), 45-52.

Rinnan, Å., van den Berg, F., & Engelsen, S. B. (2009). Review of the most common pre-processing techniques for near-infrared spectra. *Trends in Analytical Chemistry, 28*(10), 1201-1222.

Risius, H., Hahn, J., Huth, M., Tölle, R., & Korte, H. (2015). In-line estimation of falling number using near-infrared diffuse reflectance spectroscopy on a combine harvester. *Precision Agriculture, 16*(3), 261-274.

Roberts, J., & Cozzolino, D. (2016). An overview on the application of chemometrics in food science and technology—an approach to quantitative data analysis. *Food Analytical Methods, 9*(12), 3258-3267.

Rodríguez-Pulido, F. J., Barbin, D. F., Sun, D.-W., Gordillo, B., González-Miret, M. L., & Heredia, F. J. (2013). Grape seed characterization by NIR hyperspectral imaging. *Postharvest Biology and Technology, 76*, 74-82.

Romero-Cortes, T., Salgado-Cervantes, M. A., García-Alamilla, P., García-Alvarado, M. A., del C Rodríguez-Jimenes, G., Hidalgo-Morales, M., & Robles-Olvera, V. (2013). Relationship between fermentation index and other biochemical changes evaluated during the fermentation of Mexican cocoa (Theobroma cacao) beans. *Journal of the Science of Food and Agriculture, 93*(10), 2596-2604.

Rubayiza, A. B., & Meurens, M. (2005). Chemical discrimination of arabica and robusta coffees by Fourier transform Raman spectroscopy. *Journal of agricultural and food chemistry, 53*(12), 4654-4659.

Santos, J. R., Sarraguça, M. C., Rangel, A. O., & Lopes, J. A. (2012). Evaluation of green coffee beans quality using near infrared spectroscopy: A quantitative approach. *Food Chemistry, 135*(3), 1828-1835.

Santos, J. R., Viegas, O., Páscoa, R. N., Ferreira, I. M., Rangel, A. O., & Lopes, J. A. (2016). In-line monitoring of the coffee roasting process with near infrared spectroscopy: Measurement of sucrose and colour. *Food Chemistry, 208*, 103-110.

Sasic, S., Ozaki, Y., & (Eds.). (2011). *Raman, infrared, and near-infrared chemical imaging*: John Wiley & Sons.

Scheidig, C., Czerny, M., & Schieberle, P. (2007). Changes in key odorants of raw coffee beans during storage under defined conditions. *Journal of Agricultural and Food Chemistry, 55*(14), 5768-5775.

Schenker, S., Heinemann, C., Huber, M., Pompizzi, R., Perren, R., & Escher, R. (2002). Impact of roasting conditions on the formation of aroma compounds in coffee beans. *Journal of Food Science, 67*(1), 60-66.

Scholz, M. B. d. S., Kitzberger, C. S. G., Pereira, L. F. P., Davrieux, F., Pot, D., Charmetant, P., & Leroy, T. (2014). Application of near infrared spectroscopy for green coffee biochemical phenotyping. *Journal of Near Infrared Spectroscopy, 22*(6), 411-421.

Schulmerich, M. V., Walsh, M. J., Gelber, M. K., Kong, R., Kole, M. R., Harrison, S. K., McKinney, J., Thompson, D., Kull, L. S., & Bhargava, R. (2012). Protein and oil composition predictions of single soybeans by transmission Raman spectroscopy. *Journal of Agricultural and Food Chemistry, 60*(33), 8097-8102.

Semmelroch, P., & Grosch, W. (1996). Studies on character impact odorants of coffee brews. *Journal of Agricultural and Food Chemistry, 44*(2), 537-543.

Serpen, A., Capuano, E., Fogliano, V., & Gökmen, V. (2007). A new procedure to measure the antioxidant activity of insoluble food components. *Journal of Agricultural and Food Chemistry, 55*(19), 7676-7681.

Serranti, S., Cesare, D., Marini, F., & Bonifazi, G. (2013). Classification of oat and groat kernels using NIR hyperspectral imaging. *Talanta, 103*, 276-284.

Shahin, M. A., & Symons, S. J. (2008). Detection of hard vitreous and starchy kernels in amber durum wheat samples using hyperspectral imaging (GRL Number M306). *NIR news, 19*(5), 16-18.

Shahin, M. A., Symons, S. J., & Hatcher, D. W. (2014). Quantification of mildew damage in soft red winter wheat based on spectral characteristics of bulk samples: a comparison of visible-near-infrared imaging and near-infrared spectroscopy. *Food and Bioprocess Technology, 7*(1), 224-234.

Shan, J., Suzuki, T., Ogawa, Y., & Kondo, N. (2015). Coffee roasting degrees prediction in terms of weight loss with selected wavebands based on near-infrared spectroscopy. *Engineering in Agriculture, Environment and Food, 8*(4), 195-199.

Shenk, J. S., & Westerhaus, M. O. (1996). Calibration the ISI Way. In A. M. C. Davis & P. Williams (Eds.), *Near Infrared Spectroscopy: The Future Waves* (pp. 198-202). Chichester, UK: NIR Publications.

Shenk, J. S., Workman, J. J., & Westerhaus, M. O. (2001). Application of NIR spectroscopy to agricultural products. *Practical Spectroscopy Series, 27*, 419-474.

Shewry, P. R., & Halford, N. G. (2002). Cereal seed storage proteins: structures, properties and role in grain utilization. *Journal of experimental botany, 53*(370), 947-958.

Singh, C. B. (2009). Detection of insect and fungal damage and incidence of sprouting in stored wheat using near-infrared hyperspectral and digital color imaging. *Journal of Stored Products Research, 45*(3), 151-158.

Siripatrawan, U., Makino, Y., Kawagoe, Y., & Oshita, S. (2011). Rapid detection of Escherichia coli contamination in packaged fresh spinach using hyperspectral imaging. *Talanta, 85*(1), 276-281.

Sissons, M., Osborne, B., & Sissons, S. (2006). Application of near infrared reflectance spectroscopy to a durum wheat breeding programme. *Journal of Near Infrared Spectroscopy, 14*(1), 17-25.

Sivertsen, A. H. (2011). Automatic inspection of cod (Gadus Morhua L.) fillets by hyperspectral imaging. *The Artic University of Norway*.

Smail, V. W., Fritz, A. K., & Wetzel, D. L. (2006). Chemical imaging of intact seeds with NIR focal plane array assists plant breeding. *Vibrational Spectroscopy, 42*(2), 215-221.

Sonka, M., Hlavac, V., & Boyle, R. (2014). *Image processing, analysis, and machine vision*: Cengage Learning.

Speer, K., & Kölling-Speer, I. (2006). The lipid fraction of the coffee bean. *Brazilian Journal of Plant Physiology, 18*(1), 201-216.

Steiner, R. (2011). Laser-tissue interactions *Laser and IPL Technology in Dermatology and Aesthetic Medicine* (pp. 23-36): Springer.

Su, W.-H., He, H.-J., & Sun, D.-W. (2017). Non-destructive and rapid evaluation of staple foods quality by using spectroscopic techniques: a review. *Critical reviews in food science and nutrition, 57*(5), 1039-1051.

Sugiyama, T., Sugiyama, J., Tsuta, M., Fujita, K., Shibata, M., Kokawa, M., Araki, T., Nabetani, H., & Sagara, Y. (2010). NIR spectral imaging with discriminant analysis for detecting foreign materials among blueberries. *Journal of Food Engineering, 101*(3), 244-252.

Sunarharum, W. B., Williams, D. J., & Smyth, H. E. (2014). Complexity of coffee flavor: A compositional and sensory perspective. *Food Research International, 62*, 315-325.

Sunoj, S., Igathinathane, C., & Visvanathan, R. (2016). Nondestructive determination of cocoa bean quality using FT-NIR spectroscopy. *Computers and electronics in Agriculture, 124*, 234-242.

Taghizadeh, M., Gowen, A. A., & O'Donnell, C. P. (2011). Comparison of hyperspectral imaging with conventional RGB imaging for quality evaluation of Agaricus bisporus mushrooms. *biosystems engineering, 108*(2), 191-194.

Taradolsirithitikul, P., Sirisomboon, P., & Dachoupakan Sirisomboon, C. (2017). Qualitative and quantitative analysis of ochratoxin A contamination in green coffee beans using Fourier transform near infrared spectroscopy. *Journal of the Science of Food and Agriculture, 97*(4), 1260-1266.

Teye, E., & Huang, X. (2015). Novel prediction of total fat content in cocoa beans by FT-NIR spectroscopy based on effective spectral selection multivariate regression. *Food Analytical Methods, 8*(4), 945-953.

Teye, E., Huang, X., Dai, H., & Chen, Q. (2013). Rapid differentiation of Ghana cocoa beans by FT-NIR spectroscopy coupled with multivariate classification. *Spectrochimica Acta Part A: Molecular and Biomolecular Spectroscopy, 114*, 183-189.

Teye, E., Huang, X., Sam-Amoah, L. K., Takrama, J., Boison, D., Botchway, F., & Kumi, F. (2015). Estimating cocoa bean parameters by FT-NIRS and chemometrics analysis. *Food Chemistry, 176*, 403-410.

Teye, E., Huang, X., Takrama, J., & Haiyang, G. (2014). Integrating NIR spectroscopy and electronic tongue together with chemometric analysis for accurate classification of cocoa bean varieties. *Journal of Food Process Engineering, 37*(6), 560-566.

Toci, A. T., & Farah, A. (2014). Volatile fingerprint of Brazilian defective coffee seeds: corroboration of potential marker compounds and identification of new low quality indicators. *Food Chemistry, 153*, 298-314.

Toledo, P. R., Pezza, L., Pezza, H. R., & Toci, A. T. (2016). Relationship between the different aspects related to coffee quality and their volatile compounds. *Comprehensive Reviews in Food Science and Food Safety, 15*(4), 705-719.

Tolessa, K., Rademaker, M., De Baets, B., & Boeckx, P. (2016). Prediction of specialty coffee cup quality based on near infrared spectra of green coffee beans. *Talanta, 150*, 367-374.

Tran, C. D. (2003). Infrared multispectral imaging: principles and instrumentation. *Applied Spectroscopy Reviews, 38*(2), 133-153.

Tran, H. T., Vargas, C. A. C., Lee, L. S., Furtado, A., Smyth, H., & Henry, R. (2017). Variation in bean morphology and biochemical composition measured in different genetic groups of arabica coffee (Coffea arabica L.). *Tree Genetics & Genomes, 13*(3), 54.

Van Boekel, M. (2006). Formation of flavour compounds in the Maillard reaction. *Biotechnology advances, 24*(2), 230-233.
Van Hilten, H. J., Fisher, P. J., & Wheeler, M. A. (2011). *The Coffee Exporter's Guide*: International Trade Centre UNCTAD/GATT.
Velasco, L., & Möllers, C. (2002). Nondestructive assessment of protein content in single seeds of rapeseed (Brassica napus L.) by near-infrared reflectance spectroscopy. *Euphytica, 123*(1), 89-93.
Velasco, L., Möllers, C., & Becker, H. C. (1999). Estimation of seed weight, oil content and fatty acid composition in intact single seeds of rapeseed (Brassica napus} L.) by near-infrared reflectance spectroscopy. *Euphytica, 106*(1), 79-85.
Velasco, L., Pérez-Vich, B., & Fernandez-Martinez, J. M. (2004). Use of near-infrared reflectance spectroscopy for selecting for high stearic acid concentration in single husked achenes of sunflower. *Crop science, 44*(1), 93-97.
Verity, J. C. K., Hac, L., & Skerritt, J. H. (1999). Development of a field enzyme-linked immunosorbent assay (ELISA) for detection of alpha-amylase in preharvest-sprouted wheat. *Cereal Chem, 76*(5), 673-681.
Veselá, A., Barros, A. S., Synytsya, A., Delgadillo, I., Čopíková, J., & Coimbra, M. A. (2007). Infrared spectroscopy and outer product analysis for quantification of fat, nitrogen, and moisture of cocoa powder. *Analytica Chimica Acta, 601*(1), 77-86.
Vidal, M., & Amigo, J. M. (2012). Pre-processing of hyperspectral images. Essential steps before image analysis. *Chemometrics and intelligent laboratory systems, 117*, 138-148.
Vines, L. L., Kays, S. E., & Koehler, P. E. (2005). Near-infrared reflectance model for the rapid prediction of total fat in cereal foods. *Journal of Agricultural and Food Chemistry, 53*(5), 1550-1555.
Vithu, P., & Moses, J. (2016). Machine vision system for food grain quality evaluation: A review. *Trends in Food Science & Technology, 56*, 13-20.
Wang, J., Jun, S., Bittenbender, H., Gautz, L., & Li, Q. X. (2009). Fourier transform infrared spectroscopy for Kona coffee authentication. *Journal of food science, 74*(5), C385-C391.
Wang, L., Liu, D., Pu, H., Sun, D.-W., Gao, W., & Xiong, Z. (2015). Use of hyperspectral imaging to discriminate the variety and quality of rice. *Food Analytical Methods, 8*(2), 515-523.
Wang, W., Li, C., Tollner, E. W., Gitaitis, R. D., & Rains, G. C. (2012). Shortwave infrared hyperspectral imaging for detecting sour skin (Burkholderia cepacia)-infected onions. *Journal of Food Engineering, 109*(1), 38-48.
Weenen, H., & Apeldoorn, W. (1996). Carbohydrate cleavage in the Maillard reaction. *Special Publication - Royal Society of Chemistry, 197*, 211-216.
Wei, F., & Tanokura, M. (2015). Chemical changes in the components of coffee beans during roasting. *Coffee in Health and Disease Prevention, 10*, 83-91.
Weinstock, B. A., Janni, J., Hagen, L., & Wright, S. (2006). Prediction of oil and oleic acid concentrations in individual corn (Zea mays L.) kernels using near-infrared reflectance hyperspectral imaging and multivariate analysis. *Applied spectroscopy, 60*(1), 9-16.
Whitacre, E., Liver, J., Broek, R. v. d., Engelen, P. v., Remers, B., Horst, B. v. d., Tewart, M., & Jansen-Beuvink, A. (2003). Predictive Analysis of Cocoa Procyanidins Using Near-Infrared Spectroscopy Techniques. *Journal of Food Science, 68*(9), 2618-2622.
Williams. (2001). Sampling, sample preparation, and sample selection. *Practical Spectroscopy Series, 27*, 307-350.

Williams, P., Geladi, P., Fox, G., & Manley, M. (2009). Maize kernel hardness classification by near infrared (NIR) hyperspectral imaging and multivariate data analysis. *Analytica Chimica Acta, 653*(2), 121-130.

Williams, P., & Norris, K. (1987). *Near-infrared technology in the agricultural and food industries*: American Association of Cereal Chemists, Inc. Minnesota (USA). ISBN: 091325049X.

Williams, P. C., & Sobering, D. (1993). Comparison of commercial near infrared transmittance and reflectance instruments for analysis of whole grains and seeds. *Journal of Near Infrared Spectroscopy, 1*(1), 25-32.

Williams, P. J., Geladi, P., Britz, T. J., & Manley, M. (2012). Investigation of fungal development in maize kernels using NIR hyperspectral imaging and multivariate data analysis. *Journal of Cereal Science, 55*(3), 272-278.

Wintgens, J. (2009). Factors influencing the quality of green coffee. *Coffee: Growing, Processing, Sustainable Production: A Guidebook for Growers, Processors, Traders, and Researchers*, 789-809.

Wollgast, J., & Anklam, E. (2000). Review on polyphenols in Theobroma cacao: changes in composition during the manufacture of chocolate and methodology for identification and quantification. *Food Research International, 33*(6), 423-447.

Workman, J., & Weyer, L. (2012). *Practical guide and spectral atlas for interpretive near-infrared spectroscopy*: CRC Press.

Wrigley, C. (2009). Wheat: a unique grain for the world. *Wheat: chemistry and technology, 7*(American Association of Cereal Chemists, Inc (AACC)), 1-17.

Wu, D., & Sun, D.-W. (2013a). Advanced applications of hyperspectral imaging technology for food quality and safety analysis and assessment: A review—Part I: Fundamentals. *Innovative Food Science & Emerging Technologies, 19*, 1-14.

Wu, D., & Sun, D.-W. (2013b). Advanced applications of hyperspectral imaging technology for food quality and safety analysis and assessment: a review—part II: applications. *Innovative Food Science & Emerging Technologies, 19*, 15-28.

Wu, J., & Shi, C. (2004). Prediction of grain weight, brown rice weight and amylose content in single rice grains using near-infrared reflectance spectroscopy. *Field Crops Research, 87*(1), 13-21.

Xing, J., Symons, S., Hatcher, D., & Shahin, M. (2011). Comparison of short-wavelength infrared (SWIR) hyperspectral imaging system with an FT-NIR spectrophotometer for predicting alpha-amylase activities in individual Canadian Western Red Spring (CWRS) wheat kernels. *biosystems engineering, 108*(4), 303-310.

Xing, J., Symons, S., Shahin, M., & Hatcher, D. (2010). Detection of sprout damage in Canada Western Red Spring wheat with multiple wavebands using visible/near-infrared hyperspectral imaging. *biosystems engineering, 106*(2), 188-194.

Xing, J., Van Hung, P., Symons, S., Shahin, M., & Hatcher, D. (2009). Using a short wavelength infrared (SWIR) hyperspectral imaging system to predict alpha amylase activity in individual Canadian western wheat kernels. *Sensing and Instrumentation for Food Quality and Safety, 3*(4), 211-218.

Xu, J.-L., Riccioli, C., & Sun, D.-W. (2016). Efficient integration of particle analysis in hyperspectral imaging for rapid assessment of oxidative degradation in salmon fillet. *Journal of Food Engineering, 169*, 259-271.

Yang, N., Liu, C., Liu, X., Degn, T. K., Munchow, M., & Fisk, I. (2016). Determination of volatile marker compounds of common coffee roast defects. *Food Chemistry, 211*, 206-214.

Yao, H., Hruska, Z., Kincaid, R., Brown, R. L., Bhatnagar, D., & Cleveland, T. E. (2013). Detecting maize inoculated with toxigenic and atoxigenic fungal strains with fluorescence hyperspectral imagery. *biosystems engineering, 115*(2), 125-135.

Yao, H., Lewis, D., & Sun, P. (2010). Spectral preprocessing and calibration techniques. *Hyperspectral imaging for food quality analysis and control*, 45-78.

Yeretzian, C., Jordan, A., Badoud, R., & Lindinger, W. (2002). From the green bean to the cup of coffee: investigating coffee roasting by on-line monitoring of volatiles. *European food research and technology, 214*(2), 92-104.

Zamora-Rojas, E. (2013). *Control no destructivo e in situ de productos y procesos en la industria del cerdo ibérico usando censores espectrales de infrarrojo cercano.* Universidad de Córdoba.

Zhang, C., Jiang, H., Liu, F., & He, Y. (2017). Application of near-infrared hyperspectral imaging with variable selection methods to determine and visualize caffeine content of coffee beans. *Food and Bioprocess Technology, 10*(1), 213-221.

Zhang, X., & He, Y. (2013). Rapid estimation of seed yield using hyperspectral images of oilseed rape leaves. *Industrial Crops and Products, 42*, 416-420.

Zhang, X., Li, W., Yin, B., Chen, W., Kelly, D. P., Wang, X., Zheng, K., & Du, Y. (2013). Improvement of near infrared spectroscopic (NIRS) analysis of caffeine in roasted Arabica coffee by variable selection method of stability competitive adaptive reweighted sampling (SCARS). *Spectrochimica Acta Part A: Molecular and Biomolecular Spectroscopy, 114*, 350-356.

Zhang, X., Liu, F., He, Y., & Li, X. (2012). Application of hyperspectral imaging and chemometric calibrations for variety discrimination of maize seeds. *Sensors, 12*(12), 17234-17246.

Zhao, M., Esquerre, C., Downey, G., & O'Donnell, C. P. (2017). Process analytical technologies for fat and moisture determination in ground beef-a comparison of guided microwave spectroscopy and near infrared hyperspectral imaging. *Food Control, 73*, 1082-1094.

Zhao, X., Burks, T. F., Qin, J., & Ritenour, M. A. (2010). Effect of fruit harvest time on citrus canker detection using hyperspectral reflectance imaging. *Sensing and Instrumentation for Food Quality and Safety, 4*(3-4), 126-135.

Zheng, C., Sun, D.-W., & Zheng, L. (2006). Recent developments and applications of image features for food quality evaluation and inspection–a review. *Trends in Food Science & Technology, 17*(12), 642-655.

Zhu, D., Wang, C., Pang, B., Shan, F., Wu, Q., & Zhao, C. (2012). Identification of wheat cultivars based on the hyperspectral image of single seed. *Journal of Nanoelectronics and Optoelectronics, 7*(2), 167-172.

Zhu, D., Wang, K., Zhang, D., Huang, W., Yang, G., Ma, Z., & Wang, C. (2011). Quality assessment of crop seeds by near-infrared hyperspectral imaging. *Sensor Letters, 9*(3), 1144-1150.

APPENDIX

Microstructure of wheat kernels, cocoa and coffee beans.



Figure A.1. Microstructure of a wheat kernel obtained by Computed Tomography (courtesy of Campden BRI).

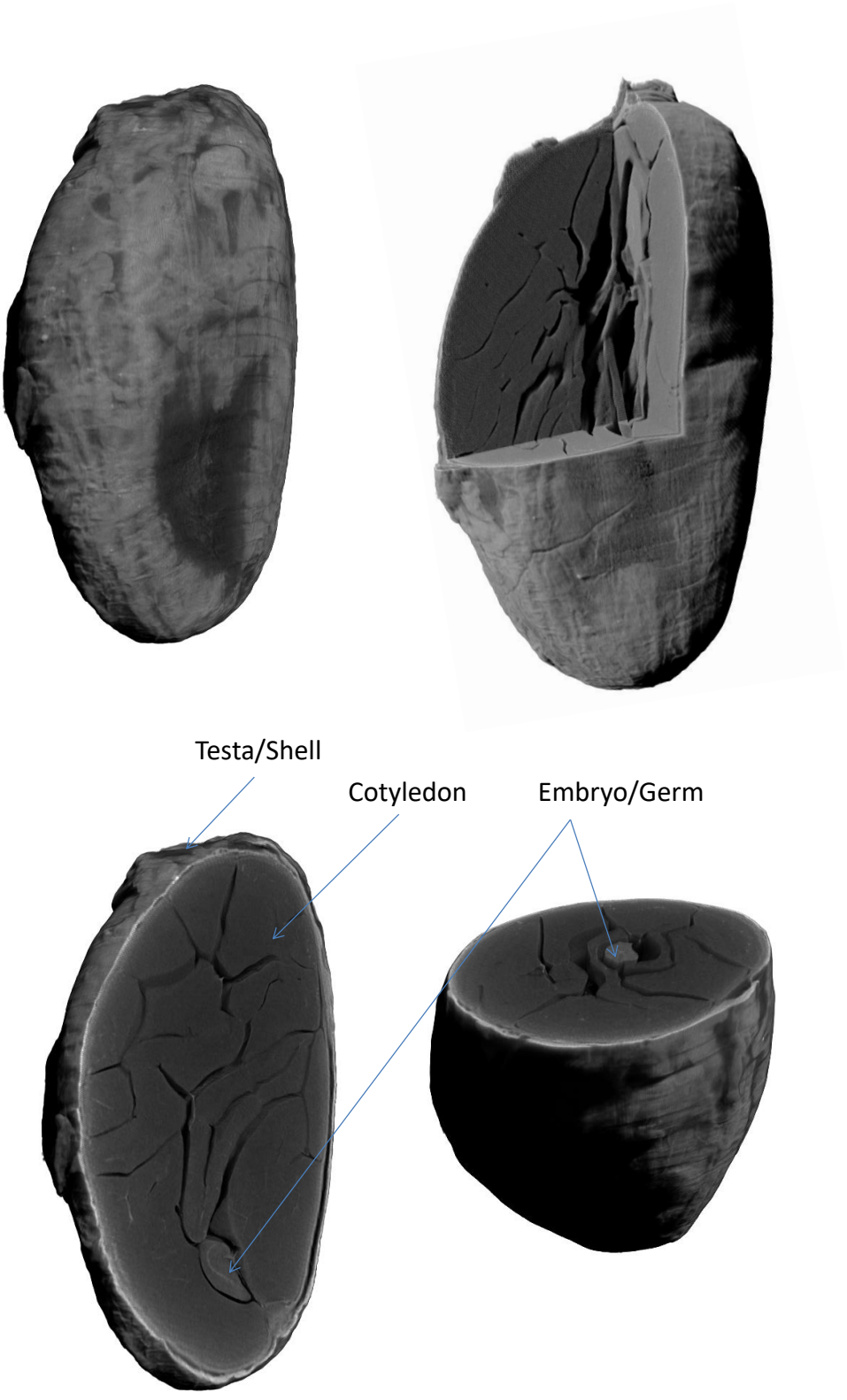


Figure A.2. Microstructure of a whole cocoa bean obtained by Computed Tomography (courtesy of Campden BRI).

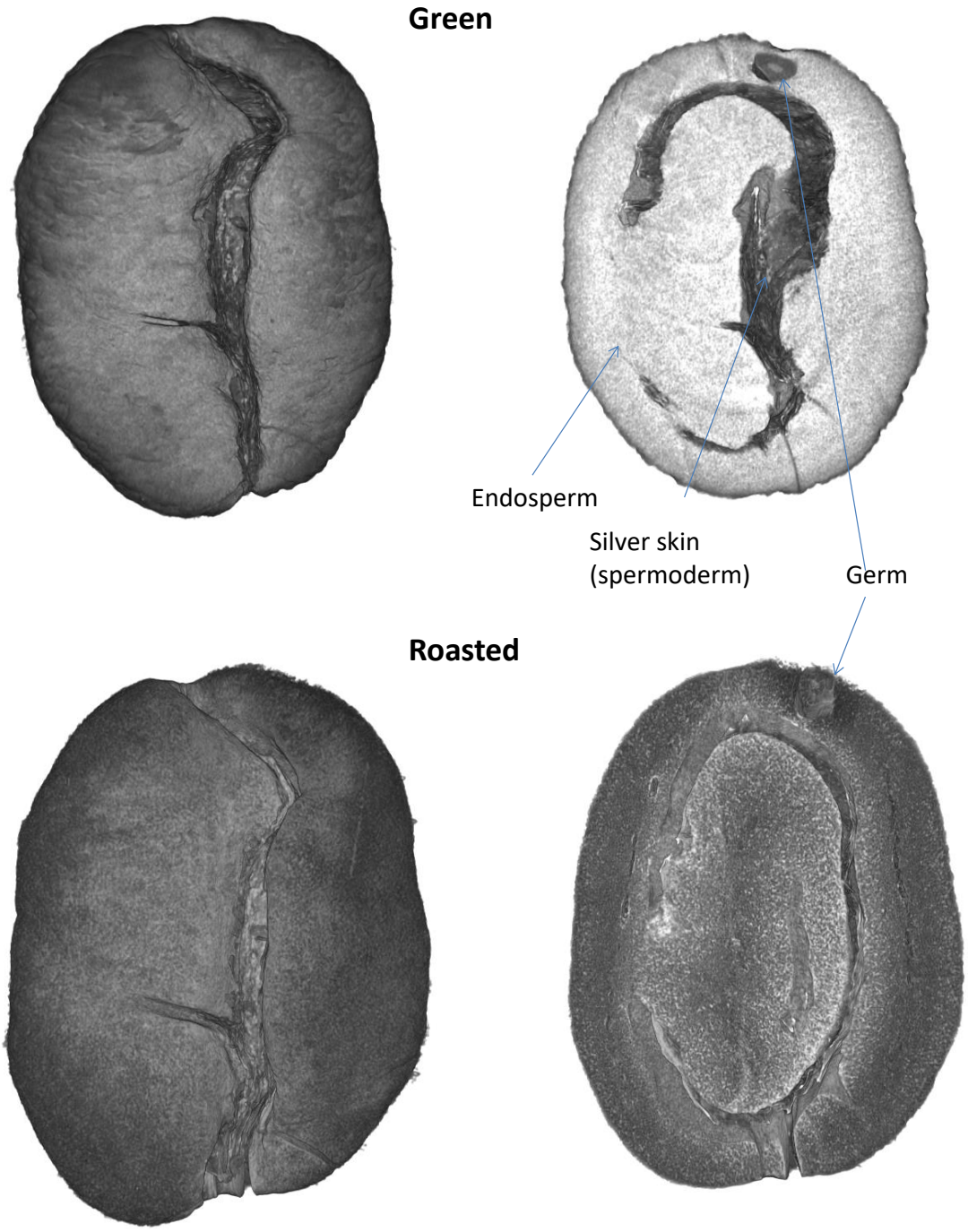


Figure A.3. Microstructure of a green and roasted coffee bean obtained by Computed Tomography. The same bean was scanned before and after roasting (courtesy of Campden BRI).

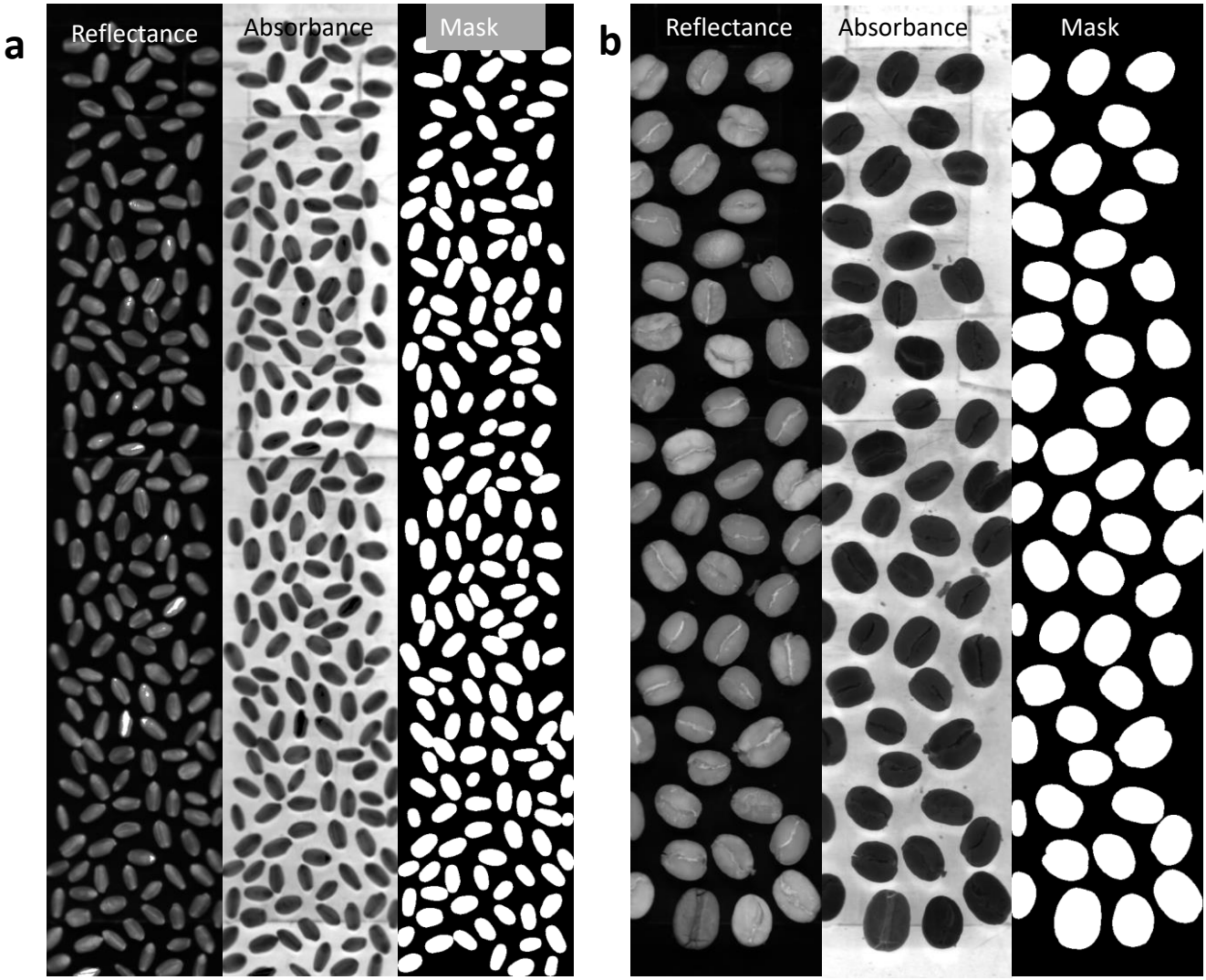


Figure A.4. Example of scanning multiple **a**) wheat kernels and **b**) coffee beans from a single batch, for validation purposes. The images show the original reflectance image at a specific spectral band (~1000 nm), the relative absorbance image (log(1/R)), and the mask applied for segmentation in order to remove the background and apply prediction calibrations to single objects.

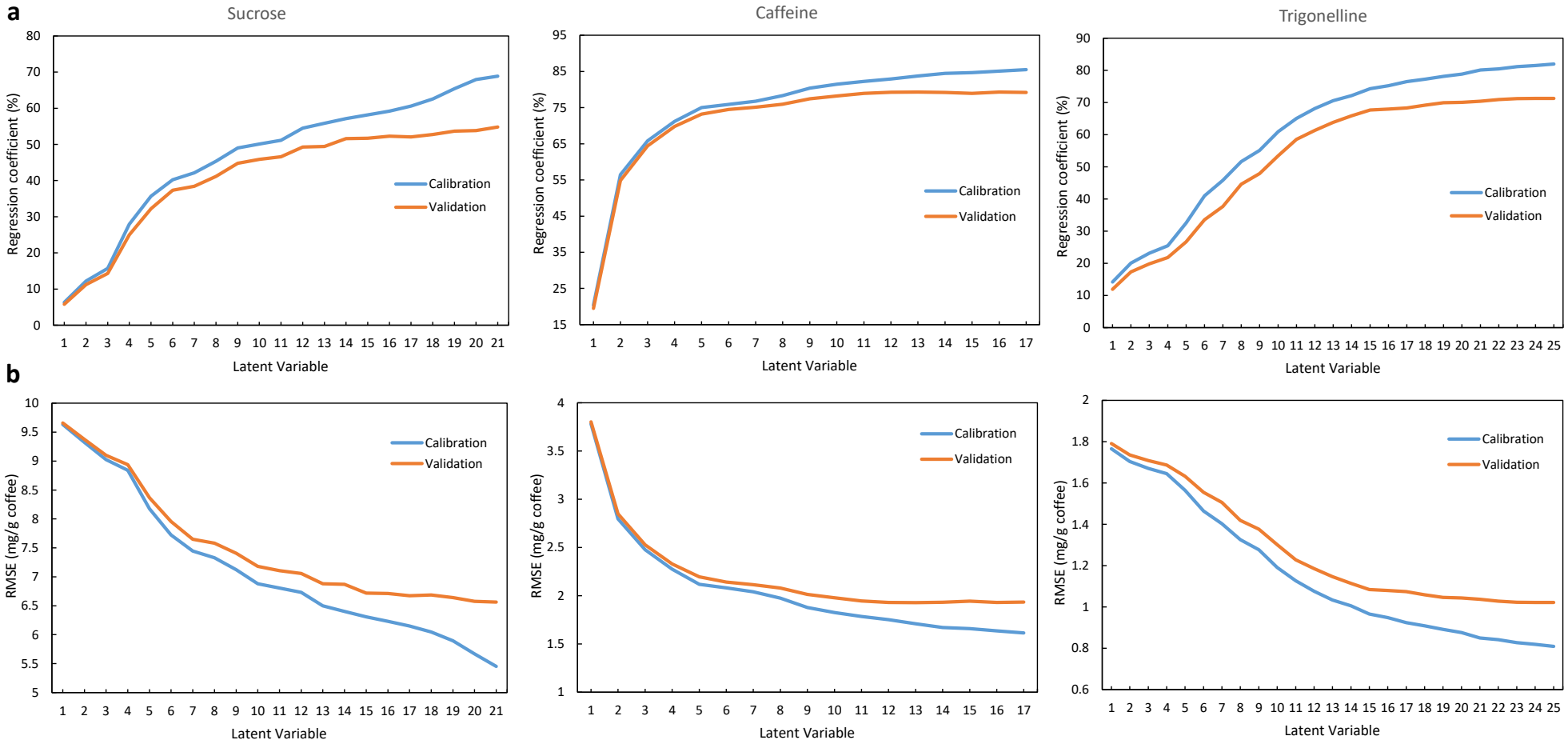


Figure A.5. **Model parameters of sucrose, caffeine and trigonelline in single green coffee beans**. Plots of (**a**) explained variance of the PLS regression models for sucrose, caffeine and trigonelline prediction; (**b**) root-mean square error (RMSE) of calibration and cross-validation for the models, depending on the number of Latent Variables (LV).

Table A.1. Chemical assignment of coffee compounds in the NIR spectral range, based on literature data (modified from Esteban-Diez et al., 2004).

Compound	Wavelength (nm)	Bond vibration
Amino acids / protein	1972/1978	N-H asymmetric stretching + amide II
	2124	N-H stretching + C=O stretching
	2142	=C-H stretching + C=C stretching (HC=CH)
Caffeine	1100/1212	C-H stretching second overtone
	1340	2 × C-H stretching + C-H deformation
	1914/1916	C=O str. second overtone (CONH)
Carbohydrates (fibre)	1212	C-H stretching second overtone
	1340	2 × C-H stretching + C-H deformation
	1718	C-H stretching first overtone (CH2)
	1838/1860	O-H stretching + 2 × C-O stretching
	2066/2096/2104	O-H stretc. + O-H def.; 2 × O-H def. + 2 × C-O stretc.
	2112	2 × O-H deformation + 2 × C-O stretching
Carbohydrates (sucrose)	1998/2008	2 × O-H deformation + C-O deformation
Carboxylic acids	1914	C=O stretching second overtone (-CO_2H)
Chlorogenic acids	1116/1120/1122	O-H stretching second overtone
	1124/1126	C-H stretching second overtone
	1908	C=O stretching second overtone (-CO_2H)
	1944/1948/1968	C=O stretching second overtone (-CO_2R)
	2066/2096/2112	O-H stretching + O-H deformation
	2142/2148/2150	=C-H stretching + C=C stretching (HC=CH)
Fatty acids	2170	2 × amide I + amide III
	1724/1728	C-H stretching first overtone (CH2)
	2150	=C-H stretching + C=C stretching (HC=CH)
	2170	CH_2 asymmetric stretching + C= stretc. (HC =CH)
Water	1934/1938/1944/1948	O-H stretching + O-H deformation

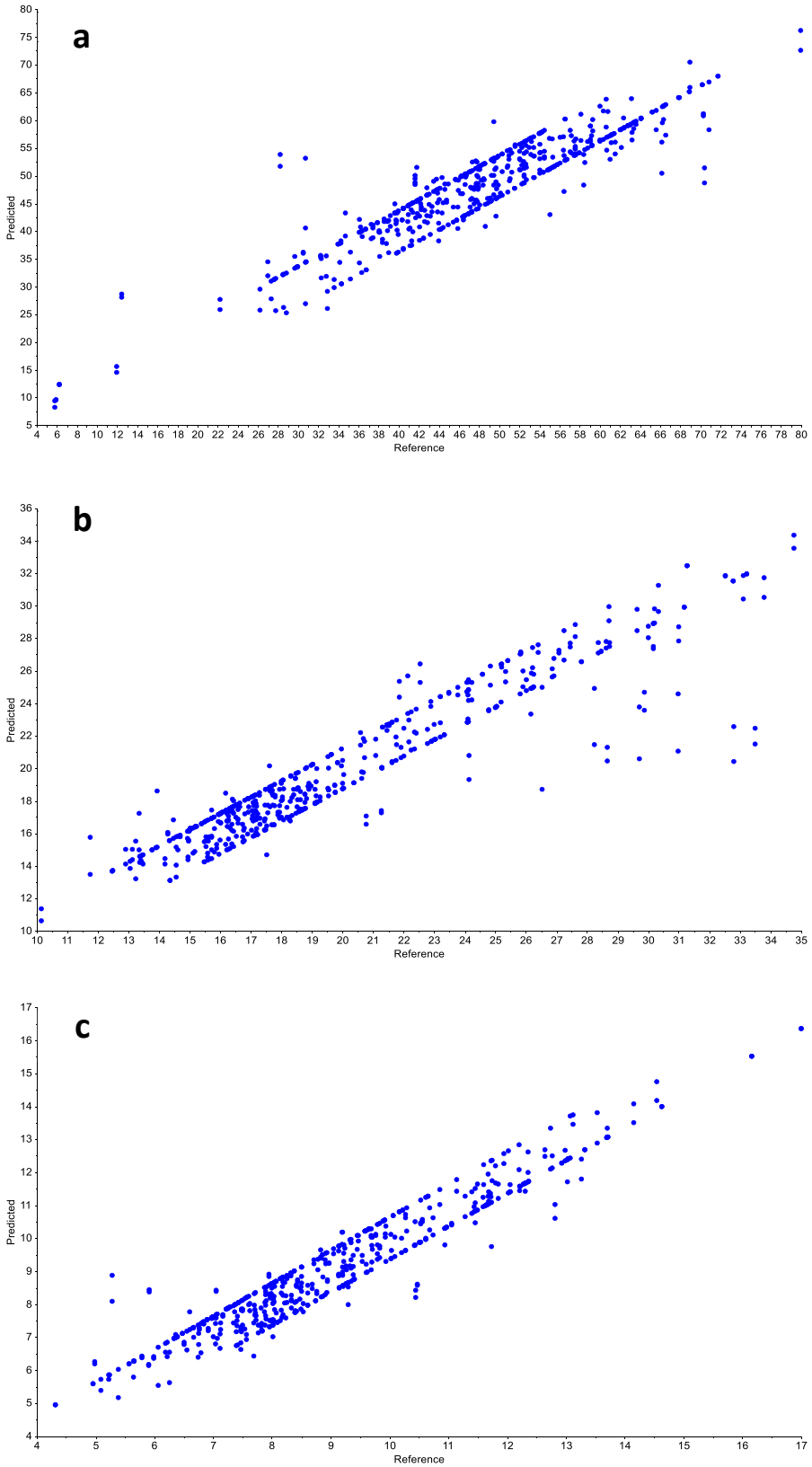


Figure A.6. HSI prediction model of green coffee constituents. Predicted vs reference measurement of (**a**) sucrose, (**b**) caffeine and (**c**) trigonelline using Support Vector Machine-Regression (SVM-R) (values expressed on dry matter basis).

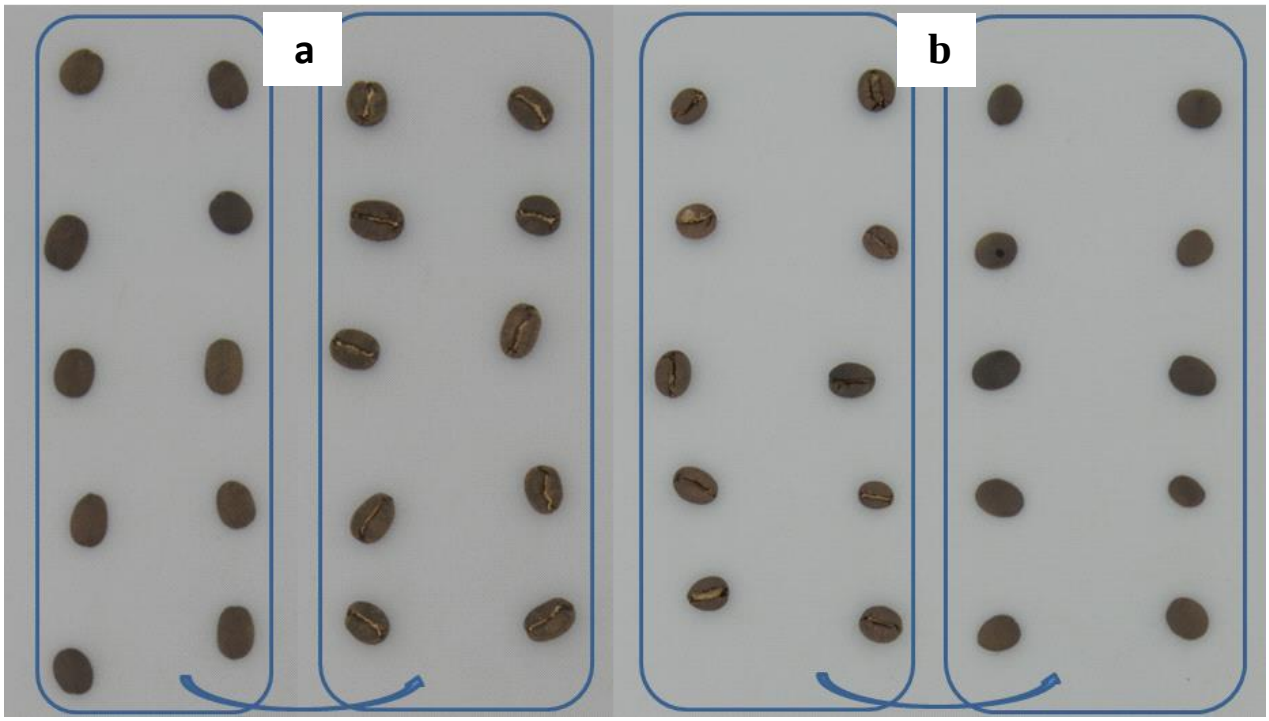


Figure A.7. Example of pictures acquired by DigiEye for coffee beans colour analysis. Pictures were acquired on both sides of the beans. **a**) Arabica and **b**) Robusta coffees from Guatemala.

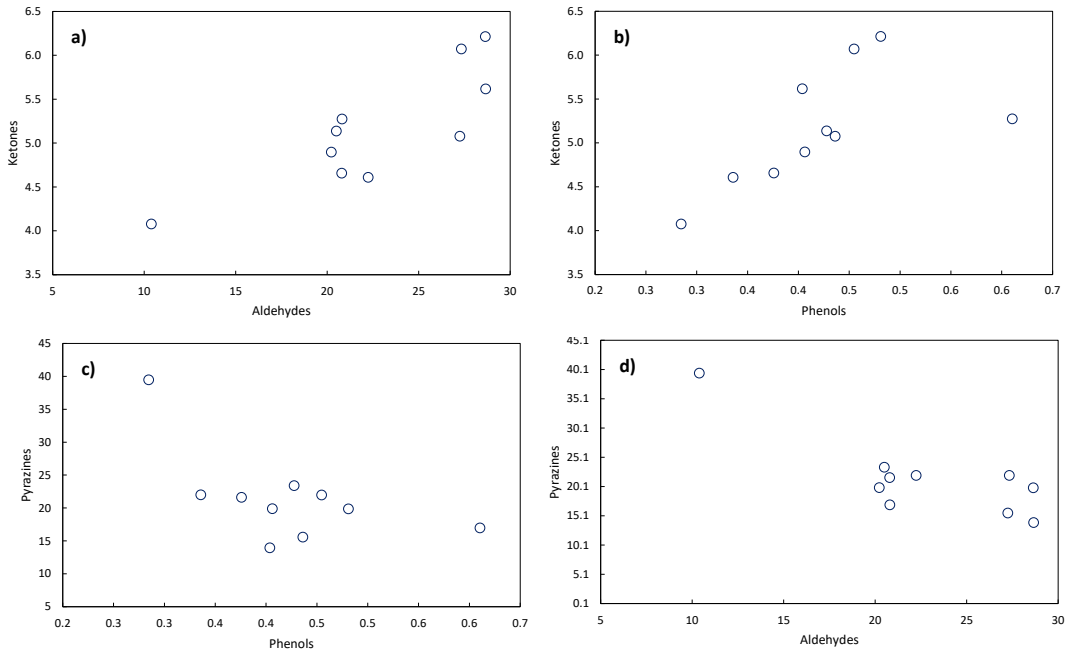


Figure A.8. Relationship between volatile compounds, grouped according to their chemical classes, predicted by HSI in single roasted coffee beans. Example on a batch of Arabica coffee, where 10 beans were scanned. (**a,b**) positive correlations, and (**c,d**) negative correlations were observed, with one bean showing dramatic differences (lower aldehydes and ketones, and higher pyrazines).

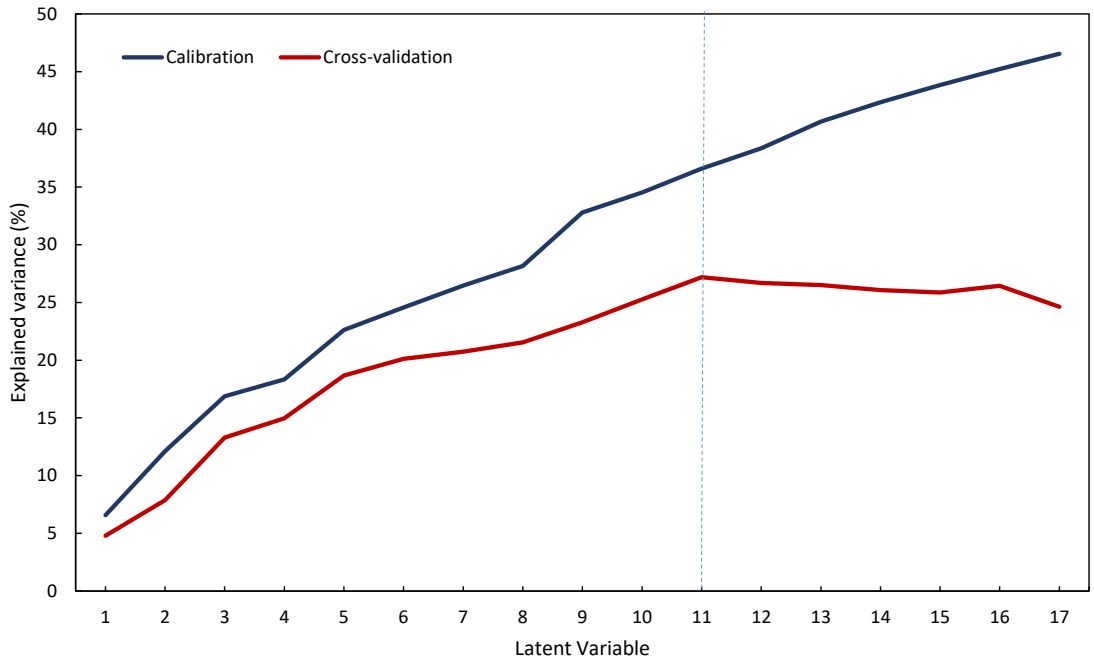


Figure A.9. Plot of explained variance depending on the number of latent variables used in PLS2 regression model for single volatile compounds in green coffee beans. The vertical line indicates the optimal LV chosen for the prediction model.

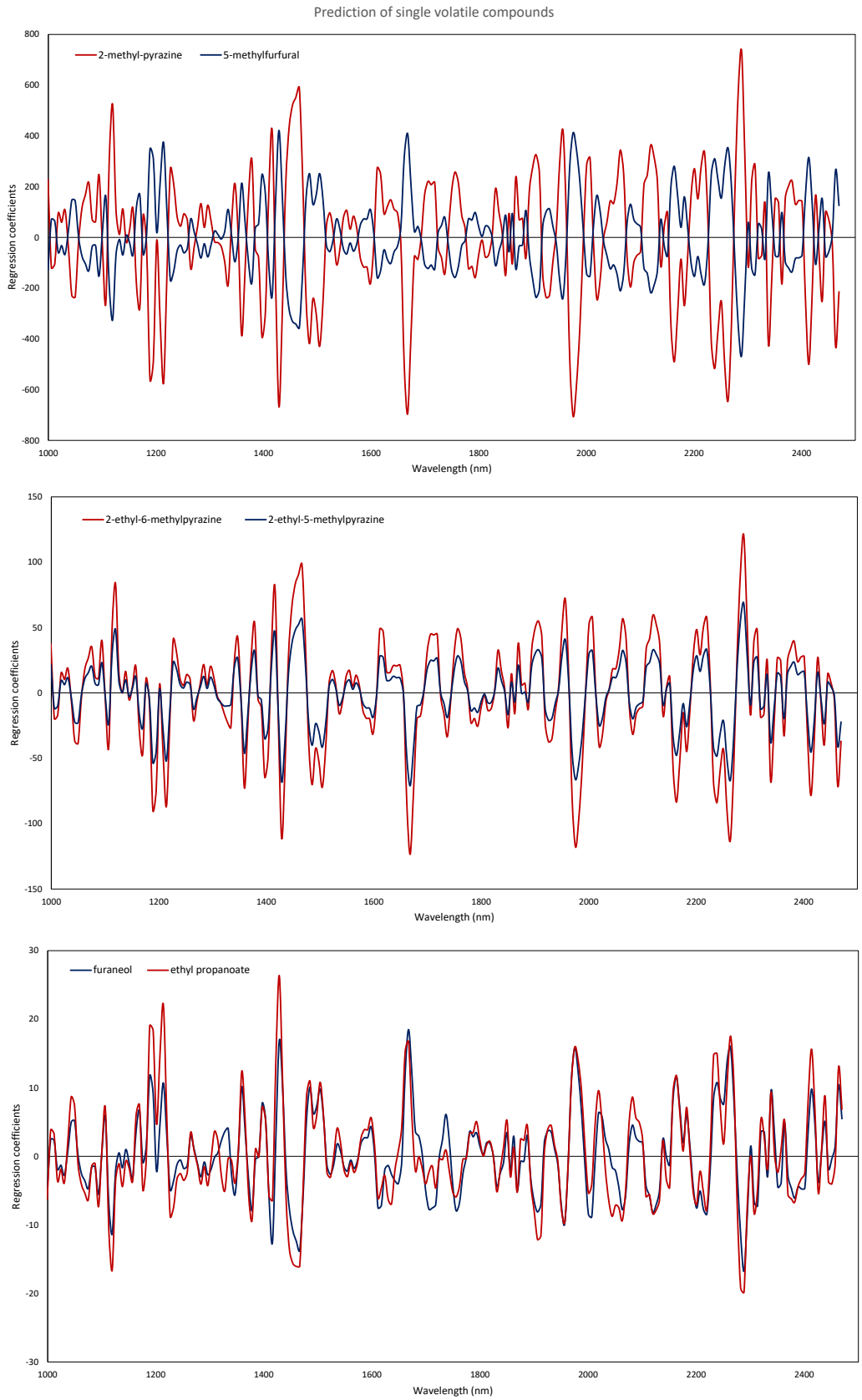


Figure A.10. PLS2 regression coefficients for HSI prediction of single volatile compounds. Example on some potent odorants in single coffee beans by scanning roasted coffee.

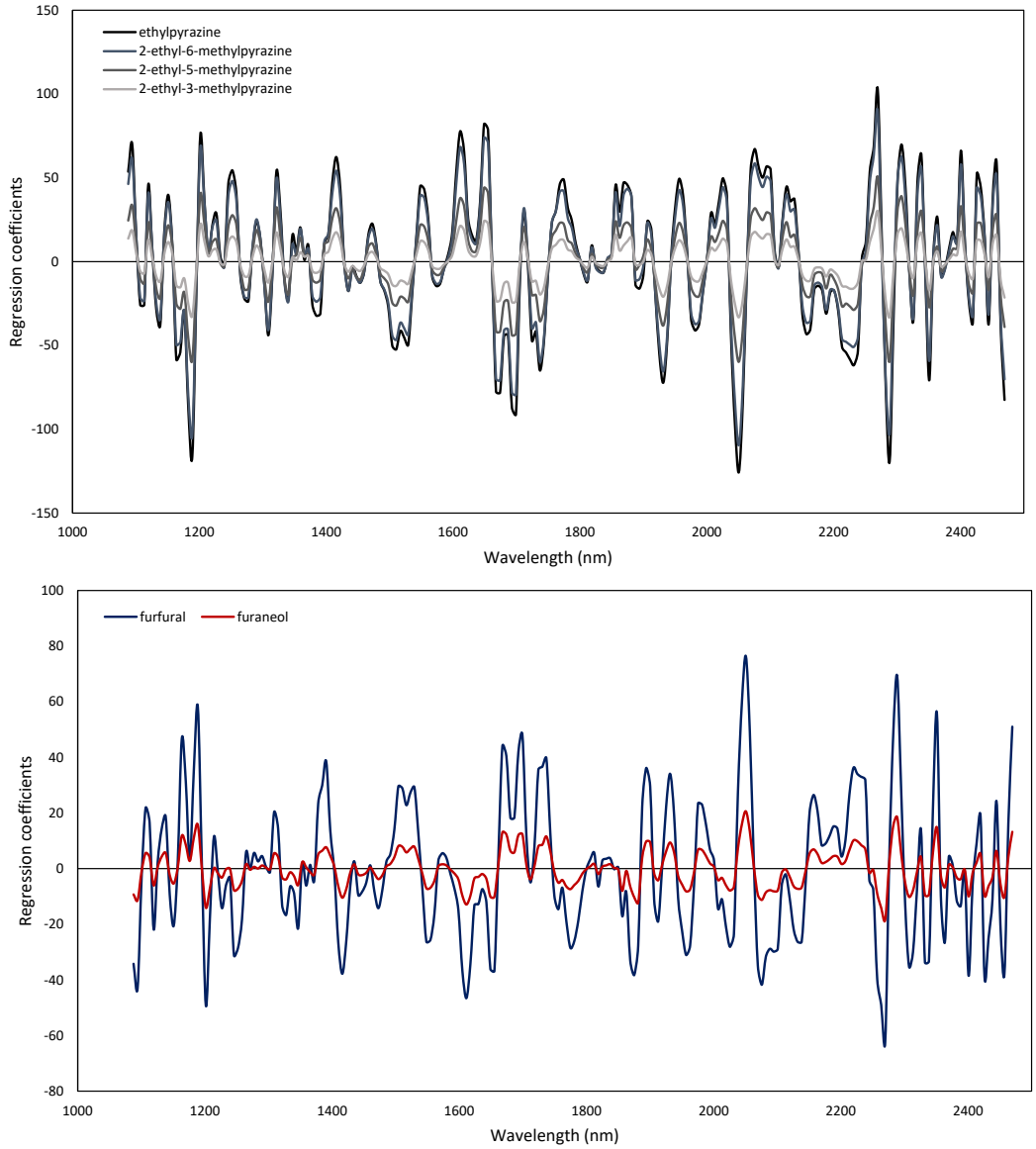


Figure A.11. PLS2 regression coefficients for HSI prediction of single volatile compounds. Example on some potent odorants in single coffee beans by scanning green coffee.

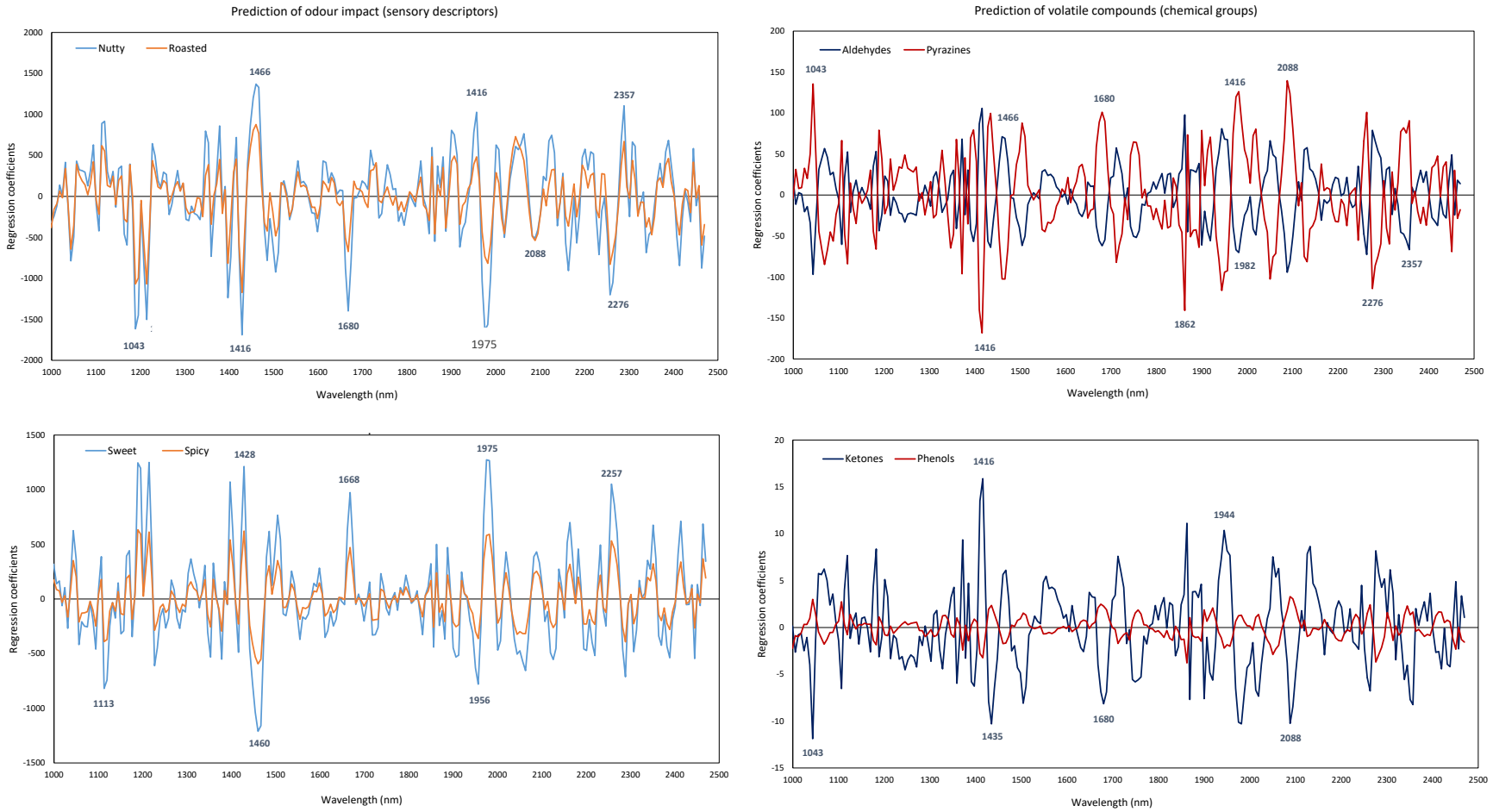


Figure A.12. Regression coefficients of the HSI prediction models in single roasted coffee beans, for (left graphs) **odour impact** and (right) volatiles compounds expressed as **chemical groups**. Spectral pre-treatment applied: 2nd derivative for predicted odour, and SNV for volatile compounds.

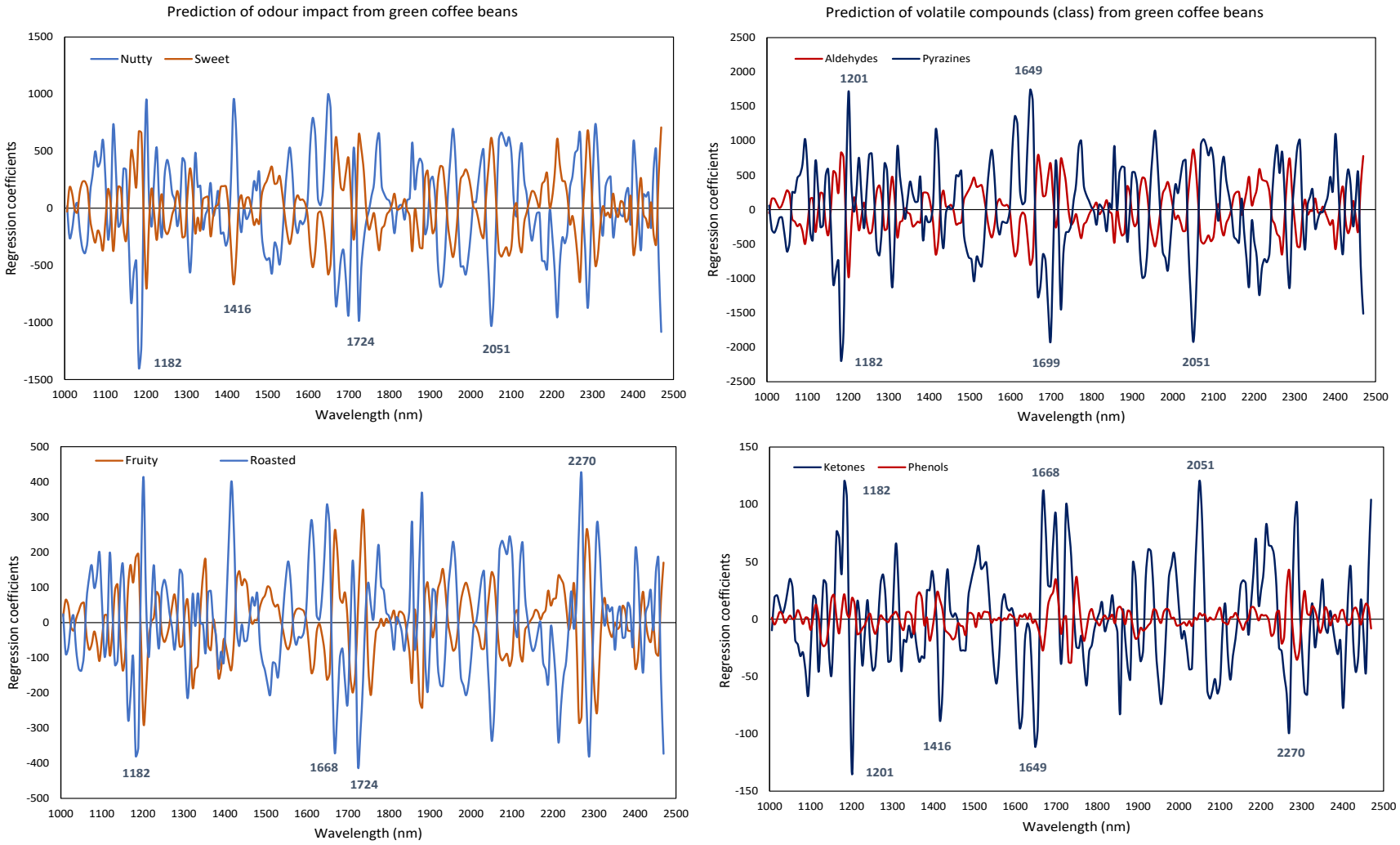


Figure A.13. Prediction of aroma generation from single green coffee beans by HSI. Left: prediction of expected **odour impact** in terms of sensory descriptors. Right: prediction of volatile compound grouped as **chemical classes**. Fruity values were multiplied by 10 for better visualisation.

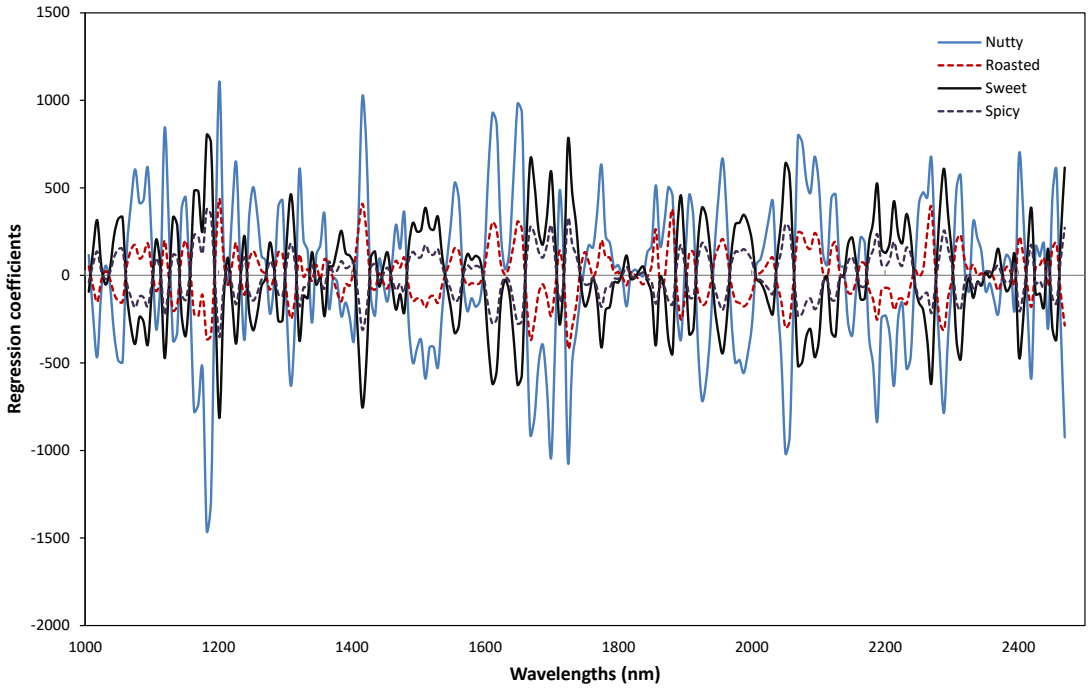


Figure A.14. Regression coefficients of the PLSR models for prediction of sensory impact in single coffee beans, built by HSI on green coffee beans.

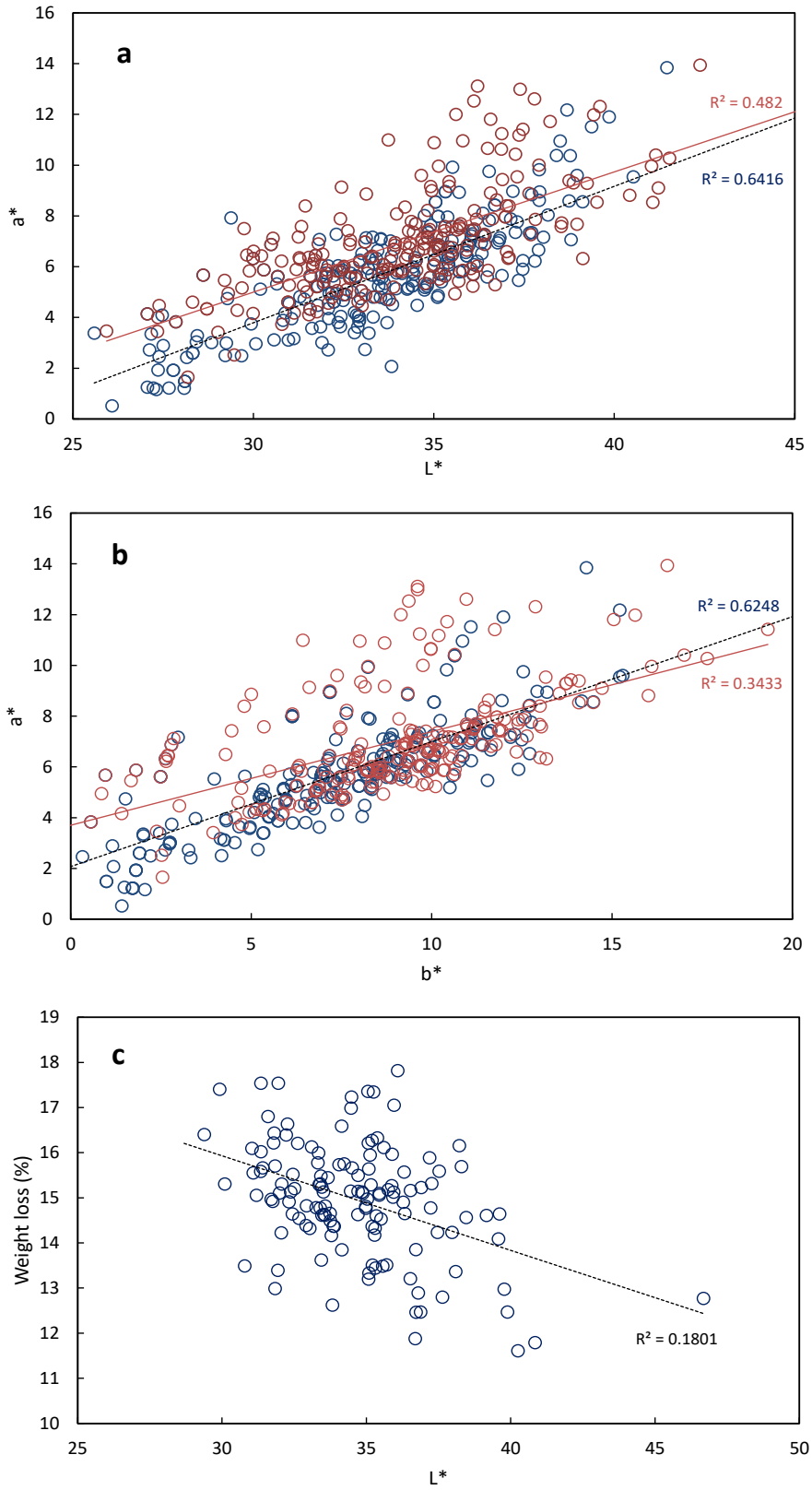


Figure A.15. Colour parameters (L* a* b* values) in single roasted coffee beans used in the present study, showing (**a,b**) the correlation among these parameters for the "up" (red) and "down" (blue) crease position of the bean. **c**) Correlation between L* value and the weight loss of single beans.